The Development of New Bioorganometallic Metallodendrimers as *in vitro* Anticancer Agents

Preshendren Govender

University of Cape Town

February 2014

The Development of New Bioorganometallic Metallodendrimers as *in vitro* Anticancer Agents

by

Preshendren Govender

Thesis Presented for the Degree of

Doctor of Philosophy

Supervisor: Associate Professor Gregory S. Smith

Department of Chemistry

University of Cape Town

South Africa

February 2014

Declaration

I declare that "**The Development of New Bioorganometallic Metallodendrimers as *in vitro* Anticancer Agents**" is my own work and to the best of my knowledge has never been reported or submitted for any degree or examination in any university. All sources of information used are cited, acknowledged and completely referenced at the end of each chapter.

I grant the University of Cape Town free license to reproduce the dissertation in whole or in-part for the purpose of research.

……..……..

Preshendren Govender

…..…/……../……..

Acknowledgements

I would like to express my appreciation and gratitude to A/Prof Gregory Smith, my research supervisor, for his constant guidance, encouragement, praise and constructive criticism throughout the project. Thank you so much for pushing me, sometimes kicking and screaming, to look at research and my work in different ways, and for opening my mind. Your support was essential for my success here.

My thanks are also extended to Prof Allan Hutton (University of Cape Town) for his help with the cyclic voltammetric experiments. I would like to acknowledge our Swiss collaborators, Prof Bruno Therrien (University of Néuchatel) for the X-ray crystallographic data and Prof Paul Dyson (Ecole Polytechnique Fédérale de Lausanne) for the anticancer and DNA binding data. Furthermore, I would like to acknowledge our German collaborators Prof Ulrich Schatzschneider for hosting me at the University of Würzburg and Mr Sandesh Pai for his help with the CO-release experiments.

I wish to acknowledge and appreciate the help provided by Mrs Deirdre Brooks for her administrative support and constant encouragement throughout my post-graduate career. I would also like to extend my thanks to the analytical staff at the University of Cape Town, Mr Pete Roberts for running the 2D-NMR experiments and Mr Gianpierro Benincasa for recording the elemental analysis data.

A heartfelt thank you to Dr Richard Gessner, Dr Peter Malatji and Dr Prinessa Chellan for proof-reading my thesis. I wish to thank my friends and colleagues, Miss Tameryn Stringer, Mr Wade Petersen, Mr Krishna Govender, Mr Kyle Fernandes, Miss Aneesa Omar and Dr Riedaa Gamieldien for our fruitful conversations. I would further like to thank the post-graduate students from the Hunter, Egan, Jardine and Chibale Research Groups for their support. Of course, I would like to thank the members of my research group, Organometallic Research, who made working in the lab a pleasure.

And finally to my family, once again Dad, Ma and Kirshia, I thank you for your unconditional love and support throughout my academic career and through another milestone in my life. Last but not least, to the love of my life, Miss Allenda Langenhoven, who played a crucial role in keeping me sane throughout my PhD career. Ally, you have taught me the real meaning of having patience, being truthful to one's self and unconditional love. Thank you for being my inspiration.

Financial support was provided by the National Research Fund (NRF-DAAD) and University of Cape Town.

"A question that sometimes drives me hazy: Am I or are the others crazy?"

Albert Einstein

Abstract

The clinical success of cisplatin and its derivatives for the treatment of different cancers has had a profound effect on the use of metal-containing agents in medicine. Despite the successes, the drawbacks of platinum-based therapy, such as drug resistance, toxicity and the emergence of unwanted side effects, have bred a need for effective and novel anticancer agents. Hence, the design and study of bioorganometallic complexes as potential therapeutic agents may eventually lead to the identification of new drug candidates. The purpose of this study was to synthesize and characterize a series of polynuclear transition-metal-containing complexes based on a (poly)propyleneimine dendritic scaffold, and investigate the *in vitro* antiproliferative activity of these complexes.

A series of new neutral and cationic *N*,*O*-ruthenium-arene, *N*,*N*- and *N*,*O*-osmium-arene metallodendrimers were successfully synthesized and characterized. This was achieved *via* the reaction of salicylaldehyde with the peripheral amine end-groups of first-, second-, third- and fourth-generation 1,4-diaminobutane poly(propylene) dendritic scaffolds, to afford polyvalent Schiff base dendritic ligands bearing salicylaldiminato functionalities on the surface. Complexation with metal-precursors $[M(\eta^6\text{-arene})Cl_2]_2$ (where M = Ru or Os and arene = *p*-cymene or hexamethylbenzene) afforded the metallodendrimers in good yield.

A second series of new cationic *N*,*O*- and *N*,*N*- ferrocenyl-derived ruthenium-arene metallodendrimers were prepared from new ferrocenyl-derived conjugates. The first step required preparation of the ferrocenyl-derived conjugates, and was achieved by reacting vinyl ferrocene with 4-bromo-2-hydroxybenzaldehyde or 5-bromo-2-pyridinecarboxaldehyde *via* a Heck coupling reaction. Schiff base condensation of first- and second-generation 1,4-diaminobutane poly(propylene) dendritic scaffolds with the ferrocenyl-conjugates afforded ferrocenyl-derived dendritic ligands. Complexation of the ferrocenyl-derived dendritic ligands with $[Ru(\eta^6\text{-}p\text{-cymene})Cl_2]_2$ produced heterometallic ferrocenyl-derived ruthenium-arene metallodendrimers. There is a direct correlation between the electron transfer capacity and anticancer activity of ferrocenyl-derived anticancer agents. The mode of action of these compounds is suggested to follow a series of redox processes which eventually results in the generation of reactive oxygen species. Consequently, electrochemical studies revealed that the *N*,*O*- ferrocenyl-derived ruthenium-arene metallodendrimers result in two irreversible redox

processes (oxidation of Fe^{II} and Ru^{II}), whilst the *N*,*N*- ferrocenyl-derived ruthenium-arene metallodendrimers display one reversible wave (*i.e.* Fe^{II}/Fe^{III}- couple) in the positive region. Hence, these systems favor the production of reactive oxygen species which in turn enhance these systems antitumor properties.

All of the metallodendrimers were isolated as air- and moisture-stable solids, which are soluble in only a handful of solvents. The mononuclear analogs were synthesized as models of the larger metallodendrimers. Single crystal X-ray diffraction, for a select number of model mononuclear complexes, confirmed the proposed molecular structure and pseudo-tetrahedral geometry around the metal ion. All dendritic ligands and complexes were fully characterized using an array of spectroscopic (^{1}H, $^{13}C\{^{1}H\}$ and $^{31}P\{^{1}H\}$ NMR, FT-IR and UV-Vis spectroscopy) and analytical (electrochemical, elemental analysis and mass spectrometry) methods.

As potential antitumor agents, the *in vitro* biological activity of all the complexes were evaluated against A2780 (cisplatin sensitive) and A2780cisR (cisplatin resistant) human ovarian carcinoma cell lines. In nanomedicine the concept of multinuclearity is used to improve the potency of therapeutic drugs, with respect to metallodendrimers, this concept is known as the dendritic effect and can be exploited by preparing dendrimer analogs of increasing dendrimer generation. Consequently, all metallodendrimers demonstrated moderate to high cytotoxic effects, with an increase in cytotoxicity observed upon increasing dendrimer generation. In particular, the fourth-generation *N*,*O*-ruthenium-arene metallodendrimers display potent activity (IC_{50} = 2 - 3 μM, A2780). The mononuclear derivatives have no significant cytotoxic effect (IC_{50} > 50 μM, A2780). Furthermore, introduction of the 1,3,5-triaza-7-phosphaadamantane ligand into the ruthenium coordination sphere displayed a vast improvement in the antitumor activity of these complexes. However, no improvement in cytotoxicity was observed when replacing ruthenium with osmium. The mode of action of platinum-based therapeutic drugs involves binding to DNA and hence, preliminary DNA binding studies in the form of NMR and gel electrophoresis experiments were performed and suggest DNA is a possible drug target.

Preliminary *in vitro* cell viability studies of the homometallic ferrocenyl-derived ligands and their heterometallic complexes revealed that both systems are moderately active against A2780 and A2780cisR human ovarian cancer cells at the 5 μM dose concentration. More specifically, four of the twelve compounds evaluated displayed enhanced activity. Furthermore, the data suggests introduction of the second metal, in the form of the ruthenium-arene moiety, does improve the activity in at least two of the heterometallic metallodendrimers compared to their homometallic dendritic ligands.

A third series of metallodendrimers bearing functionalized tricarbonylmanganese(I) CO-releasing moieties on the periphery were successfully prepared. This required preparation of bipyridylimine dendritic ligands, *via* a Schiff base condensation reaction, between first- and second-generation 1,4-diaminobutane poly(propylene) dendritic scaffolds and 4'-methyl-2,2'-bipyridine-4-carboxaldehyde. Chelation of the new bipyridylimine dendritic ligands with $[Mn(CO)_5Br]$ afforded new polynuclear tricarbonylmanganese(I) metallodendrimers. In addition, a mononuclear model complex was prepared and comprehensively studied. All complexes are air-stable solids and stable in solution for up to 16 h in the absence of light. The CO-release properties of these complexes were investigated using the myoglobin assay, and show photoactivated CO-release at 410 nm. Regardless of the generation number, the complexes released ~65 % of the total number of CO ligands per molecule, with no scaling effects observed. These CO-releasing metallodendrimers afford new ways for the targeted delivery of large amounts of carbon monoxide to cellular systems.

Publications

Journal Articles:

1. Preshendren Govender, Fabio Edafe, Banothile C. E. Makhubela, Paul J. Dyson, Bruno Therrien and Gregory S. Smith, **Neutral and Cationic Osmium(II)-Arene Metallodendrimers: Synthesis, Characterization and Anticancer Activity,** *Inorganica Chimica Acta*, **2014**, 409, 112-120.

2. Preshendren Govender, Sandesh Pai, Ulrich Schatzschneider and Gregory S. Smith, **Next Generation PhotoCORMs: Polynuclear Tricarbonylmanganese(I)-Functionalized Polypyridyl Metallodendrimers,** *Inorganic Chemistry*, **2013**, 52, 5470-5478.

3. Preshendren Govender, Lara C. Sudding, Catherine M. Clavel, Paul J. Dyson, Bruno Therrien and Gregory S. Smith, **The Influence of RAPTA Moieties on the Antiproliferative Activity of Peripheral-Functionalized Poly(salicylaldiminato) Metallodendrimers,** *Dalton Transactions*, **2013**, 42, 1267-1277.

4. Preshendren Govender, Bruno Therrien and Gregory S. Smith, **Bio-Metallodendrimers – Emerging Strategies in Metal-Based Drug Design,** *European Journal of Inorganic Chemistry*, **2012**, 2853-2862.

Conference Contributions:

1. **Poster with Oral Flash Presentation:** Preshendren Govender, Ulrich Schatzschneider and Gregory S. Smith, *Next Generation PhotoCORMs: Polynuclear Tricarbonylmanganese(I)-Functionalized Polypyridyl Metallodendrimers*, presented at the 16th Biennual SACI Inorganic Chemistry Conference, Durban, South Africa, **2013**.

2. **Poster Presentation:** Preshendren Govender and Gregory S. Smith, *The Influence of RAPTA Moieties on the Antiproliferative Activity of Peripheral-Functionalised Poly(salicylaldiminato) Dendrimers,* presented at the XXV International Conference on Organometallic Chemistry, Lisbon, Portugal, **2012**.

3. **Poster Presentation:** Preshendren Govender and Gregory S. Smith, *The Influence of RAPTA Moieties on the Antiproliferative Activity of Peripheral-Functionalised Poly(salicylaldiminato) Dendrimers,* presented at the 6th International Symposium on Bioorganometallic Chemistry, Toronto, Canada, **2012**.

4. **Poster Presentation:** Preshendren Govender and Gregory S. Smith, *Synthesis and Anticancer Studies of Ruthenium(II) Arene Complexes Coordinated to Poly(propyleneimine) Dendritic Scaffolds,* presented at the 40th South African Chemical Institute (SACI) National Convention and Federation of African Chemical Societies (FACS) Meeting, Johannesburg, South Africa, **2011**.

Abbreviations, Symbols and Units

°	degrees
°C	degrees Celsius
Å	angstrom(s)
***μ*A**	microamps
***μ*M**	micromolar
5'GMP	guanosine 5'-monophosphate
Ar	aromatic
ATR	attenuated total reflectance
br	broad
bpy	bipyridyl
$^{13}C\{^{1}H\}$	proton decoupled carbon-13
calc	calculated
CBA	cytometric bead array
CH_3CN	acetonitrile
cisR	cisplatin-resistant
CO	carbon monoxide
CORMs	CO-*releasing molecules*
COSY	correlation spectroscopy
Cp	cyclopentadienyl
Cp*	pentamethylcyclopentadienyl
cye	cymene
d	doublet
dd	doublet-doublet
D_2O	deuterated water
DAB	1,4-diaminobutane
DCM	dichloromethane

dendr	dendrimer
deoxy-Mb	deoxy-myoglobin
DMSO	dimethylsulfoxide
DMF	dimethylformamide
DNA	deoxyribonucleic acid
EA	elemental analysis
en	ethylenediamine
E*pa*	anodic potential
E*pc*	cathodic potential
EPR	enhanced permeability and retention
Eqn.	equation
ESI	electrospray ionization
EtOAc	ethyl acetate
EtOH	ethanol
Et_3N	triethylamine
$Et_3NH^+Cl^-$	triethylamine ammonium chloride
Et_2O	diethyl ether
FAB-MS	fast atom bombardment - mass spectrometry
Fc	ferrocene
FT-IR	fourier transform infrared spectroscopy
g	gram(s)
h	hour(s)
HMB	hexamethylbenzene
HPLC	high performance liquid chromatography
HR	high-resolution
HSQC	heteronuclear single quantum correlation
Hz	hertz
IC_{50}	50 % inhibitory concentration
IR	infrared

J	coupling constant
LED	light-emitting diode
Lit.	literature
m	multiplet (NMR); medium intensity (IR)
MALDI-TOF	matrix-assisted desorption/ionization - time of flight
Mb	myoglobin
Mb-CO	carboxy- myoglobin
Me	methyl
MeOH	methanol
MHz	megahertz
min	minute(s)
mL	millilitre(s)
mol	mole(s)
mmol	millimole(s)
MP	melting point
MS	mass spectrometry
m*/*z	mass to charge ratio
NFP	*N*-formylpiperidine
NMR	nuclear magnetic resonance
OC	open circular
ORTEP	Oak Ridge Thermal Ellipsoid Plot
p	para
$^{31}P\{^{1}H\}$	proton decoupled phosphorus -31
PAMAM	poly(amidoamine)
PBS	phosphate buffer solution
Pet. Ether	petroleum ether
Ph	phenyl
PhotoCORMs	Photo-activated CORMs
PPh_3	triphenylphosphine
PPI	poly(propyleneimine)

ppm	parts per million
Pr^i	isopropyl
pta (PTA)	1,3,5-triaza-7-phosphaadamantane
***p*-TSA**	*p*-toluenesulfonic acid hydrate
pyr	pyridine
q	quartet
qn	quintet
RAPTA	ruthenium-arene PTA
RP-HPLC	reverse phase-HPLC
RT	room temperature
s	singlet (NMR); strong intensity (IR)
SC	supercoiled
sep	septet
t	triplet
THF	tetrahydrofuran
TFA	trifluoroacetic acid
tpm	tris(pyrazolyl)methane)
t_R	retention time
unsubst.	unsubstituted
UV/Vis	Ultraviolet-visible
V	volts
vs.	versus
w	weak intensity (IR)

Table of Contents

Chapter 1

Introduction and Literature Review:

From Metallodrugs to Metallodendrimers for Therapy

1.1 Cancer: An Introduction 1

1.2 The Use of Metals as Therapeutic Agents 1

1.2.1 Platinum Anticancer Agents 1

1.2.2 Titanium Anticancer Agents 3

1.2.3 Gallium Anticancer Agents 4

1.2.4 Tin Anticancer Agents 4

1.2.5 Ruthenium(III) Anticancer Agents 6

1.3 Ruthenium(II) Compounds as Anticancer Agents 7

1.3.1 Organometallic Ruthenium-Based Antitumor Compounds 7

1.3.2 Proposed Mode of Cytotoxic Action of Ruthenium-Arene Compounds:

With focus on RAPTA Compounds 10

1.3.3 Multinuclear Ruthenium-Arene Compounds as Anticancer Agents 12

1.4 Ferrocene in Cancer Research 17

1.4.1 Ferrocene in Medicine:

With Focus on Ferrocenyl-Based Derivatives as Therapeutic Agents 17

1.4.2 Heterometallic and Multinuclear Ferrocenyl-Derived Anticancer Agents 19

1.5 CO-Releasing Molecules: A Therapeutic Approach 21

1.5.1 Transition Metal Carbonyl Complexes as Novel CO-Releasing

Molecules (CORMs) 22

1.5.2 Photoinduced CO-Releasing Molecules (PhotoCORMs) 27

1.5.3 PhotoCORMs as Bio-Conjugates 30

1.6 Metallodendrimers: *Metal Decorated Dendrimers for Oncology* 32

1.6.1 General Design and Synthesis of Dendrimers 32

1.6.2 Applications of Metallodendrimers:

With Focus on Nanomedicine 36

1.6.3 Metallodendrimers as Anticancer Agents 38

1.7 Closing Remarks 41

1.8 Aims and Objectives of the Thesis 42
1.8.1 General Aims 42
1.8.2 Specific Objectives 42
1.8.2.1 Synthesis 42
1.8.2.2 Biological Investigation 44
1.9 References 45

Chapter 2

Synthesis and Characterization of Neutral and Cationic Ruthenium(II)- and Osmium(II)-Arene Complexes Based on Poly(propyleneimine) Dendritic Scaffolds

2.1 Introduction 57
2.2 Synthesis and Characterization of *N*,*O*-Salicylaldiminato Ligands 59
2.2.1 ^{1}H and ^{13}C{^{1}H} NMR Spectroscopy 61
2.2.2 Infrared Spectroscopy 62
2.2.3 Elemental Analysis and Mass Spectrometry 63
2.3 Synthesis and Characterization of Neutral *N*,*O*-Ru(II)-Arene Metallodendrimers 64
2.3.1 ^{1}H and ^{13}C{^{1}H} NMR Spectroscopy 65
2.3.2 Infrared Spectroscopy 67
2.3.3 Elemental Analysis and Mass Spectrometry 67
2.4 Synthesis and Characterization of Cationic *N*,*O*-Ru(II)-Arene-PTA Metallodendrimers 68
2.4.1 ^{1}H, ^{31}P{^{1}H} and ^{13}C{^{1}H} NMR Spectroscopy 69
2.4.2 Infrared Spectroscopy 72
2.4.3 Elemental Analysis and Mass Spectrometry 72
2.5 Synthesis and Characterization of Cationic *N*,*O*-Ru(II)-Arene-PTA Mononuclear Complexes 73
2.5.1 ^{1}H, ^{31}P{^{1}H} and ^{13}C{^{1}H} NMR Spectroscopy 74
2.5.2 Infrared Spectroscopy 77
2.5.3 Elemental Analysis and Mass Spectrometry 77
2.5.4 X-ray Crystallography 77

2.6 Synthesis and Characterization of Neutral and Cationic Os(II)-Arene Complexes 79
2.6.1 ^{1}H, ^{31}P{^{1}H} and ^{13}C{^{1}H} NMR Spectroscopy 82
2.6.2 Infrared Spectroscopy 83
2.6.3 Elemental Analysis and Mass Spectrometry 84
2.6.4 X-ray Crystallography 84
2.7 Overall Summary 87
2.8 References 88

Chapter 3

Synthesis and Characterization of Heterometallic Ferrocenyl-Containing Ruthenium(II)-Arene Complexes Based on Poly(propyleneimine) Dendritic Scaffolds

3.1 Introduction 91
3.2 Synthesis and Characterization of *N*,*O*- and *N*,*N*- Ferrocenyl-Derived Conjugates 93
3.2.1 ^{1}H and ^{13}C{^{1}H} NMR Spectroscopy 96
3.2.2 Infrared Spectroscopy 98
3.2.3 Mass Spectrometry and HPLC 99
3.3 Synthesis and Characterization of Ferrocenyl-Derived *N*,*O*-Salicylaldiminato and *N*,*N*-Pyridylimine Dendritic Ligands 99
3.3.1 ^{1}H and ^{13}C{^{1}H} NMR Spectroscopy 100
3.3.2 Infrared Spectroscopy 102
3.3.3 Elemental Analysis and Mass Spectrometry 102
3.4 Synthesis and Characterization of Ferrocenyl-Derived *N*,*O*-Salicylaldiminato and *N*,*N*-Pyridylimine Monomeric Ligands 103
3.4.1 ^{1}H and ^{13}C{^{1}H} NMR Spectroscopy 103
3.4.2 Infrared Spectroscopy 105
3.4.3 Mass Spectrometry and HPLC 105
3.5 Synthesis and Characterization of Cationic Ferrocenyl-Derived *N*,*O*-Ru(II)-Arene-PTA and *N*,*N*-Ru(II)-Arene Metallodendrimers 105
3.5.1 ^{1}H, ^{31}P{^{1}H} and ^{13}C{^{1}H} NMR Spectroscopy 106
3.5.2 Infrared Spectroscopy 109
3.5.3 Elemental Analysis and Mass Spectrometry 109
3.5.4 Electrochemistry 110

3.6 Synthesis and Characterization of Cationic Ferrocenyl-Derived
N,*O*-Ru(II)-Arene-PTA and *N*,*N*-Ru(II)-Arene Mononuclear Complexes 114
3.6.1 ^{1}H, ^{31}P{^{1}H} and ^{13}C{^{1}H} NMR Spectroscopy 115
3.6.2 Infrared Spectroscopy 117
3.6.3 Mass Spectrometry and HPLC 117
3.6.4 Electrochemistry 118
3.6.5 X-ray Crystallography 120
3.7 Overall Summary 122
3.8 References 123

Chapter 4

Biological Evaluation of Ruthenium, Osmium and Ferrocenyl-Derived Metallodendrimers

4.1 Introduction 127
4.2 *In vitro* Biological Activity of Ruthenium- and Osmium-Arene
Metallodendrimers 130
4.2.1 Influence of the Number of Metal Centres:
Mononuclear vs. G_1 vs. G_2 vs. G_3 vs. G_4 132
4.2.2 Influence of the Type of Arene Ring:
p-Cymene vs. Hexamethylbenzene 139
4.2.3 Influence of the Water-Soluble Phosphine Ligand:
Neutral vs. Cationic (i.e. PTA vs. Chlorido) 142
4.2.4 Resistance 145
4.2.5 Selectivity 147
4.3 Stability of the Cationic *N*,*O*-Ruthenium-Arene-PTA Metallodendrimers
in Solution and Interactions with Nucleotides 148
4.3.1 Degradation Test 148
4.3.2 Aquatic Stability 149
4.3.3 Nucleotide Binding 151
4.4 DNA Binding Study of Neutral and Cationic *N*,*O*-Ruthenium-Arene
Metallodendrimers 152
4.5 Cell Viability Studies of Ferrocenyl-Derived Metallodendrimers 155
4.6 Overall Summary 159
4.7 References 161

Chapter 5

Synthesis, Characterization and CO-Release of Polynuclear Tricarbonylmanganese(I)-Polypyridyl Complexes Based on Poly(propyleneimine) Dendritic Scaffolds

5.1 Introduction 166
5.2 Synthesis and Characterization of Bipyridyl Ligands 168
5.2.1 ^{1}H and ^{13}C{^{1}H} NMR Spectroscopy 170
5.2.2 Infrared Spectroscopy 173
5.2.3 Elemental Analysis and Mass Spectrometry 173
5.3 Synthesis and Characterization of $Mn(CO)_3$-Functionalized Metallodendrimers 174
5.3.1 ^{1}H and ^{13}C{^{1}H} NMR Spectroscopy 175
5.3.2 Infrared Spectroscopy 177
5.3.3 Mass Spectrometry and HPLC 178
5.4 Long-Term Stability of Compounds 179
5.5 Electronic Absorption Spectra and CO-Release Properties 181
5.5.1 Absorption Maxima and Molar Extinction Coefficients 181
5.5.2 Dark Stability and CO-Release Properties 182
5.6 CO-Release Experiments with the Myoglobin Assay 184
5.6.1 Myoglobin Assay 184
5.6.2 Stability in Myoglobin Assay 185
5.6.3 Photoactivation of Myoglobin Assay Spiked with the PhotoCORM 186
5.7 Kinetics and Quantum Yield Measurements 189
5.7.1 Rate of CO-Release 189
5.7.2 Quantum Yield of CO-Release Determined by Ferrioxalate Actionometry 191
5.8 Overall Summary 192
5.9 References 193

Chapter 6

Experimental Details

6.1 General Remarks 196
6.2 Instrumentation 197

6.3 Synthesis of *N*,*O*-Salicylaldiminato Ligands 199
6.3.1 Preparation of **21**, **22** and **37** 199
6.3.2 General Procedure for the Preparation of **23** and **24** 199
6.3.2.1 DAB-G_3-$(C_7H_5NOH)_{16}$ (**23**) 199
6.3.2.2 DAB-G_4-$(C_7H_5NOH)_{32}$ (**24**) 200
6.4 Synthesis of Ru(II)- and Os(II)-Arene Precursors 200
6.5 Synthesis of Ru(II)-and Os(II)-Arene Complexes 201
6.5.1 General Procedure for the Preparation of Neutral
N,*O*-Ru(II)-Arene Metallodendrimers (**25** - **28**) 201
6.5.1.1 DAB-G_3-PPI-$\{(\eta^6$-*p*-cye)Ru$((C_7H_5NO)$-κ^2-*N*,*O*)$Cl\}_{16}$ (**25**) 201
6.5.1.2 DAB-G_4-PPI-$\{(\eta^6$-*p*-cye)Ru$((C_7H_5NO)$-κ^2-*N*,*O*)$Cl\}_{32}$ (**26**) 202
6.5.1.3 DAB-G_3-PPI-$\{(\eta^6$-HMB)Ru$((C_7H_5NO)$-κ^2-*N*,*O*)$Cl\}_{16}$ (**27**) 203
6.5.1.4 DAB-G_4-PPI-$\{(\eta^6$-HMB)Ru$((C_7H_5NO)$-κ^2-*N*,*O*)$Cl\}_{32}$ (**28**) 204
6.5.2 General Procedure for the Preparation of Cationic *N*,*O*-Ru(II)-Arene-PTA
Metallodendrimers ([**29**][PF_6]$_4$ - [**36**][PF_6]$_{32}$) 205
6.5.2.1 [DAB-G_1-PPI-$\{(\eta^6$-*p*-cye)Ru$((C_7H_5NO)$-κ^2-*N*,*O*)PTA$\}_4$][PF_6]$_4$
([**29**][PF_6]$_4$) 206
6.5.2.2 [DAB-G_2-PPI-$\{(\eta^6$-*p*-cye)Ru$((C_7H_5NO)$-κ^2-*N*,*O*)PTA$\}_8$][PF_6]$_8$
([**30**][PF_6]$_8$) 207
6.5.2.3 [DAB-G_3-PPI-$\{(\eta^6$-*p*-cye)Ru$((C_7H_5NO)$-κ^2-*N*,*O*)PTA$\}_{16}$][PF_6]$_{16}$
([**31**][PF_6]$_{16}$) 208
6.5.2.4 [DAB-G_4-PPI-$\{(\eta^6$-*p*-cye)Ru$((C_7H_5NO)$-κ^2-*N*,*O*)PTA$\}_{32}$][PF_6]$_{32}$
([**32**][PF_6]$_{32}$) 209
6.5.2.5 [DAB-G_1-PPI-$\{(\eta^6$-HMB)Ru$((C_7H_5NO)$-κ^2-*N*,*O*)PTA$\}_4$][PF_6]$_4$
([**33**][PF_6]$_4$) 210
6.5.2.6 [DAB-G_2-PPI-$\{(\eta^6$-HMB)Ru$((C_7H_5NO)$-κ^2-*N*,*O*)PTA$\}_8$][PF_6]$_8$
([**34**][PF_6]$_8$) 211
6.5.2.7 [DAB-G_3-PPI-$\{(\eta^6$-HMB)Ru$((C_7H_5NO)$-κ^2-*N*,*O*)PTA$\}_{16}$][PF_6]$_{16}$
([**35**][PF_6]$_{16}$) 212
6.5.2.8 [DAB-G_4-PPI-$\{(\eta^6$-HMB)Ru$((C_7H_5NO)$-κ^2-*N*,*O*)PTA$\}_{32}$][PF_6]$_{32}$
([**36**][PF_6]$_{32}$) 213

6.5.3 General Procedure for the Preparation of Cationic *N*,*O*-Ru(II)-Arene-PTA Mononuclear Complexes ([**38**][PF_6] & [**39**][PF_6]) 214
6.5.3.1 [$CH_3CH_2CH_2$-(η^6-*p*-cye)Ru((C_7H_5NO)-κ^2-*N*,*O*)PTA][PF_6] ([**38**][PF_6]) 214
6.5.3.2 [$CH_3CH_2CH_2$-(η^6-HMB)Ru((C_7H_5NO)-κ^2-*N*,*O*)PTA][PF_6] ([**39**][PF_6]) 215
6.5.4 Synthesis of Neutral *N*,*O*-Os(II)-Arene Complexes (**40**, **41**, **48**) 215
6.5.4.1 [DAB-G_1-PPI-{(η^6-*p*-cye)Os((C_7H_5NO)-κ^2-*N*,*O*)Cl}$_4$] (**40**) 216
6.5.4.2 [DAB-G_2-PPI-{(η^6-*p*-cye)Os((C_7H_5NO)-κ^2-*N*,*O*)Cl}$_8$] (**41**) 217
6.5.4.3 [$CH_3CH_2CH_2$-(η^6-*p*-cye)Os((C_7H_5NO)-κ^2-*N*,*O*)Cl] (**48**) 218
6.5.5 Synthesis of Cationic *N*,*O*-Os(II)-Arene-PTA Complexes ([**42**][PF_6]$_4$, [**43**][PF_6]$_8$, [**49**][PF_6]) 218
6.5.5.1 [DAB-G_1-PPI-{(η^6-*p*-cye)Os((C_7H_5NO)-κ^2-*N*,*O*)PTA}$_4$][PF_6]$_4$ ([**42**][PF_6]$_4$) 219
6.5.5.2 [DAB-G_2-PPI-{(η^6-*p*-cye)Os((C_7H_5NO)-κ^2-*N*,*O*)PTA}$_8$][PF_6]$_8$ ([**43**][PF_6]$_8$) 220
6.5.5.3 [$CH_3CH_2CH_2$-(η^6-*p*-cye)Os((C_7H_5NO)-κ^2-*N*,*O*)PTA][PF_6] ([**49**][PF_6]) 221
6.5.6 Synthesis of *N*,*N*-2-Pyridylimine Ligands (**44**, **45**, **50**) 221
6.5.7 Synthesis of Cationic *N*,*N*-Os(II)-Arene Complexes ([**46**][PF_6]$_4$, [**47**][PF_6]$_8$, [**51**][PF_6]) 222
6.5.7.1 [DAB-G1-PPI-{(η^6-*p*-cye)Os(($C_6H_5N_2$)-κ^2-*N*,*N*)Cl}$_4$][PF_6]$_4$ ([**46**][PF_6]$_4$) 222
6.5.7.2 [DAB-G_2-PPI-{(η^6-*p*-cye)Os(($C_6H_5N_2$)-κ^2-*N*,*N*)Cl}$_8$][PF_6]$_8$ ([**47**][PF_6]$_8$) 223
6.5.7.3 $CH_3CH_2CH_2$-(η^6-*p*-cye)Os(($C_6H_5N_2$)-κ^2-*N*,*N*)Cl][PF_6] ([**51**][PF_6]) 224
6.6 Synthesis of Ferrocenyl-Derived Conjugates (**53** - **55**) 225
6.6.1 Vinyl Ferrocene (**53**) 225
6.6.2 (4*E*)-(4-ferrocenyl-vinyl)-2-hydroxy-benzaldehyde (**54**) 226
6.6.3 (5*E*)-(5-ferrocenyl-vinyl)-2-pyridinecarboxaldehyde (**55**) 227

6.7 General Procedure for the Preparation of Ferrocenyl-Derived *N,O*-Salicylaldiminato Dendritic Ligands (**56** & **57**) 228
6.7.1 DAB-G_1-(4-ferrocenyl-vinyl-$C_7H_5NOH)_4$ (**56**) 228
6.7.2 DAB-G_2-(4-ferrocenyl-vinyl-$C_7H_5NOH)_8$ (**57**) 229
6.8 Synthesis of Ferrocenyl-Derived *N,N*-Pyridylimine Ligands (**58** & **59**) 230
6.8.1 DAB-G_1-(5-ferrocenyl-vinyl-$C_6H_5N_2)_4$ (**58**) 230
6.8.2 DAB-G_2-(5-ferrocenyl-vinyl-$C_6H_5N_2)_8$ (**59**) 231
6.9 Synthesis of Ferrocenyl-Derived *N,O*-Salicylaldiminato Monomeric Ligand (**60**) 232
6.9.1 (5*E*, 2*E*)-(5-ferrocenyl-vinyl)-2-((propylimino)methyl)phenol (**60**) 232
6.10 Synthesis of Ferrocenyl-Derived *N,N*-Pyridylimine Monomeric Ligands (**61**) 233
6.10.1 (5*E*, 2*E*)-*N*-((5-ferrocenyl-vinyl-pyridin-2-yl)methylene)propan-1-amine (**61**) . 233
6.11 General Procedure for the Preparation of Ferrocenyl-Derived Cationic *N,O*-Ru(II)-Arene-PTA Metallodendrimers ([**62**][$PF_6]_4$ & [**63**][$PF_6]_8$) 234
6.11.1 [DAB-G_1-PPI-{(η^6-*p*-cye)Ru((C_7H_5NO)-κ^2-*N,O*)PTA-(5-ferrocenyl-vinyl)}$_4$][$PF_6]_4$ ([**62**][$PF_6]_4$) 235
6.11.2 [DAB-G_2-PPI-{(η^6-*p*-cye)Ru((C_7H_5NO)-κ^2-*N,O*)PTA-(5-ferrocenyl-vinyl)}$_8$][$PF_6]_8$ ([**63**][$PF_6]_8$) 236
6.12 General Procedure for the Preparation of Ferrocenyl-Derived Cationic *N,N*-Ru(II)-Arene Metallodendrimers ([**64**][$PF_6]_4$ & [**65**][$PF_6]_8$) 237
6.12.1 [DAB-G_1-PPI-{(η^6-*p*-cye)Ru(($C_6H_5N_2$)-κ^2-*N,N*)Cl-(5-ferrocenyl-vinyl)}$_4$][$PF_6]_4$ ([**64**][$PF_6]_4$) 238
6.12.2 [DAB-G_2-PPI-{(η^6-*p*-cye)Ru(($C_6H_5N_2$)-κ^2-*N,N*)Cl-(5-ferrocenyl-vinyl)}$_8$][$PF_6]_8$ ([**65**][$PF_6]_8$) 239
6.13 Synthesis of Ferrocenyl-Derived Cationic *N,O*-Ru(II)-Arene-PTA Mononuclear Complex ([**66**][PF_6]) 240
6.13.1 [$CH_3CH_2CH_2$-(η^6-*p*-cye)Ru((C_7H_5NO)-κ^2-*N,O*)PTA-(5-ferrocenyl-vinyl)][PF_6] ([**66**][PF_6]) 240
6.14 Synthesis of Ferrocenyl-Derived Cationic *N,N*-Ru(II)-Arene Mononuclear Complex ([**67**][PF_6]) 241
6.14.1 [$CH_3CH_2CH_2$-(η^6-*p*-cye)Ru(($C_6H_5N_2$)-κ^2-*N,N*)Cl-(5-ferrocenyl-vinyl)][PF_6] ([**67**][PF_6]) 241
6.15 Synthesis of Bipyridyl Conjugate (**71**) 242
6.15.1 4'-Methyl-2,2'-bipyridine-4-carboxaldehyde (**71**) 242

6.16 Synthesis of Bipyridyl Ligands (**72** - **74**) 243
6.16.1 DAB-G_1-$(C_{12}H_{10}N_3)_4$ (**72**) 243
6.16.2 DAB-G_2-$(C_{12}H_{10}N_3)_8$ (**73**) 244
6.16.3 (4*E*)-*N*-((4'-methyl-[2,2'-bipyridin]-4yl)methylene)propan-1-amine (**74**) 244
6.17 Synthesis of $Mn(CO)_3$-Functionalized Complexes (**75** - **77**) 245
6.17.1 [DAB-G_1-PPI-{$(CO)_3Mn((C_{12}H_{10}N_3)$-$\kappa^2$-*N*,*N*)Br}$_4$] (**75**) 245
6.17.2 [DAB-G_2-PPI-{$(CO)_3Mn((C_{12}H_{10}N_3)$-$\kappa^2$-*N*,*N*)Br}$_8$] (**76**) 246
6.17.3 [$CH_3CH_2CH_2$-$(CO)_3Mn((C_{12}H_{10}N_3)$-$\kappa^2$-*N*,*N*)Br] (**77**) 246
6.18 Electrochemical Studies 247
6.19 X-ray Crystallography 248
6.20 NMR Experiments 252
6.20.1 Degradation Test 252
6.20.2 Aquatic Stability 252
6.20.3 Interactions with 5'GMP 252
6.21 Biological Studies 253
6.21.1 Cell Culture and Inhibition of Cell Growth 253
6.21.2 DNA Binding Study 253
6.21.3 Cell Viability Study 254
6.21.4 Myoglobin Assay 255
6.22 Ferrioxalate Actinometry 256
6.23 References 257

Chapter 7

Overall Summary, Conclusions and Future Outlook

7.1 Conclusions 258
7.1.1 Synthesis of Ruthenium-Arene and Osmium-Arene Metallodendrimers 258
7.1.2 Synthesis of Heterometallic Ferrocenyl-Derived Ruthenium-Arene Metallodendrimers 259
7.1.3 *In Vitro* Biological Activity 260
7.1.4 Synthesis and CO-Release Properties of $Mn(CO)_3$-Functionalized Metallodendrimers 262

7.2 Future Outlook 263
7.2.1 Investigating Higher Dendrimer Generations and Alternative Dendritic Scaffolds 263
7.2.2 Exploring Covalently Bound Dendrimer-Drug Conjugates 264
7.2.3 Exploring the Biology 265
7.3 References 266

Chapter 1

Introduction and Literature Review:

From Metallodrugs to Metallodendrimers for Therapy

This chapter forms part of the following publication:

Preshendren Govender, B. Therrien and G. S. Smith, **Bio-Metallodendrimers – Emerging Strategies in Metal-Based Drug Design,** *European Journal of Inorganic Chemistry*, 2012, 2853-2862.

1.1 Cancer: An Introduction

Cancer is a class of disease characterized by uncontrolled cell proliferation (*i.e.* undergoing cell division beyond the normal limits) and the ability of these cells to invade adjacent tissue, and sometimes spreading to other locations of the body *via* blood or lymph. The main types of cancers (based on mortality rate) are lung, stomach, colorectal, liver and breast cancer. These cancers can be treated by several methods such as surgery, radiotherapy and most importantly chemotherapy, which is the main treatment of this disease. Chemotherapy is the treatment of cancer with anticancer drugs that target and destroy cancer cells. In the last decade, a revolution in cancer treatment has been presented by organometallic chemists.[1, 2]

1.2 The Use of Metals as Therapeutic Agents

For the last 25 years medicinal inorganic chemistry was a new and unexplored field. However, research has flourished following the success of platinum-based anticancer agents.[3] In addition to metal-based therapies, the efficacy of organic drugs can be improved by combining them with metals.[3]

1.2.1 Platinum Anticancer Agents

The therapeutic properties of *cis*-diamminedichloridoplatinum(II) (*cis*-$[Pt(NH_3)_2Cl_2]$, cisplatin) (Figure 1.1) was accidently discovered by Barnett Rosenberg,[4, 5] in the late 1960s, whilst he was investigating the influence of an electric field on the growth of *Escherichia coli* bacteria. Cisplatin was in fact first synthesized by Michele Peyrone[6] in 1844 and was known

as Peyrone's chloride. More than a century later it became the first metal-containing anticancer drug.

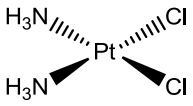

Figure 1.1 *Cisplatin the first metal-based anticancer complex discovered by Rosenberg.*[4]

Today, cisplatin is FDA approved, and is used in the treatment of a wide range of tumors,[7] in particular ovarian[8, 9] and testicular cancers.[10, 11] Cisplatin is also used in combination therapy of many other solid tumors, such as head, neck, bladder and small cell lung cancers.[12] Analogs of cisplatin (*i.e.* carboplatin and oxaliplatin, Figure 1.2), have shown great effectiveness as second-generation drugs.[13] Oxaliplatin is currently a 'billion-dollar' drug, primarily used to treat colorectal cancer.[14]

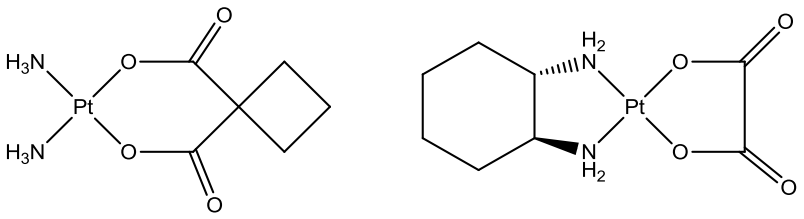

Figure 1.2 *Structures of 2nd generation Pt-based anticancer agents, carboplatin (left) and oxaliplatin (right).*[13]

Farrell and co-workers synthesized a Pt-based trinuclear complex with the general formula [*trans*, *trans*, *trans*-$(NH_3)_2$-Pt(Cl)$(CH_2)_6NH_2$Pt$(NH_3)_2NH_2(CH_2)_6NH_2$Pt-$(NH_3)_2$(Cl)][NO_3]$_4$ (BBR3464, Figure 1.3) which showed potent *in vitro* toxicity over cisplatin and its mononuclear analog.[15] BBR3464 was claimed as the first platinum-based drug with a DNA binding mode different to cisplatin.[16] Though Phase II trials of BBR3464 were not pursued further,[16] the concept of multinuclearity may assist in the improvement of the activity of potential therapeutic agents.

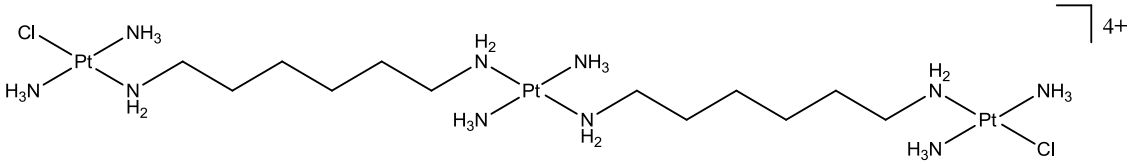

Figure 1.3 *Structure of the trinuclear Pt-based anticancer agent, BBR3464.*[15]

The clinical successes of platinum-based therapies tend to be overlooked due to the severe toxic side-effects and drug-resistance of these complexes.[12, 17] To overcome these limitations researchers have moved their attention to compounds incorporating other metals.[3]

1.2.2 Titanium Anticancer Agents

There have been two Ti^{IV} complexes explored as anticancer agents, both entered clinical trials in the 1990s. The first, is a tris-acetylacetonate derivative called Budotitane (Figure 1.4)[18] and the second, titanocene dichloride [$(\eta^5$-$C_5H_5)_2TiCl_2$] (Figure 1.4).[19] Both complexes are similar in structure to cisplatin, with both containing two labile chlorido ligands. Though the rate hydrolysis of these Ti-complexes is much faster than cisplatin, it did however lead to complications. Bound water is more acidic, which lead to the formation of hydroxo-bridged species, which in turn lead to toxic TiO_2 and hence did not complete Phase I clinical trials.[20, 21] Titanocene dichloride had more success than Budotitane, with the completion of Phase I and II clinical trials; however it was abandoned.[22] Titanocene dichloride was not approved for clinical use since it did not show significant advantages over current drugs on the market. The poor water solubility and low hydrolytic stability hampered its development.[20, 21]

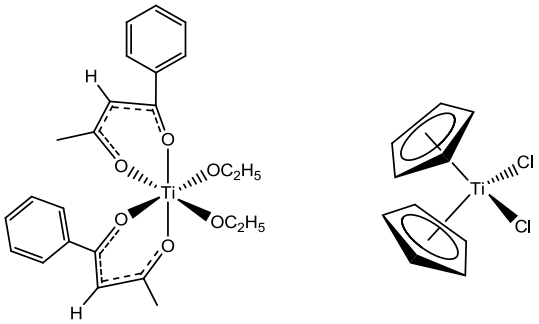

Figure 1.4 *Structures of Ti-based anticancer agents: Budotitane (left) and titanocene dichloride (right).*[18, 19]

To aid in stability of the Ti-based complexes, *ansa* derivatives of titanocene dichloride were developed (Figure 1.5)[23] and some complexes were active against 36 human tumor cell lines.[24] However, the hydrolytic stability of the complexes remained a problem, hence an alternative approach was taken. The dichlorido ligands of the *ansa* derivatives were replaced with an oxalate ligand, generating bis[(*p*-methoxybenzyl)cyclopentadienyl]-titanium(IV) oxalate (oxali-titanocene Y, Figure 1.5) which was found to be twice as potent as cisplatin towards pig kidney epithelial (LLC-PK) cells[25] and demonstrated favorable pharmacokinetic properties.

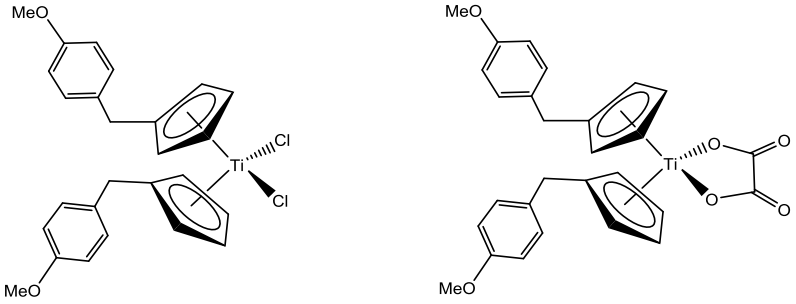

***d*ichloride titanocene derivative** **oxali-titanocene Y**

Figure 1.5 *Structures of dichloride titanocene derivative (left) and oxali-titanocene Y (right).*[23, 25]

1.2.3 Gallium Anticancer Agents

There are only a handful of gallium-based complexes used as anticancer agents,[26] namely Ganite® (gallium nitrate complex),[26] KP46 ([tris(8-quinlinolato)gallium(III)][27] and GaM (gallium maltolate, tris(3-hydroxy-2-methyl-4*H*-pyran-4onato)gallium)[28] (Figure 1.6). Ganite® is FDA approved, and used to treat cancer-related hypercalcemia, however the drug has poor bioavailability.[26] KP46 is an orally bioavailable drug, which has been through Phase I clinical trials for the treatment of solid tumors *via* S-phase cell cycle and apoptosis.[27] Though not redox active under biological conditions, Ga^{III} has similar chemistry to Fe^{III} and can be transported to cells *via* the Fe^{III} transport system (bound to serum protein transferrin).[29]

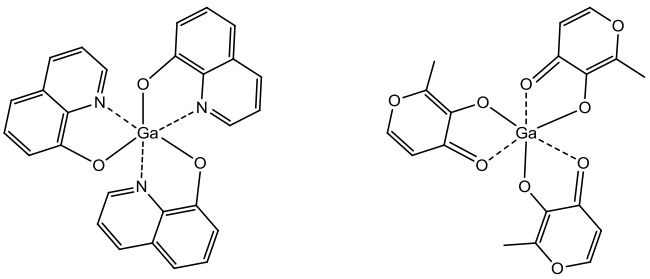

Figure 1.6 *Structures of KP46 (left) and GaM (right).*[27, 28]

1.2.4 Tin Anticancer Agents

Sn^{IV} complexes have become very attractive as therapeutic agents because of their attractive properties such as, increased water solubility, lower general toxicity than Pt-based drugs, better body clearance, fewer side-effects[30] and most importantly does not develop drug resistance.[31, 32] Recently, a tributyl complex tri-*n*-butyltin(IV)lupinylsulfide hydrogen flumarate (IST-FE 35, Figure 1.7), displayed inhibition of the implanted tumors (p388 myelomonocytic leukemia and B16-F10 melanoma) in BDF1 mice.[33, 34] Following a single dose of the drug, IST-FE 35 reduced the tumor volume by 96 % at day 11.[33, 34]

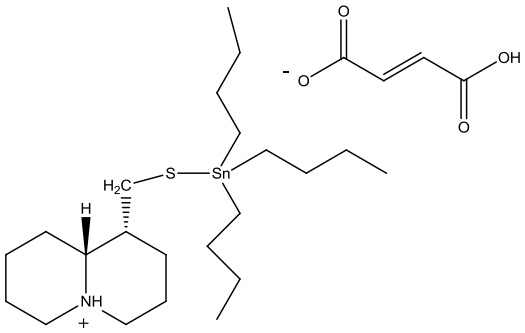

Figure 1.7 *Structure of Sn^{IV} anticancer complex, IST-FS 35.*[33, 34]

Other examples of a Sn-based antitumor agents, are the trigonal-bipyrimidal anionic tin(IV) complexes recently synthesized by Kaluderovic,[35] namely, triphenyltin(IV) chlorides containing *N*-phthaloyl-L-glycine (P-Gly), *N*-phthaloyl-L-alanine (P-AlaH), and 1,2,4-benzenetricarboxylic 1,2-anhydride (BTCH), were tested against a series of cancer cell lines. The Sn-based complexes displayed high activity in the cancer cell lines, with some of the complexes displaying IC_{50} values lower than cisplatin. The most active complex of the series (50 times more potent than cisplatin) was the organotin complex, triethylammonium (*N*-phthaloylglycinato)triphenyltin(IV) chloride [$SnPh_3$(P-Gly)Cl] (Figure 1.8), and was found to induce apoptosis *via* extrinsic pathways on DLD-1 cancer cells.[35]

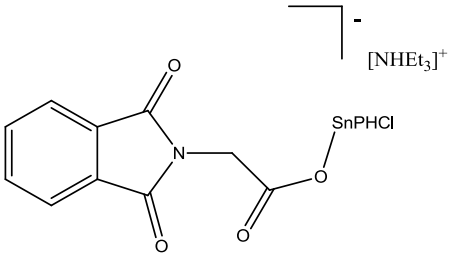

Figure 1.8 *Organotin complex $[SnPh_3(P\text{-}Gly)Cl]^-$ (where P-Gly = N-phthaloylglycinato), 50 times more potent than cisplatin and induces apoptosis.*[35]

Other metals have been used in the pursuit of potential therapeutic agents, such as gold,[36] arsenic,[37] copper,[38] zinc,[39] bismuth,[40] molybdenum.[41] However, ruthenium-based complexes have shown the most promise as anticancer agents.[42]

1.2.5 Ruthenium(III) Anticancer Agents

Soon after the discovery of the cytotoxic effects of platinum-based drugs, ruthenium compounds were investigated as potential therapeutic agents. As an alternative to platinum, ruthenium has shown favorable properties and conditions to form the basis for anticancer drug design.[13] Moreover, ruthenium is less toxic than platinum, with its biological activity attributed to its ability to mimic the behavior of iron, and bind to biomolecules, such as human serum albumin and transferrin.[43] Two inorganic Ru^{III} complexes, [ImH][*trans*-$Ru(DMSO)(Im)Cl_4$] (NAMI-A, where Im = imidazole)[44-46] and [IndH][*trans*-$Ru(Ind)_2Cl_4$] (KP1019, where Ind = indazole)[47-49] (Figure 1.9) are currently undergoing Phase II clinical trials.

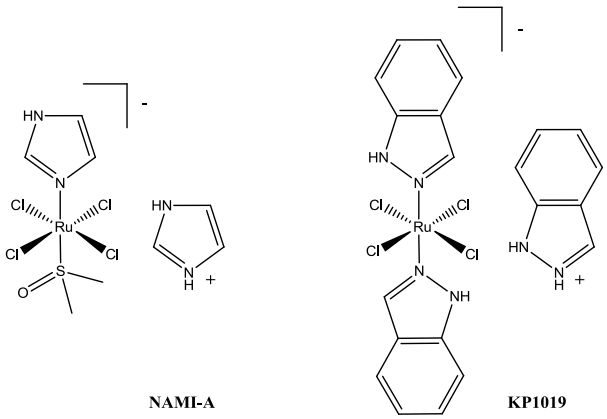

Figure 1.9 *Ru(III)-anticancer compounds, NAMI-A (left) and KP1019 (right), currently undergoing clinical trials.*

NAMI-A, synthesized by Gianni Sava, is a tetrachlorido imidazole/DMSO-Ru^{III} compound, and was the first of the two Ru^{III} complexes to enter clinical trials. NAMI-A, was found to be inactive during initial *in vitro* testing. However, *in vivo* testing showed that the drug inhibits matrix metalloproteinases and prevents metastases (tumor growth),[46] with little impact on primary tumors in animal models.[45]

KP1019, developed by Bernhard Keppler, is administered intravenously and hence binds initially to proteins in the blood stream. In fact, following cellular uptake of KP1019, it was primarily found bound to proteins (*i.e.* albumin and transferrin) and on DNA in peripheral leukocytes.[48] The side-effects seen with platinum-based anticancer agents were related to their binding to serum proteins, while KP1019 binds to transferrin, an important step in its mode of action, as it aids in the transport into the cell *via* the transition pathway.[47, 50, 51]

In recent years the focus on Ru^{III} complexes has shifted towards the development of Ru^{II} complexes, as in both cases (*i.e*. NAMI-A and KP1019) the active drug is considered a Ru^{II} species. Moreover, the Ru^{III} agents are 'activated' upon entering the cancerous cell, by reduction to the Ru^{II} species which coordinate more rapidly to biomolecules. [52, 53]

1.3 Ruthenium(II) Compounds as Anticancer Agents

Ru^{III}-based anticancer drugs such as NAMI-A, KP1019 and their derivatives, pioneered as alternatives to Pt-based therapeutic agents. However, with the +2 oxidation state proposed as the active ruthenium species, several investigations into the development of Ru^{II} compounds as anticancer agents have been pursued.[54-56]

1.3.1 Organometallic Ruthenium-Based Antitumor Compounds

In organometallic complexes, it is the metal-carbon bond which endows these coordination complexes with their unique properties. The lability of the metal-ligand bond can greatly be influenced by the presence of metal-carbon bonds, as these complexes have high *trans*-effects and *trans*-influences. Moreover, the π-bonded arene and cyclopentadienyl (Cp) ligands can act as both electron donors and π-acceptors.

Similarly to Ru^{III} complexes, Ru^{II} complexes have been extensively studied as anticancer agents.[54-56] The most widely studied organoruthenium compounds are the ruthenium-arene and ruthenium-cyclopentadienyl half-sandwich compounds, also referred to as 'piano-stool' complexes.[57] The term 'piano-stool' is derived from the orientation of the coordinating ligands around the metal centre. All these pseudo-octahedral complexes have either a Cp (η^5) or arene (η^6) ring (*i.e.* the 'seat' of the 'piano-stool'), and coordinating ligands (*i.e.* the 'legs' of the 'piano-stool'). There are three forms of binding in which the coordinating ligands can coordinate around the d^6 metal (Ru^{II}, Os^{II}, Ir^{III} or Rh^{III}) (Figure 1.10).

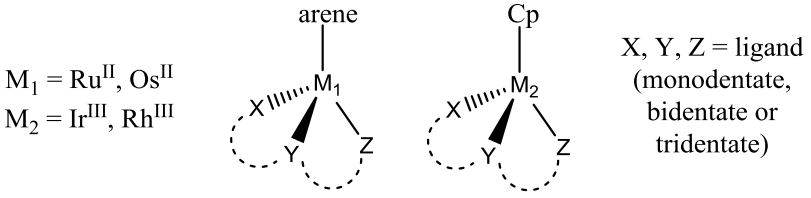

Figure 1.10 *General structures of ruthenium- and osmium-arene (left), and iridium- and rhodium-cyclopentadienyl half-sandwich (right) complexes.*

Depending on the nature of the ligand, binding can occur in a monodentate (Z), bidentate (X-Y) or tridentate (X-Y-Z) manner, in-turn generating neutral or charged (isolated as salts) complexes. The different types of coordinating ligands (X, Y, Z and arene/Cp) dictate the reactivity (labile or inert) of the complexes. The π-donor ability of the arene/Cp ligand protects the metal centre from oxidation.[1] The first half-sandwich organoruthenium antitumor agent was 1-β-hydroxyethyl-2-methyl-5-nitro-imidazole (metronidazole) coordinated to a ruthenium(II)-benzene dichlorido moiety (Figure 1.11).[58] The Ru-complex is more active *in vitro* than its base-ligand, metronidazole.[58]

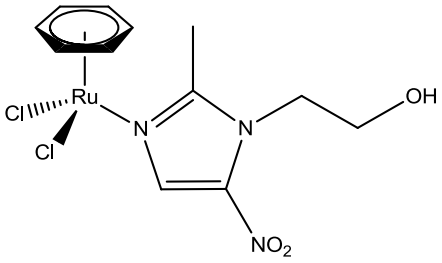

Figure 1.11 *The first organoruthenium antitumor agent.*[58]

There are two main classes of ruthenium-arene complexes developed for cytotoxicity against cancer cells. The first class was pioneered by Peter Sadler, with general formula [(η^6-arene)Ru(XY)Z]$^{n+}$ (XY are bidentate chelating ligands (*NN*, *NO*, *OO*, *SO*) and Z is a monodentate ligand (most likely a chlorido)).[3, 59-64] The second class with general formula [(η^6-arene)Ru(PTA)Cl_2] (RAPTA) (where PTA = 1,3,5-triaza-7-phosphatricyclo[3.3.1.1]decane) was pioneered by Paul Dyson.[53, 65-70]

Sadler prepared RM175, with formula [(C_6H_5Ph)Ru(en)Cl][PF_6] (en = ethylenediamine)[71] (Figure 1.12), which showed good biological activity against primary cell lines. The activity of RM175 is comparable to cisplatin against A2780 human ovarian cancer cells and displays activity against a cisplatin-resistant cell line.[72]

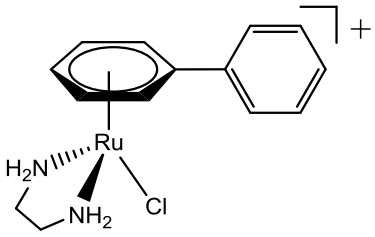

RM175

Figure 1.12 *Molecular structure of RM175.*

Sadler then replaced the ruthenium with osmium (affording AFAP51, Figure 1.13) and following a series of experiments, the authors reported ruthenium plays a key role in anti-metastatic activity.[73] AFAP-51 shows six times more potency against breast cancer cells (MCF-7) than RM175. However, the Ru^{II} derivative shows *in vivo* activity against mammary carcinoma and reduces metastasis, where AFAP-51 did not.[73] A series of structure-activity-relationship studies (SARs) were performed, replacement of the arene ring, from simple to extended arene systems (*e.g.* benzene, biphenyl or tetrahydroanthracene), afforded improvement in biological activity. Moreover, introducing other bidentate ligands (*e.g. N, N, N', N'* tetramethylethylenediamine, TMEDA), reduces activity of the complex.[74]

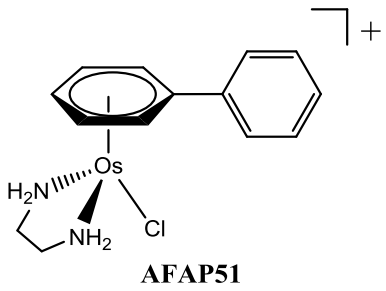

AFAP51

Figure 1.13 *Molecular structure of AFAP51.*[73]

Dyson prepared RAPTA-C, with formula [(η^6-*p*-cymene)Ru(PTA)Cl_2] (Figure 1.14), which has a similar structure to RM175. Similarly seen with NAMI-A, RAPTA-C was inactive *in vitro*, however *in vivo* experiments displayed the true potential of these drugs, as the complex showed activity against lung metastasis in CBA mice.[68] Another attractive feature of RAPTA-C, is its low toxicity compared to its Ru^{III} counterparts, hence the drug can be administered in higher dosage.[75] A study was performed where the authors replaced the ruthenium of RAPTA-C with osmium, generating the isostructural complex (Figure 1.14), and investigated the enzyme inhibition properties of the complexes.[76] The study included the Cp derivatives ($CpIr^{III}$ & $CpRh^{III}$) of RAPTA-C (Figure 1.14).

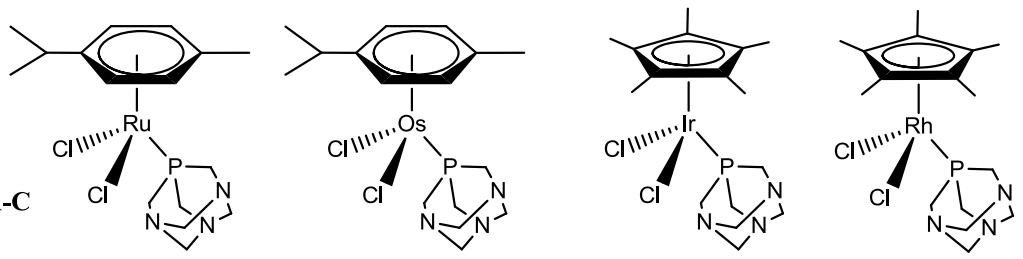

RAPTA-C

Figure 1.14 *RAPTA-C (far left) and derivatives of RAPTA-C (Os^{II}, Ir^{III}, Rh^{III}).*[76]

RAPTA-C and the Os^{II} derivative both displayed similar activity to their Ru^{III} counterparts with cytotoxicity in the lower micromolar range. However, the Cp^*Rh^{III} and Cp^*Ir^{III} derivatives were inactive. The authors attributed the poor activity of the Cp^* derivatives to the formation of weak metal-sulfur (M-S) bonds at the cathespin B active site, whilst the active-arene derivatives displayed formation of thermodynamically favoured strong M-S bonds.[76]

Following intracellular uptake, some 'piano-stool' complexes can be 'activated' *via* ligand substitution or v*ia* redox reaction, affording a more reactive species and can be called 'pro-drugs'.[43]

1.3.2 Proposed Mode of Cytotoxic Action of Ruthenium-Arene Compounds: *With focus on RAPTA Compounds*

Alessio and co-workers addressed whether or not the aromatic fragment (arene or Cp^*) is important in bringing about the biological activity of organoruthenium complexes.[77] The authors prepared half-sandwich ruthenium(II)-(1,4,7-trithiocyclononane) complexes functionalized with PTA (Figure 1.15) and compared these derivatives with known RAPTA analogs.[77]

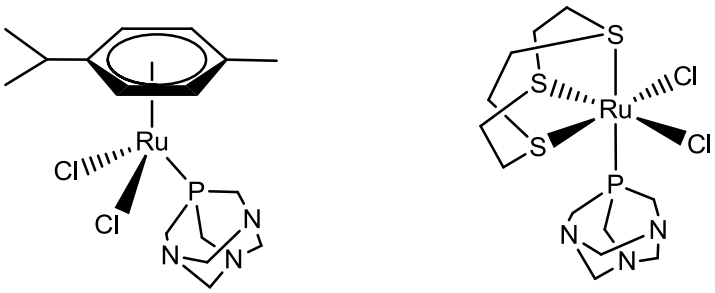

Figure 1.15 *RAPTA-C (left) and the $Ru^{II}[9]aneS_3$ derivative (right).*[77]

The results showed the arene ring is in fact not an essential feature in the biological activity of the RAPTA complexes, as the $Ru^{II}[9]aneS_3$ derivatives showed similar activity to the RAPTA analogs. Hence, the arene/Cp ligand can be replaced by a face-capping 6-electron ligand, without influence on the biological activity.[77] However, Bratsos *et al*. suggest the coordinating ligands must have low steric demand and low hydrophobic activity.[78]

These results were somewhat surprising, hence researchers focussed on investigating the mode of action of the RAPTA analogs. Unlike the classic Pt-based anticancer agents, the mechanism of action proved to be complex, involving both extra- and intra-cellular processes. Nevertheless, since metal drugs are usually prodrugs, and are activated *via* aquation following uptake into the cell, the aquation of the complexes were investigated (Scheme 1.1).[79, 80]

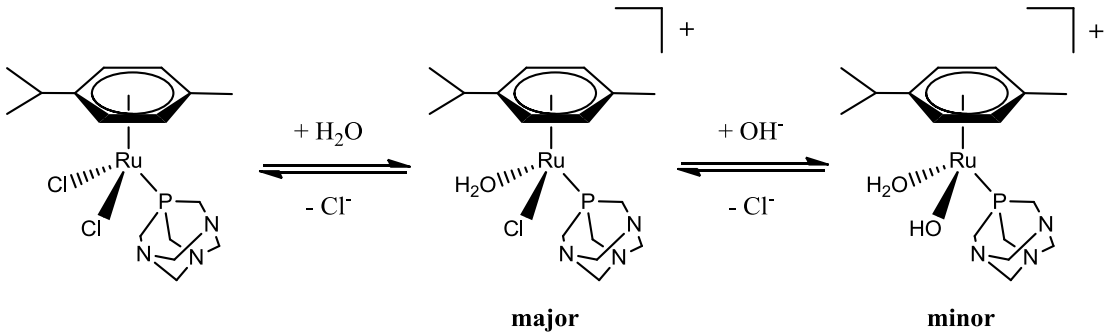

Scheme 1.1 *Hydrolysis of RAPTA-C in pure water at 1 or 2 μM concentration.*[79, 80]

RAPTA complexes have two kinetically labile chlorido ligands which undergo rapid solvent exchange. With the use of UV/Vis and $^{31}P\{^{1}H\}$ NMR spectroscopy, aquation studies of RAPTA-C were carried out.[79, 80] In 100 mM NaCl solution (simulating high chloride concentration in the blood) aquation was suppressed, and at 4 mM NaCl solution (simulation low intracellular chloride concentration) aquation occurs, to yield major and minor products (Scheme 1.1) of RAPTA-C.

These findings show aquation occurs once the drug is taken up by the cell, but is aquation necessary to bring about a biological response? Hence, the two chlorido ligands in RAPTA-C were replaced with bidentate oxalate and 1,1-cyclobutanedicarboxylate ligands, affording derivatives with formula [(η^6-*p*-cymene)Ru(PTA)(C_2O_4)] (oxaliRAPTA) and [(η^6-*p*-cymene)Ru(PTA)($C_6H_6O_4$)] (carboRAPTA) respectively (Figure 1.16).[67]

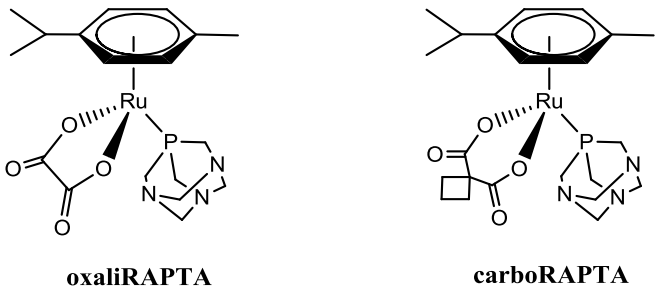

Figure 1.16 *OxaliRAPTA (left) and carboRAPTA (right).*[67]

The results were as expected, with oxaliRAPTA remaining un-aquated in pure water, whilst carboRAPTA only formed <5 % of aquation products, compared to RAPTA-C.[67] Binding to bimolecular targets were also investigated, with all three complexes showing similar binding and similar cytotoxicities against several cell lines. The authors suggest, although aquation takes place following cell uptake, it is not essential for reactions with biomolecules.[67]

There has been growing interest in tethering RAPTA-type complexes to proteins, which significantly increases the cytotoxicity of the complexes (Scheme 1.2).[70, 81]

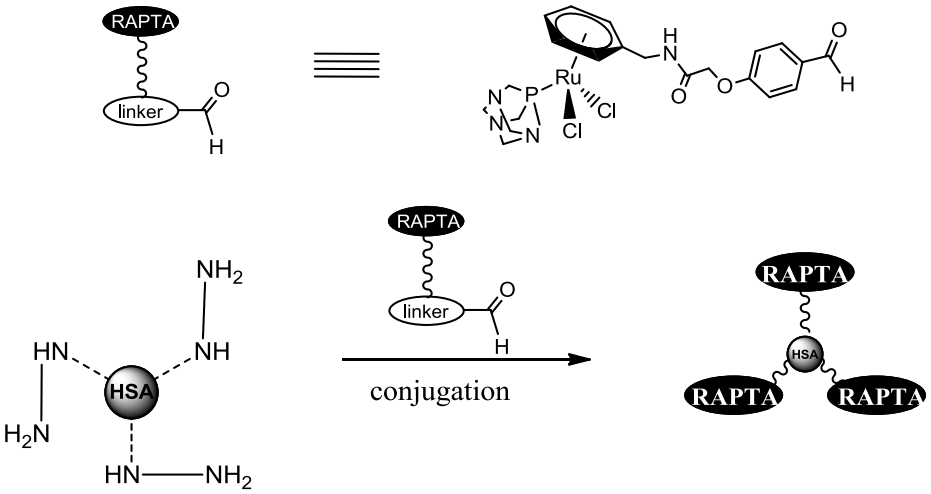

Scheme 1.2 *Strategy in tethering a RAPTA moiety to human serum albumin (HSA).*[81]

The RAPTA-like moiety was coordinated to a linker which in turn was conjugated to the carrier protein (human serum albumin, HSA) *via* hydrazone bond formation. The protein conjugate showed potent cytotoxicity (IC_{50} = 11 μM) compared to RAPTA-C (IC_{50} >300 μM) in the same cell line (A2780).[81]

Consequently, there has been growing interest in multinuclear Ru^{II} complexes as potential therapeutic agents.[53, 82]

1.3.3 Multinuclear Ruthenium-Arene Compounds as Anticancer Agents

The trinuclear Pt-based anticancer agent, BBR3464, is 2-6 orders of magnitude more active than cisplatin in cisplatin-resistant cell lines.[83] Hence, the use of multinuclear complexes as potential therapeutic agents has since been considered.

In order to improve the activity of the ruthenium-arene complexes, Keppler and co-workers, synthesized water-soluble dinuclear ruthenium-arene complexes, based on 3-hydroxy-2-methyl-pyridinone, with varied alkyl spacers (Figure 1.17).[64, 84] The dinuclear ruthenium-arene complexes were compared against Pt-based antitumor agents (*i.e.* cisplatin, carboplatin and oxaliplatin), in a series of human tumor cell lines.[64, 84] In particular, one of the dinuclear complexes has similar activity to oxaliplatin, with the mononuclear derivative (Figure 1.17) inactive in the same cell line.

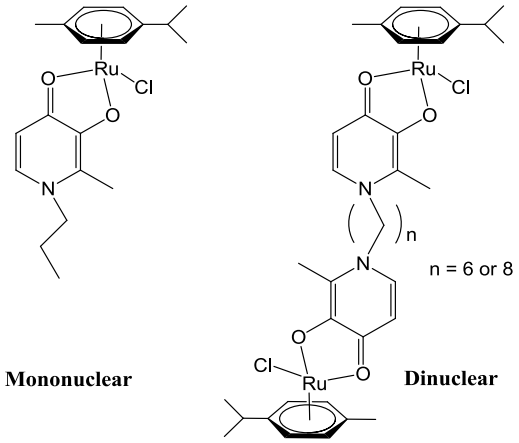

Figure 1.17 *Mononuclear (left) and dinuclear (with varying spacer lengths, right) ruthenium-arene antitumor complexes.*[64, 84]

Following initial screening of the dinuclear complexes, the authors investigated the DNA interaction using biochemical and biophysical methods.[85] Using a DNA model (in the absence of proteins), the dinuclear complexes formed intrastrand and interstrand cross-links with DNA. In some cases, the complexes cross-link two DNA duplexes and/or proteins to DNA, which has not yet been observed with other ruthenium-arene complexes. This concept of interhelical and DNA-protein cross-linking of these dinuclear complexes could exhibit a variety of biological effects and be useful in nucleic acid research.[85]

Gras and co-workers prepared a series of cationic thiophenolato-bridged diruthenium complexes with general formula $[(arene)_2Ru_2(SPh)_3]^+$ (where arene = benzene, *p*-cymene, hexamethylbenzene, C_6H_5R (where R = $(CH_2)_nOC(O)C_6H_4$-*p*-$O(CH_2)_6CH_3$ or $(CH_2)_nOC(CO)CH{=}CHC_6H_4$-*p*-$OCH_3$ and n = 2 or 4)) (Figure 1.18).[86] The thiophenolato-bridged dinuclear complexes were highly toxic against human ovarian cancer cells (A2780) and cisplatin-resistant cells (A2780cisR), with a few of the complexes in the nanomolar range.[86]

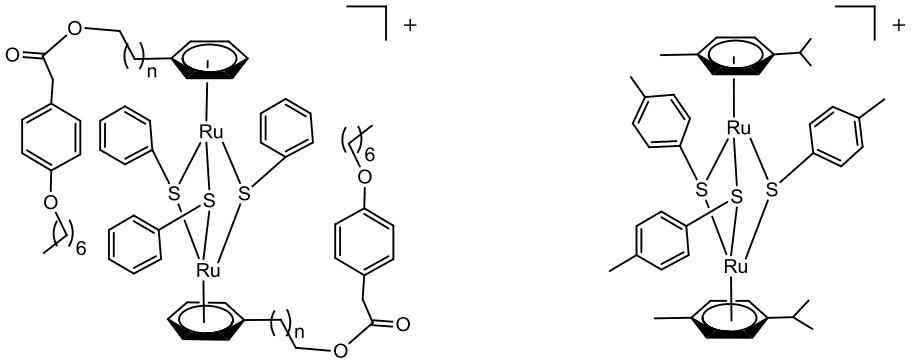

IC_{50} = 0.49 (A2780)
IC_{50} = 0.56 (A2780cisR)

IC_{50} = 0.13 (A2780)
IC_{50} = 0.08 (A2780cisR)

Figure 1.18 *Thiophenolato-bridged dinuclear ruthenium complexes, the functionalized arene derivative (left) and p-cymene derivative (right).*[86]

The authors attributed the activity of the diruthenium complexes to the phenyl or tolyl substituents on the three thiolato bridges, as analogous trishydroxythiophenolato complexes $[(\eta^6\text{-arene})_2Ru_2(S\text{-}p\text{-}C_6H_4OH)_3]Cl$ (IC_{50} values around 100 μM) are much less toxic towards cancer cells.[87]

Stringer *et al.* prepared a series of mononuclear and dinuclear ruthenium-arene complexes based on a benzaldehyde thiosemicarbazone (Figure 1.19).[88] The thiosemicarbazone moiety is known for its potent enzyme inhibition (in particular ribonucleotide reductase) and is capable of interrupting DNA replication.[89] The dinuclear complex showed enhanced biological activity (IC_{50} = 8.96 μM) in the oesophageal cancer cell line (WHCO1), over its mononuclear derivative (IC_{50} >200 μM, WHCO1).[88]

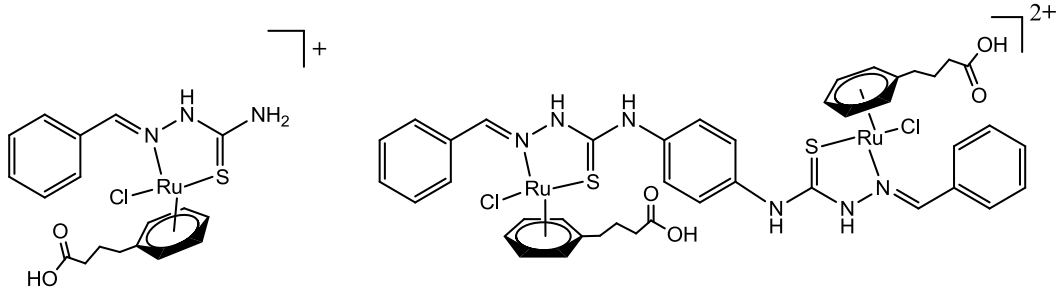

mononuclear **dinuclear**

Figure 1.19 *Ruthenium-arene thiosemicarbazone-based antitumor agents, mononuclear (left) and dinuclear (right).*[88]

A tetranuclear ruthenium-arene complex with general formula $[(p\text{-cymene})_4Ru_4(R_1)Cl_6]Cl_2$ (where R_1 = 1,2-bis(di-*N*-methylimidazol-2-ylphosphine)ethane) was prepared by Noffke and co-workers (Figure 1.20).[90] However, the cytotoxicity of the complexes are poor in several cancer cell lines (Hct116, Huh7, H411E and A2780 cells).

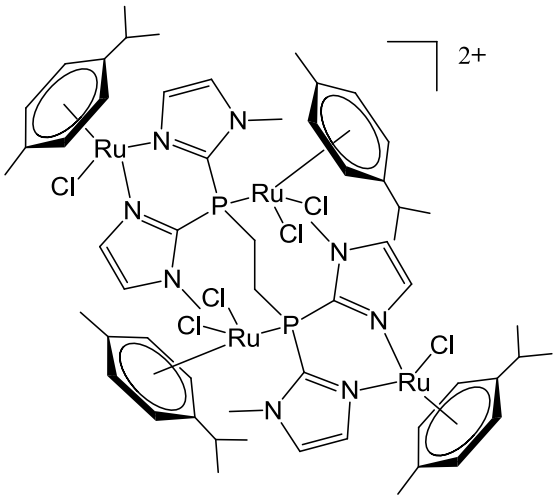

Figure 1.20 *A novel tetranuclear ruthenium-arene complex synthesized by Noffke et al.*[90]

Therrien and co-workers synthesized tetranuclear metalla-rectangles (or metalla-cycles), with moderate to excellent cytotoxicity towards human ovarian cancer cells (A2780 and A2780cisR).[91, 92] In particular, the biological activity of the tetranuclear ruthenium-arene metalla-cycles of general formula $[(\eta^6\text{-arene})_4Ru_4(\mathit{00}\cap\mathit{00})_2(N\cap N)_2]^{4+}$ (arene = *p*-cymene, hexamethylbenzene; *00*∩*00* and N∩N are linkers) (Figure 1.21), can be fine-tuned, as the size of the linker used as well as the type of arene-ligand greatly influences the activity.

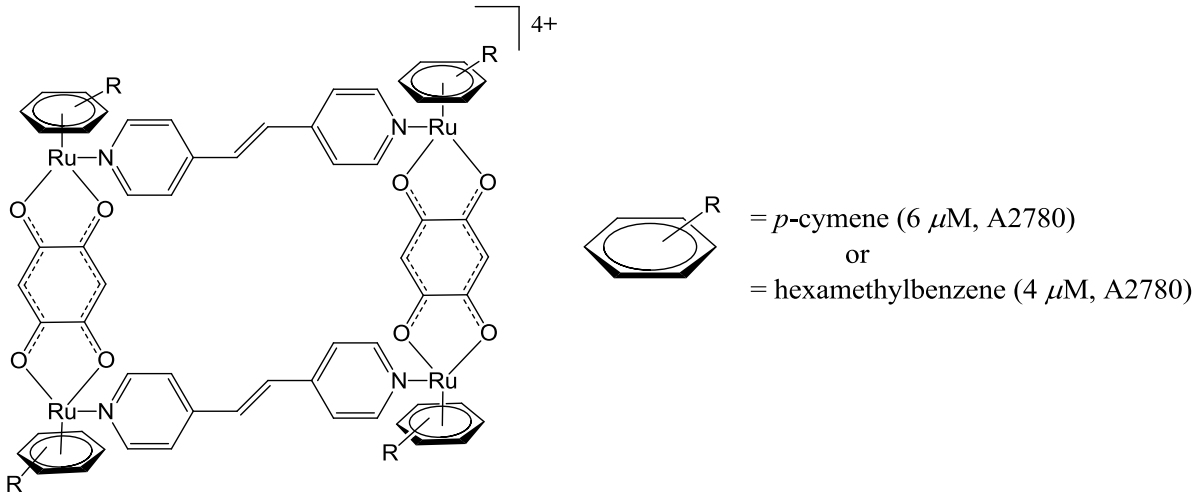

Figure 1.21 *Highly cytotoxic metalla-rectangles synthesized by Therrien et al.*[91]

Besides the ruthenium-arene tetranuclear metalla-cycles,[93] hexanuclear metalla-prisms[94] and octanuclear metalla-boxes[95, 96] have been synthesized. The hexanuclear metalla-prisms (Figure 1.22) do not show encapsulation of guest molecules, however, the complexes showed good DNA interaction and cytotoxicity in cancer cells (A2780).[97]

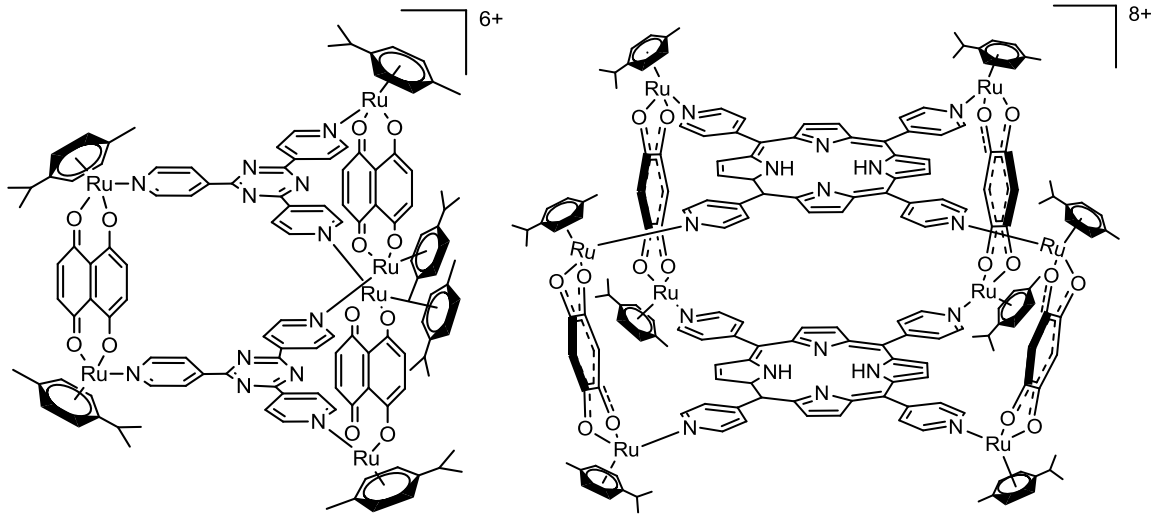

Figure 1.22 *Hexanuclear ruthenium-arene metalla-prisms (left) and octanuclear ruthenium-arene metalla-boxes.*[96, 97]

The octanuclear metalla-boxes were prepared using tetra(pyridyl)porphyrin panels, which resulted in octacationic ruthenium-arene complexes (Figure 1.22).[96] The complexes interact well with duplex and quadruplex DNA, with good cytotoxicity against human ovarian cells (A2780 and A2780cisR). More, recently these cage-like structures have been investigated as potential drug-delivery systems.[98, 99]

Synthesis of multinuclear ruthenium-arene systems is an additional strategy used to modify the mechanism of action of metal-based drugs. Another strategy to develop potent therapeutic systems is to develop heteronuclear systems, which is the incorporation of two or more different metals into one system.

1.4 Ferrocene in Cancer Research

Ferrocene was first discovered in 1951,[100, 101] however the structure was elucidated afterwards (Figure 1.23) independently by Wilkinson, Fischer and Pfab.[102, 103] The benzene inspired name 'ferrocene' was coined by Woodword and co-workers in 1952.[104] Scientists wasted no time in developing new strategies in synthesizing ferrocene and its derivatives.[105] Owing to its ease of functionalization and favorable electronic properties, a wide range of applications for these sandwich complexes were explored.[106] Stability of ferrocene in aqueous and aerobic media, the large variety of derivatives and the favorable electronic properties made ferrocene and its derivatives attractive as potential biological agents.[107, 108]

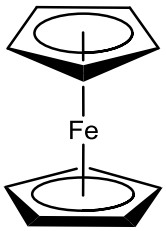

Figure 1.23 *The molecular structure of ferrocene.*

1.4.1 Ferrocene in Medicine: *With Focus on Ferrocenyl-Based Derivatives as Therapeutic Agents*

Many ferrocenyl compounds display good *in vivo* or *in vitro* activity as antitumor,[109, 110] antimalarial,[111] antifungal[112] and antiretroviral (ARV)[113] agents, and show DNA-cleavage activity.[114] Brynes *et al.* reported the first ferrocene-based anticancer complex in the late 1970s, with the compounds bearing amine or amide groups (Figure 1.24) tested against leukemia P-388 cells.[115] The ferrocenyl-derived compounds were administered to mice and the activity of these complexes were low but showed an improvement compared to the starting ligand.[115] This report clearly suggests, the incorporation of ferrocene into an appropriate biomolecule or carrier molecule, could provide the compound with enhanced anticancer activity.

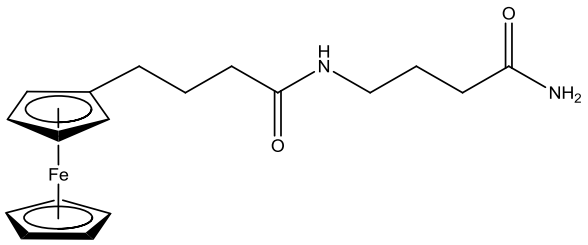

Figure 1.24 *The structure of a ferrocenyl-derived compound tested against leukemia P-388 cells.*[115]

Jaouen and co-workers developed a series of ferrocenyl derivatives and studied their activity in cancer cells.[116] The ferrocenyl derivatives, called ferrocifens (Figure 1.25), were derived from the anticancer drug tamoxifen (Figure 1.25), where one of the phenyl rings was replaced with ferrocene moiety. Derivatives of the active metabolite, hydroxytamoxifen (Figure 1.25) were also synthesized and the antiproliferative activity of these ferrocenyl derivatives investigated against breast cancer cells (MCF-7, hormone independent and MDA-MB231, hormone dependent).[117] The ferrocifens exhibited strong biological activity in both cell lines, though some were comparable to hydroxytamoxifen, others were slightly better. The authors attribute the activity to the greater lipophilicity of ferrocifens and the cytotoxicity induced by the redox-active ferrocene moiety. Furthermore, these results show that ferrocifens are the first molecules to show activity in both hormone-dependent and hormone-independent human breast cancer lines.[118]

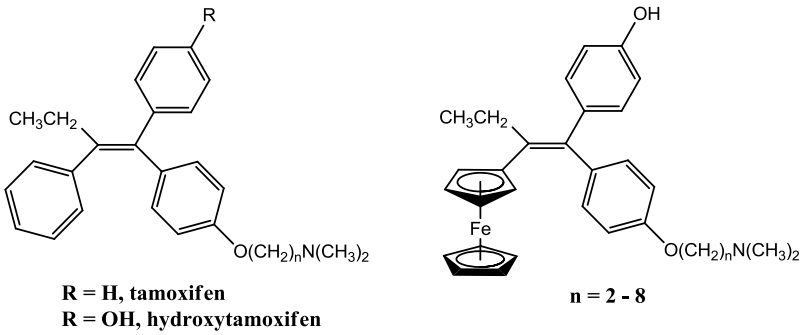

Figure 1.25 *Structures of parent drugs tamoxifen and hydroxytamoxifen (left), and the ferrocenyl-based derivatives, ferrocifens (right).*[117, 118]

The extended π-system plays an important role on the mode of action of the ferrocenyl-derived anticancer agents, with authors reporting a correlation between cytotoxicity and electron transfer capacity of these complexes.[119] The mode of action is said to originate from a series of redox processes on the ferrocenyl moiety, which results in the generation of reactive oxygen species (ROS).[119]

It has been shown that tethering the ferrocenyl moiety onto biologically active compounds increases their potency. The increase in activity has been attributed to the combined action of the organic drug and the Fenton chemistry of the Fe centre.[120]

1.4.2 Heterometallic and Multinuclear Ferrocenyl-Derived Anticancer Agents

Ferrocene has been linked to both platinum,[121-124] gold[125] and ruthenium[126, 127] in an effort to achieve a synergistic effect between the two biologically active centres. Nieto and co-workers synthesized a series of heterometallic Pt(II) compounds with *β*-aminoethylferrocenes. The compounds were tested against four cancer cell lines (HBL-100 (breast), HeLa (cervix), SW1573 (lung), WiDr (colon)). One of the *β*-aminoethylferrocenes-Pt(II) compounds (Figure 1.26) displayed good cytotoxicity in all four cell lines (IC_{50} = 1.7 - 2.3 μM), with activity in the colon cancer cell line better than the benchmark drug (cisplatin).

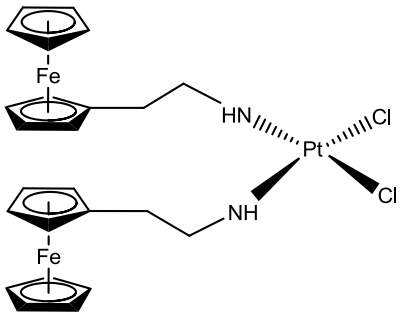

Figure 1.26 *Structure of heterometallic Pt(II)-compound with β-aminoethylferrocenes.*[123]

Recently, Dyson and co-workers prepared heterometallic phosphinoferrocene amino conjugates, incorporating the biologically active ruthenium-arene moiety (Figure 1.27).[126] These systems show moderate to good *in vitro* antitumor activity towards both the sensitive and cisplatin-resistant human ovarian cancer cell lines (A2780, IC_{50} = 4.1 μM; A2780cisR, IC_{50} = 6.9 μM).[126]

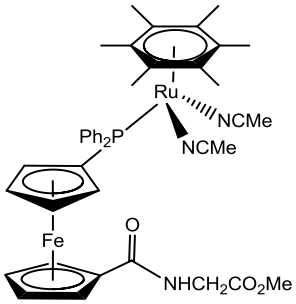

Figure 1.27 *Structure of heterometallic ruthenium-arene phosphinoferrocene amino conjugate.*[126]

As a result of the electrochemical properties and chemical stability of ferrocene, multinuclear ferrocenyl-derived polymers have been prepared and extensively investigated as prototypes for molecular electronic devices.[128, 129] Using a fast four-step synthesis, Astruc and co-workers reported the synthesis of the 54-ferrocene dendrimer (Figure 1.28).[130] The dendrimer is reversibly oxidized in dimethylformamide in a single 54-electron wave or by chemical means with NO^+, illustrating that access to precise redox-active nanoscopic molecules is possible. The resulting compound was used to modify a platinum electrode and the authors report such materials may have the potential to find uses as sensors or as molecular batteries.[130]

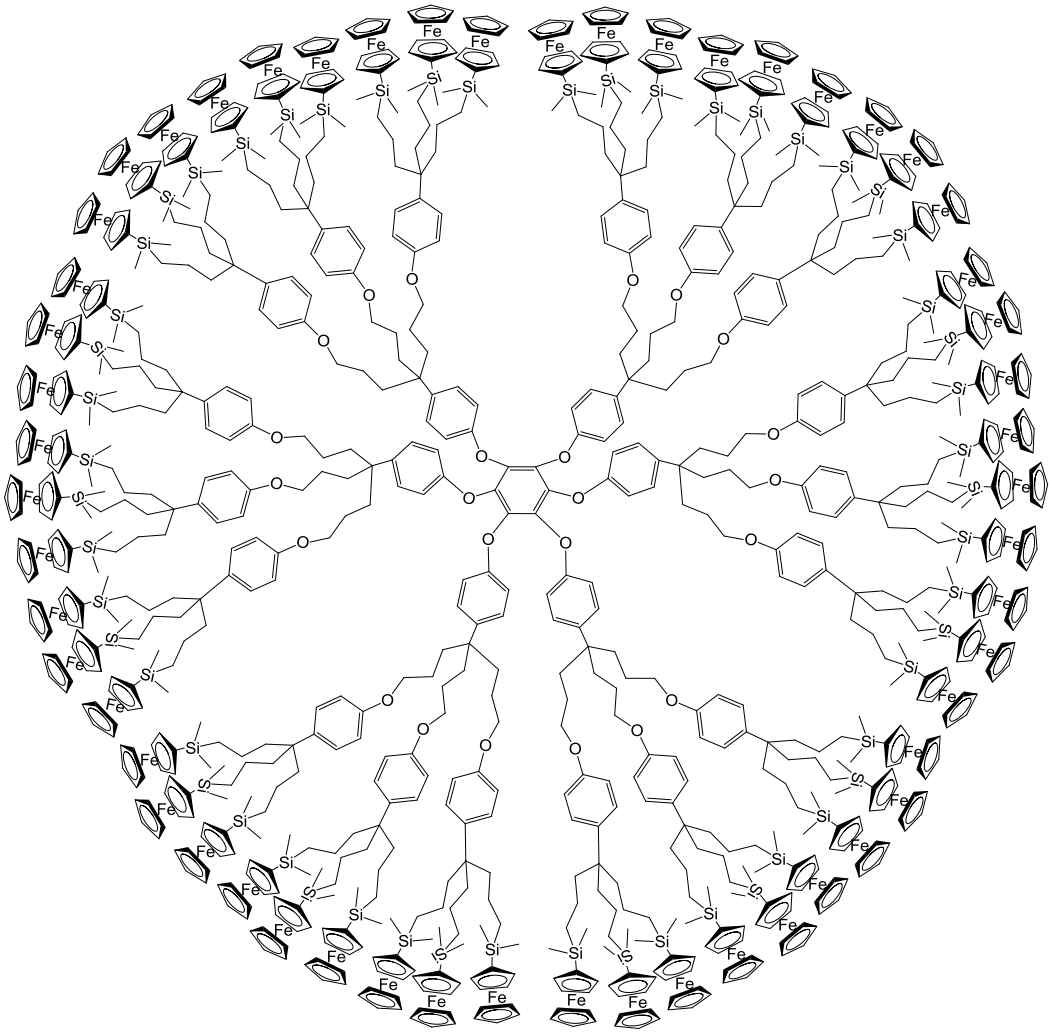

Figure 1.28 *Structure of 54-ferrocene dendrimer.*[130]

These multinuclear systems show promise as sensors and as molecular batteries, however there is a need for developing such macromolecular systems as potential anticancer agents, as there are few if not any reported.[131]

1.5 CO-Releasing Molecules: A Therapeutic Approach

For decades, the odorless, tasteless and colorless gas carbon monoxide (CO) has been viewed as highly toxic on the human oxygen transport system in the blood.[132] However, small molecules such as nitric oxide and hydrogen sulfide have shown to be important signalling molecules in human biology.[133, 134] This is also true for CO, with the major source of endogenously produced CO (86 %) in the human body obtained from the catalyzed oxidation of heme. The remaining 14 % of CO is generated from other physiological processes like photo-oxidation, lipid peroxidation, xenobiotics and bacteria. Heme oxygenase (HO) catalyzes the regiospecific conversion of heme (iron(III) protoporphyrin IX) to α-biliverdin, CO and free Fe^{3+}, *via* a multistep mechanism (Scheme 1.3).[135, 136]

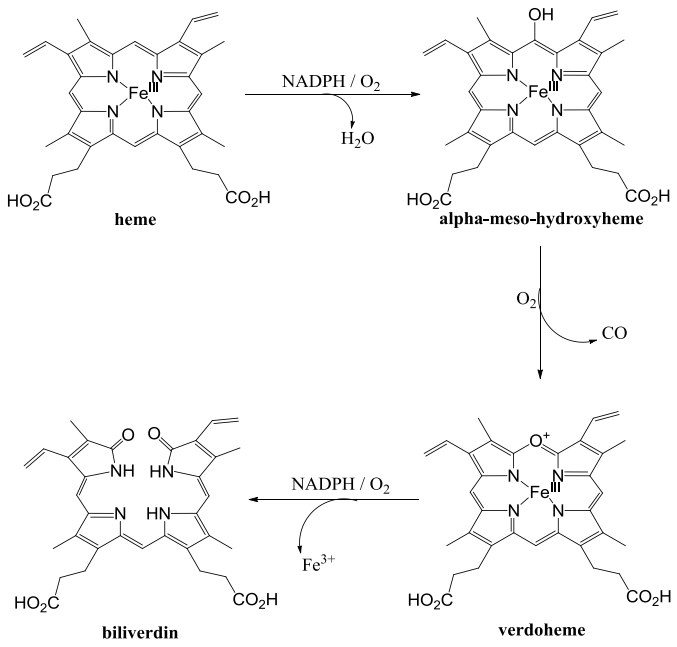

Scheme1.3 *The formation of biliverdin and CO from heme by heme oxygenase.*[135]

The first step, of the three step dioxygen activation pathway, is the regiospecific hydroxylation of heme at the *α-meso* carbon atom. The second step involves the conversion of *α-meso*-hydroxyheme to verdoheme, which occurs by the deprotonation of *α-meso*-hydroxyheme followed by binding oxygen to give a ferrous peroxy radical. The final step involves oxygen activation which cleaves the heme macrocycle to afford biliverdin and free ferrous iron.[137] The biliverdin (a green pigment) is subsequently reduced to bilirubin (a yellow pigment). This is one of the most visible enzyme reactions as it occurs during the development of bruises.

Some of the physiological effects of CO include anti-inflammatory activity, whereby it reduces allergic inflammation, protects against hyperoxia, decreases perfusion pressure in isolated human placenta and some beneficial cytoprotective activity.[138-140] The concept of delivering low concentrations of CO gas to palliate disease was a remarkable step[141] and was in line with the idea that carbon monoxide (derived from HO) endogenously contributes to important intracellular functions. Moreover, it is known that the prolonged inhalation of CO may lead to toxic side-effects imposed by the gas on the transport and delivery of oxygen[142] and rendering this approach of limited use in a therapeutic context. Thus, from a pharmacological perspective and to develop novel pharmaceutical agents suitable for therapeutic applications, it was further envisaged that this problem could be overcome by storing CO in a "stable chemical form", with the CO groups carried and supplied to cells or tissues in a more convenient fashion.[143] Indeed, the search led to transition metal carbonyl complexes of manganese, iron, or cobalt as promising lead structures.

1.5.1 Transition Metal Carbonyl Complexes as Novel CO-Releasing Molecules (CORMs)

One of the promising features of transition metal carbonyl complexes are that certain compounds are sensitive to light and under certain optimized conditions, such as the photoexcitation of metal-carbonyl complexes which leads to the dissociative loss of CO.[144] The initial experiments by Roberto Motterlini using *in vitro* and *ex vivo* systems showed that carbon monoxide liberated by $Mn_2(CO)_{10}$ led to the mitigation of coronary vasoconstriction.[145] These results provided evidence that CO can be liberated from transition metal carbonyls and delivered to cells. Thus, the term "CO-releasing molecules" (CORMs) was coined to classify the bioactive CO carriers. To study the cellular mode of action of carbon monoxide for potential therapeutic applications, interests in the use of CORMs are steadily increasing.[146]

The first CORMs to be identified were by Motterlini and co-workers, who have pioneered the development of CORMs, with the use of manganese decacarbonyl [$Mn_2(CO)_{10}$] (CORM-1)[144, 145] and the synthesis of tricarbonyldichlororuthenium(II) dimer $[Ru(CO)_3Cl_2]_2$ (CORM-2)[147] (Figure 1.29). It has been reported that [$Mn_2(CO)_{10}$] is sensitive to light and upon photo-excitation, the metal-carbonyl bond is cleaved leading to the dissociative loss of CO.[148] Due to its limited solubility in water, dimethylsulfoxide was used for investigating the CO-release behavior.[143] Motterlini *et al*. reported that in aqueous solutions [$Mn_2(CO)_{10}$] liberated CO

upon stimulation with light in a 1:1 ratio, as quantified spectrophotometrically, by measuring the conversion of deoxymyoglobin (deoxyMb) to carboxymyoglobin (MbCO).[145] More interestingly, extenuation of coronary vasoconstriction was achieved by $[Mn_2CO_{10}]$ upon stimulation with light to release CO which was not the case when the experiment was conducted in dark.[147]

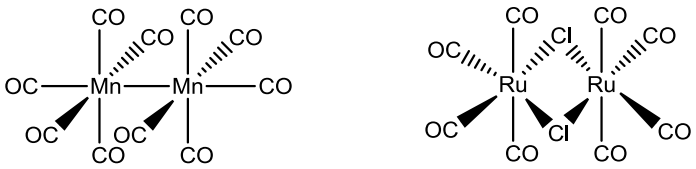

CORM-1 CORM-2

Figure 1.29 *The first CORMs identified by Motterlini and co-workers $[Mn_2(CO)_{10}]$ (CORM-1, left) and $[Ru(CO)_3Cl_2]_2$ (CORM-2, right).*[145, 147]

Ruthenium-based carbonyl complexes were explored as CORMs, as there is a wide range of coordinating ligands for this metal in aqueous solution.[149] In addition, ruthenium-based compounds have already been developed for the treatment of cancer and inflamation.[56, 150] Hence, the synthesis of CORM-2, which reacts reversibly with dimethylsulfoxide, leading to the loss of a CO group.[147] In a dimethylsulfoxide solution, CORM-2 results in a mixture of *fac*-$[Ru(CO)_3(DMSO)Cl_2]$ and *cis, cis, trans*-$[Ru(CO)_2(DMSO)_2Cl_2]$, identified as the tricarbonyl and dicarbonyl monomers respectively.[147] The $[Ru(CO)_3(DMSO)Cl_2]$ species rapidly releases CO to myoglobin and showed vasoactive properties in which the metal carbonyl compound significantly prevented the increase in arterial pressure in a rat model of acute hypertension.[143] The chemical structures, properties and carbon monoxide release profiles of some CORMs are shown in Table 1.1.[143]

Good water solubility of compounds is advantageous in the process of drug discovery and designing new therapeutic agents. As mentioned, both CORM-1 and CORM-2 are only soluble in a few organic solvents, *e.g*. dimethylsulfoxide and ethanol. The versatile chemistry of transition metals enables them to be effectively modified by coordinating biological ligands to the metal centre, in order to render the molecule more water-soluble and eventually less toxic. These key features led to the discovery of *fac*-tricarbonylchloro(glycinato)ruthenium(II) [*fac*-$Ru(CO)_3$(glycinate)Cl] complex (Figure 1.30), as the first water-soluble CORM.[151] [*fac*-$Ru(CO)_3$(glycinate)Cl] was termed CORM-3 and rapidly releases a CO group to myoglobin with $t_{½}$ <2 min and is stable in pure water with $t_{½}$ >24 h.[151]

Table 1.1 *Chemical structures, properties and CO-release profiles of some important CORMs.*

Compound	Chemical Structure	Solubility	CO-release (in PBS, PH 7.4)	Year of Identification
CORM-1 $[Mn_2(CO)_{10}]$	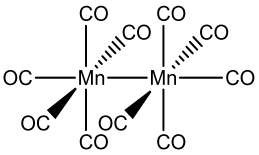	DMSO, EtOH	Light dependent Fast ($t_{1/2}$ <1 min)	2002[145]
CORM-2 $[Ru(CO)_3Cl_2]_2$	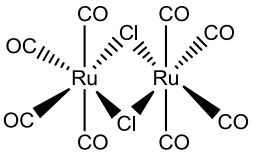	DMSO, EtOH	Solvent-assisted Fast ($t_{1/2}$ ~ 1 min)	2002[147]
CORM-3 [*fac*-Ru $(CO)_3$(glycinate)Cl]	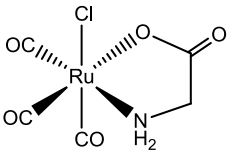	H_2O (stable at acidic pH)	Solvent-assisted Fast ($t_{1/2}$ ~ 1 min)	2003[151]
CORM-A1 $[Na_2H_3BCO_2]$	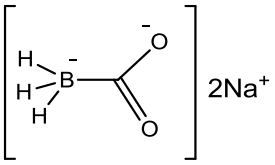	H_2O (stable at basic pH)	pH-dependent Slow ($t_{1/2}$ ~ 21 min)	2004[152]
CORM-F3 $[C_9H_5BrFeO_5]$	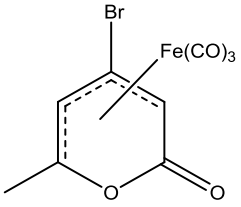	DMSO, EtOH	Induced by metal oxidation Slow ($t_{1/2}$ ~ 55 min)	2006[153]

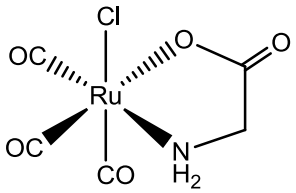

Figure 1.30 *The first water-soluble CORM identified by Motterlini and co-workers [Ru(CO)₃(glycinate)Cl] (CORM-3).*[151]

CORM-3 has a diverse solution chemistry, with hydroxide attacking one carbonyl at pH 3 giving $[Ru(CO)_2(CO_2H)(glycinate)Cl]^-$ and its isomers, which then undergo another pH-dependent reaction to give $[Ru(CO)_2(CO_2)(glycinate)Cl]^{2-}$ or

$[Ru(CO)_2(CO_2H)(OH)(glycinate)]^-$ at physiological pH, both as a mixture of isomers, (Scheme 1.4).[154]

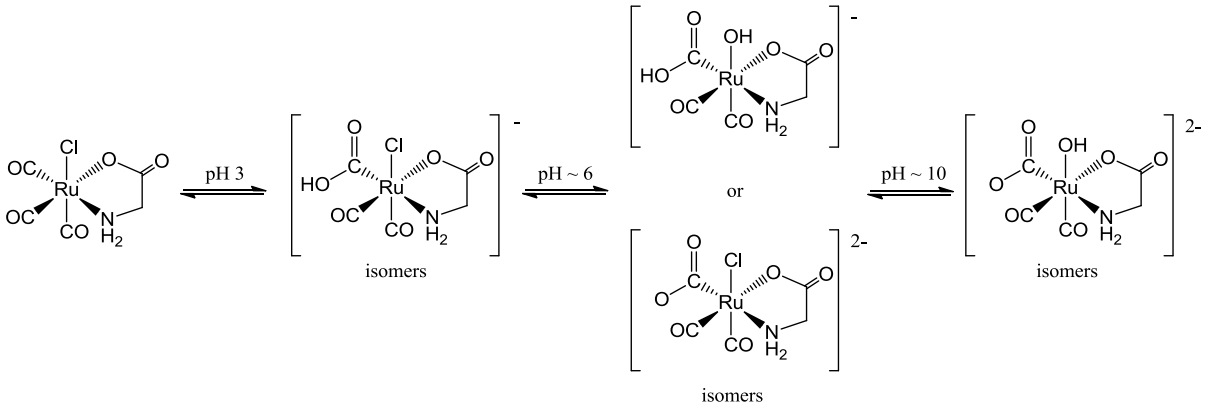

Scheme 1.4 *The pH dependence of CORM-3 in an aqueous medium.*

A detailed study showed that substituted 2-pyrones are capable of inhibiting the human ovarian cancer (A2780) and human chronic myelogenous leukemia (K562) cell lines, with IC_{50} values at sub-micromolar levels.[155] The 2-pyrone behaves as a pro-drug, where a carbonyl ring-opening reaction leads to the bioactive form.[155] Thus, the complexation of 2-pyrone in an η^4-diene-like fashion to an iron tricarbonyl unit, lead to the activation of the 2-pyrone ring-system, in-turn opening the way for the synthesis of several novel η^4-2-pyrone functionalized iron-containing carbonyl complexes. One such complex, the first iron-containing CORMs $[(\eta^4\text{-2-pyrone})Fe(CO)_3]$ (CORM-F3), which undergoes solvent-assisted CO-release, with a CO-release rate of approximately 0.19 μM/min (Figure 1.31).[153]

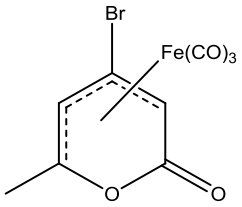

Figure 1.31 *The first iron-containing CORM $[(\eta^4\text{-2-pyrone})Fe(CO)_3]$ (CORM-F3).*[153]

Furthermore, the IC_{10} value for CORM-F3 (132 μM) indicated the concentration used for vasorelaxation (100 μM) is non-toxic and its pharmacological effect is due to the CO-release.[153] Also, it was found that CORM-F3 did not affect the cell viability of RAW246.7 murine macrophages at a concentration of 100 μM.[153] The substitution of bromine with chlorine (CORM-F8) results in a considerable loss of CO-release activity. Additionally, substitution at the 4- or 6-position with methyl groups (CORM-F11) further decreases the

ability of the compound to release CO.[156] More recently, Romão *et al.* synthesized a series of $Mo(CO)_3$-based complexes with a wide range of biomedical applications, focussing on inflammation, infection, and vasorelaxation, with a recent review detailing the requirements of CORMs for clinical applications.[157]

In addition to compounds where CO-release is induced by ligand exchange (*i.e.* with solvent or other dissolved species), enzyme-triggered CO-releasing molecules (ET-CORMs) have been developed by Schmalz and co-workers.[158-160] The concept of ET-CORMs was first introduced in 2011, with the synthesis acyloxybutadiene-irontricarbonyl complexes (Figure 1.32),[158] which are activated by enzymatic cleavage of the ester functionality.

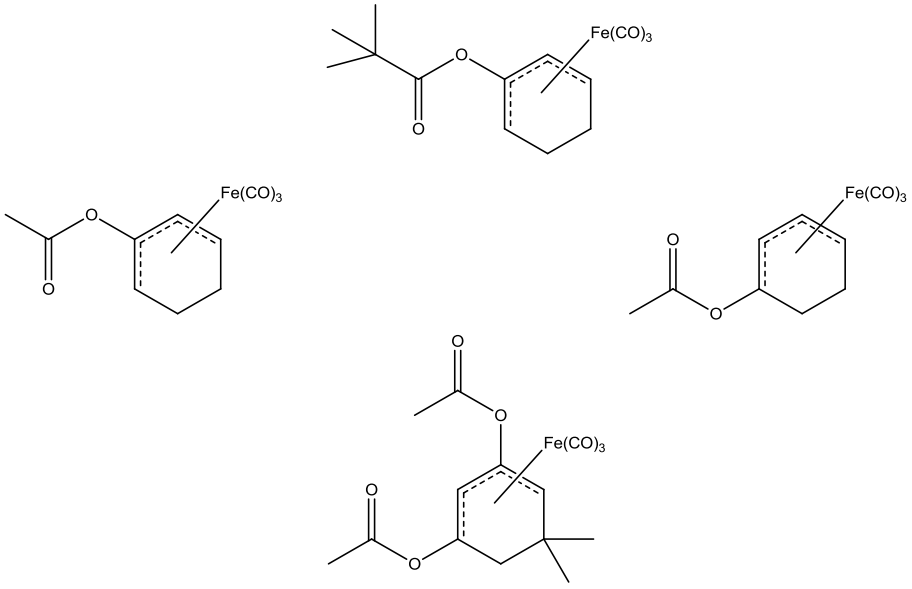

Figure 1.32 *Acyloxydiene-$Fe(CO)_3$ complexes used as ET-CORMs.*[158]

Moreover, the acyloxydiene-$Fe(CO)_3$ complexes are sufficiently stable under physiological conditions but are readily converted to the "active" species by means of enzymatic hydrolysis. The authors propose that once the acyloxydiene-$Fe(CO)_3$ complex enters the cell, cleavage of the ester function *via* enzymatic hydrolysis (usually by an intracellular esterase), triggers CO-release and generates the labile enol complex (Scheme 1.5).[159] Which is followed by oxidative decomposition (*via* a 16 electron species), in-turn leading to release of three molecules of CO, the enone ligand and the free metal ion.[159]

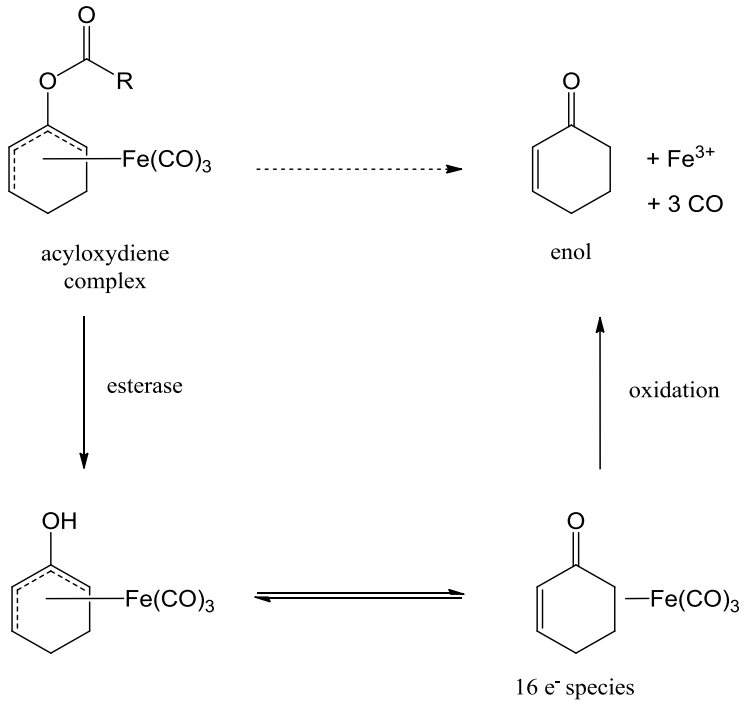

Scheme 1.5 *Proposed mechanism of action of ET-CORMs.*[159]

Other than solvent-assisted or enzyme trigger CO-release, recently photoactivation has become another important tool to induce CO-release of carbonyl-based complexes.[161]

1.5.2 Photoinduced CO-Releasing Molecules (PhotoCORMs)

Photoactivation has become an attractive tool and has gained much importance to induce biological activity of pro-drugs. Metal-carbonyl complexes are the obvious candidate as they have been known for years to release CO.[162] One such approach is photodynamic therapy (PDT), a clinical technique employing the combination of light, oxygen and a sensitizing agent to induce the photochemical degradation of unwanted cells within the body.[163-167] Medicinal PDT deals with the reactions which pharmaceuticals (drugs or diagnostic agents) undergo when exposed to UV/Visible light. The basic concept of PDT is not new, with the healing aspects of light described by the Greek historian Herodotus in the 5th Century BC, and the first use of a combination of light and a photosensitizer (eosin) to treat skin cancer took place in 1903 (Figure 1.33).[168]

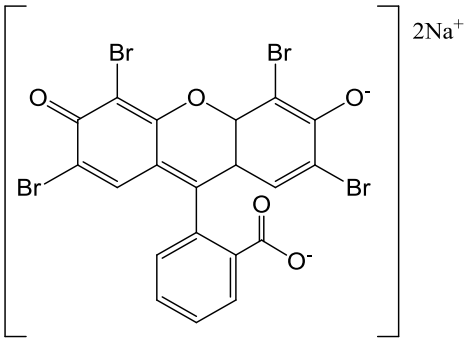

Figure 1.33 *Molecular structure of photoactivated eosin used to treat skin cancer.*[168]

Developed by Ford, Schatzschneider and others,[146, 161, 169-171] photoactivation of CORMs has become an important technique to induce CO-release (Eqn. 1.1). Photoactivation of CO-releasing molecules (PhotoCORMs) follows the selective enrichment of a dark-stable CORM prodrug, at a biological target (*e.g.* cancer site), from which carbon monoxide is only released upon irradiation. This is an attractive approach which allows for precise spatial and temporal control of the biological action of CO.[140]

Equation 1.1:

$$\mathrm{ML}_x(\mathrm{CO})_y \xrightarrow{h\nu} \mathrm{ML}_x(\mathrm{CO})_{y-1} + \mathrm{CO}$$

(where *x* and *y* are integers)

Westerhausen *et al.* report the synthesis of a iron-based water-soluble CORM, *cis*, *trans*-dicarbonylbis(cysteamine)-iron, called CORM-S1 (Figure 1.34).[172] With the use of the spectrophotometric myoglobin assay, CORM-S1 was stable in the dark for a period of time, before CO-release was photoactively initiated with 470 nm light. The authors reported the slow release ($t_{1/2}$ = 43.9 min) of CO, with two molecules of CO-released per molecule of CORM-S1. It has previously been shown that the potassium channels found in the cell membrane can be stimulated by CO.[173] Hence, CO-release was investigated utilizing the membrane patch experiment.[174] An immediate increase in current was observed when compared to the dark control.[172] This data confirmed that particular PhotoCORMs can initiate biological responses and are well suited for the use in biological systems.

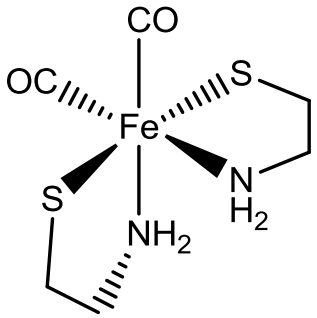

Figure 1.34 *The novel water-soluble PhotoCORM identified by Westerhausen and co-workers [Fe(cysteamine)$_2$(CO)$_2$] (CORM-S1).*[172]

Schatzschneider and co-workers reported the CO-release of a tris(pyrazolyl)methane (tpm) manganese tricarbonyl complex, [Mn(CO)$_3$(tpm)]PF$_6$ (Figure 1.35).[175] In which a manganese(I) tricarbonyl unit is coordinated by a tridentate facial tpm co-ligand. The CO-release properties of [Mn(CO)$_3$(tpm)]PF$_6$ was investigated using the spectrophotometric myoglobin assay, on the basis of changes in the Q-band region. These changes in the Q-band region are due to the formation of MbCO from deoxyMb. This CORM exhibited photoinduced release of two carbonyl ligands upon excitation at 365 nm and is also efficiently internalized by HT-29 human colon carcinoma cells. The primary photophysical process is a metal-ligand charge transfer (MLCT) transition from manganese t_{2g}-type orbitals to unoccupied orbitals with mixed metal-CO character. [Mn(CO)$_3$(tpm)]PF$_6$ is the parent compound of a family of metal-tricarbonyl complexes with functionalized tpm ligands, and was found to be inactive in the dark up to 100 μM.[175]

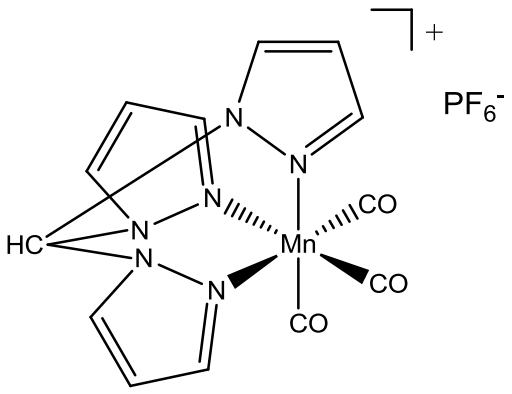

Figure 1.35 *Tris(pyrazolyl)methane (tpm) manganese tricarbonyl complex, [Mn(CO)$_3$(tpm)]PF$_6$, synthesized by Schatzschneider et al.*[175]

Furthermore, the bioavailability of $[Mn(CO)_3(tpm)]PF_6$ was quantified by measuring the cellular Mn uptake by HT-29 human colon cancer cells with atomic absorption spectroscopy (AAS).[175] In these studies, it was found that the cellular Mn content increased linearly with increasing incubation concentration, indicating a passive diffusion rather than active transport across the cell membrane.[175] The most important property of this novel CORM ($[Mn(CO)_3(tpm)]PF_6$), was the efficient reduction of cell biomass after photoactivation, comparable to that induced by established anticancer agent 5-fluorouracil (5-FU) which is in clinical use for many years. For a targeted delivery of PhotoCORMs, researchers envisaged functionalization of PhotoCORMs to biomolecules in an attempt to enable specific uptake into cancer cells.

1.5.3 PhotoCORMs as Bio-Conjugates

A common drawback of CORMs, regardless of how CO-release is brought about (*i.e.* solvent-assisted, enzyme-triggered or photoactivated), is the formation of the metal-co-ligand fragment following release of the CO ligand(s), which might possess a biological activity of its own. One strategy is thought to functionalize macromolecular systems with CORMs, thus following CO-release, the metal-co-ligand fragment remains bound to the "carrier" and eventually metabolized.

The promising results of PhotoCORM $[Mn(CO)_3(tpm)]PF_6$ (mentioned above), prompted the authors to investigate the biocompatibility and the targeted ability of this CORM.[176] Photoactive cytotoxic peptide bioconjugates (Figure 1.36) were prepared with the use of Pd-catalyzed Sonogashira cross-coupling and "click" reactions.[176] One notable feature is the functionalization of the tpm ligand allowed for the preparation of water-soluble bioconjugates. Furthermore, it was demonstrated that the CO-release behavior of the $[Mn(CO)_3(tpm)]^+$ moiety as compared to the parent CORM $[Mn(CO)_3(tpm)]PF_6$ remains unaffected after peptide conjugation.

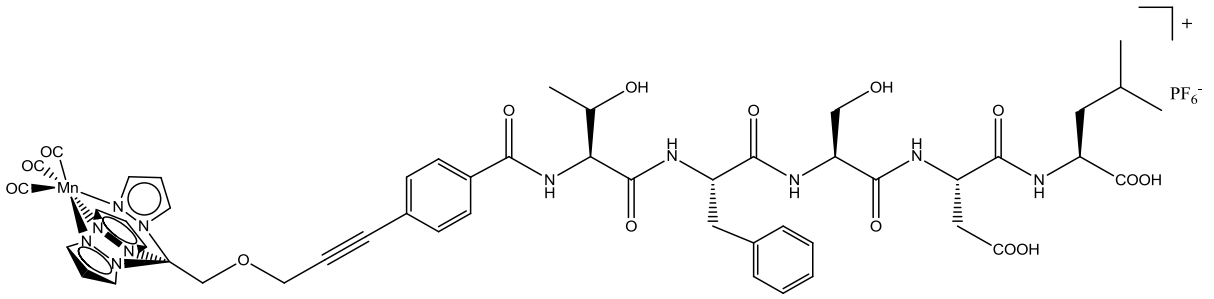

Figure 1.36 *Photoactive $[Mn(CO)_3(tpm)]^+$ functionalized bioconjugates prepared by Schatzschneider et al.*[176]

Kunz and co-workers reported the synthesis and CO-release of a novel PhotoCORM delivery vehicle, a biologically compatible polymeric carrier (2-hydroxypropyl methylacrylamide (HPMA)).[177] Here, the authors functionalized HPMA or, a biodegradable linker, bis(pyridylmethyl)ethanolamine (HPMA-PLA), with bis(pyridylmethyl)amine manganese tricarbonyl complexes (Figure 1.37).[177] Once again, the myoglobin assay was used to determine CO-release, with the polymer free complexes releasing ~ 2 CO ligands per complex following irradiation ($t_{1/2}$ = 20 min). The CO-release of the polymer conjugates was not quantifiable, although qualitatively CO-release was observed following irradiation.

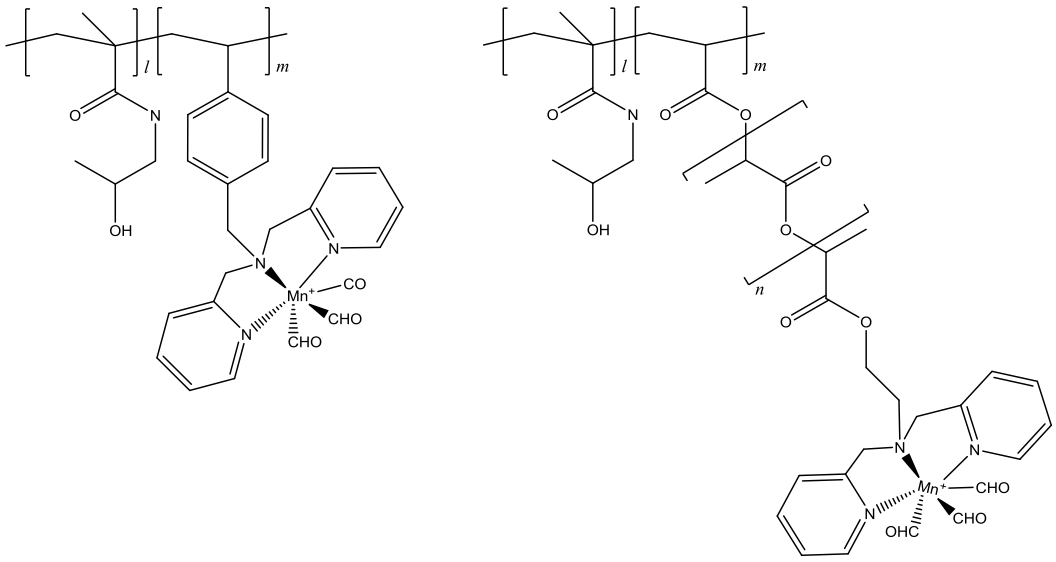

Figure 1.37 *Photoactive bis(pyridylmethyl)amine manganese tricarbonyl functionalized HPMA (left) and HPMA-PLA (right).*[177]

Furthermore, the authors investigated the *in vitro* cytotoxicity of the free complexes and polymer conjugates against human colon carcinoma (Hct116) and human heptanoma (HepG2) cell lines. Only the HPMA-PLA polymer conjugate and free styrene complex showed activity.

However, the cytotoxic effect was not brought about due to CO-release, as the free styrene complex and the HPMA-PLA polymer conjugate showed toxicity before irradiation (in the dark) and following irradiation.

Many different mononuclear CORMs systems have been reported in the literature, however, there are few if not any examples of multinuclear CORMs reported. Hence there is scope in the preparation of such multinuclear systems.

1.6 Metallodendrimers: *Metal Decorated Dendrimers for Oncology*

The term metallodendrimers is derived from the name given to metal functionalized highly branched macromolecules known as dendrimers. The term dendrimer is built from the Greek words “dendros” meaning tree, and “meros” meaning part. These complex macromolecules have well defined shape, are highly branched and are built from a central core.[178] compared to linear polymers, dendrimers can be synthesized reproducibly with low polydispersity, which is a highly discernible feature for drug delivery agents. A wide range of functionalities can be included throughout the dendritic framework (on the periphery, at the core or interspersed), which give them a wide range of applications in medicinal chemistry,[179, 180] host-guest chemistry[181, 182] and catalysis.[183-186]

1.6.1 General Design and Synthesis of Dendrimers

A dendritic scaffold has four main regions (Figure 1.38):[187]

i. the core scaffold (initiator),
ii. repeating branching units attached to the core (generation, G_n, where n can be 0 to 12),
iii. terminal groups, found on the periphery, attached to the outmost generation,
iv. void spaces (for encapsulation of small molecules).

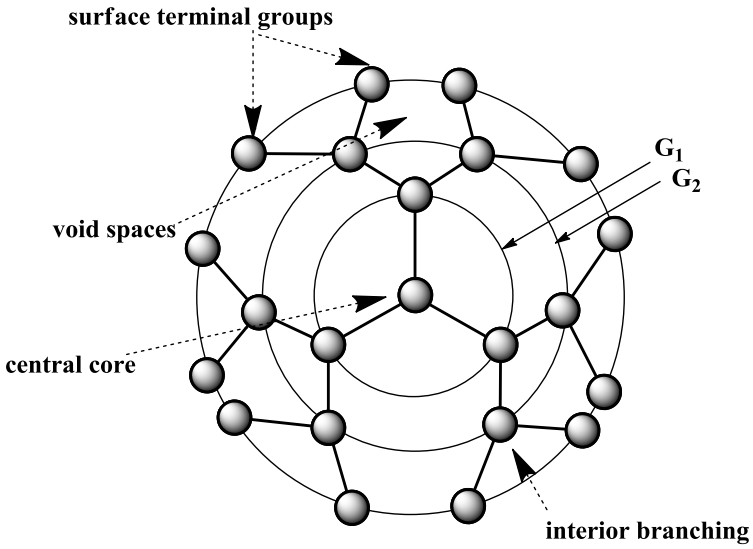

Figure 1.38 *A general schematic of the dendritic scaffold.*[187]

There are two general methods/routes in synthesizing dendrimers, namely the divergent route (building 'outwards' from a central core) and the convergent route (synthesis of dendritic-like wedges (dendrons), followed by a final coupling reaction) (Figure 1.39).[188]

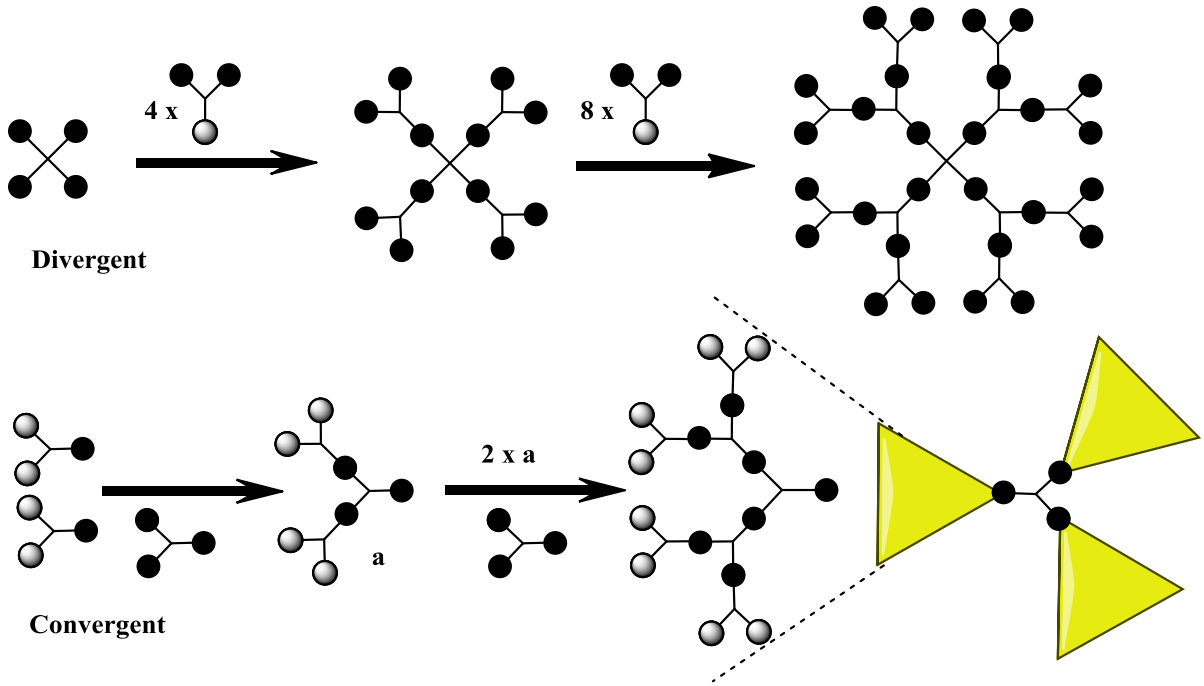

Figure 1.39 *General methods in synthesizing dendrimers, the divergent route (top) and convergent route (bottom).*[188]

The divergent synthesis can be explained by the synthesis of poly(amidoamine) (PAMAM) dendrimers, which were the first commercially available dendrimers of the dendrimer family (Scheme 1.6).[189] PAMAM synthesis is initiated by using and alkyl diamine core, such as ethylene diamine (EDA) which reacts *via* a Michael addition with methyl acrylate monomers to produce a branch intermediate. The branch intermediate is reacted with excess EDA to produce G_0 with four NH_2 surface groups, or reacted with ethanolamine to produce G_0 with four OH surface groups.[190] Synthesis of the higher generations is achieved by sequential Michael addition of methyl acrylate monomers followed by an extensive amidation reaction with EDA.

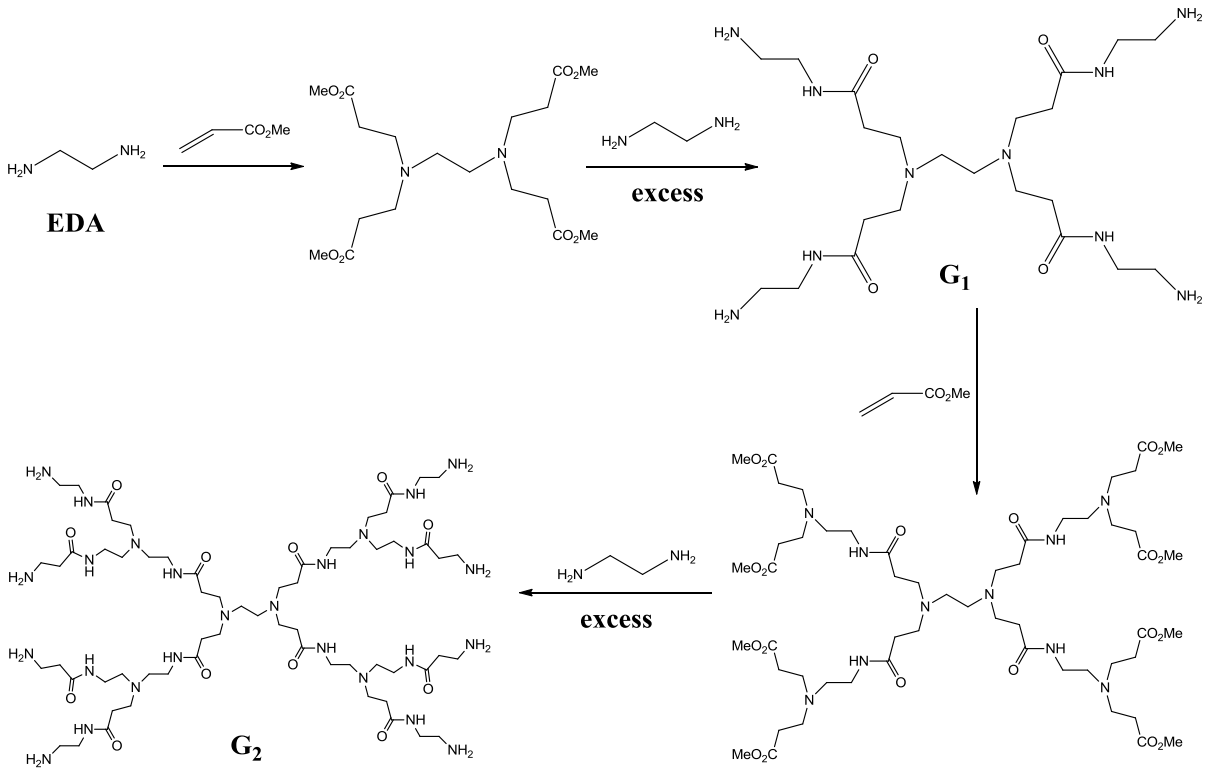

Scheme 1.6 *Synthesis of PAMAM dendrimers using the divergent synthesis.*[190]

This synthesis produced highly branched, highly ordered and monodispersed polymers. However, dendrimer growth reaches a critical point due to steric crowding of the dendritic arms, which limits development into higher generations, and results in a number of structural defects known as de Gennes dense packing effect.[191] The effect is only observed from generation 7 to generation 10, where the yields become insignificant and is attributed to steric factors.[192]

Hence, an alternate route was devised to address the deficiencies of the divergent method, namely the convergent approach. As mentioned, convergent synthesis involved building from the periphery toward a central focal point, by coupling surface units to building blocks to form the branching structure (dendron). Following the synthesis of the dendrons, each dendron is conjugated to a multifunctional core to complete the dendrimer. The convergent approach has fewer structural defects and the purification of the dendrons are simpler compared to an entire dendrimer.

Hawker and Frechet reported the synthesis of polyether dendrimers using the convergent approach (Scheme 1.7).[193] The polyether dendrimers were based on 3,5-dihydroxylbenzyl alcohol units coupled to a activated benzyl bromide, affording successive dendrons.[193]

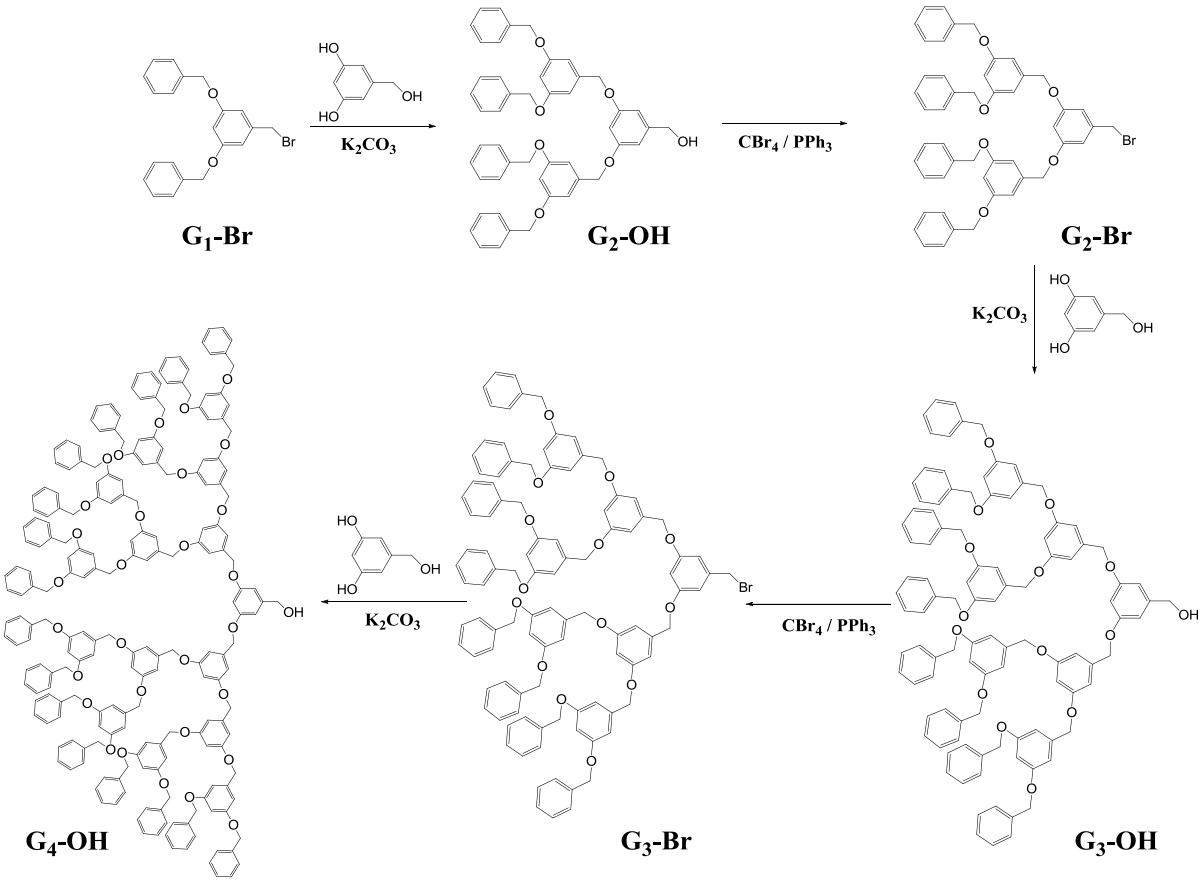

Scheme 1.7 *Synthesis of polyether dendrimers using the convergent synthesis, by Hawker and Frechet.*[193]

Early research in dendrimers mainly focussed on synthesis and characterization,[194, 195] more recently researchers have directed their focus towards functionality and applications of these macromolecules.

1.6.2 Applications of Metallodendrimers: *With Focus on Nanomedicine*

The well-defined and ordered molecular structure of dendrimers and their unique properties such as the high density and highly flexible design, the reactivity of the functional groups on the periphery, as well as the possible aqueous solubility and low toxicity offers dendrimers applications in a variety of fields. These fields include catalysis,[183-185] biosensors,[196, 197] adhesives,[198] magnetic resonance imaging,[199] and nanomedicine.[179, 180] Moreover in catalysis, the catalytically-active complex can be located throughout the dendritic framework (Figure 1.40).[178] The multinuclearity approach affords greater activity and efficiency of the metallodendrimers over their mononuclear analogs.[184, 200, 201]

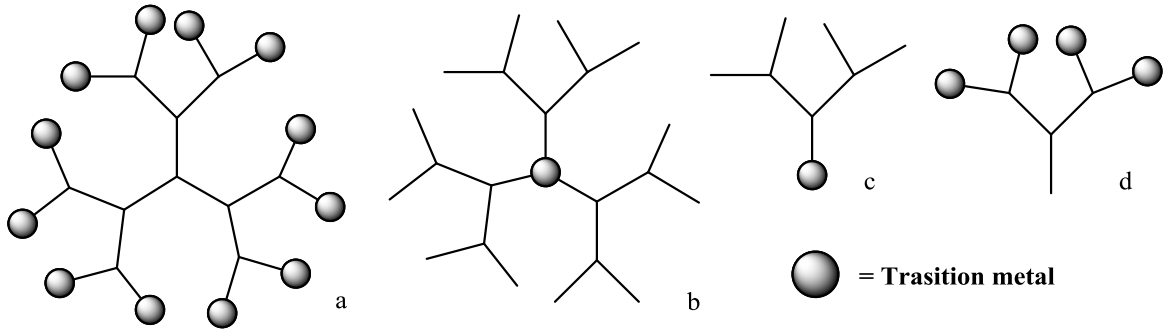

Figure 1.40 *Catalytically active transition-metals can be attached, (a) to the periphery, (b) to the core, (c) to the focal point of a dendron or (d) on the periphery of a dendron.*[178]

The concept of multinuclearity could lead to improved activity of metallodrugs. Hence, another application of metallodendrimers is the delivery of drugs. Several approaches have been used (Figure 1.38):[187]

i. physical encapsulation of the drugs into the void spaces (drawbacks, fast and uncontrolled delivery of drugs)[202]
ii. electrostatic binding between the ionic peripheral groups of the dendrimer and the drug
iii. hydrogen bonding between the peripheral functional groups and the drug
iv. and covalent linkage of the drug to the dendritic periphery or surface (known as the pro-drug approach)

Notably, in nanomedicine, the concept of multinuclearity can be applied to improve the potency of chemotherapeutic drugs. By exploiting the enhanced permeability and retention effect (EPR effect) dendrimers can be used to selectively target drug-targets.

The EPR effect is a phenomenon in which macromolecules (such as metallodendrimers), can exploit the physiological patterns of solid tumors (Figure 1.41). Metallodendrimers can accumulate at the tumor site due to an increase in blood vessel permeability (porous endothelial layer) within the cancerous cells over healthy tissues.[203, 204] The healthy endothelial layer surrounding blood vessels, restricts the size of molecules that can diffuse from the blood stream into the cells. In contrast, the endothelial layer of cancerous tissues is more porous, providing access to the surrounding tissue. Furthermore, diseased tissues have an impaired lymphatic drainage system, thus once macromolecules have entered the cancerous site they are retained for longer periods (increase in bio-availability). A tetraruthenium cluster is highly active against the polio virus, without effecting healthy cells.[83]

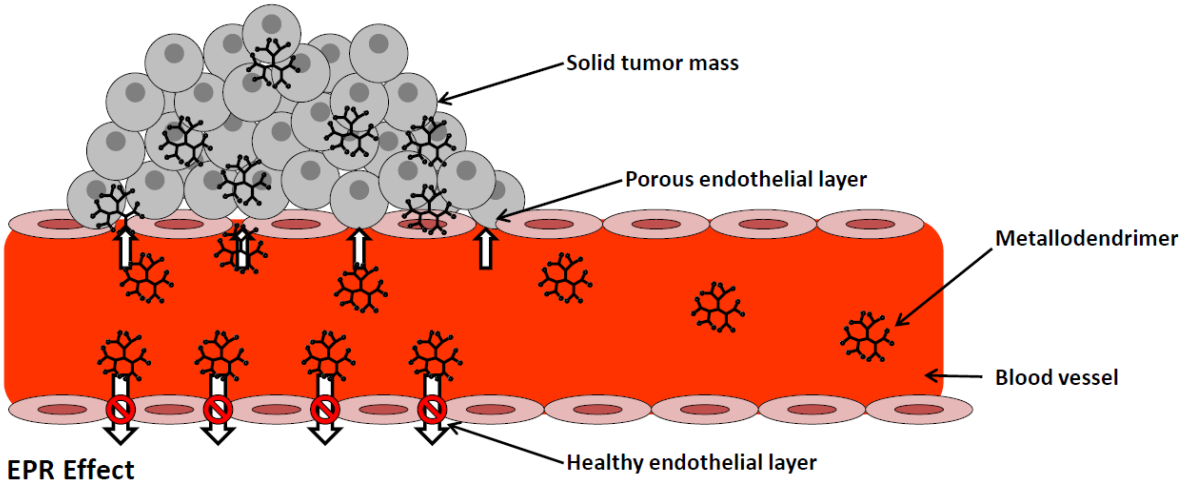

Figure 1.41 *Illustration showing the diffusion of metallodendrimers into the tumor site, explained by the phenomenon known as the EPR effect.*[203, 204]

The use of dendrimers in the field of medicine is highly developed, with a number of dendrimer conjugates reported.[205-207] However, the use of metallodrugs conjugated to dendritic frameworks is sparse, with only a handful of reports as antitumor agents [180, 187] or antimalarial agents.[208]

1.6.3 Metallodendrimers as Anticancer Agents

Following the successes of cisplatin and its analogs,[13] in particular the trinuclear Pt-based complex (BBR3464) mentioned earlier.[15] Researchers have pursued the idea of functionalizing metallodrugs onto dendritic scaffolds in an effort to improve the activity of the metallodrug. There are only a handful of metallodendrimers specifically developed to target cancerous cells and are highlighted in a recent review.[180]

It should come to no surprise that the first metallodendrimer synthesized to target cancer cells, was a tetranuclear Pt-based compound (Figure 1.42).[209] The platinum-functionalized metallodendrimer DAB(PA-tPt-Cl)$_4$ (where DAB = diaminobutane, PA = polyamine) is based on the first-generation poly(propylene) (PPI) dendritic scaffold. The Pt-metallodendrimer was synthesized to overcome problems associated with cisplatin-resistance in cancer cells:

i. deactivation of the Pt-species by intracellular thiolates and
ii. improved repair of crosslinks with DNA.

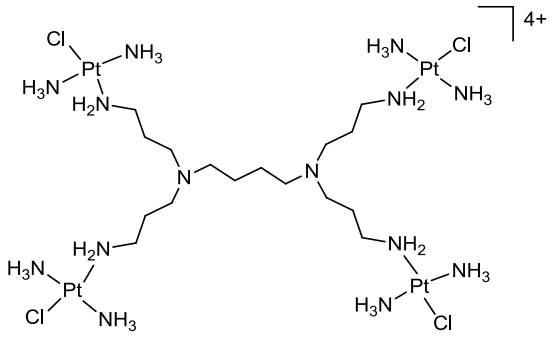

Figure 1.42 *Structure if G_1 tetranuclear Pt-functionalized metallodendrimer, DAB(PA-tPt-Cl)$_4$.*[209]

The four-armed molecule is expected to form crosslinks with DNA, which are very different from the adduct(s) formed by cisplatin. The tetranuclear complex was able to bind to four molecules of the model nucleobase, guanine-5'-monophosphate (GMP) at the N7 position, similarly seen with BBR3464. The complex showed moderate cytotoxicity against mouse leukemia cells (L1210/0, IC_{50} = 12.4 μM),[209] and was investigated against seven human cell lines (IC_{50} >9 μM).[209] The authors attribute the low activity to high charge and branching of the metallodendrimer, which would in turn impede the movement of the complex into the active site (*i.e.* crossing the cell membrane).

With the severe side-effects of platinum-based drugs,[17] researchers shifted their attention to other metals. Hence, Zhao and co-workers synthesized tetranuclear (Pt-based) and hexanuclear (Cu-based) PAMAM metallodendrimers (Figure 1.43), with the biological activity of these complexes investigated (in cisplatin-sensitive, MOLT-4, and cisplatin-resistant, MCF-7, breast cancer cells).[210]

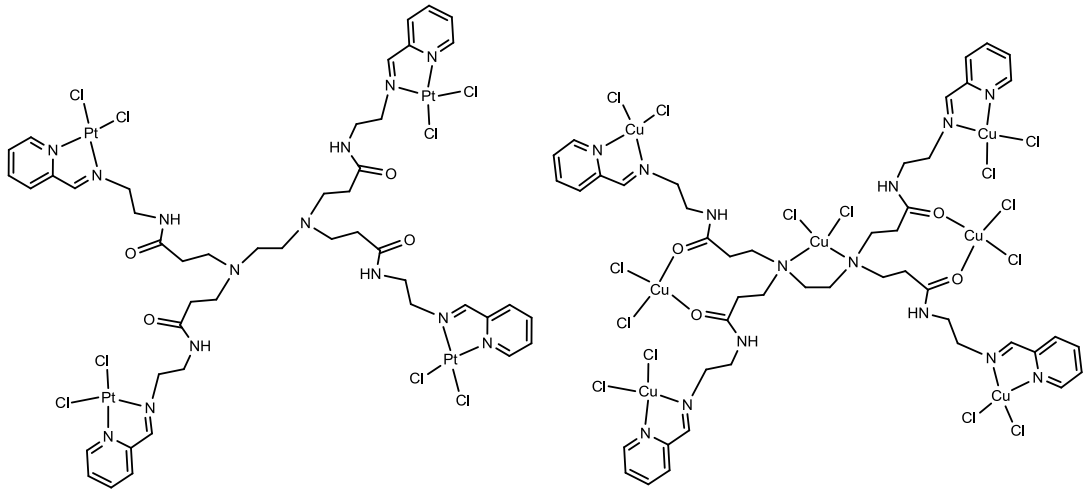

Figure 1.43 *Structure of G_1 tetranuclear Pt- (left) and Cu-functionalized (right) metallodendrimers.*[210]

The ligands showed no activity against the cancer cells, whilst the multinuclear complexes showed enhanced activity over their mononuclear derivatives. Moreover, the copper analogs displayed greater activity to their platinum analogs, with the authors attributing the low toxicity of the Pt-complexes to poor solubility in the testing medium and ability of the complexes to self-assemble (seen through SEM experiments).[210]

Stability of anticancer agents in solution is a key aspect before consideration for biological and clinical applications. Rodrigues and co-workers monitored the degradation and stability of low generation ruthenium-based poly(alkylideneamine)-nitrile metallodendrimers (Figure 1.44) by ^{31}P-NMR spectroscopy. The metallodendrimers containing the $[Ru(Cp)(PPh_3)_2]^+$ moiety was unstable at physiological temperature, as there is a release of the Ru half-sandwich. However, the metallodendrimer containing the $[Ru(dppe)_2Cl]^+$ is stable over 4 h in solution, revealing the potential of the complexes for biological applications.

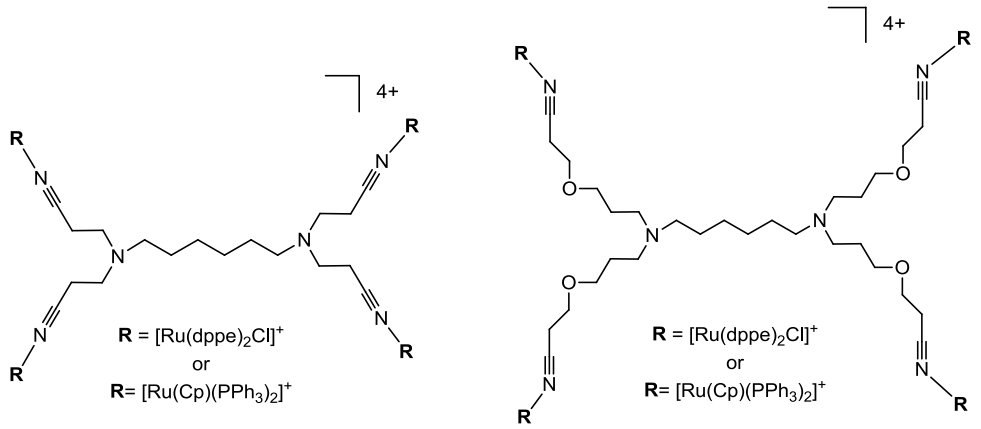

Figure 1.44 *Structure of poly(alkylideneamine)-nitrile metallodendrimers functionalized with* $[Ru(dppe)_2Cl]^+$ *or* $[Ru(Cp)(PPh_3)_2]^+$.[211]

Metallodendrimers have also shown promise as potential photodynamic therapy (PDT) agents, with the synthesis of a 32-armed ruthenium-polypyridyl functionalized PAMAM metallodendrimer, by Velders and co-workers.[212] The positively charged derivative shows promise as a PDT agent, whilst the negatively charged derivative shows promise for diagnostic fluorescence assays.

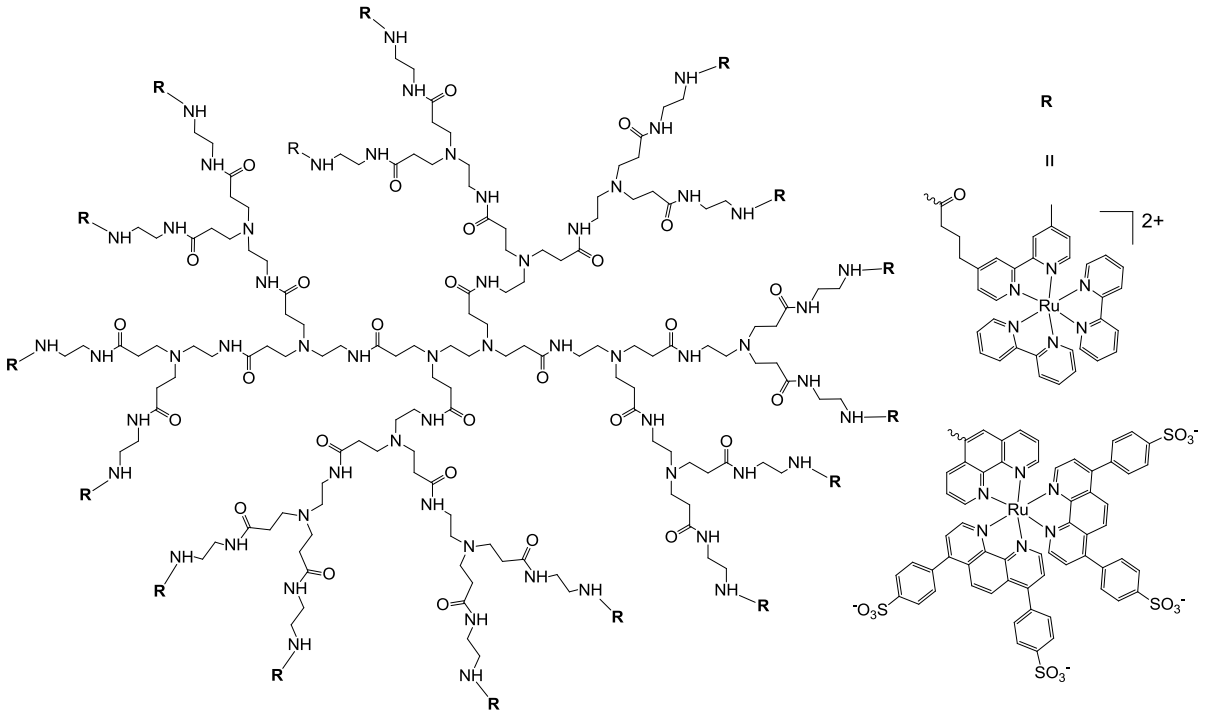

Figure 1.45 *A positively and negatively charged PAMAM polypyridyl ruthenium metallodendrimer.*[212]

Recently, a series of neutral and cationic first- and second-generation monodentate (*N*- donor) and chelating (*N*,*N*- and *N*,*O*-) ruthenium-arene metallodendrimers were prepared.[213, 214] These peripherally functionalized metallodendrimers were based on a poly(propyleneimine) dendritic scaffold and displayed increasing cytotoxicity upon increasing dendrimer generation. Furthermore, the improved activity gives good reason for the preparation of higher generation metallodendrimers, which may lead to potent antitumor compounds. The coupling of metallodrugs to dendritic scaffolds to afford bio-metallodendrimers is novel, but in recent years it has been explored, revealing a new field of metal-based biomolecules.

1.7 Closing Remarks

With the number of cases reported each year increasing exponentially, cancer is a serious threat. The severe toxicity and acquired drug resistance of current chemotherapeutics has led to an urgent need for alternative drugs. Bioorganometallic molecules have emerged as alternative compounds to address the problems presented by commercially available drugs.

Whilst there are few reports on the use of multinuclear metallodendrimers as anticancer agents, the promising results observed for mononuclear complexes, provides motivation for the investigation of their multinuclear derivatives.

1.8 Aims and Objectives of the Thesis

1.8.1 General Aims

In the light of past and recent developments, there is precedence for the development of new bioorganometallic metallodendrimers. Therefore, the aims of the project were:

- The design and synthesis of new multimeric dendritic ligands.
- The coordination of these dendritic ligands to metals (Ru, Os, Mn) to afford multinuclear metallodendrimers.
- Evaluation of these metallodendrimers for their activity as therapeutic agents.

1.8.2 Specific Objectives

1.8.2.1 Synthesis

This project dealt with the preparation of new multinuclear metallodendrimers containing ruthenium, osmium, iron or manganese *via* peripheral functionalization of a poly(propyleneimine) dendritic scaffold. The complexes were characterized using an array of spectroscopic and analytical techniques. Furthermore, to compare the biological activity of the metallodendrimers, their mononuclear analogs were also prepared. The complexes can be divided into three sub-categories, which involve the preparation of three types of ligands systems, all which were complexed with metallodrugs and their biological activity investigated.

I. The preparation of first-, second-, third- and fourth-generation metallodendrimers, where the dendritic ligand coordinates in a chelating bidentate manner to the biologically active ruthenium- or osmium-arene metal centre (Figure 1.46).

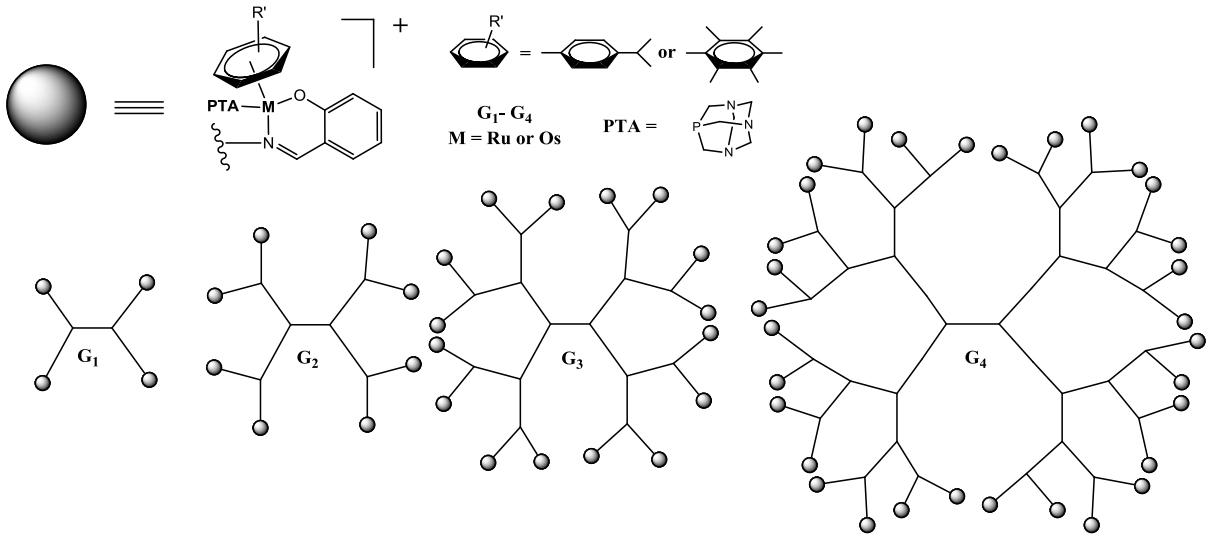

Figure 1.46 *General structures of ruthenium- and osmium-arene metallodendrimers prepared in this study.*

II. The preparation of first- and second-generation metallodendrimers, where ferrocene has been incorporated into the dendritic scaffold, to possibly influence the lipophilic nature of the complexes (Figure 1.47).

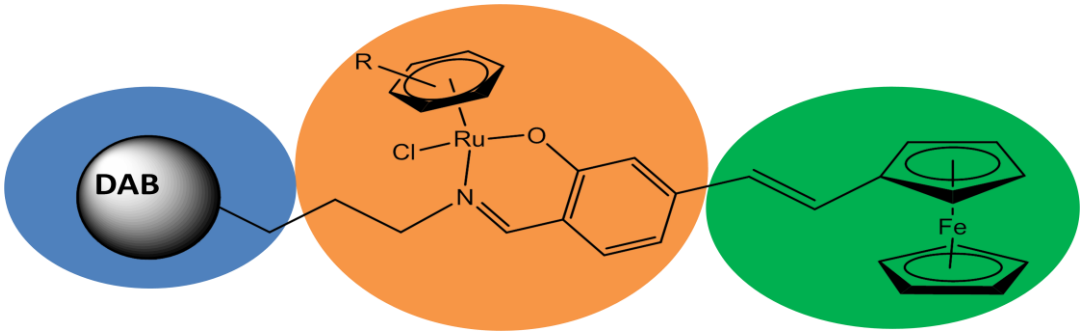

Figure 1.47 *General structure illustrating the incorporation of the ferrocene moeity onto the dendritic scaffold.*

III. The preparation of first- and second-generation metallodendrimers, where the polypyridyl dendritic ligand coordinates in a chelating bidentate manner to a CO-releasing Mn(I) precursor (Figure 1.48).

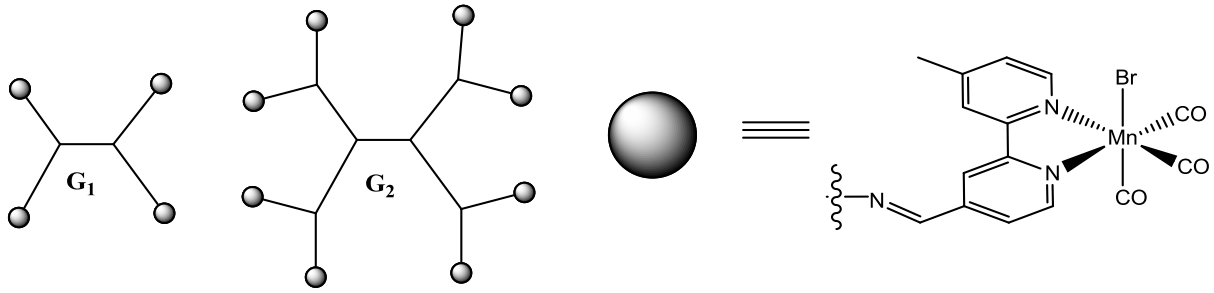

Figure 1.48 *General structures of CO-releasing polypyridyl Mn(II) metallodendrimers prepared.*

All complexes have been characterized using a variety of analytical and spectroscopic techniques, which include NMR, IR and UV-Vis spectroscopy, elemental analysis and mass spectrometry.

1.8.2.2 Biological Investigation

Following preparation of the metallodendrimers, it was necessary to investigate the *in vitro* antitumor activity of the complexes in human ovarian cancer cells (A2780 & A2780cisR). Furthermore, stability studies and DNA binding experiments were performed on the most active complexes. Eventually, structure-activity relationships were established and reported.

The CO-release properties of the manganese-based metallodendrimers were investigated. The CO-release was assessed using the myoglobin assay and complemented with investigations using infrared and UV/Vis spectroscopy during the photolysis of the complexes.

1.9 References

1. P. J. Dyson and G. Sava, *Dalton Trans.*, 2006, **16**, 1929-1933.
2. G. Jaouen, ed., *Bioorganometallics*, Wiley-VCH, Weinheim, 2006.
3. N. J. Farrer and P. J. Sadler, in *Bioinorganic Medicinal Chemistry*, ed. E. Alessio, Wiley-VCH, Weinheim, 2011, pp. 1-47.
4. B. Rosenberg, L. Vancamp and T. Krigas, *Nature*, 1965, **205**, 698-699.
5. B. Rosenberg, L. Van Camp, J. E. Trosko and V. H. Mansour, *Nature*, **1969**, 385-386.
6. M. Peyrone, *Ann. Chemie. Pharm.*, 1844, **51**, 1-29.
7. C. X. Zhang and S. J. Lippard, *Curr. Opin. Chem. Biol.*, 2003, **7**, 481-489.
8. E. Wiltshaw and B. Carr, *Rec. Res. Cancer Res.*, 1974, **48**, 178-182.
9. J. P. Neijt, W. W. ten Bokkel Huinink, M. E. van der Burg, A. T. van Oosterom, P. H. Willemse, J. B. Vermorken, A. C. van Lindert, A. P. Heintz, E. Aartsen and M. van Lent, *Eur. J. Cancer*, 1991, **27**, 1367-1372.
10. D. J. Higby, H. J. J. Wallace, D. Albert and J. F. Holland, *J. Urol.*, 1974, **112**, 100-104.
11. A. Horwich, *Br. J. Cancer.*, 1989, **59**, 156-159.
12. M. Galanski, M. A. Jakupec and B. K. Keppler, *Curr. Med. Chem.*, 2005, **12**, 2075-2094.
13. M. Gordon and S. Hollander, *J. Med. Chem.*, 1993, **24**, 209-265.
14. D. Simpson, C. Dunn, M. Curran and K. L. Goa, *Drugs*, 2003, **63**, 2127-2156.
15. C. Billecke, S. Finniss, L. Tahash, C. Miller, T. Mikkelsen, N. P. Farrell and O. Bogler, *Neuro-Oncology*, 2006, **8**, 215-226.
16. D. I. Jodrell, T. R. J. Evans, W. Steward, D. Cameron, J. Prendiville, C. Aschele, C. Noberasco, M. Lind, J. Carmichael, N. Dobbs, G. Camboni, B. Gatti and F. De Braud, *Eur. J. Cancer*, 2004, **40**, 1872-1877.
17. E. Wong and C. M. Giandomenico, *Chem. Rev.*, 1999, **99**, 2451-2466.
18. T. Pieper, K. Borsky and B. K. Keppler, in *Topics in Biological Inorganic Chemistry*, eds. M. J. Clarke and P. J. Sadler, Springer, Verlag, Berlin, 1999, vol. 1, pp. 171-199.
19. H. Köpf and P. Köpf-Maier, *Angew. Chem.*, 1979, **91**, 509-512.
20. A. Erxleben, J. Claffey and M. Tacke, *J. Inorg. Biochem.*, 2010, **104**, 390-396.
21. J. H. Toney and T. J. Marks, *J. Am. Chem. Soc.*, 1985, **107**, 947-953.
22. N. Kröger, U. R. Kleeberg, K. Mross, L. Edler and D. K. Hossfeld, *Onkologie*, 2000, **23**, 60-62.

23. N. J. Sweeney, J. Claffey, H. Muller-Bunz, C. Pampillon, K. Strohfeldt and M. Tacke, *Appl. Organomet. Chem.*, 2007, **21**, 57-65.
24. G. Kelter, N. J. Sweeney, K. Strohfeldt, H.-H. Fiebig and M. Tacke, *Anti-Cancer Drugs*, 2005, **16**, 1091-1098.
25. J. Claffey, M. Hogan, H. Müller-Bunz, C. Pampillon and M. Tacke, *Chem. Med. Chem.*, 2008, **3**, 729-731.
26. G. Bandoli, A. Dolmella, F. Tisato, M. Porchia and F. Refosco, *Coord. Chem. Rev.*, 2009, **253**, 56-77.
27. S. M. Valiahdi, P. Heffeter, M. A. Jakupec, R. Marculescu, W. Berger, K. Rappersberger and B. K. Keppler, *Melanoma Res.*, 2009, **19**, 283-293.
28. D. Chen, M. Frezza, S. R., Q. C. Cui, V. Milacic, C. N. Verani and Q. P. Dou, *Cancer Res.*, 2007, **67**, 9258-9265.
29. K. De Leon, F. Balldin, C. Watters, A. Hqmood, J. Griswold, S. Streedharan and K. P. Rumbaugh, *Antimicrobl. Agents Chemother.*, 2009, **53**, 1331-1337.
30. J. F. Lascourreges, P. Caumette and O. F. X. Donard, *Appl. Organomet. Chem.*, 2000, **14**, 98-107.
31. N. Gerasimchuk, T. maher, P. Durham, K. V. Domasevitch, J. Wilking and A. Mokhir, *Inorg. Chem.*, 2007, **46**, 7268-7284.
32. G. N. Kaluderovic and R. Paschke, *Curr. Med. Chem.*, 2011, **18**, 4738-4752.
33. A. Alama, M. Viale, M. Cilli, C. Bruzzo, F. Novelli, B. Tasso and F. Sparatore, *Invest. New Drugs*, 2009, **27**, 124-130.
34. A. Alama, B. Tasso, F. Novelli and F. Sparatore, *Drug Discov. Today*, 2009, **14**, 500-508.
35. G. N. Kaluderovic, H. Kommera, E. Hey-Hawkins, R. Paschke and S. Gómez-Ruiz, *Metallomics*, 2010, **2**, 419-428.
36. J. J. Liu, P. Galettis, A. Farr, L. Maharaj, H. Samarasinha, A. C. McGechan, B. C. Baguley, R. J. Bowen, S. J. Berners-Price and M. J. McKeage, *J. Inorg. Biochem.*, 2008, **102**, 303-310.
37. S. M. Mautlis, A. A. Morales, L. Yehiayan, C. Croutch, D. Gutman, Y. Cai, K. P. Lee and L. H. Biose, *Mol. Cancer Ther.*, 2009, **8**, 1197-1206.
38. F. Tisato, C. Marzano, M. Porchia, M. Pellei and C. Santini, *Med. Res. Rev.*, 2010, **30**, 708-749.

39. D. Magda, P. Lecane, Z. Wang, W. Hu, P. Thiemann, X. Ma, P. K. Dranchak, X. Wang, V. Lynch, W. Wei, V. Csokai, J. G. Hacia and J. L. Sessler, *Cancer Res.*, 2008, **68**, 5318-5325.
40. H. Li, C. S. Lai, J. Wu, P. C. Ho, D. de Vos and E. R. T. Tiekink, *J. Inorg. Biochem.*, 2007, **101**, 809-816.
41. T. Yamse, *J. Mater. Chem.*, 2005, **15**, 4773-4782.
42. S. Komeda and A. Casini, *Curr. Top. Med. Chem.*, 2012, **12**, 219-315.
43. M. Pongratz, P. Schluga, M. A. Jakupec, V. B. Arion, C. G. Hartinger, G. Allmaier and B. K. Keppler, *J. Anal. At. Spectrom*, 2004, **19**, 46-51.
44. G. Sava, R. Gagliardi, A. Bergamo, E. Alessio and G. Mestroni, *Anticancer Res.*, 1999, **19**, 969-972.
45. G. Sava, S. Zorzet, C. Turrin, F. Vita, M. R. Soranzo, G. Zabucchi, M. Cocchietto, A. Bergamo, S. Di Giovine, G. Pezzoni, L. Sartor and S. Garbisa, *Clin. Cancer Res.*, 2003, **9**, 1898-1905.
46. A. Bergamo, R. Gagliardi, V. Scarcia, A. Furlani, E. Alessio, G. Mestroni and G. Sava, *J. Pharmcol. Exp. Ther.*, 1999, **289**, 559-564.
47. C. G. Hartinger, S. Zorbas-Seifried, M. A. Jakupec, B. Kynast, H. Zorbas and B. K. Keppler, *J. Inorg. Biochem.*, 2006, **100**, 891-904.
48. F. Lentz, A. Drescher, A. Lindauer, H. Henke, R. A. Hilger, C. G. Hartinger, M. E. Scheulen, C. Dittrich, B. K. Keppler and U. Jaehde, *Anti-Cancer Drugs*, 2009, **20**, 97-103.
49. P. Heffeter, K. Böck, B. Atil, M. A. R. Hoda, W. Körner, C. Bartel, U. Jungwirth, B. K. Keppler, M. Micksche, W. Berger and G. Kollensperger, *J. Biol. Inorg. Chem.*, 2010, **15**, 737-748.
50. A. R. Timberbaev, C. G. Hartinger, S. S. Aleksenko and B. K. Keppler, *Chem. Rev.*, 2006, **106**, 2224-2248.
51. D. Frasca, J. Ciampa, J. Emerson, R. S. Umans and M. J. Clarke, *Met. Based Drugs*, 1996, **3**, 197-209.
52. M. J. Clarke, *Coord. Chem.*, 2003, **236**, 209-233.
53. C. G. Hartinger and P. J. Dyson, *Chem. Soc. Rev.*, 2009, **38**, 391-401.
54. A. L. Noffke, A. Habtemariam, A. M. Pizarro and P. J. Sadler, *Chem. Commun.*, 2012, **48**, 5219-5246.
55. G. Süss-Fink, *Dalton Trans.*, 2010, **39**, 1673-1688.

56. W. H. Ang, A. Casini, G. Sava and P. J. Dyson, *J. Organomet. Chem.*, 2011, **696**, 989-998.
57. A. A. Nazarov, C. G. Hartinger and P. J. Dyson, *J. Organomet. Chem.*, 2013, doi:http://dx.doi.org/10.1016/j.jorganchem.2013.09.016.
58. L. D. Dale, J. H. Tocher, T. M. Dyson, D. I. Edwards and D. A. Tocher, *Anti-Cancer Drug Des.*, 1992, **7**, 3-14.
59. W. Kandioller, C. G. Hartinger, A. A. Nazarov, C. Bartel, M. Skocic, M. A. Jakupec, V. B. Arion and B. K. Keppler, *Chem. Eur. J.*, 2009, **15**, 12283-12291.
60. S. J. Dougan and P. J. Sadler, *Chimia*, 2007, **61**, 704-715.
61. P. C. A. Bruijnincx and P. J. Sadler, *Adv. Inorg. Chem.*, 2009, **61**, 1-62.
62. A. M. Pizarro and P. J. Sadler, *Biochimie*, 2009, **91**, 1198-1211.
63. S. H. Van Rijt and P. J. Sadler, *Drug Discov. Today*, 2009, **14**, 1089-1097.
64. M. G. Mendoza-Ferri, C. G. Hartinger, M. A. Mendoza, M. Groessl, A. Egger, R. E. Eichinger, J. B. Mangrum, N. P. Farrell, M. Maruszak, P. J. Bednarski, F. Klein, M. A. Jakupec, A. A. Nazarov, K. Severin and B. K. Keppler, *J. Med. Chem.*, 2009, **52**, 916-925.
65. C. Scolaro, A. Bergamo, L. Brescacin, R. Delfino, M. Cocchietto, G. Laureneczy, T. J. Geldbach, G. Sava and P. J. Dyson, *J. Med. Chem.*, 2005, **48**, 4161-4171.
66. C. Scolaro, T. J. Geldbach, S. Rochat, A. Dorcier, C. Gossens, A. Bergamo, M. Cocchietto, I. Tavernelli, G. Sava, U. Rothlisberger and P. J. Dyson, *Organometallics*, 2006, **25**, 756-765.
67. W. H. Ang, E. Daldini, C. Scolaro, R. Scopelliti, L. Juillerat-Jeanneret and P. J. Dyson, *Inorg. Chem.*, 2006, **45**, 9006-9013.
68. P. J. Dyson, *Chimia*, 2007, **61**, 698-703.
69. A. K. Renfrew, A. D. Phillips, E. Tapavicza, R. Scopelliti, U. Rothlisberger and P. J. Dyson, *Organometallics*, 2009, **28**, 5061-5071.
70. M. Hanif, A. A. Nazarov, A. Legin, M. Groessl, V. B. Ario, M. A. Jakupec, Y. O. Tsybin, P. J. Dyson, B. K. Keppler and C. G. Hartinger, *Chem. Commun.*, 2012, 1475-1477.
71. S. M. Guichard, R. Else, E. Reid, B. Zeitin, R. E. Aird, M. Muir, M. Dodds, H. Fiebig, P. J. Sadler and D. I. Jodrell, *Biochem. Pharmacol.*, 2006, **71**, 408-415.
72. Y. K. Yan, M. Melchart, A. Habtemariam and P. J. Sadler, *Chem. Commun.*, 2005, **38**, 4764-4776.

73. A. Bergamo, A. Masi, A. F. A. Peacock, A. Habtemariam, P. J. Sadler and G. Sava, *J. Inorg. Biochem.*, 2010, **104**, 79-86.
74. V. Brabec and O. Nováková, *Drug Resist. Updat.*, 2006, **9**, 111-122.
75. W. H. Ang and P. J. Dyson, *Eur. J. Inorg. Chem.*, 2006, **20**, 4003-4018.
76. A. Casini, F. Edafe, M. Erlandsson, L. Gonsalvi, A. Ciancetta, N. Re, A. Ienco, L. Messori, M. Peruzzini and P. J. Dyson, *Dalton Trans.*, 2010, **39**, 5556-5563.
77. B. Serli, E. Zangrando, T. Gianferrara, C. Scolaro, P. J. Dyson, A. Bergamo and E. Alessio, *Eur. J. Inorg. Chem.*, 2005, 3423-3434.
78. I. Bratsos, S. Jedner, A. Bergamo, G. Sava, T. Gianferrara, E. Zangrando and E. Alessio, *J. Inorg. Biochem.*, 2008, **102**, 1120-1133.
79. C. Gossens, A. Dorcier, P. J. Dyson and U. Rothlisberger, *Organometallics*, 2007, **26**, 3969-3975.
80. C. Scolaro, C. G. Hartinger, C. S. Allardyce, B. K. Keppler and P. J. Dyson, *J. Inorg. Biochem.*, 2008, **102**, 1743-1748.
81. W. H. Ang, E. Daldini, L. Juillerat-Jeanneret and P. J. Dyson, *Inorg. Chem.*, 2007, **46**, 9048-9050.
82. G. S. Smith and B. Therrien, *Dalton Trans.*, 2011, **40**, 10793-10800.
83. C. Manzotti, G. Pratesi, E. Menta, R. Di Domenico, E. Cavalletti, H. H. Fiebig, L. R. Kelland, N. Farrell, D. Polizzi, R. Supino, G. Pezzoni and F. Zunino, *Clin. Cancer Res.*, 2000, **6**, 2626-2634.
84. M. G. Mendoza-Ferri, C. G. Hartinger, A. A. Nazarov, R. E. Eichinger, M. A. Jakupec, K. Severin and B. K. Keppler, *Organometallics*, 2009, **28**, 6260-6265.
85. O. Nováková, A. A. Nazarov, C. G. Hartinger, B. K. Keppler and V. Brabec, *Biochem. Pharmacol.*, 2009, **77**, 364-374.
86. M. Gras, B. Therrien, G. Süss-Fink, O. Zava and P. J. Dyson, *Dalton Trans.*, 2010, **39**, 10305-10313.
87. F. Chérioux, B. Therrien, S. Sadki, C. Comminges and G. Süss-Fink, *J. Organomet. Chem.*, 2005, **690**, 2365-2371.
88. T. Stringer, B. Therrien, D. T. Hendricks, H. Guzgay and G. S. Smith, *Inorg. Chem. Commun.*, 2011, **14**, 956-960.
89. D. Kovala-Demertzi, M. A. Demertzi, J. R. Miller, C. S. Frampton, J. P. Jasinski and D. X. West, *J. Inorg. Biochem.*, 2002, **92**, 137-140.
90. A. L. Noffke, M. Bongartz, W. Wätjen, P. Böhler, B. Spingler and P. C. Kunz, *J. Organomet. Chem.*, 2011, **696**, 1096-1101.

91. J. Mattsson, P. Govindaswamy, A. K. Renfrew, P. J. Dyson, P. Štěpnička, G. Süss-Fink and B. Therrien, *Organometallics*, 2009, **28**, 4350-4357.
92. N. P. E. Barry, F. Edafe and B. Therrien, *Dalton Trans.*, 2011, **40**, 7172-7180.
93. N. P. E. Barry, O. Zava, J. Furrer, P. J. Dyson and B. Therrien, *Dalton Trans.*, 2010, **39**, 5272-5277.
94. A. Pitto-Barry, N. P. E. Barry, O. Zava, R. Deschenaux, P. J. Dyson and B. Therrien, *Chem. Eur. J.*, 2011, **17**, 1966-1971.
95. N. P. E. Barry, O. Zava, P. J. Dyson and B. Therrien, *Aust. J. Chem.*, 2010, **63**, 1529-1537.
96. N. P. E. Barry, N. H. Abd Karim, R. Vilar and B. Therrien, *Dalton Trans.*, 2009, 10717-10719.
97. N. P. E. Barry, J. Furrer, J. Freudenreich, G. Süss-Fink and B. Therrien, *Eur. J. Inorg. Chem.*, 2010, 725-728.
98. N. P. E. Barry, O. Zava, P. J. Dyson and B. Therrien, *Chem. Eur. J.*, 2011, **17**, 9669-9677.
99. B. Therrien, *Top. Curr. Chem.*, 2012, **319**, 35-55.
100. T. J. Kelly and P. L. Pauson, *Nature*, 1951, **168**, 1039-1040.
101. S. A. Miller, J. A. Tebboth and J. F. Termaine, *J. Chem. Soc.*, 1952, 632-635.
102. G. Wilkinson, M. Rosenblum, M. C. Whiting and R. B. Woodword, *J. Am. Chem. Soc.*, 1952, **74**, 2125-2126.
103. E. O. Fischer and W. Z. Pfab, *Naturforsch., B: Anorg. Chem. Org. Chem. Biochem. Biophys. Biol.*, 1952, **7b**, 377-379.
104. R. B. Woodword, M. Rosenblum and M. C. Whiting, *J. Am. Chem. Soc.*, 1952, **74**, 3458-3459.
105. R. D. Adams, *J. Organomet. Chem.*, 2001, **637-639**, 1, and references cited therin.
106. C. S. Allardyce, A. Dorcier, C. Scolaro and P. J. Dyson, *Appl. Organomet. Chem.*, 2005, **19**, 1-10.
107. M. F. R. Fouda, M. M. Abd-Elzaher, R. A. Abdelsamaia and A. A. Labib, *Appl. Organomet. Chem.*, 2006, **21**, 613-625.
108. W. A. Amer, W. L., A. M. Amin, L. Ma and H. Yu, *J. Inorg. Organomet. Polym.*, 2010, **20**, 605-615.
109. C. Ornelas, *New J. Chem.*, 2011, **35**, 1973-1985.
110. S. S. Braga and A. M. S. Silva, *Organometallics*, 2013, **32**, 5626-5639.

111. C. Biot, N. Francois, L. Maciejewski, J. Brocard and D. Paulain, *Bioorg. Med. Chem. Lett.*, 2000, **10**, 839-841.
112. T. Itoh, S. Shirakami, N. Ishida, Y. Yamashita, T. Yoshida, H.-S. Kim and Y. Wataya, *Med. Chem. Lett.*, 2000, **10**, 1657-1659.
113. A. K. Kondapi, N. Satyanarayana and D. Saikrishna, *Arch. Biochem. Biophys.*, 2006, **450**, 123-132.
114. C. Baldoli, S. Maiorana, E. Licandro, G. Zinzalla and D. Perdicchia, *Org. Lett.*, 2002, **4**, 4341-4344.
115. V. J. Fiorina, R. J. Dubois and S. Brynes, *J. Med. Chem.*, 1978, **21**, 393-395.
116. A. Nguyen, A. Vessieres, E. A. Hillard, S. Top, P. Pigeon and G. Jaouen, *Chimia*, 2007, **61**, 716-724.
117. G. Jaouen, S. Top, A. Vessières, G. Lelercq, J. Quivy, L. Jin and A. C. R. Croisy, *Acad, Sci. Paris Ser. IIc.*, 2000, **3**, 89-93.
118. A. Vessières, S. Top, W. Beck, E. A. Hillard and G. Jaouen, *Dalton Trans.*, 2006, **4**, 529-541.
119. E. A. Hillard, P. Pigeon, A. Vessières, C. Amatore and G. Jaouen, *Dalton Trans.*, 2007, 5073-5081.
120. E. A. Hillard, A. Vessières, F. Le Bideau, D. Plazul, D. Spera, M. Huché and G. Jaouen, *Chem. Med. Chem.*, 2006, **1**, 551-559, and references therein.
121. W. Henderson and S. R. Alley, *Inorg. Chem. Acta.*, 2001, **322**, 106-112.
122. Rosenfeld, J. Blum, D. Gibson and A. Ramu, *Inorg. Chem. Acta.*, 1992, **201**, 219-221.
123. D. Nieto, A. M. Gonzalez-Vadillo, S. Brauna, C. J. Pastor, C. Rios-Luci, L. G. Leon, J. M. Padron, C. Navarro-Ranninger and I. Cuadrado, *Dalton Trans.*, 2012, **41**, 432-441.
124. H. Samouei, M. Rashidi and F. W. Heinemann, *J. Organomet. Chem.*, 2011, **696**, 3764-3771.
125. M. Viotte, B. Gautheron, M. M. Kubicki, I. E. Nifant'ev and S. P. Fricker, *Met.-Based Drugs*, 1995, **2**, 311-326.
126. J. Tauchman, G. Süss-Fink, P. Štěpnička, O. Zava and P. J. Dyson, *J. Organomet. Chem.*, 2013, **723**, 233-238.
127. M. Auzias, B. Therrien, G. Süss-Fink, P. Štěpnička, W. H. Ang and P. J. Dyson, *Inorg. Chem.*, 2008, **47**, 578-583.
128. C. Engtrakul and L. R. Sita, *Nano Lett.*, 2001, **1**, 541-549.
129. M. A. Hussein and A. M. Asiri, *Des. Monomers Polym.*, 2012, **15**, 207-251.

130. S. Nlate, J. Ruiz, J.-C. Blais and D. Astruc, *Chem. Commun.*, 2000, 417.
131. I. Angurell, O. Rossell and M. Seco, *Inorg. Chim. Acta*, 2014, **409**, 2-11.
132. R. Foresti and R. Motterlini, *Curr. Drug Targets*, 2010, **11**, 1595-1604.
133. Y. C. Hou, A. Janczuk and P. G. Wang, *Current Pharmaceutical Design*, 1999, **5**, 417-441.
134. L. Li, P. Rose and P. K. Morre, *Annu. Rev. Pharmacol. Toxicol.*, 2011, **51**, 169-187.
135. B. E. Mann and R. Motterlini, *Chem. Commun.*, 2007, 4197-4208.
136. R. Tenhunen, H. S. Marver and R. Schmid, *J. Biol. Chem.*, 1969, **244**, 6388-6394.
137. T. Matsui, M. Furukawa, M. Unno, T. Tomita and M. Ikeda-Saito, *J. Biol. Chem.*, 2005, **280**, 2981-2989.
138. M. Stupfel and G. Bouley, *Ann. N. Y. Acad. Sci.*, 1970, **174**, 342-368.
139. S. W. Ryter, L. E. Otterbein, D. Morse and A. M. K. Choi, *Mol. Cell Biochem.*, 2002, 234-235.
140. U. Schatzschneider, *Eur. J. Inorg. Chem.*, 2010, 1451-1467.
141. L. E. Otterbein, F. H. Bach, J. Alam, M. Soares, H. Tao Lu, M. Wysk, R. J. Davis, R. A. Flavell and A. M. K. Choi, *Nat. Med.*, 2000, **6**, 422-428.
142. C. A. Piantadosi, *Antioxid. Redox. Signal.*, 2002, **4**, 259-270.
143. R. Motterlini, B. E. Mann and R. Foresti, *Expert Opin. Invest. Drugs.*, 2005, **14**, 1305-1318.
144. M. S. Wrighton and D. S. Ginley, *J. Am. Chem. Soc.*, 1975, **97**, 2065-2072.
145. R. Motterlini, R. Foresti and C. J. Green, in *Carbon Monoxide and Cardiovascular Function*, ed. R. Wang, CRC Press, Boca Raton, Fl, 2002, pp. 249-271.
146. R. Alberto and R. Motterlini, *Dalton Trans.*, 2007, **17**, 1651-1660.
147. R. Motterlini, J. E. Clark, R. Foresti, P. Sarathchandra, B. E. Mann and C. J. Green, *Circ. Res.*, 2002, **90**, e17-e24.
148. A. F. Hepp and M. S. Wrighton, *J. Am. Chem. Soc.*, 1983, **105**, 5934-5935.
149. M. J. Clarke, *Coord. Chem. Rev.*, 2002, **232**, 69-93.
150. S. P. Fricker, E. Slade, N. A. Powell, O. J. Vaughan, G. R. Henderson, B. A. Murrer, I. L. Megson, S. K. Bisland and F. W. Flitney, *Br. J. Pharmacol.*, 1997, **122**, 1441-1449.
151. J. E. Clark, P. Naughton, S. Shurey, C. J. Green, T. R. Johnson, B. E. Mann, R. Foresti and R. Motterlini, *Circ. Res.*, 2003, **93**, e2-e8.
152. R. Motterlini, P. Sawle, J. Hammad, S. Bains, R. Alberto, R. Foresti and C. J. Green, *FASEB J.*, 2005, **19**, 284-286.

153. I. J. S. Fairlamb, A.-K. Duhme-Klair, J. M. Lynam, B. E. Moulton, C. T. O' Brien, P. Sawle, J. Hammad and R. Motterlini, *Bioorg. Med. Chem. Lett.*, 2006, **16**, 995-998.
154. T. R. Johnson, B. E. Mann, I. P. Teasdale, H. Adams, R. Foresti, C. J. Green and R. Motterlini, *Dalton Trans.*, 2007, 1500-1508.
155. I. J. S. Fairlamb, L. R. Marrison, J. M. Dickinson, F.-J. Lu and J. P. Schmidt, *Bioorg. Med. Chem.*, 2004, **12**, 4285-4299.
156. P. Sawle, J. Hammad, I. J. S. Fairlamb, B. E. Moulton, C. T. O' Brien, J. M. Lynam, A.-K. Duhme-Klair, R. Foresti and R. Motterlini, *J. Pharmcol. Exp. Ther.*, 2006, **318**, 403-410.
157. C. C. Romão, W. A. Blättler, J. D. Seixas and G. J. L. Bernardes, *Chem. Soc. Rev.*, 2012, **41**, 3571-3583.
158. S. Romanski, B. Kraus, U. Schatzschneider, J.-M. Neudörfl, S. Amslinger and H.-G. Schmalz, *Angew. Chem. Int. Ed.*, 2011, **50**, 2392-2396.
159. S. Romanski, B. Kraus, M. Guttentag, W. Schlundt, H. Rücker, A. Adler, J.-M. Neudörfl, R. Alberto, S. Amslinger and H.-G. Schmalz, *Dalton Trans.*, 2012, **41**, 13862-13875.
160. S. Romanski, H. Rücker, E. Stamellou, M. Guttentag, J.-M. Neudörfl, R. Alberto, S. Amslinger, B. Yard and H.-G. Schmalz, *Organometallics*, 2012, **31**, 5800-5809.
161. U. Schatzschneider, *Inorg. Chim. Acta*, 2011, **374**, 19-23.
162. M. S. Wrighton, *Chem. Rev.*, 1974, **74**, 401-431.
163. D. Crespy, K. Landfester, U. S. Schubert and A. Schiller, *Chem. Commun.*, 2010, **46**, 6651-6662.
164. H. Ali and J. E. van Lier, *Chem. Rev.*, 1999, **99**, 2379-2450.
165. S. B. Brown, E. A. Brown and I. Walker, *Lancet Oncol.*, 2004, **5**, 497-508.
166. K. Szacilowski, W. Macyk, A. Drzewiecka-Matuszek, M. Brindell and G. Stochel, *Chem. Rev.*, 2005, **105**, 2647-2694.
167. R. Ackroyd, C. Kelty, N. Brown and M. Reed, *Photochem. Photobiol.*, 2001, **74**, 656-669.
168. H. I. Pass, *J. Natl. Cancer Inst.*, 1993, **85**, 443-456.
169. R. D. Rimmer, H. Richter and P. C. Ford, *Inorg. Chem.*, 2010, **49**, 1180-1185.
170. R. D. Rimmer, A. E. Pierri and P. C. Ford, *Coord. Chem. Rev.*, 2012, **256**, 1509-1519.
171. A. E. Pierri, A. Pallaoro, G. Wu and P. C. Ford, *J. Am. Chem. Soc.*, 2012, **134**, 18197-18200.

172. R. Kretschmer, G. Gessner, H. Görls, S. H. Heinemann and M. Westerhausen, *J. Inorg. Biochem.*, 2011, **105**, 6-9.
173. S. W. Hou, R. Xu, S. H. Heinemann and T. Hoshi, *Proc. Natl. Acad. Sci. USA*, 2008, **105**, 4039-4043.
174. G. Gessner, R. Heller, T. Hoshi and S. H. Heinemann, *Eur. J. Pharmacol.*, 2007, **555**, 185-193.
175. J. Niesel, A. Pinto, H. W. Peindy N'Dongo, K. Merz, I. Ott, R. Gust and U. Schatzschneider, *Chem. Commun.*, 2008, 1798-1800.
176. H. Pfeiffer, A. Rojas, J. Niesel and U. Schatzschneider, *Dalton Trans.*, 2009, 4292-4298.
177. N. E. Brückmann, M. Wahl, G. J. Reiß, M. Kohns, W. Wätjen and P. C. Kunz, *Eur. J. Inorg. Chem.*, 2011, 4571-4577.
178. G. E. Oosterom, J. N. H. Reek, P. C. J. Kamer and P. W. N. M. van Leeuwen, *Angew. Chem. Int. Ed.*, 2001, **40**, 1828-1849.
179. H. Yang and W. J. J. Kao, *Biomater. Sci. Polym. Ed.*, 2006, **17**, 3-19.
180. P. Govender, B. Therrien and G. S. Smith, *Eur. J. Inorg. Chem.*, 2012, 2853-2862.
181. R. E. Bauer, C. G. J. Clark and K. Müllen, *New J. Chem.*, 2007, **31**, 1275-1283.
182. J. Hu, T. Xu and Y. Cheng, *Chem. Rev.*, 2012, **112**, 3856-3891.
183. D. Astruc, *Pure Appl. Chem.*, 2003, **75**, 461-481.
184. A. W. Bosman, H. W. Janssen and E. W. Meijer, *Chem. Rev.*, 1999, **99**, 1665-1668.
185. S.-H. Hwang, C. D. Shreiner, C. N. Moorefield and G. R. Newkome, *New J. Chem.*, 2007, **31**, 1192-1217.
186. R. S. Bagul and N. Jayaraman, *Inorg. Chim. Acta*, 2014, **409**, 34-52.
187. S. El Kazzouli, N. El Brahmi, S. Mignani, M. Bousmina, M. Zablocka and J.-P. Majoral, *Curr. Med. Chem.*, 2012, **19**, 4995-5010.
188. B. Klajnert and M. Bryszewska, *Acta Biochim. Polonica*, 2001, **48**, 199-208.
189. R. Esfand and D. A. Tomalia, *Drug Discov. Today*, 2001, **6**, 427-436.
190. L. J. Twyman, A. E. Beezer, R. Esfand, M. J. Hardy and J. C. Mitchell, *Tetrahedron Lett.*, 1999, **40**, 1743-1746.
191. D. A. Tomalia, A. M. Naylor and W. Goddard III, *Angew. Chem. Int. Ed.*, 1990, **29**, 138-175.
192. J. D. Eichman, A. U. Bielinska, J. F. Kukowaksa-Latallo and J. R. Backer, *Pharm. Sci. Technol. Today*, 2000, **3**, 232-245.
193. C. J. Hawker and J. M. J. Fréchet, *J. Am. Chem. Soc.*, 1990, **112**, 7638-7647.

194. D. A. Tomalia, H. Baker, J. R. Dewald, M. Hall, G. Kallos, S. Martin, J. Roeck, J. Ryder and P. Smith, *Macromolecules*, 1986, **19**, 2466-2469.
195. G. R. Newkome, Z. Yao, G. R. Baker and V. K. Gupta, *Org. Chem.*, 1985, **50**, 2003-2004.
196. Z.-M. Liu, Y. Yang, H. Wang, Y.-L. Liu, G.-L. Shen and R.-Q. Yu, *Sensor. Actuat. B: Chem.*, 2005, 394-400.
197. O. A. Arotiba, A. Ignaszak, R. Malgas, A. Al-Ahmed, P. G. L. Baker, S. F. Mapolie and E. I. Iwuhoa, *Electrochem. Acta*, 2007, **53**, 1689-1696.
198. R. Mezzenga, L. Boogh and J.-A. E. Manson, *61*, Comp. Sci. Technol., 787-795.
199. R. Misselwitz, H. Schmitt-Willich, W. Ebert, T. Frenzel and H.-J. Weinmann, *Magn. Res. Mater. Biol. Phys. Med.*, 2001, **12**, 128-134.
200. M. T. Reetz, G. Lohmer and R. Schwickardi, *Angew. Chem. Int. Ed. Engl.*, 1997, **36**, 1526-1529.
201. M. T. Reetz, *Top. Catal.*, 1997, **4**, 187-200.
202. M. A. Mintzer and M. W. Grinstaff, *Chem. Soc. Rev.*, 2011, **40**, 173-190.
203. D. F. Baban and L. W. Seymour, *Adv. Drug Delivery Rev.*, 1998, **34**, 109-119.
204. H. Maeda, J. Wu, T. Sawa, Y. Matsumura and K. Hori, *J. Controlled Release*, 2000, **65**, 271-284.
205. M. P. Toraskar, V. G. Pande and V. J. Kadam, *Int. J. Res. in Pharm.*, 2011, **1**, 1100-1107.
206. S. Chandra, S. Dietrich, H. Lang and D. Bahadur, *J. Mater. Chem.*, 2011, **21**, 5729-5737.
207. H. Lang and B. Luhmann, *Adv. Mater.*, 2001, **13**, 1523-1540.
208. S. D. Khanye, J. Gut, P. J. Rosenthal, K. Chibale and G. S. Smith, *J. Organomet. Chem.*, 2011, **696**, 3296-3300.
209. B. A. Jansen, J. v. d. Zwan, J. Reedijk, H. d. Dulk and J. Brouwer, *Eur. J. Inorg. Chem.*, 1999, **9**, 1429 - 1433.
210. X. Zhao, A. C. J. Loo, P. P.-F. Lee, T. T. Y. Tan and C. K. Chu, *J. Inorg. Biochem.*, 2010, **104**, 105-110.
211. J. Rodrigues, M. G. Jardim, J. Figueira, M. Gouveia, H. Tomás and K. Rissanen, *New J. Chem.*, 2011, **35**, 1938-1943.
212. A. Ruggi, C. Beekman, D. Wasserberg, V. Subramaniam, D. N. Reinhoudt, F. W. B. v. Leeuwen and A. H. Velders, *Chem. Eur. J.*, 2011, **17**, 464-467.

213. P. Govender, N. C. Antonels, J. Mattsson, A. K. Renfrew, P. J. Dyson, J. R. Moss, B. Therrien and G. S. Smith, *J. Organomet. Chem.*, 2009, **694**, 3470-3476.

214. P. Govender, A. K. Renfrew, C. M. Clavel, P. J. Dyson, B. Therrien and G. S. Smith, *Dalton Trans.*, 2011, **40**, 1158-1167.

Chapter 2

Synthesis and Characterization of Neutral and Cationic Ruthenium(II)- and Osmium(II)-Arene Complexes Based on Poly(propyleneimine) Dendritic Scaffolds

This chapter forms part of the following publications:

Preshendren Govender, L. C. Sudding, C. M. Clavel, P. J. Dyson, B. Therrien and G. S. Smith, **The Influence of RAPTA Moieties on the Antiproliferative Activity of Peripheral-Functionalized Poly(salicylaldiminato) Metallodendrimers,** *Dalton Transactions*, 2013, 42, 1267-1277.

Preshendren Govender, F. Edafe, B. C. E. Makhubela, P. J. Dyson, B. Therrien and G. S. Smith, **Neutral and Cationic Osmium(II)-Arene Metallodendrimers: Synthesis, Characterization and Anticancer Activity,** *Inorganica Chimica Acta*, 2014, 409, 112-120.

2.1 Introduction

Despite the successes of cisplatin and other platinum-based derivatives, the drawbacks of platinum-based chemotherapeutics, such as drug resistance, side-effects and toxicity, have motivated investigations towards the preparation of complexes based on other metals as effective anticancer agents.[1, 2] Most noteworthy and relevant to this study, is the development of half-sandwich organometallic ruthenium-arene complexes with potent anticancer activity, of general formula [(η^6-arene) Ru(X)(Y)(Z)], where X and Y are bidentate chelating groups (*NN*, *NO*, *OO* or *SO*), or two monodentate ligands, and Z a monodentate moiety, often a leaving group.[3-6] A host of derivatives have been synthesized, which include incorporation of paullones,[7, 8] pyr(id)ones,[9] ethylenediamine (en),[3, 10] or 1,3,5-triaza-7-phosphatricyclo-[3.3.1.1.]decane (PTA),[11, 12] to the ruthenium coordination ion.

Metallodendrimers have been investigated as potential therapeutic agents,[13] as their multivalency may lead to increased interactions between a dendrimer-drug conjugate and a target bearing multiple receptors. A series of monodentate (*N*- donor) and chelating (*N*,*N*- and *N*,*O*-) ruthenium-arene (where arene = *p*-cymene or hexamethylbenzene) first- and second-

generation metallodendrimers, based on a poly(propyleneimine) dendritic scaffold have previously been reported (Figure 2.1).[14, 15] The chelating ruthenium-arene metallodendrimers **5** - **12** show superior *in vitro* antitumor activity over the monodentate ruthenium-arene metallodendrimers **1** - **4**, with the second-generation cationic *N*,*N*-ruthenium-hexamethylbenzene metallodendrimer **8** displaying the greatest activity. A clear correlation between the size dependency of the metallodendrimer and cytotoxicity was also observed. For this reason, it was envisaged that investigation into the synthesis of higher generations of ruthenium-arene metallodendrimers may lead to more potent antitumor agents. Furthermore, half-sandwich rhodium- and iridium-analogs **13** - **20**, of the mentioned ruthenium-arene metallodendrimers **5** - **12**, were reported recently, and displayed moderate to good activity *in vitro* (Figure 2.1).[16]

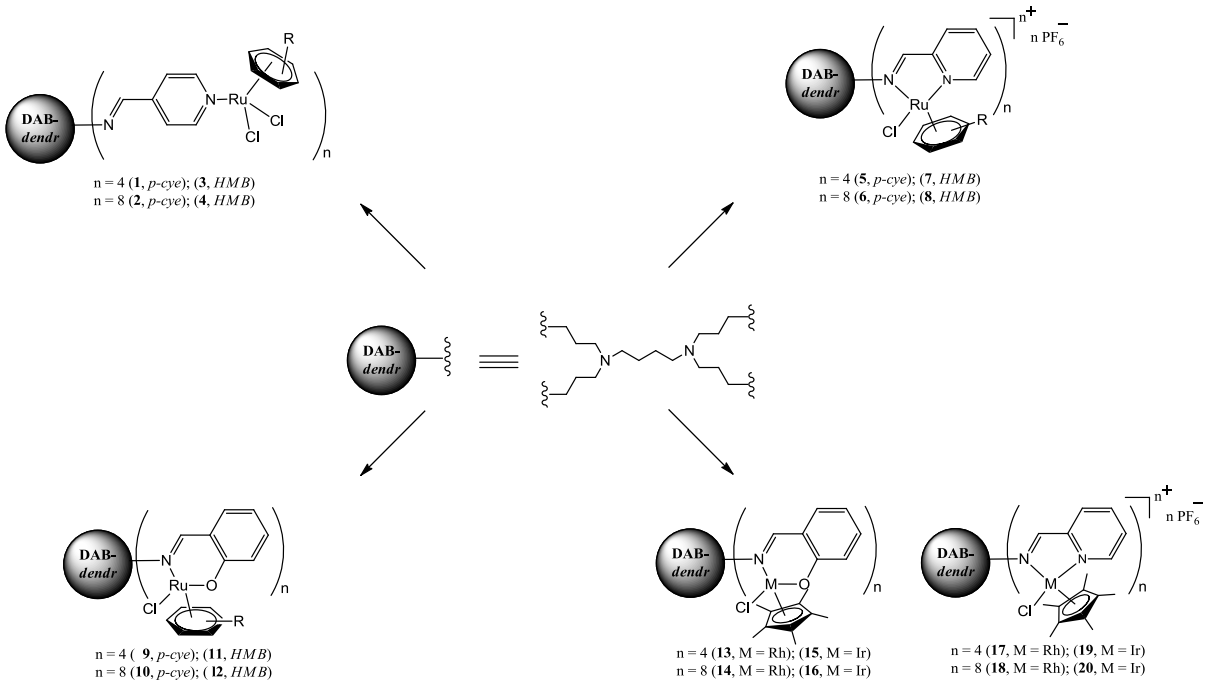

Figure 2.1 *A series of neutral and cationic half-sandwich ruthenium-arene, rhodium-Cp* and iridium-Cp* (where Cp* = pentamethylcyclopentadienyl) metallodendrimers **1** - **20**..*

Eventually, the design and synthesis of these various metallodendrimers will form an important structure-activity study, which will give valuable insights into the mode of action of these potential therapeutic agents.

In this chapter, the synthesis and characterization of novel ruthenium- and osmium-arene metallodendrimers is described. A rationale for the synthesis of this class of compounds and the use of a series of dendritic scaffolds is discussed. Several spectroscopic and analytical techniques were employed to confirm and elucidate the proposed structures, and are described. The biological activity of these metallodendrimers and their mononuclear analogs is discussed in Chapter 4.

2.2 Synthesis and Characterization of *N,O*-Salicylaldiminato Ligands

First- and second-generation *N,O*-salicylaldiminato dendritic ligands, DAB-**G$_1$**-PPI-($C_7H_5NOH)_4$ (**21**) and DAB-**G$_2$**-PPI-$(C_7H_5NOH)_8$ (**22**), were synthesized using known methods.[17] As an extended study the third- and fourth-generation *N,O*-salicylaldiminato dendritic ligands **23** and **24** are new compounds and hence are discussed below.

N,O-salicylaldiminato dendritic ligands **23** and **24** were prepared by reacting salicylaldehyde with the appropriate dendritic scaffold (DAB-**G$_3$**-PPI-$(NH_2)_8$ for **23** or DAB-**G$_4$**-PPI-$(NH_2)_{32}$ for **24**) (Scheme 2.1) *via* a Schiff base condensation reaction (Scheme 2.2, general mechanism) using modified literature reported methodologies.[17]

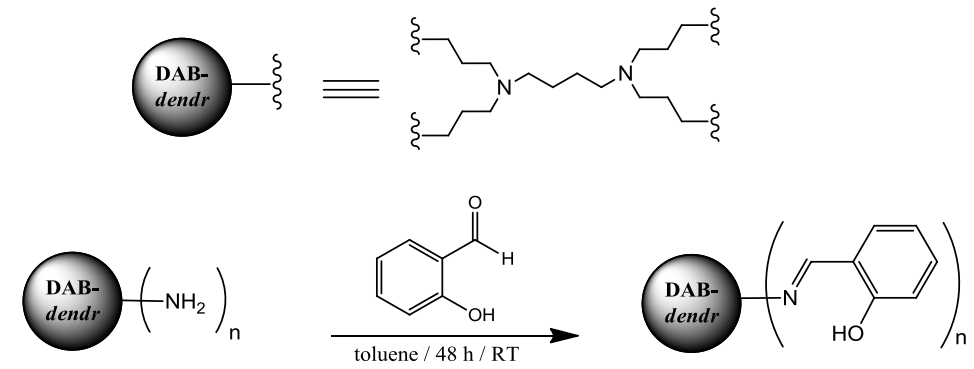

n = 4 (DAB-**G$_1$**-PPI-$(NH_2)_4$)
n = 8 (DAB-**G$_2$**-PPI-$(NH_2)_8$)
n = 16 (DAB-**G$_3$**-PPI-$(NH_2)_{16}$)
n = 32 (DAB-**G$_4$**-PPI-$(NH_2)_{32}$)

n = 4 (**21**)
n = 8 (**22**)
n = 16 (**23**)
n = 32 (**24**)

Scheme 2.1 *Synthesis of N,O-salicylaldiminato dendritic ligands **21** - **24**.*

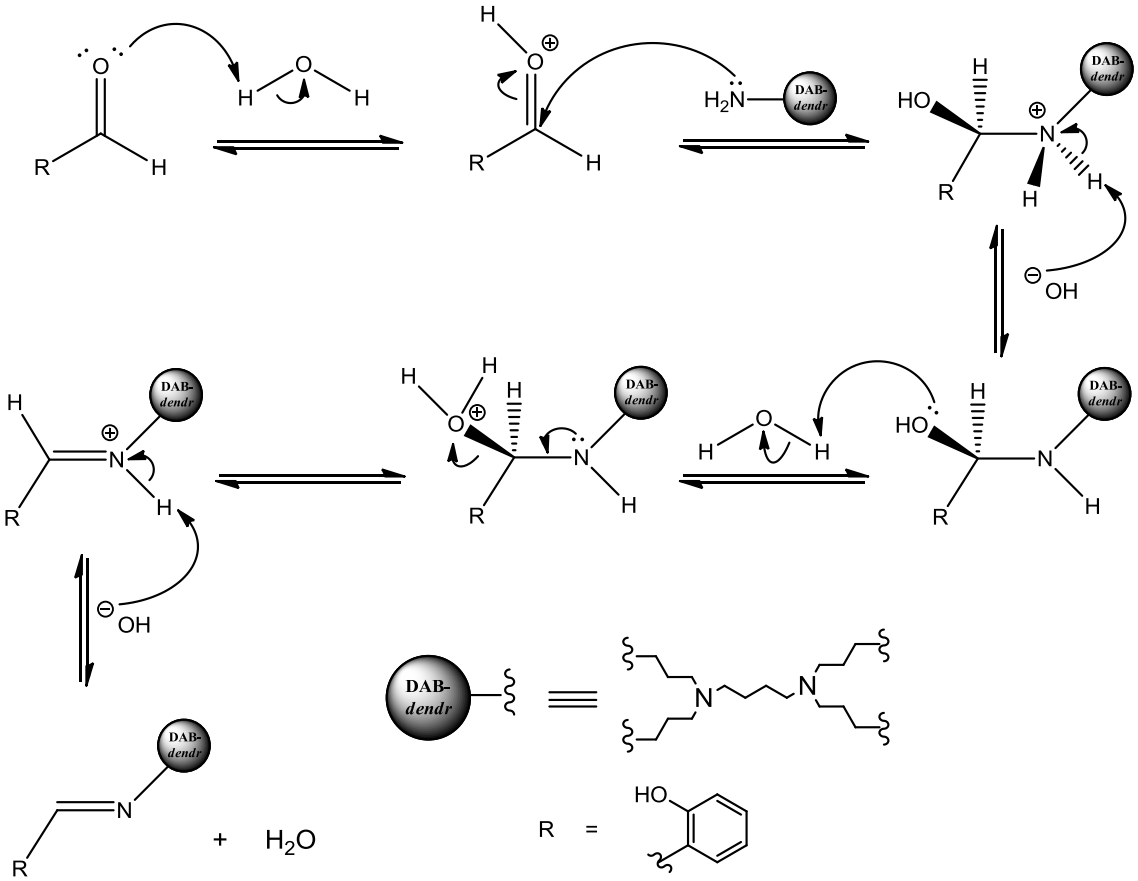

Scheme 2.2 *Mechanistic outline of a general Schiff base condensation reaction.*

The reactants were stirred for 48 h in toluene, at room temperature, in the presence of anhydrous $MgSO_4$, which is used as a drying agent to remove water formed as a by-product in the reaction. Following filtration and removal of the solvent, a liquid-liquid (water/dichloromethane) extraction was employed to remove unreacted starting material. The dendritic ligands **23** and **24** were isolated as yellow-orange oils, in moderate to low yields (Table 2.1). The oils are soluble in most organic solvents such as dichloromethane, methanol, toluene, diethyl ether and dimethylsulfoxide. Spectroscopic (^{1}H NMR, ^{13}C{^{1}H} NMR and IR spectroscopy) and analytical data (elemental analysis and mass spectrometry) confirmed the proposed structures.

Table 2.1 *Physical appearance and percentage yield for dendritic ligands **23** and **24**.*

Compound	Physical Appearance	Yield [%]
23	Orange-yellow oil	71
24	Orange oil	40

2.2.1 ^{1}H and ^{13}C{^{1}H} NMR Spectroscopy

The ^{1}H and ^{13}C{^{1}H} NMR spectra of **23** and **24** were recorded in deuterated chloroform ($CDCl_3$) and are consistent with literature reported values for the first- and second-generation *N,O*-salicylaldiminato analogs,[17] in as far as a reasonable comparison could be made.

The ^{1}H NMR spectra of **23** (Figure 2.2) and **24** show a distinct downfield shift in the signal assigned to aliphatic CH_2 protons adjacent to the imine nitrogen, observed at 3.56 ppm for **23** and 3.53 ppm for **24**. The downfield shift is attributed to the electron withdrawing effects imposed by the imine moiety. The aliphatic protons at the core and on the branches of the dendritic ligands appear between 1.30 ppm and 3.60 ppm.

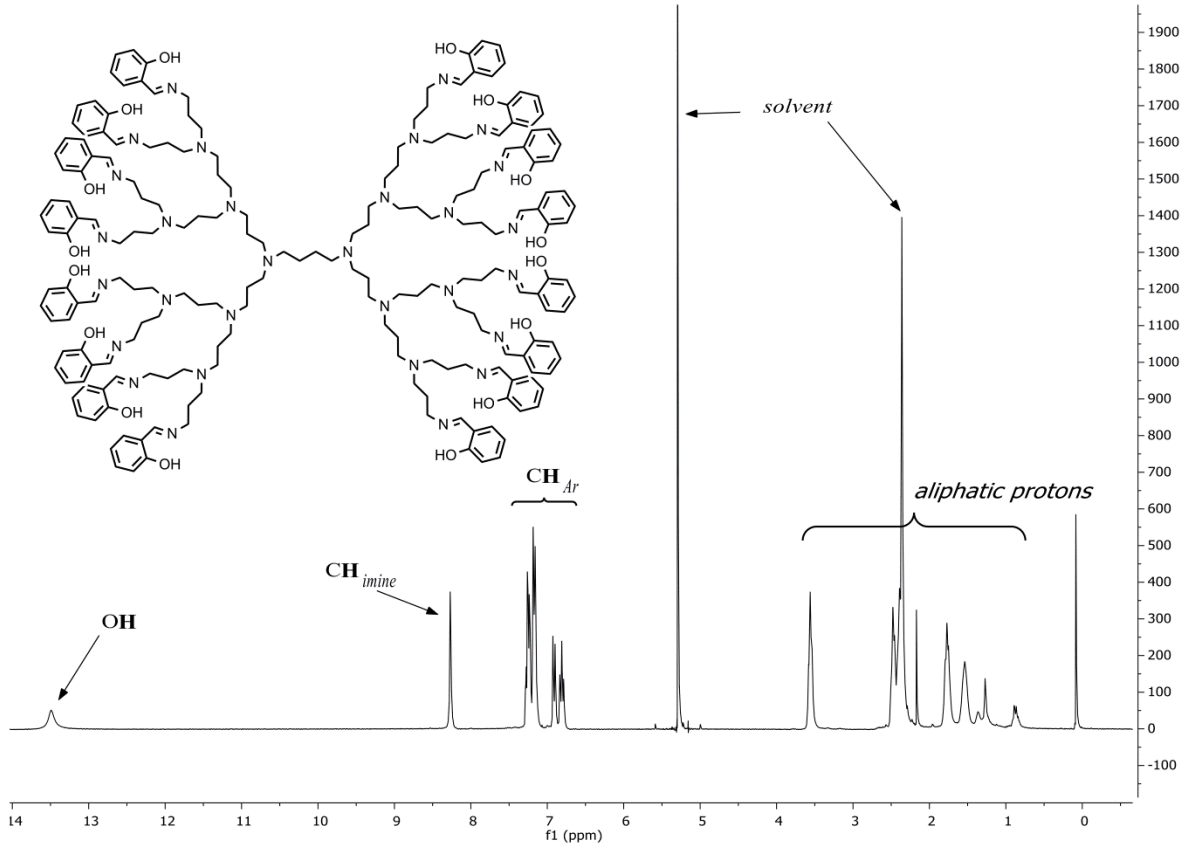

Figure 2.2 *^{1}H NMR spectrum of fourth-generation N,O-dendritic ligand **23** in $CDCl_3$.*

Dendritic ligands **23** and **24** show complex ^{1}H NMR spectra, with peak broadening and overlapping of signals in the aliphatic region, and is attributed to the multi-functionality of the dendrimers and to the sensitivity of the NMR machine. The dendritic arms have many degrees of freedom and hence the ^{1}H NMR spectrum displays broadened peaks. Low temperature ^{1}H NMR is an alternate method to improve the quality and/or resolution of the ^{1}H NMR spectra of **23** and **24**, but these experiments were not performed. The aromatic protons resonate in a

similar range to the monomeric ligand $CH_3CH_2CH_2(C_7H_5NOH)$ (discussed in Section 2.5),[18] between 6.8 ppm and 7.3 ppm for both **23** and **24**. The imine and hydroxyl protons of **23** and **24** are assigned to the singlet and broad singlet at ~8.3 ppm and ~13.5 ppm respectively (Table 2.2).

Table 2.2 *Selected spectroscopic and analytical data for dendritic ligands **23** and **24**.*

Compound	^{1}H NMR (imine, OH) [ppm][a]	^{13}C{^{1}H} NMR (imine) [ppm][a]	IR (imine) [cm^{-1}][b]	MS ([M]$^+$) [*m*/*z*][c]
23	8.27, 13.50	164.9	1634	3354
24	8.27, 13.48	164.8	1634	6844

[a] Recorded in $CDCl_3$,
[b] Recorded in NaCl solution cells in CH_2Cl_2,
[c] MALDI-TOF-MS

The ^{13}C{^{1}H} NMR spectra of **23** and **24** displayed the expected carbon peaks for each compound. No significant changes were observed in the chemical shifts of the signals when moving from the third-generation **23** to the fourth-generation **24**. Signals for the aliphatic carbons are seen between 24 - 57 ppm and for the aromatic carbons between 117 - 161 ppm for both **23** and **24**. The chemical shifts of the signals assigned to the aromatic and imine carbons of **23** and **24** (Table 2.2), are comparable to the chemical shifts reported for the first- and second- generation analogs.[17]

2.2.2 Infrared Spectroscopy

Along with ^{1}H and ^{13}C{^{1}H} NMR spectroscopy, infrared spectroscopy was used to assist in identifying the C=N stretching vibration, indicative of a successful Schiff base condensation reaction. The dendritic ligands **23** and **24** were recorded in dichloromethane in NaCl solution cells. The appearance of a strong stretching vibration at 1634 cm^{-1} for **23** and **24** (Table 2.2) suggests successful condensation of the carbonyl and the amine functionalities. The stretching vibration at 1634 cm^{-1} is assigned to the $(C=N)_{imine}$ bond and is comparable to the first- and second- generation dendritic ligands **21** and **22**.[17] For **23** and **24**, a broad band at ~2950 cm^{-1} is observed and indicated the presence of the hydroxyl functionality. The absence of the carbonyl (~1700 cm^{-1}) and amine (~3300 cm^{-1}) stretching vibrations suggest tautomerism did not occur (Scheme 2.3).[19]

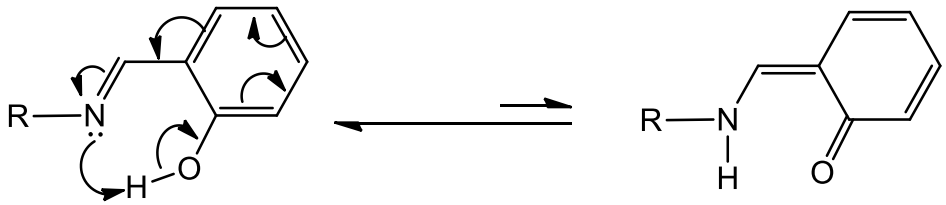

Scheme 2.3 *Tautomerism of the hydroxyimine (left) to the keto-amine (right).*

2.2.3 Elemental Analysis and Mass Spectrometry

The elemental analysis data for **23** and **24** was initially found outside acceptable limits and was ascribed to the inclusion of solvent(s). Following extensive drying under vacuum, the presence of solvent was consistently observed in the ^{1}H NMR spectrum of **23** and **24**. Recalculation of percentages with the inclusion of three molecules of water (for **23**) and one molecule of toluene (for **24**) brought the experimental data within acceptable limits. This phenomenon is observed with other poly(propyleneimine) dendrimers functionalized at the periphery with organic and inorganic moeities.[15, 20]

Further evidence for the formation of **23** and **24** is supported by MALDI-TOF mass spectrometry data, which shows the parent molecular ion peak $[M]^{+}$ in the spectrum of each ligand, at *m/z* = 3354 and *m/z* = 6844 for **23** and **24** (Figure 2.3) respectively (Table 2.2).

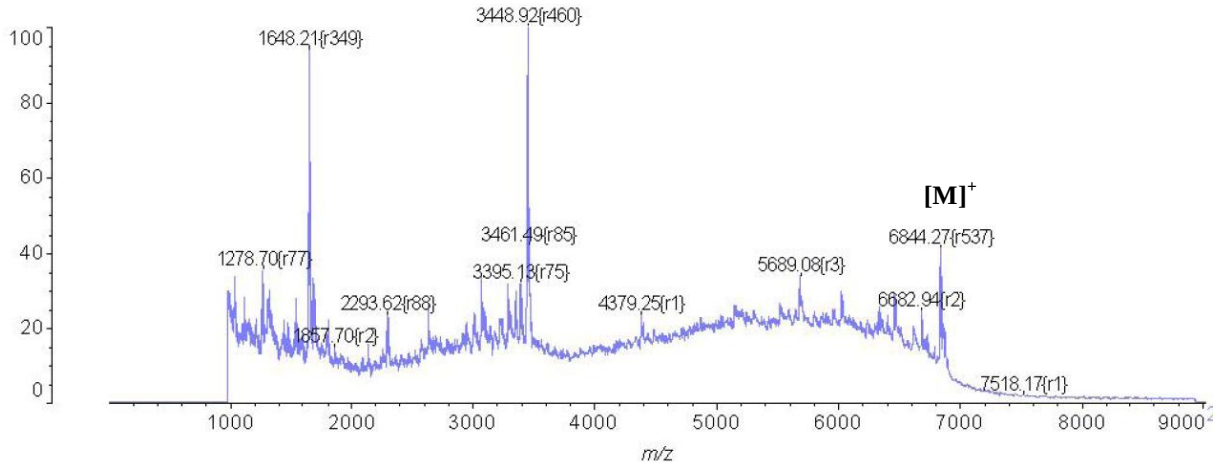

Figure 2.3 *MALDI-TOF mass spectrum of N,O-dendritic ligand **24**.*

2.3 Synthesis and Characterization of Neutral *N,O*-Ru(II)-Arene Metallodendrimers

The synthesis of the first- and second- generation neutral *N,O*-ruthenium-arene metallodendrimers **9 - 12** were previously reported by our group (Figure 2.1).[15] The same methodology was employed in the synthesis of the third- and fourth-generation analogs **25 - 28**, and is discussed below.

The synthesis of the new neutral *N,O*-ruthenium-arene metallodendrimers **25 - 28** involved two reactions. The first reaction, was the preparation of the appropriate ruthenium dimer, ($[Ru(\eta^6\text{-}p\text{-}Pr^iC_6H_4Me)Cl_2]_2$ & $[Ru(\eta^6\text{-}C_6Me_6)Cl_2]_2$), following literature reported procedures.[21, 22] The second reaction involved the bridge-splitting reaction of the dendritic ligands **23** and **24** with either the $[Ru(\eta^6\text{-}p\text{-}Pr^iC_6H_4Me)Cl_2]_2$ or $[Ru(\eta^6\text{-}C_6Me_6)Cl_2]_2$ dimer, in the presence of a weak base, to afford dendritic complexes **25 - 28** (Scheme 2.4).

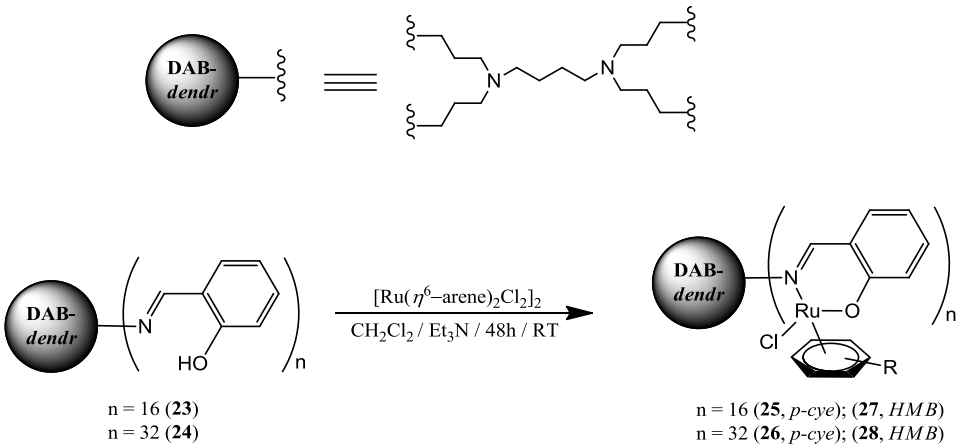

Scheme 2.4 *Synthesis of neutral N,O-Ru(II)-arene metallodendrimers **25 - 28**.*

The bridge-splitting reaction was first attempted without the addition of a base, and following the workup of the reaction, only starting materials were observed. Consequently, prior to addition of the ruthenium dimer, a weak base (triethylamine) was added to deprotonate the hydroxyl group. The reactions were stirred in dichloromethane for 48 h at room temperature, filtered and the solvent removed resulting in a crude solid. The crude solids were purified by low temperature precipitation from dichloromethane, to afford the *p*-cymene derivatives (**25** and **26**) as yellow-brown solids and hexamethylbenzene derivatives (**27** and **28**) as orange solids in 68 - 91 % yields (Table 2.3).

Table 2.3 *Physical appearance and percentage yield for dendritic complexes **25 - 28**.*

Compound	Physical Appearance	Yield [%]	Melting Point [ºC]
25	Yellow-brown solid	91	[a]62
26	Yellow-brown solid	89	[a]81
27	Orange solid	84	179 - 189
28	Orange solid	68	[a]183

[a] Decompose without melting

Dendritic complexes **25 - 28** are non-hygroscopic, air-stable and soluble in dimethylsulfoxide, acetone, acetonitrile, tetrahydrofuran, dichloromethane, chloroform, toluene, methanol and insoluble in non-polar solvents. The hexamethylbenzene derivatives **27** and **28** are more thermally stable (melting points >150 ºC) compared to their *p*-cymene counterparts **25** and **26**, which decompose without melting between 60 and 80 ºC (Table 2.3).

2.3.1 ^{1}H and ^{13}C{^{1}H} NMR Spectroscopy

The proposed chelation of the imine nitrogen and the phenolic oxygen to the ruthenium ion was confirmed by ^{1}H NMR spectroscopy. The ^{1}H NMR spectra of **25 - 28** were recorded in $CDCl_3$ and display characteristic peaks for the coordination of the dendritic ligands **23** and **24** to the ruthenium-arene (where arene = *p*-cymene or hexamethylbenzene) moiety. The ^{1}H NMR spectra of **25 - 28** showed broadened peaks (similarly observed in the ^{1}H NMR spectra of **23** and **24**), with many of the peaks overlapping and/or coalescing, due to the multinuclearity of these dendritic systems.

There are distinctive shifts in signals assigned to the imine proton and protons on the aromatic ring of **25 - 28**, and is attributed to the electronic influences brought about by the chelation of the imine nitrogen and phenolic oxygen to the ruthenium ion. There is an upfield shift in the imine singlet from ~8.3 (in **23** and **24)** to ~8.1 ppm for **25 - 28** (Table 2.4), and an absence in the broad peak (~13.5 ppm) assigned to the proton on the hydroxyl moiety (in **23** and **24)**. These two observations confirm deprotonation of the phenolic oxygen and coordination of the both the imine nitrogen and phenolic oxygen to the ruthenium ion. Coordination of **23** and **24**, generates a chiral centre around the ruthenium ion, which is brought on by the four different groups on the ruthenium ion. The formation of the chiral centre explains the doubling of signals observed in the ^{1}H NMR spectra of **25 - 28**, and this in turn generates diastereotopic protons on the dendritic 'arms' of complexes **25 - 28**. Diastereotopic protons on the carbon

adjacent to the imine nitrogen, display two sets of broad multiplets in the ranges 1.8 - 2.8 ppm and 4.0 - 4.5 ppm for **25 - 28**.

Table 2.4 *Selected spectroscopic and analytical data for dendritic complexes **25 - 28**.*

Compound	^{1}H NMR (imine) [ppm][a]	^{13}C{^{1}H} NMR (imine) [ppm][a]	IR (C=N)$_{imine}$ (complex, ligand) [cm^{-1}][b]	MS (fragment, assignment) [*m*/*z*][c]
25	8.05	164.7	1621, 1634	845.1812 [M-9Cl]$^{9+}$
26	8.08	164.9	1621, 1634	580.9363 [M-26Cl]$^{26+}$
27	8.18	165.8	1617, 1634	[d]8080 [M-Cl]$^{+}$
28	8.16	166.0	1618, 1634	630.0355 [M+26H]$^{26+}$

[a] Recorded in $CDCl_3$,
[b] Recorded in NaCl solution cells in CH_2Cl_2,
[c] HR-ESI-TOF-MS,
[d] MALDI-TOF-MS

*^{1}H NMR spectra of p-cymene derivatives (**25**, **26**)*

In the ^{1}H NMR spectra of **25** and **26**, the methyl protons on the isopropyl group (*i.e.* on the *p*-cymene ring) exhibit one broad multiplet per methyl group. The two broad multiplets are observed at ~1.0 ppm and ~1.1 ppm and are assigned to the diastereotopic methyl groups of the isopropyl functionality, and attributed to the formation of the asymmetric centre. A broader multiplet for **25** and **26** is observed between 3.1 - 3.2 ppm and is assigned to the single proton on the isopropyl functionality. Two broad doublets for **25** and **26** are observed between 6.3 - 6.8 ppm and are assigned to the aromatic protons on the *p*-cymene ring.

*^{1}H NMR spectra of hexamethylbenzene derivatives (**27**, **28**)*

The ^{1}H NMR spectra of **27** and **28** show a singlet in the range of 1.8 - 3.8 ppm, and is assigned to the methyl protons on the hexamethylbenzene ring.

^{13}C{^{1}H} NMR spectra of **25 - 28** were recorded in $CDCl_3$ and similar chemical shifts for signals assigned to aromatic carbons were observed. Extra signals were seen in the aliphatic region for the higher generation complexes **26** and **28**, and were assigned to the aliphatic carbons on the dendritic 'arms'. The ^{13}C{^{1}H} NMR spectra of **25 - 28** are similar to the spectra of **23** and **24**, with expected shifts observed for the imine and pyridyl carbons (Table 2.4) due to coordination to the ruthenium ion. ^{13}C{^{1}H} NMR spectra of **25 - 28** show signals for the aromatic carbons in the range of 114 - 135 ppm. The ^{13}C{^{1}H} NMR spectra of the *p*-cymene derivatives **25** and **26** display a range of signals between 19 - 23 ppm and 31 - 100

ppm, and are assigned to the carbon atoms on the *p*-cymene moiety. The $^{13}C\{^{1}H\}$ NMR spectra of the hexamethylbenzene derivatives **27** and **28** show signals at 16 ppm and ~90 ppm for the sp^3 carbon and sp^2 carbon on the hexamethylbenzene ring respectively.

2.3.2 Infrared Spectroscopy

Further evidence for the coordination of the dendritic ligands **23** and **24** *via* the imine nitrogen to the ruthenium ion, is illustrated in the infrared spectra of **25** - **28**. A distinct shift in the $(C=N)_{imine}$ stretching vibration from ~1634 cm^{-1} (for the ligand) to 1621 cm^{-1} for **25** and **26**, and to ~1617 cm^{-1} for **27** and **28** is observed (Table 2.4 and Figure 2.4). Furthermore, the absence in the stretching vibration at ~2950 cm^{-1} (due to the $(O-H)_{hydroxyl}$ in the ligand) confirmed the absence of the hydroxyl proton and suggests formation of a σ-bond with the ruthenium ion, for **25** - **28.**

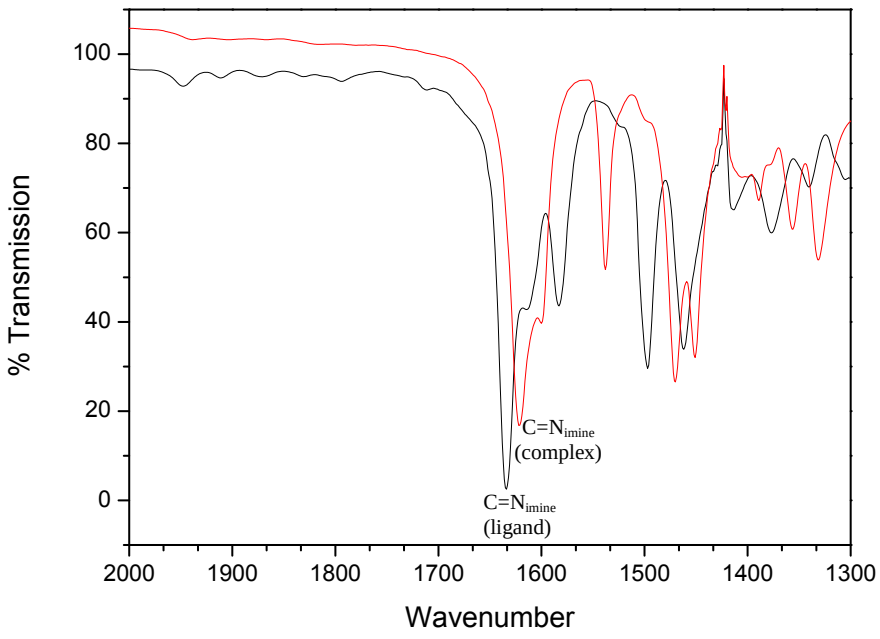

Figure 2.4 *Overlaid infrared spectra of dendritic ligand **23** (black) and metallodendrimer **25** (red) recorded in NaCl solutions cells in dichloromethane.*

2.3.3 Elemental Analysis and Mass Spectrometry

The synthesis of **25** - **28** involves deprotonation of the hydroxyl group, prior to coordination to the ruthenium moiety, which affords $Et_3NH^+Cl^-$ as a by-product (also observed in the ^{1}H NMR spectra). Thus, theoretical values were recalculated with the inclusion of solvent

molecules and/or inorganic salts (*i.e.* $Et_3NH^+Cl^-$). The re-calculated percentages correlate well with the experimental values.

Positive-ion MALDI-TOF mass spectral data for metallodendrimers **25**, **26** and **28** and HR-ESI mass spectral data for metallodendrimer **27** were consistent with the proposed structures. The mass spectral data further supported elemental analysis data for **25 - 28**, with the base-peaks listed in Table 2.4.

2.4 Synthesis and Characterization of Cationic *N,O*-Ru(II)-Arene-PTA Metallodendrimers

A series of new first-, second-, third- and fourth-generation cationic *N,O*-Ru(II)-arene-PTA metallodendrimers [**29**][PF_6]$_4$ - [**36**][PF_6]$_{32}$ were prepared. The synthesis involved a one-pot reaction of the ruthenium dimer [Ru(η^6-arene)Cl_2]$_2$ (arene = *p*-Pr^iC_6H_4Me or C_6Me_6) and the appropriate salicylaldiminato dendritic ligand **21** - **24** (Scheme 2.5). Prior to addition of the ruthenium dimer, triethylamine was added to deprotonate the hydroxyl group. Following formation of the anion and splitting of the ruthenium dimer, the reaction mixture was filtered and the water-soluble ligand PTA (1,3,5-triaza-7-phosphatricyclo[3.3.1.1.] decane) was added.

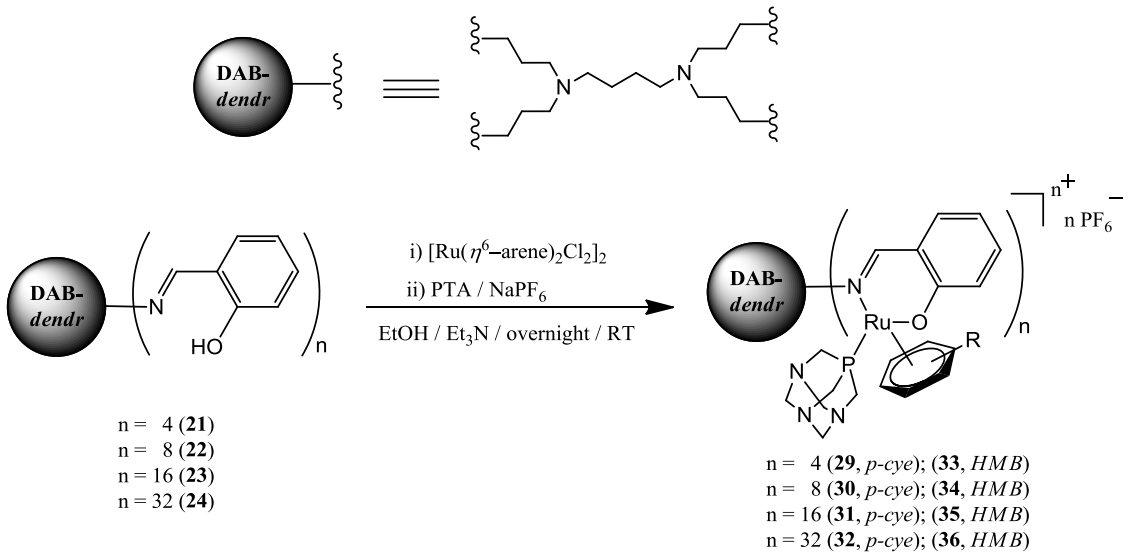

n = 4 (**21**)
n = 8 (**22**)
n = 16 (**23**)
n = 32 (**24**)

n = 4 (**29**, *p-cye*); (**33**, *HMB*)
n = 8 (**30**, *p-cye*); (**34**, *HMB*)
n = 16 (**31**, *p-cye*); (**35**, *HMB*)
n = 32 (**32**, *p-cye*); (**36**, *HMB*)

Scheme 2.5 *Synthesis of cationic N,O-Ru(II)-arene-PTA metallodendrimers [**29**][PF_6]$_4$ - [**36**][PF_6]$_{32}$.*

The PTA ligand displaced the chlorido ligand, which in turn generated a cationic species. Attempts to isolate **29** - **36** as chlorido derivatives were not successful. The chlorido products were hygroscopic and hence difficult to isolate. These products form an oily residue when exposed to air. Hence, **29** - **36** were stabilized as hexafluorophosphate salts. This was achieved *via* an anion exchange using $NaPF_6$ and the products isolated as yellow, thermally stable, solids in high yields (Table 2.5). Metallodendrimers [**29**][PF_6]$_4$ - [**36**][PF_6]$_{32}$ are non-hygroscopic, air-stable and soluble in dimethylsulfoxide, acetone and acetonitrile.

Table 2.5 *Physical appearance, percentage yield and melting point for dendritic complexes [**29**][PF_6]$_4$ - [**36**][PF_6]$_{32}$.*

Compound	Physical Appearance	Yield [%]	Melting Point [ºC]
[**29**][PF_6]$_4$	Yellow solid	94	[a]272
[**30**][PF_6]$_8$	Mustard solid	90	[a]275
[**31**][PF_6]$_{16}$	Mustard solid	88	259 - 281
[**32**][PF_6]$_{32}$	Mustard solid	78	195 - 199
[**33**][PF_6]$_4$	Yellow solid	91	[a]224
[**34**][PF_6]$_8$	Yellow solid	93	[a]203
[**35**][PF_6]$_{16}$	Yellow solid	88	[a]200
[**36**][PF_6]$_{32}$	Yellow solid	78	[a]196

[a] Decompose without melting

Coordination of the ligand occurred *via* the imine nitrogen and the phenolic oxygen, and the proposed structures were confirmed by analytical and spectroscopic techniques.

2.4.1 ^{1}H, ^{31}P{^{1}H} and ^{13}C{^{1}H} NMR Spectroscopy

Compared to the neutral metallodendrimers **9** - **12** and **25** - **28,**[15] the ^{1}H NMR spectra of the cationic metallodendrimers [**29**][PF_6]$_4$ - [**36**][PF_6]$_{32}$ show a general downfield shift in signals due to the cationic nature of these complexes. Broadened peaks are observed in the ^{1}H NMR spectra of [**29**][PF_6]$_4$ - [**36**][PF_6]$_{32}$, with many of the peaks overlapping and/or coalescing, due to the multinuclear nature of the complexes (Figure 2.5). The broadening of peaks is more noticeable with the third- and fourth-generation derivatives. Chirality induced by the ruthenium ion is evident by the appearance of two broad multiplets assigned to the diastereotopic protons on the carbon adjacent to the imine nitrogen (between 3.0 - 4.0 ppm), of complexes [**29**][PF_6]$_4$ - [**36**][PF_6]$_{32}$. Two multiplets observed between 4.1 and 4.6 ppm in the ^{1}H NMR spectra are assigned to the PTA ligand. A small upfield shift in the singlet

assigned to the imine proton from 8.27 ppm (in the ligand) to between 8.1 - 8.2 ppm, and the disappearance in the broad singlet at ~13.5 ppm (phenolic proton on the ligand) for [**29**][PF_6]$_4$ - [**36**][PF_6]$_{32}$ is observed (Table 2.6). Furthermore, this evidence suggests coordination occurs *via* the imine nitrogen and phenolic oxygen.

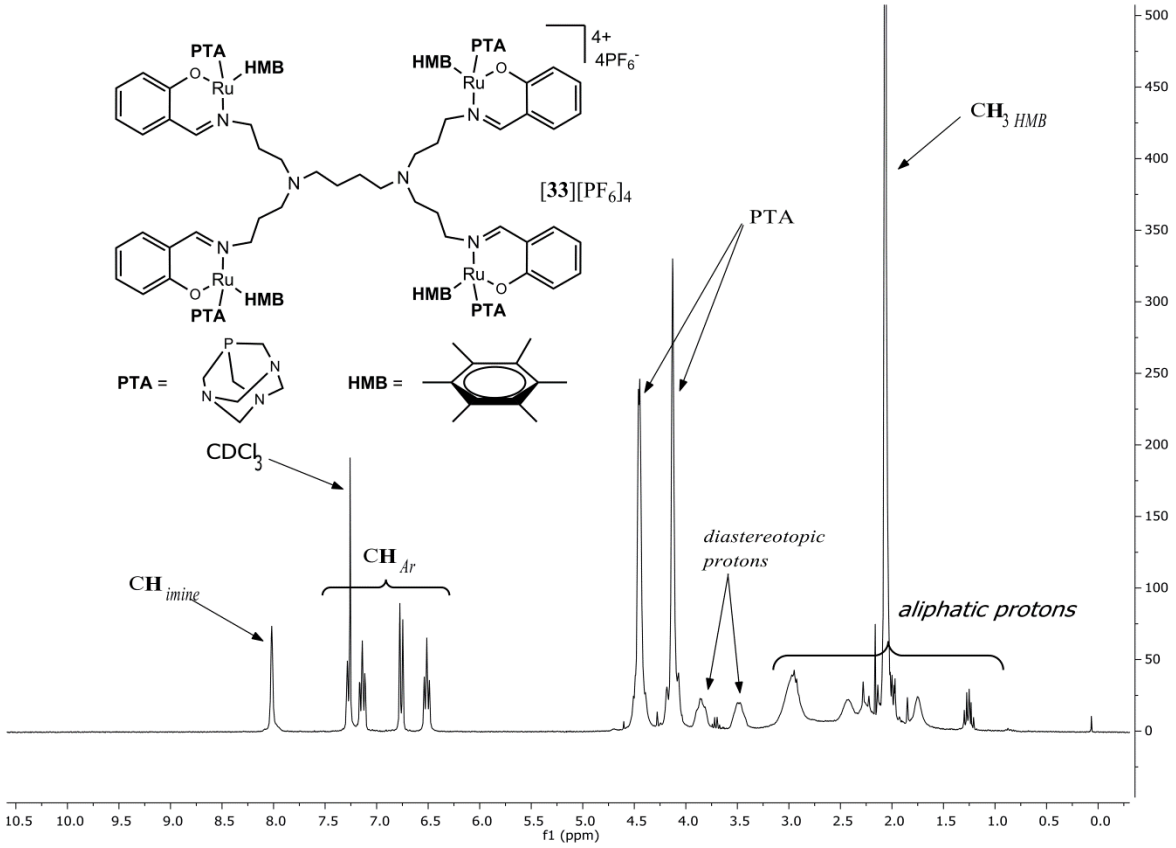

Figure 2.5 *^{1}H NMR spectrum of first-generation N,O-Ru(II)-hexamethylbenzene-PTA metallodendrimer [**33**][PF_6]$_4$ in $(CD_3)_2CO$.*

*^{1}H NMR spectra of p-cymene derivatives ([**29**][PF_6]$_4$ - [**32**][PF_6]$_{32}$)*

Metallodendrimers [**29**][PF_6]$_4$ - [**32**][PF_6]$_{32}$ show a loss of two-fold symmetry of the *p*-cymene moiety upon coordination of the bidentate *N*,*O*-dendritic ligand. This feature in turn results in the methyl protons of the isopropyl group exhibiting two broad multiplets in the range of 1.0 - 1.3 ppm, and a broad multiplet observed at ~3.5 ppm assigned to the single proton of the isopropyl group. The aromatic protons of the *p*-cymene ring display four broad multiplets in the range of 5.6 - 6.5 ppm.

*^{1}H NMR spectra of hexamethylbenzene derivatives ([**33**][PF$_6$]$_4$ - [**36**][PF$_6$]$_{32}$)*

Metallodendrimers [**33**][PF$_6$]$_4$ - [**36**][PF$_6$]$_{32}$ exhibit a singlet at ~2.1 ppm assigned to the methyl protons of the hexamethylbenzene ring.

The ^{31}P{^{1}H} NMR spectra of [**29**][PF$_6$]$_4$ - [**36**][PF$_6$]$_{32}$ attests to the purity of the complexes as a singlet in the range of -47 - -26 ppm is observed (Table 2.6), suggesting a single phosphine species is present. Furthermore, these chemical shifts are comparable to structurally similar mononuclear RAPTA complexes reported in the literature.[23]

Table 2.6 *Selected spectroscopic and analytical data for dendritic complexes [**29**][PF$_6$]$_4$ - [**36**][PF$_6$]$_{32}$.*

Compound	^{1}H NMR (imine) [ppm][a]	^{13}C{^{1}H} NMR (imine) [ppm][a]	^{31}P{^{1}H} NMR (PTA) [ppm][a]	MS (fragment, assignment) [*m/z*][b]
[**29**][PF$_6$]$_4$	8.20	166.9	-32.5	575.6148 $[M]^{4+}$ (where M = [**29**][PF$_6$]$_4$ - 4PF$_6$)
[**30**][PF$_6$]$_8$	8.21	166.7	-32.3	540.1608 $[M+H]^{9+}$ (where M = [**30**][PF$_6$]$_8$ - 8PF$_6$)
[**31**][PF$_6$]$_{16}$	8.21	167.0	-26.2	617.1169 $[M]^{16+}$ (where M = [**31**][PF$_6$]$_{16}$ - 16PF$_6$)
[**32**][PF$_6$]$_{32}$	8.10	166.7	-26.6	603.1587 $[M]^{32+}$ (where M = [**32**][PF$_6$]$_{32}$ - 32PF$_6$)
[**33**][PF$_6$]$_4$	8.02	165.5	-41.0	603.7332 $[M+2H]^{4+}$ (where M = [**33**][PF$_6$]$_4$ - 4PF$_6$)
[**34**][PF$_6$]$_8$	8.02	165.4	-40.8	451.1324 $[M+3H]^{11+}$ (where M = [**34**][PF$_6$]$_8$ - 8PF$_6$)
[**35**][PF$_6$]$_{16}$	8.00	165.3	-40.6	629.2938 $[M]^{16+}$ (where M = [**35**][PF$_6$]$_{16}$ - 16PF$_6$)
[**36**][PF$_6$]$_{32}$	8.16	170.2	-40.4	596.1664 $[M+2H]^{34+}$ (where M = [**36**][PF$_6$]$_{32}$ - 32PF$_6$)

[a] Recorded in $(CD_3)_2CO$
[b] HR-ESI-TOF-MS

^{13}C{^{1}H} NMR spectra for metallodendrimers [**29**][PF$_6$]$_4$ - [**36**][PF$_6$]$_{32}$ showed the expected number of signals for the proposed structure. There is an increase in the number of signals observed as the generation number is increased. The increase in signals is attributed to the increase in the number aliphatic carbons (*i.e.* carbons found on the dendritic 'arms') as the generation number is increased. Signals assigned to the carbons at the dendritic 'core' and on

the dendritic 'arms' were observed in the range of 21 - 69 ppm. A singlet is observed for the imine carbon in the range of 165 - 170 ppm (Table 2.6). The CH_2 groups of the PTA ligand is observed at ~51 ppm and ~72 ppm for the *p*-cymene derivatives [**29**][PF_6]$_4$ - [**32**][PF_6]$_{32}$, whilst signals for the hexamethylbenzene derivatives [**33**][PF_6]$_4$ - [**36**][PF_6]$_{32}$ were observed at ~49 ppm and ~73 ppm in the $^{13}C\{^1H\}$ NMR spectra.

2.4.2 Infrared Spectroscopy

The infrared spectra of [**29**][PF_6]$_4$ - [**36**][PF_6]$_{32}$ display a shift in the $(C=N)_{imine}$ absorption band for the uncoordinated dendritic ligands (~1650 cm^{-1}) to lower wavenumbers for the metal complex (~1618 cm^{-1}), which further supports coordination of imine nitrogen to the ruthenium ion. These shifts can be explained by the synergic effect,[24] where the $(C=N)_{imine}$ bond experiences electron-withdrawing effects from the coordinated ruthenium and the aromatic ring, which in turn weakens the $(C=N)_{imine}$ bond and pushes the stretching vibration to a lower wavenumber. The disappearance in the $(O\text{-}H)_{hydroxyl}$ stretching vibration suggests the dendritic ligands coordinate through the phenolic oxygen, similarly observed for the neutral metallodendrimers **9** - **12** and **25** - **28**.

2.4.3 Elemental Analysis and Mass Spectrometry

Similarly observed with **25** - **28**, the metallodendrimers [**29**][PF_6]$_4$ - [**36**][PF_6]$_{32}$ displayed elemental analysis percentages outside acceptable limits, and these were ascribed to possible solvent inclusion (even after extensive drying) and/or encapsulation of inorganic salts (*i.e.* $Et_3NH^+Cl^-$), which is observed in the ^1H NMR spectrum of these complexes. This is a result of the phenomenon whereby dendritic arms fold back onto one another, in turn trapping small molecules, and is also observed in other poly(propyleneimine) dendrimers functionalized at the periphery with organic groups.[20] Synthesis of metallodendrimers [**29**][PF_6]$_4$ - [**36**][PF_6]$_{32}$ involves deprotonation of the hydroxyl group, prior to coordination to the ruthenium moiety, which in turn yields $Et_3NH^+Cl^-$ as a by-product (similarly observed with metallodendrimers **25** - **28**). Recalculation of the percentages with the inclusion of $Et_3NH^+Cl^-$ and/or ethanol (reaction solvent) gave percentages within acceptable limits.

The ^1H, $^{13}C\{^1H\}$, $^{31}P\{^1H\}$ NMR and IR spectral data was supported by HR-ESI-MS data, which showed $[M]^{16+}$ as the highest molecular weight fragment for [**31**][PF_6]$_{16}$ and [**35**][PF_6]$_{16}$, whilst $[M]^{32+}$ was observed for [**32**][PF_6]$_{32}$. The highest molecular weight fragments for the rest of the dendritic salts in this series are listed in Table 2.6.

2.5 Synthesis and Characterization of Cationic *N,O*-Ru(II)-Arene-PTA Mononuclear Complexes

The new mononuclear complexes [**38**][PF_6] and [**39**][PF_6] were synthesized as models of the larger metallodendrimers [**29**][PF_6]$_4$ - [**36**][PF_6]$_{32}$ in order to compare size dependency on the antiproliferative activity (discussed in Chapter 4). The synthesis of the *p*-cymene [**38**][PF_6] and hexamethylbenzene [**39**][PF_6] derivatives involved a two-step process. The first step was synthesis of the monomeric ligand (*E*)-2-((propylimino)methyl)phenol **37**, *via* a Schiff base condensation reaction, by following literature reported methods (Scheme 2.6).[18]

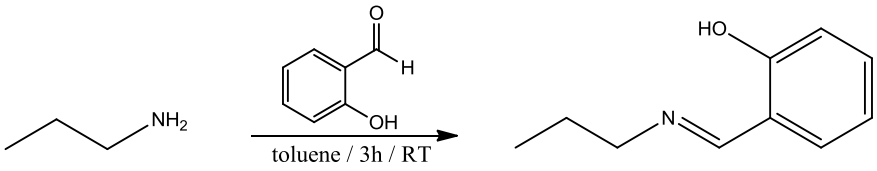

37

Scheme 2.6 *Synthesis of monomeric ligand (E)-2-((propylimino)methyl)phenol **37**.*

The second step involved the bridge-splitting reaction of the appropriate ruthenium dimer with monomeric ligand **37**. Complex **38** and **39** were isolated as hexafluorophosphate salts *via* a one-pot reaction of the [Ru(η^6-arene)Cl_2]$_2$ (arene = *p*-Pr^iC_6H_4Me or C_6Me_6) with the monomeric ligand **37**, in the presence of triethylamine, followed by the addition of PTA and sodium hexafluorophosphate (Scheme 2.7).

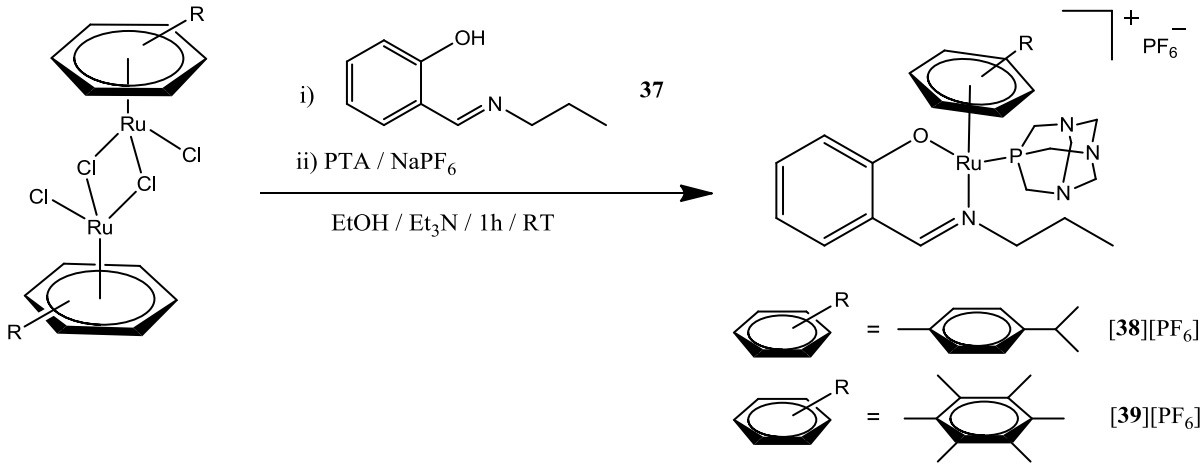

Scheme 2.7 *Synthesis of cationic N,O-Ru(II)-arene-PTA mononuclear complexes [**38**][PF_6] and [**39**][PF_6].*

Complexes [**38**][PF_6] and [**39**][PF_6] were isolated as thermally stable yellow solids in relatively high yields and are soluble in dimethylsulfoxide, acetone, acetonitrile and chloroform.

2.5.1 ^{1}H, ^{31}P{^{1}H} and ^{13}C{^{1}H} NMR Spectroscopy

^{1}H NMR spectroscopy was used to assist in providing evidence for the coordination of the imine nitrogen and phenolic oxygen to the ruthenium ion. The ^{1}H NMR spectra of complexes [**38**][PF_6] and [**39**][PF_6] was recorded in acetone-d_6 and showed all the relevant peaks for the proposed structures. Following coordination of ligand **37** to the ruthenium ion, there is a absence in the broad singlet assigned to the hydroxyl proton (~13.5 ppm in the ^{1}H NMR of **37**) and an upfield shift in the singlet assigned to the imine proton at 8.32 ppm (in **37**) to 8.13 ppm for both [**38**][PF_6] and [**39**][PF_6] (Table 2.7).

Table 2.7 *Selected spectroscopic and analytical data for mononuclear complexes [**38**][PF_6] and [**39**][PF_6].*

Compound	^{1}H NMR (imine) [ppm][a]	^{13}C{^{1}H} NMR (imine) [ppm][a]	^{31}P{^{1}H} NMR (PTA) [ppm][a]	IR (C=N)$_{imine}$ (complex, ligand) [cm^{-1}][b]	MS (fragment, assignment) [*m/z*][c]
[**38**][PF_6]	8.13	166.9	-33.0	1619, 1635	566 [M-CYE]$^{+}$
[**39**][PF_6]	8.13	165.2	-41.6	1618, 1635	283 [M-PF_6]$^{+}$

[a] Recorded in $(CD_3)_2CO$
[b] Recorded as KBr pellet
[c] ESI-MS

Similarly seen with the cationic metallodendrimers [**29**][PF_6]$_4$ - [**36**][PF_6]$_{32}$, the protons on the propyl chain are diastereotopic and this is attributed to the chiral nature of the molecule. Hence, two multiplets (integrating for one proton per signal) in the range of 3.8 - 4.1 ppm for [**38**][PF_6] (Figure 2.6) and in the range of 3.6 - 3.8 ppm for [**39**][PF_6] (Figure 2.7), is observed.

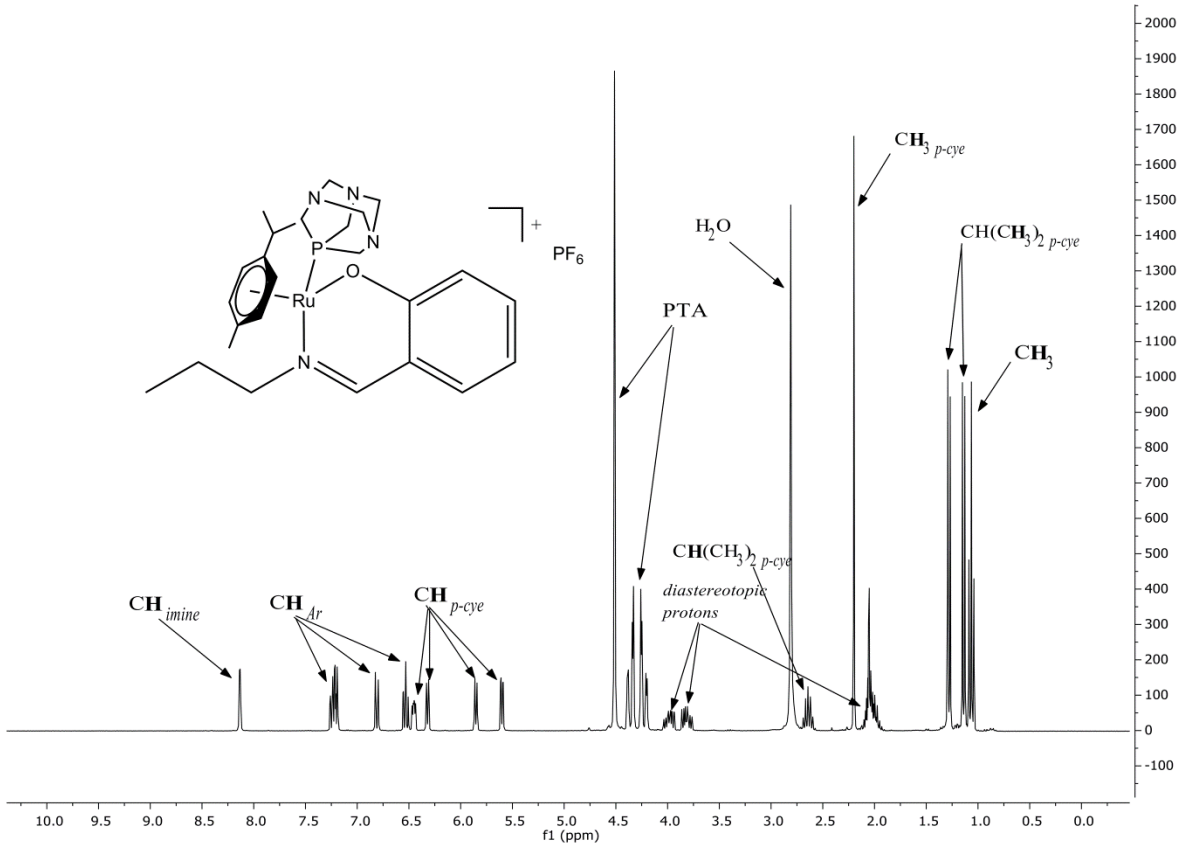

Figure 2.6 *^{1}H NMR spectrum for the mononuclear N,O-Ru(II)-p-cymene-PTA complex [**38**][PF_6] in $(CD_3)_2CO$.*

*^{1}H NMR spectra of p-cymene derivative ([**38**][PF_6])*

The asymmetric nature of the ruthenium centre results in a loss of 2-fold symmetry around the arene ring. Hence the diastereotopic methyl groups on the isopropyl moiety are observed as two doublets. Furthermore, each doublet integrates for three protons, with a coupling constant of ^3J = 3.7 Hz per doublet. The three doublets and one multiplet observed in the range of 5.6 - 6.5 ppm corresponds to the aromatic protons of the *p*-cymene ring, with coupling constants around ^3J = 5 Hz. A multiplet is observed at 2.6 ppm for [**38**][PF_6] and is assigned to the single proton on the isopropyl functionality.

*^{1}H NMR spectra of hexamethylbenzene derivative ([**39**][PF_6])*

A singlet is observed at 2.06 ppm, integrates for 18 protons, and is assigned to the CH_3 groups on the hexamethylbenzene ring.

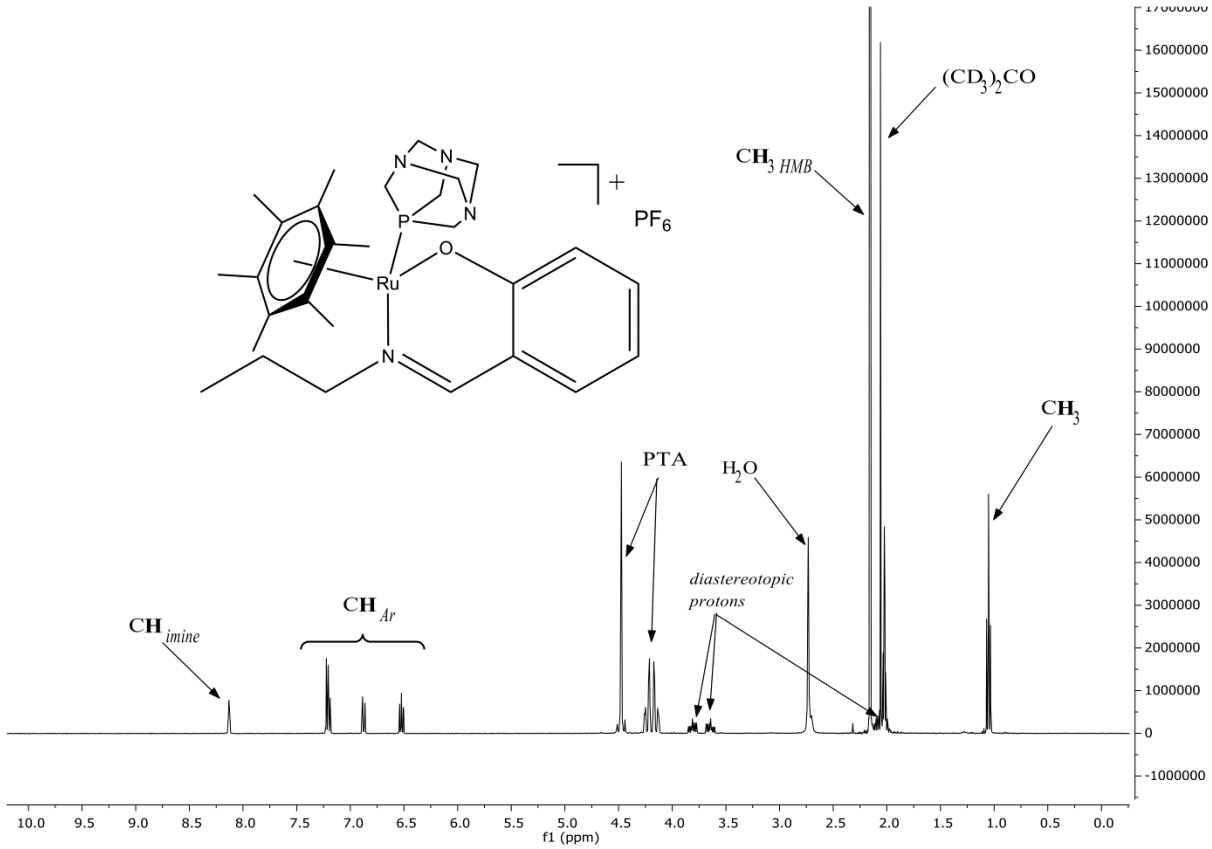

Figure 2.7 *^{1}H NMR spectrum for the mononuclear N,O-Ru(II)-hexamethylbenzene-PTA complex [**39**][PF_6] in $(CD_3)_2CO$.*

The ^{1}H NMR spectra of [**38**][PF_6] and [**39**][PF_6] display two doublets and a singlet in the range of 4.2 - 4.5 ppm and is assigned to the two types of CH_2 protons on the PTA moiety. The 6 protons of -P-CH_2-N- are represented as a singlet at ~4.5 ppm (Figure 2.6 and Figure 2.7). This signal is usually represented as a doublet in the free ligand, with P-H coupling ($^{2}J_{P\text{-}H}$ = 10.5 Hz). However, the $J_{P\text{-}H}$ coupling is reduced to a negligible value (with no coupling observed in the ^{1}H NMR spectra) following coordination to the ruthenium ion, as observed in other PTA complexes.[25, 26] Whilst the 6 protons of -N-CH_2-N- display an AB spin system centred at ~4.2 ppm (Figure 2.6 and Figure 2.7), which is assigned to the N-CH_{ax}-N and N-CH_{eq}-N protons on the PTA ligand, and has previously been observed in other transition metal-PTA complexes.[27-29]

The ^{31}P{^{1}H} NMR spectra shows a singlet at -33.0 ppm and 41.6 ppm for [**38**][PF_6] and [**39**][PF_6] respectively (Table 2.7). Furthermore, this suggests a single coordinated phosphine species is present (PTA) and also attests to the purity these complexes.

$^{13}C\{^{1}H\}$ NMR spectra for [**38**][PF_6] and [**39**][PF_6] gave the expected number of carbon signals for the proposed structure. There is a downfield shift in the singlet assigned to the imine carbon, and is observed at 164 ppm (in ligand **37**) to 165 ppm for [**38**][PF_6] and 167 ppm for [**39**][PF_6] The appearance of two singlets at ~50 ppm and ~73 ppm, confirms coordination of the PTA ligand to the ruthenium ion, for both [**38**][PF_6] and [**39**][PF_6].

2.5.2 Infrared Spectroscopy

Complexes [**38**][PF_6] and [**39**][PF_6] display a shift in the $C{=}N_{imine}$ stretching vibration to lower wavenumbers, form 1635 cm^{-1} (in the ligand **37**) to ~1619 cm^{-1} (Table 2.7), similarly observed with metallodendrimers [**29**][PF_6]$_4$ - [**36**][PF_6]$_{32}$.

2.5.3 Elemental Analysis and Mass Spectrometry

The elemental analysis results are consistent with the proposed structures of [**38**][PF_6] and [**39**][PF_6]. ESI mass spectrometry data depicted molecular ion peaks with a loss of the *p*-cymene moiety and the loss of the PF_6 counter-ion for complexes [**38**][PF_6] and [**39**][PF_6] respectively (Table 2.7). In addition to spectroscopic and analytical data, single crystal X-ray diffraction analysis of [**38**][PF_6] and [**39**][PF_6] confirm the bidentate coordination of the ligand to the ruthenium ion.

2.5.4 X-ray Crystallography

Single-crystal X-ray diffraction of [**38**][PF_6] and [**39**][PF_6] confirms the expected pseudo-tetrahedral or “piano-stool” geometry around the Ru(II) ion, and the coordination of the salicylaldiminato ligand **37** in a bidentate-chelating mode through its phenolic oxygen and imine nitrogen (Figure 2.8). In both these mononuclear complexes, the metal centre is stereogenic, however [**38**][PF_6] and [**39**][PF_6] are obtained as racemic mixtures. Crystallographic details can be found in Chapter 6, summarized in Table 6.1.

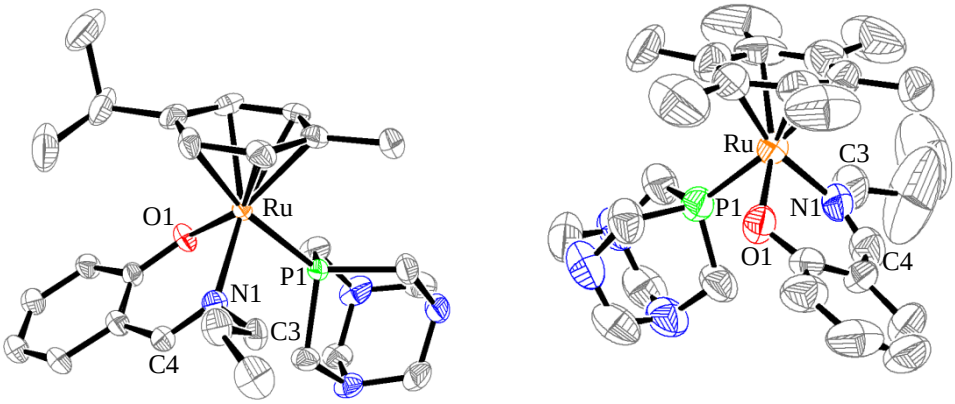

Figure 2.8 *ORTEP representations of mononuclear cations [**38**][PF_6] (left) and [**39**][PF_6] (right). Thermal ellipsoids are drawn at the 50 % probability level. The PF_6^- counter-ion and hydrogen atoms have been omitted for clarity.*

The geometrical parameters of [**38**][PF_6] and [**39**][PF_6] are comparable to those observed in other *N,O*-ruthenium-arene complexes,[30, 31] and selected geometrical parameters are listed in Table 2.8. The Ru-P distances in [**38**][PF_6] and [**39**][PF_6] are comparable to those observed in analogous ruthenium-arene-PTA compounds.[23, 32] In [**38**][PF_6], the ruthenium ion is situated ~1.728 Å from the centroid of the *p*-cymene ligand and in [**39**][PF_6] the distance is ~1.732 Å from the centroid of the hexamethylbenzene ligand.

Table 2.8 *Selected average bond lengths and bond angles in [**38**][PF_6] and [**39**][PF_6].*

	[**38**][PF_6]	[**39**][PF_6]
	interatomic distances (Å)	
Ru1-N1	2.080(7)	2.063(6)
Ru1-O1	2.074(6)	2.058(5)
Ru1-P1	2.320(2)	2.325(2)
C4-C5	1.448(13)	1.421(10)
C4-N1	1.280(11)	1.272(9)
N1-C3	1.499(11)	1.479(9)
Ru–centroid	~1.728	~1.732
	[**38**][PF_6]	[**39**][PF_6]
	angles (°)	
N1-Ru1-O1	87.0(3)	87.7(2)
N1-Ru1-P1	86.7(2)	86.7(2)
O1-Ru1-P1	79.8(2)	79.7(2)
C5-C4-N1	126.8(8)	127.6(7)
C4-N1-C3	113.5(8)	117.1(7)

2.6 Synthesis and Characterization of Neutral and Cationic Os(II)-Arene Complexes

In order to investigate whether the type of metal has influence on the biological activity, new osmium analogs of the ruthenium complexes were prepared. In the synthesis of the neutral and cationic Os(II)-arene complexes, only the *p*-cymene analogs were synthesized.

The methodology employed in the synthesis of the neutral *N,O*-osmium-arene metallodendrimers (**40**, **41**) and cationic *N,O*-osmium-arene-PTA metallodendrimers ([**42**][PF_6]$_4$, [**43**][PF_6]$_8$) were similar to the methods employed in the synthesis of their ruthenium analogs mentioned. The neutral metallodendrimers **40** and **41** were synthesized by reacting the dendritic scaffolds **21** (for **40**) or **22** (for **41**) with [Os(η^6-*p*-Pr^{i}C$_6$H$_4$Me)Cl$_2$]$_2$ in dichloromethane (Scheme 2.8), in the presence of triethylamine. The neutral metallodendrimers **40** and **41** were afforded as yellow solids, in moderate to high yields (Table 2.9) and soluble in most polar organic solvents.

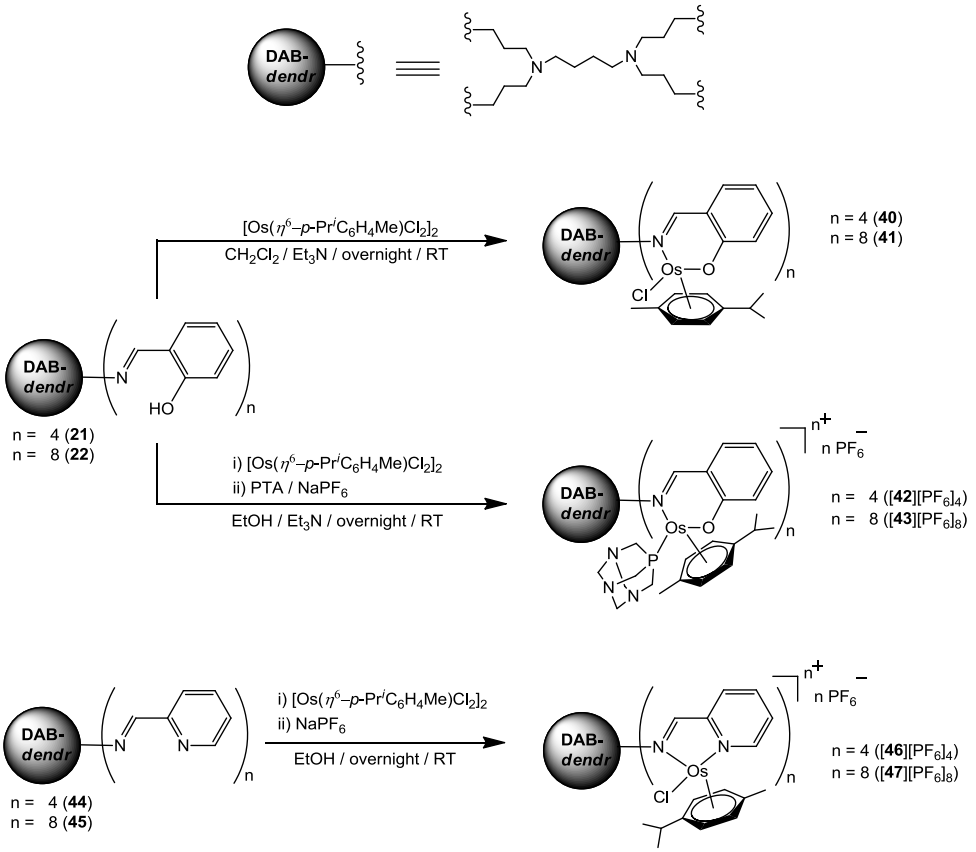

Scheme 2.8 *Synthesis of osmium metallodendrimers* ***40*** *-* ***[43]*** *[PF_6]$_8$,* ***[46]*** *[PF_6]$_4$ and* ***[47]*** *[PF_6]$_8$.*

Table 2.9 *Physical appearance, percentage yield and melting point for osmium complexes **40** - [**43**][PF_6]$_8$, [**46**][PF_6]$_4$, [**47**][PF_6]$_8$, **48**, [**49**][PF_6] and [**51**][PF_6].*

Compound	Physical Appearance	Yield [%]	Melting Point [ºC]
40	Mustard-yellow solid	88	[a]151
41	Mustard-yellow solid	52	[a]165
48	Orange-yellow solid	48	226-231
[**42**][PF_6]$_4$	Yellow solid	95	185-188
[**43**][PF_6]$_8$	Yellow solid	54	179-182
[**49**][PF_6]	Orange-yellow solid	54	226-231
[**46**][PF_6]$_4$	Dark orange solid	72	[a]194
[**47**][PF_6]$_8$	Yellow-brown solid	76	[a]193
[**51**][PF_6]	Red solid	62	[a]181

[a] Decompose without melting

The cationic *N,O*-osmium-arene-PTA metallodendrimers [**42**][PF_6]$_4$ and [**43**][PF_6]$_8$ were synthesized by a one-pot reaction of the dendritic ligand **21** (for [**42**][PF_6]$_4$) or **22** (for [**43**][PF_6]$_8$) with [Os(η^6-*p*-Pr^iC_6H_4Me)Cl_2]$_2$, followed by the addition of PTA, and stabilized as the hexafluorophosphate salt *via* a cation-exchange reaction (Scheme 2.8). Cationic metallodendrimers [**42**][PF_6]$_4$ and [**43**][PF_6]$_8$ were isolated as thermally stable yellow solids, in moderate to high yields (Table 2.9) and are soluble in acetone, acetonitrile and dimethylsulfoxide.

The synthesis of the cationic *N,N*-osmium dendritic complexes [**46**][PF_6]$_4$ and [**47**][PF_6]$_8$ involved a two-step synthesis. The first step in the synthesis was the preparation of the first- and second-generation iminopyridyl dendritic ligands **44** and **45** *via* Schiff base condensation reaction described by Smith *et al.*[33, 34] The second step in the synthesis afforded [**46**][PF_6]$_4$ and [**47**][PF_6]$_8$ as hexafluorophosphate salts, by reacting the dendritic ligands **44** (for [**46**][PF_6]$_4$) or **45** (for [**47**][PF_6]$_8$) and [Os(η^6-*p*-Pr^iC_6H_4Me)Cl_2]$_2$, and followed by a metathesis reaction with $NaPF_6$ (Scheme 2.8). The cationic metallodendrimers [**46**][PF_6]$_4$ and [**47**][PF_6]$_8$ were isolated as thermally stable orange-red solids, in moderate yields (Table 2.9) and are soluble in acetone, acetonitrile and dimethylsulfoxide. Attempts to synthesize the cationic *N,N*-osmium-*p*-cymene-PTA metallodendrimers proved futile, as abstraction of the chlorido ligand was difficult.

In order to compare size dependency on the biological activity (discussed in Chapter 4), mononuclear derivatives **48**, [**49**][PF_6] and [**51**][PF_6] of the osmium metallodendrimers were synthesized. These were prepared in a similar manner to the mononuclear ruthenium analogs mentioned. The neutral and cationic mononuclear complexes **48**, [**49**][PF_6] and [**51**][PF_6] were prepared from the known salicylaldiminato and iminopyridyl monomeric ligands **37** and **50**.[18, 35] Cleavage of [Os(η^6-*p*-Pr^{i}C$_6$H$_4$Me)Cl$_2$]$_2$ dimer with the monomeric ligands **37** or **50** afforded the neutral osmium complex **48** as a yellow solid, whilst the cationic complexes [**49**][PF_6] and [**51**][PF_6] were isolated as yellow and red hexafluorophosphate salts respectively (Scheme 2.9, Table 2.9).

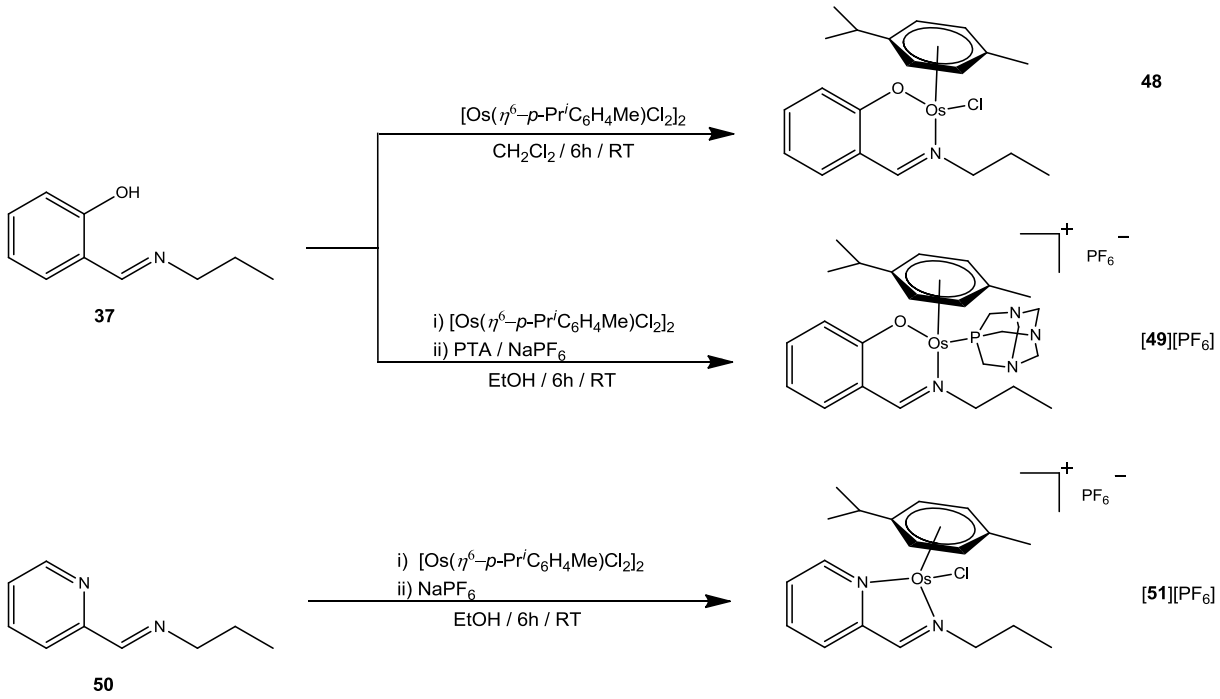

Scheme 2.9 *Synthesis of mononuclear neutral and cationic osmium complexes **48**, [**49**][PF_6] and [**51**][PF_6].*

The neutral and cationic osmium complexes were characterized with a series of spectroscopic and analytical techniques.

2.6.1 ^{1}H, ^{31}P{^{1}H} and ^{13}C{^{1}H} NMR Spectroscopy

*^{1}H and ^{13}C{^{1}H} NMR spectra of N,O-Os(II)-arene complexes (**40**, **41**, **48**)*

The ^{1}H NMR spectra of the neutral complexes **40**, **41** and **48** confirm coordination of the *N,O*-ligand to the osmium ion. Notable features include the disappearance of the broad singlet (~13.5 ppm) assigned to the hydroxyl proton of the *N,O*-ligand and an upfield shift in the imine signal from ~8.3 ppm (in the *N,O*-ligand) to ~7.8 ppm for complexes **40**, **41** and **48**. The aliphatic protons at the dendritic core and on the dendritic branches, for **40** and **41**, display broadened resonance signals, with some of the signals coalescing. This was attributed to the high nuclearity of the dendritic complex and fluxionality of the dendritic arms. Peak broadening was also observed in the analogous ruthenium-*p*-cymene metallodendrimers **9** - **12** (Figure 2.1).[15] Signals observed in the ^{1}H NMR spectrum of the mononuclear complex **48** are more discernable and well-resolved. Similarly observed with the ruthenium-arene complexes described above, there is a loss of two-fold symmetry about the *p*-cymene moiety upon coordination of the bidentate *N,O*-salicylaldiminato ligand, and as a result, the methyl protons of the isopropyl group appear as two broad doublets (1.0 - 1.2 ppm). Hence, the diastereotopic protons on the aliphatic carbon (adjacent to the imine nitrogen) are assigned to two broad multiplets in the range of 4.0 - 4.4 ppm for metallodendrimers **40** and **41**, with a similar resonance observed for the mononuclear derivative **48**. ^{13}C{^{1}H} NMR spectral data display the expected number of signals for the proposed structure of neutral complexes **40**, **41** and **48**.

*^{1}H, ^{31}P{^{1}H} and ^{13}C{^{1}H} NMR spectra of N,O-Os(II)-arene-PTA complexes ([**42**][PF_6]$_4$, [**43**][PF_6]$_8$, [**49**][PF_6])*

In comparison to the mentioned neutral complexes **40**, **41** and **48**, introduction of the PTA ligand to the osmium ion generates a positively charged species, which in turn results in an overall downfield shift in signals observed in the ^{1}H NMR spectra of the cationic derivatives [**42**][PF_6]$_4$, [**43**][PF_6]$_8$ and [**49**][PF_6]. Replacement of the chlorido ligand with the PTA ligand retains chirality at the osmium centre. Hence, the methyl protons of the *p*-cymene moiety appears as two distinct doublets (~1.1 ppm & ~1.3 ppm), and the diastereotopic protons on the aliphatic carbon (adjacent to the imine nitrogen) are observed as two multiplets (3.9 - 4.2 ppm). The aromatic protons on the *p*-cymene moiety, of the neutral metallodendrimers **40** and **41**, are assigned to two broad multiplets (5.6 - 5.7 ppm) in the ^{1}H NMR spectrum. However, this pattern was not observed with the cationic metallodendrimers [**42**][PF_6]$_4$ and [**43**][PF_6]$_8$, these protons on the *p*-cymene ring were assigned to four broad multiplets in the range 5.5 -

6.3 ppm, with signals for the mononuclear complex [**49**][PF_6] appearing slightly more downfield. $^{31}P\{^1H\}$ NMR spectroscopy was used to further confirm purity of [**42**][PF_6]$_4$, [**43**][PF_6]$_8$ and [**49**][PF_6], as only a singlet was observed at -71 ppm, with similar values reported for structurally related complexes.[36, 37] The expected number of signals were observed in the $^{13}C\{^1H\}$ NMR spectra for the proposed structures of [**42**][PF_6]$_4$, [**43**][PF_6]$_8$ and [**49**][PF_6].

*^1H and $^{13}C\{^1H\}$ NMR spectra of N,N-Os(II)-arene complexes ([**46**][PF_6]$_4$, [**47**][PF_6]$_8$, [**51**][PF_6])*

As expected, signals in the ^1H NMR spectra for the cationic *N*,*N*-complexes [**46**][PF_6]$_4$, [**47**][PF_6]$_8$ and [**51**][PF_6] are comparable to previously reported isostructural ruthenium analogs **5** - **8** (Figure 2.1), with some of the chemical shifts almost identical.[15] The ^1H NMR spectra of [**46**][PF_6]$_4$, [**47**][PF_6]$_8$ and [**51**][PF_6] depict a loss of a 2-fold symmetry at the osmium ion, similarly observed with the above mentioned neutral (**25** - **28**) and cationic ([**29**][PF_6]$_4$ - [**36**][PF_6]$_{32}$) ruthenium complexes, and hence a similar splitting pattern is observed. The $^{13}C\{^1H\}$ NMR spectra of [**46**][PF_6]$_4$, [**47**][PF_6]$_8$ and [**41**][PF_6] display the expected number of signals.

2.6.2 Infrared Spectroscopy

The infrared spectra of neutral complexes **40**, **41** and **48** depict a shift in the $C{=}N_{imine}$ stretching vibration from ~1635 cm^{-1} (for the *N*,*O*-ligand) to lower wavenumbers at ~1618 cm^{-1}, further suggesting coordination of the imine nitrogen. Furthermore, a stretching vibration in the infrared spectra was observed at the same frequency (~1618 cm^{-1}) for the *N*,*N*-osmium complexes [**46**][PF_6]$_4$, [**47**][PF_6]$_8$ and [**51**][PF_6] and was also ascribed to the $C{=}N_{imine}$ bond (Figure 2.9). Whilst the infrared spectra of the cationic *N*,*O*-osmium-PTA complexes [**42**][PF_6]$_4$, [**43**][PF_6]$_8$ and [**49**][PF_6] depicted a stretching vibration at ~1613 cm^{-1} and was assigned to the $C{=}N_{imine}$ bond.

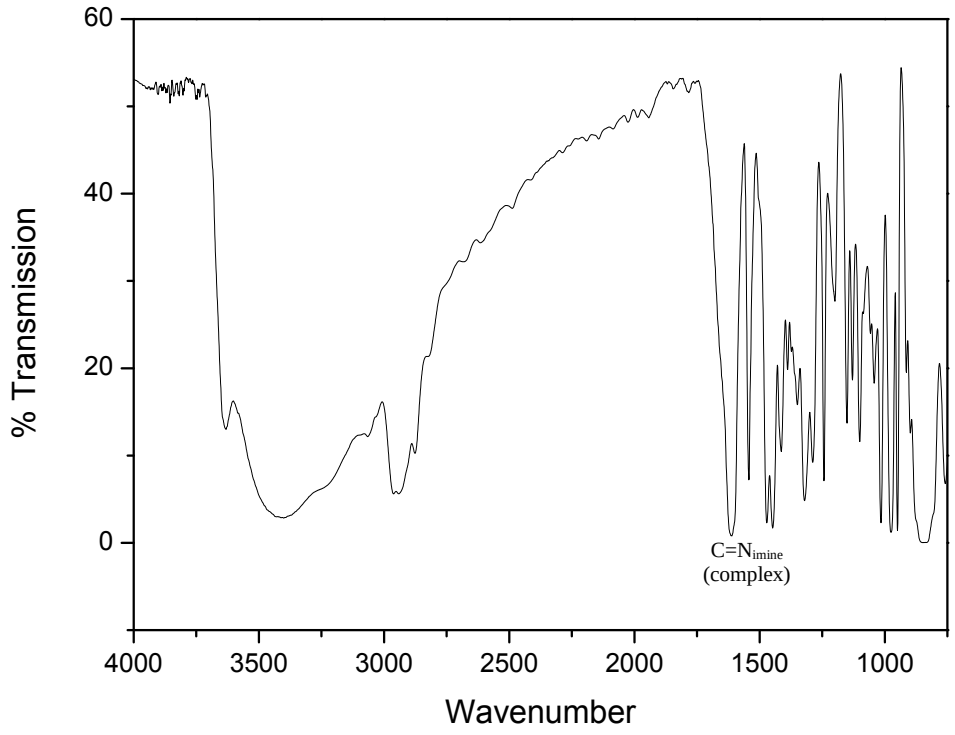

Figure 2.9 *Infrared spectrum of cationic metallodendrimer [**46**][PF$_6$]$_4$ recorded as a KBr pellet.*

2.6.3 Elemental Analysis and Mass Spectrometry

Similarly observed with the ruthenium metallodendrimers mentioned above, elemental analysis data for the osmium metallodendrimers were initially outside acceptable limits. Recalculation of the percentages with the inclusion of salts and/or solvent molecules gave percentages of the osmium metallodendrimers **40** - [**43**][PF$_6$]$_8$, [**46**][PF$_6$]$_4$ and [**47**][PF$_6$]$_8$ within acceptable limits. HR-ESI-TOF mass spectrometry data confirmed the proposed structures of metallodendrimers **40** - [**43**][PF$_6$]$_8$, [**46**][PF$_6$]$_4$ and [**47**][PF$_6$]$_8$. Positive-ion mass (ESI-MS) spectral data was consistent with the proposed structures of the mononuclear complexes **48**, [**49**][PF$_6$] and [**51**][PF$_6$].

2.6.4 X-ray Crystallography

The proposed structures of the mononuclear complexes **48**, [**49**][PF$_6$] and [**51**][PF$_6$] were further confirmed by single-crystal X-ray diffraction on crystals grown by slow evaporation of a concentrated solution of **48** in dichloromethane, or from either slow diffusion of hexane into a dichloromethane solution of [**49**][PF$_6$], or slow diffusion of diethyl ether into an acetone solution of [**51**][PF$_6$]. Mononuclear complex **48** crystallized in the orthorhombic

space group *Pbca* as two independent structures (**48A** and **48B**) in the asymmetric unit, and [**49**][PF_6] and [**51**][PF_6] crystallized in the triclinic space group *P* -1. ORTEP drawings of the molecular structures of **48**, [**49**][PF_6] and [**51**][PF_6] are illustrated in Figures 2.10 and 2.11. The molecular structures of **48A**, **48B**, [**49**][PF_6] and [**51**][PF_6] display the characteristic 'piano-stool' geometry and further confirms coordination of the bidentate-chelating salicylaldiminato (**37**) or iminopyridyl (**50**) ligands, through the imine nitrogen and phenolic oxygen or pyridyl nitrogen respectively. Crystallographic details can be found in the experimental Chapter 6, summarized in Table 6.2.

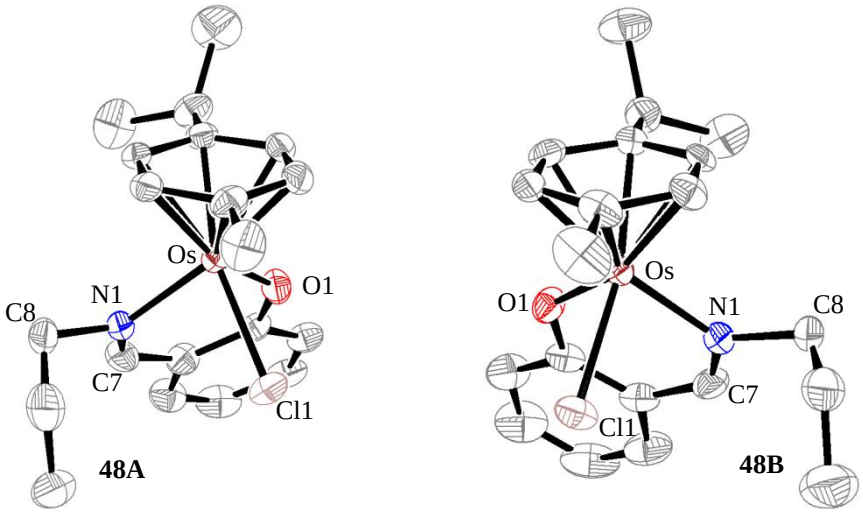

Figure 2.10 *ORTEP representations of mononuclear complexes **48** (two independent complexes **48A** (left) and **48B** (right)). Thermal ellipsoids are drawn at the 50 % probability level. Hydrogen atoms have been omitted for clarity.*

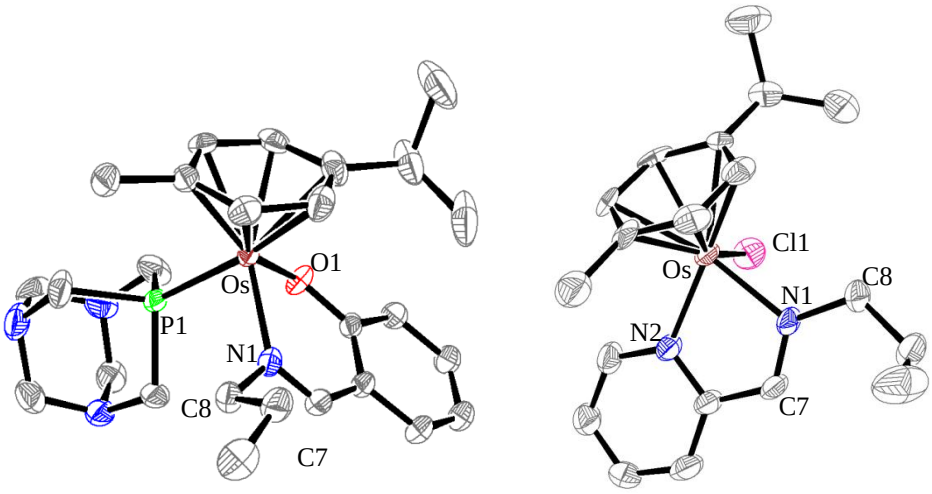

Figure 2.11 *ORTEP representations of mononuclear complexes [**49**][PF_6] (left) and [**51**][PF_6] (right). Thermal ellipsoids are drawn at the 50 % probability level. The PF_6^- counter-ion and hydrogen atoms have been omitted for clarity.*

Selected geometrical parameters of complexes **48A, 48B** and [**51**][PF_6] are listed in Table 2.10 and are comparable to those observed in other *N,O*- or *N,N*-osmium-arene complexes.[38-40] The Os-P bond distance in [**49**][PF_6] is comparable to other structurally similar osmium-arene-PTA complexes.[37] Expected structural similarities between these Os-complexes and previously reported ruthenium analogs are observed, such that the Os-Cl bond distance of [**51**][PF_6] (2.390 Å) is identical to the Ru-Cl bond distance (2.391 Å).[15] This feature is seen with the Os-P bond distance of [**49**][PF_6] and the Ru-P bond distance of the ruthenium-arene-PTA complex [**48**][PF_6] mentioned.

Table 2.10 *Selected average bond lengths and bond angles in **48A**, **48B**, [**49**][PF_6] and [**51**][PF_6].*

	48A	**48B**	[**49**][PF_6]	[**51**][PF_6]
	interatomic distances (Å)			
Os1-N1$_{imine}$	2.097(4)	2.092(4)	2.104(4)	2.089(7)
Os1-N2$_{pyr}$	-	-	-	2.075(8)
Os1-O1	2.069(3)	2.063(3)	2.084(3)	-
Os1-P1	-	-	2.326(1)	-
Os1-Cl1	2.428(1)	2.435(1)	-	2.390(2)
C7-N1$_{imine}$	1.291(6)	1.286(6)	1.292(6)	1.319(12)
C8-N1$_{imine}$	1.430(7)	1.428(7)	1.490(6)	1.451(12)
Os–centroid	~1.650	~1.654	~1.720	~1.691
	48A	**48B**	[**49**][PF_6]	[**51**][PF_6]
	angles (°)			
N1$_{imine}$-Os1-O1	88.3(1)	87.9(1)	86.4(1)	-
N1$_{imine}$-Os1-P1	-	-	86.8(1)	-
O1-Os1-P1	-	-	79.6(1)	-
O1-Os1-Cl1	83.0(1)	83.9(1)	-	-
N1$_{imine}$-Os1-N2$_{pyr}$	-	-	-	76.9(3)
N1$_{imine}$-Os1-Cl1	85.2(1)	84.2(1)	-	85.8(2)
N2$_{pyr}$-Os1-Cl1	-	-	-	84.7(2)
C6-C7-N1$_{imine}$	129.6(5)	129.1(5)	127.6(5)	118.3(8)
C7-N1$_{imine}$-C8	115.8(4)	115.2(4)	114.4(4)	123.9(8)

A study of their *in vitro* antitumor activity has been undertaken and the results are discussed in Chapter 4.

2.7 Overall Summary

A series of new neutral and cationic *N*,*O*-ruthenium-arene metallodendrimers have been successfully synthesized and characterized using a series a spectroscopic and analytical techniques, namely ^{1}H, $^{13}C\{^{1}H\}$ NMR, infrared, mass spectrometry and elemental analysis. Their mononuclear analogs were prepared and characterized. Single crystal X-ray diffraction was utilized to further confirm the proposed structures and illustrate the mode of coordination is in-fact through the imine nitrogen and phenolic oxygen.

A second series of new neutral and cationic *N*,*N*- and *N*,*O*-osmium-arene metallodendrimers have successfully been prepared, with spectroscopic and analytical methods used to corroborate proposed structures. Once again, mononuclear derivatives of the osmium-arene analogs were prepared and characterized, with single crystal X-ray diffraction on these complexes further confirming the proposed molecular structure.

2.8 References

1. N. Pabla and Z. Dong, *Kidney Int.*, 2008, **73**, 994-1007.
2. E. Wong and C. M. Giandomenico, *Chem. Rev.*, 1999, **99**, 2451-2466.
3. A. L. Noffke, A. Habtemariam, A. M. Pizarro and P. J. Sadler, *Chem. Commun.*, 2012, **48**, 5219-5246.
4. G. S. Smith and B. Therrien, *Dalton Trans.*, 2011, **40**, 10793-10800.
5. C. G. Hartinger and P. J. Dyson, *Chem. Soc. Rev.*, 2009, **38**, 391-401.
6. G. Süss-Fink, *Dalton Trans.*, 2010, **39**, 1673-1688.
7. W. F. Schmid, R. O. John, V. B. Arion, M. A. Jakupec and B. K. Keppler, *Organometallics*, 2007, **26**, 6643-6652.
8. G. Mühlgassner, C. Bartel, W. F. Schmid, M. A. Jakupec, V. B. Arion and B. K. Keppler, *J. Inorg. Biochem.*, 2012, **116**, 180-187.
9. W. Kandioller, A. Kurzwernhart, M. Hanif, S. M. Meier, H. Henke, B. K. Keppler and C. G. Hartinger, *J. Organomet. Chem.*, 2011, **696**, 999-1010.
10. A. M. Pizarro, A. Habtemariam and P. J. Sadler, *Activation Mechanisms for Organometallic Anticancer Complexes*, Springer, Berlin, 2010.
11. W. H. Ang, A. Casini, G. Sava and P. J. Dyson, *J. Organomet. Chem.*, 2011, **696**, 989-998.
12. A. Casini, C. G. Hartinger, A. A. Nazarov and P. J. Dyson, *Top. Organomet. Chem.*, 2010, **32**, 57-80.
13. P. Govender, B. Therrien and G. S. Smith, *Eur. J. Inorg. Chem.*, 2012, 2853-2862.
14. P. Govender, N. C. Antonels, J. Mattsson, A. K. Renfrew, P. J. Dyson, J. R. Moss, B. Therrien and G. S. Smith, *J. Organomet. Chem.*, 2009, **694**, 3470-3476.
15. P. Govender, A. K. Renfrew, C. M. Clavel, P. J. Dyson, B. Therrien and G. S. Smith, *Dalton Trans.*, 2011, **40**, 1158-1167.
16. R. Payne, P. Govender, B. Therrien, C. M. Clavel, P. J. Dyson and G. S. Smith, *J. Organomet. Chem.*, 2013, **729**, 20-27.
17. R. Malgas, S. F. Mapolie, S. O. Ojwach, G. S. Smith and J. Darkwa, *Catal. Commun.*, 2008, **9**, 1612-1617.
18. M. A. Torzilli, S. Colquhoun, D. Doucet and R. H. Beer, *Polyhedron*, 2002, **21**, 697-704.
19. H. H. Freedman, *J. Am. Chem. Soc.*, 1961, **83**, 2900-2905.

20. J. F. G. A. Jansen, E. M. E. de Brabander-van den Berg and E. W. Meijer, *Science*, 1994, **266**, 1226-1269.
21. M. A. Bennett and A. K. Smith, *J. Chem. Soc., Dalton Trans.*, 1974, **2**, 233-241.
22. M. A. Bennett, T. W. Matheson, G. B. Robertson, A. K. Smith and P. A. Tucker, *Inorg. Chem.*, 1980, **19**, 1014-1021.
23. W. H. Ang, E. Daldini, C. Scolaro, R. Scopelliti, L. Juillerat-Jeanneret and P. J. Dyson, *Inorg. Chem.*, 2006, **45**, 9006-9013.
24. C. Elschenbroich and A. Salzer, *Organometallics - A Concise Introduction*, 2nd edn., VCH Publishers Inc., New York, 1992.
25. P. Smolenski, F. P. Pruchnik, Z. Ciunik and T. Lis, *Inorg. Chem.*, 2003, **42**, 3318-3322.
26. F. P. Pruchnik, P. Smolenski, E. Galdecka and Z. Galdecki, *New J. Chem.*, 1998, **22**, 1395-1398.
27. P. Smolenski and A. J. L. Pombeiro, *Dalton Trans.*, 2008, 87-91.
28. R. Schibli, K. V. Katti, W. A. Volkert and C. L. Barnes, *Inorg. Chem.*, 1998, **37**, 5306-5312.
29. P. Smolenski, C. Dinoi, M. F. C. Guedes da Silva and A. J. L. Pombeiro, *J. Organomet. Chem.*, 2008, **693**, 2338-2344.
30. P. Govindaswamy, B. Therrien, G. Süss-Fink, P. Štěpnička and J. Ludvík, *J. Organomet. Chem.*, 2007, **692**, 1661-1671.
31. T.-T. Thai, B. Therrien and G. Süss-Fink, *J. Organomet. Chem.*, 2009, **694**, 3973-3981.
32. A. K. Renfrew, A. D. Phillips, E. Tapavicza, R. Scopelliti, U. Rothlisberger and P. J. Dyson, *Organometallics*, 2009, **28**, 5061-5071.
33. G. Smith, R. Chen and S. Mapolie, *J. Organomet. Chem.*, 2003, **673**, 111-115.
34. G. S. Smith and S. F. Mapolie, *J. Mol. Catal A: Chem.*, 2004, **213**, 187-192.
35. J. Cloete and S. F. Mapolie, *J. Mol. Catal A: Chem.*, 2006, **243**, 221-225.
36. A. K. Renfrew, A. D. Phillips, A. E. Egger, C. G. Hartinger, S. S. Bosquain, A. A. Nazarov, B. K. Keppler, L. Gonsalvi, M. Peruzzini and P. J. Dyson, *Organometallics*, 2009, **28**, 1165-1172.
37. A. Dorcier, P. J. Dyson, C. Gossens, U. Rothlisberger, R. Scopelliti and I. Tavernelli, *Organometallics*, 2005, **24**, 2114-2123.
38. A. F. A. Peacock, S. Parsons and P. J. Sadler, *J. Am. Chem. Soc.*, 2006, **129**, 3348-3357.

39. W. Ginzinger, G. Mühlgassner, V. B. Arion, M. A. Jakupec, A. Roller, M. Galanski, M. Reithofer, W. Berger and B. K. Keppler, *J. Med. Chem.*, 2012, **55**, 3398-3413.

40. Y. Fu, A. Habtemariam, A. M. B. H. Basri, D. Braddick, G. J. Clarkson and P. J. Sadler, *Dalton Trans.*, 2011, **40**, 10553-10562.

Chapter 3

Synthesis and Characterization of Heterometallic Ferrocenyl-Containing Ruthenium(II)-Arene Complexes Based on Poly(propyleneimine) Dendritic Scaffolds

3.1 Introduction

Apart from ruthenium-based anticancer agents, the introduction of a second metal in the preparation of heterometallic complexes as potential anticancer agents has flourished.[1-5] One such metal is iron or more specifically the iron-based organometallic complex, ferrocene.[6] Ferrocene-based molecules have become very attractive in the field of medicinal chemistry and more specifically as promising anticancer agents,[7-9] with the activity of these complexes attributed to their favorable electronic properties and ease of functionalization.[10, 11] Furthermore, simple derivatives of ferrocene display good activity *in vitro*, with inhibition of tumors observed *in vivo*.[12, 13] In the pursuit for new tamoxifen-like drugs, Jaouen and co-workers synthesized ferrocifens or 1-[4-(2-dimethylaminoethoxy)]-1-(phenyl-2-ferrocenylbut-1-ene) (Figure 3.1), which are highly active ferrocenyl-derivatives of the purely organic breast cancer drug tamoxifen.[14, 15] The increase in activity is attributed to the dual action of the organic drug and the Fenton chemistry (*i.e.* formation of singlet oxygen) of the Fe centre.[16, 17]

This effect is observed with a number of biologically active molecules.[18] Such an example is ferroquine (Figure 3.1), the ferrocenyl-based derivative of chloroquine, which displays an increased efficacy towards chloroquine-resistant malaria strains.[19-22] Furthermore, Edwards *et al.* reported the coupling of ferrocene to penicillin and cephalosporin which improved the antibacterial activity (Figure 3.1).[23-25]

In an effort to develop cytotoxic anticancer agents, ferrocene derivatives have been coupled with gold,[26] silver,[27] palladium,[1] rhodium[28] and iridium[28] in order to achieve a synergistic effect between the two active metals. The coupling of the two metals displayed cytotoxicities (in various cancer cell lines) comparable to the benchmark drug cisplatin. Bimetallic

ferrocenyl-derived gold(I)-phosphine complexes display activity against human ovarian cancer cells (A2780). The most potent ferrocenyl-derived gold complex (Figure 3.1) in the series displays better activity than cisplatin, with cytotoxicities in the nanomolar range.[26]

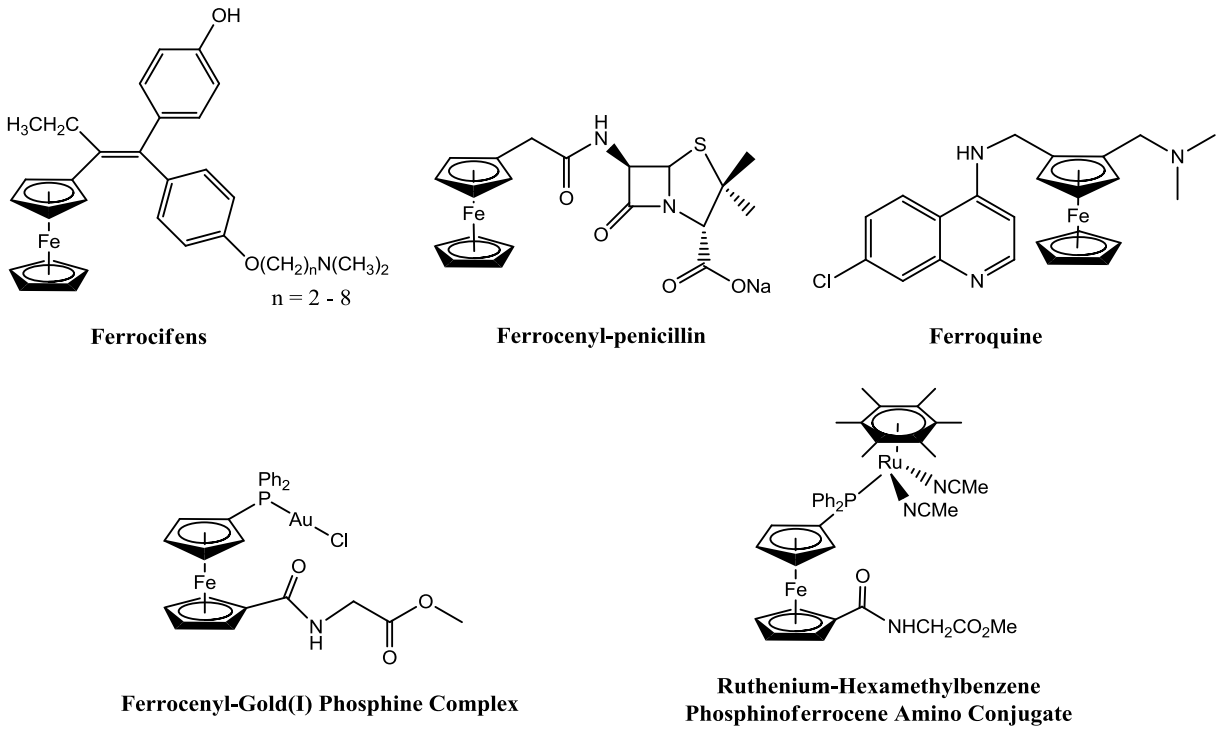

Figure 3.1 *Various ferrocenyl-derived anticancer compounds.*

As mentioned, ruthenium compounds are tolerated well *in vivo* and exhibit lower toxicity than their platinum counterparts.[29] It is proposed that the activity of Ru(III) complexes is brought about by reduction of the complex to the more active Ru(II) species *in vivo*.[30] This has, in part, triggered the development of half-sandwich organometallic ruthenium(II)-arene complexes as anticancer agents.[31-33] However, there are only a handful of reports where ruthenium and iron are coupled within the same molecule and investigated for anticancer activity.[34-36] The majority of ferrocenyl-derived ruthenium-arene derivatives display moderate activity compared to cisplatin. However, a heterobimetallic ruthenium-hexamethylbenzene phosphinoferrocene amino conjugate (Figure 3.1) displays activity in the low micromolar range (~4 μM in A2780),[34] further providing motivation for this study.

The coupling of the ferrocene to biologically active molecules or the preparation of new ferrocenyl-based anticancer agents is clearly an attractive field. Furthermore, the stability of ferrocene in aqueous and aerobic media, the ability to prepare a large variety of derivatives, and its favorable electrochemical properties has become a promising molecule for biological applications.[37]

In light of these findings, this chapter describes the synthesis and characterization of novel cationic ferrocenyl-derived ruthenium-arene metallodendrimers. The rationale for the synthesis of this class of compounds is to attempt to increase the lipophilic nature of these molecules, by coupling the ferrocenyl moiety to the ruthenium-arene metallodendrimers described in Chapter 2, in an effort to improve the antitumor activity of these complexes. Furthermore, Chapter 4 discusses the antitumor activity of the ruthenium-arene metallodendrimers reported in Chapter 2, with the cationic derivatives displaying the best activity in the series. Hence, only cationic ferrocenyl-derived ruthenium-arene metallodendrimers were prepared. Several spectroscopic and analytical techniques were employed to confirm and elucidate the proposed structure of the metallodendrimers and mononuclear analogs, and are described. The biological activity of these metallodendrimers and their mononuclear analogs is discussed in Chapter 4.

3.2 Synthesis and Characterization of *N,O*- and *N,N*- Ferrocenyl-Derived Conjugates

Synthesis of the ferrocenyl-derived conjugates required the preparation of vinyl ferrocene **53**. Two efficient routes are known in the preparation of **53**. The first route involves dehydration of 1-ferrocenylethanol using aluminium oxide,[38] whilst the second route proceeds *via* a Wittig reaction from ferrocene carboxaldehyde **52** in tetrahydrofuran (Scheme 3.1).[39] The second route, *via* a Wittig reaction, was chosen as this reported higher yields.[39, 40] The phosphonium ylide was formed by treating methyltriphenylphosphonium iodide with *n*-BuLi, and treated with **52** to form vinyl ferrocene **53** in a yield of 86 % (Scheme 3.1). The ^{1}H NMR spectrum of **53**, shows an absence in the singlet at ~10 ppm, usually assigned to the proton on aldehyde moiety of **52**, and the appearance of three doublet-of-doublets (5.02, 5.33 & 6.45 ppm) which are assigned to the three protons on the alkene moiety of **53**. Further confirmation for the presence of the alkene in **53** can be observed in the infrared spectrum with the appearance of

the stretching vibration at 1627 cm^{-1} ($C{=}C_{alkene}$ bond). The melting point of **53** (Mp: 48 - 49 ^{o}C) was obtained and attests to the purity of the compound as-well-as corresponds well with literature reports (Lit. Mp: 49 - 50 ^{o}C).[41]

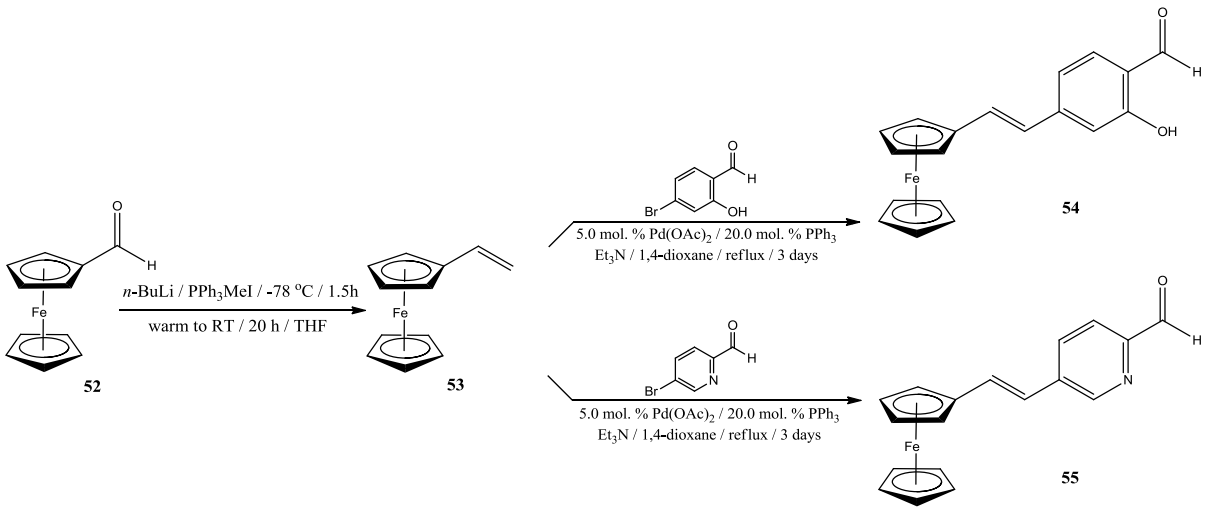

Scheme 3.1 *Synthesis of N,O- and N,N-ferrocenyl-derived conjugates **53** - **55**.*

The new ferrocenyl-derived conjugates (4*E*)-(4-ferrocenyl-vinyl)-2-hydroxy-benzaldehyde **54** and (5*E*)-(5-ferrocenyl-vinyl)-2-pyridinecarboxaldehyde **55** were prepared *via* a Heck coupling reaction of **53** and the appropriate aryl-bromide (Scheme 3.1).

The method followed was described by Reyes *et al.*,[42] whereby **53** was coupled with 4-bromobenzaldehyde **56** in dimethylformamide and triethylamine, with tri-*o*-tolylphosphine (POT) and palladium acetate as a catalyst, to afford (*E*)-(4-ferrocenyl-vinyl)benzaldehyde **57** (Scheme 3.2).

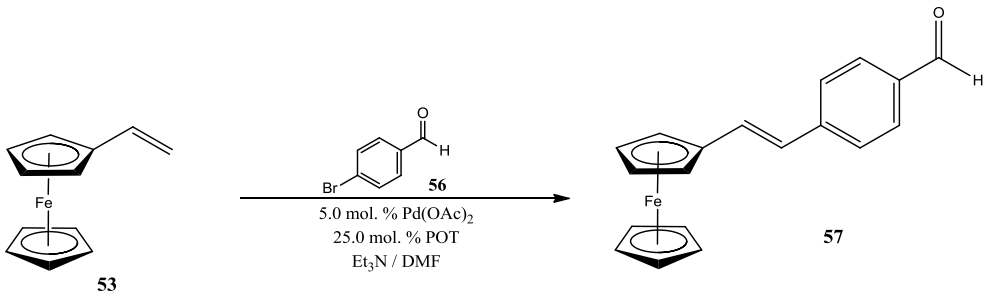

Scheme 3.2 *Synthesis of (E)-(4-ferrocenyl-vinyl)benzaldehyde **57** reported by Reyes et al.*[42]

However, to mimic the structure of previously synthesized metallodendrimers described in Chapter 2, a site for chelation of the ruthenium centre is required. Hence, coupling of **53** with 4-bromo-2-hydroxybenzaldehyde or 5-bromo-2-pyridinecarboxaldehyde afforded **54** and **55** respectively (Scheme 3.1). In the synthesis of **54** and **55**, the method described by Reyes *et al.* was modified slightly, with 1,4-dioxane as the solvent, triphenylphosphine instead of POT, palladium acetate as the catalyst and a stoichiometric amount of triethylamine as the base

The Heck reaction is an important reaction in both scientific (preparation of olefins, dienes and other unsaturated compounds)[43-47] and industrial (preparation of dyes, UV screens and pharmaceuticals)[48, 49] chemistry, as it is one of the key reactions used in C-C bond formation. Hence, it is also important to understand how these catalytic reactions take place. The Heck reaction (also known as the Mizoroki-Heck reaction) is typically carried out with a palladium catalyst, a catalytic amount of the tertiary phosphine and a stoichiometric amount of a weak base (Scheme 3.3).[50-54] The Pd-catalyzed reaction is typically used to couple aryl- or vinyl-halides and activated alkenes.

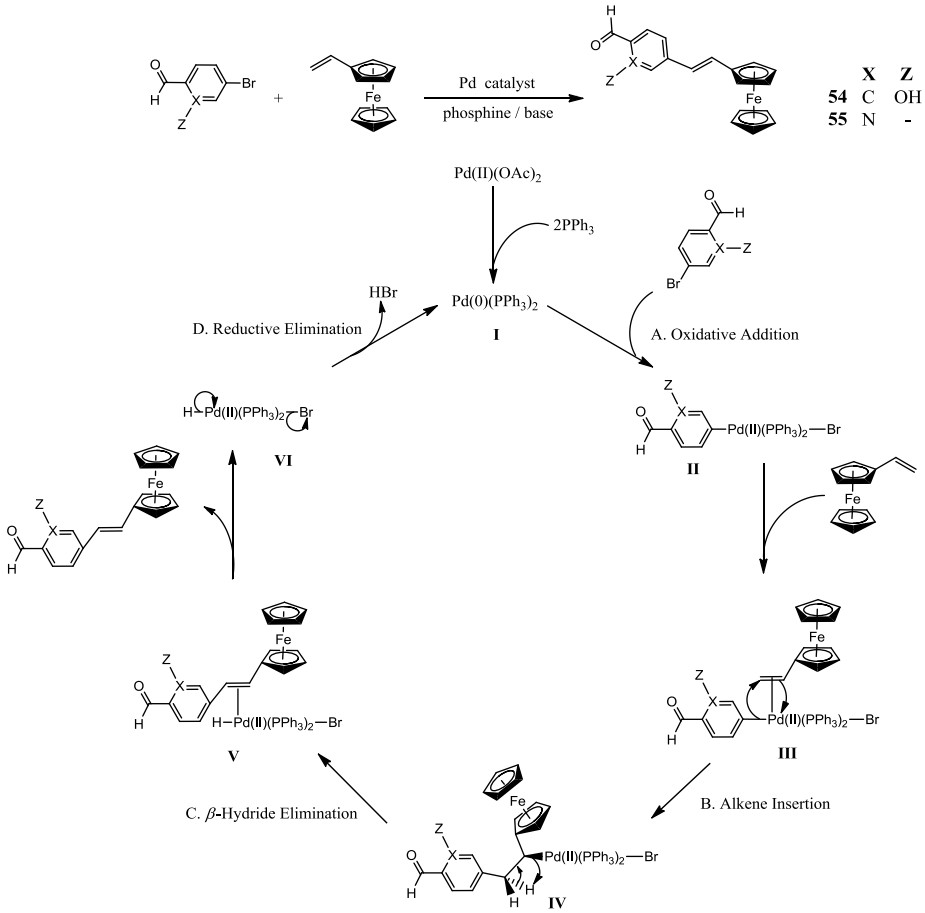

Scheme 3.3 *Catalytic cycle describing the interconversion of the oxidation sates during the course of the palladium catalyzed Heck C-C coupling reaction.*

The first step in the Heck reaction (also known as the pre-activation step, Scheme 3.3), involves reduction of the Pd(II) catalyst into the Pd(0) active species **I**, *via* a multiple ligand exchange with the phosphine ligand. The second step, involves an oxidative addition reaction of the aryl-halide to the coordinatively unsaturated complex **I**, generating a *σ*-alkenyl- or *σ*-aryl- palladium(II) complex **II**. The next step involves formation of the *π*-complex **III,** by rapid coordination of the alkene to the electrophilic Pd-coordination sphere. Alkene insertion or syn addition follows, whereby a new C-C bond is formed generating complex **IV**. *β*-Hydride elimination is next and generates a new *π*-complex **V**. The final step (drawn as two steps), is a reductive elimination step, whereby the *π*-complex **V** liberates the desired alkene and a hydridopalladium halide complex **VI**, which, with the aid of a base, regenerates the Pd(0) active species **I**.[55]

The Pd-catalyst, triphenylphosphine, triethylamine, **53** and the appropriate aldehyde were heated under reflux for 3 days, to afford **54** or **55** as purple solids in low yields (10 - 25 %). **54** and **55** are soluble in most organic solvents such as dichloromethane, methanol, toluene, diethyl ether and dimethylsulfoxide. Spectroscopic (^{1}H NMR, ^{13}C{^{1}H} NMR and IR spectroscopy) and analytical data (HPLC and mass spectrometry) confirmed the integrity of the new ferrocenyl-derived conjugates.

3.2.1 ^{1}H and ^{13}C{^{1}H} NMR Spectroscopy

The ^{1}H and ^{13}C{^{1}H} NMR spectra of the new ferrocenyl-derived conjugates **54** and **55** were recorded in deuterated chloroform, and affirms the coupling of the two starting materials. The characteristic singlet for the presence of a highly deshielded proton on an aldehyde functionality is observed for both **54** (Figure 3.2) and **55** (Figure 3.3) at ~10 ppm. In the ^{1}H NMR spectrum of **54**, a singlet is observed at ~11.1 ppm and is assigned to the phenolic proton. The characteristic AA'BB'-type spin system for monosubstituted ferrocenyl-derived derivatives, which is a singlet (~4.2 ppm) integrating for five protons and two triplets (~4.4 ppm & ~4.5 ppm) integrating for two protons each, is observed in the ^{1}H NMR spectrum for both **54** and **55**. Similar chemical shifts and coupling constants are consistent for structurally similar monosubstituted ferrocenyl-derived complexes.[56, 57]

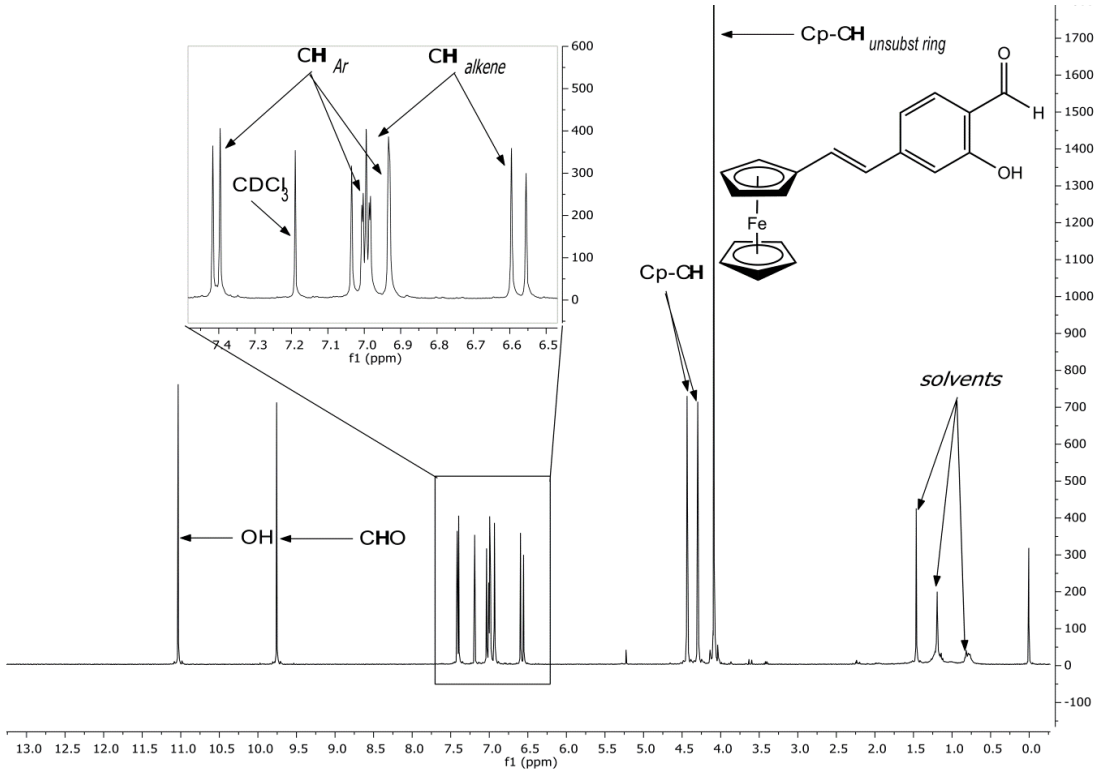

Figure 3.2 *^{1}H NMR spectrum of (4E)-(4-ferrocenyl-vinyl)-2-hydroxy-benzaldehyde **54** in $CDCl_3$.*

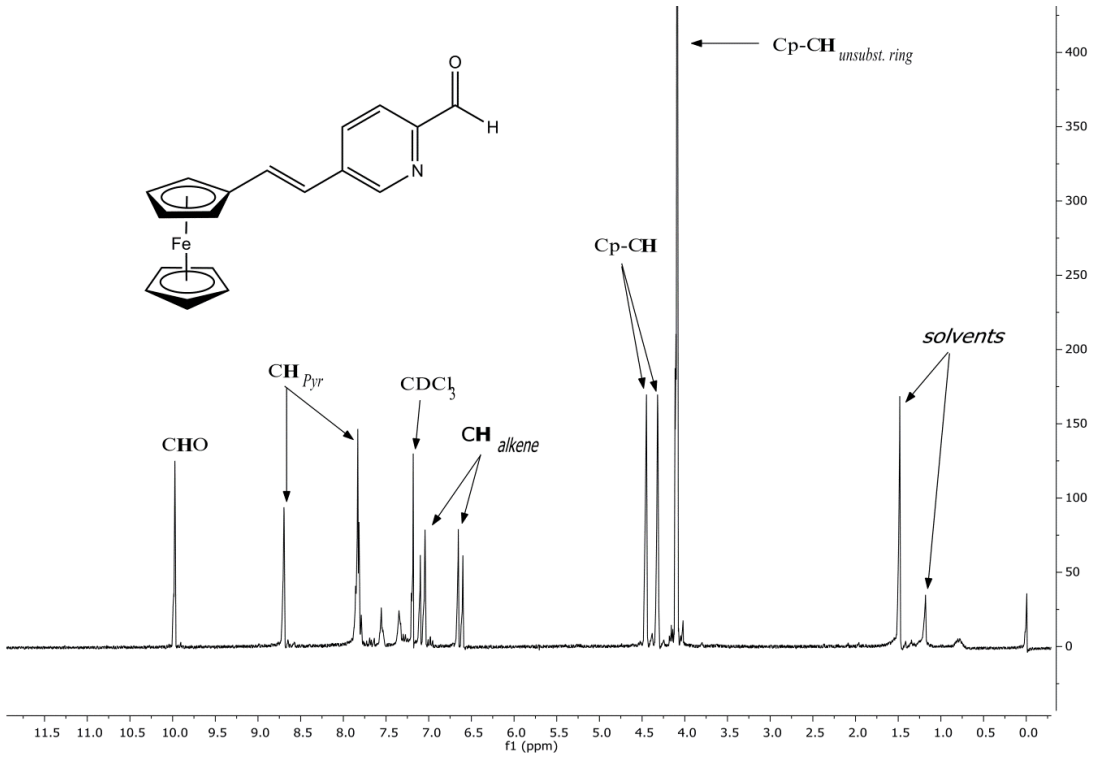

Figure 3.3 *^{1}H NMR spectrum of (5E)-(5-ferrocenyl-vinyl)-2-pyridinecarboxaldehyde **55** in $CDCl_3$.*

The disappearance of the three doublet-of-doublets (observed in the ^{1}H NMR spectrum of **53**) and the appearance of the two doublets (~6.7 ppm and ~7.1 ppm), are assigned to the two protons on the alkene moiety for both **54** and **55** and suggest C-C bond formation. The two doublets have a coupling constant of $^{3}J_{HH}$ = ~16 Hz each, suggesting that the alkene moieties of **54** and **55** adopt a *trans* confirmation rather than a *cis* confirmation, as typical coupling constants for a *cis* confirmation would be much lower ($^{3}J_{HH}$ = ~9 Hz) (Figure 3.4).[58] Hence, the *E*-isomer formed exclusively, as signals for the *Z*-isomer was not observed in the ^{1}H NMR spectrum of **54** and **55**. A similar coupling constant (*i.e.* $^{3}J_{HH}$ = 16 Hz) was reported by Yang *et al*., for the structurally similar compound (4*E*)-(4-ferrocenyl-vinyl)-pyridne.[56]

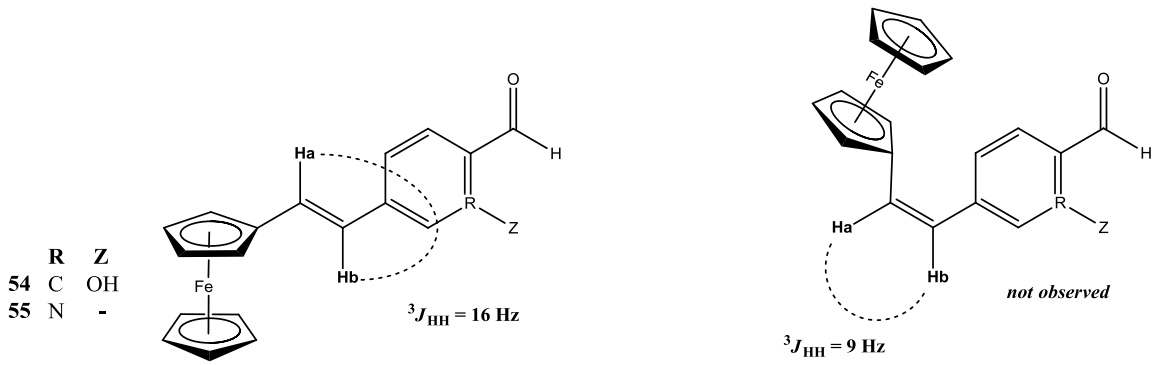

Figure 3.4 *E and Z forms of ferrocenyl-derived conjugates **54** and **55**, with the cis isomer (right) not observed.*

The ^{13}C{^{1}H} NMR spectrum of the ferrocenyl-derived conjugates **54** and **55** are similar, with some of the signals displaying identical chemical shifts. The 2D-HSQC NMR spectrum of **54** and **55** was utilized in the assignment of the signals in ^{13}C{^{1}H} spectrum. Three signals in the range of 65 - 70 ppm are observed for **54** and **55** and assigned to the carbons on both the substituted and unsubstituted Cp rings.

3.2.2 Infrared Spectroscopy

The infrared spectrum of **54** and **55** were recorded as pure solids using the ATR technique. A strong sharp stretching vibration is observed at 1614 cm^{-1} and 1575 cm^{-1} for **54** and **55** respectively, and is assigned to the C=C bond of the alkene moiety. This observation confirms successful C-C bond formation *via* the Heck reaction. The stretching vibrations observed at 1652 cm^{-1} and 1703 cm^{-1} are assigned to the C=O bond of **54** and **55** respectively. Furthermore, an extra stretching vibration is observed in the IR spectrum of **55**, at 1629 cm^{-1}, and is assigned to the C=N bond of the pyridyl ring.

3.2.3 Mass Spectrometry and HPLC

HR-ESI mass spectrometry was also used to characterize **54** and **55** in the positive-ion mode. The mass spectrum of **54** and **55** gave a base peak for $[M+H]^+$ ions at m/z = 333.0562 and m/z = 318.0580 respectively and are consistent with the proposed structures.

Analytical-HPLC traces were obtained for **54** and **55**, with single peaks observed at t_R = 17 min and t_R = 16 min respectively and attests the purity of these compounds.

3.3 Synthesis and Characterization of Ferrocenyl-Derived *N,O*-Salicylaldiminato and *N,N*-Pyridylimine Dendritic Ligands

The third step in the synthesis involved preparation of two new ferrocenyl-derived *N,O*-salicylaldiminato dendritic ligands **56** and **57** and two new ferrocenyl-derived *N,N*-pyridylimine dendritic ligands **58** and **59**. The dendritic ligands **56** - **59** were prepared *via* a Schiff base condensation of **54** (for **56** & **57**) or **55** (for **58** & **59**) with the amino groups of DAB-**G$_1$**-$(NH_2)_4$ (for **56** & **58**) or of DAB-**G$_2$**-$(NH_2)_8$ (for **57** & **59**) in dichloromethane overnight (Scheme 3.4), with purification involving precipitation from petroleum ether (40 - 60 °C). The dendritic ligands **56** - **59**, were isolated as orange solids in moderate yields (50 - 65 %).

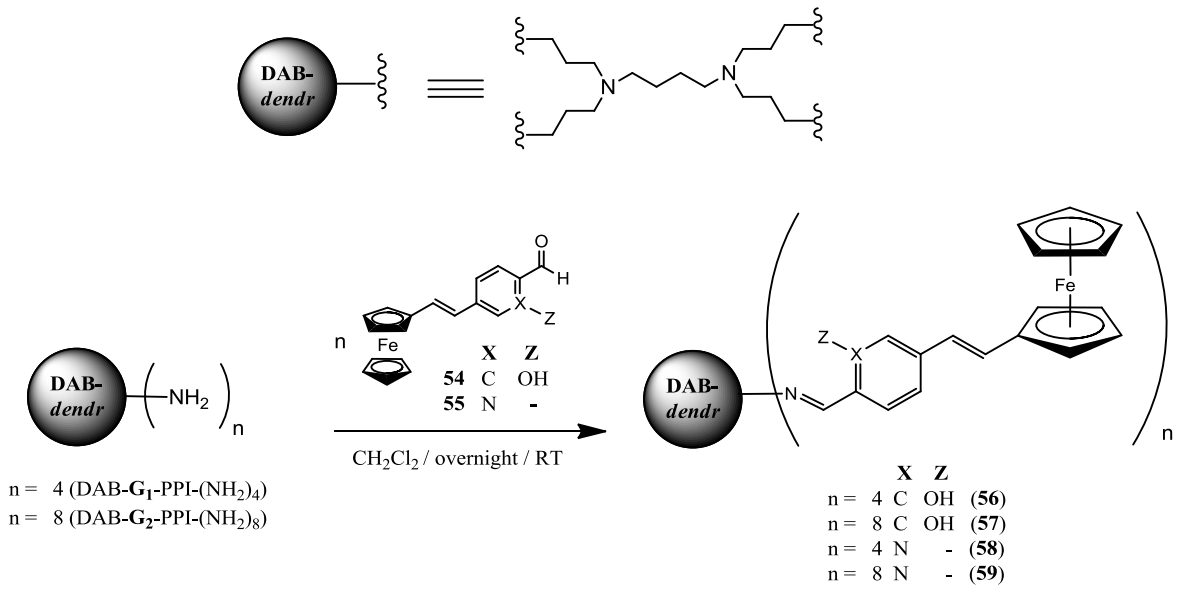

Scheme 3.4 *Synthesis of ferrocenyl-derived N,O-salicylaldiminato and N,N-pyridylimine dendritic ligands* ***56 - 59****.*

The ligands **56 - 59** are air- and moisture-stable, are soluble in a handful of solvents, such as dichloromethane, chloroform, acetonitrile and dimethylsulfoxide, and not soluble in protic and non-polar solvents. These compounds were characterized using ^{1}H and ^{13}C{^{1}H} NMR spectroscopy, infrared spectroscopy, elemental analysis and mass spectrometry.

3.3.1 ^{1}H and ^{13}C{^{1}H} NMR Spectroscopy

The ^{1}H and ^{13}C{^{1}H} NMR data of **56 - 59** were recorded in deuterated chloroform and display overlapping and broadening of signals, similarly observed with the dendritic ligands previously mentioned in Chapter 2. The ^{1}H NMR spectrum of **56 - 59** (Figures 3.5 and 3.6) shows an absence of the singlet at ~10 ppm (C**H**O proton of **54** & **55**) with an appearance of a broad singlet at ~8.2 ppm (for **56** & **57**) and ~8.4 ppm (for **58** & **59**), which is assigned to the proton on the newly formed imine bond. Typically, the signals for the aliphatic protons on the dendritic core and dendritic arms appear in the region between 1.4 - 3.7 ppm for **56 - 59**. The two doublets at ~6.7 ppm and ~7.0 ppm, with coupling constants of $^{3}J_{HH}$ = ~16 Hz, are assigned to the protons on the alkene moiety of **56 - 59**.

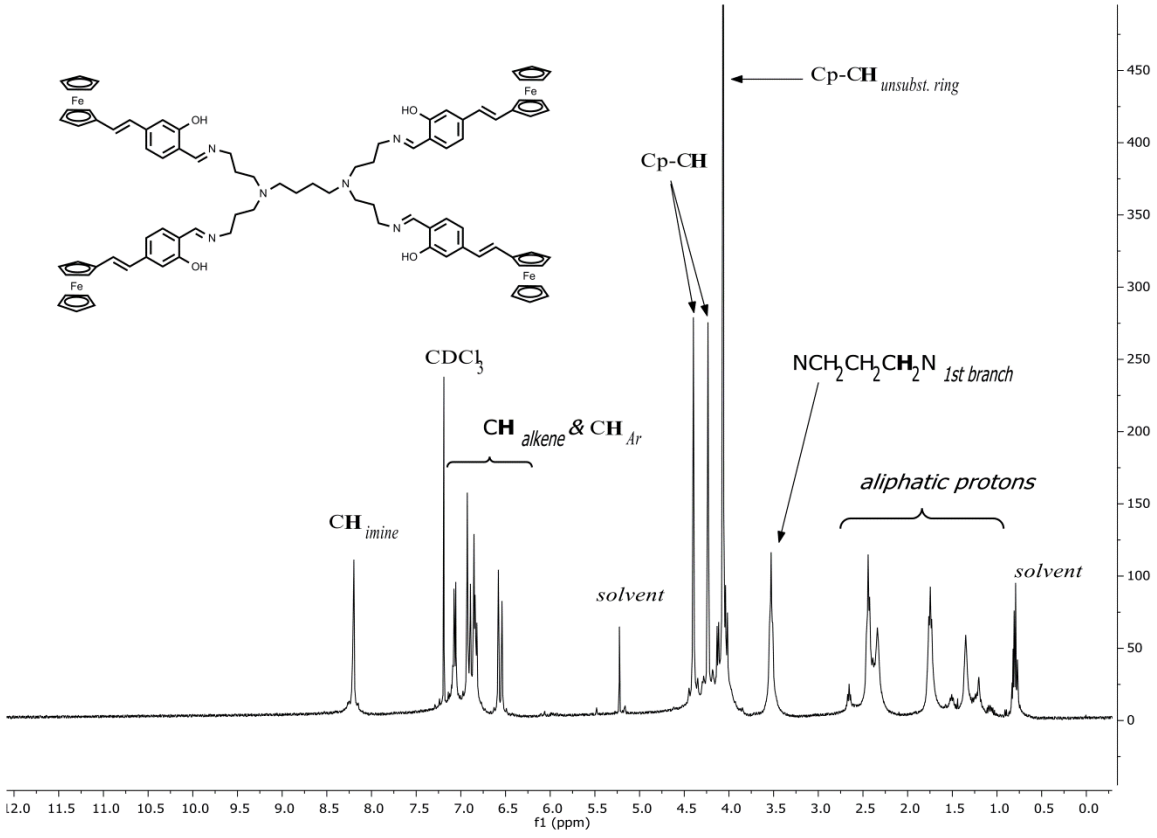

Figure 3.5 *^{1}H NMR spectrum of first-generation ferrocenyl-derived N,O-salicylaldiminato dendritic ligand **56** in $CDCl_3$.*

Broad signals are observed in the region of 6.9 - 7.1 ppm (for **56** & **57**) and 7.8 - 8.6 ppm (for **58** & **59**), and are assigned to the aromatic and pyridyl protons respectively. Unlike the *N*,*O*-salicylaldiminato dendritic ligands **21** - **24** mentioned in Chapter 2, the ^{1}H NMR spectrum of **56** and **57** did not display a broad singlet (typically ~13.5 ppm), which is usually assigned to the phenolic proton. This was attributed to possible solvent exchanges, though usually expected in deuterated dimethylsulfoxide and deuterated acetone, and not in deuterated chloroform.

The ^{13}C{^{1}H} spectrum for **56** - **59** display the expected number of signals in both the aromatic and aliphatic region. The singlet observed in the ^{13}C{^{1}H} spectrum for the ferrocenyl-derived conjugates **54** and **55**, at ~195 ppm and ~193 ppm respectively (assigned to the carbonyl carbon) was not observed in the spectrum of **56** - **59**. This observation confirms formation of the imine bond, as a singlet at ~164 ppm (for **56** & **57**) and at ~162 ppm (for **58** & **59**) is observed in the ^{13}C{^{1}H} NMR spectrum, and is assigned to the carbon atom of the imine bond.

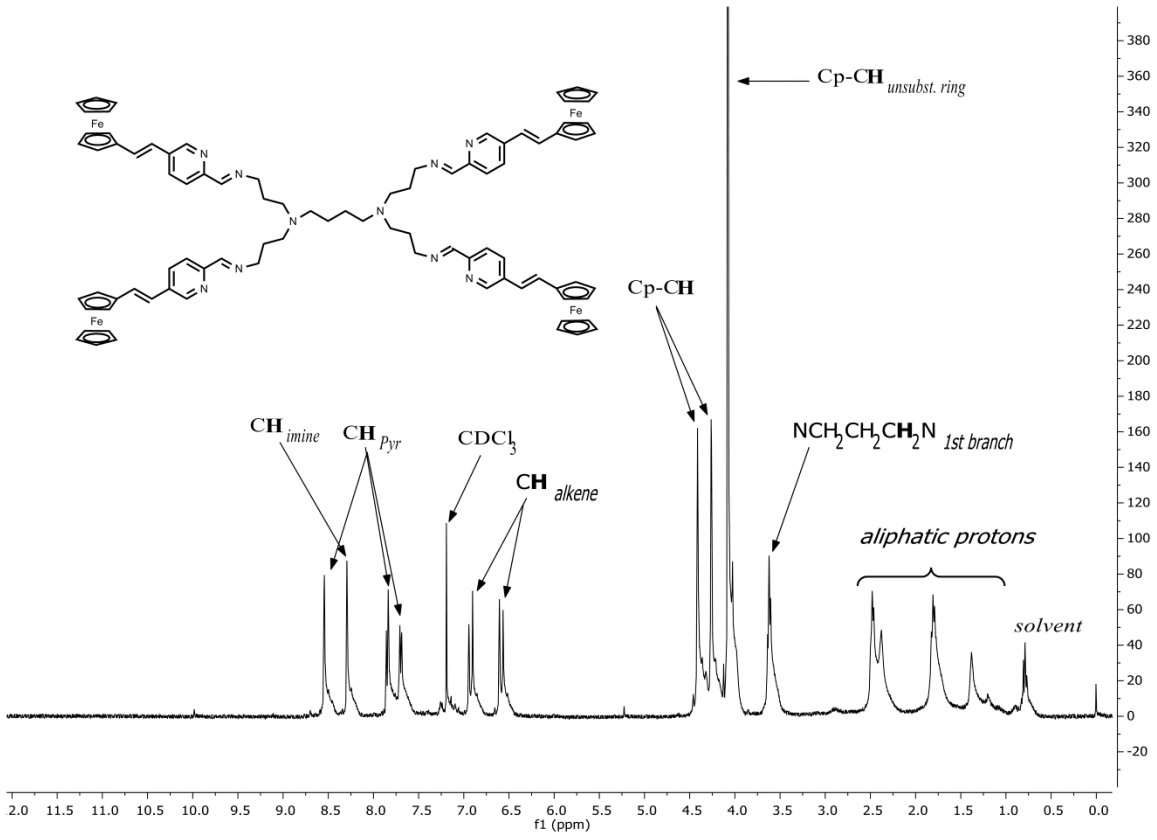

Figure 3.6 *^{1}H NMR spectrum of first-generation ferrocenyl-derived N,N-pyridylimine dendritic ligand **58** in $CDCl_3$.*

3.3.2 Infrared Spectroscopy

The infrared spectra of **56 - 59** was recorded as pure solids using the ATR technique, with the results further confirming the formation of the imine bond. The infrared spectrum of dendritic ligands **56** and **55** display a strong broad stretching vibration at ~1610 cm^{-1} and is assigned to both the C=N and C=C bonds of the imine and alkene moieties respectively. However, dendritic ligands **58** and **59** display two bands of medium intensity, at ~1580 cm^{-1} and ~1640 cm^{-1}, and are assigned to the alkene and imine bonds respectively. Furthermore, **58** and **59** display an extra stretching vibration at 1628 cm^{-1}, and is assigned to the C=N bond of the pyridyl ring.

3.3.3 Elemental Analysis and Mass Spectrometry

Following extensive drying of **56 - 59**, satisfactory elemental diffraction was not obtained, as percentages obtained were outside acceptable limits and is ascribed to possible solvent inclusions. The inclusion of small molecules has been observed with purely organic dendrimers, as the free rotation of the dendritic arms allows for folding onto one another in turn trapping small molecules.[59] Recalculation of the C, H and N percentages obtained for **56 - 59** with the inclusion of dichloromethane (reaction solvent, observed in the ^{1}H NMR spectrum, ~ 5 mols of dichloromethane) gave percentages within acceptable limits.

HR-ESI mass spectrometry was used to confirm the proposed structures of **56 - 59**, and the molecular ion peaks are listed in (Table 3.1). All complexes exhibited a base peak corresponding to a charged complex, with both **56** and **58** displaying a triply charged complex $[M+3H]^{3+}$ at m/z = 525.1727 and at m/z = 500.0750 respectively.

Table 3.1 *Mass spectral data for ferrocenyl-derived dendritic ligands **56 - 59**.*

Compound	MS (fragment, assignment) [m/z][a]
56	525.1727 $[M+3H]^{3+}$
57	822.8010 $[M+4H]^{4+}$
58	500.0750 $[M+3H]^{3+}$
59	633.1572 $[M+5H]^{5+}$

[a] HR-ESI-TOF-MS

3.4 Synthesis and Characterization of Ferrocenyl-Derived *N,O*-Salicylaldiminato and *N,N*-Pyridylimine Monomeric Ligands

The monomeric ligands **60** and **61** were synthesized in a similar manner to their dendritic derivatives **56 - 59**, by reacting *n*-propylamine with **54** and **55** (Scheme 3.5), *via* a Schiff base condensation reaction. Following purification over a small pad of silica (2 cm in height), the new monomeric ligands **60** and **61** were isolated as orange-red solids in 56 % and 71 % yield respectively.

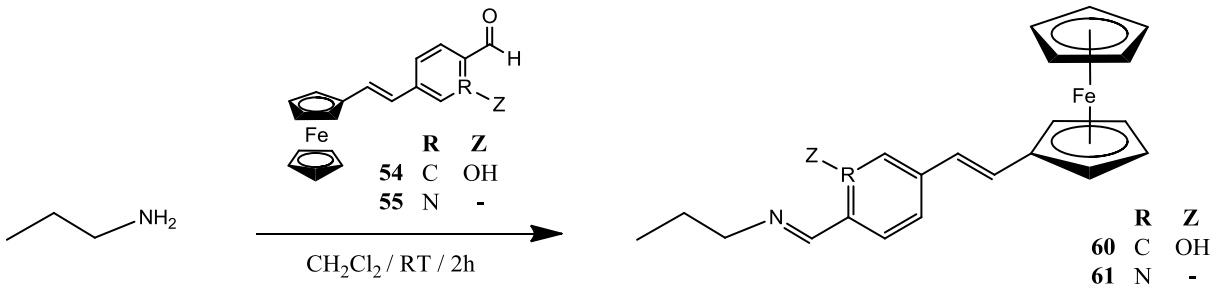

Scheme 3.5 *Synthesis of monomeric ligands (5E, 2E)-(5-ferrocenyl-vinyl)-2-((propylimino)methyl)phenol **60** and (5E, 2E)-N-((5-ferrocenyl-vinyl-pyridin-2-yl)methylene)propan-1-amine **61**.*

3.4.1 ^{1}H and ^{13}C{^{1}H} NMR Spectroscopy

The Schiff base reaction used in the synthesis of monomeric ligands **60** and **61** was confirmed by ^{1}H and ^{13}C{^{1}H} NMR spectroscopy, recorded in deuterated chloroform. The ^{1}H NMR spectrum of **60** (Figure 3.7) and **61** (Figure 3.8) exhibit a signal integrating for one proton, at 8.3 ppm, and are assigned to the imine proton. The singlet (at 4.1 ppm) and the two doublets (at 4.3 ppm & 4.5 ppm), integrating for five and two protons (for each doublet) respectively, and are assigned to the protons on the ferrocenyl functionality for both **60** and **61**. Signals for the aliphatic protons are observed at 1.0 ppm (triplet), 1.7 ppm (multiplet) and 3.6 ppm (multiplet). The signals for the aromatic protons (for **60**) and pyridyl protons (for **61**) are observed in the range of 6.9 - 7.2 ppm and 7.7 - 8.6 ppm respectively. Similarly observed for the dendritic ligands **56** and **55**, no broad signal for the hydroxyl proton was observed for **60**.

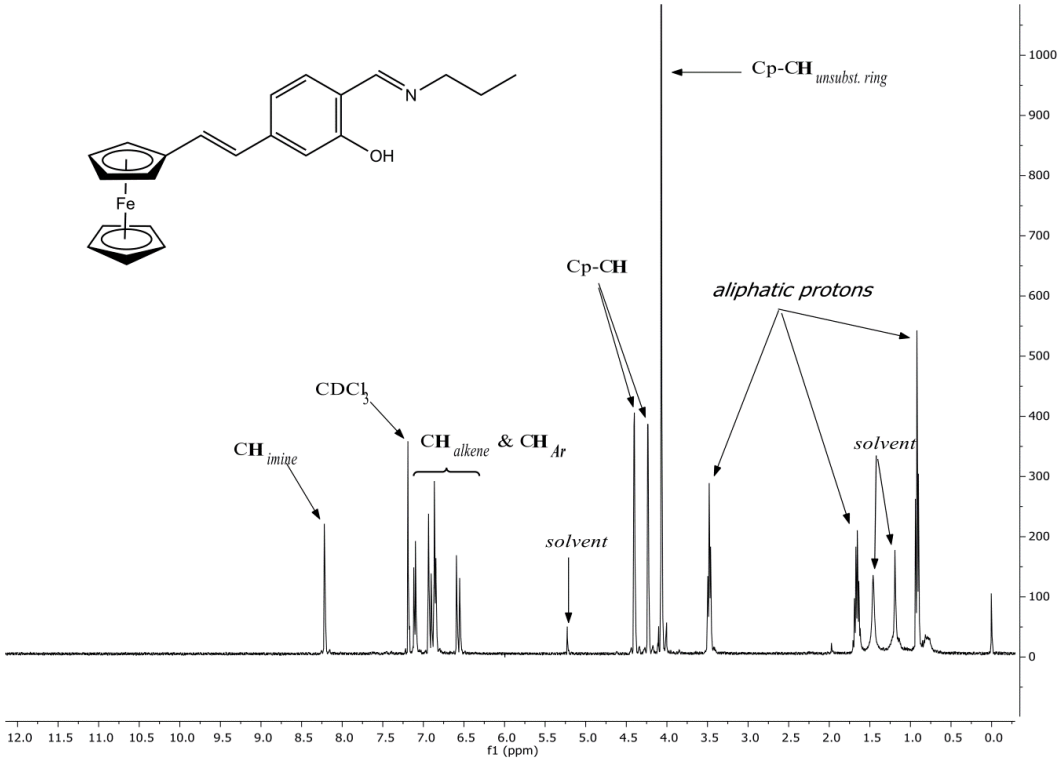

Figure 3.7 *^1H NMR spectrum of monomeric ligand (5E, 2E)-(5-ferrocenyl-vinyl)-2-((propylimino)methyl)phenol **60** in $CDCl_3$.*

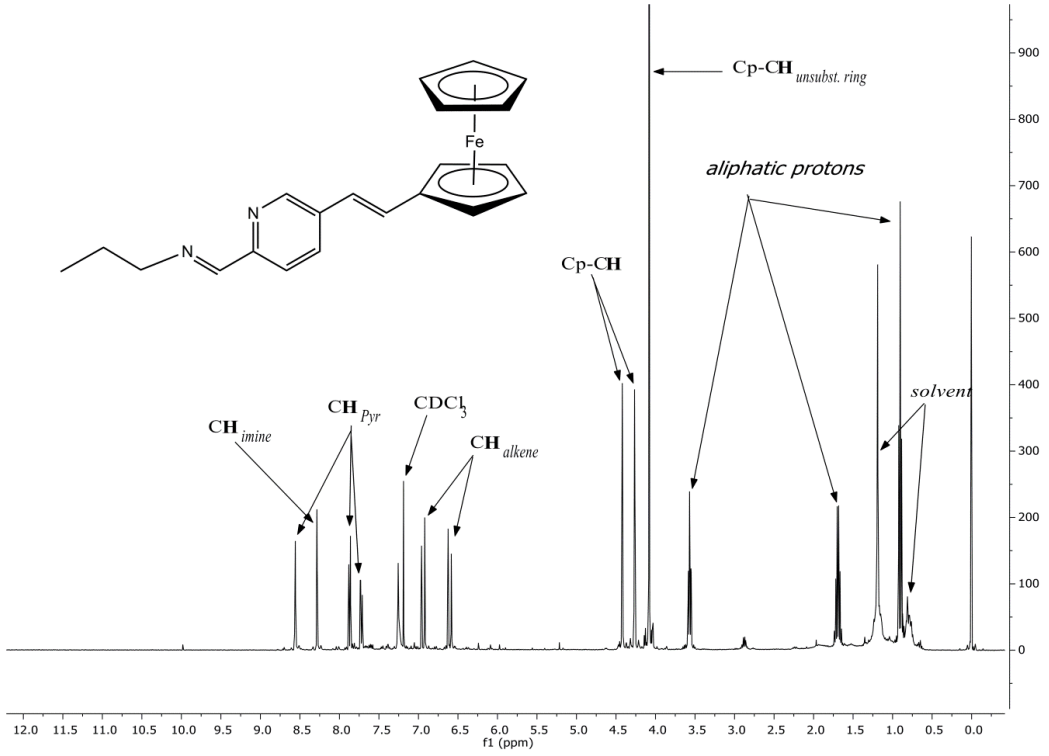

Figure 3.8 *^1H NMR spectrum of monomeric ligand (5E, 2E)-N-((5-ferrocenyl-vinyl-pyridin-2-yl)methylene)propan-1-amine **61** in $CDCl_3$.*

All the relevant signals for the carbon atoms are observed in the $^{13}C\{^{1}H\}$ NMR spectrum of **60** and **61**. In particular, signals for the imine carbon (~160 ppm) and two alkene carbons (~123 ppm & ~125 ppm) were observed.

3.4.2 Infrared Spectroscopy

Monomeric ligand **60** displays a broad stretching vibration at 1607 cm^{-1} and is assigned to the alkene and imine bonds. Whilst **61** displayed three stretching vibrations at 1579 cm^{-1}, 1630 cm^{-1} and 1643 cm^{-1}, and are assigned to the alkene, pyridyl and imine bonds respectively.

3.4.3 Mass Spectrometry and HPLC

HR-ESI mass spectral data for **60** and **61** displays a base peak for a charged complex $[M+H]^+$ at m/z = 374.1206 and at m/z = 359.1208 respectively. This data further confirms the proposed structures of **60** and **61**.

In addition, the purity of the monomeric ligands **60** and **61** was determined using high performance liquid chromatography (HPLC), with single peaks observed at t_R = ~18 min.

3.5 Synthesis and Characterization of Cationic Ferrocenyl-Derived *N,O*-Ru(II)-Arene-PTA and *N,N*-Ru(II)-Arene Metallodendrimers

A similar approach, used in the synthesis of non-ferrocenyl-based metallodendrimers prepared in Chapter 2, was followed in the preparation of metallodendrimers [**62**][PF_6]$_4$ - [**65**][PF_6]$_8$. The appropriate dendritic ligand was initially reacted with [Ru(η^6-*p*-Pr^iC_6H_4Me)Cl_2]$_2$ in ethanol at room temperature. However, this method proved to be unsuccessful for the synthesis of [**62**][PF_6]$_4$ - [**65**][PF_6]$_8$, most likely due to the poor solubility of the dendritic ligands **56** - **59** in ethanol.

The metallodendrimers [**62**][PF_6]$_4$ - [**65**][PF_6]$_8$ were therefore synthesized by reacting the appropriate first- or second-generation dendritic ligand (**56** - **59**) with the ruthenium precursor [Ru(η^6-*p*-Pr^iC_6H_4Me)Cl_2]$_2$ in an ethanol:dichloromethane (50:50 % *v*/*v*) mixture at room temperature (Scheme 3.6).

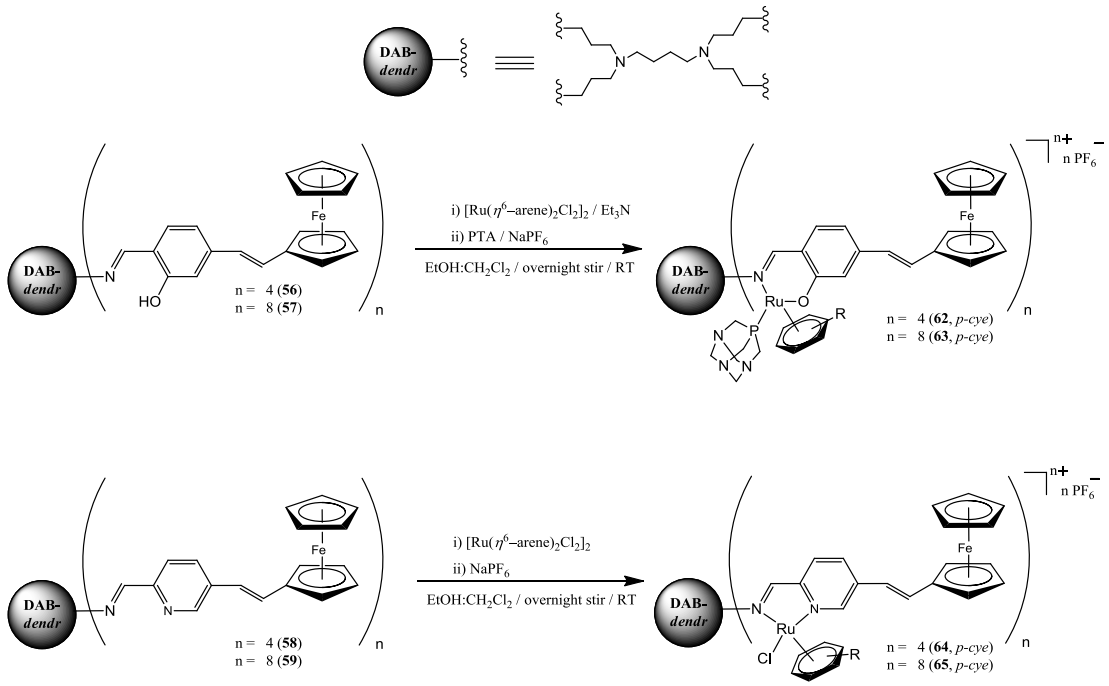

Scheme 3.6 *Synthesis of cationic ferrocenyl-derived N,O-Ru(II)-Arene-PTA and N,N-Ru(II)-Arene metallodendrimers [**62**][PF_6]$_4$ - [**65**][PF_6]$_8$.*

For the *N,O*-salicylaldiminato dendritic ligands **56** and **57**, triethylamine was added to remove the phenolic proton, which was followed by complexation with [Ru(η^6-*p*-Pr^{i}C$_6$H$_4$Me)Cl$_2$]$_2$ in a one-pot *in situ* reaction. The water-soluble PTA ligand was added to displace the chlorido ligand, in turn generating a cationic species.

Compounds **62** - **65** were isolated as hexafluorophosphate salts, *via* a metathesis reaction with $NaPF_6$, to afford orange solids ([**62**][PF_6]$_4$ & [**63**][PF_6]$_8$) or dark purple solids ([**64**][PF_6]$_4$ & [**65**][PF_6]$_8$), in good yields (72 - 85 %). Compounds [**62**][PF_6]$_4$ - [**65**][PF_6]$_8$ are non-hygroscopic, air- and moisture-stable solids, can be stored on the bench-top for more than five months and are soluble in dimethylsulfoxide, acetone and dimethylformamide, and partially soluble in acetonitrile.

Chelation of the ligands to the metal centre, as well as purity of the metallodendrimers, were confirmed by spectroscopic (^{1}H, ^{13}C{^{1}H} NMR and infrared spectroscopy) and analytical techniques (elemental analysis and mass spectrometry).

3.5.1 ^{1}H, ^{31}P{^{1}H} and ^{13}C{^{1}H} NMR Spectroscopy

The ^{1}H NMR data of the metallodendrimers [**62**][PF_6]$_4$ - [**65**][PF_6]$_8$ was recorded in deuterated acetone. Comparison of the ^{1}H NMR spectrum of [**62**][PF_6]$_4$ - [**65**][PF_6]$_8$ to its

corresponding dendritic ligand reveals an overall downfield shift in the broadened signals (in the range of 1.3 - 4.0 ppm) associated with the aliphatic protons of the dendritic core or on the dendritic arms. This downfield shift is attributed to the incorporation of the metal ion onto the ligand, which in turn generates a charged species further influencing the overall chemical shift of signals. Confirmation for the chelation of the dendritic ligand to the ruthenium ion is attributed to a slight downfield shift in the imine signal from ~8.0 ppm (for **56** & **57**) and ~8.3 ppm (for **58** & **59**) to ~8.1 ppm (for [**62**][PF_6]$_4$ (Figure 3.9) & [**63**][PF_6]$_8$) and ~8.9 ppm (for [**64**][PF_6]$_4$ (Figure 3.10) & [**65**][PF_6]$_8$) respectively. Upon coordination of the dendritic ligand to the ruthenium ion, [**62**][PF_6]$_4$ - [**65**][PF_6]$_8$ results in a loss of two-fold symmetry of the *p*-cymene moiety. This results in the methyl protons of the isopropyl group exhibiting two broad multiplets in the range of 1.1 - 1.3 ppm (for [**62**][PF_6]$_4$ - [**65**][PF_6]$_8$), with a broad multiplet observed at ~2.6 ppm assigned to the single proton on the isopropyl group. The protons on the substituted and un-substituted ferrocenyl functionality are assigned to the broad singlet and two broad doublets in the region 4.0 - 4.4 ppm for [**62**][PF_6]$_4$ - [**65**][PF_6]$_8$. The protons on the alkene moiety appear at ~6.7 ppm and 7.1 ppm for [**62**][PF_6]$_4$ and [**63**][PF_6]$_8$, whilst they appear at ~6.7 ppm and 7.6 ppm for [**64**][PF_6]$_4$ and [**65**][PF_6]$_8$.

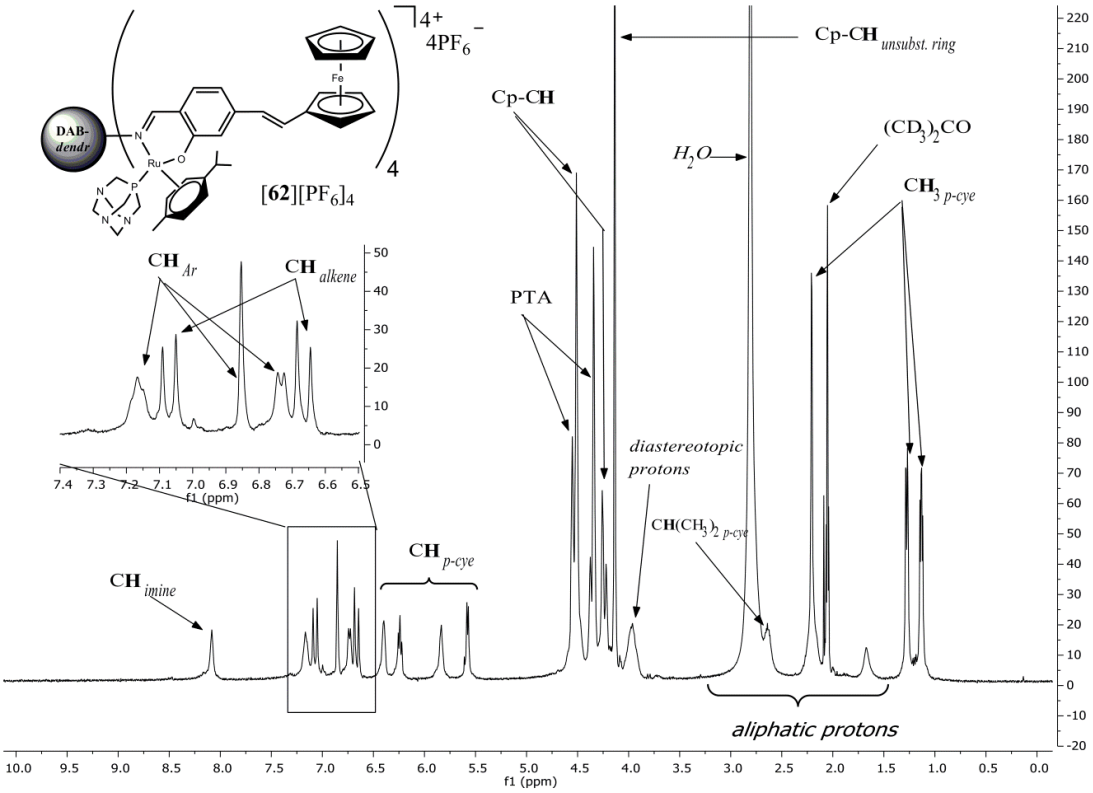

Figure 3.9 *^{1}H NMR spectrum for [DAB-**G$_1$**-PPI-{(η^6-p-cye)Ru((C_7H_5NO)-κ^2-N,O)PTA-(5-ferrocenyl-vinyl)}$_4$][PF_6]$_4$ ([**62**][PF_6]$_4$) in $(CD_3)_2CO$.*

*^{1}H NMR spectra of N,O-Ru(II)-arene-PTA metallodendrimers ([**62**][PF$_6$]$_4$ & [**63**][PF$_6$]$_8$)*

The ^{1}H NMR spectrum of metallodendrimers [**62**][PF$_6$]$_4$ (Figure 3.9) and [**63**][PF$_6$]$_8$ show signals in the range of 5.5 - 7.2 ppm and are assigned to the aromatic protons. The signals for the protons on the PTA ligand (4.1 - 4.6 ppm) overlap with the broad signals assigned to the protons on the ferrocenyl functionality and the diastereotopic protons (as a result of chirality induced by the ruthenium ion) on the aliphatic carbon adjacent to the imine nitrogen. Furthermore, the signals for the PTA ligand display the typical splitting pattern for an AB spin system, and correlates well with splitting patterns observed with other PTA complexes in the iterature.[60, 61]

Four multiplets observed at around 5.5, 5.8, 6.2 and 6.4 ppm, are assigned to the aromatic protons on the *p*-cymene ring.

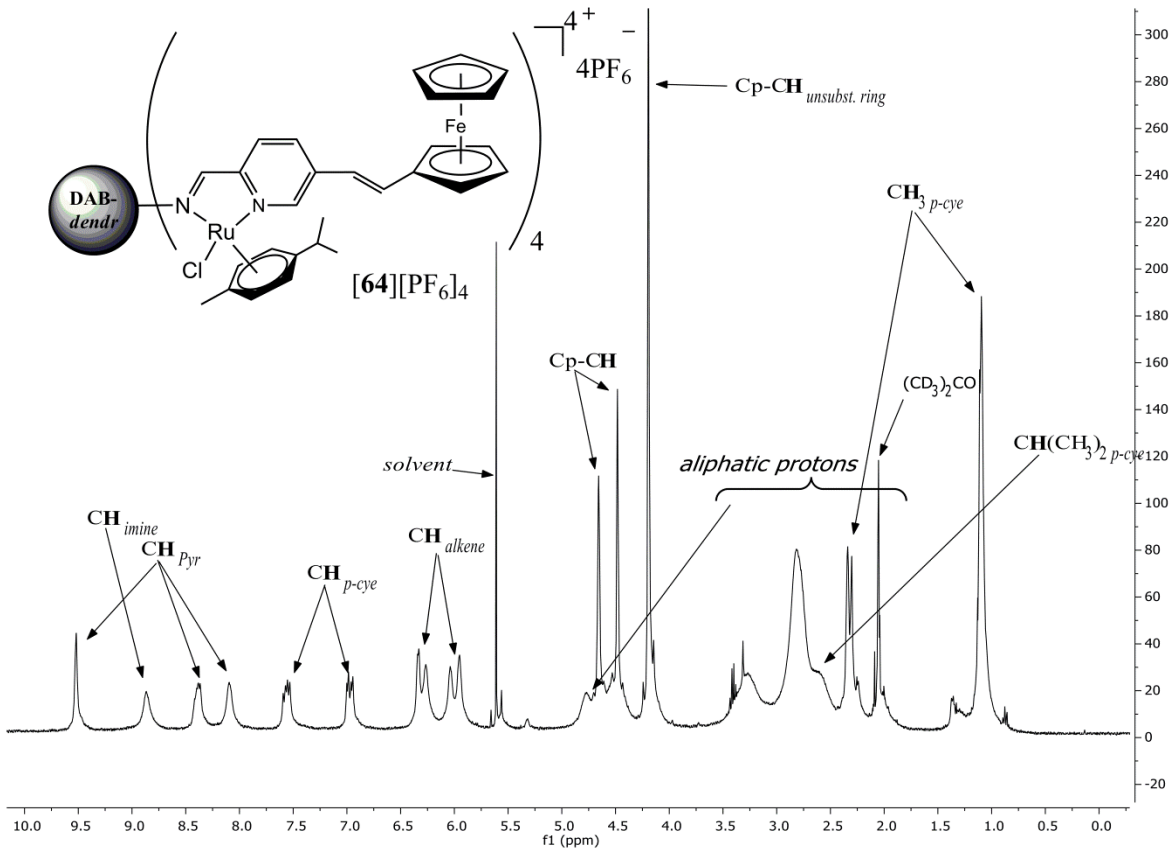

Figure 3.10 *^{1}H NMR spectrum for [DAB-**G$_1$**-PPI-{(η^6-p-cye)Ru((C$_6$H$_5$N$_2$)-κ^2-N,N)Cl-(5-ferrocenyl-vinyl)}$_4$][PF$_6$]$_4$ ([**64**][PF$_6$]$_4$) in (CD$_3$)$_2$CO.*

*^{1}H NMR spectra of N,N-Ru(II)-arene metallodendrimers ([**64**][PF$_6$]$_4$ & [**65**][PF$_6$]$_8$)*

Chirality induced by the ruthenium ion results in the appearance of two broad multiplets (4.4 - 4.8 ppm) assigned to the diastereotopic protons on the aliphatic carbon adjacent to the imine nitrogen for [**64**][PF$_6$]$_4$ (Figure 3.10) and [**65**][PF$_6$]$_8$. These broad multiplets overlap with the two broad doublets assigned to the protons on the substituted ferrocenyl functionality, with the protons on the un-substituted ferrocenyl functionality appear as a singlet at 4.2 ppm. Three multiplets at around 8.1, 8.4 and 9.5 ppm are assigned to the protons on the pyridyl ring, with the signals for the aromatic protons on the *p*-cymene ring appearing at ~6.0 ppm and ~6.3 ppm for [**64**][PF$_6$]$_4$ and [**65**][PF$_6$]$_8$.

The ^{31}P{^{1}H} NMR spectrum of [**62**][PF$_6$]$_4$ and [**63**][PF$_6$]$_8$ display a singlet at ~-32 ppm, suggesting a single phosphine species and further attests to the purity of the complexes. In addition, a high-field septet ~-144.0 ppm, assigned to the phosphorus atom of the PF$_6$ counter-ion, which couples to the six fluorine atoms with $^{1}J_{P\text{-}F}$ = 711 Hz. Similar splitting pattern and coupling constant are reported for other hexafluorophosphate salts.[62, 63]

The ^{13}C{^{1}H} NMR data for [**62**][PF$_6$]$_4$ - [**65**][PF$_6$]$_8$ were recorded in deuterated acetone with the expected number of signals for the carbon atoms observed. Furthermore, extra signals (due to the ruthenium-arene functionalization) for the carbon atoms of the *p*-cymene moiety are also observed for [**62**][PF$_6$]$_4$ - [**65**][PF$_6$]$_8$. In addition, metallodendrimers [**62**][PF$_6$]$_4$ and [**63**][PF$_6$]$_8$ display two singlets for the carbon atoms of the PTA ligand in the range of 51 - 72 ppm, confirming coordination to the ruthenium ion and displacement of the chlorido ligand.

3.5.2 Infrared Spectroscopy

Infrared data of metallodendrimers [**62**][PF$_6$]$_4$ - [**65**][PF$_6$]$_8$ were obtained using the ATR technique. Upon coordination of the ligand to the ruthenium ion, a distinct shift in the C=C$_{alkene}$ and C=N$_{imine}$ stretching vibration is observed from ~1613 cm^{-1} (for **56** & **57**) to ~1590 cm^{-1} (for [**62**][PF$_6$]$_4$ & [**63**][PF$_6$]$_8$). A similar shift to lower wavenumbers of the C=N$_{imine}$ stretching vibration for metallodendrimers [**64**][PF$_6$]$_4$ and [**65**][PF$_6$]$_8$, from ~1640 cm^{-1} (for **58** & **59**) to ~1625 cm^{-1}, is observed.

3.5.3 Elemental Analysis and Mass Spectrometry

Similarly observed for the dendritic ligands **56** - **59**, satisfactory elemental analysis was not obtained for [**62**][PF$_6$]$_4$ - [**65**][PF$_6$]$_8$, as percentages obtained were outside acceptable limits.

However, recalculation of the C, H and N percentages obtained for [**62**][PF_6]$_4$ - [**65**][PF_6]$_8$ with the inclusion of dichloromethane (reaction solvent, observed in the ^{1}H NMR spectrum, between 3 - 9 moles) resulted in percentages within acceptable limits.

In addition, HR-ESI mass spectrometry was also used to characterize metallodendrimers [**62**][PF_6]$_4$ - [**65**][PF_6]$_8$, with the spectral data listed in Table 3.2. The first-generation metallodendrimers [**62**][PF_6]$_4$ and [**64**][PF_6]$_4$ exhibited a base peak corresponding to a 6+ and 5+ charged ions respectively. Whilst the second-generation derivatives [**63**][PF_6]$_8$ and [**65**][PF]$_8$ depicted a multi-charged ion complex and a molecular ion peak in the mass spectrum respectively.

Table 3.2 *Mass spectral data for dendritic ligands [**62**][PF_6]$_4$ - [**65**][PF_6]$_8$.*

Compound	**MS (fragment, assignment) [*m*/*z*]**[a]
[**62**][PF_6]$_4$	628.1917 $[M+2H]^{6+}$ (where M = [**62**][PF_6]$_4$ - 4PF_6)
[**63**][PF_6]$_8$	247.1670 $[M+18H]^{26+}$ (where M = [**63**][PF_6]$_8$ - 8PF_6)
[**64**][PF_6]$_4$	649.1115 $[M+H]^{5+}$ (where M = [**64**][PF_6]$_4$ - 4PF_6)
[**65**][PF_6]$_8$	667.4059 $[M]^{8+}$ (where M = [**65**][PF_6]$_8$ - 8PF_6)

[a] HR-ESI-TOF-MS

3.5.4 Electrochemistry

The different σ-donating and π-accepting capacities of the dendritic ligands **56** - **59** influence the oxidation potentials of the Ru^{II} centres. Furthermore, these potentials provide insight on the basic character of the ligands in the complexes. Previous reports suggest, ligands that favour oxidation of the ferrocenyl moiety can produce reactive oxygen species, which have the ability to disrupt lipid membranes and in turn influence the antitumor activity of the complexes.[64-66] Hence, to investigate such possible correlations in the current systems and to provide further characterization of the complexes, the metallodendrimers [**62**][PF_6]$_4$ - [**65**][PF_6]$_8$ were studied by cyclic voltammetry at a Pt disc working electrode in acetonitrile, containing [*n*-Bu_4N][ClO_4] as the background electrolyte, a platinum wire auxiliary electrode and a Ag/Ag^+ reference electrode. A comparison of the relevant electrochemical data is given in Table 3.3.

Table 3.3 *Electrochemical data of metallodendrimers [**62**][PF_6]$_4$ - [**65**][PF_6]$_8$ and ferrocene (**Fc**).*

	Fe^{II} / Fe^{III}						
Compound	E_{pa} **[V]**	E_{pc} **[V]**	ΔE_p **[V]**[a]	$E_{1/2}$ **[V]**[b]	$\Delta E_{1/2}$ **[V]**[c]	i_{pa} / i_{pc}	E_{pa} **(Ru) [V]**
[**62**][PF_6]$_4$	0.16	n.o.	-	-	-	-	0.98
[**63**][PF_6]$_8$	0.17	n.o.	-	-	-	-	0.98
[**64**][PF_6]$_4$	0.23	0.15	0.08	0.19	0.07	1.14	n.o.
[**65**][PF_6]$_8$	0.22	0.15	0.07	0.19	0.07	1.46	n.o.
Fc	0.17	0.07	0.10	0.12	0	0.99	-

[a] $\Delta E_p = E_{pa} - E_{pc}$, where E_{pa} and E_{pc} are the anodic and cathodic peak potentials vs. Ag/AgCl respectively.
[b] $E_{1/2} = (E_{pa} + E_{pc})/2$
[c] $\Delta E_{1/2} = E_{1/2}$(Fc-compound) - $E_{1/2}$(Fc)
Electrochemical studies were measured in CH_3CN at a scan rate of 100 mVs^{-1} ([**62**][PF_6]$_4$ & [**63**][PF_6]$_8$) and 50 mVs^{-1} ([**64**][PF_6]$_4$ & [**65**][PF_6]$_8$), and referenced to Ag/Ag^+.
The $E_{1/2}$ potentials of [**62**][PF_6]$_4$ - [**65**][PF_6]$_8$ are quoted relative to ferrocene/ferrocenium couple of a sample containing only ferrocene.
n.o. = clear peak not observed.
[*n*-Bu_4N][ClO_4] was used as the background electrolyte.

The free ferrocene standard exhibits a one-electron reversible wave with $E_{1/2}$ = 0.12 V for Fc/Fc^+ couple relative to the Ag/Ag^+ reference electrode. First- and second-generation metallodendrimers display similar voltammetric behaviours in acetonitrile, and hence representative cyclic voltammograms are shown in Figure 3.11 and Figure 3.12 for the first-generation *N,O*-ruthenium-arene-PTA metallodendrimer [**62**][PF_6]$_4$ and *N,N*-ruthenium-arene-PTA metallodendrimer [**64**][PF_6]$_4$, respectively.

*Cyclic voltammograms of N,O-Ru(II)-arene-PTA metallodendrimers ([**62**][PF_6]$_4$ & [**63**][PF_6]$_8$)*

The redox potentials of [**62**][PF_6]$_4$ and [**63**][PF_6]$_8$ were measured at a scan rate of 100 mVs^{-1} and ferrocene was used as the internal standard. Both [**62**][PF_6]$_4$ (Figure 3.11, *bottom*) and [**63**][PF_6]$_8$ exhibit similar voltammograms with two irreversible waves in the positive region. The ferrocene oxidation ($Fe^{II} \rightarrow Fe^{III}$) wave appears at E_{pa} = 0.16 V and 0.17 V for [**62**][PF_6]$_4$ and [**63**][PF_6]$_8$ respectively. In principle, the more electron-donating groups coordinated to the metal centre, the more facile the oxidation and *vice versa*. Hence, a second redox event for the oxidation of the ruthenium centre ($Ru^{II} \rightarrow Ru^{III}$) appears at 0.98 V for both [**62**][PF_6]$_4$ and [**63**][PF_6]$_8$,[67] and is electrochemically irreversible, suggesting thermodynamic instability of the oxidation products.[68, 69]

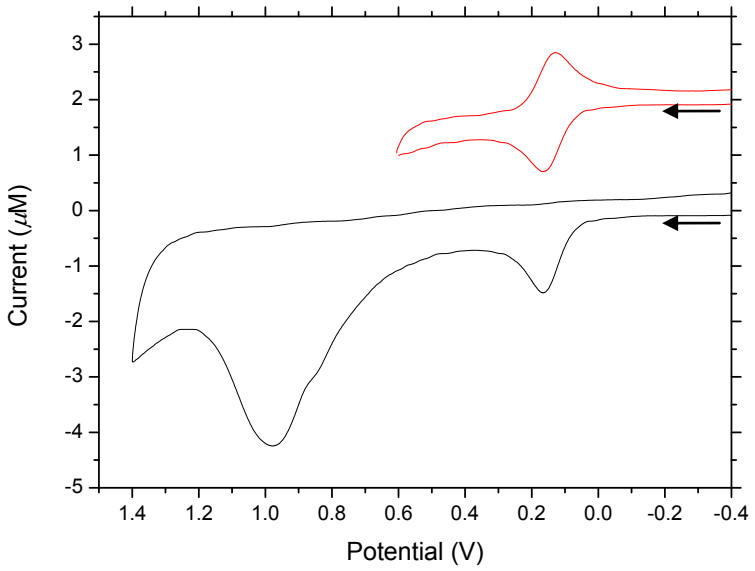

Figure 3.11 *Cyclic voltammogram of [**62**][PF_6]$_4$ showing a partial (top) and a full scan (bottom), as recorded in acetonitrile at a Pt disc-electrode (scan rate: 100 mVs^{-1}). The partial voltammogram is shifted by +2 μA to avoid overlap. [n-Bu_4N][ClO_4] was used as the background electrolyte.*

When scanned with the switching potential set just after the first oxidation wave, the reversible one-electron ferrocene/ferrocenium redox potential is observed for both [**62**][PF_6]$_4$ (Figure 3.11, *top*) and [**63**][PF_6]$_8$. Unlike other ruthenium-iron heterometallic systems,[34, 36, 68, 70-72] where an irreversible wave for the ruthenium centre and a reversible wave for the ferrocenyl moiety are common, here this is not observed. However, the electrochemical studies performed on the reported ruthenium-iron heterometallic systems found in the literature, were performed using different conditions (*i.e.* background electrolyte, reaction solvent and/or the compound counter-ion), and hence effect the oxidation/reduction processes compared. In the present study, the electrochemical data suggest oxidation of the ruthenium centre influences and prevents reduction of the ferrocenium species, resulting in two irreversible redox processes observed for [**62**][PF_6]$_4$ and [**63**][PF_6]$_8$.

*Cyclic voltammograms of N,N-Ru(II)-arene metallodendrimers ([**64**][PF_6]$_4$ & [**65**][PF_6]$_8$)*

The redox potentials of [**64**][PF_6]$_4$ and [**65**][PF_6]$_8$ were measured at a scan rate of 50 mVs^{-1} and are given versus the ferrocene couple. Due to the partial solubility of [**64**][PF_6]$_4$ and [**65**][PF_6]$_8$ in acetonitrile, a slower scan rate was chosen, as faster scan rates did not produce smooth cyclic voltammograms. The cyclic voltammogram for [**64**][PF_6]$_4$ (Figure 3.12) and [**65**][PF_6]$_8$ exhibit one reversible wave in the positive region and is assigned to the Fe^{II}/Fe^{III} couple.[36, 72]

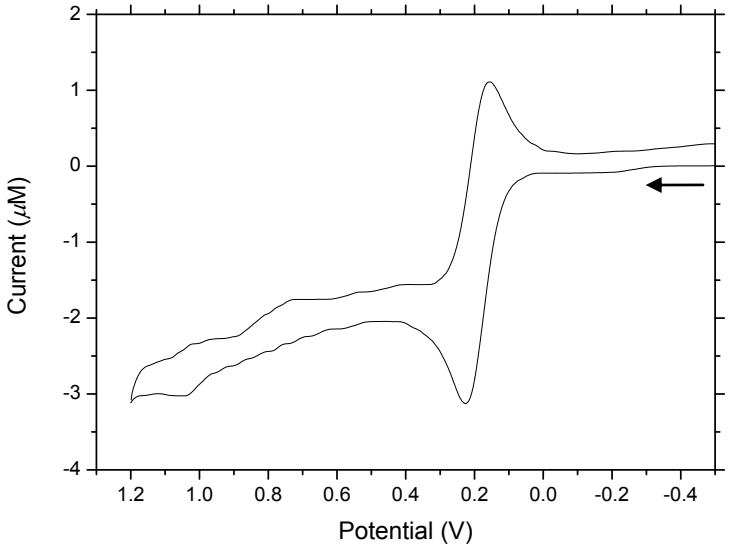

Figure 3.12 *Cyclic voltammogram of [**64**][PF_6]$_4$ showing a full scan, as recorded in acetonitrile at a Pt disc-electrode (scan rate: 50 mVs^{-1}). [n-Bu_4N][ClO_4] was used as the background electrolyte.*

Furthermore, current ratios (i_{pa}/i_{pc}) are close to unity suggesting these are one-electron redox potentials. However, there was no oxidation of Ru^{II} observed and is attributed to the electron withdrawing nature of the chlorido ligand, thereby lowering the electron density at the ruthenium centre, making the Ru-oxidation more difficult. As expected the ferrocene/ferrocenium redox potential of the first- and second-generation metallodendrimers [**64**][PF_6]$_4$ and [**65**][PF_6]$_8$ are nearly identical Table 3.3. In comparison to free ferrocene ($E_{1/2}$ = 0.12 V), the ferrocenyl moiety of [**64**[PF_6]$_4$ and [**65**][PF_6]$_8$ is more difficult to oxidize ($E_{1/2}$ = 0.19 V), and is attributed to the electron-withdrawing effects from the alkene moiety, the ruthenium centre and the overall positive charge of the complexes. This was similarly demonstrated for monosubstituted ferrocenyl-derived complexes containing electron-withdrawing groups bonded to the ferrocene ring.[73]

3.6 Synthesis and Characterization of Cationic Ferrocenyl-Derived *N,O*-Ru(II)-Arene-PTA and *N,N*-Ru(II)-Arene Mononuclear Complexes

In order to compare size dependency on the biological activity (discussed in Chapter 4), mononuclear derivatives [**66**][PF_6] and [**67**][PF_6] of the ferrocenyl-derived ruthenium-arene metallodendrimers were prepared. Two equivalents of the monomeric ligand **60** or **61** were reacted with one equivalent of the ruthenium-arene dimer [Ru(η^6-*p*-Pr^iC_6H_4Me)Cl_2]$_2$ by stirring at room temperature in an ethanol:dichloromethane (50:50 % *v*/*v*) (Scheme 3.7), in the presence of triethylamine (for preparation of [**66**][PF_6]). PTA was added to the reaction mixture containing the *N,O*-salicylaldiminato ligand **60**, which displaced the chlorido ligand and generated a cationic complex. The new mononuclear complexes [**66**][PF_6] and [**67**][PF_6] were isolated as orange and dark-purple hexafluorophosphate salts respectively, and have similar solubilities in polar solvents to their dendritic counterparts [**62**][PF_6]$_4$ - [**65**][PF_6]$_8$.

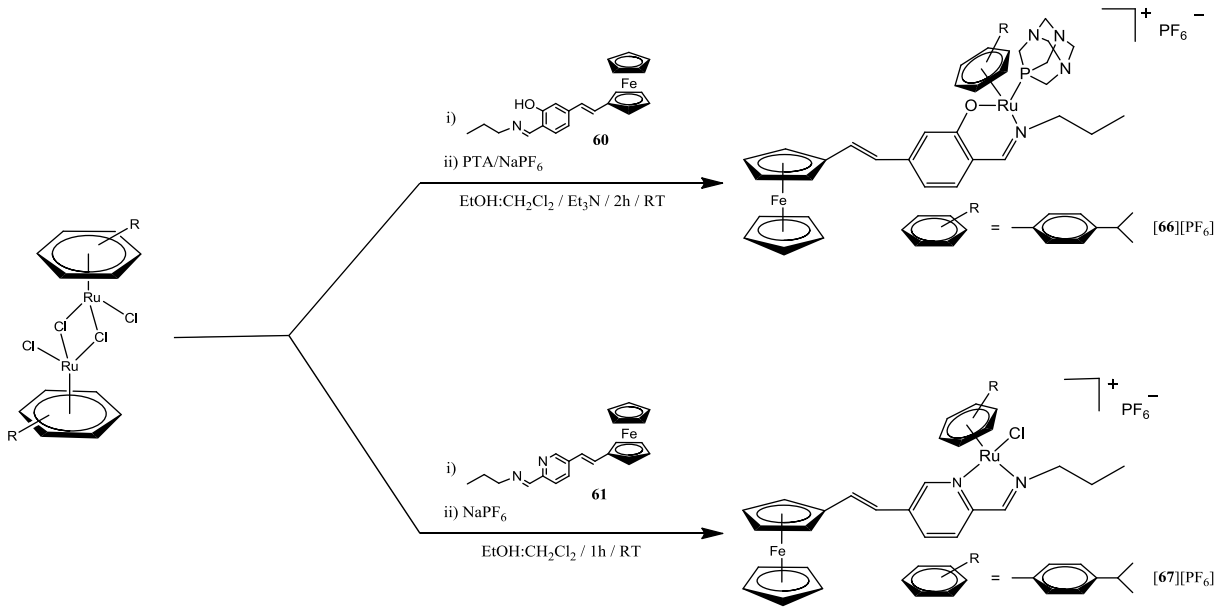

Scheme 3.7 *Synthesis of [$CH_3CH_2CH_2$-(η^6-p-cye)Ru((C_7H_5NO)-κ^2-N,O)PTA-(5-ferrocenyl-vinyl)][PF_6] [**66**][PF_6] and [$CH_3CH_2CH_2$-(η^6-p-cye)Ru(($C_6H_5N_2$)-κ^2-N,N)Cl-(5-ferrocenyl-vinyl)][PF_6] [**67**][PF_6].*

The two mononuclear complexes were characterized using a number of spectroscopic and analytical techniques.

3.6.1 ^{1}H, ^{31}P{^{1}H} and ^{13}C{^{1}H} NMR Spectroscopy

The ^{1}H NMR data of [**66**][PF_6] and [**67**][PF_6] were recorded in deuterated acetone. The ^{1}H NMR spectrum shows an upfield shift in the proton singlet assigned to the imine proton from ~8.3 ppm (for **60** & **61**) to ~8.1 ppm for [**66**][PF_6] (Figure 3.13) and a downfield shift to ~8.7 ppm for [**67**][PF_6] (Figure 3.14), suggesting coordination of the ligand to the ruthenium ion. Confirmation for the chiral nature of the molecule can be attributed to the appearance of two sets of multiplets (integrating for two protons per set) in the range of 2.0 - 2.1 ppm and 3.8 - 4.6 ppm, and are assigned to the diastereotopic protons on the propyl chain of [**66**][PF_6] and [**67**][PF_6]. Furthermore, the loss of 2-fold symmetry around the arene ring results in the methyl protons on the isopropyl group of the *p*-cymene moiety, to resonate as two doublets ($^{3}J_{HH}$ = 6.9 Hz) in the range of 1.1 - 1.3 ppm for [**66**][PF_6] and [**67**][PF_6]. The two doublets in the range of 6.6 - 7.6 ppm, with a coupling constant of $^{3}J_{HH}$ = 16.0 Hz, is assigned to the two protons on the alkene moiety. The protons on the un-substituted ferrocenyl ring resonates ~4.2 ppm as a singlet, whilst the protons on the monosubstituted Cp ring resonate as two doublets ($^{3}J_{HH}$ = 1.9 Hz) ~4.4 ppm and ~4.7 ppm for [**66**][PF_6] and [**67**][PF_6].

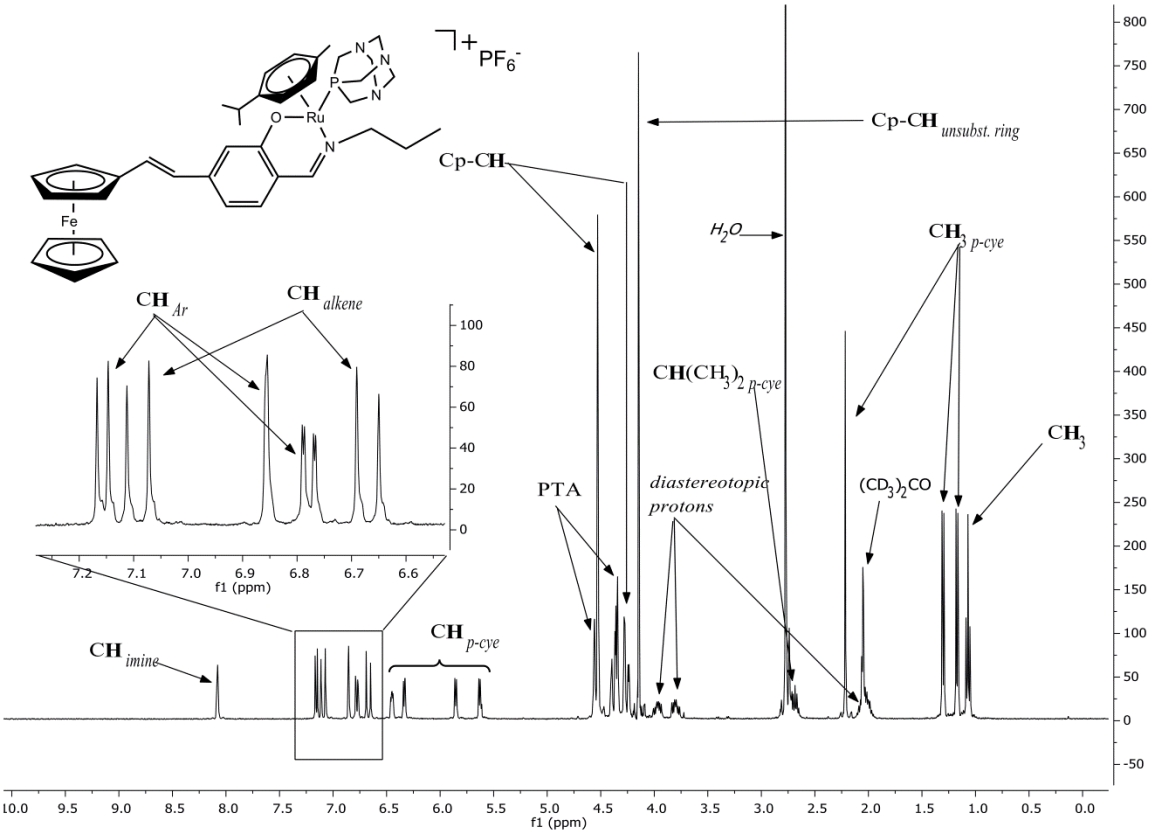

Figure 3.13 *^{1}H NMR spectrum for [$CH_3CH_2CH_2$-(η^6-p-cye)Ru((C_7H_5NO)-κ^2-N,O)PTA-(5-ferrocenyl-vinyl)][PF_6] [**66**][PF_6] in $(CD_3)_2CO$.*

*^{1}H NMR spectrum of N,O-Ru(II)-arene-PTA mononuclear complex [**66**][PF_6]*

The aromatic protons of [**66**][PF_6] appear as two doublets ($^3J_{HH}$ = 8.1 Hz) and one singlet, at ~6.9 ppm and ~7.2 ppm respectively. Due to the loss of two-fold symmetry around the arene ring, the four aromatic protons on the arene ring appear as three doublets (5.6 - 6.3 ppm) and one multiplet (~6.5 ppm). Similarly observed with the first- and second- generation derivatives ([**62**][PF_6]$_4$ & [**63**][PF_6]$_8$), protons on the PTA moiety display an AB-spin system, with two doublets and one singlet observed in the range 1.3 - 4.5 ppm. Furthermore, as a result of the chirality induced by the ruthenium metal centre, diastereotopic protons on the propyl chain are observed in the range of 3.8 - 4.0 ppm and 2.0 - 2.1 ppm.

*^{1}H NMR spectra of N,N-Ru(II)-arene mononuclear complex [**67**][PF_6]*

The pyridyl protons of [**67**][PF_6] appear as two doublets ($^3J_{HH}$ = 8.3 Hz) and one singlet, at ~8.1 ppm and ~9.6 ppm respectively. Once again, the diastereotopic protons of the CH_2 groups on the propyl chain are observed in the range of 4.4 - 4.6 ppm and 2.0 - 2.1 ppm.

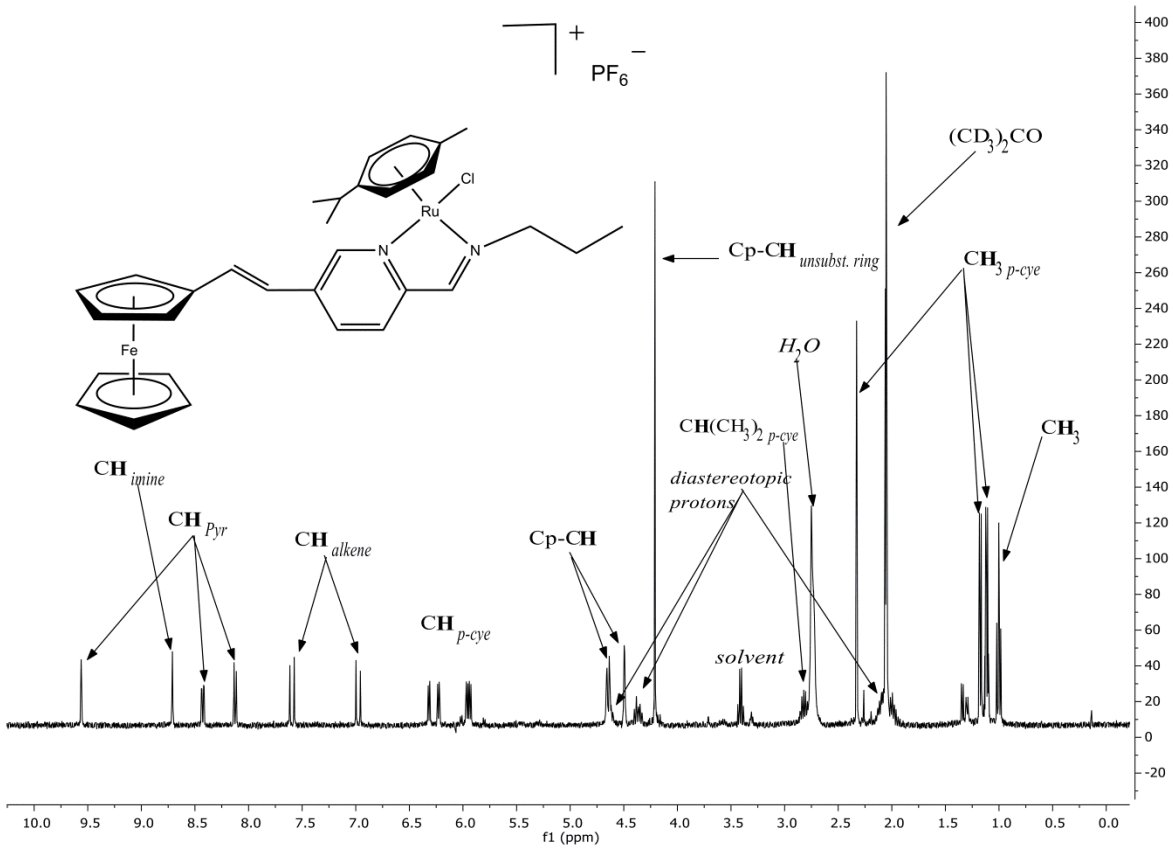

Figure 3.14 *^{1}H NMR spectrum for [$CH_3CH_2CH_2$-(η^6-p-cye)Ru(($C_6H_5N_2$)-κ^2-N,N)Cl-(5-ferrocenyl-vinyl)][PF_6] ([**67**][PF_6]) in $(CD_3)_2CO$.*

$^{31}P\{^{1}H\}$ NMR spectroscopy was used to confirm purity of [**66**][PF_6], as a singlet is observed at -33 ppm, suggesting a single coordinated phosphine species (PTA). Furthermore, similar values are observed for the first- and second- generation derivatives [**62**][PF_6]$_4$ and [**63**][PF_6]$_8$. A septet ($^{1}J_{P\text{-}F}$ = 707.7 Hz) is observed ~-144 ppm for both complexes and is assigned to the phosphine atom on the hexafluorophosphate counter-ion.

$^{13}C\{^{1}H\}$ NMR spectral data for [**66**][PF_6] and [**67**][PF_6] display the expected number of signals for the proposed structure. In particular, the imine carbon signal shifts downfield from ~164 ppm (for **60**) and ~162 ppm (for **61**) to ~166 ppm for both [**66**][PF_6] and [**67**][PF_6].

3.6.2 Infrared Spectroscopy

The infrared spectrum for [**66**][PF_6] and [**67**][PF_6] displays a stretching vibration for the C=C_{alkene} at ~1587 cm^{-1}. Similarly observed for the first- and second- generation derivatives ([**62**][PF_6]$_4$ - [**65**][PF_6]$_8$), the C=N_{imine} stretching vibration appears ~1619 cm^{-1} and ~1625 cm^{-1} for [**66**][PF_6] and [**67**][PF_6] respectively.

3.6.3 Mass Spectrometry and HPLC

The HR-ESI mass spectral data for [**66**][PF_6] (Figure 3.15) and [**67**][PF_6], confirm the proposed structures, as both display a base peak for the molecular ion at *m*/*z* = 765.1958 and at *m*/*z* = 629.0955 respectively.

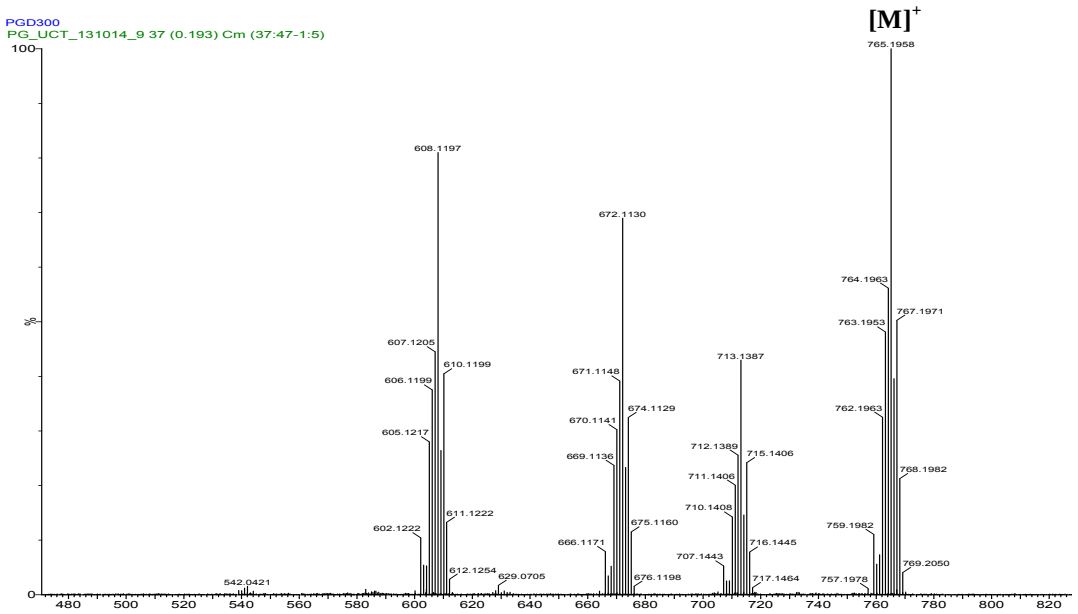

Figure 3.15 *HR-ESI-TOF mass spectrum for [$CH_3CH_2CH_2$-(η^6-p-cye)Ru((C_7H_5NO)-κ^2-N,O)PTA-(5-ferrocenyl-vinyl)][PF_6] [**66**][PF_6].*

Analytical-HPLC traces were obtained for [**66**][PF_6] and [**67**][PF_6], with single peaks observed at t_R = ~16 min, and attests to the purity of the mononuclear complexes.

3.6.4 Electrochemistry

The redox potentials of [**66**][PF_6] and [**67**][PF_6] were measured at a scan rate of 100 mVs^{-1} and 50 mVs^{-1} respectively, and ferrocene was used as the internal standard. Electrochemical data of [**66**][PF_6] and [**67**][PF_6] are listed in Table 3.4.

Table 3.4 *Electrochemical data of mononuclear complexes [**66**][PF_6], [**67**][PF_6] and ferrocene (**Fc**).*

	Fe^{II} / Fe^{III}						
Compound	E_{pa} **[V]**	E_{pc} **[V]**	ΔE_p **[V]**[a]	$E_{1/2}$ **[V]**[b]	$\Delta E_{1/2}$ **[V]**[c]	i_{pa} / i_{pc}	E_{pa} **(Ru) [V]**
[**66**][PF_6]	0.18	n.o.	-	-	-	-	0.97
[**67**][PF_6]	0.23	0.16	0.07	0.20	0.08	0.98	n.o.
Fc	0.17	0.07	0.1	0.12	0	0.99	-

[a] $\Delta E_p = E_{pa} - E_{pc}$, where E_{pa} and E_{pc} are the anodic and cathodic peak potentials vs. Ag/AgCl respectively.
[b] $E_{1/2} = (E_{pa} + E_{pc})/2$
[c] $\Delta E_{1/2} = E_{1/2}$(Fc-compound) - $E_{1/2}$(Fc)
Electrochemical studies were measured in CH_3CN at a scan rate of 100 mVs^{-1} ([**62**][PF_6]$_4$ & [**63**][PF_6]$_8$) and 50 mVs^{-1} ([**64**][PF_6]$_4$ & [**65**][PF_6]$_8$), and referenced to Ag/Ag^+.
The $E_{1/2}$ potentials of [**62**][PF_6]$_4$ - [**65**][PF_6]$_8$ are quoted relative to ferrocene/ferrocenium couple of a sample containing only ferrocene.
n.o. = clear peak not observed.
[*n*-Bu_4N][ClO_4] was used as the background electrolyte.

*Cyclic voltammograms of N,O-Ru(II)-arene-PTA mononuclear complex [**66**][PF_6] and N,N-Ru(II)-arene mononuclear complex [**67**][PF_6]*

The cyclic voltammogram for [**66**][PF_6] (Figure 3.16, *bottom*) shows two irreversible waves at E_{pa} = 0.18 V and 0.97 V for the oxidation of the ferrocenyl moiety and the ruthenium centre respectively, and is attributed to the thermodynamic instability of the oxidation products.[68, 69] Setting the switching potential just after the first oxidation wave (E_{pa} = 0.18 V) and re-scanning, results in a reversible one-electron ferrocene/ferrocenium redox potential for [**66**][PF_6] (Figure 3.16, *top*), similarly observed with metallodendrimers [**62**][PF_6]$_4$ and [**63**][PF_6]$_8$. Two shoulder peaks are observed in the cyclic voltammogram for [**66**][PF_6], which are not assigned, at ~0.88 V (full scan) and at ~0.45 V (partial scan).

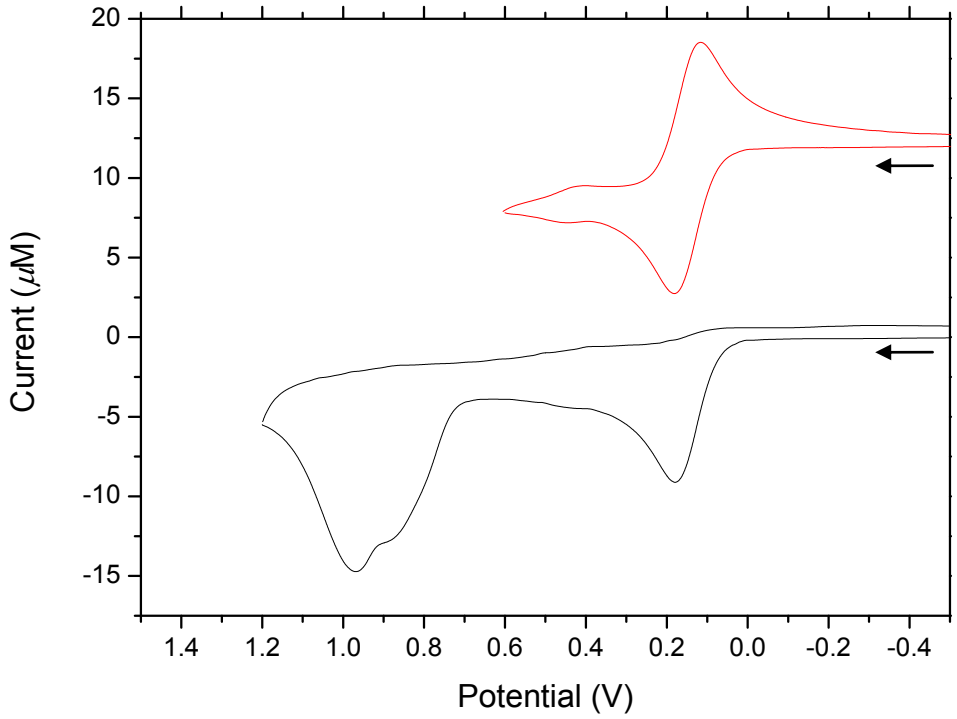

Figure 3.16 *A partial (top) and full (bottom) cyclic voltammogram of [**66**][PF_6] as recorded in acetonitrile at a Pt disc-electrode (scan rate:100 mVs^{-1}). The partial voltammogram is shifted by +12 μA to avoid overlap. [n-Bu_4N][ClO_4] was used as the background electrolyte.*

Whilst the cyclic voltammogram for [**67**][PF_6] (Figure 3.17) exhibits one reversible wave ($E_{1/2}$ = 0.20 V) and is assigned to the Fe^{II}/Fe^{III} couple.[36, 72] No oxidation of the ruthenium centre was observed in the cyclic voltammogram of [**67**][PF_6]. This is attributed to the electron-withdrawing nature of the chlorido ligand, making it difficult to oxidize the metal centre. As expected, both [**66**][PF_6] and [**67**][PF_6], exhibit similar cyclic voltammograms and wave potentials compared to their dendritic counterparts [**62**][PF_4]$_4$ - [**65**][PF_6]$_8$.

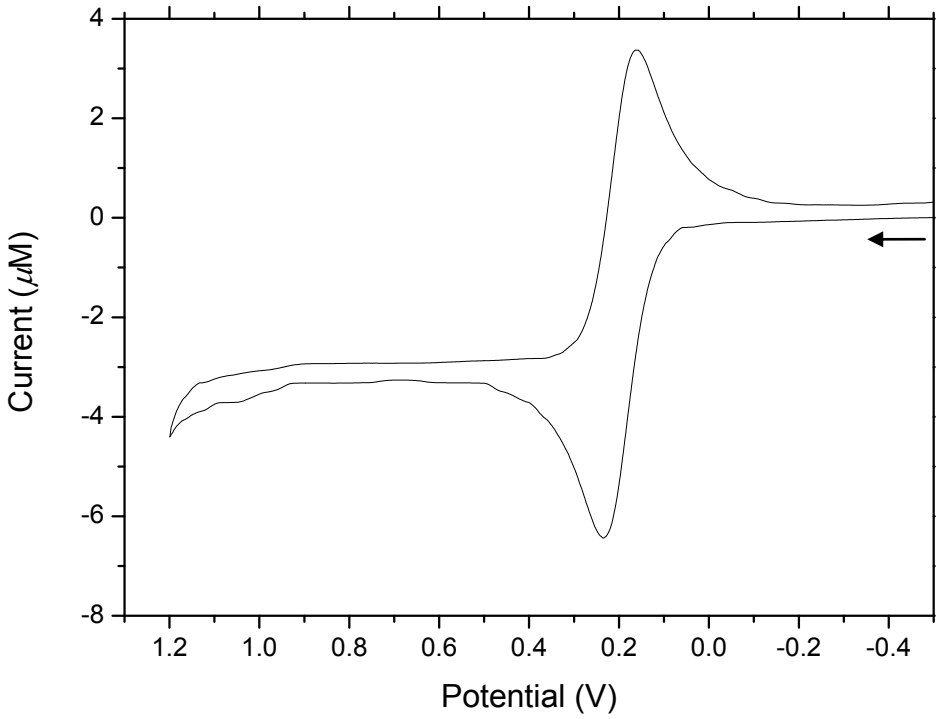

Figure 3.17 *Full cyclic voltammogram of [**67**][PF_6] as recorded in acetonitrile at a Pt disc-electrode (scan rate: 50 mVs^{-1}). [n-Bu_4N][ClO_4] was used as the background electrolyte.*

3.6.5 X-ray Crystallography

The molecular structure of the mononuclear complex [**66**][PF_6] was elucidated by a single-crystal X-ray diffraction. Crystals were grown by slow evaporation of a solution of [**66**][PF_6] in acetone, and crystallized in the monoclinic space group *P* 2_1/c. ORTEP drawing for the solvate [**66**][PF_6]·H_2O is shown in Figure 3.18, with the ferrocene adopting an eclipsed confirmation and the *E*-conformation of the vinylic carbon-carbon double bond is further confirmed. The ruthenium atom of [**66**][PF_6] is coordinated to the nitrogen and the oxygen atoms of the Schiff base ligand, to the phosphorus atom of the PTA ligand and to the η^6-*p*-cymene ligand, thus leading to a typical pseudo-tetrahedral or "piano-stool" conformation. Crystallographic details can be found in Chapter 6, summarized in Table 6.3.

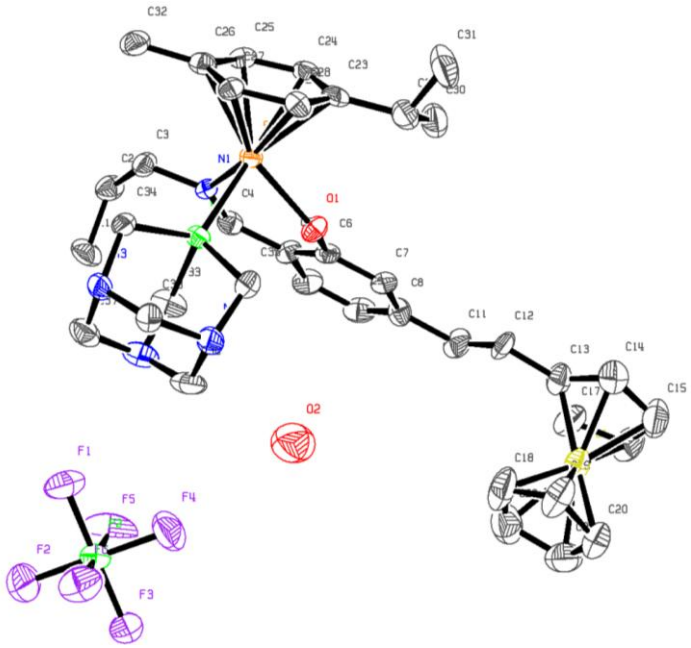

Figure 3.18 *ORTEP representations of mononuclear solvate cation [**66**][PF_6]·H_2O. Thermal ellipsoids are drawn at the 50 % probability level. Hydrogen atoms have been omitted for clarity.*

Selected geometric data for [**66**][PF_6]·H_2O are listed in Table 3.5. The average distance between the ruthenium and carbon atoms of the η^6-*p*-cymene ring is 1.73 Å, comparable to the mononuclear ruthenium-arene analogs [**38**][PF_6] and [**39**][PF_6] mentioned in Chapter 2, and that of related ruthenium-*p*-cymene complexes reported in the literature.[74] The Ru-P distance in [**66**][PF_6] is comparable to that observed in analogous ruthenium-arene-PTA compounds.[75, 76]

Table 3.5 *Selected average bond lengths and bond angles in [**66**][PF_6]·H_2O.*

	[**66**][PF_6]·H_2O
	interatomic distances (Å)
Ru1-N1	2.096(5)
Ru1-O1	2.068(5)
Ru1-P1	2.305(2)
C4-C5	1.46(1)
C4-N1	1.273(8)
N1-C3	1.48(1)
C11-C12	1.33(1)
Ru–centroid	~1.730
	[**66**][PF_6]·H_2O
	angles (°)
N1-Ru1-O1	87.5(2)
N1-Ru1-P1	86.8(1)
O1-Ru1-P1	80.5(1)
C5-C4-N1	127.2(6)
C4-N1-C3	119.2(6)
C11-C12-C13	125.1(8)
C8-C11-C12	126.5(7)

A study of their *in vitro* antitumor activity has been undertaken and the results are discussed in Chapter 4.

3.7 Overall Summary

New cationic *N*,*O*- and *N*,*N*- ferrocenyl-derived ruthenium-arene metallodendrimers have been successfully synthesized from new ferrocenyl-derived conjugates. All complexes were characterized using an array of spectroscopic and analytical techniques, which confirmed formation of the desired compounds. Their mononuclear analogs were prepared and characterized. Electrochemical studies were performed, revealing that the *N*,*O*-Ru(II)-arene-PTA complexes result in two irreversible redox processes (oxidation of the Fe^{II} & Ru^{II} centres), whilst the *N*,*N*-Ru(II)-arene complexes display one reversible wave (Fe^{II}/Fe^{III}-couple) in the positive region. Single crystal X-ray diffraction was utilized to further confirm the proposed structures and illustrate the mode of coordination, through *N*,*O*- and *N*,*N*-donor atoms.

3.8 References

1. N. Lease, V. Vasilevski, M. Carreira, A. de Almeida, M. Sanau, P. Hirva, A. Casini and M. Contel, *J. Med. Chem.*, 2013, **56**, 5806-5818.
2. M. P. Donzello, E. Viola, C. Ercolani, Z. Fu, D. Futur and K. M. Kadish, *Inorg. Chem.*, 2012, **51**, 12548-12559.
3. J. F. Gonzalez-Pantoja, M. Stem, A. A. Jarzecki, E. Royo, E. Robles-Escajeda, A. Varela-Ramirez, R. J. Aguilera and M. Contel, *Inorg. Chem.*, 2011, **50**, 11099-11110.
4. F. Pelletier, V. Comte, A. Massard, M. Wenzel, S. Toulot, P. Richard, M. Picquet, P. Le Gendre, O. Zava, F. Edafe, A. Casini and P. J. Dyson, *J. Med. Chem.*, 2010, **53**, 6923-6933.
5. M. Wenzel, B. Bertrand, M. J. Eymin, V. Comte, J. A. Harvey, P. Richard, M. Groessl, O. Zava, H. Amrouche, P. D. Harvey, P. Le Grande, M. Picquet and A. Casini, *Inorg. Chem.*, 2011, **50**, 9472-9480.
6. K. Heinze and H. Lang, *Organometallics*, 2013, **32**, 5623-5625.
7. D. R. van Staveren and N. Metzler-Nolte, *Chem. Rev.*, 2004, **104**, 5931-5985.
8. M. F. R. Fouda, M. M. Abd-Elzaher, R. A. Abdelsamaia and A. A. Labib, *Appl. Organomet. Chem.*, 2006, **21**, 613-625.
9. S. S. Braga and A. M. S. Silva, *Organometallics*, 2013, **32**, 5626-5639.
10. P. Pigeon, S. Top, A. Vessières, M. Huché, E. A. Hillard, E. Salmon and G. Jaouen, *J. Med. Chem.*, 2005, **48**, 2814-2821.
11. A. Vessières, S. Top, W. Beck, E. A. Hillard and G. Jaouen, *Dalton Trans.*, 2006, **4**, 529-541.
12. L. V. Popova, V. N. Babin, Y. A. Belousov, Y. S. Nekrasov, A. E. Snegueva, N. P. Borodina, G. M. Shaposhnikova, O. B. Bychenko and P. M. Raevskii, *Appl. Organomet. Chem.*, 1993, **7**, 85-94.
13. P. Köpf-Maier, H. Köpf and E. W. Neuse, *J. Cancer. Res. Clin.*, 1984, **108**, 336-340.
14. A. Nguyen, A. Vessieres, E. A. Hillard, S. Top, P. Pigeon and G. Jaouen, *Chimia*, 2007, **61**, 716-724.
15. S. Top, A. Vessières, C. Cabestaing, I. Laios, G. Leclereq, C. Provot and G. Jaouen, *J. Organomet. Chem.*, 2001, **637-639**, 500-506.
16. E. A. Hillard, A. Vessières, F. Le Bideau, D. Plazul, D. Spera, M. Huché and G. Jaouen, *Chem. Med. Chem.*, 2006, **1**, 551-559, and references therein.
17. P. Wardman and L. P. Candeias, *Radiat. Res.*, 1996, **145**, 523-531.

18. B. Lal, A. Badshah, A. A. Altaf, N. Khan and S. Ullah, *Appl. Organomet. Chem.*, 2011, **25**, 843-855.
19. C. Biot, G. Glorian, L. A. Maciejewski, J. S. Brocard, O. Domarle, G. Blampain, P. Millet, A. J. Georges, H. Abessolo, D. Dive and J. Lebibi, *J. Med. Chem.*, 1997, **40**, 3715-3718.
20. C. Biot, L. Delhaes, C. M. N. Diaye, L. A. Maciejewski, D. Camus, D. Dive and J. S. Brocard, *Bioorg. Med. Chem.*, 1999, **7**, 2843-2847.
21. C. Biot, L. Delhaes, D. Tarmelli, I. Forfar-Bares, L. A. Maciejewski, M. Boyce, G. Nowogrocki, J. S. Brocard, N. Basilico, P. Olliaro and T. J. Egan, *Mol. Pharm.*, 2005, **2**, 185-193.
22. L. Delhaes, C. Biot, L. Berry, P. Delcourt, L. A. Maciejewski, D. Camus, J. S. Brocard and D. Dive, *Chem. Bio. Chem.*, 2002, **3**, 418-423.
23. D. I. Edwards, R. Epton and G. Marr, *J. Organomet. Chem.*, 1975, **85**, C23-C25.
24. D. I. Edwards, R. Epton and G. Marr, *J. Organomet. Chem.*, 1976, **122**, C49-C53.
25. D. I. Edwards, R. Epton and G. Marr, *J. Organomet. Chem.*, 1979, **168**, 259-272.
26. J. Schulz, J. Tauchman, I. Císařová, T. Riedel, P. J. Dyson and P. Stěpnička, *J. Organomet. Chem.*, 2014, **751**, 604-609.
27. H. Goitia, Y. Nieto, D. Villacampa, C. Kasper, A. Laguna and C. Gimeno, *Organometallics*, 2013, **32**, 6069-6078.
28. J. Rajput, J. R. Moss, A. T. Hutton, D. T. Hendricks, C. E. Arendse and C. Imrie, *J. Organomet. Chem.*, 2004, **689**, 1553-1568.
29. M. Gordon and S. Hollander, *J. Med. Chem.*, 1993, **24**, 209-265.
30. M. J. Clarke, F. C. Zhu and D. R. Frasca, *Chem. Rev.*, 1999, **99**, 2511-2533.
31. A. L. Noffke, A. Habtemariam, A. M. Pizarro and P. J. Sadler, *Chem. Commun.*, 2012, **48**, 5219-5246.
32. G. Süss-Fink, *Dalton Trans.*, 2010, **39**, 1673-1688.
33. W. H. Ang, A. Casini, G. Sava and P. J. Dyson, *J. Organomet. Chem.*, 2011, **696**, 989-998.
34. J. Tauchman, G. Süss-Fink, P. Štěpnička, O. Zava and P. J. Dyson, *J. Organomet. Chem.*, 2013, **723**, 233-238.
35. M. Auzias, J. Gueniat, B. Therrien, G. Süss-Fink, A. K. Renfrew and P. J. Dyson, *J. Organomet. Chem.*, 2009, **694**, 855-861.
36. M. Auzias, B. Therrien, G. Süss-Fink, P. Štěpnička, W. H. Ang and P. J. Dyson, *Inorg. Chem.*, 2008, **47**, 578-583.

37. C. Ornelas, *New J. Chem.*, 2011, **35**, 1973-1985.
38. F. S. Arimoto and A. C. J. Haven, *J. Am. Chem. Soc.*, 1955, **77**, 6295-6297.
39. M. Gallei, R. Klein and M. Rehahn, *Macromolecules*, 2010, **43**, 1844-1854.
40. W.-Y. Liu, Q.-H. Xu, Y.-X. Ma, Y.-M. Liang, N.-L. Dong and D.-P. Guan, *J. Organomet. Chem.*, 2001, **625**, 128-131.
41. A. Sonoda, I. Moritani, T. Saraie and T. Wada, *Tetrahedron Lett.*, 1969, 2943-2946.
42. M. I. Reyes, R. A. Vazquez Gracia, T. Klimova, E. Klimova, L. Ortiz-Frade and M. Matinez Gracia, *Inorg. Chim. Acta*, 2008, **361**, 1597-1605.
43. R. F. Heck, in *Comprehensive Organic Synthesis*, eds. B. M. Trost and I. Flemming, Oxford, New York, 1991, vol. 4.
44. A. De Meijere and F. E. Meyer, *Angew. Chem., Int. Ed. Engl.*, 1994, **33**, 2379-2411.
45. G. T. Crisp, *Chem. Soc. Rev.*, 1998, **27**, 427-436.
46. W. Cabri, I. Candiani, A. Bedeschi and R. Santi, *J. Org. Chem.*, 1992, **57**, 3558-3563.
47. W. Cabri, I. Candiani, S. De Bernardinis, F. Francalanci and S. Penco, *J. Org. Chem.*, 1991, **56**, 5796-5800.
48. S. C. Stinson, *Chem. Eng. News*, 1999, **18**, 81.
49. L. M. Jarvis, *Chem. Eng. News*, 2006, **84**, 14.
50. A. F. Littke and G. C. Fu, *Org. Synth.*, 2005, **81**, 63-71.
51. S. P. Dudek, H. D. Sikes and C. E. D. Chidsey, *J. Am. Chem. Soc.*, 2001, **123**, 8033-8038.
52. E. Turac, E. Sahmetlioglu, A. Demircan and L. Toppare, *J. Appl. Polym. Sci.*, 2012, **126**, 808-814.
53. E. G. Morales-Espinoza, K. E. Sanchez-Montes, E. Klimova, E. Klimova, I. V. Lijanova, J. L. Maldonado, G. Ramos-Ortiz, S. Hernandez-Ortega and M. Martinez-Gracia, *Molecules*, 2010, **15**, 2564-2575.
54. C. Amatore, S. Gazard, E. Maisonhaute, C. Pebay, B. Schollhorn, J.-L. Syssa-Magale and J. D. Wadhawan, *Eur. J. Inorg. Chem.*, 2007, 4035-4042.
55. A. de Meijere and F. Diederich, *Metal-Catalyzed Cross-Coupling Reactions*, Wiley-VCH, Weinheim, 2004.
56. Y.-F. Yang, Y. Chen, T. Xie and Y.-M. Liang, *Synth. Commun.*, 2002, **32**, 2627-2631.
57. M. Kurihara, H. Sano, M. Murata and H. Nishihara, *Inorg. Chem. Commun.*, 2001, **40**, 4-5.
58. D. H. Williams and I. Fleming, in *Spectroscopic Methods in Organic Chemistry*, McGraw-Hill Book Company Ltd., United Kingdom, 1989, Table 3.27.

59. J. F. G. A. Jansen, E. M. E. de Brabander-van den Berg and E. W. Meijer, *Science*, 1994, **266**, 1226-1269.
60. P. Smolenski, F. P. Pruchnik, Z. Ciunik and T. Lis, *Inorg. Chem.*, 2003, **42**, 3318-3322.
61. F. P. Pruchnik, P. Smolenski, E. Galdecka and Z. Galdecki, *New J. Chem.*, 1998, **22**, 1395-1398.
62. S. C. Peake, M. Fild, M. J. C. Hewson and R. Schmutzler, *Inorg. Chem.*, 1971, **10**, 2723-2727.
63. G. R. Miller, H. A. Resing, F. L. Vogel, A. Pron, T. C. Wy and D. Billaud, *J. Phys. Chem.*, 1980, **84**, 3333-3335.
64. N. Chavian, H. Vezin, D. Dive, N. Touati, J. F. Paul, E. Buisine and C. Biot, *Mol. Pharm.*, 2008, **5**, 710-716.
65. F. Dubar, S. Bohic, C. Slomianny, J. C. Morin, P. Thomas, H. Kalamou, Y. Guerardel, P. Cloetens, J. Khalife and C. Biot, *Chem. Commun.*, 2012, **48**, 910-912.
66. C. Biot, W. Castro, C. Y. Botte and M. Navarro, *Dalton Trans.*, 2012, **41**, 6335-6349.
67. L. C. Matsinha, P. Malatji, A. T. Hutton, G. A. Venter, S. F. Mapolie and G. S. Smith, *Eur. J. Inorg. Chem.*, 2013, 4318-4326.
68. J. Tauchman, B. Therrien, G. Süss-Fink and P. Štěpnička, *Organometallics*, 2012, **31**, 3985-3994.
69. J.-F. Mai and Y. Yamamoto, *J. Organomet. Chem.*, 1998, **560**, 223-232.
70. P. Štěpnička and R. Gyepes, *Organometallics*, 1997, **16**, 5089-5095.
71. T. Sixt, M. Sieger, M. J. Krafft, D. Bubrin, J. Fiedler and W. Kaim, *Organometallics*, 2010, **29**, 5511-5516.
72. B. Therrien, L. Vieille-Petit, J. Jeanneret-Gris, P. Štěpnička and G. Süss-Fink, *J. Organomet. Chem.*, 2004, **689**, 2456-2463.
73. C. Lopez, R. Bosque, S. Perez, A. Roig, E. Molins, X. Solans and M. Font-Bardia, *J. Organomet. Chem.*, 2006, **691**, 475-484.
74. P. Govender, A. K. Renfrew, C. M. Clavel, P. J. Dyson, B. Therrien and G. S. Smith, *Dalton Trans.*, 2011, **40**, 1158-1167.
75. A. K. Renfrew, A. D. Phillips, E. Tapavicza, R. Scopelliti, U. Rothlisberger and P. J. Dyson, *Organometallics*, 2009, **28**, 5061-5071.
76. W. H. Ang, E. Daldini, C. Scolaro, R. Scopelliti, L. Juillerat-Jeanneret and P. J. Dyson, *Inorg. Chem.*, 2006, **45**, 9006-9013.

Chapter 4

Biological Evaluation of Ruthenium, Osmium and Ferrocenyl-Derived Metallodendrimers

This chapter forms part of the following publications:

Preshendren Govender, L. C. Sudding, C. M. Clavel, P. J. Dyson, B. Therrien and G. S. Smith, **The Influence of RAPTA Moieties on the Antiproliferative Activity of Peripheral-Functionalized Poly(salicylaldiminato) Metallodendrimers,** *Dalton Transactions*, 2013, 42, 1267-1277.

Preshendren Govender, F. Edafe, B. C. E. Makhubela, P. J. Dyson, B. Therrien and G. S. Smith, **Neutral and Cationic Osmium(II)-Arene Metallodendrimers: Synthesis, Characterization and Anticancer Activity,** *Inorganica Chimica Acta*, 2014, 409, 112-120.

4.1 Introduction

Drug resistance, side-effects and toxicity are major disadvantages of Pt-based anticancer agents, and hence studies towards the use of other platinum-group metals for effective therapeutic agents were persued.[1, 2] Ruthenium(III) complexes, namely NAMI-A {H_2Im[*trans*-$RuCl_4$(DMSO)(Him)] (Him = imidazole)}[3] and KP1019 {H_2Ind[*trans*-$RuCl_4(Hind)_2$] (Hind = indazole),[4, 5] have shown promise in phase I clinical trials, with the former NAMI-A active against solid metastases and currently in a phase II study. The latter, KP1019, displays superior activity against metastasis and primary tumors, and in particular towards colorectal tumors. However, it has been suggested that the activity of these Ru(III) prodrugs is brought about by *in vivo* reduction into the activated Ru(II) species.[6] This has triggered the development of half-sandwich organometallic ruthenium(II)-arene complexes for the exploration as anticancer agents. Furthermore, due to their structural diversity, such as the hydrophobic arene ring (which facilitates diffusion of the drug through the cell membrane) and the various bonding modes (where the remaining coordination sites are usually occupied by mono-, bi-, or tri-dentate ligands) offer these complexes diverse biological properties. A host of derivatives have been synthesized which include incorporation of paullones,[7, 8] pyr(id)ones,[9] ethylenediamine (en),[10, 11] or 1,3,5-triaza-7-

phosphatricyclo-[3.3.1.1.]decane (PTA),[12, 13] to the ruthenium-arene coordination sphere, with all the complexes displaying moderate to potent *in vitro* antitumor activity.

RAPTA compounds of general formula [(η^6-arene)Ru(PTA)Cl_2] (Figure 4.1), display activity against the TS/A mouse adenocarcinoma cancer cell line, and no selectivity towards HBL-100 human mammary cells.[14] The RAPTA compounds display moderate activity, but are very effective *in vivo* against metastatic[14] and primary tumors.[15] Furthermore, the activity of the RAPTA compounds are comparable to the Ru(III)-anticancer drug NAMI-A. Ruthenium-arene-metronidazole complex [(η^6-C_6H_6)Ru(metronidazole)Cl_2] (where metronidazole is used in the treatment of rosacea, a dermatological condition), was the first of its kind to combine organometallic ruthenium with a bioactive ligand (Figure 4.1).[16] This type of structure-activity relationship has been explored by Keppler and co-workers, where paullones, which are known inhibitors of cyclin-dependent kinases and glycogen synthase kinase-3, have been coupled with organometallic ruthenium (Figure 4.1).[7] These complexes display high antiproliferative activity in three cell lines, making them potential candidates as metal-based anticancer drugs.

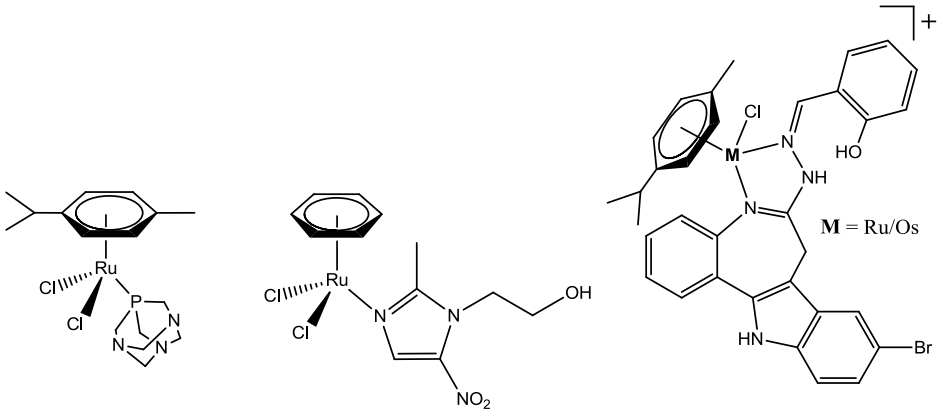

RAPTA-C **[(η^6–C_6H_6)Ru(metronidazole)Cl_2]** **[(*p*-cymene)M(paullone)Cl]Cl**

Figure 4.1 *Structures of organometallic ruthenium-arene complexes of interest as anticancer agents.*[7, 14, 16]

Since the discovery of the trinuclear platinum-based anticancer drug, BBR3464 [*trans*, *trans*, *trans*-$(NH_3)_2$-Pt(Cl)$(CH_2)_6NH_2$Pt$(NH_3)_2NH_2(CH_2)_6NH_2$Pt-$(NH_3)_2$(Cl)][NO_3]$_4$ (Figure 4.2),[17] the concept of multinuclearity has not been extensively explored towards development of new anticancer agents.[18, 19] Remarkably, tethering RAPTA-type complexes to macromolecules such as proteins, significantly increases their cytotoxicity.[20, 21] Consequently, there is growing

interest in the development of multinuclear ruthenium(II) complexes as potential anticancer agents.[18, 19]

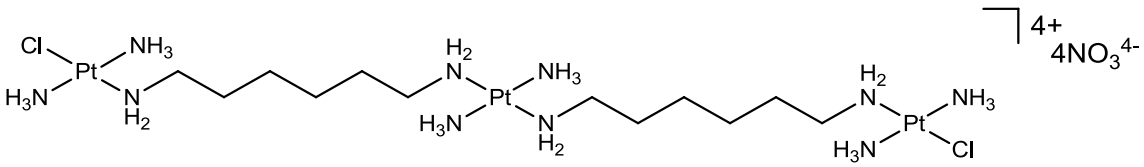

BBR3464

Figure 4.2 *Structure of the trinuclear Pt-based anticancer drug BBR3464.*[17]

Only recently have metallodendrimers been investigated as potential therapeutic agents.[22] A wide range of functionalities may be introduced onto the periphery of these macromolecules allowing them to be modified for specific applications in medicinal chemistry,[23] host-guest chemistry[24] and catalysis.[25, 26] Notably, in medicinal chemistry, the concept of multinuclearity can be used to improve the potency of chemotherapeutic drugs and the application of metallodendrimers can also be used to selectively target tumors by exploiting the enhanced permeability and retention (EPR) effect.[27] The EPR effect results in the passive accumulation of macromolecules in cancerous tissues, further increasing the therapeutic index while decreasing side effects.[28] Another utility of metallodendrimers are their multivalency which potentially leads to increased interactions between a dendrimer-drug conjugate and a target bearing multiple receptors.

Recently, a series of monodentate (*N*-) and chelating bidentate (*N,N*- and *N,O*-) ruthenium-arene first- and second-generation metallodendrimers based on poly(propyleneimine) dendritic scaffolds were prepared.[29, 30] The chelating bidentate ruthenium-arene metallodendrimers show superior *in vitro* antitumor activity over their monodentate counterparts, with the octanuclear cationic *N,N*-ruthenium-hexamethylbenzene metallodendrimer displaying the greatest activity. A clear correlation between the size dependency of the metallodendrimer, cytotoxicity and DNA damage was observed.

In this chapter, the *in vitro* pharmacological evaluation of the neutral and cationic chelating bidentate ruthenium- and osmium-arene metallodendrimers, as well as the ferrocenyl-derived ruthenium-arene derivatives for antitumor activity will be discussed (Figure 4.3).

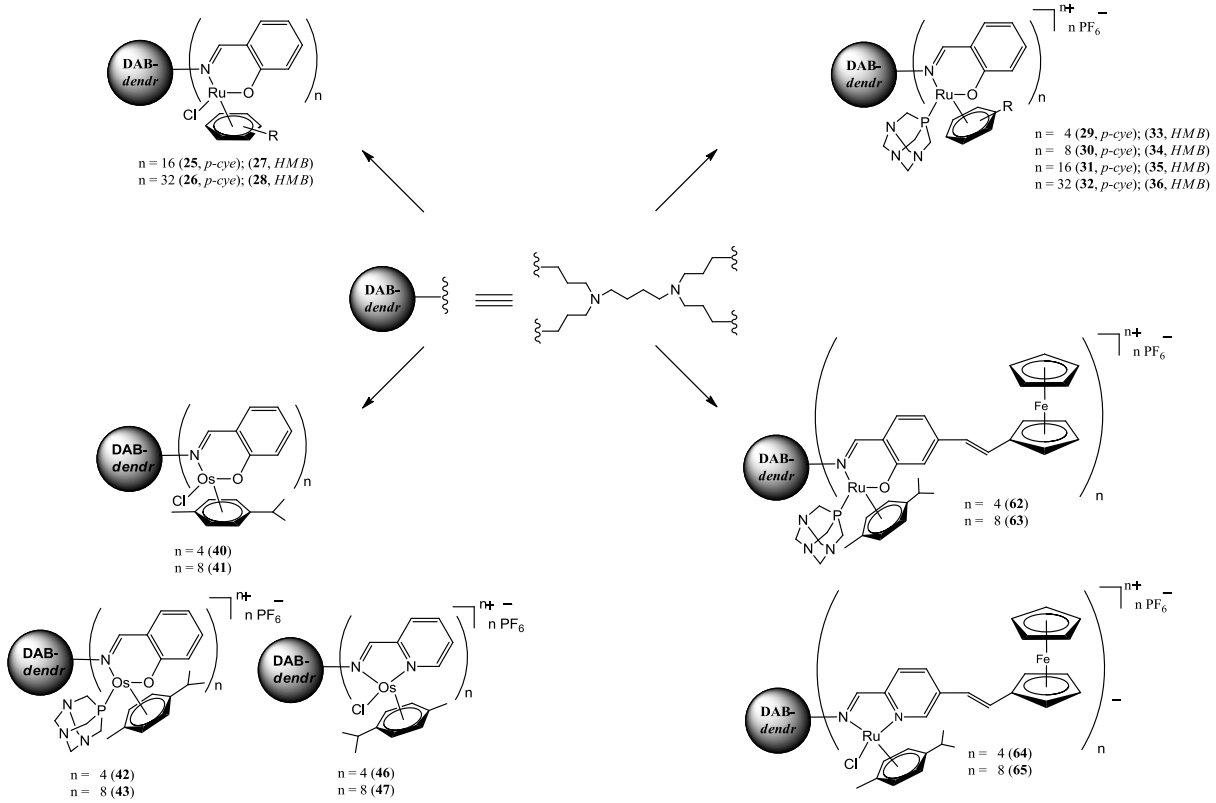

Figure 4.3 *Neutral and cationic chelating bidentate ruthenium- and osmium-arene metallodendrimers prepared in this study.*

4.2 *In vitro* Biological Activity of Ruthenium- and Osmium-Arene Metallodendrimers

With the established tumor-inhibiting properties of ruthenium-arene-PTA complexes,[31] and the current interest in metallodendrimers for biological applications, the *in vitro* biological activity of the neutral *N,O*-ruthenium-arene metallodendrimers (**25** - **28**, Figure 4.3) and cationic *N,O*-ruthenium-arene-PTA metallodendrimers ([**29**][PF_6]$_4$ - [**36**][PF_6]$_{32}$, Figure 4.3) were evaluated against cisplatin-sensitive (A2780) and cisplatin-resistant (A2780*cis*R) human ovarian cancer cell lines, and selected compounds were tested against model human embryonic kidney (HEK) cells (Table 4.1 & Table 4.2).

Table 4.1 *IC_{50} values of neutral N,O-Ru-arene complexes determined against A2780 and A2780cisR human ovarian cancer cells.*

				IC_{50} [μM][a]		
Compound	**Metal**	**n[b]**	**Arene**	**A2780[c]**	**A2780cisR[c]**	**RI[d]**
68	Ru	1	*p*-cye	49 ± 2.3	47 ± 0.8	1.0
9	Ru	4	*p*-cye	50 ± 1.4	52 ± 0.8	1.0
10	Ru	8	*p*-cye	22 ± 1.2	15 ± 1.4	0.7
25	Ru	16	*p*-cye	6.0 ± 1.0	13.2 ± 1.4	2.2
26	Ru	32	*p*-cye	2.9 ± 0.1	9.9 ± 1.2	3.4
69	Ru	1	HMB	19 ± 1.8	18 ± 0.8	0.9
11	Ru	4	HMB	27 ± 1.3	25 ± 1.3	0.9
12	Ru	8	HMB	10 ± 0.3	9 ± 0.2	0.9
27	Ru	16	HMB	2.1 ± 0.1	2.1 ± 0.1	1.0
28	Ru	32	HMB	1.6 ± 0.1	2.1 ± 0.1	1.3
cisplatin	Pt	1	-	1.5	25	16.7

[a] IC_{50} values of **68**, **69**, **9 - 12** taken from reference 30, [b] *n* = number of metals present in the complex, [c] IC_{50} value ± standard error, [d] RI, resistance index = IC_{50} of A2780cisR/IC_{50} of A2780.

Table 4.2 *IC_{50} values of cationic N,O-Ru-arene-PTA complexes determined against A2780 and A2780cisR human ovarian cancer cells, and healthy HEK cells.*

				IC_{50} [μM]					
Compound	**Metal**	**n[a]**	**Arene**	**A2780[b]**	**A2780cisR[b]**	**RI[c]**	**HEK**	**SI_{A2780}[d]**	**$SI_{A2780cisR}$[e]**
[**38**][PF_6]	Ru	1	*p*-cye	>200	82.0 ± 6.0	0.4	115.6	0.6	1.4
[**29**][PF_6]$_4$	Ru	4	*p*-cye	174.0 ± 40	72.8 ± 1.6	0.4	122.1	0.7	1.7
[**30**][PF_6]$_8$	Ru	8	*p*-cye	9.3 ± 0.4	19.3 ± 0.2	2.1	53.2	5.9	2.7
[**31**][PF_6]$_{16}$	Ru	16	*p*-cye	1.4 ± 0.4	3.6 ± 0.2	2.6	12	8.6	3.3
[**32**][PF_6]$_{32}$	Ru	32	*p*-cye	0.8 ± 0.1	2.7 ± 0.1	3.4	2.6	3.3	1.0
[**39**][PF_6]	Ru	1	HMB	38.0 ± 3.4	93.0 ± 7.0	2.4	59.7	1.6	0.6
[**33**][PF_6]$_4$	Ru	4	HMB	8.9 ± 2.8	25.0 ± 5.0	2.8	89.6	10.1	3.6
[**34**][PF_6]$_8$	Ru	8	HMB	6.2 ± 0.3	11.8 ± 1.1	1.9	20.9	3.4	1.8
[**35**][PF_6]$_{16}$	Ru	16	HMB	2.9 ± 0.1	2.0 ± 0.1	0.7	6.4	2.2	3.2
[**36**][PF_6]$_{32}$	Ru	32	HMB	2.0 ± 0.1	1.1 ± 0.1	0.6	2.3	1.2	2.1
cisplatin	Pt	1	-	1.5	25	16.7	-	-	-

[a] *n* = number of metals present in the complex, [b] IC_{50} value ± standard error, [c] RI, resistance index = IC_{50} of A2780cisR/IC_{50} of A2780, [d] SI_{A2780}, selectivity index = IC_{50} of HEK/IC_{50} of A2780, [e] $SI_{A2780cisR}$, selectivity index = IC_{50} of HEK/IC_{50} of A2780cisR.

To perform an extensive investigation, Chapter 2 described the preparation and characterization of neutral and cationic osmium-arene salicylaldiminato derivatives (**40** - [**43**][PF_6]$_8$, [**46**][PF_6]$_4$, [**47**][PF_6]$_8$, Figure 4.3). Parts of this chapter discuss the antiproliferative activity of these osmium derivatives against A2780 and A2780*cis*R human ovarian cancer cells (Table 4.3).

Table 4.3 *IC_{50} values of neutral and cationic osmium-arene complexes determined against A2780 and A2780cisR human ovarian cancer cells.*

				IC_{50} [μM]	
Compound	**Metal**	**n**[a]	**Arene**	**A2780**[b]	**A2780cisR**[b]
48	Os	1	*p*-cye	58.1 ± 13.3	90.4 ± 11.7
40	Os	4	*p*-cye	>200	>200
41	Os	8	*p*-cye	insoluble	insoluble
[**49**][PF_6]	Os	1	*p*-cye	>200	>200
[**42**][PF_6]$_4$	Os	4	*p*-cye	166.7 ± 12.5	>200
[**43**][PF_6]$_8$	Os	8	*p*-cye	16.4 ± 12.5	43.5 ± 2.7
[**51**][PF_6]	Os	1	*p*-cye	120.7 ± 2.4	65.7 ± 16.3
[**46**][PF_6]$_4$	Os	4	*p*-cye	151.5 ± 20.2	>200
[**47**][PF_6]$_8$	Os	8	*p*-cye	24.6 ± 4.8	27.5 ± 5.2
cisplatin	Pt	1	-	1.5	25

[a] *n* = number of metals present in the complex. [b] IC_{50} value ± standard error.

In order to compare size dependency on the *in vitro* biological activity, the synthesis and characterization of mononuclear analogs of the metallodendrimers were described in Chapter 2. Furthermore, their antitumor activities were evaluated against A2780 and A2780cisR human ovarian cancer cell lines and are described here. The un-complexed *N,O*-salicylaldiminato dendritic ligands were not tested.

4.2.1 Influence of the Number of Metal Centres: *Mononuclear vs. G_1 vs. G_2 vs. G_3 vs. G_4*

Neutral N,O-Ruthenium-Arene Complexes

The *in vitro* antitumor activity of the third- and fourth-generation neutral ruthenium-arene metallodendrimers **25** - **28** was evaluated against A2780 and A2780cisR human ovarian cancer cells, and compared with the activity of the first- and second-generation derivatives (**9** -**12**) and mononuclear analogs (**68** & **69**) taken from reference 30 (Figure 2.1 *in Chapter 2*). The general activity of the neutral ruthenium-arene complexes increases when moving from the mononuclear analog to the higher dendrimer generations, for both cell lines (A2780 &

A2780cisR), and for both the *p*-cymene (Figure 4.4, *left*) and hexamethylbenzene (Figure 4.4, *right*) derivatives. The fourth-generation metallodendrimers **26** and **28** display the best activity in both the A2780 (IC_{50} = 2.9 μM and 1.6 μM respectively) and A2780cisR (IC_{50} = 9.9 μM and 2.1 μM respectively) cell lines. Furthermore, fourth-generation derivatives **26** and **28** display higher cytotoxicity compared to structurally similar mononuclear *N,O*-bidentate complexes reported by Grgurić-Šipka and co-workers.[32] The correlation between size of the metallodendrimer and the increase in antitumor activity, previously observed for **9** - **12**,[30] is observed with metallodendrimers **25** - **28**.

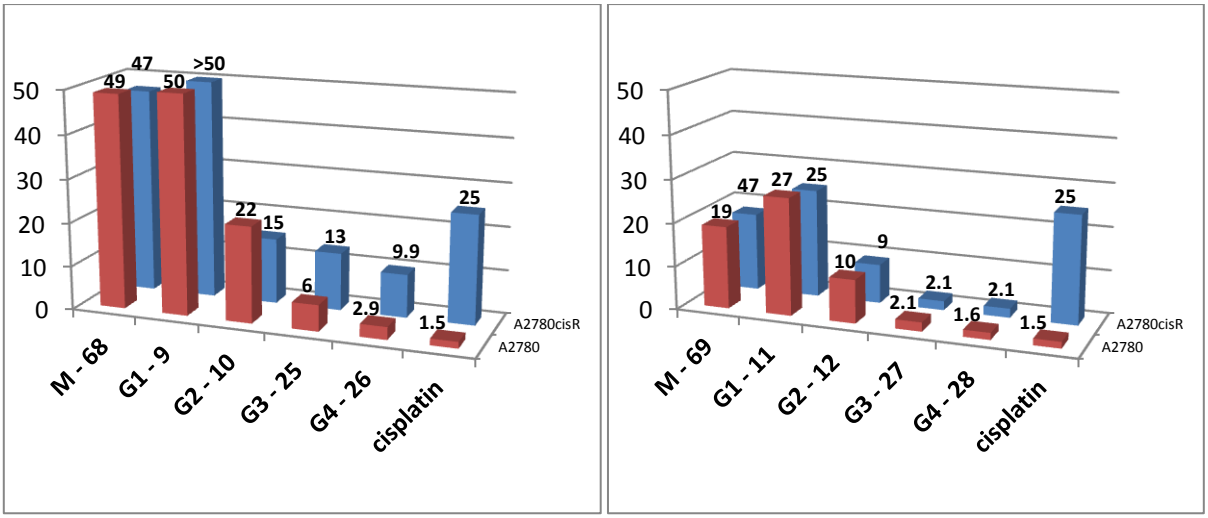

Figure 4.4 *Effect of the number of metal centres (Ru-p-cymene complexes - left; Ru-HMB complexes - right) on the antitumor activity against A2780 and A2780cisR human ovarian cancer cells, with **68**, **69**, **9** - **12**, **25** - **28**. IC_{50} values of **68**, **69**, **9** - **12** taken from reference 30.*

Previous work within our research group describes the preparation of a series of first- and second-generation monodentate ruthenium(II)-arene (arene = *p*-cymene or hexamethylbenzene) 4-iminopyridyl-based poly(propyleneimine) metallodendrimers (Figure 4.5), and their *in vitro* cytotoxicity investigated against A2780 human ovarian cancer cells.[29] These complexes showed a lower cytotoxicity compared to cisplatin, however, a clear correlation between the size of the compound and the cytotoxicity was similarly observed, with the second-generation octanuclear analog displaying the best activity of the series.

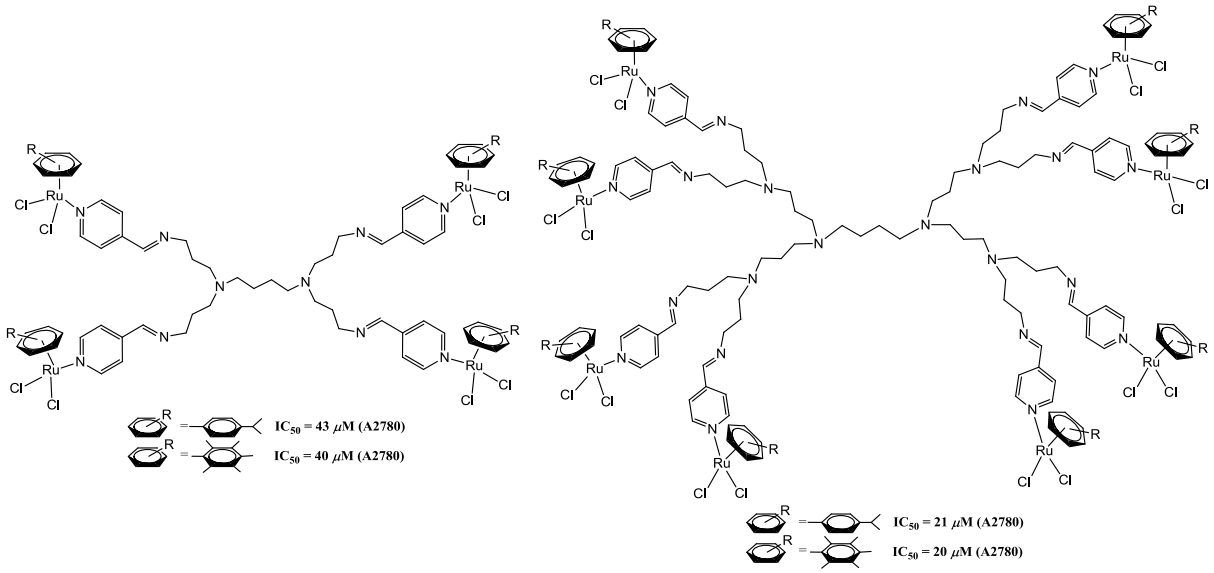

Figure 4.5 *Molecular structure of first- (left) and second-generation (right) monodentate ruthenium-arene metallodendrimers based on a 4-iminopyridyl-poly(propyleneimine) dendritic scaffold and IC_{50} values of complexes against A2780 human ovarian cancer cells.*

Cationic N,O-Ruthenium-Arene-PTA Complexes

A similar trend observed with the neutral *N,O*-ruthenium-arene metallodendrimers [**25** - **28**] is observed with the cationic *N,O*-ruthenium-arene-PTA metallodendrimers [**29**][PF_6]$_4$ - [**36**][PF_6]$_{32}$ (Figure 4.6). Essentially the mononuclear analogs [**38**][PF_6] (Figure 4.6, *left*) and [**39**][PF_6] (Figure 4.6, *right*) display no activity (IC_{50} >30 μM) in both the A2780 and A2780cisR cell lines. However, the higher generation metallodendrimers display a remarkable improvement in activity, in both cell lines, with the fourth-generation metallodendrimers [**32**][PF_6]$_{32}$ and [**36**][PF_6]$_{32}$ the most active of the series. Metallodendrimer [**32**][PF_6]$_{32}$ (IC_{50} = 0.8 μM in A2780; 2.7 μM in A2780cisR) shows enhanced cytotoxicity compared to the benchmark drug cisplatin (IC_{50} = 1.5 μM in A2780; 25 μM in A2780cisR).

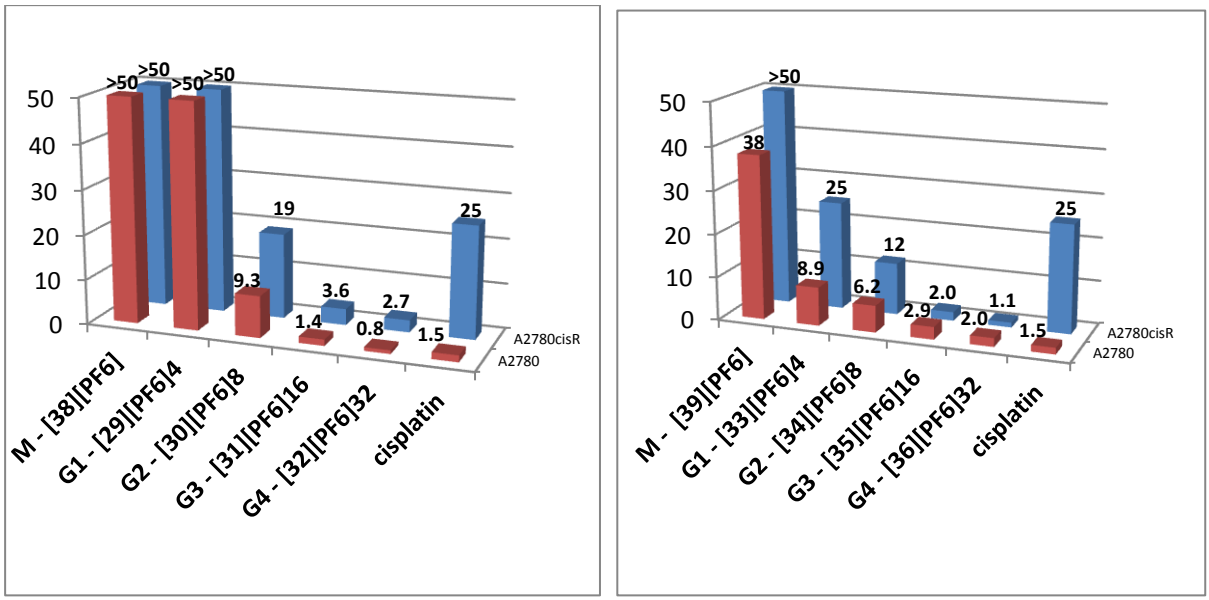

Figure 4.6 *Effect of the number of metal centres (Ru-p-cymene complexes - left; Ru-HMB complexes - right) on the antitumor activity against A2780 and A2780cisR human ovarian cancer cells, with* ***[29]***$[PF_6]_4$ *-* ***[36]***$[PF_6]_{32}$*,* ***[38]***$[PF_6]$ *and* ***[39]***$[PF_6]$*.*

Metallodendrimer **[32]**$[PF_6]_{32}$ shows promising cytotoxicity compared to other multinuclear metallodendrimers.[22] Though not tested in the same cell line, such examples include the tetranuclear platinum complex (IC_{50} = 12.4 μM in L1210/0, mouse leukemia cells) based on the butanediamine poly(propyleneimine) dendrimer, functionalized with cisplatin-derived moieties (Figure 4.7, *left*),[33] and the multinuclear copper complex (IC_{50} = 8.7 μM in Chang liver cells), based on the poly(amidoamine) dendrimer (Figure 4.7, *right*).[34] Once again a clear correlation between the size dependency of the metallodendrimer and cytotoxicity is observed.

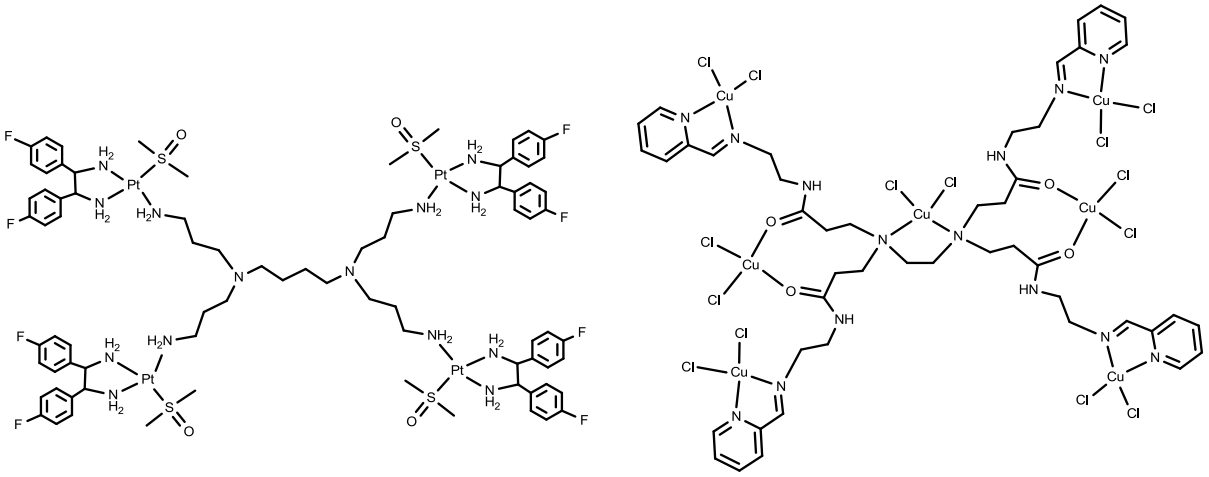

IC_{50} =12.4 μM (L1210/0) **IC_{50} = 8.7 μM (Chang Liver Cells)**

Figure 4.7 *Molecular structure of tetranuclear platinum-based metallodendrimer (left) and multinuclear copper-based metallodendrimer (right), and IC_{50} values of compounds.*[33, 34]

Neutral and Cationic Osmium-Arene Complexes

Osmium, found in the same group as ruthenium, is thought to have similar chemical and biological properties. Hence, osmium analogs of potent ruthenium(III)-anticancer drugs, namely NAMI-A[35] and KP1019,[36] were prepared by Sava and Keppler respectively. The antiproliferative activity of the osmium-analog of NAMI-A is comparable to its ruthenium derivative, with enhanced activity in the human cancer cell line (HT-10) observed, and markedly inert towards substitution reactions in the form of hydrolysis and DNA base interaction.[35] Whilst the cytotoxicity of the osmium-analog of KP1019 is inactive in three cell lines (*i.e.* A549, CH1, SW480) and is attributed to their poor solubility in the testing medium (1 % dimethylsulfoxide:water).[36] This is no surprise, with the low-spin d^6 characteristic of 3rd row transition metal ions, osmium complexes are usually considered inert in comparison to their ruthenium derivatives.[37-42]

Nevertheless, the biological activities of the neutral and cationic osmium-arene complexes were evaluated. The cytotoxicity of the neutral *N,O*-osmium-arene complexes **40**, **41** and **48**, and cationic *N,O*-osmium-arene-PTA complexes [**42**][PF_6]$_4$, [**43**][PF_6]$_8$ and [**49**][PF_6], and cationic *N,N*-osmium-arene complexes [**46**][PF_6]$_4$, [**47**][PF_6]$_8$ and [**51**][PF_6] were tested *in vitro* against both the A2780 and A2780cisR cell lines (Figure 4.8). Replacing ruthenium with osmium results in a drastic decrease in biological activity, as the mononuclear complexes **48**,

[**49**][PF_6] and [**51**][PF_6], and first-generation derivatives **40**, [**42**][PF_6]$_4$ and [**46**][PF_6]$_4$ display no activity (IC_{50} >50 μM) in both cell lines. The cytotoxicity of the second-generation metallodendrimer **41** was not obtained due to poor solubility of the complex in the cell culture, with the second-generation metallodendrimers [**43**][PF_6]$_8$ (IC_{50} = 16.4 μM in A2780; 43.5 μM in A2780cisR) and [**47**][PF_6]$_8$ (IC_{50} = 24.6 μM in A2780; 27.5 μM in A2780cisR) display modest activity compared to cisplatin.

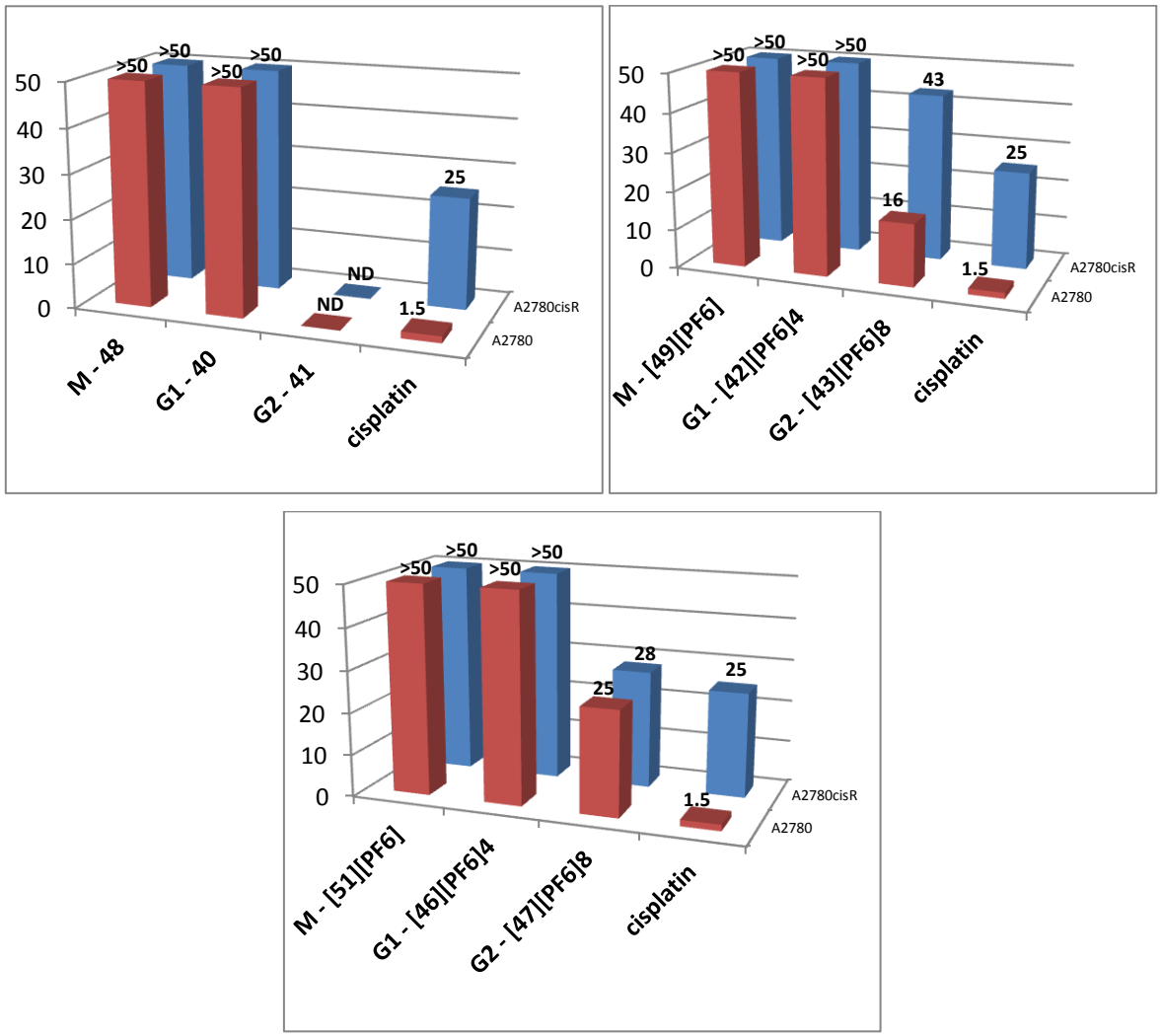

Figure 4.8 *Effect of the number of metal centres (neutral N,O-Os-p-cymene complexes - top left; cationic N,O-Os-p-cymene-PTA complexes - top right; cationic N,N-Os-p-cymene complexes - bottom centre) on the antitumor activity against A2780 and A2780cisR human ovarian cancer cells. ND = Not Done.*

The pseudo-tetrahedral shape of organometallic ruthenium and osmium derivatives are almost identical, which triggered the investigation by Meggers and co-workers on the correlation between shape and function of two isostructural ruthenium and osmium complexes (Figure 4.9).[43] The two organometallic osmium and ruthenium metal ions functionalized to protein kinase inhibitor scaffolds show almost identical biological activities in melanoma cells (1205 Lu).[43]

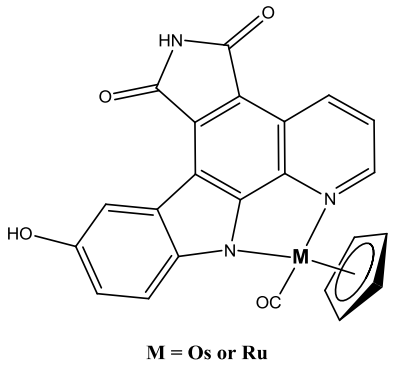

Figure 4.9 *Molecular structure of the isostructural osmium and ruthenium complex.*[43]

Despite the structural similarities between the current series of neutral and cationic osmium-arene and ruthenium-arene complexes presented in this study, there is no vast improvement in the cytotoxicity of the complexes when replacing ruthenium with osmium, in-fact there is a drastic decrease in activity. The observed low activity may be attributed to the poor solubility in the testing media, similarly observed for the osmium-analog of KP1019.[36]

The neutral and cationic *N,O*-osmium-arene metallodendrimers presented here are new, and following an extensive search of the literature, these osmium-based complexes are the first metallodendrimers evaluated as potential anticancer agents. However, multinuclear osmium complexes have been reported,[44] where the authors describe the synthesis of hexanuclear osmium-arene metalla-prisms, with focus on encapsulation of inorganic and organic guest molecules (Figure 4.10). Similarly observed to their ruthenium metalla-prisms,[45] the osmium analogs enhance the anticancer activities of the encapsulated drug. The improvement in activity is attributed to better solubility of the encapsulated drugs, leading to increased cellular internalization.

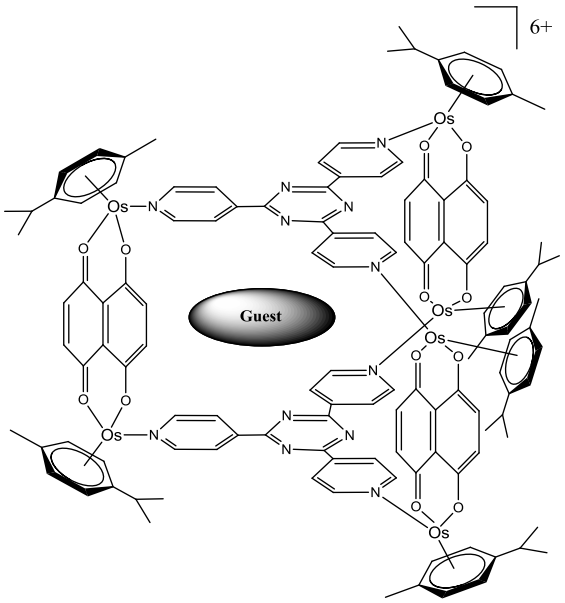

Figure 4.10 *Molecular structure of hexanuclear osmium-arene metalla-prism.*[44]

4.2.2 Influence of the Type of Arene Ring: *p-Cymene vs. Hexamethylbenzene*

Neutral N,O-Ruthenium-Arene Complexes

To investigate whether a structure-activity-relationship exists between the current series of metallodendrimers **25** - **28**, the *p*-cymene ligand was replaced with the hexamethylbenzene ligand. The arene ring of ruthenium-arene complexes is an important feature in the mode of action, in particular towards the inhibition of tumor growth.[46, 47] IC_{50} values of the neutral third- and fourth-generation metallodendrimers **25** - **28**, along with the first- and second-generation derivatives **9** - **12** and the mononuclear analogs **68** and **69** taken from reference 30 (Figure 4.11), are compared.

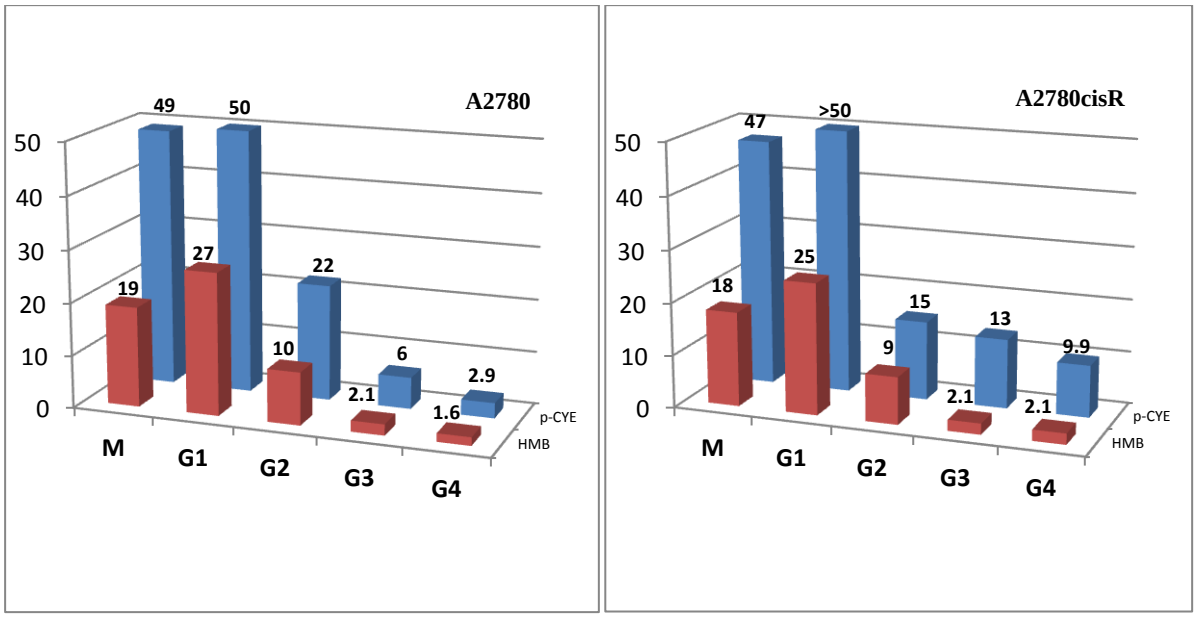

Figure 4.11 *Effect of the arene ring on the antitumor activity against A2780 (left) and A2780cisR (right) human ovarian cancer cells, with neutral N,O-Ru-arene complexes: M (**68**, **69**); G1 (**9**, **11**); G2 (**10**, **12**); G3 (**25**, **27**) and G4 (**26**, **28**). IC_{50} values for complexes **68**, **69** and **9** - **12** are taken from reference 30.*

The neutral *N,O*-ruthenium-hexamethylbenzene metallodendrimers (**11**, **12**, **27**, **28**) display better activity in the A2780 (Figure 4.11, *left*) and A2780cisR (Figure 4.11, *right*) cell lines, compared to their *p*-cymene counter-parts (**9**, **10**, **25**, **26**). It is suggested that the hexamethylbenzene ligand improves lipophilicity of the complex, thereby enhancing the uptake into cells, and plays a role in biomolecular interactions and recognition processes, such as hydrophobic interactions between the arene ring and DNA, specifically in the form of strong arene-nucleobase π-π stacking interactions.[47]

Cationic N,O-Ruthenium-Arene-PTA Complexes

However, the cationic hexamethylbenzene metallodendrimers [**33**][PF_6]$_4$ - [**36**][PF_6]$_{32}$ do not show an improvement in cytotoxicity in comparison to the *p*-cymene derivatives [**29**][PF_6]$_4$ - [**32**][PF_6]$_{32}$ in the A2780 cell line (Figure 4.12, *left*). However, a small improvement in cytotoxicity is observed in the cisplatin-resistant cell line (A2780cisR) for the hexamethylbenzene analogs (in some cases only) over their *p*-cymene counterparts (Figure 4.12, *right*).

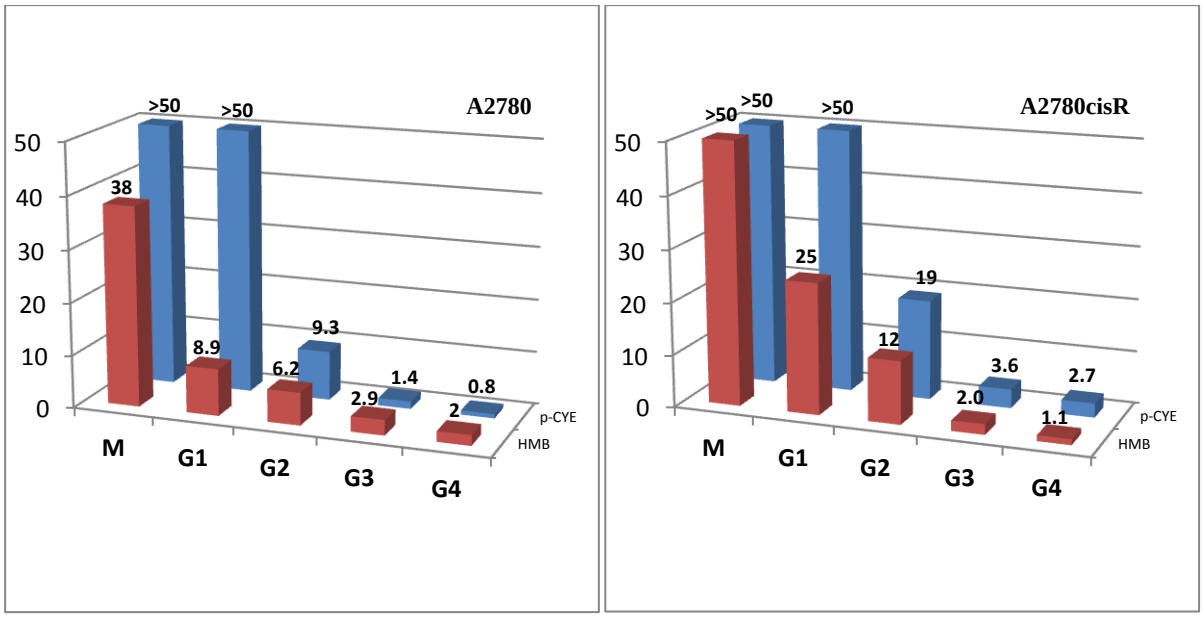

Figure 4.12 *Effect of the arene ring on the antitumor activity against A2780 (left) and A2780cisR (right) human ovarian cancer cells, with cationic N,O-Ru-arene-PTA complexes: M ([**38**][PF$_6$], [**39**][PF$_6$]); G1 ([**29**][PF$_6$]$_4$, [**33**][PF$_6$]$_4$); G2 ([**30**][PF$_6$]$_8$, [**34**][PF$_6$]$_8$); G3 ([**31**][PF$_6$]$_{16}$, [**35**][PF$_6$]$_{16}$) and G4 ([**32**][PF$_6$]$_{32}$, [**36**][PF$_6$]$_{32}$).*

The similar trend is observed with reported cationic *N,N*-ruthenium-arene complexes, containing the 2-(pyridine-2-yl)thiazole ligand, with the hexamethylbenzene derivatives displaying better activity over the *p*-cymene derivatives (Figure 4.13, *top left*).[48] Furthermore, the hexamethylbenzene-octanuclear metallarectangle synthesized by Therrien *et al.*, display 50 % better activity over its *p*-cymene derivative (Figure 4.13, *top right*).[49] Furthermore, Sadler and co-workers reported an increase in cytotoxicity, with an increase in the size of the arene ring system in the order, arene = benzene < *p*-cymene < biphenyl < dihydroanthracene < tetrahydroanthracene (Figure 4.13, *bottom centre*).[50]

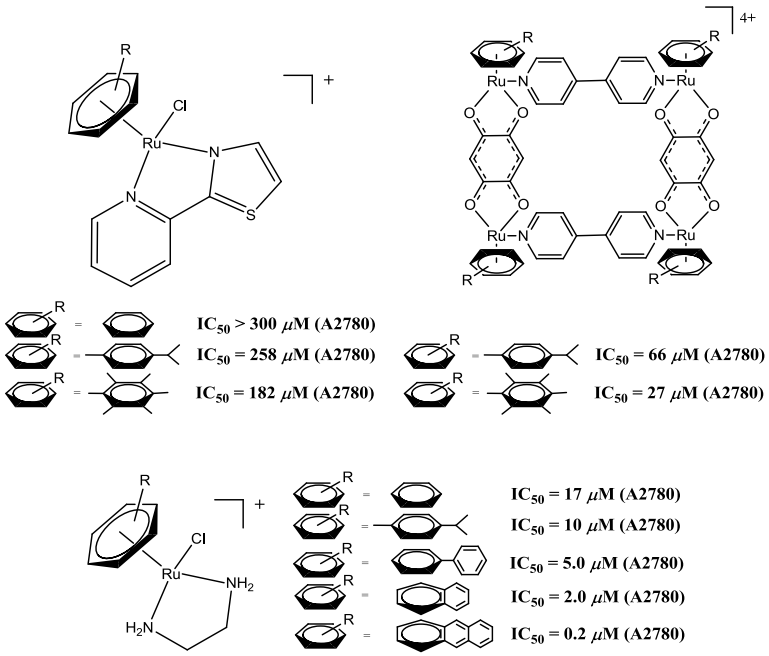

Figure 4.13 *Molecular structures of ruthenium-arene complexes, with varying arene rings, and IC_{50} values of the compounds in A2780 human ovarian cancer cells.*[48-50]

4.2.3 Influence of the Water-Soluble Phosphine Ligand:

Neutral vs. Cationic (i.e. PTA vs. Chlorido)

In order to improve interactions between the drug and DNA, it was thought to synthesize cationic complexes, to improve simple electrostatic interactions between the cationic complex and the negatively charged phosphate groups on the surface of DNA (possible drug target).[51] It was thought to abstract the chlorido ligand from the previously reported first- and second-generation neutral *N,O*-ruthenium-arene metallodendrimers (**9** - **12**),[29] and the newly prepared third- and fourth-generation derivatives **25** - **28**, and introduce the water-soluble PTA ligand into the coordination sphere, in turn generating cationic metallodendrimers [**29**][PF_6]$_4$ - [**36**][PF_6]$_{32}$. Furthermore, with the established tumor inhibiting properties of the RAPTA complexes, and the targeting of metastatic tumors in CBA mice,[31, 52] the introduction of the PTA moiety would make for an interesting investigation towards the mode of action of the complexes.

In general the cationic metallodendrimers [**29**][PF_6]$_4$ - [**36**][PF_6]$_{32}$ display a vast improvement in biological activity in the A2780 cell line, over their neutral counter-parts **9** - **12** and **25** - **28**, for both *p*-cymene (Figure 4.14, *left*) and hexamethylbenzene (Figure 4.14, *right*) derivatives. The fourth-generation cationic *N,O*-ruthenium *p*-cymene metallodendrimer [**32**][PF_6]$_{32}$ (IC_{50} = 0.8 μM in A2780) displays a two-fold increase in activity over its neutral chlorido-derivative

26 (IC_{50} = 2.9 μM in A2780). The hexamethylbenzene metallodendrimer [**36**][PF_6]$_{32}$ displays the same activity to its neutral derivative **28** (IC_{50} ~ 2 μM in A2780).

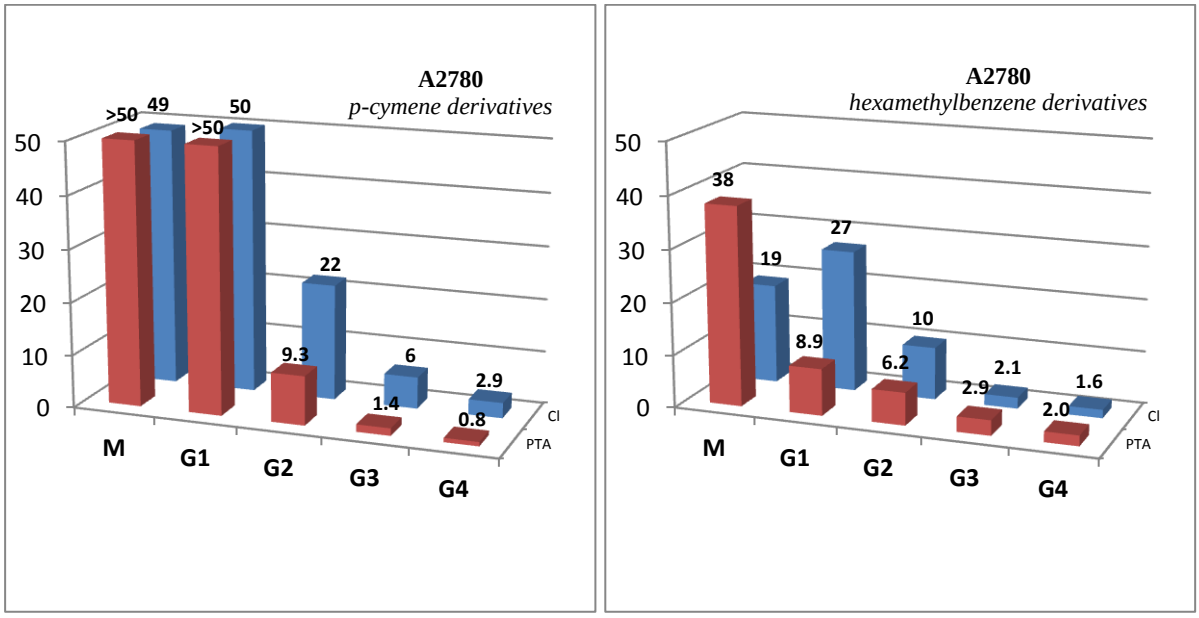

Figure 4.14 *Effect of the charge on the antitumor activity against A2780 human ovarian cancer cells (p-cymene derivatives - left; hexamethylbenzene derivatives - right), with neutral N,O-Ru-arene complexes and cationic N,O-Ru-arene-PTA complexes. IC_{50} values of neutral complexes **68**, **69** and **9** - **12** is taken from reference 30.*
*p-cymene derivatives: M ([**38**][PF_6], **68**); G1 ([**29**][PF_6]$_4$, **9**); G2 ([**30**][PF_6]$_8$, **10**); G3 ([**31**][PF_6]$_{16}$, **25**) and G4 ([**32**][PF_6]$_{32}$, **26**).*
*hexamethylbenzene derivatives: M ([**39**][PF_6], **69**); G1 ([**33**][PF_6]$_4$, **11**); G2 ([**34**][PF_6]$_8$, **12**); G3 ([**35**][PF_6]$_{16}$, **27**) and G4 ([**36**][PF_6]$_{32}$, **28**).*

Moreover, in the A2780cisR cell line the cationic *p*-cymene metallodendrimers [**29**][PF_6]$_4$ - [**32**][PF_6]$_{32}$, display better activity than their neutral *p*-cymene counterparts **9**, **10**, **25** and **26** (Figure 4.15, *left*). In particular the third- and fourth-generation cationic derivatives [**31**][PF_6]$_{16}$ (IC_{50} = 3.6 μM in A2780cisR) and [**32**][PF_6]$_{32}$ (IC_{50} = 2.7 μM in A2780cisR), display superior activity over the neutral derivatives **25** (IC_{50} = 13.2 μM in A2780cisR) and **26** (IC_{50} = 9.9 μM in A2780cisR). Whilst the cationic hexamethylbenzene-derived second-, third- and fourth-generation metallodendrimers [**34**][PF_6]$_8$ (IC_{50} = 12 μM in A2780cisR), [**35**][PF_6]$_{16}$ (IC_{50} = 2.0 μM in A2780cisR) and [**36**][PF_6]$_{32}$ (IC_{50} = 1.1 μM in A2780cisR), display comparable cytotoxicities to the neutral hexamethylbenzene derivatives **12** (IC_{50} = 9.0 μM in A2780cisR), **27** (IC_{50} = 2.1 μM in A2780cisR) and **28** (IC_{50} = 2.1 μM in A2780cisR), in the A2780cisR cell line.

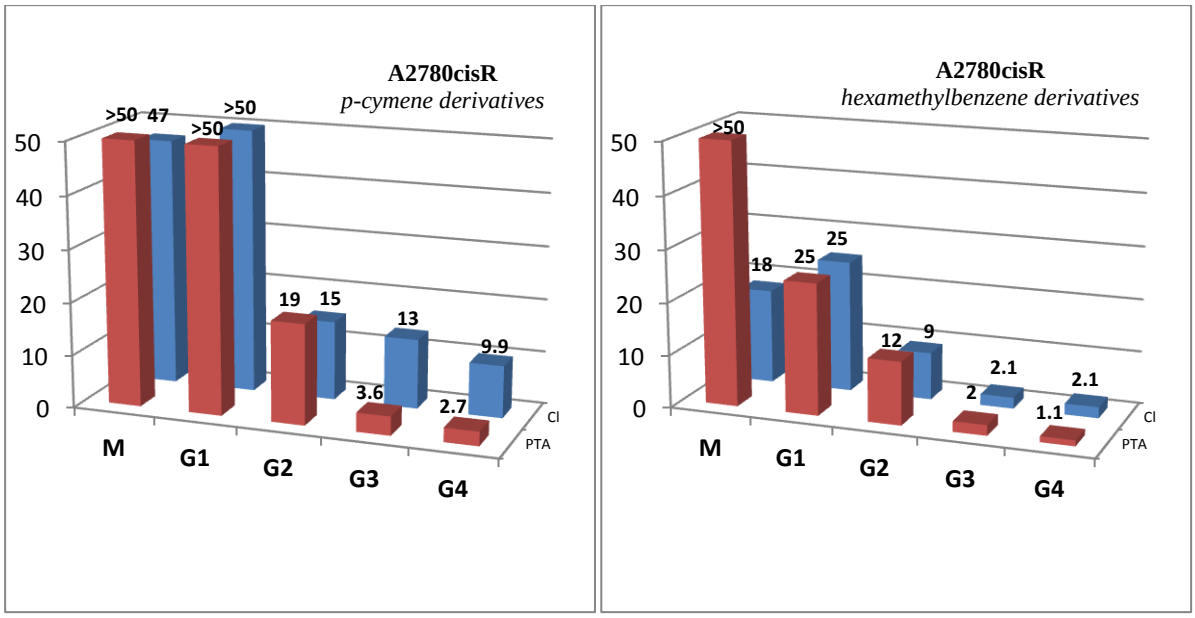

Figure 4.15 *Effect of the charge on the antitumor activity against A2780cisR human ovarian cancer cells (p-cymene derivatives - left; hexamethylbenzene derivatives - right), with neutral N,O-Ru-arene complexes and cationic N,O-Ru-arene-PTA complexes. IC_{50} values of neutral complexes **68**, **69** and **9** - **12** is taken from reference 30.*

*p-cymene derivatives: M ([**38**][PF_6], **68**); G1 ([**29**][PF_6]$_4$, **9**); G2 ([**30**][PF_6]$_8$, **10**); G3 ([**31**][PF_6]$_{16}$, **25**) and G4 ([**32**][PF_6]$_{32}$, **26**).*

*hexamethylbenzene derivatives: M ([**39**][PF_6], **69**); G1 ([**33**][PF_6]$_4$, **11**); G2 ([**34**][PF_6]$_8$, **12**); G3 ([**35**][PF_6]$_{16}$, **27**) and G4 ([**36**][PF_6]$_{32}$, **28**).*

It does appear that the PTA ligand improves the pharmacological properties of the metallodendrimers, at least *in vitro*, leading to an improvement in cytotoxicity. The *in vitro* antitumor activity of the above mentioned metallodendrimers is moderate to good compared to cisplatin. However, *in vitro* potency appears not to be a prerequisite in particular for ruthenium-arene drugs.[38] RAPTA complexes exhibit low activity *in vitro* but possess very good antimetastatic activity *in vivo*.[14, 15]

4.2.4 Resistance

The mean resistance index (RI) was calculated by the IC_{50} of A2780cisR cells/IC_{50} of A2780 cells for the neutral *N,O*-ruthenium-arene complexes (Table 4.1) and the cationic *N,O*-ruthenium-arene-PTA complexes (Table 4.2). The RI values relate to how resistant the compounds are in the cisplatin-sensitive cell line (A2780) compared to the cisplatin-resistant cell line (A2780cisR).

Resistance of Neutral N,O-Ruthenium-Arene Complexes

The neutral *N,O*-ruthenium-arene complexes display similar activity in both the A2780 and A2780cisR cell lines, with RI values approximately equal to 1 (Table 4.1), with the exception of metallodendrimers **25** (RI = 2.2) and **26** (RI = 3.4) which display moderate resistance in the A2780cisR cells. However, this resistance is modest in comparison to cisplatin-resistance (RI = 16.7). In general, the neutral *N,O*-ruthenium-*p*-cymene metallodendrimers display an increase in resistance with an increase in dendrimer generation, whilst the neutral *N,O*-ruthenium-hexamethylbenzene metallodendrimers display no cross-resistance to cisplatin (Figure 4.16).

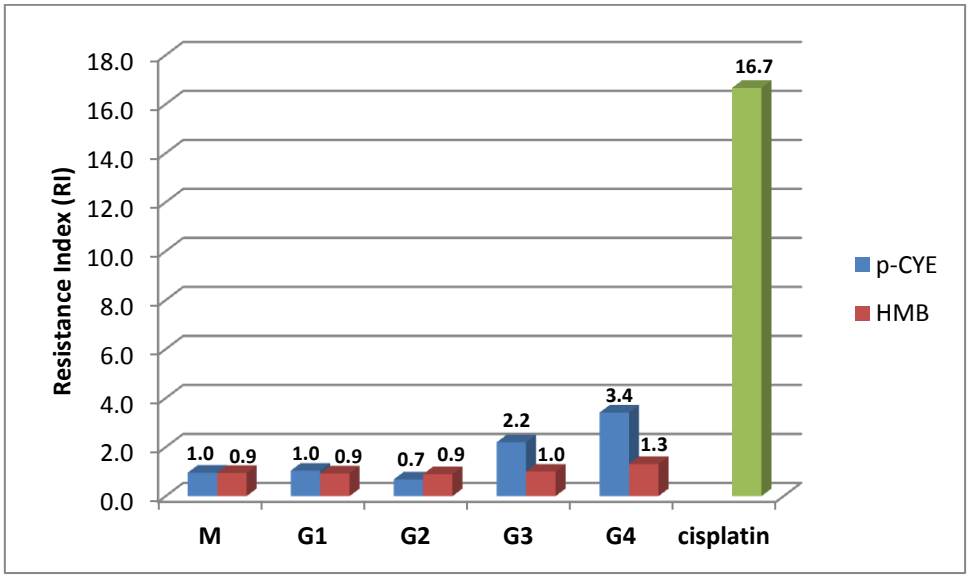

Figure 4.16 *Effect of changing the arene ligand from p-cymene to hexamethylbenzene on the cytotoxicity against A2780 and A2780cisR cells (plotted as a resistance index RI = IC_{50} of A2780 cells / IC_{50} of A2780cisR cells) for complexes: M (**68**, **69**); G1 (**9**, **11**); G2 (**10**, **12**); G3 (**25**, **27**); G4 (**26**, **28**) and cisplatin.*

Resistance of Cationic N,O-Ruthenium-Arene-PTA Complexes

The cationic *N,O*-ruthenium-arene-PTA complexes are active in both the A2780 and A2780cisR human ovarian cancer cells, with moderate RI values listed in Table 4.2. There is a small increase in resistance of the cationic ruthenium-*p*-cymene-PTA metallodendrimers [**29**][PF_6]$_4$ - [**32**][PF_6]$_{32}$ with an increase in dendrimer generation (Figure 4.17). However, there is a decrease in resistance of the cationic ruthenium-hexamethylbenzene-PTA metallodendrimers [**33**][PF_6]$_4$ - [**36**][PF_6]$_{32}$ with an increase in dendrimer generation towards A2780cisR cells.

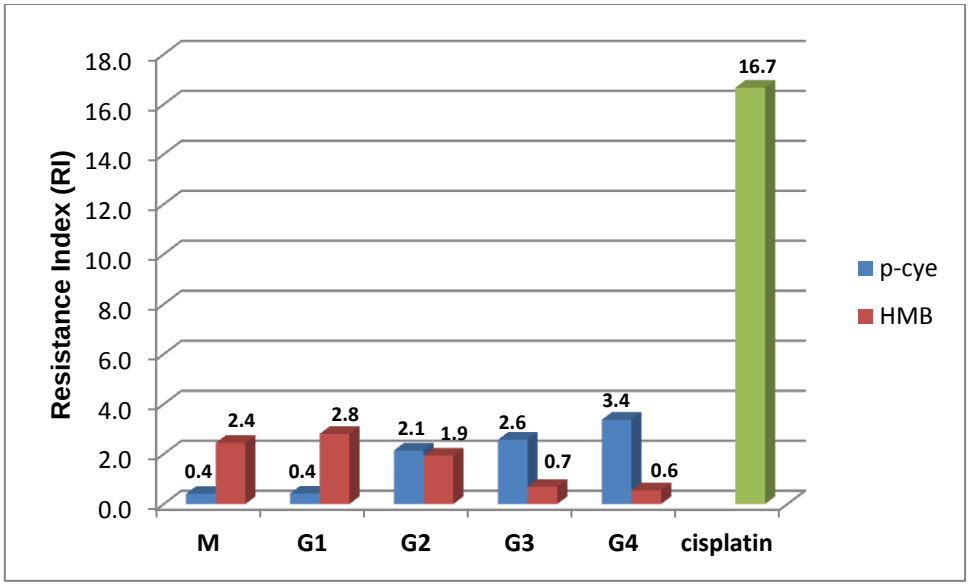

Figure 4.17 *Effect of changing the arene ligand from p-cymene to hexamethylbenzene on the cytotoxicity against A2780 and A2780cisR cells (plotted as a resistance index RI = IC_{50} of A2780 cells / IC_{50} of A2780cisR cells) for complexes: M ([**38**][PF_6], [**39**][PF_6]); G1 ([**29**][PF_6]$_4$, [**33**][PF_6]$_4$); G2 ([**30**][PF_6]$_8$, [**34**][PF_6]$_8$); G3 ([**31**][PF_6]$_{16}$, [**35**][PF_6]$_{16}$); G4 ([**32**][PF_6]$_{32}$, [**36**][PF_6]$_{32}$) and cisplatin.*

Generally, both the neutral and cationic ruthenium-arene metallodendrimers display no cross resistance to cisplatin, in other words, the cytotoxicities are similar in both cell lines. Furthermore, this indicates that these types of systems are markedly less susceptible to the same resistance mechanisms that inhibit cisplatin-activity against A2780cisR cells.[53]

4.2.5 Selectivity

Selectivity of Cationic N,O-Ruthenium-Arene-PTA Complexes

Before drugs can be considered for biological applications, evaluation of their selectivity for cancerous cells over non-tumorigenic cells is extremely important. Hence, the *in vitro* biological activity of the *N,O*-cationic ruthenium-arene metallodendrimers against model human embryonic kidney (HEK) cells was elucidated (Figure 4.18).

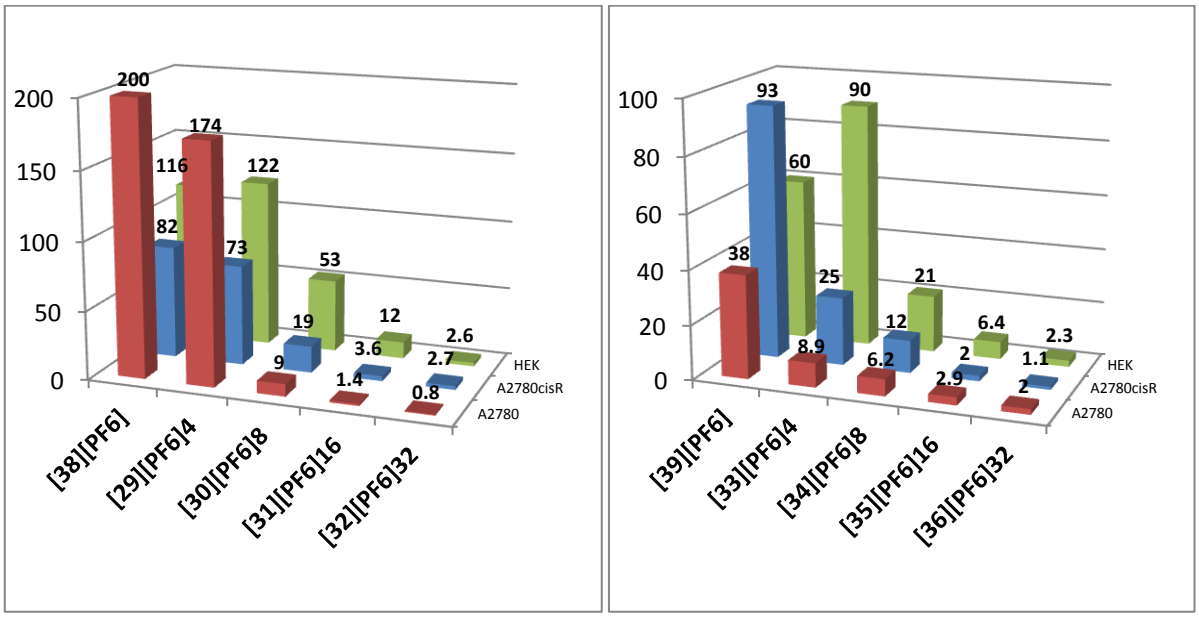

Figure 4.18 *Effect of arene ring (cationic N,O-Ru-p-cymene-PTA complexes - left; cationic N,O-Ru-hexamethylbenzene-PTA complexes - right) on the selectivity for cancer cells, with* ***[29]*** *$[PF_6]_4$ -* ***[36]*** *$[PF_6]_{32}$,* ***[38]*** *$[PF_6]$ and* ***[39]*** *$[PF_6]$.*

With the exception of [**29**]$[PF_6]_4$, the multinuclear complexes are consistently selective towards the cancer cells (A2780 & A2780cisR) over the non-tumorigenic cells. More specifically, the first-generation *p*-cymene metallodendrimer [**33**]$[PF_6]_4$ displays good selectivity for the A2780 (IC_{50} = 8.9 μM) and A2780cisR (IC_{50} = 25 μM) over the HEK cells (IC_{50} = 90 μM). However, the selectivity is not ideal and therefore synthesis of heterometallic ferrocenyl-derived ruthenium-arene metallodendrimers were prepared and described in Chapter 3. Furthermore, ferrocene is considered non-toxic and its one-electron reversible oxidation to the cytotoxic ferrocenium cation makes it a promising candidate in the development of therapeutic agents.

4.3 Stability of the Cationic *N,O*-Ruthenium-Arene-PTA Metallodendrimers in Solution and Interactions with Nucleotides

4.3.1 Degradation Test

It is important to understand the stability of drugs in solution before they can be considered for any biological applications. Hence, to investigate the influence of the bidentate chelating *N,O*-dendritic ligands on the stability of the cationic *N,O*-ruthenium-arene metallodendrimers in solution, time degradation studies on selected complexes were investigated using $^{31}P\{^{1}H\}$ NMR spectroscopy. The hexamethylbenzene derivatives display the best activity, hence first-generation metallodendrimer [**33**][PF_6]$_4$; and its mononuclear analog [**39**][PF_6] were selected, and will be used as a preliminary study to model the behavior of the higher generation metallodendrimers in deuterated dimethylsulfoxide. To monitor degradation or the release of metallofragments, the complexes were prepared at a concentration of 0.043 mg.μL^{-1}, and $^{31}P\{^{1}H\}$ NMR experiments (Figure 4.19 and 4.20) were performed at 37 ºC (physiological temperature).

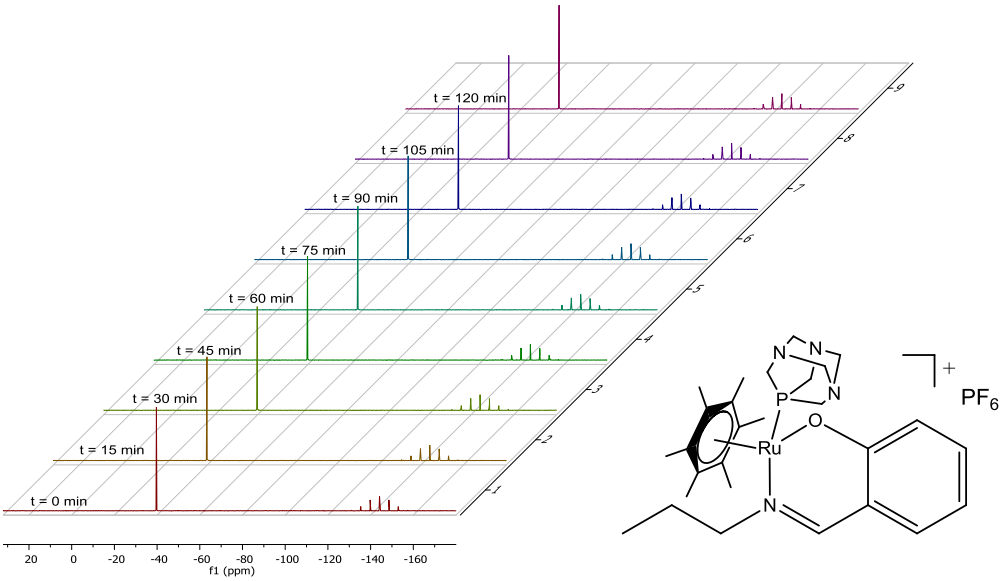

Figure 4.19 *$^{31}P\{^{1}H\}$ NMR spectra of the mononuclear complex [**39**][PF_6] recorded at 37 ºC in $(CD_3)_2SO$ at different time intervals.*

Metallodendrimer [**33**][PF_6]$_4$ and mononuclear derivative [**39**][PF_6] displayed good stability in deuterated dimethylsulfoxide, with no signs of degradation signals observed in the $^{31}P\{^1H\}$ NMR spectrum over the 2h period. In addition, this shows that the complexes are stable in deuterated dimethylsulfoxide during the time period between preparation of the compound stock solutions and dosing of the cancer cells in the assay.

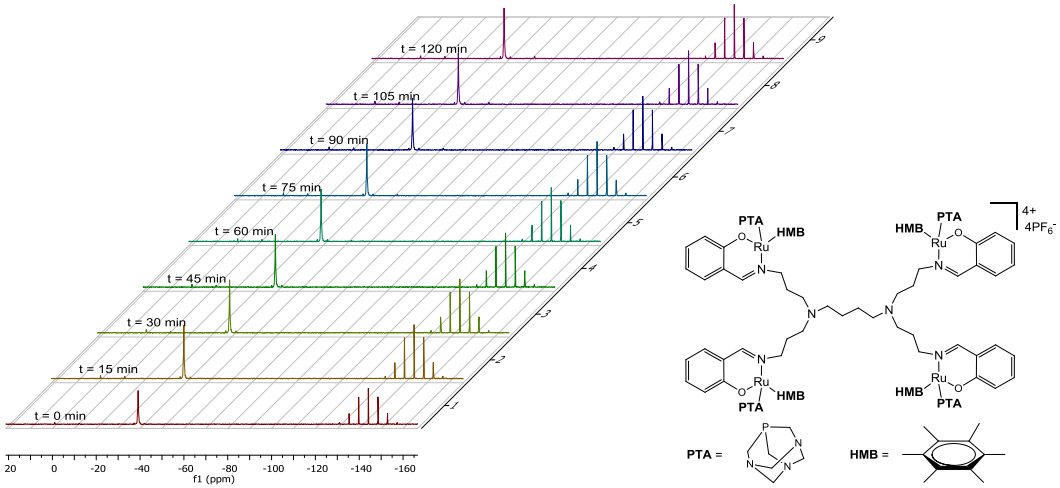

Figure 4.20 *$^{31}P\{^1H\}$ NMR spectra of the metallodendrimer [**33**][PF_6]$_4$ recorded at 37 ºC in $(CD_3)_2SO$ at different time intervals.*

4.3.2 Aquatic Stability

It is important to know the identity of the compound that reaches the cell, and accordingly, the aqueous chemistry of the complexes is important. Following uptake into the cell, it has been reported that ruthenium-arene-PTA complexes are activated *via* aquation, generating the aqua species. This is said to be the 'active' form of the complex (Scheme 4.1) and the formation of the aqua species can be monitored by NMR spectroscopy.[54, 55]

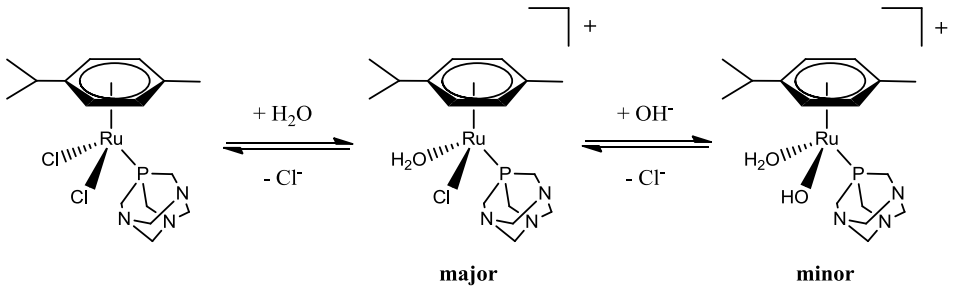

Scheme 4.1 *Hydrolysis of RAPTA-C in pure water.*[54, 55]

In order to study the influence of the chelating *N,O*-dendritic ligand on the behavior of the *N,O*-ruthenium-arene complexes in an aqueous solution, the first-generation *N,O*-ruthenium-hexamethylbenzene-PTA metallodendrimer [**33**][PF_6]$_4$, used to model the higher generation metallodendrimers, was dissolved in D_2O:$(CD_3)_2SO$ (95:5 % *v*/*v*) and the complex monitored by ^1H and $^{31}P\{^1H\}$NMR spectroscopy (Figure 4.21).

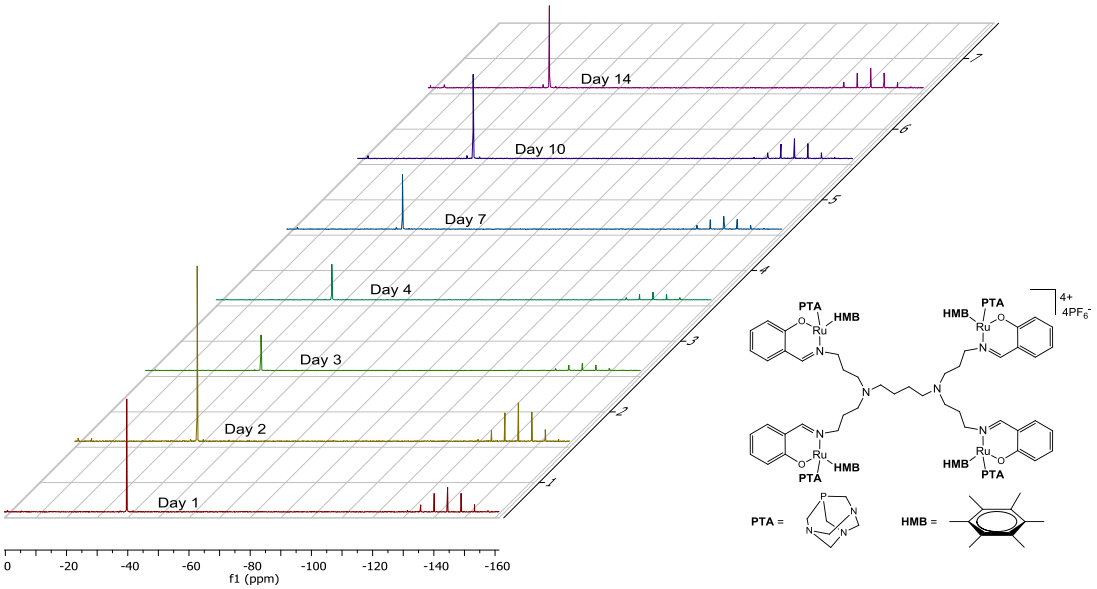

Figure 4.21 *$^{31}P\{^1H\}$ NMR spectra of the metallodendrimer [**33**][PF_6]$_4$ recorded at 37 ºC in D_2O:$(CD_3)_2SO$ (95:5) over 14 days.*

As expected, introduction of the *N,O*-chelate ligand resulted in enhanced stability of the complex. Metallodendrimer [**33**][PF_6]$_4$ is stable over the 14 days with no side-products or aqua-species observed. A similar result was observed by Hanif and co-workers, where a series of dichloride carbohydrate-ruthenium-arene derivatives formed mono aqua species within a few hours.[56] However, exchange of the chlorido ligands by *O,O*-biscarboxylato chelate ligands resulted in enhanced stability of the complexes.[57]

Ideally this type of experiment should be performed under biological conditions (in a buffered solution, at pH 7.4) and in NaCl solutions representative of blood plasma (100 mM) and intracellular (4 mM) concentrations.[14] Nevertheless, the higher generation cationic ruthenium-arene metallodendrimers display good cytotoxicity *in vitro*, and this preliminary investigation suggests the activity may not have been brought on by the formation of the aqua-species and these complexes operate *via* a different mode of action to that of the RAPTA series.

4.3.3 Nucleotide Binding

Though the *N,O*-ruthenium-arene-PTA complexes are inert in water, it has been reported that in the presence of other ligands (such as those found in biological media), these reactions may occur more readily.[56, 58] In particular, the binding of ruthenium-arene complexes to proteinaceous targets is thought to be an important step in the mechanism of action of these complexes,[59-64] though they also have a strong affinity towards DNA.[64, 65] Furthermore, mechanistic studies on the interaction between RAPTA complexes and DNA suggest that these complexes preferentially bind to the purine base, guanine.[66, 67] Hence, the interaction between [**39**][PF_6] (used to model the higher generation metallodendrimers) and nucleotide guanosine 5'-monophosphate (5'GMP) in D_2O:$(CD_3)_2SO$ (95:5 % *v/v*) was monitored by ^1H and $^{31}P\{^1H\}$ NMR spectroscopy. Essentially the mixtures were incubated at 37 ºC for 2h before preliminary NMR experiments were performed. The ^1H NMR spectrum (Figure 4.22) of the mixture shows a downfield shift in the signal assigned to the H8 atom from 8.22 ppm (for free 5'GMP) to 8.64 ppm (for adduct), and is attributed to the formation of the Ru-HMB-5'GMP adduct. Furthermore, this suggests coordination of the 5'GMP to the ruthenium centre *via* the *N*7 atom, with similar shifts in signals observed for other Ru(II) complexes.[66]

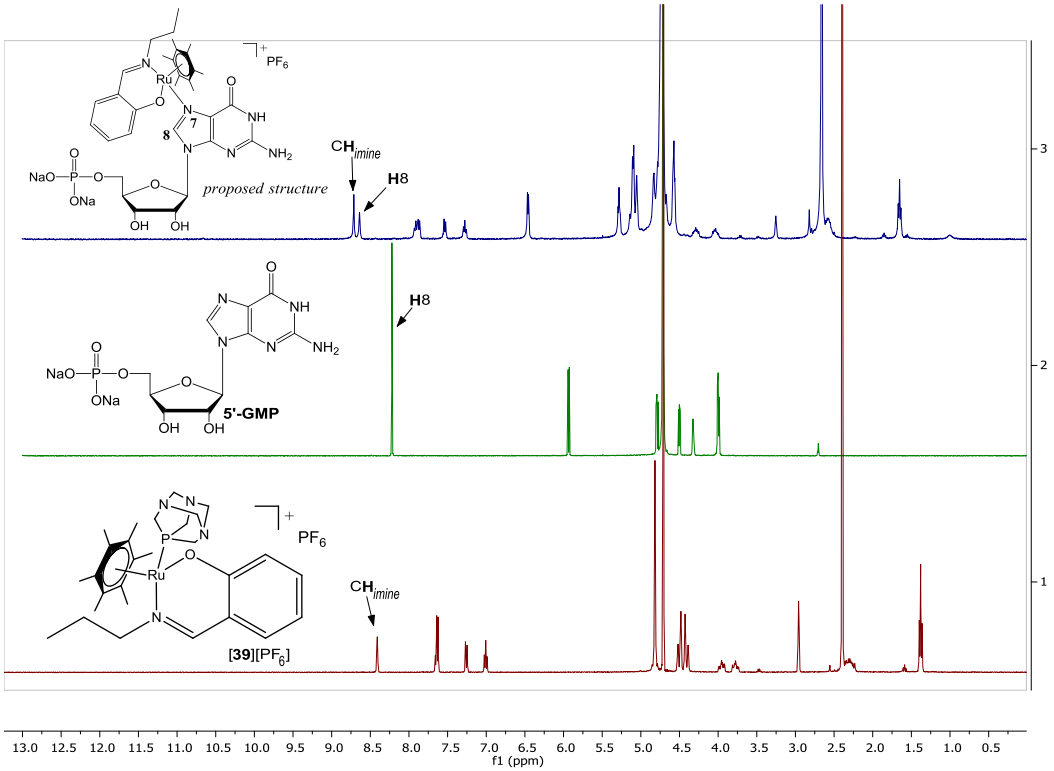

Figure 4.22 *^1H NMR spectra of [**39**][PF_6] (bottom), 5'GMP (middle), and a mixture of [**33**][PF_6] and 5'GMP (ratio 1:1, top) recorded at 37 ºC in D_2O:$(CD_3)_2SO$ (95:5 % v/v) after 2h of incubation. The residual water signal is visible ~4.7 ppm.*

Prior to reaction(s) with biomolecular targets, hydrolysis is considered an essential step in the mechanism of action of ruthenium and platinum complexes.[4, 68] However, for [**39**][PF_6], although hydrolysis was not observed, binding of the *N*7 atom of 5'GMP to the Ru(II) centre is observed. This property has been observed for similar chelating bidentate Ru(II) complexes,[57] and hence hydrolysis may not be a prerequisite, as the biological activity may appear to be brought on by covalent bonding to biomolecular targets. Using the mononuclear complexes [**39**][PF_6] to model the higher generation metallodendrimers, this preliminary investigation suggests these types of systems do bind to the *N*7 atom of the purine base, 5'GMP, *via* the ruthenium centre. Therefore, DNA represents a suitable binding partner for this class of compounds.

4.4 DNA Binding Study of Neutral and Cationic *N,O*-Ruthenium-Arene Metallodendrimers

DNA is a potential drug target for ruthenium-arene drugs and is an important target in cancer therapy.[69] Furthermore, the most cytotoxic ruthenium drugs act as DNA intercalators upon coordination to the suitable ancillary ligand.[70] In order to correlate the antiproliferative activity of the neutral and cationic *N,O*-ruthenium-arene systems to possible interactions with DNA, the compounds were incubated with plasmid DNA for 24 hours and analyzed by gel electrophoresis. As mentioned, DNA is a possible biomolecular target for anticancer drugs and hence the interactions between both the neutral and cationic ruthenium-arene complexes with DNA were investigated.

Gel electrophoresis was employed for the DNA binding studies and is a technique used to separate DNA based on its mobility in an electric field. Mobility of the DNA is primarily based on size. Hence, the larger the DNA adducts the slower the migration of the DNA band down the gel matrix (agarose gel). Typically, the metal complex is incubated with the plasmid DNA and then separated by electrophoresis. This process involves the connection of opposite ends of the gel plate to a power source, which in turn is used to initiate migration of the DNA. Following electrophoresis, the gel is stained with ethidium bromide (staining agent) and the bands analyzed with an UV gel scanner. Incubation of the metal complex with DNA may result in DNA damage which will alter the pattern of migration (*i.e.* retardation of the band).

DNA binding studies were performed by incubating plasmid DNA in the presence of the ruthenium-arene metallodendrimers (**25** - [**36**][PF_6]$_{32}$), their mononuclear analogs ([**38**][PF_6] & [**39**][PF_6]) and cisplatin (cisPt) for 24 h at 37 °C at different metal center/DNA base pair ratios (r = 0.25 and 0.5). The entire series was evaluated as this type of experiment can accommodate the evaluation of several complexes simultaneously. The resulting mixtures were separated by gel electrophoresis and the resulting gels are shown in Figure 4.23.

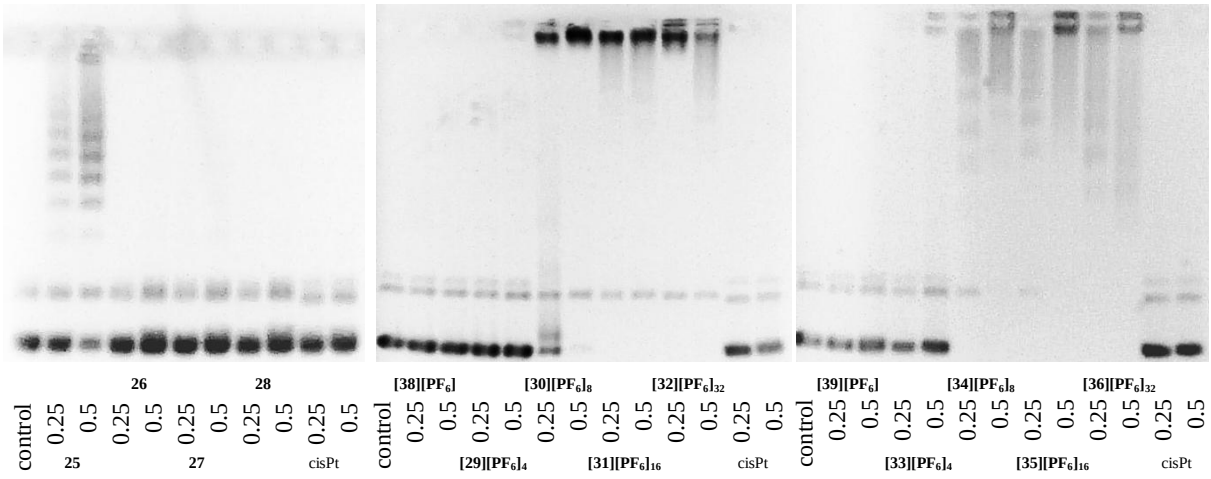

Figure 4.23 *Comparison of DNA damage induced by (from left to right on each gel): (left) the neutral N,O-ruthenium-arene-chlorido complexes **25** - **28** and cisplatin (cisPt: reference compound), (middle) the cationic N,O-ruthenium-p-cymene-PTA complexes [**38**][PF_6], [**29**][PF_6]$_4$ - [**32**][PF_6]$_{32}$ and cisPt, (right) the cationic N,O-ruthenium-hexamethylbenzene-PTA complexes [**39**][PF_6], [**33**][PF_6]$_4$ to [**36**][PF_6]$_{32}$ and cisPt, for 24 h at different metal centre:DNA base pair ratios (r = 0.25 and 0.5); visualized by electrophoretic DNA migration in an agarose gel. Control is DNA alone.*

The cleaving ability of all the compounds was assessed by their efficiency to convert supercoiled *p*BR322 DNA into nicked DNA, while the third form, linear DNA, was not observed by gel electrophoresis. Significant differences between the neutral *N,O*-ruthenium-arene metallodendrimers (**25** - **28**) and the cationic *N,O*-ruthenium-arene-PTA metallodendrimers ([**29**][PF_6]$_4$ - [**36**][PF_6]$_{32}$) were observed. The metallodendrimers bearing chlorido ligands do not seem to interact with DNA (with the exception of **25**). Whilst the metallodendrimers bearing the PTA ligand, which contain eight or more metal centres, appears to form extensive DNA aggregates that are unable to migrate in the gel.

The reason for ready interaction of the cationic *N,O*-ruthenium-arene-PTA metallodendrimers (G_2, G_3 & G_4) with the plasmid DNA is not known. Three possible reasons for this interaction are therefore proposed; firstly there exists negatively charged phosphate groups on the surface of the DNA helix, which in turn allows for electrostatic interactions between these negatively charged groups and the positive chargers on the cationic complexes (Figure 4.24). Furthermore, Eichman and co-workers formed purely organic PAMAM dendrimer-DNA adducts, which resulted from ionic interactions between the negatively charged DNA and the positively charged dendrimer, that were used for gene transfer.[51] Kim *et al.* report the synthesis of argentine-rich PAMAM-based dendrimers, which are able to electrostatically self-assemble with plasmid DNA, forming nanometer-scale complexes.[71]

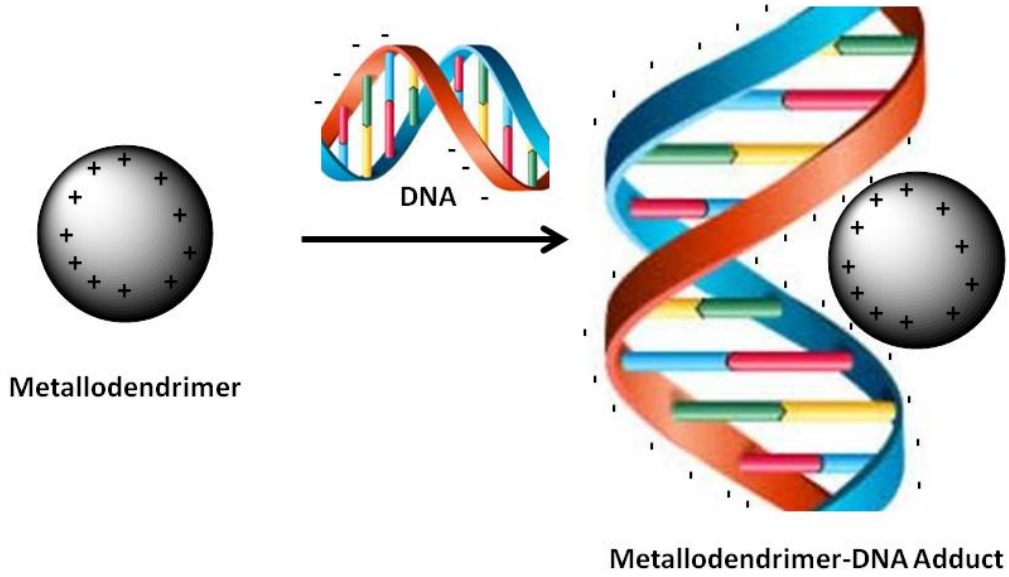

Figure 4.24 *Schematic diagram illustrating the ionic interaction between the positively charged metallodendrimer and the negatively charged DNA back-bone.*[72]

Secondly, the DAB-dendritic scaffold resembles that of naturally occurring polyamines, which are known for their biological activity.[73] Naturally occurring polyamines such as spermidine and putrescine have the ability to interact with nucleic acids of DNA and inhibit DNA replication.[74]

Finally, Sadler and co-workers extensively studied the mechanism of action of a series of ruthenium-arene complexes bearing substituted arenes or arenes with extended π-systems, with particular focus on the interaction between the arene ring and DNA.[70] Studies showed the arene ring provides a hydrophobic face for the complex and enhances π-π stacking interactions between the arene ring and DNA bases. Furthermore, the biomolecular interactions increased with an increase in size of the coordinated arene.

Moreover, there could be a cooperative effect between these possible modes-of-action, resulting in the formation of DNA aggregates and high cytotoxicity of these cationic *N*,*O*-ruthenium-arene metallodendrimers.

4.5 Cell Viability Studies of Ferrocenyl-Derived Metallodendrimers

Research in the medical field is focussed towards the design of new drugs which are active against a wide range of cancers and have fewer side-effects than well-established Pt-based drugs. Ferrocene has gained considerable attention due to it being neutral, chemically stable in an aqueous media and non-toxic. It is easily derivatized and many ferrocenyl-based derivatives display cytotoxic,[75, 76] antitumor,[77, 78] antimalarial[79] and antifungal[80] properties. The activity of these complexes are attributed to their favorable electronic properties and ease of functionalization.[81, 82]

Ferrocene has been linked with both platinum[83, 84] and gold[85] centres, in an attempt to achieve a synergistic effect between the two metals and potentially target multiple drug targets. Similarly, cationic heterometallic *N*,*O*- and *N*,*N*-ruthenium-*p*-cymene metallodendrimers, bearing the ferrocene moiety ([**62**][PF_6]$_4$ - [**65**][PF_6]$_8$, Figure 4.3) were synthesized and discussed in Chapter 3. Preliminary *in vitro* cell viability studies of the ligands and their complexes were evaluated against A2780 and A2780cisR human ovarian cancer cells and is described (Table 4.4).

Cell viability studies involve the use of a viability assay which is used to determine the ability of cells to maintain or recover its viability. In short, by dosing the cells with the test substance at a specific concentration, the cells and the test substance are incubated over a period time and the percentage viable cells then measured. The lower the percentage viability value obtained the more active the test substances are at the specific test concentration.

Table 4.4 *Cell viability values of the ferrocenyl-derived ligands and their heterometallic complexes determined against A2780 and A2780cisR human ovarian cancer cells after 96 h of exposure to the compound.*

				Cell Viability at 5 μM [%]	
Compound	**Metal**	**n**[a]	**Arene**	**A2780**[b]	**A2780cisR**[b]
60	Fe	1	-	7.8 ± 10.1	18.6 ± 4.7
56	Fe	4	-	42.3 ± 34.2	37.3 ± 19.5
57	Fe	8	-	21.1 ± 15.3	36.8 ± 21.7
61	Fe	1	-	26.0 ± 19.4	24.9 ± 20.6
58	Fe	4	-	31.3 ± 28.4	29.4 ± 16.5
59	Fe	8	-	23.0 ± 18.7	30.8 ± 21.5
[**66**][PF_6]	Fe-Ru	1	*p*-cye	70.3 ± 16.0	54.6 ± 5.8
[**62**][PF_6]$_4$	Fe-Ru	4	*p*-cye	-2.3 ± 5.6	-4.3 ± 1.5
[**63**][PF_6]$_8$	Fe-Ru	8	*p*-cye	5.5 ± 12.6	-1.8 ± 4.2
[**67**][PF_6]	Fe-Ru	1	*p*-cye	12.0 ± 9.6	25.5 ± 8.9
[**64**][PF_6]$_4$	Fe-Ru	4	*p*-cye	86.1 ± 26.3	59.9 ± 12.7
[**65**][PF_6]$_8$	Fe-Ru	8	*p*-cye	107.6 ± 97.8	42.5 ±13.1

[a] *n* = number of metals present in the complex.
[b] Cell viability ± standard deviation

The cell viability studies of the ferrocenyl-derived compounds were initially performed at 20 μM and 10 μM dose concentrations, however many of the compounds displayed potent activity, with no structure-activity relationships observed. After lowering the dose concentration to 5 μM, generally both the ferrocenyl-derived ligands **56** - **61** and ferrocenyl-derived ruthenium-*p*-cymene complexes [**62**][PF_6]$_4$ - [**67**][PF_6] are active in both the A2780 and A2780cisR cell lines (Figure 4.25), with the A2780 cell line being the most sensitive and showing no cross resistance to cisplatin.

The moderate results and the large error bars obtained for the ferrocenyl-derived ligands were attributed to the poor solubility of the ligands in the culture medium, with precipitation of the compounds observed at higher concentrations. Nevertheless, the ferrocenyl-derived *N*,*O*- and *N*,*N*- ligands **56 - 59** and **61** display moderate activity in both cell lines, with the monomeric ferrocenyl-derived *N*,*O*-salicylaldiminato ligand **60** displaying good activity (Figure 4.25). However, there is no correlation between the size of the dendritic ligand and the activity observed.

More specifically, it seems the first- and second-generation ferrocenyl-derived *N*,*O*-ruthenium-*p*-cymene-PTA metallodendrimers [**62**][PF_6]$_4$ and [**63**][PF_6]$_8$ are the most active of the heterometallic series (Figure 4.25). There is an increase in activity observed when moving from the mononuclear analog [**66**][PF_6] to the higher generation dendritic derivatives [**62**][PF_6] and [**63**][PF_6]. Furthermore, introduction of the ruthenium-arene moiety does improve the activity in at least two of the metallodendrimers, [**62**][PF_6]$_4$ and [**63**][PF_6]$_8$, and can be attributed to possible transmembrane interactions and increased bioavailability brought on by the ferrocene moiety.[86]

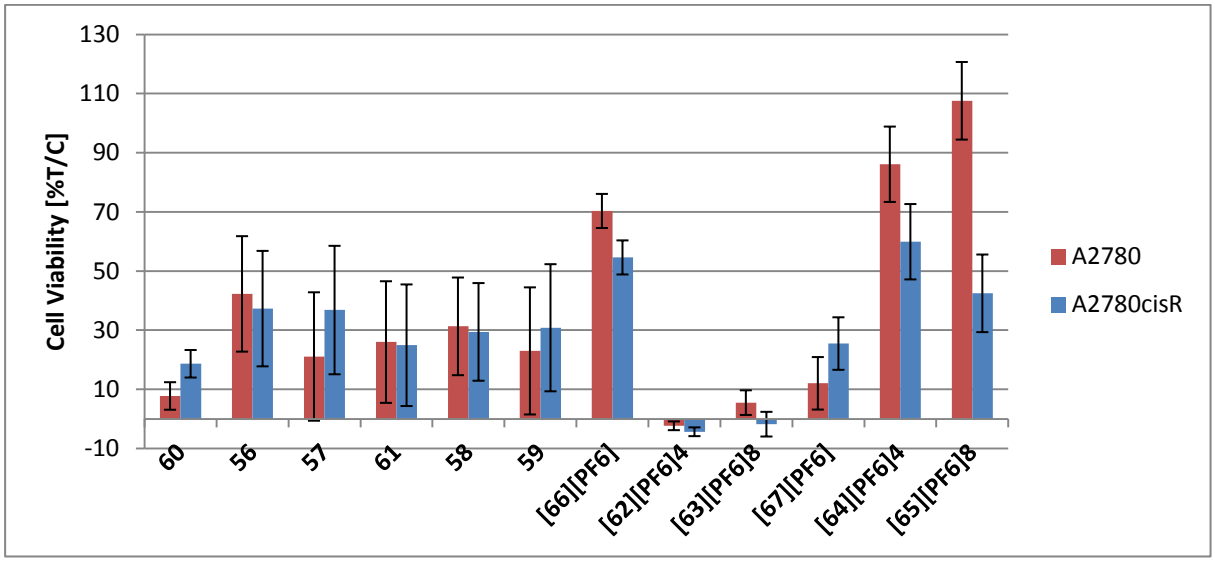

Figure 4.25 *Plot of percentage cell viability against A2780 and A2780cisR cells for ferrocenyl-derived ligands and their complexes: M (**60**, **61**, [**66**][PF_6], [**67**][PF_6]); G1 (**56**, **58**, [**62**][PF_6]$_4$, [**64**][PF_6]$_4$) and G2 (**57**, **59**, [**63**][PF_6]$_8$, [**65**][PF_6]$_8$). Treated cells that grew slower and/or were less viable than the control cells display a negative percent change in cell viability.*

A similar trend was observed by Auzias *et al.*, where ferrocenyl-derived ruthenium-arene complexes displayed improved *in vitro* antitumor activity against A2780 human ovarian cancer cells compared to their ferrocenyl-derived ligands (Figure 4.26).[87]

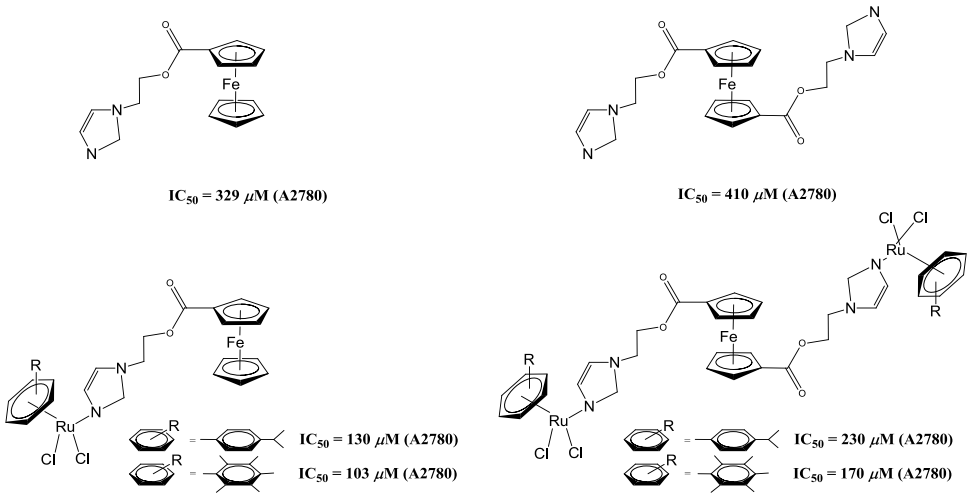

Figure 4.26 *Molecular structures of ferrocenyl-derived ligands and ferrocenyl-derived ruthenium-arene complexes, and IC_{50} values of the compounds in A2780 human ovarian cancer cells.*[87]

This improvement in activity is not observed for the ferrocenyl-derived *N*,*N*-ruthenium-*p*-cymene metallodendrimers [**64**][PF_6]$_4$ and [**65**][PF_6]$_8$ compared to their ferrocenyl-derived dendritic ligands **58** and **59**, with the mononuclear analog [**67**][PF_6] displaying better activity in both cell lines (Figure 4.25).

A direct comparison cannot be made between these heterometallic ferrocenyl-derived ruthenium-arene metallodendrimers mentioned and the homometallic ruthenium-arene-PTA metallodendrimers discussed in Chapter 2. Hence, the next step in the biological evaluation of the heterometallic ferrocenyl-derived ruthenium-arene metallodendrimers is to determine the IC_{50} values of the most active compounds and compare them with the values obtained for the homometallic ruthenium-arene-PTA systems. These experiments could not be performed at the time of submission and will eventually be performed.

4.6 Overall Summary

The neutral *N,O*-ruthenium-arene metallodendrimers **25** - **28** exhibit moderate to high antiproliferative activity against both the A2780 and A2780cisR human ovarian cancer cell lines, particularly the second (**10**, **12**), third (**25**, **27**) and fourth (**26**, **28**) generation derivatives. The neutral *N,O*-ruthenium-hexamethylbenzene derivatives (**11**, **12**, **27**, **28**) display better activity, in both the A2780 and A2780cisR cell lines, compared to their *p*-cymene counter-parts (**9**, **10**, **25**, **26**). Furthermore, the neutral *N,O*-ruthenium-hexamethylbenzene metallodendrimers display no cross-resistance to cisplatin. All of the neutral *N,O*-ruthenium-arene metallodendrimers demonstrate lower toxicity against human embryonic kidney (HEK) cells.

The cationic *N,O*-ruthenium-arene-PTA metallodendrimers [**29**][PF_6]$_4$ - [**36**][PF_6]$_{32}$ display a similar trend in activity to their neutral derivatives (**9** - **12**, **25** - **28**), with an increase in biological activity observed with increase in dendrimer generation. Furthermore, incorporation of the PTA moiety resulted in a vast improvement in the biological activity of these complexes. With an increase in dendrimer generation, there is a decrease in resistance of the cationic ruthenium-hexamethylbenzene-PTA metallodendrimers [**33**][PF_6]$_4$ - [**36**][PF_6]$_{32}$ towards A2780cisR cells. These multinuclear complexes are consistently selective for cancer cells over the healthy cells.

The introduction of the *N,O*-chelate ligand resulted in an enhanced stability of the complexes in solution, suggesting hydrolysis may not be a prerequisite in the mode of action of these complexes. Hence, preliminary NMR experiments confirmed the coordination of the 5'GMP to the ruthenium centre *via* the *N*7 atom and it appears covalent binding to biomolecules might be a prerequisite for these compounds to exhibit their activity. The metallodendrimers bearing chlorido ligands do not seem to interact with DNA, whilst the higher generation metallodendrimers bearing the PTA ligand, appear to form extensive DNA aggregates that are unable to migrate in the gel.

The neutral and cationic osmium-arene complexes (**40** - [**43**][PF_6]$_8$, [**46**][PF_6]$_4$, [**47**][PF_6]$_8$), displayed no improvement in the cytotoxicity of the complexes when replacing ruthenium with osmium.

Preliminary cell viability studies performed on the ferrocenyl-derived ligands **56** - **61** and ferrocenyl-derived ruthenium-*p*-cymene-PTA complexes [**62**][PF_6]$_4$ - [**67**][PF_6] are active at the 5 μM dose concentration in both the A2780 and A2780cisR cell lines. The complexes displayed no cross resistance to cisplatin. The first- and second-generation ferrocenyl-derived *N,O*-ruthenium-*p*-cymene-PTA metallodendrimers [**62**][PF_6]$_4$ and [**63**][PF_6]$_8$ are the most active of the series.

The activity of the neutral and cationic ruthenium-arene metallodendrimers could be improved through suitable modification of the ligand structure and/or preparing higher dendrimer generations of the active compounds. Modification of the arene ring, with more extended arene ring systems, could present an enhanced biological activity. Furthermore, though only a handful of these complexes display poor cytotoxicity *in vitro*, they may display effective *in vivo* activity against metastasis cells, similarly observed for the ruthenium-based anticancer drugs RAPTA-C[14, 15] and NAMI-A.[88, 89]

4.7 References

1. N. Pabla and Z. Dong, *Kidney Int.*, 2008, **73**, 994-1007.
2. E. Wong and C. M. Giandomenico, *Chem. Rev.*, 1999, **99**, 2451-2466.
3. A. Bergamo and G. Sava, *Dalton Trans.*, 2007, **13**, 1267-1272.
4. C. G. Hartinger, S. Zorbas-Seifried, M. A. Jakupec, B. Kynast, H. Zorbas and B. K. Keppler, *J. Inorg. Biochem.*, 2006, **100**, 891-904.
5. C. G. Hartinger, M. A. Jakupec, S. Zorbas-Seifried, M. Groessl, A. Egger, W. Berger, H. Zorbas, P. J. Dyson and B. K. Keppler, *Chem. Biodivers.*, 2008, **5**, 2140-2155.
6. M. J. Clarke, F. C. Zhu and D. R. Frasca, *Chem. Rev.*, 1999, **99**, 2511-2533.
7. W. F. Schmid, R. O. John, V. B. Arion, M. A. Jakupec and B. K. Keppler, *Organometallics*, 2007, **26**, 6643-6652.
8. G. Mühlgassner, C. Bartel, W. F. Schmid, M. A. Jakupec, V. B. Arion and B. K. Keppler, *J. Inorg. Biochem.*, 2012, **116**, 180-187.
9. W. Kandioller, A. Kurzwernhart, M. Hanif, S. M. Meier, H. Henke, B. K. Keppler and C. G. Hartinger, *J. Organomet. Chem.*, 2011, **696**, 999-1010.
10. A. L. Noffke, A. Habtemariam, A. M. Pizarro and P. J. Sadler, *Chem. Commun.*, 2012, **48**, 5219-5246.
11. A. M. Pizarro, A. Habtemariam and P. J. Sadler, *Activation Mechanisms for Organometallic Anticancer Complexes*, Springer, Berlin, 2010.
12. W. H. Ang, A. Casini, G. Sava and P. J. Dyson, *J. Organomet. Chem.*, 2011, **696**, 989-998.
13. A. Casini, C. G. Hartinger, A. A. Nazarov and P. J. Dyson, *Top. Organomet. Chem.*, 2010, **32**, 57-80.
14. C. Scolaro, A. Bergamo, L. Brescacin, R. Delfino, M. Cocchietto, G. Laureneczy, T. J. Geldbach, G. Sava and P. J. Dyson, *J. Med. Chem.*, 2005, **48**, 4161-4171.
15. S. Chatterjee, S. Kundu, A. Bhattacharyya, C. G. Hartinger and P. J. Dyson, *J. Biol. Inorg. Chem.*, 2008, **13**, 1149-1155.
16. L. D. Dale, T. M. Dyson, D. A. Tocher, J. H. Tocher and D. I. Edwards, *Anti-Cancer Drug Des.*, 1989, **4**, 295-302.
17. D. I. Jodrell, T. R. J. Evans, W. Steward, D. Cameron, J. Prendiville, C. Aschele, C. Noberasco, M. Lind, J. Carmichael, N. Dobbs, G. Camboni, B. Gatti and F. De Braud, *Eur. J. Cancer*, 2004, **40**, 1872-1877.
18. G. S. Smith and B. Therrien, *Dalton Trans.*, 2011, **40**, 10793-10800.

19. C. G. Hartinger, A. D. Phillips and A. A. Nazarov, *Curr. Top. Med. Chem.*, 2011, **11**, 2688-2702.
20. W. H. Ang, E. Daldini, L. Juillerat-Jeanneret and P. J. Dyson, *Inorg. Chem.*, 2007, **46**, 9048-9050.
21. M. Hanif, A. A. Nazarov, A. Legin, M. Groessl, V. B. Ario, M. A. Jakupec, Y. O. Tsybin, P. J. Dyson, B. K. Keppler and C. G. Hartinger, *Chem. Commun.*, 2012, 1475-1477.
22. P. Govender, B. Therrien and G. S. Smith, *Eur. J. Inorg. Chem.*, 2012, 2853-2862.
23. H. Yang and W. J. J. Kao, *Biomater. Sci. Polym. Ed.*, 2006, **17**, 3-19.
24. R. E. Bauer, C. G. J. Clark and K. Müllen, *New J. Chem.*, 2007, **31**, 1275-1283.
25. D. Astruc, *Pure Appl. Chem.*, 2003, **75**, 461-481.
26. A. W. Bosman, H. W. Janssen and E. W. Meijer, *Chem. Rev.*, 1999, **99**, 1665-1668.
27. D. F. Baban and L. W. Seymour, *Adv. Drug Delivery Rev.*, 1998, **34**, 109-119.
28. R. Duncan, *STP Pharmacol. Sci.*, 1996, 237-263.
29. P. Govender, N. C. Antonels, J. Mattsson, A. K. Renfrew, P. J. Dyson, J. R. Moss, B. Therrien and G. S. Smith, *J. Organomet. Chem.*, 2009, **694**, 3470-3476.
30. P. Govender, A. K. Renfrew, C. M. Clavel, P. J. Dyson, B. Therrien and G. S. Smith, *Dalton Trans.*, 2011, **40**, 1158-1167.
31. P. J. Dyson and G. Sava, *Dalton Trans.*, 2006, **16**, 1929-1933.
32. S. Grgurić-Šipka, I. Ivanović, G. Rakić, N. Todorović, N. Gligorijević, S. Radulović, V. B. Arion, B. K. Keppler and Z. L. Tešić, *Eur. J. Med. Chem.*, 2010, **45**, 1051-1058.
33. T. Kapp, A. Dullin and R. Gust, *J. Med. Chem.*, 2006, **49**, 1182-1190.
34. X. Zhao, A. C. J. Loo, P. P.-F. Lee, T. T. Y. Tan and C. K. Chu, *J. Inorg. Biochem.*, 2010, **104**, 105-110.
35. B. Cebrián-Losantos, A. A. Krokhin, I. N. Stepanenko, R. Eichinger, M. A. Jakupec, V. B. Arion and B. K. Keppler, *Inorg. Chem.*, 2007, **46**, 5023-5033.
36. G. E. Büchel, I. N. Stepanenko, M. Hejl, M. A. Jakupec, B. K. Keppler and V. B. Arion, *Inorg. Chem.*, 2011, **50**, 7690-7697.
37. A. Dorcier, W. H. Ang, S. Bolano, L. Gonsalvi, L. Juillerat-Jeanneret, G. Laurenezy, M. Peruzzini, A. D. Phillips, F. Zanobini and P. J. Dyson, *Organometallics*, 2006, **25**, 4090-4096.
38. M. Hanif, H. Henke, S. M. Meier, S. Martic, M. Labib, W. Kandioller, M. A. Jakupec, V. B. Arion, H.-B. Kraatz, B. K. Keppler and C. G. Hartinger, *Inorg. Chem.*, 2010, **49**, 7953-7963.

39. A. F. A. Peacock, S. Parsons and P. J. Sadler, *J. Am. Chem. Soc.*, 2006, **129**, 3348-3357.
40. S. H. Van Rijt, A. J. Hebden, T. Amaresekera, R. J. Deeth, G. J. Clarkson, S. Parsons, P. C. McGowan and P. J. Sadler, *J. Med. Chem.*, 2009, **52**, 7753-7764.
41. S. H. Van Rijt, A. F. A. Peacock, R. D. L. Johnstone, S. Parsons and P. J. Sadler, *Inorg. Chem.*, 2009, **48**, 1753-1762.
42. M. Hanif, A. A. Nazarov, C. G. Hartinger, W. Kandioller, M. A. Jakupec, V. B. Ario, P. J. Dyson and B. K. Keppler, *Dalton Trans.*, 2010, **39**, 7345-7352.
43. J. Maksimoska, D. S. Williams, G. E. Atilla-Gokcumen, K. S. M. Smalley, P. J. Carroll, R. D. Webster, P. Filippakopoulos, S. Knapp, M. Herlyn and E. Meggers, *Chem. Eur. J.*, 2008, **14**, 4816-4822.
44. N. P. E. Barry, O. Zava, P. J. Dyson and B. Therrien, *J. Organomet. Chem.*, 2012, **705**, 1-6.
45. N. P. E. Barry and B. Therrien, *Eur. J. Inorg. Chem.*, 2009, 4695-4700.
46. R. E. Morris, R. E. Aird, P. D. S. Murdoch, H. Chen, J. Cummings, N. D. Hughes, S. Parsons, A. Parkin, G. Boyd, D. I. Jodrell and P. J. Sadler, *J. Med. Chem.*, 2001, **44**, 3616-3621.
47. H. Chen, J. A. Parkinson, S. Parsons, R. A. Coxall, R. O. Gould and P. J. Sadler, *J. Am. Chem. Soc.*, 2002, **124**, 3064-3082.
48. M. Gras, B. Therrien, G. Süss-Fink, O. Zava and P. J. Dyson, *Dalton Trans.*, 2010, **39**, 10305-10313.
49. J. Mattsson, P. Govindaswamy, A. K. Renfrew, P. J. Dyson, P. Štěpnička, G. Süss-Fink and B. Therrien, *Organometallics*, 2009, **28**, 4350-4357.
50. R. E. Aird, J. Cummings, A. A. Ritchie, M. Muir, R. E. Morris, H. Chen and P. J. Sadler, *Br. J. Cancer.*, 2002, **86**, 1652-1657.
51. J. D. Eichman, A. U. Bielinska, J. F. Kukowaksa-Latallo and J. R. Backer, *Pharm. Sci. Technol. Today*, 2000, **3**, 232-245.
52. P. J. Dyson, *Chimia*, 2007, **61**, 698-703.
53. H. R. Bhat, S. K. Gupta and U. P. Singh, *RSC Advances*, 2012, **2**, 12690-12695.
54. C. Scolaro, C. G. Hartinger, C. S. Allardyce, B. K. Keppler and P. J. Dyson, *J. Inorg. Biochem.*, 2008, **102**, 1743-1748.
55. C. Gossens, A. Dorcier, P. J. Dyson and U. Rothlisberger, *Organometallics*, 2007, **26**, 3969-3975.

56. I. Berger, M. Hanif, A. A. Nazarov, C. G. Hartinger, R. O. John, M. L. Kuznetsov, M. Groessl, F. Schmitt, O. Zava, F. Biba, V. B. Arion, M. Galanski, M. A. Jakupec, L. Juillerat-Jeanneret, P. J. Dyson and B. K. Keppler, *Chem. Eur. J.*, 2008, **14**, 9046-9057.
57. M. Hanif, S. M. Meier, W. Kandioller, A. Bytzek, M. Hejl, C. G. Hartinger, A. A. Nazarov, V. B. Arion, M. A. Jakupec, P. J. Dyson and B. K. Keppler, *J. Inorg. Biochem.*, 2011, **105**, 224-231.
58. W. H. Ang, E. Daldini, C. Scolaro, R. Scopelliti, L. Juillerat-Jeanneret and P. J. Dyson, *Inorg. Chem.*, 2006, **45**, 9006-9013.
59. W. H. Ang, L. J. Parker, D. L. A., L. Juillerat-Jeanneret, C. J. Morton, M. Lo Bello, M. W. Parker and P. J. Dyson, *Angew. Chem. Int. Ed.*, 2009, **48**, 3854-3857.
60. A. Casini, C. Gabbiani, F. Sorrentino, M. Pia Rigobello, A. Bindoli, T. J. Geldbach, A. Marrone, N. Re, C. G. Hartinger, P. J. Dyson and L. Messori, *J. Med. Chem.*, 2008, **51**, 6773-6781.
61. A. Casini, C. Gabbiani, E. Michelucci, G. Pieraccini, G. Moneti, P. J. Dyson and L. Messori, *J. Biol. Inorg. Chem.*, 2009, **14**, 761-770.
62. A. Casini, A. Karotki, C. Gabbiani, F. Rugi, M. Vasak, L. Messori and P. J. Dyson, *Metallomics*, 2009, **1**, 434-441.
63. M. Groessl, M. Terenghi, A. Casini, L. Elviri, R. Lobinski and P. J. Dyson, *J. Anal. At. Spectrom*, 2010, **25**, 305-313.
64. A. E. Egger, C. G. Hartinger, A. K. Renfrew and P. J. Dyson, *J. Biol. Inorg. Chem.*, 2010, **15**, 919-927.
65. M. Groessl, Y. O. Tsybin, C. G. Hartinger, B. K. Keppler and P. J. Dyson, *J. Biol. Inorg. Chem.*, 2010, **15**, 677-688.
66. A. Dorcier, C. G. Hartinger, R. Scopelliti, R. H. Fish, B. K. Keppler and P. J. Dyson, *J. Inorg. Biochem.*, 2008, **102**, 1066-1076.
67. A. Dorcier, P. J. Dyson, C. Gossens, U. Rothlisberger, R. Scopelliti and I. Tavernelli, *Organometallics*, 2005, **24**, 2114-2123.
68. M. Galanski, M. A. Jakupec and B. K. Keppler, *Curr. Med. Chem.*, 2005, **12**, 2075-2094.
69. F. Wang, J. Bella, J. A. Parkinson and P. J. Sadler, *J. Biol. Inorg. Chem.*, 2005, **10**, 147-155.
70. H.-K. Liu and P. J. Sadler, *Acc. Chem. Res.*, 2011, **44**, 349-359.

71. J.-B. Kim, J. S. Choi, K. Nam, M. Lee, J.-S. Park and J.-K. Lee, *J. Controlled Release*, 2006, **114**, 110-117.
72. R. K. Tekade, P. V. Kumar and N. K. Jain, *Chem. Rev.*, 2009, **109**, 49-87.
73. G. Karigiannis and D. Papaioannou, *Eur. J. Inorg. Chem.*, 2000, 1841-1863.
74. R. A. Casero Jr. and P. M. Woster, *J. Med. Chem.*, 2009, **52**, 4551-4573.
75. P. Meunier, I. Ouattara, B. Gautheron and J. Tirouflet, *Eur. J. Med. Chem.*, 1991, **26**, 351-362.
76. S. Top, J. Tang, A. Vessières, D. Carrez, C. Provot and G. Jaouen, *Chem. Commun.*, 1996, 955-956.
77. P. Köpf-Maier, H. Köpf and E. W. Neuse, *Angew. Chem., Int. Ed. Engl.*, 1984, **23**, 456-457.
78. P. Köpf-Maier and H. Köpf, *Drugs Future*, 1986, **11**, 297-320.
79. C. Biot, N. Francois, L. Maciejewski, J. Brocard and D. Paulain, *Bioorg. Med. Chem. Lett.*, 2000, **10**, 839-841.
80. T. Itoh, S. Shirakami, N. Ishida, Y. Yamashita, T. Yoshida, H.-S. Kim and Y. Wataya, *Med. Chem. Lett.*, 2000, **10**, 1657-1659.
81. P. Pigeon, S. Top, A. Vessières, M. Huché, E. A. Hillard, E. Salmon and G. Jaouen, *J. Med. Chem.*, 2005, **48**, 2814-2821.
82. A. Vessières, S. Top, W. Beck, E. A. Hillard and G. Jaouen, *Dalton Trans.*, 2006, **4**, 529-541.
83. W. Henderson and S. R. Alley, *Inorg. Chem. Acta.*, 2001, **322**, 106-112.
84. Rosenfeld, J. Blum, D. Gibson and A. Ramu, *Inorg. Chem. Acta.*, 1992, **201**, 219-221.
85. M. Viotte, B. Gautheron, M. M. Kubicki, I. E. Nifant'ev and S. P. Fricker, *Met.-Based Drugs*, 1995, **2**, 311-326.
86. C. Ornelas, *New J. Chem.*, 2011, **35**, 1973-1985.
87. M. Auzias, J. Gueniat, B. Therrien, G. Süss-Fink, A. K. Renfrew and P. J. Dyson, *J. Organomet. Chem.*, 2009, **694**, 855-861.
88. S. Zorzet, A. Bergamo, M. Cocchietto, A. Sorc, B. Gava, E. Alessio, E. Iengo and G. Sava, *J. Pharmcol. Exp. Ther.*, 2000, **295**, 927-933.
89. G. Sava, S. Zorzet, C. Turrin, F. Vita, M. R. Soranzo, G. Zabucchi, M. Cocchietto, A. Bergamo, S. Di Giovine, G. Pezzoni, L. Sartor and S. Garbisa, *Clin. Cancer Res.*, 2003, **9**, 1898-1905.

Chapter 5

Synthesis, Characterization and CO-Release of Polynuclear Tricarbonylmanganese(I)-Polypyridyl Complexes Based on Poly(propyleneimine) Dendritic Scaffolds

This chapter forms part of the following publication:

Preshendren Govender, S. Pai, U. Schatzschneider and G. S. Smith, **Next Generation PhotoCORMs: Polynuclear Tricarbonylmanganese(I)-Functionalized Polypyridyl Metallodendrimers,** *Inorganic Chemistry*, 2013, 52, 5470-5478.

5.1 Introduction

More than half a century ago, it was found that carbon monoxide (CO) is constantly formed in small quantities in humans,[1] and has been viewed as highly toxic due to its deleterious effects on the oxygen transport system within the human body.[2] Over the last 10 years, the interest in the biological effects of carbon monoxide has greatly increased, and it is now established in the medical literature that CO does have a major role in mammals as a signalling molecule.[3, 4]

There is growing interest in the use of CO-*releasing molecules* (CORMs) as a stable solid storage form of CO,[5] which is much easier to handle than the toxic gas itself, to eventually investigate the potential therapeutic applications and the biological mode of action at a molecular level.[6] Transition-metal carbonyl complexes are a natural choice as CO-prodrugs and a number of trigger mechanisms to initiate CO-release from the metal coordination sphere have been developed, namely solvent-assisted CO-release and enzyme-triggered CO-release.[7-11] Another important technique is light-induced CO-release in photo-activated CORMs (PhotoCORMs).[5, 12-15]

Light has been used to induce a biological response in “caged” complexes (Figure 5.1), as well as in the context of photodynamic therapy (PDT), where light is used to initiate the production of singlet oxygen by photosensitisers. However, a more well-defined spectrum of cellular targets was required in the form a light-activated ‘active’ species. Hence the synthesis

of light-activated water-soluble molybdenum-containing CORMs [Mo(C≡CCR^{1}R^{2}OH)(η^5-C_5H_5)$(CO)_3$] (**68**, where R = R^1 = Me or R = Me, R^1 = Ph) was pursued (Figure 5.1).[16] The light-activated release of carbonyl ligands and the efficient cellular uptake by HT-29 human colon cancer cells of a Mn-functionalized CORM, *i.e.* $[Mn(CO)_3(tpm)]PF_6$ (**69**, where tpm = tris(pyrazolyl)methane) (Figure 5.1),[17] prompted the investigation into the biocompatibility and the targeting ability of this CORM. Hence, Schatzschneider and co-workers conjugated amino acids and model peptides (**70**) with the $[Mn(CO)_3(tpm)]^+$ *via* Sonogashira cross-coupling and "click" reactions, for a more targeted approach (Figure 5.1).[18] However, incorporation to the bioconjugate did not alter the CO-release properties of the metal carbonyl moiety.

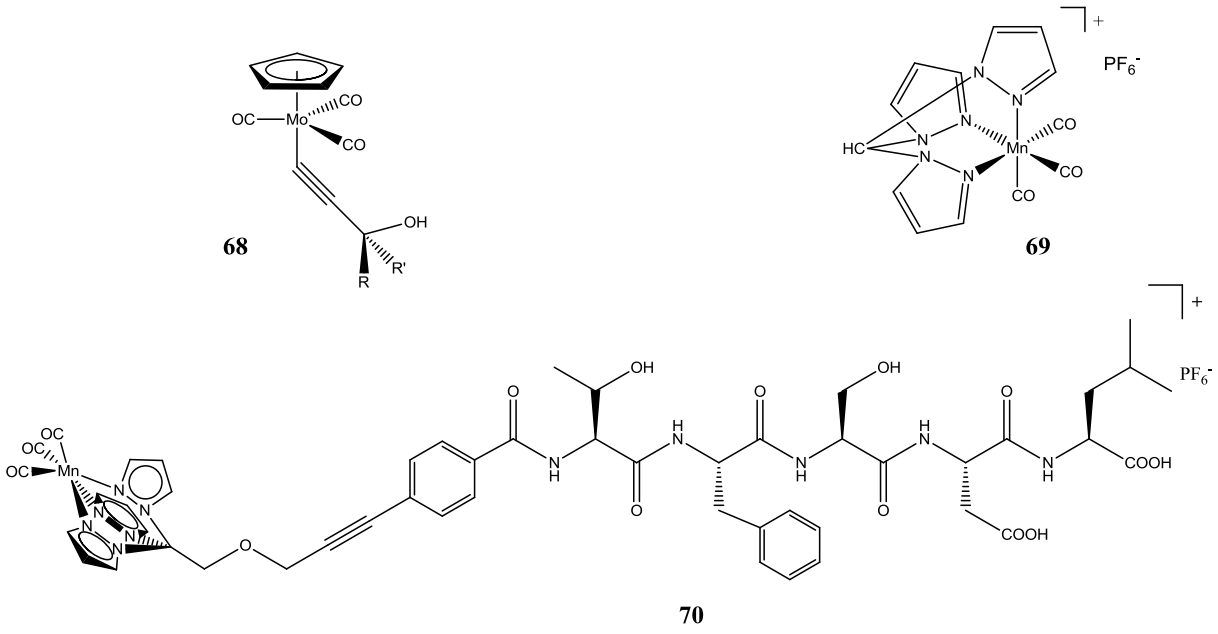

Figure 5.1 *Light-activated CO-releasing molecules.*[16-18]

A common problem with all reported CORMs, is the fact that in addition to the CO liberated, there is always an inevitable formation of a metal-coligand fragment, which might possess a biological activity of its own. One strategy to address this problem is based on systems in which the metal-ligand moiety generated after CO-release remains bound to a macromolecular carrier. In addition to different polymeric materials,[19] dendrimers are an attractive choice for this purpose due to their monodisperse nature and facile preparation. As previously mentioned, such macromolecules are known to passively accumulate in cancerous tissue due to the enhanced permeability and retention (EPR) effect.[20]

In this chapter the synthesis and characterization of novel tetranuclear and octanuclear $Mn(CO)_3$-functionalized CO-releasing metallodendrimers based on polypyridyl dendritic scaffolds is described. The complexes were comprehensively characterized by analytical and spectroscopic methods, and are described. The CO-release of the metallodendrimers was investigated using the myoglobin assay[21] and is discussed. In addition, a mononuclear analog was synthesized as a model of the larger metallodendrimers in order to study potential size-dependent scaling effects on the photoactivated CO-release.

5.2 Synthesis and Characterization of Bipyridyl Ligands

The synthesis of the bipyridyl ligands required the preparation of 4'-methyl-2,2'-bipyridine-4-carboxaldehyde **71** *via* an oxidation reaction with selenium dioxide in 1,4-dioxane (Scheme 5.1).[22-24] Compound **71** was isolated as a white solid in a moderate yield, with the experimental data listed in Chapter 6. The appearance of the singlet at ~10 ppm (CHO proton) in the ^{1}H NMR spectrum and the stretching vibration at ~1700 cm^{-1} (C=O bond) in the infrared spectrum, assigned to the aldehyde functionality, confirms the integrity of **71**.

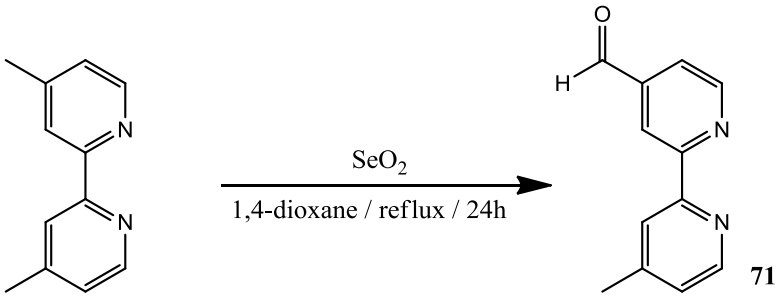

Scheme 5.1 *Synthesis of 4'-methyl-2,2'-bipyridine-4-carboxaldehyde **71**.*

The *N*,*N*-bipyridylimine dendritic ligands **72** and **73** were prepared *via* a Schiff base condensation reaction of **71** with DAB-$\mathbf{G_1}$-PPI-$(NH_2)_4$ (for **72**) or DAB-$\mathbf{G_2}$-PPI-$(NH_2)_8$ (for **73**) in dichloromethane for 48 h (Scheme 5.2). **72** and **73** were isolated as red-brown oils in high yields (89 - 90 %).

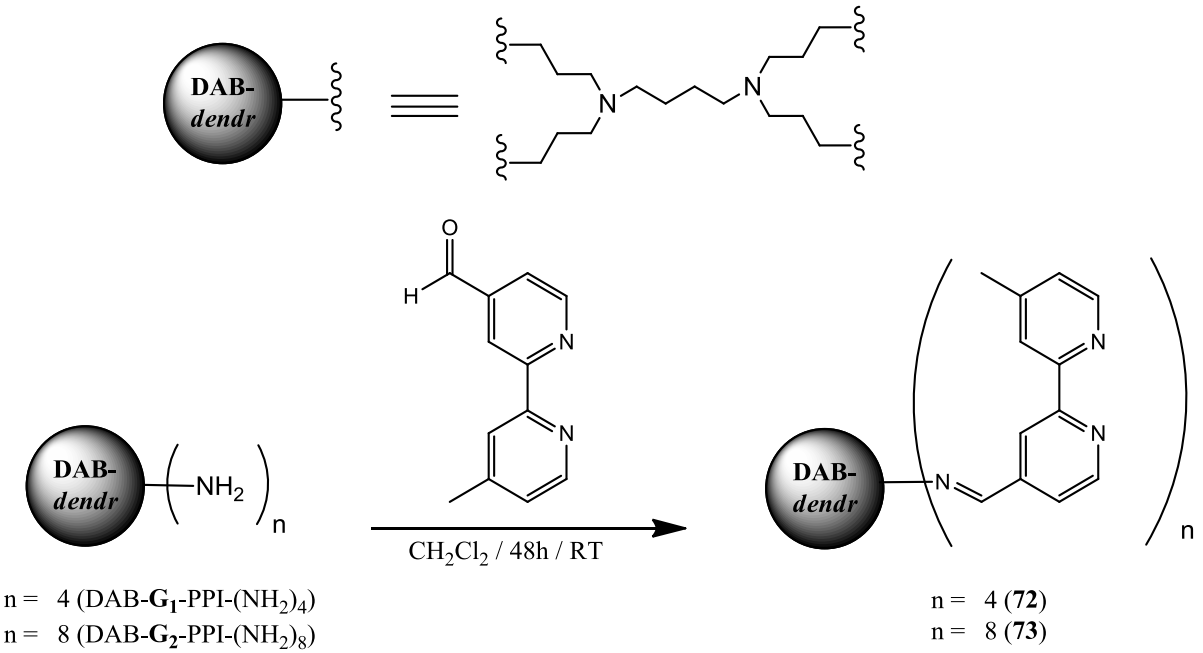

Scheme 5.2 *Synthesis of N,N-bipyridylimine dendritic ligands **72** and **73**.*

Similarly, the *N,N*-bipyridylimine monomeric ligand **74** was prepared by reacting *n*-propylamine and **71** (Scheme 5.3), to afford **74** as a dark yellow oil in a moderate yield. The oils **72 - 74** are soluble in most organic solvents such as dichloromethane, methanol, toluene, diethyl ether and dimethylsulfoxide. Spectroscopic (^{1}H NMR, ^{13}C{^{1}H} NMR and IR spectroscopy) and analytical data (elemental analysis and mass spectrometry) confirmed the integrity of the new ligands.

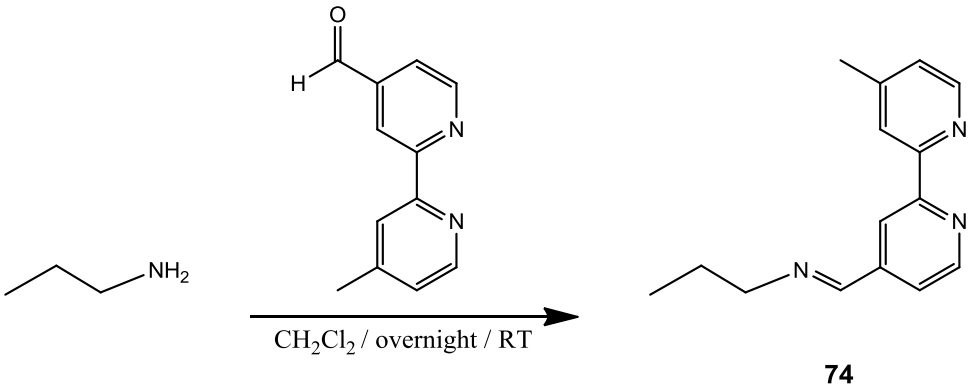

Scheme 5.3 *Synthesis of monomeric N,N-bipyridylimine monomeric ligand **74**.*

5.2.1 ^{1}H and ^{13}C{^{1}H} NMR Spectroscopy

The ^{1}H and ^{13}C{^{1}H} NMR data of **72 - 74** was recorded in deuterated chloroform. A broad singlet at ~8.3 ppm in the ^{1}H NMR spectra for **72** (Figure 5.2) and **73**, which integrates for four and eight protons respectively, is assigned to the imine proton (Table 5.1) and confirms formation of the Schiff base. Additional broad multiplets are observed between 1.4 and 3.7 ppm in the ^{1}H NMR spectra for **72** and **73**, are assigned to the aliphatic protons of the core and arms of the dendritic ligands. The characteristic sharp singlet at ~2.4 ppm, for **72** and **73**, is assigned to the protons on the methyl group.

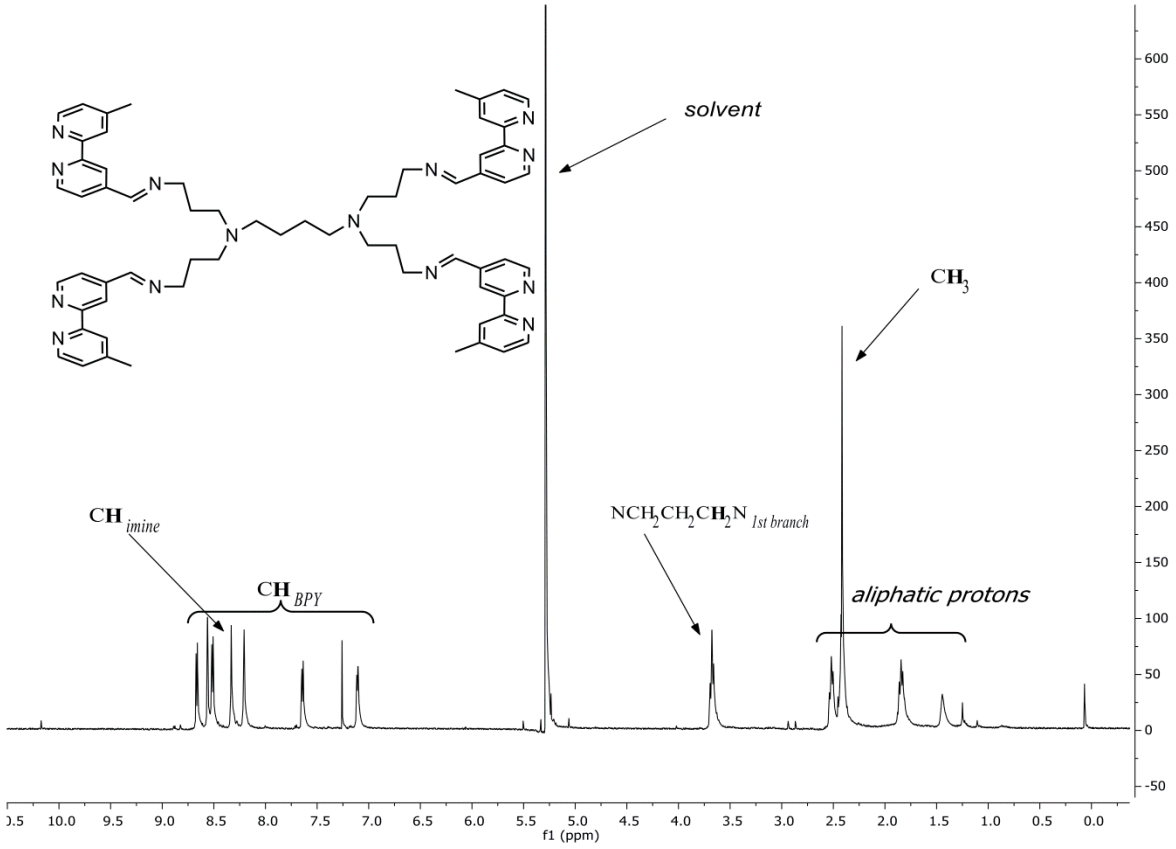

Figure 5.2 *^{1}H NMR spectrum of first-generation N,N-bipyridylimine dendritic ligand* ***72*** *in $CDCl_3$.*

Table 5.1 *Selected spectroscopic and analytical data for ligands **72** - **74**.*

Compound	^{1}H NMR (imine) [ppm][a]	^{13}C{^{1}H} NMR (imine) [ppm][a]	IR (imine) [cm^{-1}][b]	MS ([fragment]$^{+}$) [*m*/*z*][c]
72	8.33	159.3	1648	1038.79 $[M+H]^{+}$
73	8.30	159.2	1648	560.25 $[M+4H]^{4+}$
74	8.32	159.1	1649	239.28 $[M]^{+}$ [d]

[a]Recorded in $CDCl_3$
[b]Recorded in NaCl solution cells in CH_2Cl_2
[c]HR-ESI-TOF-MS
[d]EI-MS

Similar trends and splitting patterns are observed in the ^{1}H NMR spectrum of **74** (Figure 5.3, Table 5.1). The signals observed for the aliphatic protons on the propyl chain appear upfield, with the CH_2 protons closest to the imine moiety assigned to the broad triplet observed at ~3.7 ppm.

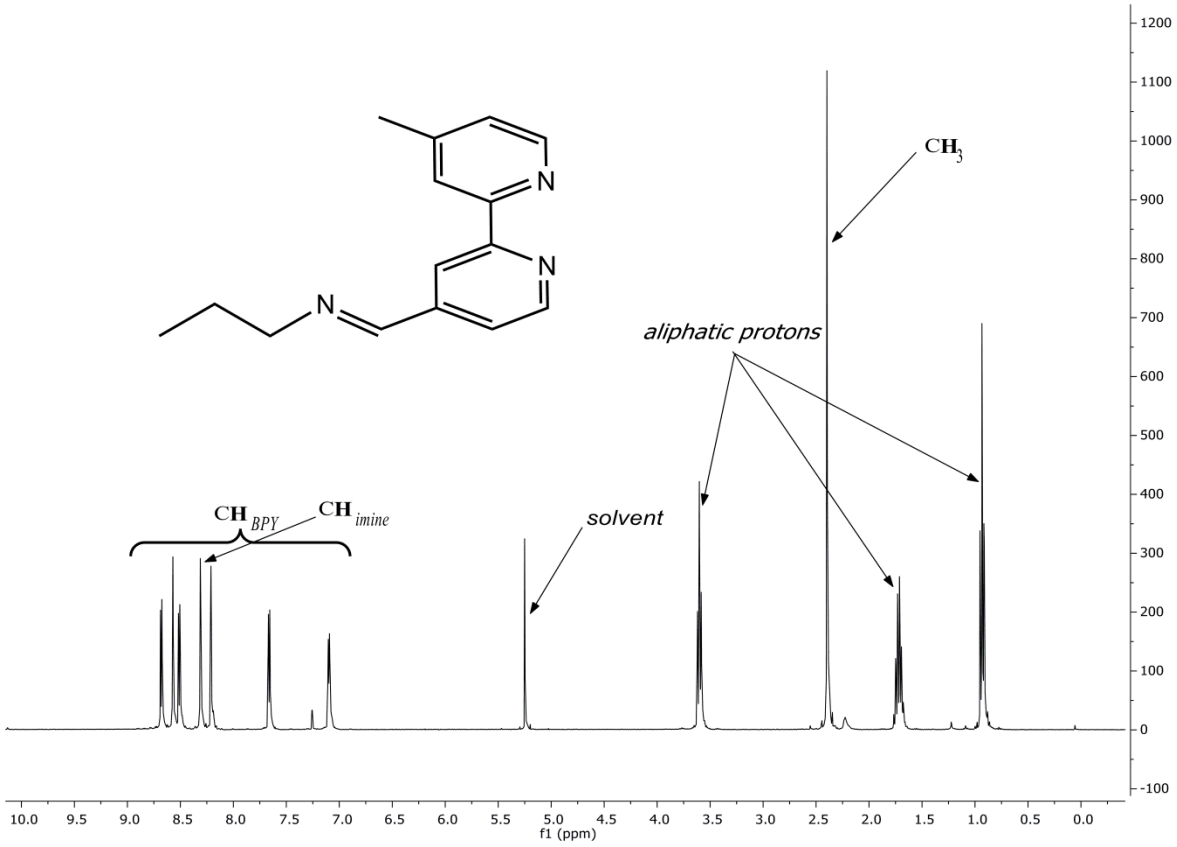

Figure 5.3 *^{1}H NMR spectrum of monomeric N,N-bipyridylimine ligand **74** in $CDCl_3$.*

Several peaks are observed in the aromatic region, of the ^{1}H NMR spectrum of **72** - **74**, between 7.0 and 9.0 ppm and are assigned to the protons on the bpy (bipyridyl) moieties. With aid of the 2D-COSY NMR spectrum (Figure 5.4) of **74**, assignments of the aromatic signals of the protons on the bpy moiety and the imine proton are assigned and are listed in Chapter 6.

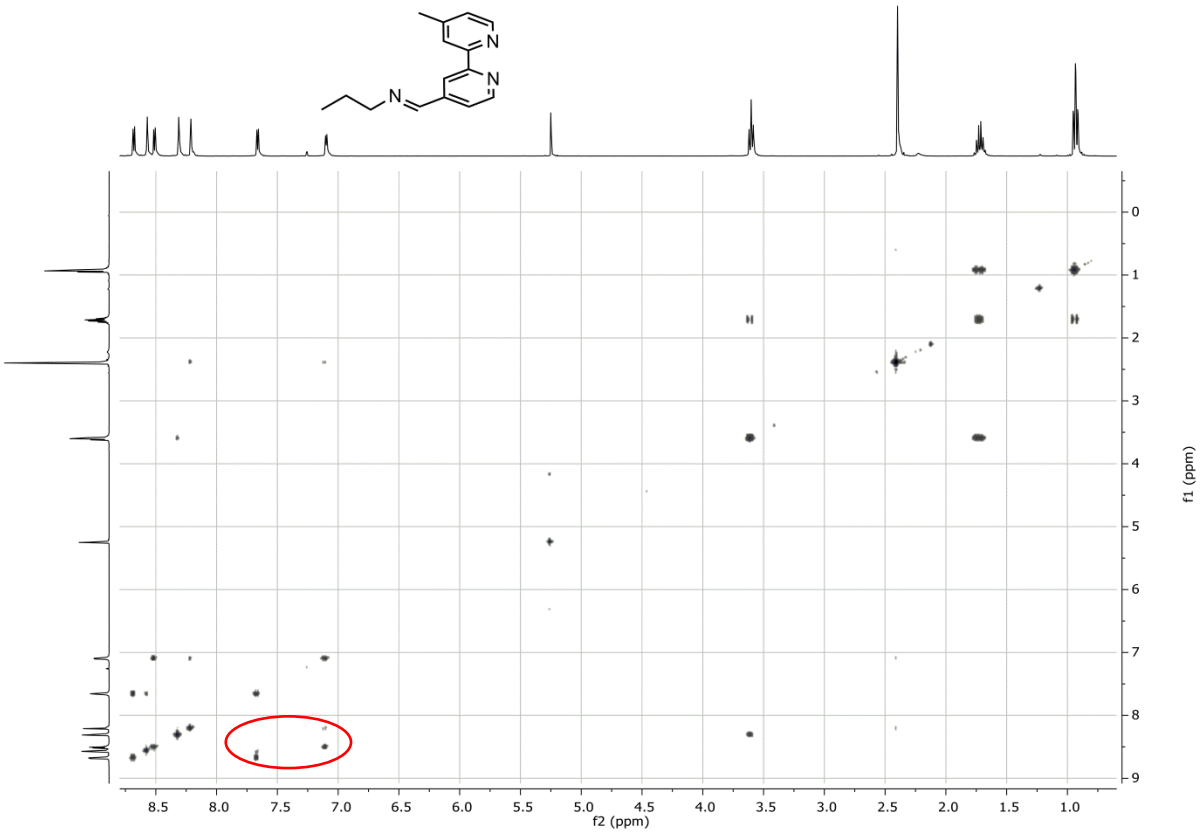

Figure 5.4 *2D-COSY NMR spectrum of the N,N-bipyridylimine monomeric ligand **74** in $CDCl_3$.*

The ^{13}C{^{1}H} NMR data of **72** - **74** gave the expected carbon peaks for each compound (Table 5.1). No significant changes were observed in the chemical shifts of the signals observed when moving from the first-generation **72** to the second-generation **73**. Signals for the aliphatic carbons are observed between 20 - 60 ppm and aromatic carbons seen between 120 - 160 ppm for **72** - **74**. In the ^{13}C{^{1}H} NMR spectra of **72** - **74**, four singlets of medium intensity are observed between 144 ppm and 158 ppm and are assigned to the quaternary carbons of the bpy moiety (Figure 5.5).

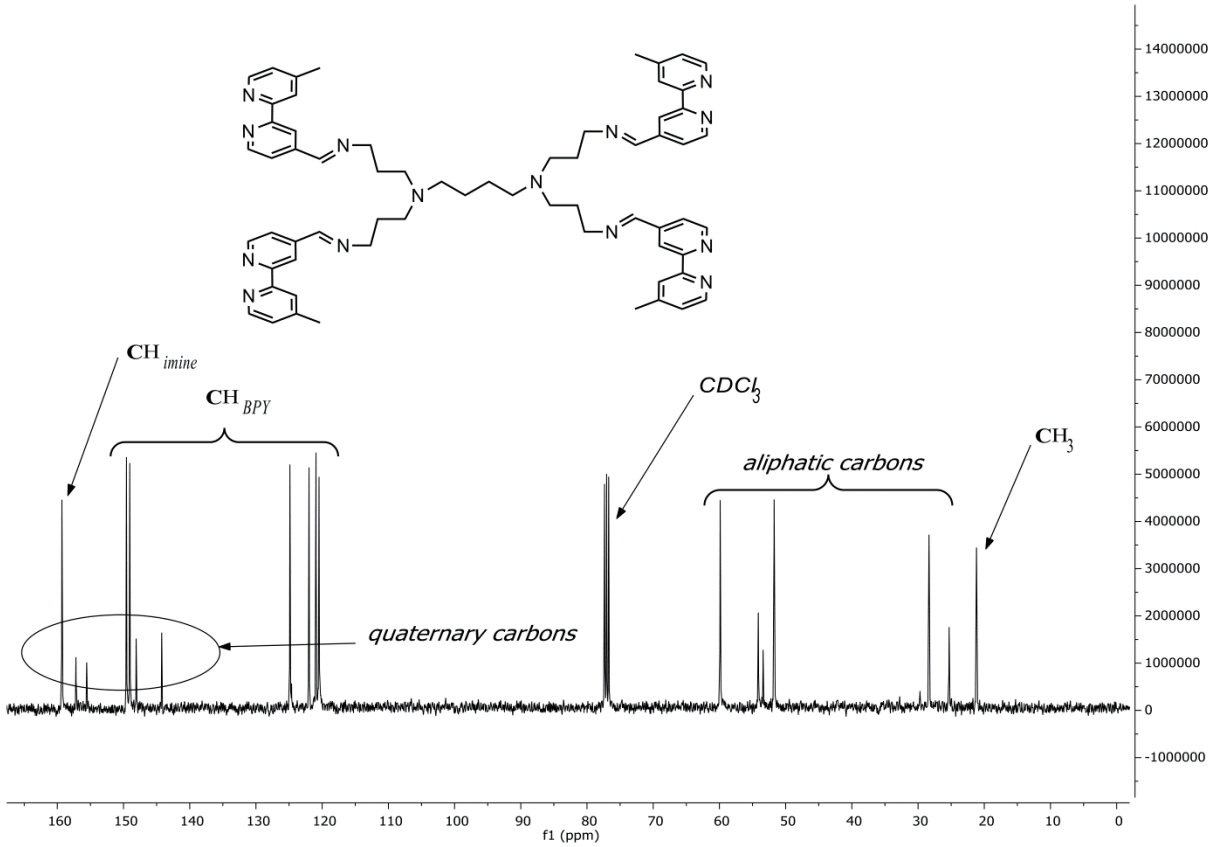

Figure 5.5 *$^{13}C\{^{1}H\}$ NMR spectrum of the first-generation N,N-bipyridylimine dendritic ligand **72** in $CDCl_3$.*

5.2.2 Infrared Spectroscopy

Along with ^{1}H and $^{13}C\{^{1}H\}$ NMR, formation of the imine bond is confirmed by the diagnostic C=N absorption band at ~1648 cm^{-1} in the infrared spectrum for ligands **72** - **74** (Table 5.1). An absorption band at ~1600 cm^{-1} is observed and was attributed to the C=N bond present in the bpy moiety.

5.2.3 Elemental Analysis and Mass Spectrometry

Elemental analysis and mass spectrometry analysis (Table 5.1) confirmed the integrity of the new ligands **72** - **74**. Following extensive drying, elemental analysis data were found within acceptable limits for **72** - **74**, with no solvent inclusion observed. HR-ESI-mass spectrometry analysis showed the highest molecular weight fragment of $[M+H]^{+}$ and $[M+4H]^{4+}$ for **72** and **73** respectively, whilst the EI-MS data for **74** displayed a peak for $[M]^{+}$.

5.3 Synthesis and Characterization of $Mn(CO)_3$-Functionalized Metallodendrimers

The tricarbonylmanganese(I) functionalized tetranuclear **75**, octanuclear **76** and mononuclear **77** complexes were synthesized *via* reaction of manganese pentacarbonyl bromide [$Mn(CO)_5Br$] and ligands **72**, **73** and **74** respectively in dichloromethane at room temperature, under the exclusion of light (*i.e.* in the dark) (Scheme 5.4 and Scheme 5.5).

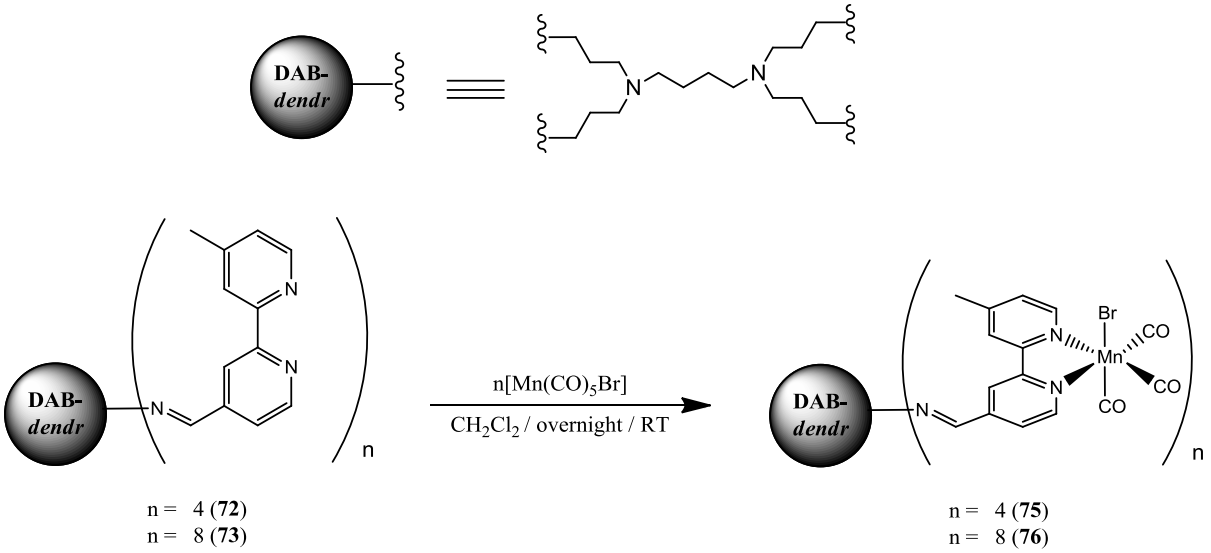

Scheme 5.4 *Synthesis of tricarbonylmanganese(I) functionalized tetranuclear (**75**) and octanuclear (**76**) metallodendrimers.*

The workup was performed with minimal exposure to light. Precipitation with diethyl ether, afforded the crude products **75** and **76** as yellow-orange solids in moderate yield. Heptane was used to precipitate **77** as an orange solid in low yield. Complexes **75** - **77** were purified with RP-HPLC using a gradient of 5 - 90 % acetonitrile/water with 0.1 % TFA, and are soluble in most polar solvents.

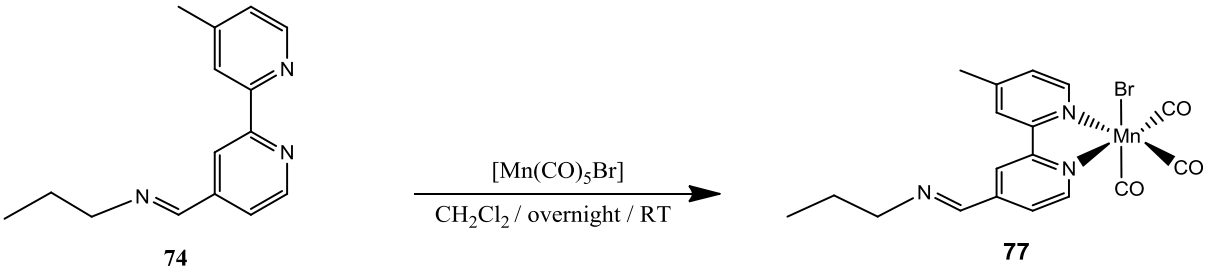

Scheme 5.5 *Synthesis of tricarbonylmanganese(I) functionalized mononuclear complex **77**.*

5.3.1 ^{1}H and ^{13}C{^{1}H} NMR Spectroscopy

The ^{1}H NMR spectra of complexes **75 - 77** were recorded in deuterated dimethylsulfoxide and showed all the relevant peaks for the proposed structures. Broad overlapping signals (possibly due to the fact that the Mn(I) centre is paramagnetic) are observed in the ^{1}H NMR spectra of **75** (Figure 5.6) and **76** and are assigned to the aliphatic protons of the dendritic core and arms, characteristically seen with other similar metallodendrimers.[25-28]

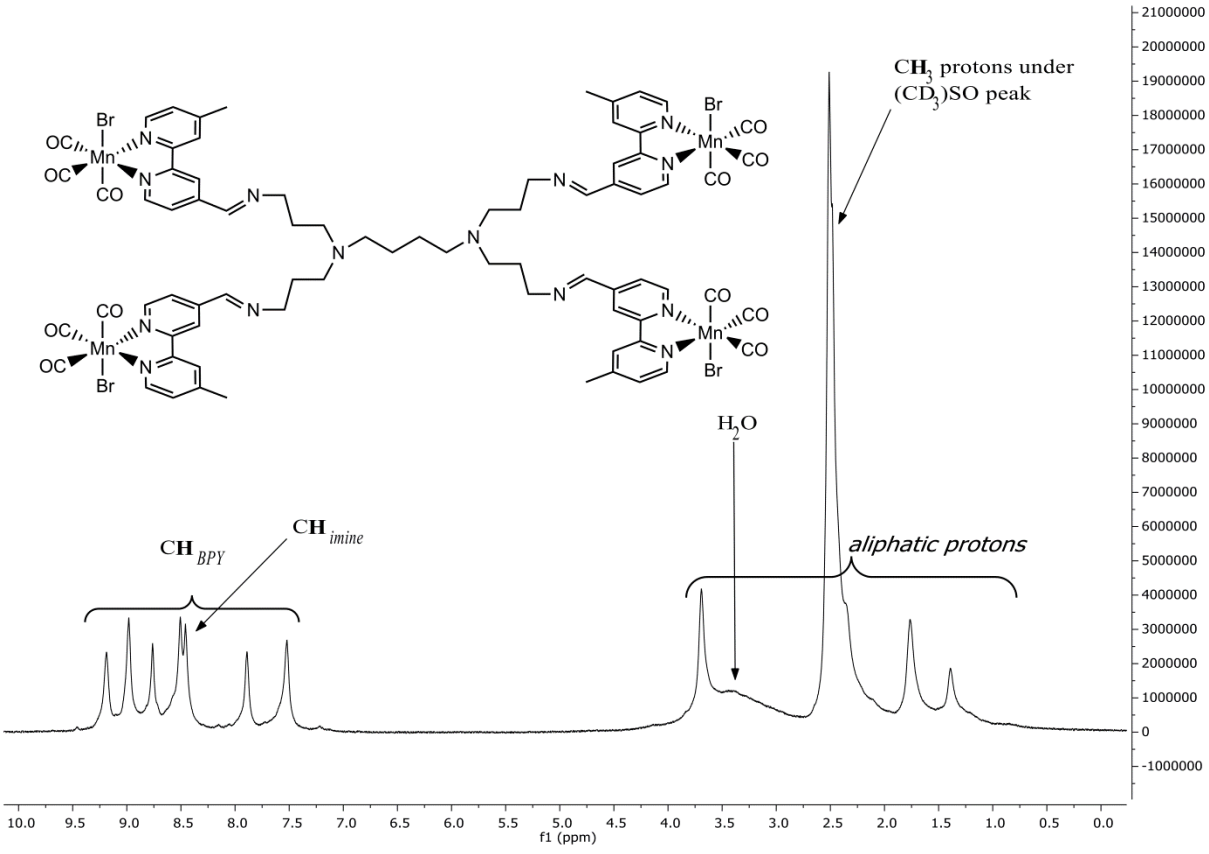

Figure 5.6 *^{1}H NMR spectrum of the first-generation tricarbonylmanganese(I) functionalized metallodendrimer **75** in $(CD_3)_2SO$.*

There is a small downfield shift in the signal assigned to the imine proton form ~8.3 ppm in the ligands **72 - 74** to ~8.5 ppm in the complexes **75 - 77** (Table 5.2). However, the shift is not large enough to suggest coordination of the manganese moiety occurs at the imine nitrogen. Additionally, there is a downfield shift in the two doublets, assigned to protons adjacent to the pyridyl nitrogen, from ~8.5 ppm and ~8.7 ppm in the ligand to ~9.0 ppm and ~9.3 ppm in the complexes **75 - 77**. The shift in signals suggests coordination occurs in a bidentate manner at both the bipyridyl nitrogens, rather than in a monodentate coordination at the imine nitrogen.

Table 5.2 *Selected spectroscopic and analytical data for tricarbonylmanganese(I) functionalized complexes **75 - 77**.*

Compound	^{1}H NMR (imine) [ppm][a]	^{13}C{^{1}H} NMR (imine) [ppm][a]	IR (imine) [cm^{-1}][b]	MS ([fragment]$^{+}$) [*m*/*z*][c]
75	8.46	158.0	1644	961.57 $[M+2H]^{2+}$
76	8.43	157.8	1644	1344.59 $[M+3H]^{3+}$
77	8.53	158.2	1644	462.02 $[M+H]^{+}$

[a]Recorded in $(CD_3)_2SO$
[b]Recorded as pure solids (ATR)
[c]HR-ESI-TOF-MS

^{13}C{^{1}H} NMR spectra for complexes **75 - 77** were recorded in deuterated dimethylsulfoxide and gave the expected number of carbon signals for the proposed structures. Similarly, shifts in the signals observed in the ^{1}H NMR spectra for complexes **75 - 77**, were observed in the ^{13}C{^{1}H} NMR spectra. As expected, the singlet assigned to the carbon atom of the imine functionality remains constant at ~158 ppm in both the ligands **72 - 74** and the complexes **75 - 77** (Table 5.2). Furthermore, three singlets observed in the ^{13}C{^{1}H} NMR spectrum (Figure 5.7) at about 220, 221, and 223 ppm also confirm the presence and integrity of the $Mn(CO)_3$ functionality.

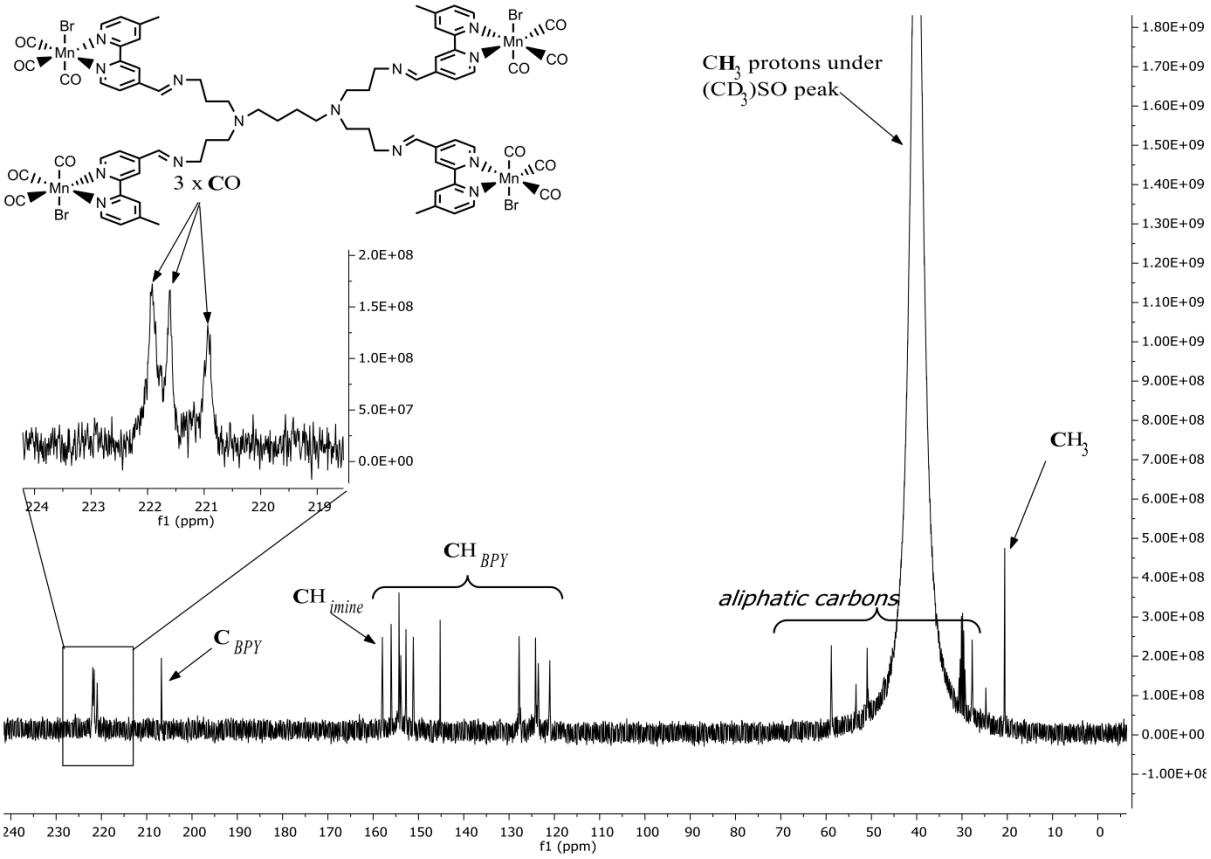

Figure 5.7 *$^{13}C\{^{1}H\}$ NMR spectrum of the first-generation tricarbonylmanganese(I) functionalized metallodendrimer **75** in $(CD_3)_2SO$, with expansion of three singlets inset.*

5.3.2 Infrared Spectroscopy

The infrared spectrum of complexes **75** - **77** were recorded as pure solids using the ATR technique. Three strong stretching vibrations are observed at about 1900 cm^{-1}, 1920 cm^{-1} and 2020 cm^{-1} and are assigned to the C≡O stretching vibrations of the manganese functionality (Figure 5.8). These stretching vibrations are comparable with other manganese-tricarbonyl mononuclear complexes reported.[29-31] The shift to higher wavenumbers of the stretching vibration assigned to the C=N group of the bpy moiety, from ~1600 cm^{-1} (ligand) to ~1620 cm^{-1} (complex), indicates that complexation occurred *via* the two pyridyl nitrogen atoms and not *via* the imine nitrogen atom, as there is no shift in the stretching vibration of the imine bond (constant at ~1650 cm^{-1}).

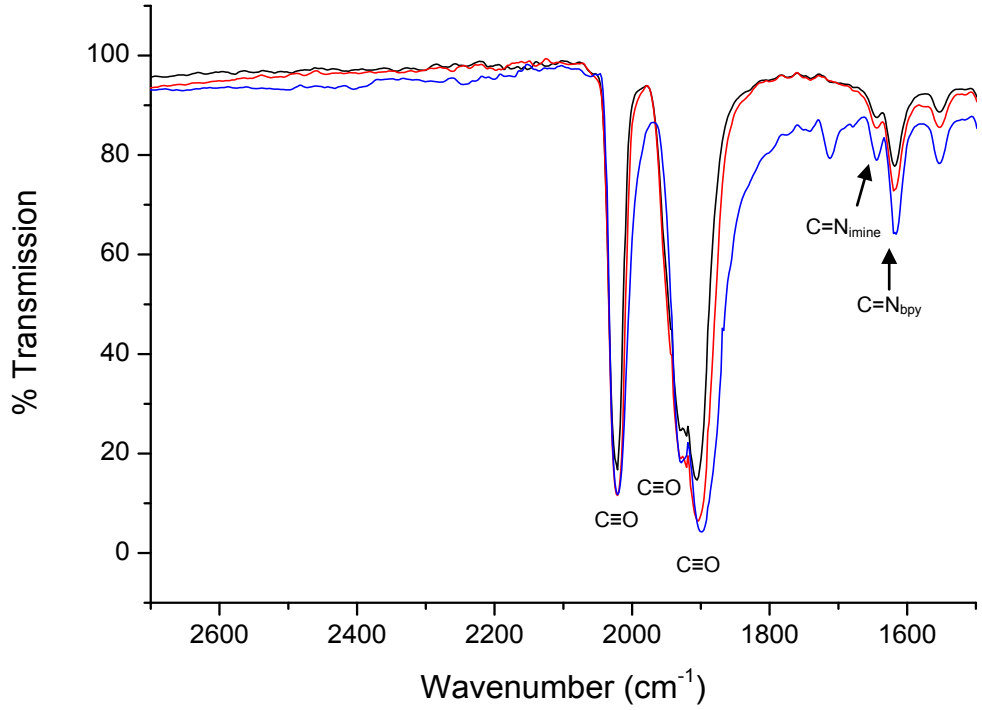

Figure 5.8 *IR (ATR) spectra of tricarbonylmanganese(I) functionalized complexes **75** (black), **76** (red) and **77** (blue).*

5.3.3 Mass Spectrometry and HPLC

HR-ESI-TOF mass spectrometric data further confirmed the structural integrity of metallodendrimers **75** and **76**. Mass spectral data of **75** and **76** displayed the highest molecular weight fragment of $[M+2H]^{2+}$ and $[M+3H]^{3+}$ respectively, whilst the mass spectral data for **77** displayed a peak for $[M+H]^{+}$ (Table 5.2). Elemental analysis data for **75** - **77** were not obtained due to the instability of the complexes (discussed in section 5.4), and hence analytical-HPLC traces were obtained of **75** - **77**. Single peaks (t_R = ~23 min) are observed in the analytical-HPLC traces of **75** (Figure 5.9) - **77**, and further attests to the purity of the metal complexes. The smaller shoulder peak in the analytical-HPLC trace for 75 was attributed to trace impurities present in the sample.

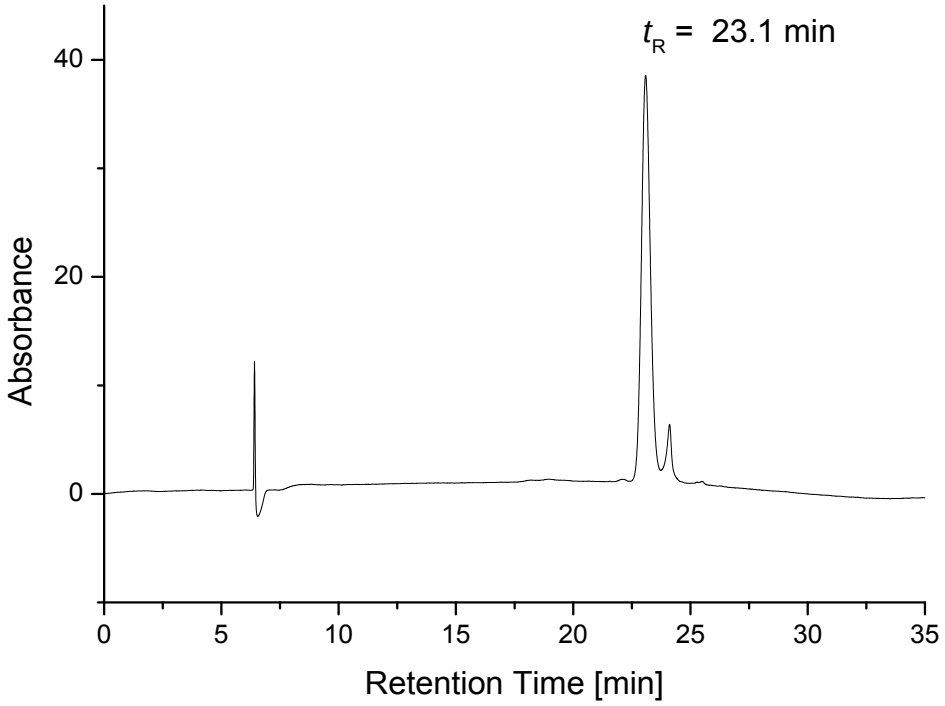

Figure 5.9 *Analytical HPLC trace of metallodendrimer **75** with a gradient of acetonitrile/water 5 - 90 %, over 35 min, flow rate of 0.6 mL/min, showing one major peak at t_R = 23.1 min.*

5.4 Long-Term Stability of Compounds

When compounds **75** - **77** are exposed to natural daylight for an extended period of time, a pronounced decrease in the intensity of the signals for the $Mn(CO)_3$ moiety between 2025 cm^{-1} and 1900 cm^{-1} is observed in the infrared spectra (Figure 5.10). This is indicative of significant structural changes in the metal-carbonyl group and a first indicator of the CO-release from these compounds. In addition, dimethylsulfoxide solutions of the complexes lose their bright orange colour and become a dark brown colour with a brown precipitate (possibly manganese dioxide), following prolonged exposure to natural daylight (Figure 5.11). The dark stability of the compounds **75** - **77** will be discussed in section 5.5.2.

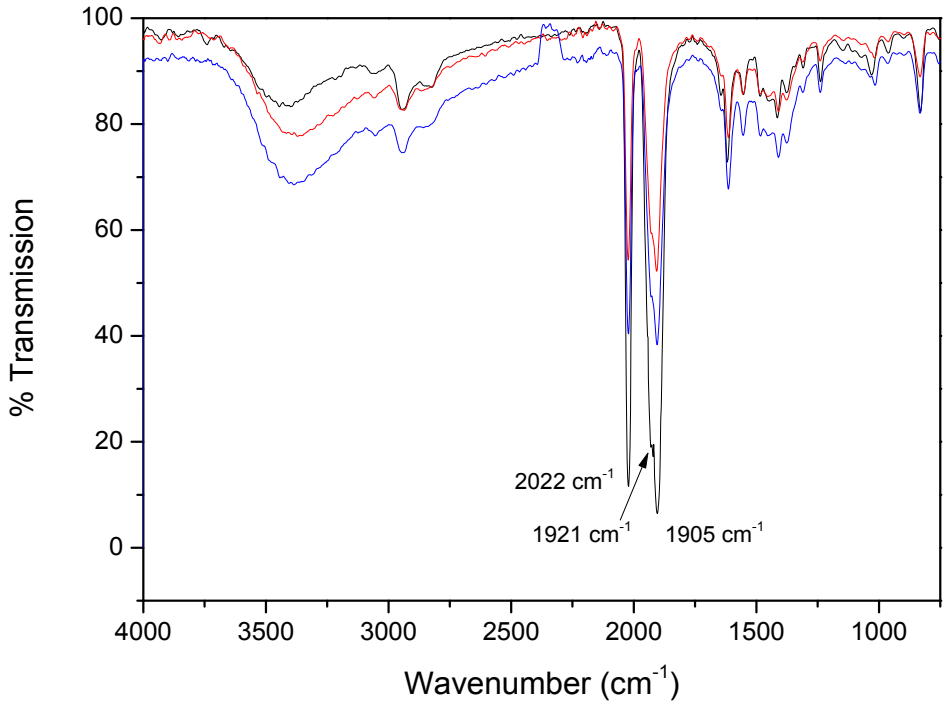

Figure 5.10 *IR (ATR) spectra of metallodendrimer **75** for a freshly prepared sample (black) and after exposure to natural daylight for 1.5 h (blue) and 24 h (red).*

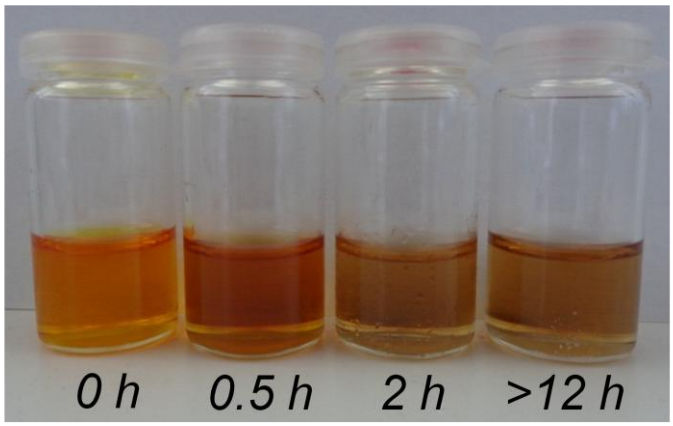

Figure 5.11 *Photograph of metallodendrimer **75** (DMSO solution) following exposure to natural daylight for set time intervals.*

5.5 Electronic Absorption Spectra and CO-Release Properties

5.5.1 Absorption Maxima and Molar Extinction Coefficients

The absorbance maxima and molar extinction coefficients of complexes **75** - **77** were determined in a mixture of dimethylsulfoxide and water (10:90 % *v*/*v*). Two broad bands are observed for all compounds **75** - **77** at ~300 nm (λ_1) and, at somewhat lower intensity, in the range of 370 nm to 450 nm (λ_2) (Figure 5.12). Assignments of the bands are based on structurally similar mononuclear complexes reported in the literature.[32, 33]

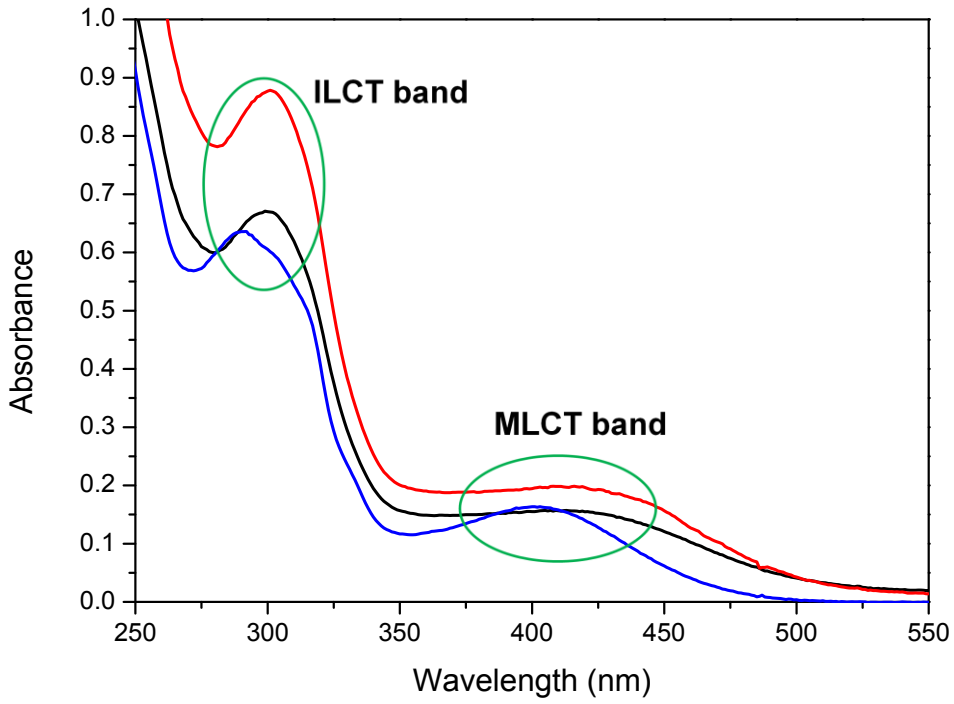

Figure 5.12 *Overlay of the electronic absorption spectra of complexes* ***75*** *(black),* ***76*** *(red), and* ***77*** *(blue) in dimethylsulfoxide/water (10:90 % v/v).*

The absorption band at λ_1 is assigned to the intraligand charge-transfer (ILCT) band and is attributed to the spin allowed intraligand $\pi \rightarrow \pi^*$ transitions of the bpy moiety. The absorption band at λ_2 is assigned to the metal-ligand charge-transfer (MLCT) band. The position of the low-energy MLCT transition at λ_2 increases slightly upon moving from **75** to **76**, by about 10 nm, while the higher energy ILCT band at λ_1 remains unchanged. The absorption maxima and the molar extinction coefficients are listed in Table 5.3. The increase in molar extinction coefficients for both bands is more pronounced, on moving from the mononuclear compound **77** to the metallodendrimers **75** and **76**. There is an increase in the molar extinction coefficient by a factor of ~3.3, on moving from mononuclear **77** to metallodendrimer **76**, and the molar

extinction coefficient further doubles on moving from **75** to **76**, which is expected when comparing the increase in the number of manganese-tricarbonyl groups per compound. This confirms the linear scaling of the optical properties with increasing dendrimer generation.

Table 5.3 *Absorption maxima and molar extinction coefficient of complexes **75** - **77**.*

Compound	Absorption maxima λ_1 [nm]	ε_1 [$M^{-1}cm^{-1}$][a]	Absorption maxima λ_2 [nm]	ε_2 [$M^{-1}cm^{-1}$][a]
75	300	47 717 ± 1413	410	10 371 ± 550
76	300	91 606 ± 657	420	18 799 ± 818
77	290	13 278 ± 370	400	3 527 ± 194

[a] Molar extinction coefficient ± standard error

5.5.2 Dark Stability and CO-Release Properties

As discussed in Section 5.4, exposure of compounds **75** - **77** to natural daylight resulted in the compounds undergoing structural changes (Figure 5.8). Hence, to obtain insight into the photoinduced CO-release and the dark stability of compounds **75** - **77**, the complexes were incubated in a dimethylsulfoxide/water (10:90 % *v*/*v*) solution in the absence of light. The complexes were incubated for a 16 h (**75** (Figure 5.13 and Figure 5.14) and **76** only) and 15 h (**77** only) period in the dark and the absorbance measured every 30 min. All three compounds showed good dark stability in the aqueous solution with only negligible spectral fluctuations observed at around 300 and 410 nm.

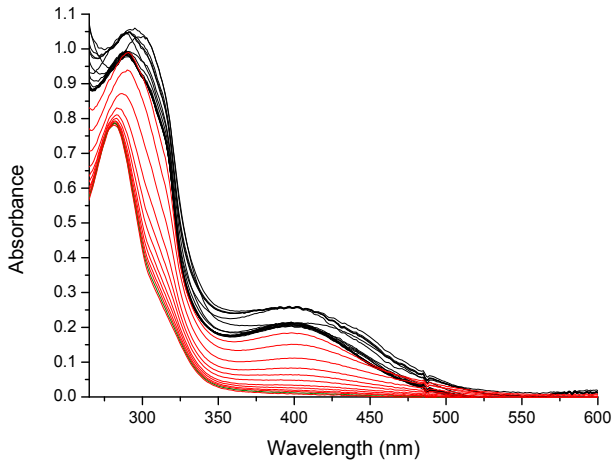

Figure 5.13 *UV/Vis spectral traces of metallodendrimer **75** in dimethylsulfoxide/water (10:90 % v/v) during incubation in the dark (0 to 16 h, black) followed by photoactivation with a LED array at 410 nm for 12 min (red).*

The compounds were then irradiated with a custom-made LED cluster at 410 nm, coincident with the MLCT absorption maximum λ_2. Irradiations were interrupted in 1 min intervals to measure the absorbance of the compounds **75** - **77**. In stark contrast, irradiation at 410 nm resulted in a pronounced decrease of the broad band centered at around 400 nm to almost zero towards the end of the experiment and a blue-shift of the peak at around 300 nm. Plateau values were reached after about 10 - 15 min with no further spectral changes upon extended irradiation.

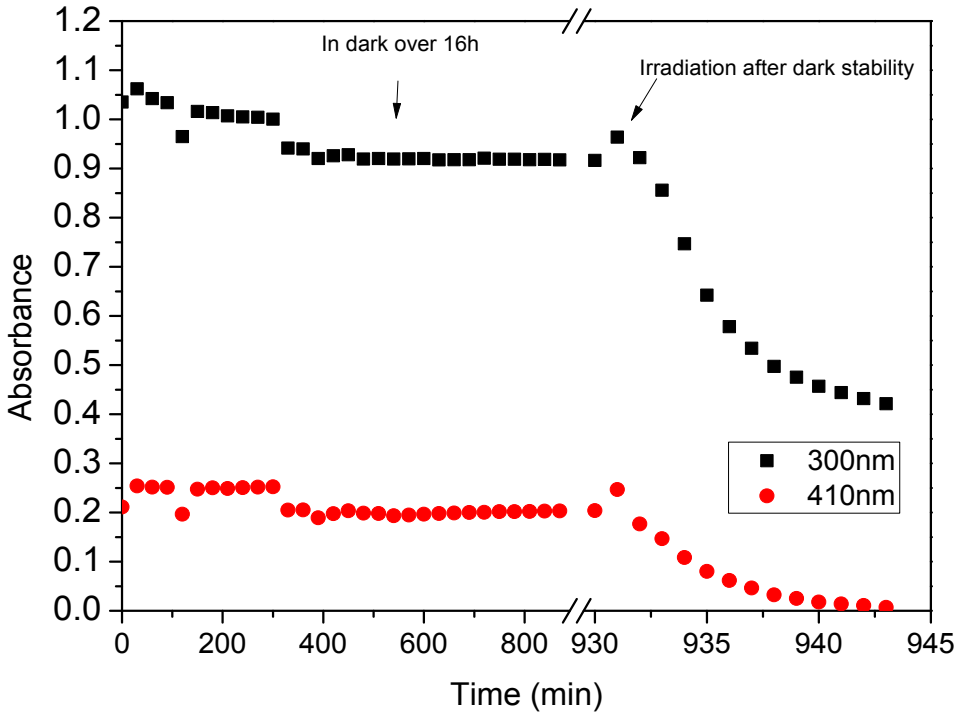

Figure 5.14 *Change of absorption at selected wavelengths with increasing incubation time in the dark (0 to 16 h) and after subsequent photoactivation with a LED array at 410 nm for 12 min for a solution of dendrimer **75** in dimethylsulfoxide/water (10:90 % v/v), as monitored by UV/Vis spectroscopy.*

5.6 CO-Release Experiments with the Myoglobin Assay

5.6.1 Myoglobin Assay

The CO-release from compounds **75 - 77** was studied using the standard myoglobin assay,[21] which is based on the UV-Vis spectroscopic detection of the conversion of deoxy-Mb (deoxy-myoglobin) to Mb-CO (carboxy-myoglobin).[34, 35] The myoglobin assay is not the only method developed for determining the amount and rate of CO-released from compounds, as head space analysis by GC is also used.[36, 37] However, the myoglobin assay remains the principal method and was first reported by Motterlini and co-workers in 2002.[21] The method basically involves the release of CO-ligands by the complex into solution, which in-turn binds to the deoxy-Mb, instantly converting it into Mb-CO (rate constant, k = 0.38 μMs^{-1}, and binding constant = 16.9 μM^{-1}).[34] The conversion can be monitored, by observing changes in the Q-band region, by UV-Vis spectroscopic analysis (Figure 5.15).

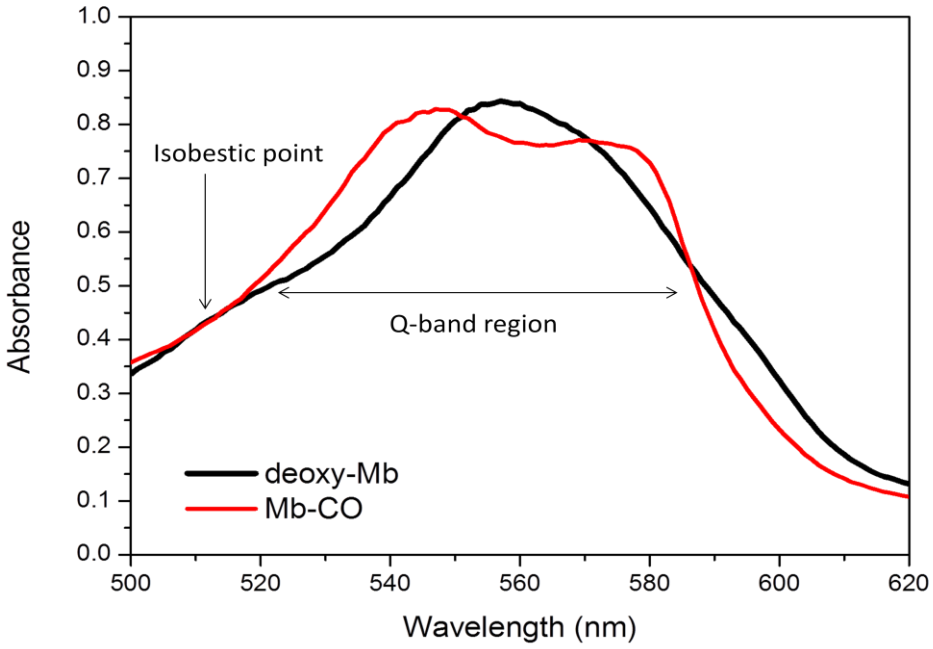

Figure 5.15 *UV-Vis spectra of the deoxy-Mb and Mb-CO in the Q-band region.*

Monitoring spectral changes at 540 nm, the proportion of deoxy-Mb converted to Mb-CO can be obtained with the use of the Beer-Lambert law and the overall concentration of deoxy-Mb (determined using the known extinction coefficient of ε_{540} = 15.4 $mM^{-1}cm^{-1}$).[38] Hence, the concentration of Mb-CO can be calculated, which represents the quantity of CO-released by the complex at each spectral change.

5.6.2 Stability in Myoglobin Assay

Prior to the irradiation experiments (conducted in the dark), the stability of compounds **75** - **77** in 0.1 M phosphate buffer (PBS, pH 7.4) under the reducing conditions of the myoglobin assay was monitored using UV/Vis spectroscopy. Spectral changes were monitored at four wavelengths in the Q-band region, over a 16 h period, which include 540 nm and 577 nm (formation of Mb-CO), 557 nm (formation of deoxy-Mb) and 510 nm (isobestic point). The isobestic point (point of intersection of UV-Vis spectral traces of the two interconverting species) should remain constant throughout the experiment (*i.e.* during the dark and irradiation). The two metallodendrimers **75** (Figures 5.16) and **76** showed negligible spectral changes over a 16 h period at the four wavelengths. Indicating that no CO-release to myoglobin occurs in the dark during this time and is a good indicator of the suitability of these compounds as photoactivatable CO-prodrugs.

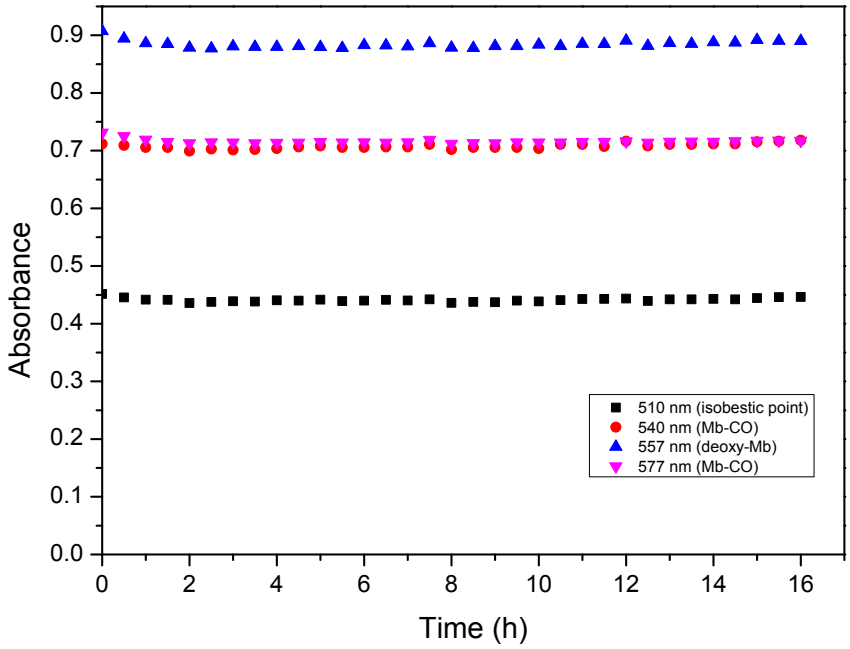

Figure 5.16 *Change of absorption at selected wavelengths with increasing incubation time in the dark (0 to 16 h) for a solution of metallodendrimer **75** (4 µM) in 0.1 M PBS at pH 7.4 in the presence of myoglobin (60 µM) and sodium dithionite (10 mM) under a dinitrogen atmosphere as monitored by UV/Vis spectroscopy.*

For the mononulcaer derivative **77**, some minor fluctuations were observed in the above mentioned spectral regions, in particular during the first few hours of incubation, but since these affected all wavelengths monitored to the same degree, they are probably rather indicative of some precipitation, due to poor solubility, than a general instability of the compound.

5.6.3 Photoactivation of Myoglobin Assay Spiked with the PhotoCORM

For photoactivation studies, a custom-made LED cluster with an emission wavelength of 410 nm, matching the MLCT band, was used and setup as in Figure 5.17. The violet light photoactivation of the present compounds **75** - **77** is quite an attractive feature, since most PhotoCORMs reported to date only show sensitivity to light at shorter wavelengths (315-365 nm).[16, 29, 30, 39, 40] For deep tissue penetration, an excitation wavelength of larger than 600-700 nm would be ideal, which would also minimize potential photodamage to healthy cells.[41] By suitable modification of the substituents in the 4-position of the bpy ligand, it is anticipated that the excitation wavelength can be further shifted towards the red.[42]

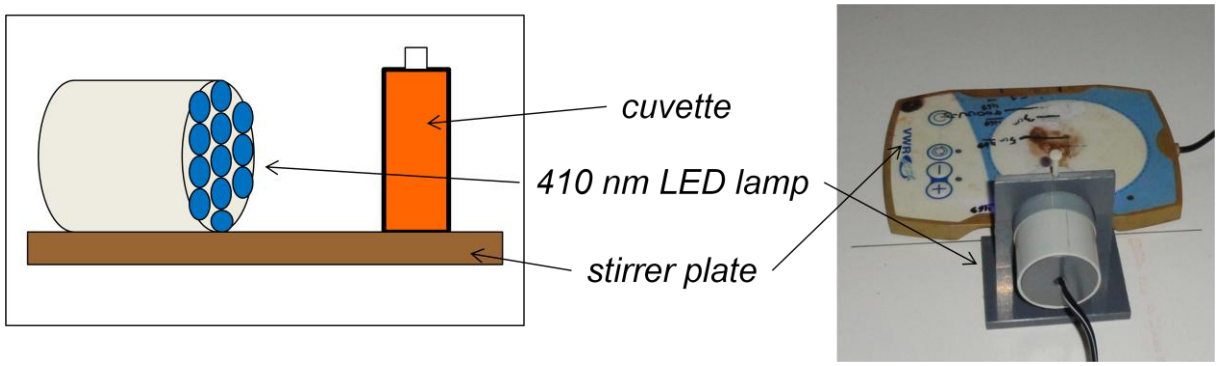

Figure 5.17 *Setup of photoactivation experiment (right) and schematic of the setup (left).*

A solution of myoglobin in 0.1 M PBS buffer was degassed by bubbling with dinitrogen and reduced by addition of sodium dithionite, followed by the addition of a solution of compounds **75**, **76**, or **77** in dimethylsulfoxide/water (10:90 % *v*/*v*) was prepared. The photoexcitation of the freshly prepared solutions at 410 nm leads to pronounced changes in the Q-band region of the Mb absorption. The band at 557 nm slowly decreases in intensity while two new bands at 540 and 577 nm slowly increases in intensity for complexes, which is characteristic for the conversion of deoxy-Mb to Mb-CO (Figure 5.18).

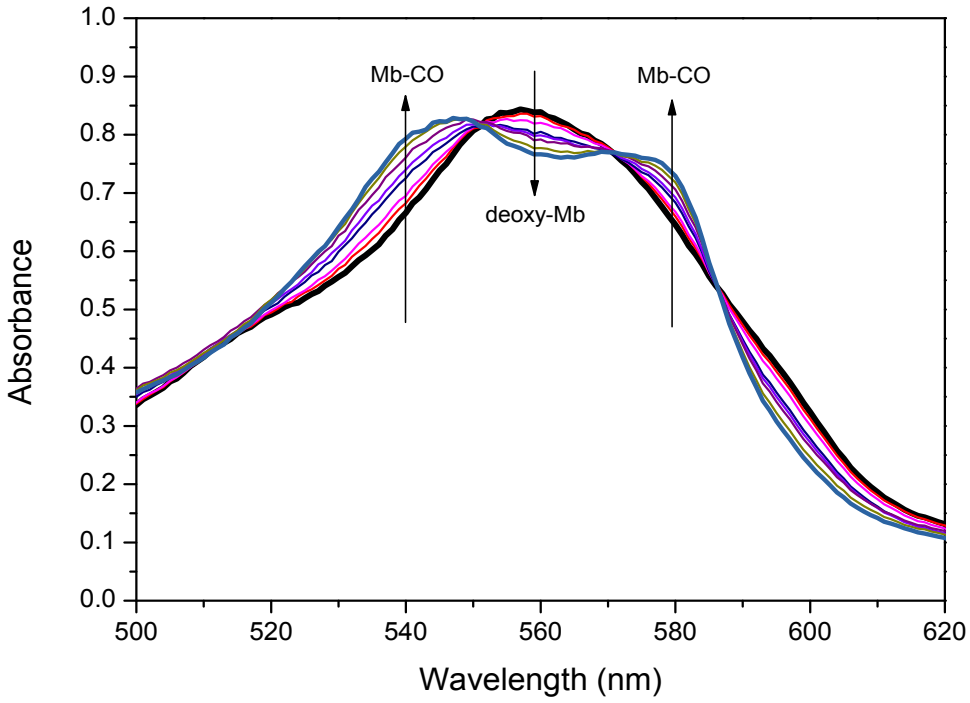

Figure 5.18 *Change of absorption in the Q-band region of myoglobin with increasing irradiation time at 410 nm for a solution of metallodendrimer **75** (4 µM) in 0.1 M PBS pH 7.4 in the presence of myoglobin (60 µM) and sodium dithionite (10 mM) under a dinitrogen atmosphere as monitored by UV/Vis spectroscopy.*

The concentration of Mb-CO in solution was determined from the absorption data by application of the Beer-Lambert law with an assumption that the total concentration of the myoglobin remains constant throughout the whole assay and using the molar extinction coefficient for Mb-CO of ε_{540} = 15.4 $(mM)^{-1}L^{-1}$.[38] Since the concentration of deoxy-Mb has to be fixed to keep the absorption in the Q-band region <1, an excess of deoxy-Mb over the total amount of potentially labile CO in compounds **75** - **77** was always maintained. When 4 μM of **75** was added to 60 μM of deoxy-Mb, the CO-release profile of complex **75** upon photoactivation (Figure 5.18) indicates that approximately eight CO-ligands are released per molecule of **75** (Table 5.4).

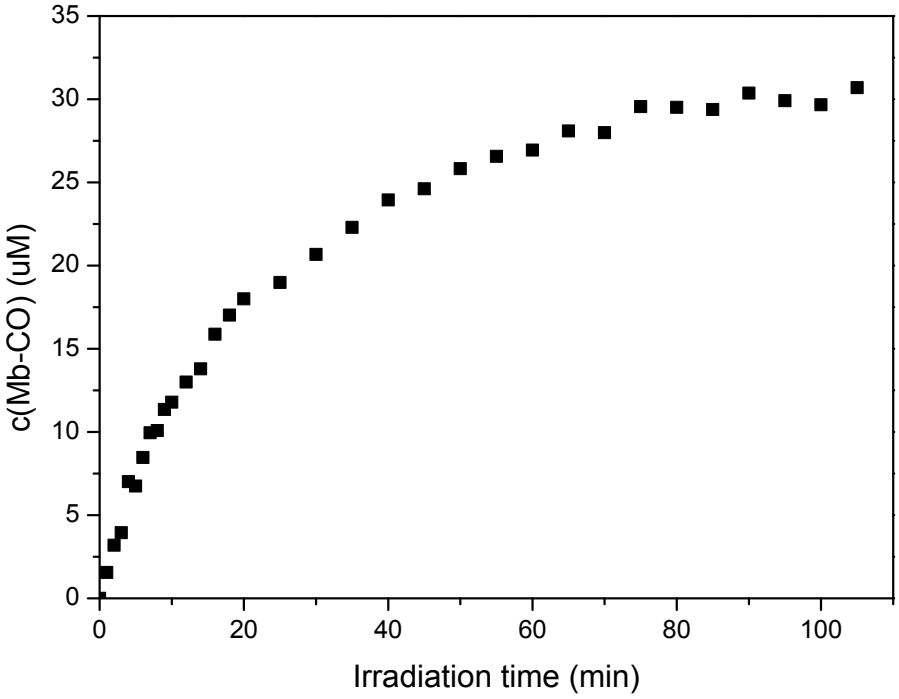

Figure 5.19 *Amount of Mb-CO in µM formed with increasing irradiation time at 410 nm for a solution of metallodendrimer* ***75*** *(4 µM) in 0.1 M PBS pH 7.4 in the presence of myoglobin (60 µM) and sodium dithionite (10 mM) under a dinitrogen atmosphere as determined from UV/Vis spectroscopy.*

Second-generation metallodendrimer **76** (2 μM) released a significantly higher number of CO-ligands, about 15 equivalents (Table 5.4). For the mononuclear model complex **77** (10 μM), about two CO-ligands per molecule were released upon exhaustive photoactivation (Table 5.4).

Table 5.4 *CO-release data of complexes* ***75*** *-* ***77****.*

Compound	Conc. of MbCO [μM][a]	Eq. of CO-released[b, c]	Percentage CO-released [%][c]
75	30.24 ± 0.08	7.56 ± 0.02	63.0
76	30.47 ± 0.31	15.24 ± 0.15	63.5
77	20.29 ± 3.03	1.51 ± 0.07	50.5

[a] Conc. of MbCO ± standard error.
[b] Eq. of CO-released ± standard error.
[c] Per molecule

While the absolute number of CO-ligands liberated from the molecules increases from about 1.5 to 15.2 when comparing **75 - 77**, interestingly, the proportional amount of CO-released versus the remaining bound CO stays remarkably constant, with an average value of ~65 % for the two metallodendrimers (**75**, **76**) and ~51 % for the mononuclear complex **77** (Table 5.4). Thus, under the conditions of the myoglobin assay, a maximum of two out of the three CO-ligands per metal carbonyl moiety are photolabile. Furthermore, this data indicates that the CO-release from each $Mn(CO)_3$ moiety in the metallodendrimers does not seem to be a cooperative process due to the linear scaling.

5.7 Kinetics and Quantum Yield Measurements

5.7.1 Rate of CO-Release

The CO-release studies showed on average the metallodendrimers **75** and **76** released ~65 % per molecule, whilst the mononuclear complex **77** released ~51 % of CO per molecule. The half-life ($t_{1/2}$) in this study is defined as the time taken for compounds **75 - 77** to release 50 % of the total CO-ligands present per molecule. For an effective CO-releasing molecule the $t_{1/2}$ ideally needs to be less than 2 h, as the higher $t_{1/2}$ is unlikely to result in a high enough CO-concentration within the cell, due to the CO circulation within the body and insufficient binding with heme.[12] The CO-release profile follows a pseudo first-order behavior and hence the $t_{1/2}$ of each complex **75 - 77** was calculated, by fitting a 1st order exponential growth curve (Equation 5.1).

$$y = y_o + Ae^{x/t_1} \quad \text{Eqn. 5.1}$$

$$c(MbCO) = A_1 e^{t/t_1} + Y_o \quad \text{Eqn. 5.2}$$

$$Y_o/_2 = A_1 e^{t_{1/2}/t_1} + Y_o \quad \text{Eqn. 5.3}$$

$$t_{1/2} = t_1 \ln\left[\frac{-Y_o}{2A_1}\right] \quad \text{Eqn. 5.4}$$

$$Half\ life = \frac{ln2}{k} \ (1^{st} \text{ order}) \quad \text{Eqn. 5.5}$$

Substitution of the relevant symbols and rearrangement of the equation afforded Equation 5.2. Y_o is the y-variable where the graph plateaus. Therefore, the concentration of Mb-CO (c(MbCO)) at $t_{1/2}$ is $^{Yo}/_{2}$, and $t = t_{1/2}$, to afford Equation 5.3. Rearrangement of Equation 5.3 and placing $t_{1/2}$ as the subject of the formula, afforded Equation 5.4. t_1, Y_o and A_1 was obtained from the exponential growth curve plot of complexes **75** - **77**, and hence $t_{1/2}$ was calculated and listed in Table 5.5.

Table 5.5 *Kinetic data of complexes **75** - **77**.*

Compound	Half-life, $t_{1/2}$ [min][a, b]	Rate constant, k_{CO} [s^{-1}][c]	Quantum yield, Φ_{410}[d]
75	14.54 ± 0.25	7.95×10^{-4}	$(2.66 \pm 0.16)\times10^{-3}$
76	16.84 ± 0.56	6.86×10^{-4}	$(2.71 \pm 0.49)\times10^{-3}$
77	7.41 ± 0.24	1.56×10^{-3}	$(3.15 \pm 0.27)\times10^{-3}$

[a] Determined under the conditions of the myoglobin assay.
[b] Half life ± standard error
[c] Determined from UV/Vis spectral studies in DMSO/water solution .
[d] Calculated using a photon flux of the LED array determined as $(9.9 \pm 0.4)\times10^{-9}$ Einstein·s^{-1}

Metallodendrimers **75** and **76** displayed a $t_{1/2}$ of 14.5 min and 16.8 min respectively, whilst the mononuclear complex **77** displayed a significantly shortened $t_{1/2}$ of 7.4 min, way below the threshold $t_{1/2}$ of 2 h. Compared to the tricarbonyl manganese(I)-PTA PhotoCORM ($t_{1/2}$ = 93.0 min) synthesized by Mohr *et al*. the $t_{1/2}$ of these complexes **75** - **77** is faster.[31] However, compared to one of the first PhotoCORMs reported, $[Mn(tpm)(CO)_3]^+$ (where tpm = tris(pyrazolyl)methane, $t_{1/2}$ = 10 min), the $t_{1/2}$ is comparable.[17]

All three compounds follow a pseudo first-order behavior, and hence using Equation 5.5, the CO-release rate (k_{CO}) for each complex **75** - **77** was calculated and is listed in Table 5.5. The k_{CO} is comparable to $[Mn(tpm)(CO)_3]^+$,[17] but is relatively faster than other manganese-functionalized PhotoCORMs.[29, 43] CO-release rates are comparable to other metal carbonyl complexes such as the iron compound $[Fe(CO)(N4Py)](ClO_4)_2$.[44]

5.7.2 Quantum Yield of CO-Release Determined by Ferrioxalate Actionometry

The quantum yield is defined as the moles of Mb-CO formed by moles of photons produced by the light source (*i.e.* photon flux). As the photons delivered by a light source vary, a large photon flux will increase the CO-release rate, whilst a small photon flux will do the reverse. To avoid this problem, the quantum yield is measured and is used to compare CO-release of PhotoCORMs. The photon flux is defined as the number of quanta (photon flow) passing through the cuvette per second, and can be determine by ferrioxalate actinometry.[45, 46] Ferrioxalate actinometry involves the photoreduction of potassium ferrioxalate $K_3[Fe(C_2O_4)_3]\cdot 3H_2O$ (Scheme 5.6).

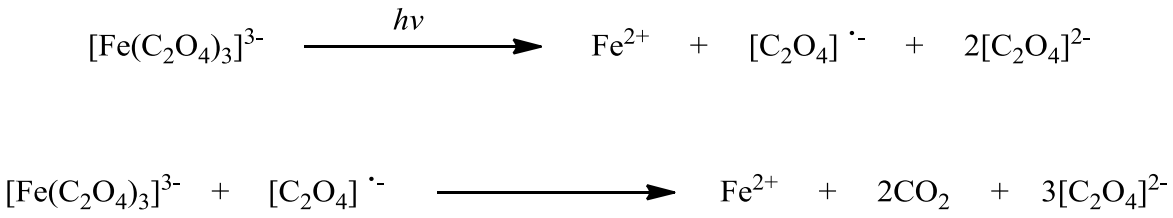

Scheme 5.6 *Photoreduction of potassium ferrioxalate, $K_3[Fe(C_2O_4)_3]\cdot 3H_2O$.*

The quantity of ferrous ions formed during the irradiation period is monitored by the conversion to the coloured tris-phenanthroline complex $[Fe(phen)_3]^{2+}$ (where phen = phenanthroline) (Scheme 5.7).

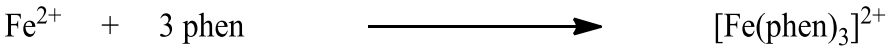

Scheme 5.7 *Formation of tris-phenanthroline complex, $[Fe(phen)_3]^{2+}$.*

With the use of UV/Vis spectroscopy and the molar extinction coefficient of $[Fe(phen)_3]^{2+}$ (11100 $Lmol^{-1}cm^{-1}$), the moles of Fe^{2+} ions was determined at λ_{max} = 510 nm.[47] The photon flux was calculated using Equation 5.6, where Φ_p is the photon flux (Einstein.s^{-1}), t is the irradiation time and Φ_λ is the quantum yield of ferrous ion production at the irradiation wavelength.

$$Photon\ Flux\ (\Phi_p) = \frac{moles\ of\ Fe^{2+}}{t\ .\Phi_\lambda} \quad \text{Eqn. 5.6}$$

$$Quantum\ Yield\ (\Phi) = \frac{moles\ of\ MbCO\ formed}{moles\ of\ photons\ formed} \quad \text{Eqn. 5.7}$$

The quantum yield of the complexes could now be calculated using Equation 5.7, where 1 Einstein = 1 mol of photon, and are listed in Table 5.5. While the values of Φ are essentially identical for metallodendrimers **75** and **76** at about 2.7×10^{-3}, again indicating that scaling effects do not play any role in these systems. For the model compound **77**, a slightly larger value of 3.2×10^{-3} was determined. These values are much lower than reported for other metal carbonyl complexes by one to two orders of magnitude.[13, 29, 48] However, one has to take into account the experiments were not carried out in pure solvent, but rather under the conditions of the myoglobin assay, using an excitation wavelength of 410 nm, in a spectral region where substantial absorption of the heme protein leads to considerable inner filter effects.

5.8 Overall Summary

First- and second-generation polypyridyl metallodendrimers, bearing four and eight tricarbonylmanganese(I) end groups, were successfully synthesized and purified using preparative HPLC. The complexes were characterized using a series a spectroscopic and analytical techniques, namely ^{1}H, ^{13}C{^{1}H} NMR, infrared and mass spectrometry. In addition, a mononuclear model complex was prepared for comparison.

All three complexes are stable in solution and in air for an extended period of time in the absence of light. However, upon photoactivation at 410 nm using a custom-made LED light source, CO-release studies with the myoglobin assay show that at least two of the three carbonyl ligands per $Mn(CO)_3$ moiety can be liberated under these conditions. The half-life and quantum yield of CO-release are similar for the first- and second-generation metallodendrimers, indicating that no scaling effects are operative in these systems and that each $[Mn(bpy)(CO)_3Br]$ end group behaves independently from the others. Furthermore, the total amount of CO-released per molecular unit increases with the dendrimer generation, reaching a value of 15 CO per molecule of the second-generation metallodendrimer.

5.9 References

1. T. Sjostrand, *Scand. J. Clin. Lab. Invest.*, 1949, **1**, 201-214.
2. R. Foresti and R. Motterlini, *Curr. Drug Targets*, 2010, **11**, 1595-1604.
3. Y. C. Hou, A. Janczuk and P. G. Wang, *Current Pharmaceutical Design*, 1999, **5**, 417-441.
4. L. Li, P. Rose and P. K. Morre, *Annu. Rev. Pharmacol. Toxicol.*, 2011, **51**, 169-187.
5. R. Alberto and R. Motterlini, *Dalton Trans.*, 2007, **17**, 1651-1660.
6. T. R. Johnson, B. E. Mann, J. E. Clarke, R. Foresti, C. J. Green and R. Motterlini, *Angew. Chem. Int. Ed.*, 2003, **42**, 3722-3729.
7. I. J. S. Fairlamb, A.-K. Duhme-Klair, J. M. Lynam, B. E. Moulton, C. T. O' Brien, P. Sawle, J. Hammad and R. Motterlini, *Bioorg. Med. Chem. Lett.*, 2006, **16**, 995-998.
8. I. J. S. Fairlamb, J. M. Lynam, B. E. Moulton, I. E. Taylor, A.-K. Duhme-Klair, P. Sawle and R. Motterlini, *Dalton Trans.*, 2007, 3603-3605.
9. S. Romanski, B. Kraus, U. Schatzschneider, J.-M. Neudörfl, S. Amslinger and H.-G. Schmalz, *Angew. Chem. Int. Ed.*, 2011, **50**, 2392-2396.
10. S. Romanski, B. Kraus, M. Guttentag, W. Schlundt, H. Rücker, A. Adler, J.-M. Neudörfl, R. Alberto, S. Amslinger and H.-G. Schmalz, *Dalton Trans.*, 2012, **41**, 13862-13875.
11. S. Romanski, H. Rücker, E. Stamellou, M. Guttentag, J.-M. Neudörfl, R. Alberto, S. Amslinger, B. Yard and H.-G. Schmalz, *Organometallics*, 2012, **31**, 5800-5809.
12. U. Schatzschneider, *Inorg. Chim. Acta*, 2011, **374**, 19-23.
13. R. D. Rimmer, H. Richter and P. C. Ford, *Inorg. Chem.*, 2010, **49**, 1180-1185.
14. R. D. Rimmer, A. E. Pierri and P. C. Ford, *Coord. Chem. Rev.*, 2012, **256**, 1509-1519.
15. A. E. Pierri, A. Pallaoro, G. Wu and P. C. Ford, *J. Am. Chem. Soc.*, 2012, **134**, 18197-18200.
16. W.-Q. Zhang, A. J. Atkin, I. J. S. Fairlamb, A. C. Whitwood and J. M. Lynam, *Organometallics*, 2011, **30**, 4643-4654.
17. J. Niesel, A. Pinto, H. W. Peindy N'Dongo, K. Merz, I. Ott, R. Gust and U. Schatzschneider, *Chem. Commun.*, 2008, 1798-1800.
18. H. Pfeiffer, A. Rojas, J. Niesel and U. Schatzschneider, *Dalton Trans.*, 2009, 4292-4298.
19. N. E. Brückmann, M. Wahl, G. J. Reiß, M. Kohns, W. Wätjen and P. C. Kunz, *Eur. J. Inorg. Chem.*, 2011, 4571-4577.

20. D. Peer, J. M. Karp, S. Hong, O. C. Farokhzad, R. Margalit and R. Langer, *Nature Nanotechnol.*, 2007, **2**, 751-760.
21. R. Motterlini, J. E. Clark, R. Foresti, P. Sarathchandra, B. E. Mann and C. J. Green, *Circ. Res.*, 2002, **90**, e17-e24.
22. B. M. Peek, G. T. Ross, S. W. Edwards, G. J. Meyer, T. J. Meyer and B. W. Erickson, *Int. J. Peptide Protein Res.*, 1991, **38**, 114-123.
23. C. Busche, P. Comba, A. Mayboroda and H. Wadepohl, *Eur. J. Inorg. Chem.*, 2010, 1295-1302.
24. L. D. Ciana, I. Hamachi and T. J. Meyer, *J. Org. Chem.*, 1989, **54**, 1731-1735.
25. P. Govender, A. K. Renfrew, C. M. Clavel, P. J. Dyson, B. Therrien and G. S. Smith, *Dalton Trans.*, 2011, **40**, 1158-1167.
26. P. Govender, N. C. Antonels, J. Mattsson, A. K. Renfrew, P. J. Dyson, J. R. Moss, B. Therrien and G. S. Smith, *J. Organomet. Chem.*, 2009, **694**, 3470-3476.
27. P. Govender, L. C. Sudding, C. M. Clavel, P. J. Dyson, B. Therrien and G. S. Smith, *Dalton Trans.*, 2013, **42**, 1267-1277.
28. R. Payne, P. Govender, B. Therrien, C. M. Clavel, P. J. Dyson and G. S. Smith, *J. Organomet. Chem.*, 2013, **729**, 20-27.
29. M. A. Gonzalez, M. A. Yim, S. Cheng, A. Moyes, A. J. Hobbs and P. K. Mascharak, *Inorg. Chem.*, 2012, **51**, 601-608.
30. P. C. Kunz, W. Huber, A. Rojas, U. Schatzschneider and B. Spingler, *Eur. J. Inorg. Chem.*, 2009, 5358-5366.
31. F. Mohr, J. Niesel, U. Schatzschneider and C. W. Lehmann, *Z. Anorg. Allg. Chem.*, 2012, **638**, 543-546.
32. M.-J. Li, X. Liu, Y.-Q. Shi, R.-J. Xie, Q.-H. Wei and G.-N. Chen, *Dalton Trans.*, 2012, **41**, 10612-10618.
33. R. R. Andrea, W. G. J. De Lange, D. J. Stufkens and A. D. Oskam, *Inorg. Chim. Acta*, 1988, **149**, 77-84.
34. A. J. Atkin, J. M. Lynam, B. E. Moulton, P. Sawle, R. Motterlini, N. M. Boyle, M. T. Pryce and I. J. S. Fairlamb, *Dalton Trans.*, 2011, **40**, 5755-5761.
35. S. McLean, B. E. Mann and R. K. Poole, *Anal. Biochem.*, 2012, **427**, 36-40.
36. C. Peng, *Chromatographia*, 1990, **29**, 347-350.
37. H. J. Vreman and D. K. Stevenson, *Anal. Biochem.*, 1988, **168**, 31-38.
38. E. Antonini and M. Brunori, in *Frontiers of Biology*, eds. A. Neuberger and E. L. Tatum, North-Holland, Amsterdam, 1971, p. 19.

39. G. Dördelmann, H. Pfeiffer, A. Birkner and U. Schatzschneider, *Inorg. Chem.*, 2011, **50**, 4362-4367.
40. J. S. Ward, J. M. Lynam, J. W. B. Moir, D. E. Sanin, A. P. Mountford and I. J. S. Fairlamb, *Dalton Trans.*, 2012, **41**, 10514-10517.
41. K. Szacilowski, W. Macyk, A. Drzewiecka-Matuszek, M. Brindell and G. Stochel, *Chem. Rev.*, 2005, **105**, 2647-2694.
42. H. Pfeiffer, T. Sowik and U. Schatzschneider, *J. Organomet. Chem.*, 2013, **734**, 17-24.
43. S. H. Crook, B. E. Mann, A. J. H. M. Meijer, H. Adams, P. Sawle, D. Scapens and R. Motterlini, *Dalton Trans.*, 2011, **40**, 4230-4235.
44. C. S. Jackson, S. Schmitt, Q. Ping Dou and J. J. Kodanko, *Inorg. Chem.*, 2011, **50**, 5336-5338.
45. C. G. Hatchard and C. A. Parker, *Proc. Roy. Soc. A.*, 1956, **235**, 518-536.
46. C. A. Parker, *Proc. Roy. Soc. A.*, 1953, **220**, 104-116.
47. R. R. Sauers, S. D. Van Arnuma and A. A. Scimone, *Green Chem.*, 2004, **6**, 578-582.
48. S. Wieland and R. van Eldik, *J. Phys. Chem.*, 1990, **94**, 5865-5870.

Chapter 6

Experimental Details

6.1 General Remarks

All reactions were performed under an inert atmosphere using a dual vacuum/nitrogen line and standard Schlenk-line techniques unless stated otherwise. All reaction solvents were dried by heating under reflux and under an inert atmosphere, over the appropriate drying agent and all samples were dried under vacuum.

2-pyridinecarboxaldehyde, salicylaldehyde, *n*-propylamine, DAB-$\mathbf{G_1}$-PPI-$(NH_2)_4$ (where DAB = 1,4-diaminobutane and PPI = poly(propyleneimine), ferrocene carboxaldehyde, sodium hexafluorophosphate, hexamethylbenzene, 4,4'-dimethyl-2,2'-bipyridyl, myoglobin from horse skeletal muscle and nucleotide guanosine 5'-monophosphate (5'GMP) were purchased from Sigma-Aldrich; α-Phellandrene was purchased from Fluka; DAB-$\mathbf{G_2}$-PPI-$(NH_2)_8$, DAB-$\mathbf{G_3}$-PPI-$(NH_2)_{16}$, DAB-$\mathbf{G_4}$-PPI-$(NH_2)_{32}$ was purchased from SyMO-Chem; Manganese pentacarbonyl bromide $[Mn(CO)_5Br]$ was purchased from Strem Chemicals and used without further purification. Ruthenium(III)trichloride trihydrate and osmium(III)trichloride trihydrate was obtained as a generous donation from Johnson Matthey/Anglo-American Platinum Limited. Deuterated solvents were purchased from Sigma-Aldrich.

Reaction progress and product mixtures were monitored by thin-layer chromatography (TLC) on precoated silica-gel F_{254} plates in a suitable solvent system, using the ascending technique; the plates were viewed under a UV light. Column chromatography was carried out with 60 Å silica-gel (70-230 mesh ASTM).

6.2 Instrumentation

Infrared (IR) spectra were measured on a Perkin-Elmer Spectrum 100 FT-IR spectrometer as KBr pellets or in NaCl solution cells in DCM or as pure solid samples using a Nicolet 380 FT-IR-Spectrometer equipped with a SMART iTR ATR unit. Intensity of stretching vibrations are marked as strong (s), medium (m) and weak (w). Melting points (MPs) were determined using a Büchi Melting Point Machine B -540.

Nuclear magnetic resonance (NMR) spectra were recorded on a Varian Unity XR400 spectrometer (^{1}H: 399.95 MHz; ^{13}C{^{1}H}: 100.58 MHz; ^{31}P{^{1}H}: 161.90 MHz) or Varian Mercury XR300 spectrometer (^{1}H: 300.08 MHz; ^{13}C{^{1}H}: 75.46 MHz; ^{31}P{^{1}H}: 121.47 MHz) or Bruker Biospin GmbH spectrometer (^{1}H: 400.22 MHz; ^{13}C{^{1}H}: 100.65 MHz; ^{31}P{^{1}H}: 162.00 MHz) at ambient temperature. Chemical shifts δ in ppm indicate a downfield shift relative to tetramethylsilane (TMS) and were referenced relative to the signal of the solvent.[1] Coupling constants J are given in Hz. Individual peaks are marked as singlet (s), doublet (d), doublet-of-doublet (dd), triplet (t), or multiplet (m).

Electron impact mass spectrometry (EI-MS) was carried out on a JEOL GCmateII mass spectrometer. Electrospray ionisation-mass spectrometry (ESI-MS) was carried out on a Waters Synapt mass spectrometer. Data were recorded in positive ion mode. Matrix assisted laser desorption time-of-flight (MALDI-TOF) mass spectra were carried out at the Tokyo Institute of Technology on a Bruker Daltonics Ultraflex MALDI TOF/TOF mass spectrometer using Fluka 87884 *trans*-2-[3-(4-tert-butylphenyl)-2-methyl-2-propenylidene]malonitrile (DCTB) as the matrix, equipped with a nitrogen laser and operated at an accelerating voltage of 25 kV.

Elemental analysis (C, H, N) was carried out using a Thermo Flash 1112 Series CHNS-O Analyser. For certain metallodendrimers, the analyses are outside acceptable limits, and are ascribed to the encapsulation of solvent molecules and/or other inorganic salts by the dendritic compounds.

HPLC analysis was performed on a Dionex Ultimate 3000 instrument equipped with a ReproSil 100 column (C_{18}, 5 μm, 4.6 mm or 10 mm diameter, 250 mm length) using a linear gradient of 5 - 90 % CH_3CN/H_2O or $MeOH/H_2O$ containing 0.1 % TFA as the eluent over 40 min at a flow rate of 0.6 mL/min for analytical and 3.0 mL/min for preparative chromatography, respectively.

Absorption spectra were measured using an Agilent 8453 UV/Vis diode array spectrophotometer in quartz cuvettes (d = 1 cm).

6.3 Synthesis of *N,O*-Salicylaldiminato Ligands

6.3.1 Preparation of 21, 22 and 37

DAB-**G$_1$**-PPI-(C$_7$H$_5$NOH)$_4$ (**21**), DAB-**G$_2$**-PPI-(C$_7$H$_5$NOH)$_8$ (**22**) and (*E*)-2-((propylimino)methyl)phenol (**37**) were prepared from known literature reported procedures.[2, 3]

6.3.2 General Procedure for the Preparation of 23 and 24

Salicyldehyde (1.06 mL, 9.94 mmol for **23**, 1.07 mL, 10.1 mmol for **24**) was added dropwise to a solution of DAB-**G$_3$**-PPI-(NH$_2$)$_{16}$ (1.04 g, 0.619 mmol for **23**) or DAB-**G$_4$**- PPI-(NH$_2$)$_{32}$ (1.10 g, 0.314 mmol for **24**) in toluene (20.0 mL). The reaction was stirred for 48 h at room temperature. The solvent was removed under vacuum affording a yellow oil. The oil was dissolved in DCM (30.0 mL) and washed with distilled H_2O (8 × 50 mL). The organic layer was dried over anhydrous $MgSO_4$ (~10 g) and filtered. The solvent was removed under reduced pressure and the resulting oil dried *in vacuo*.

6.3.2.1 DAB-G$_3$-(C$_7$H$_5$NOH)$_{16}$ (23)

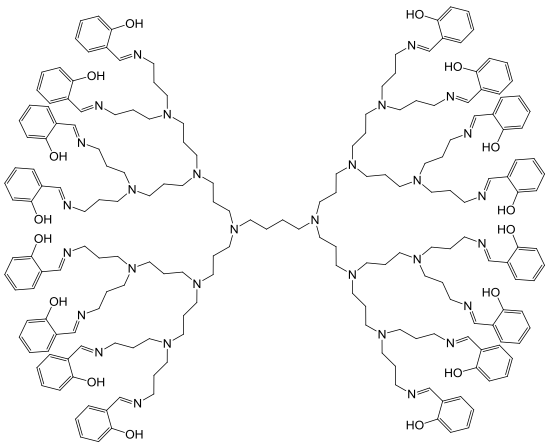

Orange-yellow oil. **Yield**: 1.47 g, 70.9 %. **IR** (NaCl cells, DCM): ν (cm^{-1}) = 1634 (s, imine, C=N); 2950 (s, hydroxyl, O-H). **^{1}H NMR** ($CDCl_3$): δ (ppm) = 1.36, 1.54, 1.77, 2.39, 2.48 (br m, 144H, NC**H**$_2$CH$_2$ *core*, NCH$_2$C**H**$_2$ *core*, NC**H**$_2$CH$_2$CH$_2$N *1st branch*, NCH$_2$C**H**$_2$CH$_2$N *1st branch*, NCH$_2$CH$_2$C**H**$_2$N *1st branch*, NC**H**$_2$CH$_2$CH$_2$N *2nd branch*, NCH$_2$C**H**$_2$CH$_2$N *2nd branch*, NCH$_2$CH$_2$C**H**$_2$N *2nd branch*, NC**H**$_2$CH$_2$CH$_2$N *3rd branch*, NCH$_2$C**H**$_2$CH$_2$N *3rd branch*), 3.56 (m, 32H, NCH$_2$CH$_2$C**H**$_2$N *3rd branch*), 6.81 (br t, 16H, Ar), 6.91 (br d, 16H, Ar), 7.17 (br d, 16H, Ar), 7.26 (br t, 16H, Ar), 8.27 (s, 16H, C**H** *imine*), 13.50 (br s, 16H, O**H**). **^{13}C{^{1}H} NMR** ($CDCl_3$): δ (ppm) = 24.5, 24.7, 28.5, 51.5, 52.1, 52.3, 57.4 (**C**H$_2$); 116.9, 118.4, 131.1, 132.0 (**C**H *Ar*); 118.8, 161.3 (**C** *Ar*); 164.9 (**C**H *imine*). **Elemental analysis** for $C_{200}H_{272}N_{30}O_{16}.3H_2O$ (3406.587): Found C, 70.42; H, 8.21; N, 12.62 %; calcd. C, 70.52; H, 8.05; N, 12.34 %. **MS** (MALDI-TOF, *m*/*z*): 3354 [M]$^+$.

6.3.2.2 DAB-G_4-$(C_7H_5NOH)_{32}$ (24)

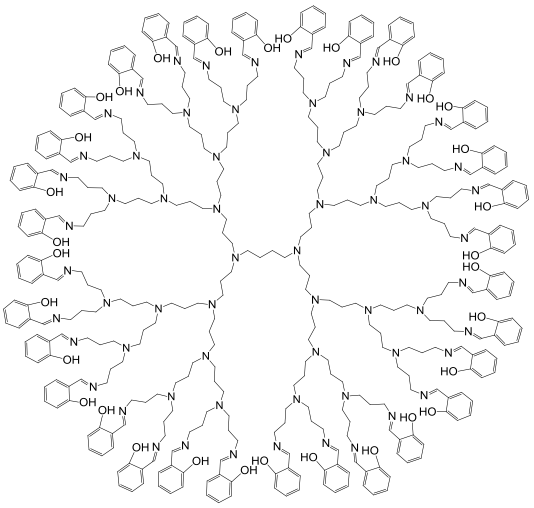

Orange oil. **Yield**: 0.858 g, 39.9 %. **IR** (NaCl cells, DCM): ν (cm^{-1}) = 1634 (s, imine, C=N); 2949 (s, hydroxyl, O-H). **^{1}H NMR** ($CDCl_3$): δ (ppm) = 1.35, 1.52, 1.74, 2.38, 2.45 (br m, 304H, NC**H**$_2$CH$_2$ *core*, NCH$_2$C**H**$_2$ *core*, NC**H**$_2$CH$_2$CH$_2$N *1st branch*, NCH$_2$C**H**$_2$CH$_2$N *1st branch*, NCH$_2$CH$_2$C**H**$_2$N *1st branch*, NC**H**$_2$CH$_2$CH$_2$N *2nd branch*, NCH$_2$C**H**$_2$CH$_2$N *2nd branch*, NCH$_2$CH$_2$C**H**$_2$N *2nd branch*, NC**H**$_2$CH$_2$CH$_2$N *3rd branch*, NCH$_2$C**H**$_2$CH$_2$N *3rd branch*, NCH$_2$CH$_2$C**H**$_2$N *3rd branch*, NC**H**$_2$CH$_2$CH$_2$N *4th branch*, NCH$_2$C**H**$_2$CH$_2$N *4th branch*), 3.53 (m, 64H, NCH$_2$CH$_2$C**H**$_2$N *4th branch*), 6.79 (br t, 32H, Ar), 6.89 (br d, 32H, Ar), 7.17 (br d, 32H, Ar), 7.26 (br t, 32H, Ar), 8.27 (s, 32H, C**H** *imine*), 13.48 (br s, 32H, O**H**). **^{13}C{^{1}H} NMR** ($CDCl_3$): δ (ppm) = 24.4, 24.5, 28.5, 51.4, 52.0, 52.3 (**C**H$_2$); 116.9, 118.4, 131.1, 132.0 (**C**H *Ar*); 118.8, 161.2 (**C** *Ar*); 164.8 (**C**H *imine*). **Elemental analysis** for $C_{408}H_{558}N_{62}O_{32}.1C_7H_8$ (6935.438): Found C, 70.62; H, 8.32; N, 12.96 %; calcd. C, 70.66; H, 8.11; N, 12.52 %. **MS** (MALDI-TOF, *m*/*z*): 6844 $[M]^+$.

6.4 Synthesis of Ru(II)- and Os(II)-Arene Precursors

$[Ru(\eta^6\text{-}p\text{-}Pr^iC_6H_4Me)Cl_2]_2$, $[Ru(\eta^6\text{-}C_6Me_6)Cl_2]_2$ and $[Os(\eta^6\text{-}p\text{-}Pr^iC_6H_4Me)Cl_2]_2$ were prepared from known literature reported procedures.[4-6]

6.5 Synthesis of Ru(II)-and Os(II)-Arene Complexes

6.5.1 General Procedure for the Preparation of Neutral *N,O*-Ru(II)-Arene Metallodendrimers (25 - 28)

Triethylamine (0.0720 mL, 0.519 mmol for **25 - 28**) was added dropwise to a stirring solution of **23** (0.108 g, 0.0323 mmol for **25** and **27**) or **24** (0.109 g, 0.0160 mmol for **26** and **28**) in dry EtOH (25.0 mL). The yellow suspension was stirred at room temperature for 0.5 h. [Ru(η^6-*p*-Pr^{i}C$_6$H$_4$Me)Cl$_2$]$_2$ (0.158 g, 0.258 mmol for **25** and **26**) or [Ru(η^6-C$_6$Me$_6$)Cl$_2$]$_2$ (0.196 g, 0.289 mmol for **27** and **28**) was added to the reaction mixture and allowed to stir for 48 h at room temperature. The reaction mixture was filtered and the solvent removed from the filtrate under reduced pressure, yielding a solid. The solid residue was dissolved in a minimum amount of DCM and the products were precipitated with hexane. The products were purified by low temperature precipitation from DCM with hexane.

6.5.1.1 DAB-G$_3$-PPI-{(η^6-*p*-cye)Ru((C$_7$H$_5$NO)-κ^2-*N,O*)Cl}$_{16}$ (25)

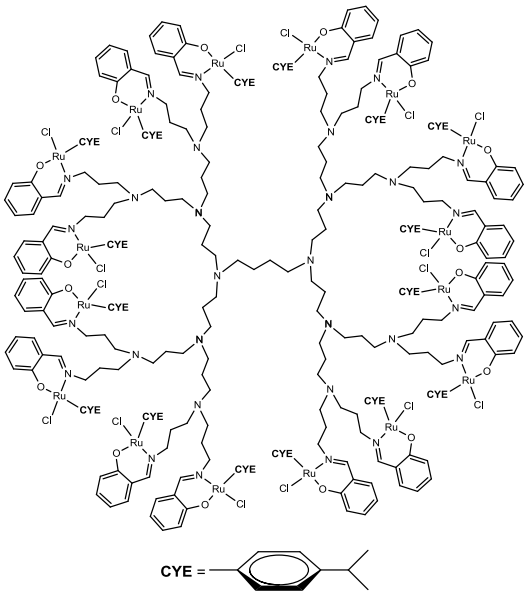

Yellow-brown solid. **Yield**: 0.233 g, 91.1 %. **IR** (NaCl cells, DCM): ν (cm^{-1}) = 1621 (s, imine, C=N). **^{1}H NMR** (CDCl$_3$): δ (ppm) = 1.01 & 1.12 (br m, 96H, CH(C**H**$_3$)$_{2\ p\text{-}cye}$), 1.77 - 2.74 (overlapping m, 240H, NC**H**$_2$CH$_2$ *core*, NCH$_2$C**H**$_2$ *core*, NC**H**$_2$CH$_2$CH$_2$N *1st branch*, NCH$_2$C**H**$_2$CH$_2$N *1st branch*, NCH$_2$CH$_2$C**H**$_2$N *1st branch*, NC**H**$_2$CH$_2$CH$_2$N *2nd branch*, NCH$_2$C**H**$_2$CH$_2$N *2nd branch*, NCH$_2$CH$_2$C**H**$_2$N *2nd branch*, NC**H**$_2$CH$_2$CH$_2$N *3rd branch*, NCH$_2$C**H**$_2$CH$_2$N *3rd branch*, C**H**$_{3\ p\text{-}cye}$), 3.11 (br m, 16H, C**H**(CH$_3$)$_{2\ p\text{-}cye}$), 4.12 & 4.41 (br m, 32H, NCH$_2$CH$_2$C**H**$_2$N *3rd branch*), 5.23 (br d, 32H, Ar$_{p\text{-}cye}$), 5.42 (br d, 32H, Ar$_{p\text{-}cye}$), 6.33 (br m, 16H, Ar), 6.81 (br m, 16H, Ar), 7.07 (br m, 32H, H$_{16}$, Ar), 8.05 (br s, 16H, C**H** *imine*). **^{13}C{^{1}H} NMR** (CDCl$_3$): δ (ppm) = 18.9, 22.3, 22.8 (**C**H$_{3\ p\text{-}cye}$); 21.7, 22.1, 25.2, 25.6, 30.8, 51.0, 66.9, 67.4 (**C**H$_2$); 30.5, 80.6, 81.4, 83.3, 87.6 (**C**H *p-cye*); 98.4, 100.2 (**C** *p-cye*); 114.0, 121.9, 134.6, 135.4 (**C**H *Ar*); 119.2, 164.8 (**C** *Ar*), 164.7 (**C**H *imine*). **Elemental analysis** for C$_{376}$H$_{544}$N$_{30}$O$_{16}$Cl$_{16}$Ru$_{16}$.8DCM.8Et$_3$NH$^+$Cl$^-$ (9705.677): Found C, 46.14; H, 6.50; N, 3.98 %; calcd. C, 46.53; H, 5.65; N, 4.33 %. **MS** (HR-ESI-TOF, *m*/*z*): 845.1812 [M-9Cl]$^{9+}$. **MP**: 62 ºC (decompose without melting).

6.5.1.2 DAB-G_4-PPI-{(η^6-*p*-cye)Ru((C_7H_5NO)-κ^2-*N*,*O*)Cl}$_{32}$ (26)

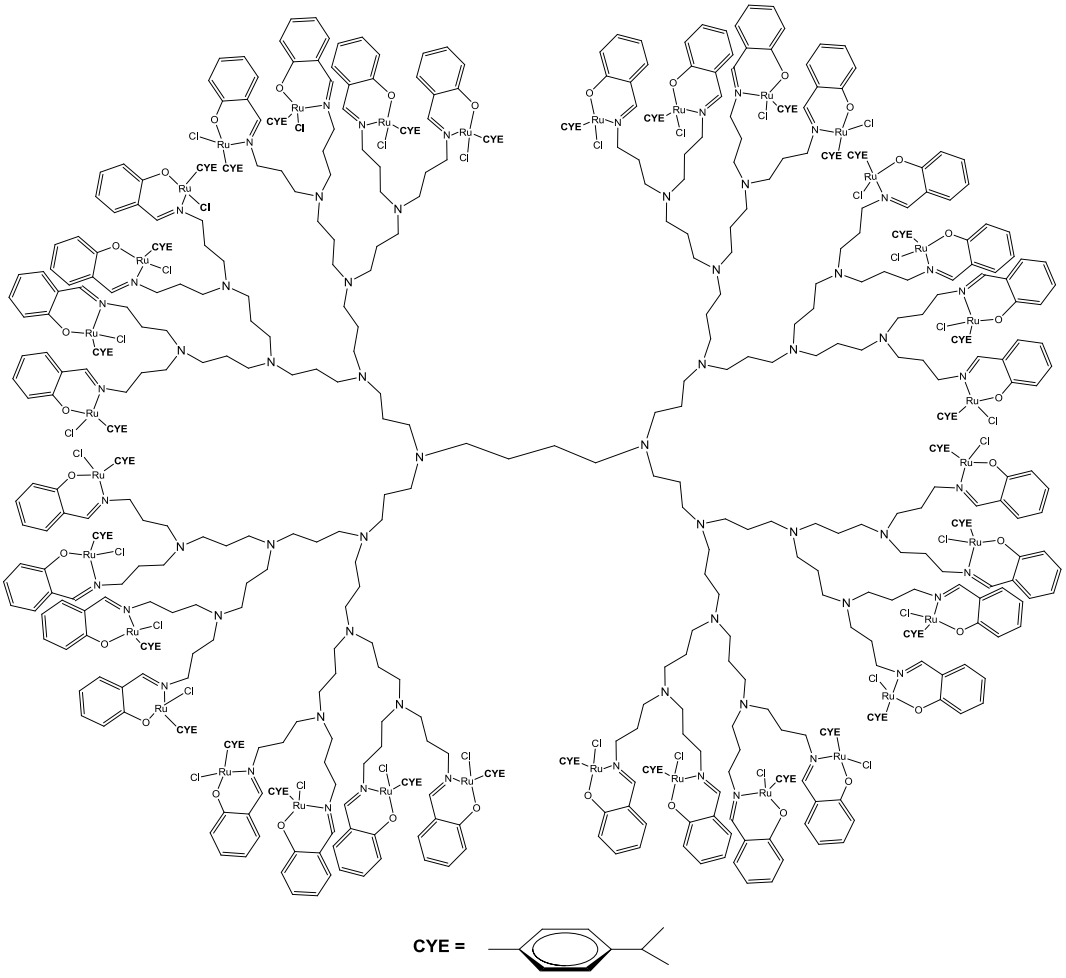

Yellow-brown solid. **Yield**: 0.227 g, 88.7 %. **IR** (NaCl cells, DCM): ν (cm^{-1}) = 1621 (s, imine, C=N). **^{1}H NMR** ($CDCl_3$): δ (ppm) = 0.98 & 1.09 (br m, 192H, CH(C**H**$_3$)$_{2\ p\text{-}cye}$), 1.93 - 2.60 (overlapping m, 400H, NC**H**$_2$CH$_2$ *core*, NCH$_2$C**H**$_2$ *core*, NC**H**$_2$CH$_2$CH$_2$N *1st branch*, NCH$_2$C**H**$_2$CH$_2$N *1st branch*, NCH$_2$CH$_2$C**H**$_2$N *1st branch*, NC**H**$_2$CH$_2$CH$_2$N *2nd branch*, NCH$_2$C**H**$_2$CH$_2$N *2nd branch*, NCH$_2$CH$_2$C**H**$_2$N *2nd branch*, NC**H**$_2$CH$_2$CH$_2$N *3rd branch*, NCH$_2$C**H**$_2$CH$_2$N *3rd branch*, NCH$_2$CH$_2$C**H**$_2$N *3rd branch*, NC**H**$_2$CH$_2$CH$_2$N *4th branch*, NCH$_2$C**H**$_2$CH$_2$N *4th branch*, C**H**$_3$ *p-cye*), 3.20 (br m, 32H, C**H**(CH$_3$)$_{2\ p\text{-}cye}$), 4.11 & 4.42 (br m, 64H, NCH$_2$CH$_2$C**H**$_2$N *4th branch*), 5.24 (br d, 64H, Ar$_{p\text{-}cye}$), 5.40 (br d, 64H, Ar$_{p\text{-}cye}$), 6.33 (br m, 32H, Ar), 6.80 (br m, 32H, Ar), 7.10 (br m, 64H, Ar), 8.08 (br s, 32H, C**H** *imine*). **^{13}C{^{1}H} NMR** ($CDCl_3$): δ (ppm) = 18.9, 22.3, 22.8 (**C**H$_3$ *p-cye*); 21.7, 25.2, 30.8, 50.5, 51.2, 67.0 (**C**H$_2$); 30.5, 80.6, 81.4, 83.3, 87.6 (**C**H *p-cye*); 98.3, 100.2 (**C** *p-cye*); 114.0, 121.8, 134.6, 135.6 (**C**H *Ar*); 119.3, 164.6 (**C** *Ar*), 164.9 (**C**H *imine*). **Elemental analysis** for $C_{760}H_{1104}N_{62}O_{32}Cl_{32}Ru_{32}$.10DCM.20$Et_3NH^+Cl^-$ (19592.596): Found C, 46.34; H, 5.22; N, 3.75 %; calcd. C, 46.59; H, 5.68; N, 4.43 %. **MS** (HR-ESI-TOF, *m*/*z*): 580.9363 $[M\text{-}26Cl]^{26+}$. **MP**: 81 ºC (decompose without melting).

6.5.1.3 DAB-G_3-PPI-{(η^6-HMB)Ru((C_7H_5NO)-κ^2-*N*,*O*)Cl}$_{16}$ (27)

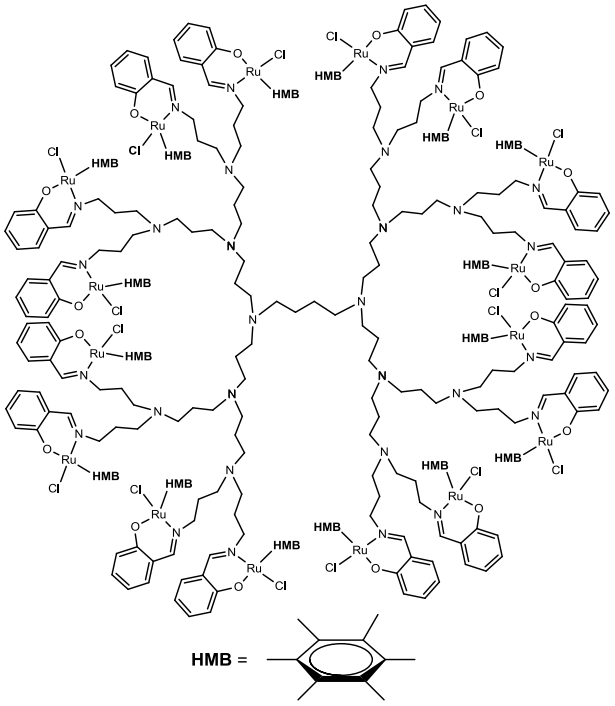

Orange solid. **Yield**: 0.245 g, 84.1 %. **IR** (NaCl cells, DCM): ν (cm^{-1}) = 1617 (s, imine, C=N). **^{1}H NMR** ($CDCl_3$): δ (ppm) = 1.74 (br m, 4H, $NCH_2C\mathbf{H}_{2\ core}$), 1.75 - 3.79 (overlapping br m, 428H, $NC\mathbf{H}_2CH_{2\ core}$, $NC\mathbf{H}_2CH_2CH_2N_{\ 1st\ branch}$, $NCH_2C\mathbf{H}_2CH_2N_{\ 1st\ branch}$, $NCH_2CH_2C\mathbf{H}_2N_{\ 1st\ branch}$, $NC\mathbf{H}_2CH_2CH_2N_{\ 2nd\ branch}$, $NCH_2C\mathbf{H}_2CH_2N_{\ 2nd\ branch}$, $NCH_2CH_2C\mathbf{H}_2N_{\ 2nd\ branch}$, $NC\mathbf{H}_2CH_2CH_2N_{\ 3rd\ branch}$, $NCH_2C\mathbf{H}_2CH_2N_{\ 3rd\ branch}$, $C\mathbf{H}_{3\ HMB}$), 3.94 & 4.11 (br m, 32H, $NCH_2CH_2C\mathbf{H}_2N_{\ 3rd\ branch}$), 6.42 (br m, 16H, Ar), 6.85 (br m, 16H, Ar), 7.08 (br m, 32H, Ar), 8.18 (br s, 16H, $C\mathbf{H}_{\ imine}$). **^{13}C{^{1}H} NMR** ($CDCl_3$): δ (ppm) = 15.8 ($\mathbf{C}H_{3\ HMB}$); 16.2, 20.8, 21.3, 25.5, 46.0, 50.0, 50.4, 51.6, 62.3 ($\mathbf{C}H_2$); 89.6 ($\mathbf{C}_{\ HMB}$); 114.5, 123.5, 133.9, 134.9 ($\mathbf{C}H_{\ Ar}$); 122.1, 165.0 ($\mathbf{C}_{\ Ar}$); 165.8 ($\mathbf{C}H_{\ imine}$). **Elemental analysis** for $C_{392}H_{544}N_{30}O_{16}Cl_{16}Ru_{16}.10DCM.4Et_3NH^+Cl^-$ (9517.109): Found C, 49.00; H, 6.05; N, 3.44 %; calcd. C, 48.47; H, 5.76; N, 4.42 %. **MS** (MALDI-TOF, *m*/*z*): 8080 $[M\text{-}Cl]^+$. **MP**: 179 - 189 ºC.

6.5.1.4 DAB-G_4-PPI-{(η^6-HMB)Ru((C_7H_5NO)-κ^2-*N*,*O*)Cl}$_{32}$ (28)

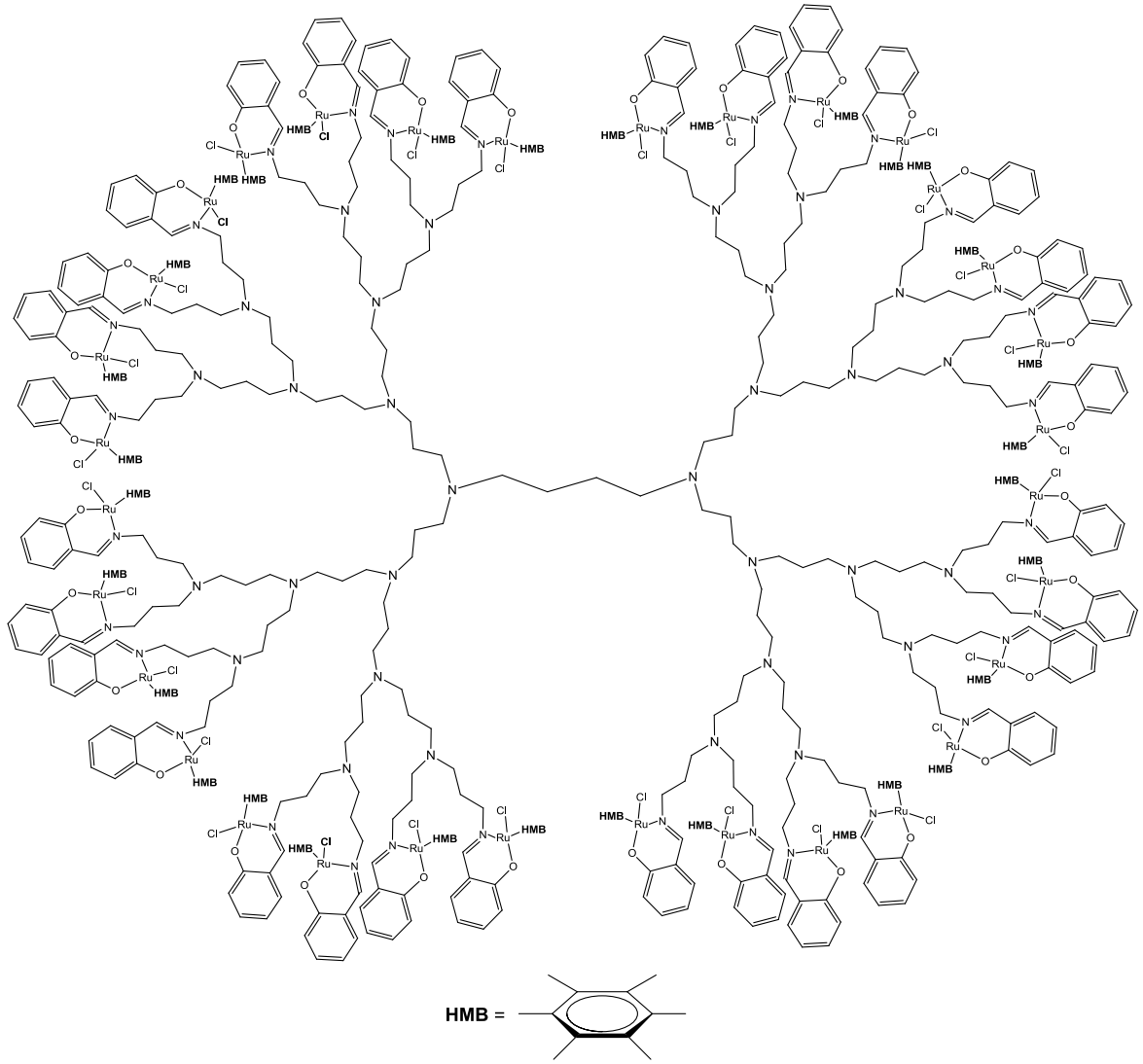

Orange solid. **Yield**: 0.167 g, 68.2 %. **IR** (NaCl cells, DCM): ν (cm^{-1}) = 1618 (s, imine, C=N). **^{1}H NMR** ($CDCl_3$): δ (ppm) = 1.85 (br m, 4H, $NCH_2C\mathbf{H}_{2\ core}$), 1.90 - 3.14 (overlapping br m, 876H, $NC\mathbf{H}_2CH_{2\ core}$, $NC\mathbf{H}_2CH_2CH_2N_{\ 1st\ branch}$, $NCH_2C\mathbf{H}_2CH_2N_{\ 1st\ branch}$, $NCH_2CH_2C\mathbf{H}_2N_{\ 1st\ branch}$, $NC\mathbf{H}_2CH_2CH_2N_{\ 2nd\ branch}$, $NCH_2C\mathbf{H}_2CH_2N_{\ 2nd\ branch}$, $NCH_2CH_2C\mathbf{H}_2N_{\ 2nd\ branch}$, $NC\mathbf{H}_2CH_2CH_2N_{\ 3rd\ branch}$, $NCH_2C\mathbf{H}_2CH_2N_{\ 3rd\ branch}$, $NCH_2CH_2C\mathbf{H}_2N_{\ 3rd\ branch}$, $NC\mathbf{H}_2CH_2CH_2N_{\ 4th\ branch}$, $NCH_2C\mathbf{H}_2CH_2N_{\ 4th\ branch}$, $C\mathbf{H}_{3\ HMB}$), 3.88 & 4.06 (br m, 64H, $NCH_2CH_2C\mathbf{H}_2N_{\ 4th\ branch}$), 6.38 (br m, 32H, Ar), 6.79 (br m, 32H, Ar), 7.04 (br m, 32H, Ar), 7.14 (br m, 32H, Ar), 8.16 (br s, 32H, $C\mathbf{H}_{\ imine}$). **^{13}C{^{1}H} NMR** ($CDCl_3$): δ (ppm) = 15.8 ($\mathbf{C}H_{3\ HMB}$); 20.9, 25.6, 35.1, 50.1, 62.3 ($\mathbf{C}H_2$); 91.2 ($\mathbf{C}_{\ HMB}$); 114.3, 123.7, 133.8, 134.8 ($\mathbf{C}H_{\ Ar}$); 122.0, 164.8 ($\mathbf{C}_{\ Ar}$); 166.0 ($\mathbf{C}H_{\ imine}$). **Elemental analysis** for $C_{792}H_{1104}N_{62}Cl_{32}O_{32}Ru_{32}$.12DCM.17$Et_3NH^+Cl^-$ (19733.856): Found C, 48.34; H, 6.37; N, 4.14 %; calcd. C, 48.21; H, 5.64; N, 4.40 %. **MS** (HR-ESI-TOF, *m*/*z*): 630.0355 $[M+26H]^{26+}$. **MP**: 183 ºC (decompose without melting).

6.5.2 General Procedure for the Preparation of Cationic *N,O*-Ru(II)-Arene-PTA Metallodendrimers ([29][PF_6]$_4$ - [36][PF_6]$_{32}$)

Triethylamine (0.083 mL, 0.596 mmol for [**29**][PF_6]$_4$ and [**33**][PF_6]$_4$; 0.075 mL, 0.541 mmol for [**30**][PF_6]$_8$ and [**34**][PF_6]$_8$; 0.080 mL, 0.599 mmol for [**31**][PF_6]$_{16}$ and [**35**][PF_6]$_{16}$; 0.060 mL, 0.493 mmol for [**32**][PF_6]$_{32}$ and [**36**][PF_6]$_{32}$) was added dropwise to a stirred solution of ligand **21** (0.108 g, 0.147 mmol for [**29**][PF_6]$_4$ and [**33**][PF_6]$_4$) or **22** (0.108 g, 0.067 mmol for [**30**][PF_6]$_8$ and [**34**][PF_6]$_8$) or **23** (0.125 g, 0.037 mmol for [**31**][PF_6]$_{16}$ and [**35**][PF_6]$_{16}$) or **24** (0.105 g, 0.054 mmol for [**32**][PF_6]$_{32}$ and [**36**][PF_6]$_{32}$) in EtOH (50 mL). The resulting yellow suspension was allowed to stir at room temperature for 0.5 h. Next, [Ru(η^6-*p*-Pr^iC_6H_4Me)Cl_2]$_2$ (0.185 g, 0.596 mmol for [**29**][PF_6]$_4$; 0.167 g, 0.272 mmol for [**30**][PF_6]$_8$; 0.183 g, 0.299 mmol for [**31**][PF_6]$_{16}$; 0.151 g; 0.246 mmol for [**32**][PF_6]$_{32}$) or [Ru(η^6-C_6Me_6)Cl_2]$_2$ (0.215 g, 0.318 mmol for [**33**][PF_6]$_4$; 0.199 g, 0.294 mmol for [**34**][PF_6]$_8$; 0.172 g, 0.254 mmol for [**35**][PF_6]$_{16}$; 0.161 g, 0.237 mmol for [**36**][PF_6]$_{32}$) was added to the reaction mixture. The reaction mixture was stirred overnight at room temperature and then the reaction mixture was filtered and PTA (0.094 g, 0.596 mmol for [**29**][PF_6]$_4$ and [**33**][PF_6]$_4$; 0.085 g, 0.541 mmol for [**30**][PF_6]$_8$ and [**34**][PF_6]$_8$; 0.094 g, 0.599 mmol for [**31**][PF_6]$_{16}$ and [**35**][PF_6]$_{16}$; 0.078 g, 0.493 mmol for [**32**][PF_6]$_{32}$ and [**36**][PF_6]$_{32}$) was added to the filtrate. The solution was stirred for 6 h and filtered by gravity, the filtrate reduced to ~5 mL. $NaPF_6$ (0.100 g, 0.596 mmol for [**29**][PF_6]$_4$ and [**33**][PF_6]$_4$; 0.091 g, 0.541 mmol for [**30**][PF_6]$_8$ and [**34**][PF_6]$_8$; 0.101 g, 0.599 mmol for [**31**][PF_6]$_{16}$ and [**35**][PF_6]$_{16}$; 0.083 g, 0.493 mmol for [**32**][PF_6]$_{32}$ and [**36**][PF_6]$_{32}$) was added and the reaction was stirred at 0 ºC for 1 h, which resulted in the formation of a solid. The solid was isolated by filtration, washed with cold EtOH, followed by Et_2O and dried under reduced pressure.

6.5.2.1 [DAB-G_1-PPI-{(η^6-*p*-cye)Ru((C_7H_5NO)-κ^2-*N*,*O*)PTA}$_4$][PF_6]$_4$ ([29][PF_6]$_4$)

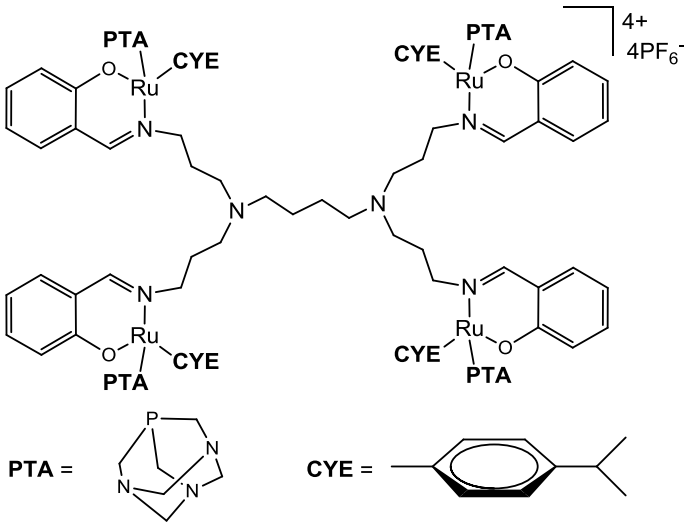

Yellow solid. **Yield**: 0.400 g, 94.3 %. **IR** (KBr pellets): ν (cm^{-1}) = 1618 (s, imine, C=N). **^{1}H NMR** ($(CD_3)_2CO$): δ (ppm) = 1.01 & 1.26 (br d, ^3J = 6.5 Hz, 24H, CH(C**H**$_3$)$_{2\ p\text{-}cye}$), 1.75 - 1.92 (overlapping m, 12H, NCH$_2$C**H**$_{2\ core}$, NCH$_2$C**H**$_2$CH$_2$N$_{branch}$), 2.22 (s, 12H, C**H**$_{3\ p\text{-}cye}$), 2.40 - 2.44 (overlapping m, 12H, NC**H**$_2$CH$_{2\ core}$, NC**H**$_2$CH$_2$CH$_2$N$_{branch}$), 2.61 (br m, 4H, C**H**(CH$_3$)$_{2\ p\text{-}cye}$), 3.98 & 4.09 (br m, 8H, NCH$_2$CH$_2$C**H**$_2$N$_{branch}$), 4.32 (m, 24H, PTA), 4.53 (m, 24H, PTA), 5.56 (br d, ^3J = 6.0 Hz, 4H, Ar$_{p\text{-}cye}$), 5.94 (br d, 4H, Ar$_{p\text{-}cye}$), 6.27 (m, 4H, Ar$_{p\text{-}cye}$), 6.42 (m, 4H, Ar$_{p\text{-}cye}$), 6.49 (t, ^3J = 6.5 Hz, 4H, Ar), 6.79 (d, ^3J = 8.3 Hz, 4H, Ar), 7.22 (m, 8H, Ar), 8.20 (s, 4H, C**H**$_{imine}$). **^{13}C{^{1}H} NMR** ($(CD_3)_2CO$): δ (ppm) = 17.9, 20.8, 21.4 (**C**H$_{3\ p\text{-}cye}$); 21.7, 53.7, 68.1 (**C**H$_2$); 51.0, 72.4 (**C**H$_{2\ PTA}$); 30.6, 83.2, 87.8, 88.8, 91.7 (**C**H$_{p\text{-}cye}$); 97.2, 121.3 (**C**$_{p\text{-}cye}$); 115.2, 122.1, 135.2, 135.4 (**C**H$_{Ar}$); 119.0, 164.2 (**C**$_{Ar}$), 166.9 (**C**H$_{imine}$). **^{31}P{^{1}H} NMR** ($(CD_3)_2CO$): δ (ppm) = -32.5 (s, PTA), -144.1 (sep, ^1J = 709.5 Hz, **P**F$_6$). **Elemental analysis** for $C_{108}H_{156}N_{18}O_4P_8F_{24}Ru_4$.9EtOH (3293.182): Found C, 38.94; H, 4.93; N, 7.76 %; calcd. C, 39.39; H, 4.77; N, 7.66 %. **MS** (HR-ESI-TOF, *m/z*): 575.6148 $[M]^{4+}$ (where M = [**29**][PF_6]$_4$ - 4PF_6). **MP**: 272 ºC (decompose without melting).

6.5.2.2 [DAB-G_2-PPI-{(η^6-*p*-cye)Ru((C_7H_5NO)-κ^2-*N*,*O*)PTA}$_8$][PF_6]$_8$ ([**30**][PF_6]$_8$)

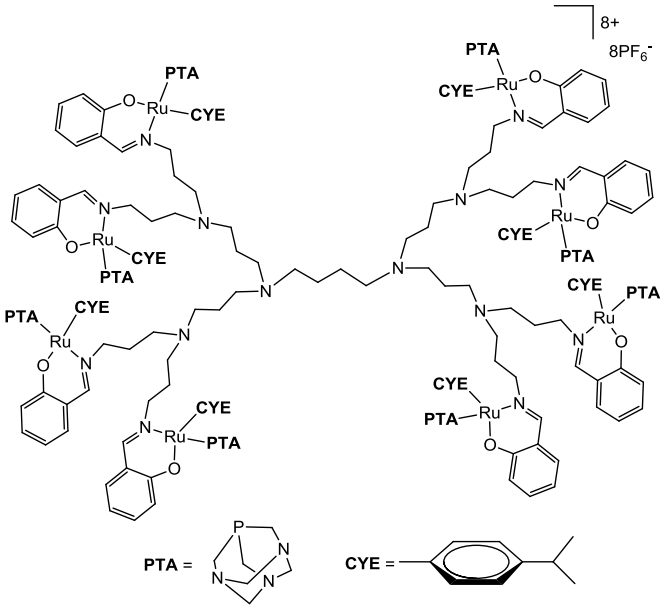

Mustard solid. **Yield**: 0.363 g, 89.6 %. **IR** (KBr pellets): ν (cm^{-1}) = 1618 (s, imine, C=N). **^{1}H NMR** ($(CD_3)_2CO$): δ (ppm) = 1.09 & 1.24 (br d, 48H, $CH(CH_3)_{2\ p\text{-}cye}$), 1.96 - 2.78 (overlapping m, 64H, $NCH_2CH_{2\ core}$, $NCH_2CH_{2\ core}$, $NCH_2CH_2CH_2N_{\ 1st\ branch}$, $NCH_2CH_2CH_2N_{\ 1st\ branch}$, $NCH_2CH_2CH_2N_{\ 1st\ branch}$, $NCH_2CH_2CH_2N_{\ 2nd\ branch}$, $NCH_2CH_2CH_2N_{\ 2nd\ branch}$), 2.22 (s, 24H, $CH_{3\ p\text{-}cye}$), 3.57 (br m, 8H, $CH(CH_3)_{2\ p\text{-}cye}$), 3.92 & 4.08 (br m, 16H, $NCH_2CH_2CH_2N_{\ 2nd\ branch}$), 4.28 (m, 48H, PTA), 4.55 (m, 48H, PTA), 5.51 (br m, 8H, Ar $_{p\text{-}cye}$), 5.90 (br m, 8H, Ar $_{p\text{-}cye}$), 6.23 (br m, 8H, Ar $_{p\text{-}cye}$), 6.42 (br m, 8H, Ar $_{p\text{-}cye}$), 6.49 (br t, 8H, Ar), 6.78 (br d, 8H, Ar), 7.23 (m, 16H, Ar), 8.21 (br s, 8H, $CH_{\ imine}$). **^{13}C{^{1}H} NMR** ($(CD_3)_2CO$): δ (ppm) = 18.0, 20.8, 21.4 ($CH_{3\ p\text{-}cye}$); 52.3, 68.3 (CH_2); 51.1, 72.4 ($CH_{2\ PTA}$); 30.6, 82.7, 87.7, 88.8, 92.0 ($CH_{\ p\text{-}cye}$); 96.8, 121.4 ($C_{\ p\text{-}cye}$); 115.1, 122.1, 135.2, 135.4 ($CH_{\ Ar}$); 119.1, 164.3 ($C_{\ Ar}$); 166.7 ($CH_{\ imine}$). **^{31}P{^{1}H} NMR** ($(CD_3)_2CO$): δ (ppm) = -32.3 (s, PTA), -144.1 (sep, ^1J = 710.5 Hz, PF_6). **Elemental analysis** for $C_{232}H_{360}N_{38}O_8P_{16}F_{48}Ru_8$.20EtOH (6993.138): Found C, 39.86; H, 5.49; N, 7.95 %; calcd. C, 40.11; H, 5.22; N, 7.66 %. **MS** (HR-ESI-TOF, *m*/*z*): 540.1608 $[M+H]^{9+}$ (where M = [**30**][PF_6]$_8$ - 8PF_6). **MP**: 275 ºC (decompose without melting).

6.5.2.3 [DAB-G_3-PPI-{(η^6-*p*-cye)Ru((C_7H_5NO)-κ^2-*N*,*O*)PTA}$_{16}$][PF_6]$_{16}$ ([**31**][PF_6]$_{16}$)

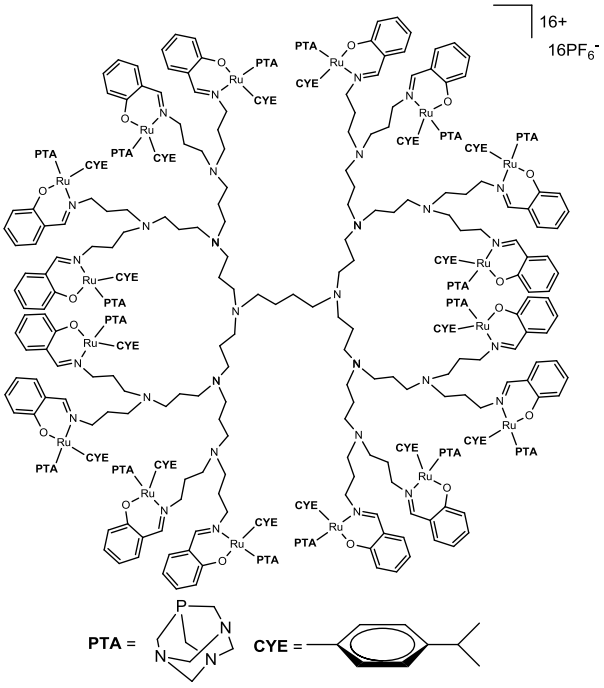

Mustard solid. **Yield**: 0.398 g, 87.5 %. **IR** (KBr pellets): ν (cm^{-1}) = 1618 (s, imine, C=N). **^{1}H NMR** ($(CD_3)_2CO$): δ (ppm) = 1.11 & 1.29 (br d, 96H, CH(C**H**$_3$)$_2$ *p-cye*), 1.99 - 3.16 (overlapping m, 144H, NC**H**$_2$CH$_2$ *core*, NCH$_2$C**H**$_2$ *core*, NC**H**$_2$CH$_2$CH$_2$N *1st branch*, NCH$_2$C**H**$_2$CH$_2$N *1st branch*, NCH$_2$CH$_2$C**H**$_2$N *1st branch*, NC**H**$_2$CH$_2$CH$_2$N *2nd branch*, NCH$_2$C**H**$_2$CH$_2$N *2nd branch*, NCH$_2$CH$_2$C**H**$_2$N *2nd branch*, NC**H**$_2$CH$_2$CH$_2$N *3rd branch*, NCH$_2$C**H**$_2$CH$_2$N *3rd branch*), 2.22 (s, 48H, C**H**$_3$ *p-cye*), 3.32 (br m, 16H, C**H**(CH$_3$)$_2$ *p-cye*), 3.90 & 4.03 (br m, 32H, NCH$_2$CH$_2$C**H**$_2$N *3rd branch*), 4.25 (m, 96H, PTA), 4.56 (m, 96H, PTA), 5.43 (br m, 16H, Ar *p-cye*), 5.85 (br m, 16H, Ar *p-cye*), 6.15 (br m, 16H, Ar *p-cye*), 6.26 (br m, 16H, Ar *p-cye*), 6.59 (br m, 16H, Ar), 6.87 (br m, 16H, Ar), 7.34 (br m, 32H, Ar), 8.21 (br s, 16H, C**H** *imine*). **^{13}C{^{1}H} NMR** ($(CD_3)_2CO$): δ (ppm) = 18.1, 20.8, 21.4 (**C**H$_3$ *p-cye*); 55.6, 60.8, 67.2, 72.8 (**C**H$_2$); 50.9, 72.3 (**C**H$_2$ *PTA*); 30.6, 82.6, 87.9, 88.8, 92.0 (**C**H *p-cye*); 96.6, 121.4 (**C** *p-cye*); 115.2, 122.2, 135.3, 135.3 (**C**H *Ar*); 119.5, 164.3 (**C** *Ar*); 167.0 (**C**H *imine*). **^{31}P{^{1}H} NMR** ($(CD_3)_2CO$): δ (ppm) = -26.2 (s, PTA), -138.6 (sep, ^1J = 709.2 Hz, **P**F$_6$). **Elemental analysis** for $C_{472}H_{736}N_{78}O_{16}P_{32}F_{96}Ru_{16}$.55EtOH (14725.394): Found C, 38.17; H, 4.09; N, 7.34 %; calcd. C, 38.50; H, 5.04; N, 7.42 %. **MS** (HR-ESI-TOF, *m*/*z*): 617.1169 $[M]^{16+}$ (where M = [**31**][PF_6]$_{16}$ - 16PF_6). **MP**: 259 - 281 ºC.

6.5.2.4 [DAB-G_4-PPI-{(η^6-*p*-cye)Ru((C_7H_5NO)-κ^2-*N*,*O*)PTA}$_{32}$][PF_6]$_{32}$ ([**32**][PF_6]$_{32}$)

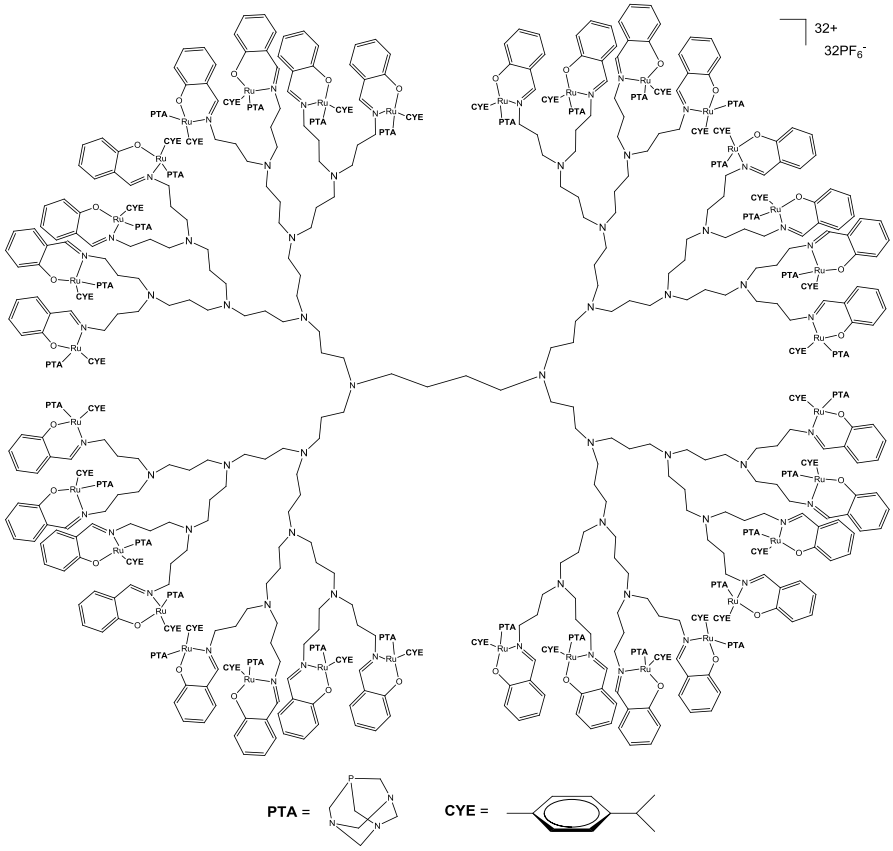

Mustard solid. **Yield**: 0.297 g, 78.7 %. **IR** (KBr pellets): ν (cm^{-1}) = 1618 (s, imine, C=N). **^{1}H NMR** ($(CD_3)_2CO$): δ (ppm) = 1.13 & 1.29 (br d, 192H, CH(C**H**$_3$)$_2$ *p-cye*), 1.75 - 3.02 (overlapping m, 304H, NC**H**$_2$CH$_2$ *core*, NCH$_2$C**H**$_2$ *core*, NC**H**$_2$CH$_2$CH$_2$N *1st branch*, NCH$_2$C**H**$_2$CH$_2$N *1st branch*, NCH$_2$CH$_2$C**H**$_2$N *1st branch*, NC**H**$_2$CH$_2$CH$_2$N *2nd branch*, NCH$_2$C**H**$_2$CH$_2$N *2nd branch*, NCH$_2$CH$_2$C**H**$_2$N *2nd branch*, NC**H**$_2$CH$_2$CH$_2$N *3rd branch*, NCH$_2$C**H**$_2$CH$_2$N *3rd branch*, NCH$_2$CH$_2$C**H**$_2$N *3rd branch*, NC**H**$_2$CH$_2$CH$_2$N *4th branch*, NCH$_2$C**H**$_2$CH$_2$N *4th branch*), 2.17 (br s, 96H, C**H**$_3$ *p-cye*), 3.15 (br m, 32H, C**H**(CH$_3$)$_2$ *p-cye*), 3.82 & 3.91 (br m, 64H, NCH$_2$CH$_2$C**H**$_2$N *4th branch*), 4.21 (m, 384H, PTA), 4.54 (m, 384H, PTA), 5.42 (br m, 32H, Ar$_{p\text{-cye}}$), 5.73 (br m, 32H, Ar$_{p\text{-cye}}$), 6.12 (br m, 32H, Ar$_{p\text{-cye}}$), 6.22 (br s, 32H, Ar$_{p\text{-cye}}$), 6.60 (br m, 32H, Ar), 6.89 (br m, 32H, Ar), 7.29 (br m, 64H, Ar), 8.10 (br s, 32H, C**H** *imine*). **^{13}C{^{1}H} NMR** ($(CD_3)_2CO$): δ (ppm) = 18.0, 20.8, 21.4 (**C**H$_3$ *p-cye*); 50.4 52.3, 68.2, 72.8 (**C**H$_2$); 50.9, 72.3 (**C**H$_2$ *PTA*); 30.6, 82.6, 87.6, 88.9, 92.0 (**C**H *p-cye*); 96.7, 121.4 (**C** *p-cye*); 115.2, 122.2, 135.3, 135.4 (**C**H *Ar*); 119.3, 164.3 (**C** *Ar*); 166.7 (**C**H *imine*). **^{31}P{^{1}H} NMR** ($(CD_3)_2CO$): δ (ppm) = -26.6 (s, PTA), -144.0 (sep, ^1J = 711.1 Hz, **P**F_6). **Elemental analysis** for $C_{952}H_{1488}N_{158}O_{32}P_{64}F_{192}Ru_{32}$.12EtOH.38$Et_3NH^+Cl^-$ (30307.105): Found C, 40.48; H, 5.75; N, 7.45 %; calcd. C, 40.38; H, 5.12; N, 7.56 %. **MS** (HR-ESI-TOF, *m*/*z*): 603.1587 $[M]^{32+}$ (where M = [**32**][PF_6]$_{32}$ - 32PF_6). **MP**: 195 - 199 ºC.

6.5.2.5 [DAB-G_1-PPI-{(η^6-HMB)Ru((C_7H_5NO)-κ^2-*N*,*O*)PTA}$_4$][PF_6]$_4$ ([**33**][PF_6]$_4$)

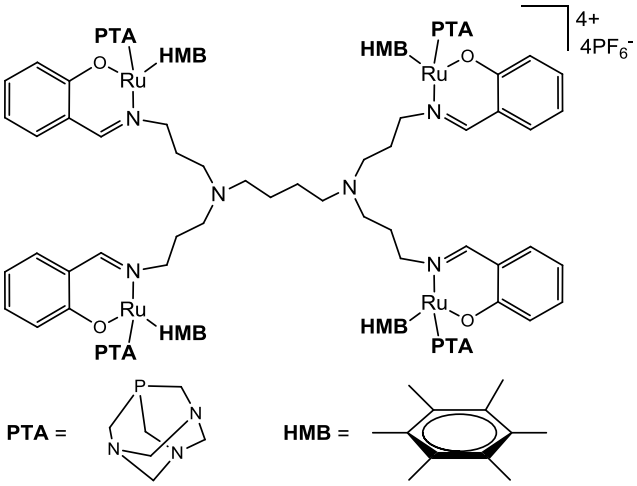

Yellow solid. **Yield**: 0.422 g, 90.8 %. **IR** (KBr pellets): ν (cm^{-1}) = 1618 (s, imine, C=N). **^{1}H NMR** ($(CD_3)_2CO$): δ (ppm) = 1.75 (overlapping m, 12H, $NCH_2C\mathbf{H}_{2\ core}$, $NCH_2C\mathbf{H}_2CH_2N_{\ branch}$), 2.07 (br s, 72H, $C\mathbf{H}_{3\ HMB}$), 2.42 (br m, 4H, $NC\mathbf{H}_2CH_{2\ core}$), 2.95 (br m, 8H, $NC\mathbf{H}_2CH_2CH_2N_{\ branch}$), 3.49 & 3.85 (br m, 8H, $NCH_2CH_2C\mathbf{H}_2N_{\ branch}$), 4.13 (m, 24H, PTA), 4.45 (m, 24H, PTA), 6.51 (t, ^3J = 7.3 Hz, 4H, Ar), 6.76 (d, ^3J = 8.4 Hz, 4H, Ar), 7.14 (t, ^3J = 7.0 Hz, 4H, Ar), 7.27 (br d, 4H, Ar), 8.02 (s, 4H, $C\mathbf{H}_{\ imine}$). **^{13}C{^{1}H} NMR** ($(CD_3)_2CO$): δ (ppm) = 16.3 ($\mathbf{C}H_{3\ HMB}$); 22.3, 26.3, 50.7, 53.0, 64.3 ($\mathbf{C}H_2$); 49.5, 73.0 ($\mathbf{C}H_{2\ PTA}$); 99.4 ($\mathbf{C}_{\ HMB}$); 115.9, 123.2, 134.7, 136.0 ($\mathbf{C}H_{\ Ar}$); 122.2, 164.3 ($\mathbf{C}_{\ Ar}$); 165.5 ($\mathbf{C}H_{\ imine}$). **^{31}P{^{1}H} NMR** ($(CD_3)_2CO$): δ (ppm) = -41.0 (s, PTA), -144.4 (sep, ^1J = 714.5 Hz, $\mathbf{P}F_6$). **Elemental analysis** for $C_{116}H_{172}N_{18}O_4P_8F_{24}Ru_4$.10EtOH (3451.465): Found C, 40.29; H, 5.15; N, 7.33 %; calcd. C, 40.37; H, 5.02; N, 7.30 %. **MS** (HR-ESI-TOF, *m*/*z*) 603.7332 $[M]^{4+}$ (where M = [**33**][PF_6]$_4$ - 4PF_6). **MP**: 224 ºC (decompose without melting).

6.5.2.6 [DAB-G_2-PPI-{(η^6-HMB)Ru((C_7H_5NO)-κ^2-*N*,*O*)PTA}$_8$][PF_6]$_8$ ([34][PF_6]$_8$)

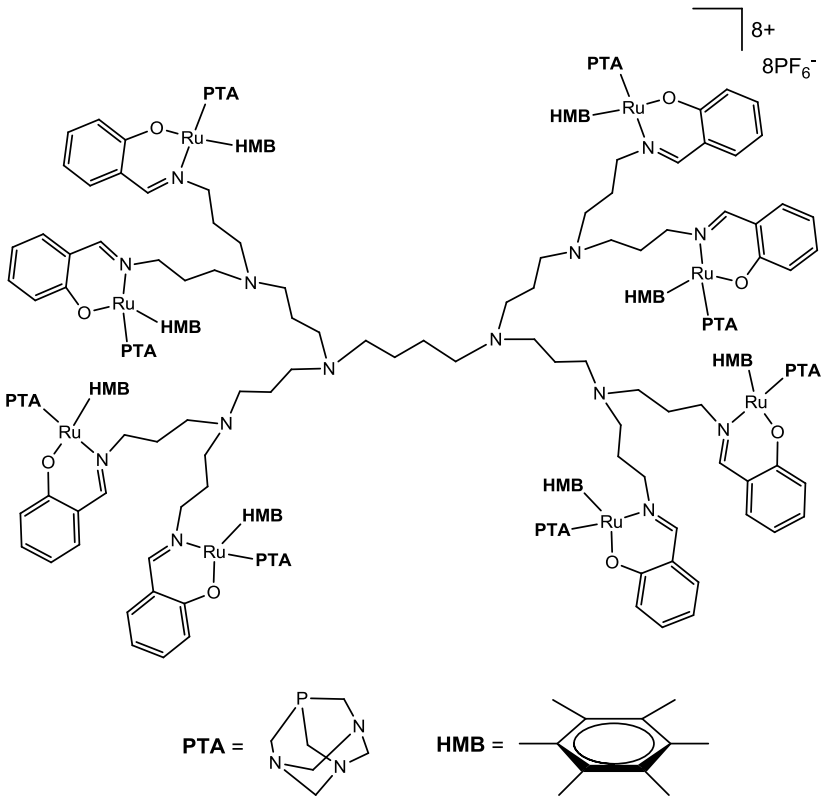

Yellow solid. **Yield**: 0.413 g, 92.7 %. **IR** (KBr pellets): ν (cm^{-1}) = 1619 (s, imine, C=N). **^{1}H NMR** ($(CD_3)_2CO$): δ (ppm) = 1.95 - 3.11 (overlapping m, 64H, NCH_2CH_2 *core*, NCH_2CH_2 *core*, $NCH_2CH_2CH_2N$ *1st branch*, $NCH_2CH_2CH_2N$ *1st branch*, $NCH_2CH_2CH_2N$ *1st branch*, $NCH_2CH_2CH_2N$ *2nd branch*, $NCH_2CH_2CH_2N$ *2nd branch*), 2.05 (br s, 144H, CH_3 *HMB*), 3.51 & 3.82 (br m, 16H, $NCH_2CH_2CH_2N$ *2nd branch*), 4.12 (m, 48H, PTA), 4.45 (m, 48H, PTA), 6.49 (br t, 8H, Ar), 6.76 (d, ^3J = 8.3 Hz, 8H, Ar), 7.13 (t, ^3J = 7.3 Hz, 8H, Ar), 7.25 (br d, 8H, Ar), 8.02 (br s, 8H, CH *imine*). **^{13}C{^{1}H} NMR** ($(CD_3)_2CO$): δ (ppm) = 16.3 (CH_3 *HMB*); 18.4, 20.8, 27.2, 29.7, 50.1, 51.0, 58.4, 64.7 (CH_2); 49.4, 72.8 (CH_2 *PTA*); 99.4 (C *HMB*); 115.8, 123.2, 134.6, 135.9 (CH *Ar*); 122.2, 164.3 (C *Ar*); 165.4 (CH *imine*). **^{31}P{^{1}H} NMR** ($(CD_3)_2CO$): δ (ppm) = -40.8 (s, PTA), -144.4 (sep, ^1J = 714.6 Hz, PF_6). **Elemental analysis** for $C_{240}H_{360}N_{38}O_8P_{16}F_{48}Ru_8$.20EtOH (7043.158): Found C, 40.62; H, 5.76; N, 7.60 %; calcd. C, 40.93; H, 5.15; N, 7.56 %. **MS** (HR-ESI-TOF, *m*/*z*): 451.1324 $[M+3H]^{11+}$ (where M = [**34**][PF_6]$_8$ - 8PF_6). **MP**: 203 ºC (decompose without melting).

6.5.2.7 [DAB-G_3-PPI-{(η^6-HMB)Ru((C_7H_5NO)-κ^2-*N*,*O*)PTA}$_{16}$][PF_6]$_{16}$ ([**35**][PF_6]$_{16}$)

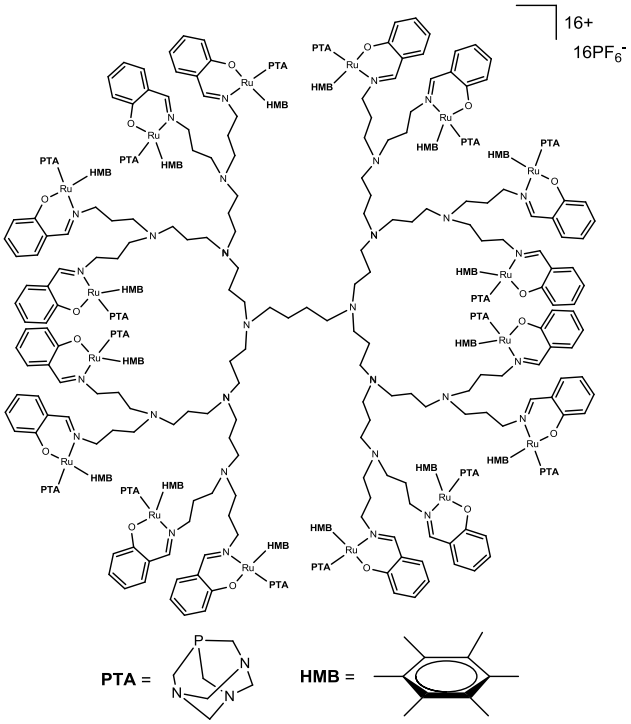

Yellow solid. **Yield**: 0.346 g, 88.1 %. **IR** (KBr pellets): ν (cm^{-1}) = 1618 (s, imine, C=N). **^{1}H NMR** ($(CD_3)_2CO$): δ (ppm) = 1.41 - 3.14 (overlapping m, 144H, NCH_2CH_2 *core*, NCH_2CH_2 *core*, $NCH_2CH_2CH_2N$ *1st branch*, $NCH_2CH_2CH_2N$ *1st branch*, $NCH_2CH_2CH_2N$ *1st branch*, $NCH_2CH_2CH_2N$ *2nd branch*, $NCH_2CH_2CH_2N$ *2nd branch*, $NCH_2CH_2CH_2N$ *2nd branch*, $NCH_2CH_2CH_2N$ *3rd branch*, $NCH_2CH_2CH_2N$ *3rd branch*), 2.03 (br s, 288H, CH_3 *HMB*), 3.49 & 3.79 (br m, 32H, $NCH_2CH_2CH_2N$ *3rd branch*), 4.09 (m, 96H, PTA), 4.42 (m, 96H, PTA), 6.46 (br t, 16H, Ar), 6.75 (br d, 16H, Ar), 7.12 (br t, 16H, Ar), 7.21 (br d, 16H, Ar), 8.00 (br s, 16H, CH *imine*). **^{13}C{^{1}H} NMR** ($(CD_3)_2CO$): δ (ppm) = 15.7 (CH_3 *HMB*); 21.3, 50.4, 50.9, 64.7 (CH_2); 49.3, 72.4 (CH_2 *PTA*); 99.4 (**C** *HMB*); 115.3, 123.6, 134.5, 145.3 (CH *Ar*); 122.3, 164.8 (**C** *Ar*); 165.3 (CH *imine*). **^{31}P{^{1}H} NMR** ($(CD_3)_2CO$): δ (ppm) = -40.6 (s, PTA), -144.3 (sep, ^1J = 714.8 Hz, PF_6). **Elemental analysis** for $C_{488}H_{736}N_{78}O_{16}P_{32}F_{96}Ru_{16}$.37EtOH (14088.339): Found C, 41.31; H, 5.64; N, 7.67 %; calcd. C, 41.60; H, 5.27; N, 7.75 %. **MS** (HR-ESI-TOF, *m*/*z*): 629.2938 $[M]^{16+}$ (where M = [**35**][PF_6]$_{16}$ - 16PF_6). **MP**: 200 ºC (decompose without melting).

6.5.2.8 [DAB-G_4-PPI-{(η^6-HMB)Ru((C_7H_5NO)-κ^2-*N*,*O*)PTA}$_{32}$][PF_6]$_{32}$ ([**36**][PF_6]$_{32}$)

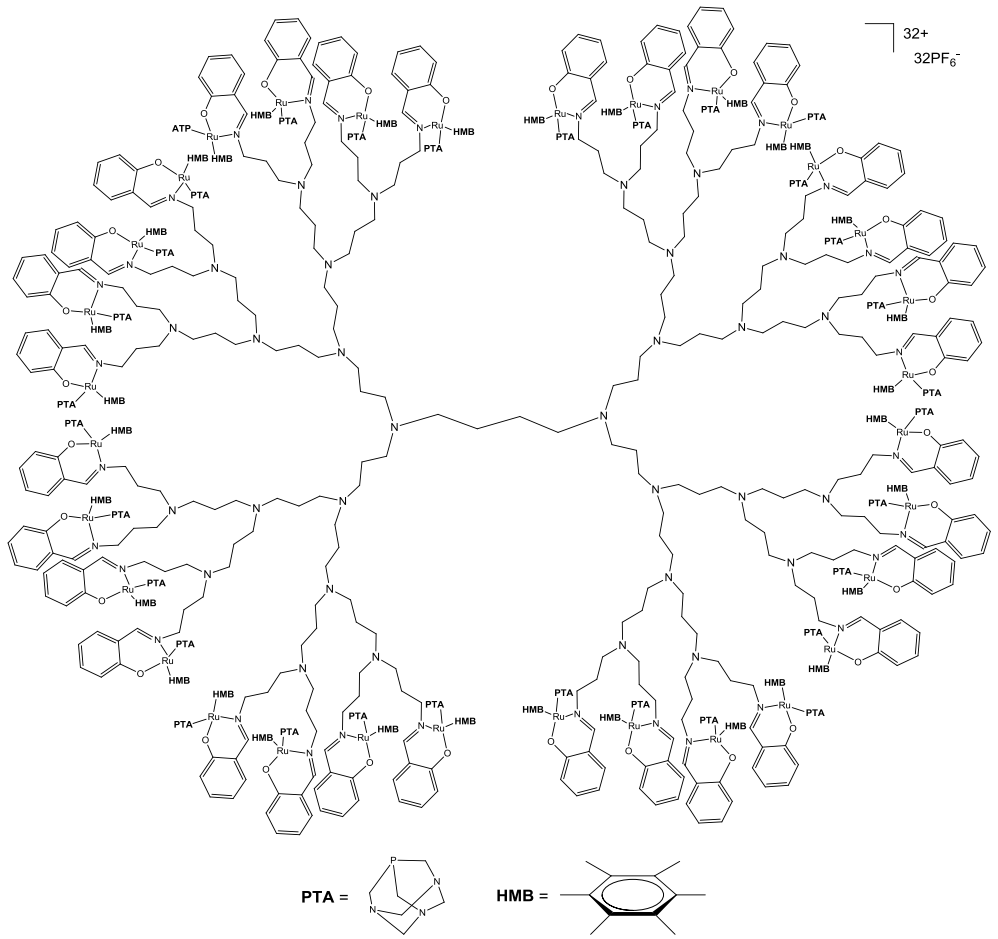

Yellow solid. **Yield**: 0.289 g, 78.3 %. **IR** (KBr pellets): ν (cm^{-1}) = 1617 (s, imine, C=N). **^{1}H NMR** ($(CD_3)_2CO$): δ (ppm) = 2.08 - 3.31 (overlapping br m, 880H, NC**H**$_2$CH$_2$ *core*, NCH$_2$C**H**$_2$ *core*, NC**H**$_2$CH$_2$CH$_2$N *1st branch*, NCH$_2$C**H**$_2$CH$_2$N *1st branch*, NCH$_2$CH$_2$C**H**$_2$N *1st branch*, NC**H**$_2$CH$_2$CH$_2$N *2nd branch*, NCH$_2$C**H**$_2$CH$_2$N *2nd branch*, NCH$_2$CH$_2$C**H**$_2$N *2nd branch*, NC**H**$_2$CH$_2$CH$_2$N *3rd branch*, NCH$_2$C**H**$_2$CH$_2$N *3rd branch*, NCH$_2$CH$_2$C**H**$_2$N *3rd branch*, NC**H**$_2$CH$_2$CH$_2$N *4th branch*, NCH$_2$C**H**$_2$CH$_2$N *4th branch*, C**H**$_3$ *HMB*), 3.64 & 4.86 (br m, 64H, NCH$_2$CH$_2$C**H**$_2$N *4th branch*), 4.17 (m, 96H, PTA), 4.47 (m, 96H, PTA), 6.48 (br m, 32H, Ar), 6.82 (br m, 32H, Ar), 7.18 (br m, 32H, Ar), 7.29 (br m, 32H, Ar), 8.16 (br s, 32H, C**H** *imine*). **^{13}C{^{1}H} NMR** ($(CD_3)_2CO$): δ (ppm) = 20.6 (**C**H$_3$ *HMB*); 25.9, 55.2, 55.7, 69.6 (**C**H$_2$); 54.0, 77.3 (**C**H$_2$ *PTA*); 104.3 (**C** *HMB*); 120.1, 128.4, 139.3, 140.2 (**C**H *Ar*); 127.1, 169.6 (**C** *Ar*); 170.2 (**C**H *imine*). **^{31}P{^{1}H} NMR** ($(CD_3)_2CO$): δ (ppm) = -40.4 (s, PTA), -144.0 (sep, ^1J = 711.2 Hz, **P**F_6). **Elemental analysis** for $C_{984}H_{1488}N_{158}O_{32}P_{64}F_{192}Ru_{32}$.8EtOH.29$Et_3NH^+Cl^-$ (29268.312): Found C, 40.48; H, 5.75; N, 7.45 %; calcd. C, 40.38; H, 5.12; N, 7.56 %. **MS** (HR-ESI-TOF, *m*/*z*): 596.1664 $[M+2H]^{34+}$ (where M = [**36**][PF_6]$_{32}$ - 32PF_6). **MP**: 196 ºC (decompose without melting).

6.5.3 General Procedure for the Preparation of Cationic *N,O*-Ru(II)-Arene-PTA Mononuclear Complexes ([38][PF_6] & [39][PF_6])

To a stirred solution of **37** (0.120 g, 0.736 mmol for [**38**][PF_6] and [**39**][PF_6]) in EtOH (50 mL), triethylamine (0.108 mL, 0.772 mmol for [**38**][PF_6] and [**39**][PF_6]) was added dropwise. The resulting yellow suspension was stirred at room temperature for 0.5 h. [Ru(η^6-*p*-Pr^iC_6H_4Me)Cl_2]$_2$ (0.225 g, 0.368 mmol for [**38**][PF_6]) or [Ru(η^6-C_6Me_6)Cl_2]$_2$ (0.232 g, 0.343 mmol for [**39**][PF_6]) was added to the reaction mixture and stirred for 0.5 h. The reaction mixture was filtered, then PTA (0.121 g, 0.772 mmol for [**38**][PF_6] and [**39**][PF_6]) was added to the filtrate and the reaction stirred for 1 h. The orange-yellow solution was filtered and the filtrate reduced to ~5 mL. $NaPF_6$ (0.130 g, 0.773 mmol for [**38**][PF_6] and **[39**][PF_6]) was added to the filtrate and stirred for 1 h, resulting in the formation of a solid. The product was isolated by filtration, washed with cold EtOH, followed by Et_2O and dried under vacuum. Crystals for X-ray diffraction were obtained by slow diffusion of EtOH (for [**38**][PF_6]) or hexane (for [**39**][PF_6]) into a concentrated DCM solution of the complex.

6.5.3.1 [$CH_3CH_2CH_2$-(η^6-*p*-cye)Ru((C_7H_5NO)-κ^2-*N,O*)PTA][PF_6] ([38][PF_6])

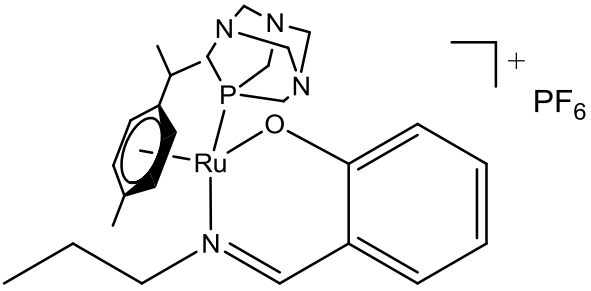

Yellow solid. **Yield**: 0.431 g, 83.7 %. **IR** (KBr pellets): ν (cm^{-1}) = 1619 (s, imine, C=N). **^{1}H NMR** ($(CD_3)_2CO$): δ (ppm) = 1.06 (t, ^3J = 7.3 Hz, 3H, $NCH_2CH_2C\mathbf{H}_3$), 1.14 & 1.23 (d, ^3J = 6.9 Hz, 6H, $CH(C\mathbf{H}_3)_{2\ p\text{-}cye}$), 2.00 & 2.08 (m, 2H, $NCH_2C\mathbf{H}_2CH_3$), 2.20 (s, 3H, $C\mathbf{H}_{3\ p\text{-}cye}$), 2.64 (m, 1H, $C\mathbf{H}(CH_3)_{2\ p\text{-}cye}$), 3.81 & 3.98 (m, 2H, $NC\mathbf{H}_2CH_2CH_3$), 4.23 and 4.36 (2d, 6H, PTA), 4.51 (s, 6H, PTA), 5.61 (d, ^3J = 4.8 Hz, 1H, $Ar_{p\text{-}cye}$), 5.85 (d, ^3J = 5.4 Hz, 1H, $Ar_{p\text{-}cye}$), 6.32 (d, ^3J = 4.9 Hz, 1H, $Ar_{p\text{-}cye}$), 6.45 (m, 1H, $Ar_{p\text{-}cye}$), 6.53 (t, ^3J = 6.5 Hz, 1H, Ar), 6.81 (d, ^3J = 8.3 Hz, 1H, Ar), 7.22 (m, 2H, Ar), 8.13 (s, 1H, $C\mathbf{H}_{\ imine}$). **^{13}C{^{1}H} NMR** ($(CD_3)_2CO$): δ (ppm) = 10.7 ($\mathbf{C}H_3$); 17.9, 21.0, 21.6 ($\mathbf{C}H_{3\ p\text{-}cye}$); 24.8, 72.3 ($\mathbf{C}H_2$); 51.3, 72.6 ($\mathbf{C}H_{2\ PTA}$); 30.8, 83.7, 97.7, 89.1, 91.5 ($\mathbf{C}H_{\ p\text{-}cye}$); 95.6, 121.4 ($\mathbf{C}_{\ p\text{-}cye}$); 115.3, 121.4, 122.6, 135.6 ($\mathbf{C}H_{\ Ar}$); 118.4, 164.4 ($\mathbf{C}_{\ Ar}$); 166.9 ($\mathbf{C}H_{\ imine}$). **^{31}P{^{1}H} NMR** ($(CD_3)_2CO$): δ (ppm) = -33.0 (s, PTA), -144.2 (sep, ^1J = 707.9 Hz, $\mathbf{P}F_6$). **Elemental analysis** for $C_{26}H_{38}N_4OP_2F_6Ru$ (699.619): Found C, 44.69; H, 5.43; N, 7.96 %; calcd. C, 44.64; H, 5.47; N, 8.01 %. **MS** (ESI, *m*/*z*): 566 $[M\text{-}CYE]^+$. **MP**: 248 ºC (decompose without melting).

6.5.3.2 [$CH_3CH_2CH_2$-(η^6-HMB)Ru((C_7H_5NO)-κ^2-*N*,*O*)PTA][PF_6] ([39][PF_6])

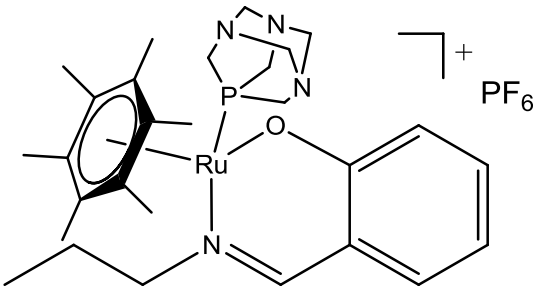

Yellow solid. **Yield**: 0.422 g, 84.6 %. **IR** (KBr pellets): ν (cm^{-1}) = 1618 (s, imine, C=N). **^{1}H NMR** ($(CD_3)_2CO$): δ (ppm) = 1.05 (t, ^3J = 7.3 Hz, 3H, $NCH_2CH_2C\mathbf{H}_3$), 2.02 (m, 2H, $NCH_2C\mathbf{H}_2CH_3$), 2.06 (s, 18H, $C\mathbf{H}_{3\ HMB}$), 3.64 & 3.81 (m, 2H, $NC\mathbf{H}_2CH_2CH_3$), 4.19 (m, 6H, PTA), 4.47 (s, 6H, PTA), 6.52 (t, ^3J = 6.8 Hz, 1H, Ar), 6.87 (d, ^3J = 9.6 Hz, 1H, Ar), 7.21 (m, 2H, Ar), 8.13 (s, 1H, $C\mathbf{H}_{imine}$). **^{13}C{^{1}H} NMR** ($(CD_3)_2CO$): δ (ppm) = 10.4 ($\mathbf{C}H_3$); 15.7 ($\mathbf{C}H_{3\ HMB}$); 23.5, 68.8 ($\mathbf{C}H_2$); 49.3, 72.6 ($\mathbf{C}H_{2\ PTA}$); 99.5 ($\mathbf{C}_{HMB}$); 115.3, 123.7, 134.6, 135.1 ($\mathbf{C}H_{Ar}$); 122.1, 164.6 ($\mathbf{C}_{Ar}$); 165.2 ($\mathbf{C}H_{imine}$). **^{31}P{^{1}H} NMR** ($(CD_3)_2CO$): δ (ppm) = -41.6 (s, PTA), -148.6 (sep, ^1J = 707.3 Hz, $\mathbf{P}F_6$). **Elemental analysis** for $C_{28}H_{42}N_4OP_2F_6Ru$ (727.673): Found C, 46.19; H, 5.79; N, 7.74 %; calcd. C, 46.22; H, 5.82; N, 7.70 %. **MS** (ESI, *m*/*z*): 283 [M-PF_6]$^+$. **MP**: 248 ºC (decompose without melting).

6.5.4 Synthesis of Neutral *N*,*O*-Os(II)-Arene Complexes (40, 41, 48)

Triethylamine (0.042 mL, 0.303 mmol for **40**; 0.032 mL, 0.231 mmol for **41**; 0.047 mL, 0.334 mmol for **48**) was added to a stirred solution of **21** (0.055 g, 0.075 mmol for **40**) or **22** (0.046 g, 0.029 mmol for **41**) or **37** (0.052 g, 0.318 mmol for **48**) in DCM (30 mL). The reaction mixture was stirred for 0.5 h. This was followed by the addition of [Os(η^6-*p*-Pr^iC_6H_4Me)Cl_2]$_2$ (0.121 g, 0.153 mmol for **40**; 0.092 g, 0.116 mmol for **41**; 0.126 g, 0.159 mmol for **48**) and the reaction stirred overnight (for **40** and **41**) or for 6 h (for **48**). The reaction mixture was filtered and the filtrate washed with distilled H_2O (5 x 50 mL). The organic layer was isolated, dried over $MgSO_4$ (~10 g) and filtered. The filtrate was reduced to ~10 mL and the desired product precipitated with hexane. The solid was filtered, washed with cold hexane, followed by excess Et_2O and dried *in vacuo*. Crystals of complex **48** were obtained by slow evaporation of a concentrated DCM solution of this complex.

6.5.4.1 [DAB-G_1-PPI-{(η^6-*p*-cye)Os((C_7H_5NO)-κ^2-*N*,*O*)Cl}$_4$] (40)

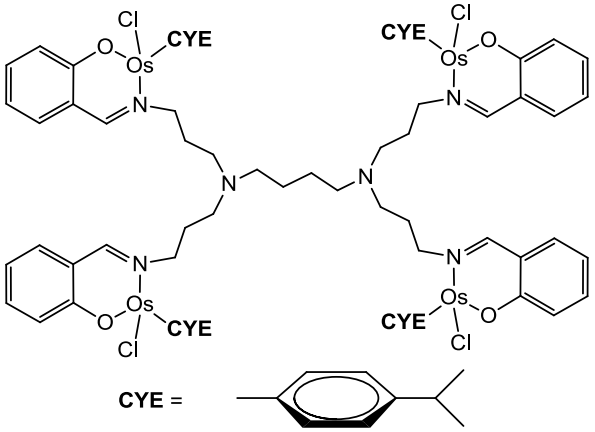

Mustard-yellow solid. **Yield**: 0.142 g, 87.5 %. **IR** (NaCl cells, DCM): ν (cm^{-1}) = 1618 (s, imine, C=N). **^{1}H NMR** ($CDCl_3$): δ (ppm) = 1.08 & 1.21 (br d, 24H, CH(C**H**$_3$)$_2$ *p-cye*), 1.47 - 2.10 (overlapping m, 12H, NCH$_2$C**H**$_2$ *core*, NCH$_2$C**H**$_2$CH$_2$N *branch*), 2.28 (s, 12H, C**H**$_3$ *p-cye*), 2.43 - 3.04 (overlapping m, 16H, NC**H**$_2$CH$_2$ *core*, NC**H**$_2$CH$_2$CH$_2$N *branch*, C**H**(CH$_3$)$_2$ *CYE*), 4.09 & 4.22 (br m, 8H, NCH$_2$CH$_2$C**H**$_2$N *branch*), 5.46 (br m, 8H, Ar *p-cye*), 5.70 (br m, 8H, Ar *p-cye*), 6.44 (br m, 4H, Ar), 6.85 (br m, 4H, Ar), 6.99 (br m, 4H, Ar), 7.20 (br m, 4H, Ar), 7.75 (br s, 4H, C**H** *imine*). **^{13}C{^{1}H} NMR** ($CDCl_3$): δ (ppm) = 19.0, 22.2, 23.4 (**C**H$_3$ *p-cye*); 24.4, 25.7, 51.4, 53.4, 69.6 (**C**H$_2$); 31.1, 71.1, 72.7, 74.1, 80.0 (**C**H *p-cye*); 90.0, 90.6 (**C** *p-cye*); 114.7, 121.2, 135.1, 135.5 (**C**H *Ar*); 119.4, 163.7 (**C** *Ar*), 163.0 (**C**H *imine*). **Elemental analysis** for $C_{84}H_{108}N_6O_4Cl_4Os_4.2Et_3NH^+Cl^-$ (2443.852): Found C, 41.88; H, 6.39; N, 3.47 %; calcd. C, 41.28; H, 4.45; N, 3.44 %. **MS** (HR-ESI-TOF, *m*/*z*): 688.3991 $[M]^{3+}$ (where M = **40** - 3Cl). **MP**: 151 ºC (decompose without melting).

6.5.4.2 [DAB-G_2-PPI-{(η^6-*p*-cye)Os((C_7H_5NO)-κ^2-*N*,*O*)Cl}$_8$] (41)

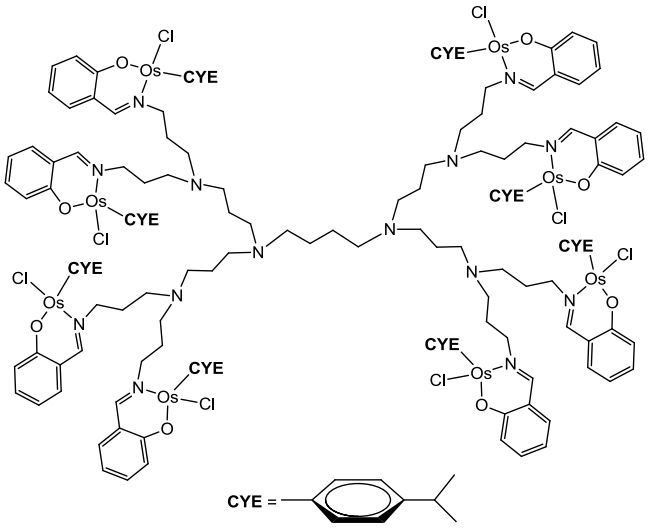

Mustard-yellow solid. **Yield**: 0.0662 g, 51.7 %. **IR** (NaCl cells, DCM): ν (cm^{-1}) = 1617 (s, imine, C=N). **^{1}H NMR** ($CDCl_3$): δ (ppm) = 1.05 & 1.17 (br m, 48H, $CH(CH_3)_2$), 1.59 - 2.82 (overlapping m, 64H, NCH_2CH_2 *core*, NCH_2CH_2 *core*, $NCH_2CH_2CH_2N$ *1st branch*, $NCH_2CH_2CH_2N$ *1st branch*, $NCH_2CH_2CH_2N$ *1st branch*, $NCH_2CH_2CH_2N$ *2nd branch*, $NCH_2CH_2CH_2N$ *2nd branch*), 2.30 (br s, 24H, CH_3 *p-cye*), 3.18 (br m, 8H, $CH(CH_3)_2$ *p-cye*), 4.18 & 4.37 (br m, 16H, $NCH_2CH_2CH_2N$ *2nd branch*), 5.61 (br d, 16H, Ar *p-cye*), 5.72 (br d, 16H, Ar *p-cye*), 6.42 (br m, 8H, Ar), 6.82 (br m, 8H, Ar), 7.19 (br m, 16H, Ar), 8.09 (br s, 8H, CH *imine*). **^{13}C{^{1}H} NMR** ($CDCl_3$): δ (ppm) = 19.1, 22.3, 23.8 (CH_3 *p-cye*); 25.2, 49.2, 52.4, 68.7 (CH_2); 31.2, 70.9, 73.0, 73.6, 79.9 (CH *p-cye*); 90.2, 91.0 (C *p-cye*); 114.8, 121.2, 135.0, 135.3 (CH *Ar*); 119.5, 163.6 (C *Ar*); 162.7 (CH *imine*). **Elemental analysis** for $C_{176}H_{232}N_{14}O_8Cl_8Os_8.4H_2O.5Et_3NH^+Cl^-$ (5237.644): Found C, 40.36; H, 5.68; N, 3.58 %; calcd. C, 40.36; H, 4.46; N, 3.74 %. **MS** (HR-ESI-TOF, *m*/*z*): 604.1675 $[M]^{7+}$ (where M = **41** - 7Cl). **MP**: 165 ºC (decompose without melting).

6.5.4.3 [$CH_3CH_2CH_2$-(η^6-*p*-cye)Os((C_7H_5NO)-κ^2-*N*,*O*)Cl] (48)

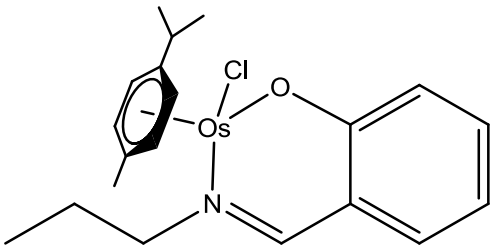

Orange-yellow solid. **Yield**: 0.080 g, 48.3 %. **IR** (NaCl cells, DCM): ν (cm^{-1}) = 1617 (s, imine, C=N). **^{1}H NMR** ($CDCl_3$): δ (ppm) = 1.01 (t, ^3J = 7.4 Hz, 3H, $NCH_2CH_2C\mathbf{H}_3$), 1.14 & 1.26 (d, ^3J = 6.8 Hz, 6H, $CH(C\mathbf{H}_3)_{2\ p\text{-}cye}$), 1.90 & 2.01 (br m, 2H, $NCH_2C\mathbf{H}_2CH_3$), 2.30 (s, 3H, $C\mathbf{H}_{3\ p\text{-}cye}$), 2.65 (m, 1H, $C\mathbf{H}(CH_3)_{2\ p\text{-}cye}$), 3.98 & 4.20 (m, 2H, $NC\mathbf{H}_2CH_2CH_3$), 5.40 (d, ^3J = 5.3 Hz, 2H, $Ar_{p\text{-}cye}$), 5.74 (m, 2H, $Ar_{p\text{-}cye}$), 6.44 (t, ^3J = 6.9 Hz, 1H, Ar), 6.87 (d, ^3J = 8.5 Hz, 1H, Ar), 6.94 (d, ^3J = 7.8 Hz, 1H, Ar), 7.22 (m, 1H, Ar), 7.70 (s, 1H, $C\mathbf{H}_{\ imine}$). **^{13}C{^{1}H} NMR** ($CDCl_3$): δ (ppm) = 11.5 ($\mathbf{C}H_3$); 18.7, 22.2, 23.3 ($\mathbf{C}H_{3\ p\text{-}cye}$); 24.5, 73.2 ($\mathbf{C}H_2$); 31.1, 71.6, 72.2, 74.2, 78.0 ($\mathbf{C}H_{\ p\text{-}cye}$); 89.5, 91.4 ($\mathbf{C}_{\ p\text{-}cye}$); 114.7, 121.4, 134.2, 135.0 ($\mathbf{C}H_{\ Ar}$); 119.5, 164.0 ($\mathbf{C}_{\ Ar}$); 161.6 ($\mathbf{C}H_{\ imine}$). **Elemental analysis** for $C_{20}H_{26}NOClOs$ (522.114): Found C, 45.98; H, 5.05; N, 2.65 %; calcd. C, 46.01; H, 5.02; N, 2.68 %. **MS** (ESI, *m*/*z*): 488 $[M\text{-}Cl]^+$. **MP**: 226 - 231 ºC.

6.5.5 Synthesis of Cationic *N*,*O*-Os(II)-Arene-PTA Complexes ([42][PF_6]$_4$, [43][PF_6]$_8$, [49][PF_6])

Triethylamine (0.083 mL, 0.596 mmol for [**42**][PF_6]$_4$; 0.042 mL, 0.303 mmol for [**43**][PF_6]$_8$; 0.077 mL, 0.551 mmol for [**49**][PF_6]) was added to a stirred suspension of **21** (0.108 g, 0.147 mmol for [**42**][PF_6]$_4$) or **22** (0.060 g, 0.376 mmol for [**43**][PF_6]$_8$) or **37** (0.086 g, 0.524 mmol for [**49**][PF_6]) in EtOH (30 mL). The reaction mixture was stirred for 0.5 h. This was followed by the addition of [Os(η^6-*p*-Pr^iC_6H_4Me)Cl_2]$_2$ (0.239 g, 0.302 mmol for [**42**][PF_6]$_4$; 0.120 g, 0.152 mmol for [**43**][PF_6]$_8$; 0.207 g, 0.262 mmol for [**49**][PF_6]) and the reaction stirred overnight (for [**42**][PF_6]$_4$ and [**43**][PF_6]$_8$) or for 6 h (for [**49**][PF_6]). The reaction mixture was filtered, the filtrate reduced to ~10 mL and PTA (0.094 g, 0.596 mmol for [**42**][PF_6]$_4$; 0.048 g, 0.303 mmol for [**43**][PF_6]$_8$; 0.087 g, 0.551 mmol for [**49**][PF_6]) was added. The reaction mixture was stirred for 6 h, filtered and the filtrate reduced ~5 mL. $NaPF_6$ (0.100 g, 0.596 mmol for [**42**][PF_6]$_4$; 0.051 g, 0.303 mmol for [**43**][PF_6]$_8$; 0.093 g, 0.551 mmol for [**49**][PF_6]) was added to the reaction mixture and stirred for 0.5 h, which resulted in the precipitation of a solid. The solid was filtered, washed with cold EtOH and excess Et_2O. The solid was dissolved in 20 mL acetone. The solution was filtered over Celite® and the filtrate reduced. The desired product was precipitated with Et_2O and dried under reduced pressure. Crystals of complex [**49**][PF_6] were obtained by slow diffusion of hexane into a concentrated DCM solution of the complex.

6.5.5.1 [DAB-G_1-PPI-{(η^6-*p*-cye)Os((C_7H_5NO)-κ^2-*N*,*O*)PTA}$_4$][PF_6]$_4$ ([**42**][PF_6]$_4$)

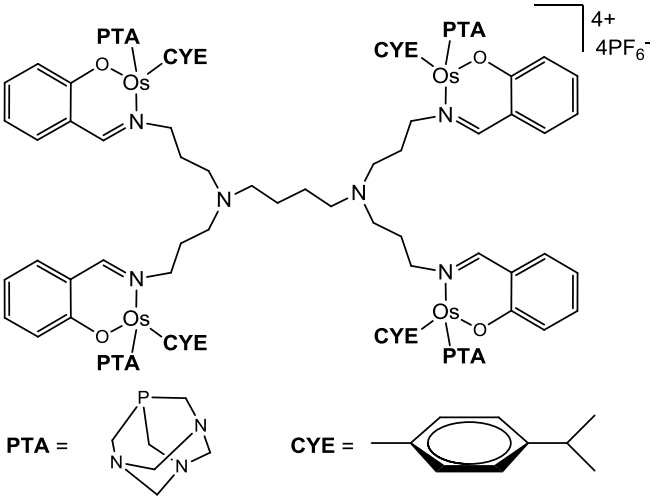

Yellow solid. **Yield**: 0.450 g, 94.5 %. **IR** (KBr pellets): ν (cm^{-1}) = 1611 (s, imine, C=N). **^{1}H NMR** ($(CD_3)_2CO$): δ (ppm) = 0.97 & 1.16 (br d, ^3J = 6.9 Hz, 24H, $CH(CH_3)_{2\ p\text{-}cye}$), 1.48 - 2.11 (overlapping m, 12H, $NCH_2CH_{2\ core}$, $NCH_2CH_2CH_2N_{branch}$), 2.25 (s, 12H, $CH_{3\ p\text{-}cye}$), 2.39 - 2.97 (overlapping m, 16H, $NCH_2CH_{2\ core}$, $NCH_2CH_2CH_2N_{branch}$, $CH(CH_3)_{2\ p\text{-}cye}$), 3.99 (br m, 8H, $NCH_2CH_2CH_2N_{branch}$), 4.11 (m, 24H, PTA), 4.34 (m, 24H, PTA), 5.63 (br d, ^3J = 5.5 Hz, 4H, $Ar_{p\text{-}cye}$), 5.94 (br m, 4H, $Ar_{p\text{-}cye}$), 6.08 (m, 4H, $Ar_{p\text{-}cye}$), 6.34 (br m, 4H, $Ar_{p\text{-}cye}$), 6.39 (t, ^3J = 7.3 Hz, 4H, Ar), 6.62 (br d, ^3J = 8.5 Hz, 4H, Ar), 7.18 (br t, ^3J = 6.8 Hz, 8H, Ar), 8.07 (br s, 4H, CH_{imine}). **^{13}C{^{1}H} NMR** ($(CD_3)_2CO$): δ (ppm) = 18.0, 20.7, 21.1 ($CH_{3\ p\text{-}cye}$); 52.1, 53.6, 70.8 (CH_2); 50.1, 72.1 ($CH_{2\ PTA}$); 30.1, 73.8, 79.3, 80.0, 82.9 ($CH_{p\text{-}cye}$); 89.5, 121.4 ($C_{p\text{-}cye}$); 115.7, 120.7, 134.7, 135.2 (CH_{Ar}); 111.7, 164.1 (C_{Ar}), 162.5 (CH_{imine}). **^{31}P{^{1}H} NMR** ($(CD_3)_2CO$): δ (ppm) = -71.2 (s, PTA), -144.1 (sep, ^1J = 709.8 Hz, PF_6). **Elemental analysis** for $C_{108}H_{156}N_{18}O_4P_8F_{24}Os_4.EtOH.Et_3NH^+Cl^-$ (3556.580): Found C, 36.21; H, 5.37; N, 7.06 %; calcd. C, 36.47; H, 4.42; N, 7.09 %. **MS** (HR-ESI-TOF, *m*/*z*): 632.8656 $[M]^{4+}$ (where M = [**42**][PF_6]$_4$ - 4PF_6). **MP**: 185 - 188 ºC.

6.5.5.2 [DAB-G_2-PPI-{(η^6-*p*-cye)Os((C_7H_5NO)-κ^2-*N*,*O*)PTA}$_8$][PF_6]$_8$ ([**43**][PF_6]$_8$)

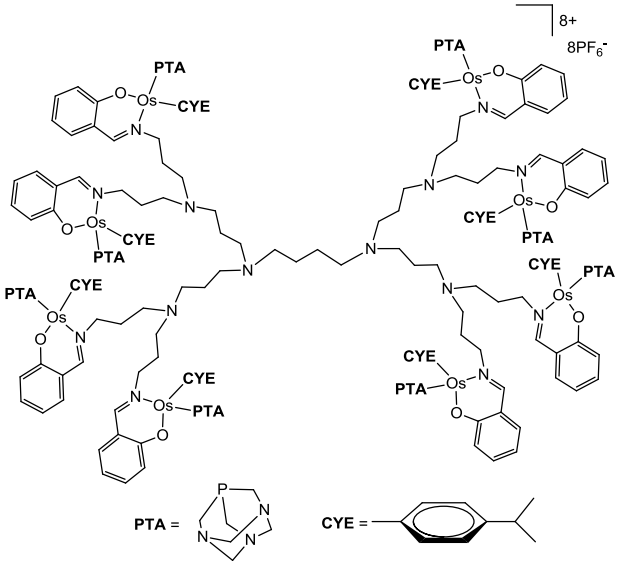

Yellow solid. **Yield**: 0.137 g, 54.0 %. **IR** (KBr pellets): ν (cm^{-1}) = 1614 (s, imine, C=N). **^{1}H NMR** ($(CD_3)_2CO$): δ (ppm) = 0.95 & 1.15 (br d, 48H, $CH(CH_3)_2$ *p-cye*), 1.74 - 2.17 (overlapping m, 28H, NCH_2CH_2 *core*, $NCH_2CH_2CH_2N$ *1st branch*, $NCH_2CH_2CH_2N$ *2nd branch*), 2.24 (s, 24H, CH_3 *p-cye*), 2.34 - 3.13 (overlapping m, 44H, NCH_2CH_2 *core*, $NCH_2CH_2CH_2N$ *1st branch*, $NCH_2CH_2CH_2N$ *1st branch*, $NCH_2CH_2CH_2N$ *2nd branch*, $CH(CH_3)_2$ *p-cye*), 3.92 (br m, 16H, $NCH_2CH_2CH_2N$ *2nd branch*), 4.09 (m, 48H, PTA), 4.36 (m, 48H, PTA), 5.58 (br m, 8H, Ar *p-cye*), 5.89 (br m, 8H, Ar *p-cye*), 6.04 (br m, 8H, Ar *p-cye*), 6.33 (br m, 8H, Ar *p-cye*), 6.38 (br t, 8H, Ar), 6.61 (br d, 8H, Ar), 7.17 (br m, 16H, Ar), 8.05 (br s, 8H, CH *imine*). **^{13}C{^{1}H} NMR** ($(CD_3)_2CO$): δ (ppm) = 18.0, 20.7, 21.1 (CH_3 *p-cye*); 50.9, 71.1 (CH_2); 50.9, 72.1 (CH_2 *PTA*); 30.0, 73.4, 79.2, 79.9, 83.2 (CH *p-cye*); 89.1, 121.5 (C *p-cye*); 115.7, 120.7, 134.7, 135.1 (CH *Ar*); 111.9, 164.0 (C *Ar*); 162.5 (CH *imine*). **^{31}P{^{1}H} NMR** ($(CD_3)_2CO$): δ (ppm) = -70.9 (s, PTA), -144.0 (sep, ^1J = 710.2 Hz, PF_6). **Elemental analysis** for $C_{224}H_{328}N_{38}O_8P_{16}F_{48}Os_8$.12EtOH (7071.325): Found C, 41.68; H, 5.53; N, 7.30 %; calcd. C, 41.58; H, 5.63; N, 7.43 %. **MS** (HR-ESI-TOF, *m*/*z*): 650.3942 $[M]^{8+}$ (where M = [**43**][PF_6]$_8$ - 8PF_6). **MP**: 179 - 182 ºC

6.5.5.3 [$CH_3CH_2CH_2$-(η^6-*p*-cye)Os((C_7H_5NO)-κ^2-*N*,*O*)PTA][PF_6] ([49][PF_6])

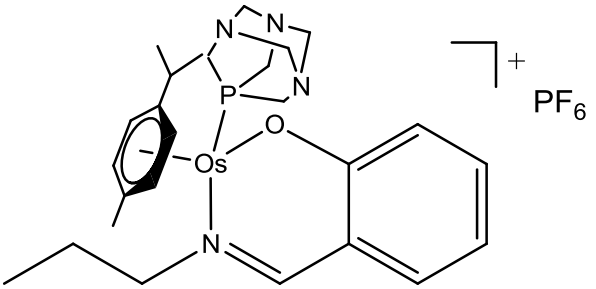

Orange-yellow solid. **Yield**: 0.222 g, 53.8 %. **IR** (KBr pellets): ν (cm^{-1}) = 1613 (s, imine, C=N). **^{1}H NMR** ($(CD_3)_2CO$): δ (ppm) = 1.05 (t, ^3J = 7.4 Hz, 3H, $NCH_2CH_2C\mathbf{H}_3$), 1.21 & 1.31 (d, ^3J = 6.9 Hz, 6H, $CH(C\mathbf{H}_3)_{2\ p\text{-}cye}$), 1.94 - 2.06 (br m, 2H, $NCH_2C\mathbf{H}_2CH_3$), 2.34 (s, 3H, $C\mathbf{H}_{3\ p\text{-}cye}$), 2.58 (m, 1H, $C\mathbf{H}(CH_3)_{2\ p\text{-}cye}$), 3.97 & 4.17 (m, 2H, $NC\mathbf{H}_2CH_2CH_3$), 4.23 (m, 6H, PTA), 4.45 (m, 6H, PTA), 5.79 (dd, ^3J = 5.7 Hz, J = 1.2 Hz, 1H, $Ar_{p\text{-}cye}$), 5.99 (d, ^3J = 5.7 Hz, 1H, $Ar_{p\text{-}cye}$), 6.26 (dd, ^3J = 5.7 Hz, J = 1.1 Hz, 1H, $Ar_{p\text{-}cye}$), 6.48 (m, 1H, $Ar_{p\text{-}cye}$), 6.55 (t, ^3J = 6.9 Hz, 1H, Ar), 6.77 (d, ^3J = 8.5 Hz, 1H, Ar), 7.25 (dd, ^3J = 6.0 Hz, J = 1.8 Hz, 1H, Ar), 7.32 (t, ^3J = 6.8 Hz, 1H, Ar), 8.13 (s, 1H, $C\mathbf{H}_{\ imine}$). **^{13}C{^{1}H} NMR** ($(CD_3)_2CO$): δ (ppm) = 10.2 ($\mathbf{C}H_3$); 17.9, 21.0, 21.5 ($\mathbf{C}H_{3\ p\text{-}cye}$); 25.0, 74.9 ($\mathbf{C}H_2$); 50.4, 72.4 ($\mathbf{C}H_{2\ PTA}$); 30.4, 74.6, 79.2, 80.4, 82.6 ($\mathbf{C}H_{\ p\text{-}cye}$); 90.7, 121.7 ($\mathbf{C}_{\ p\text{-}cye}$); 116.0, 121.0, 134.8, 135.4 ($\mathbf{C}H_{\ Ar}$); 111.2, 162.7 ($\mathbf{C}_{\ Ar}$); 164.4 ($\mathbf{C}H_{\ imine}$). **^{31}P{^{1}H} NMR** ($(CD_3)_2CO$): δ (ppm) = -71.6 (s, PTA), -148.5 (sep, ^1J = 707.6 Hz, $\mathbf{P}F_6$). **Elemental analysis** for $C_{26}H_{38}N_4OP_2F_6Os$ (788.774): Found C, 39.53; H, 4.94; N, 7.01 %; calcd. C, 39.59; H, 4.86; N, 7.10 %. **MS** (EI, *m*/*z*): 566 [M-PTA-PF_6]$^+$. **MP**: 226 - 231 ºC.

6.5.6 Synthesis of *N*,*N*-2-Pyridylimine Ligands (44, 45, 50)

DAB-$\mathbf{G_1}$-PPI-$(C_6H_5N_2)_4$ (**44**), DAB-$\mathbf{G_2}$-PPI-$(C_6H_5N_2)_8$ (**45**) and (*E*)-*N*-(pyridine-2-ylmethylene)propan-1-amine (**50**) were prepared from known literature reported procedures.[7-9]

6.5.7 Synthesis of Cationic *N,N*-Os(II)-Arene Complexes ([46][PF$_6$]$_4$, [47][PF$_6$]$_8$, [51][PF$_6$])

Ligand **44** (0.068 g, 0.101 mmol for [**26**][PF$_6$]$_4$) or **45** (0.066 g, 0.044 mmol for [**47**][PF$_6$]$_8$) or **50** (0.154 g, 0.301 mmol for [**51**][PF$_6$]) was added to a stirred suspension of [Os(η^6-*p*-Pr^{i}C$_6$H$_4$Me)Cl$_2$]$_2$ (0.164 g, 0.208 mmol for [**46**][PF$_6$]$_4$; 0.142 g, 0.180 mmol for [**47**][PF$_6$]$_8$; 0.116 g, 0.147 mmol for [**51**][PF$_6$]) in EtOH (30 mL). The reaction was stirred overnight (for [**46**][PF$_6$]$_4$ and [**47**][PF$_6$]$_8$) or for 6 h (for [**51**][PF$_6$]). The reaction mixture was filtered, NaPF$_6$ (0.069 g, 0.410 mmol for [**46**][PF$_6$]$_4$; 0.060 g, 0.357 mmol for [**47**][PF$_6$]$_8$; 0.051 g, 0.301 mmol for [**41**][PF$_6$]) was added to the filtrate and the reaction mixture stirred for 0.5 h. This resulted in the precipitation of a solid, which was filtered, washed with cold EtOH and excess Et$_2$O. The solid was dissolved in 20 mL acetone. The solution was filtered over Celite® and the filtrate reduced. The desired product was precipitated with Et$_2$O and dried under vacuum. Crystals of complex [**51**][PF$_6$] were obtained by slow diffusion of Et$_2$O into a concentrated acetone solution of the complex.

6.5.7.1 [DAB-G1-PPI-{(η^6-*p*-cye)Os((C$_6$H$_5$N$_2$)-κ^2-*N,N*)Cl}$_4$][PF$_6$]$_4$ ([46][PF$_6$]$_4$)

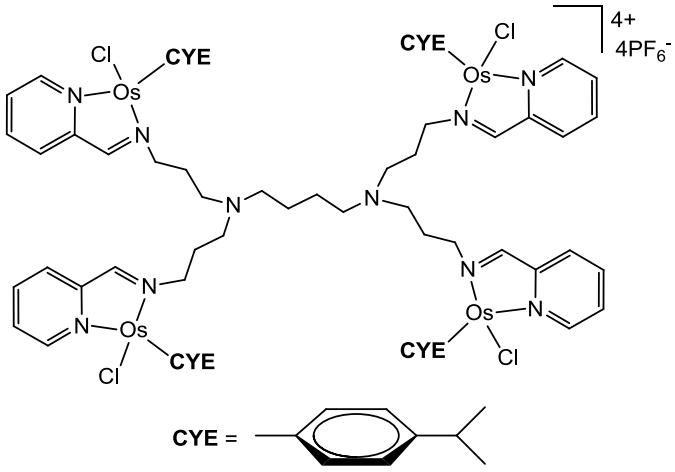

Dark orange solid. **Yield**: 0.197 g, 72.4 %. **IR** (KBr pellets): ν (cm^{-1}) = 1617 (s, imine, C=N), 1598 (s, pyridyl, C=N). **^{1}H NMR** ((CD$_3$)$_2$CO): δ (ppm) = 1.02 (br m, 24H, CH(C**H**$_3$)$_2$ *p-cye*), 1.29 (br m, 4H, NCH$_2$C**H**$_2$ *core*,), 1.93 - 2.18 (overlapping m, 12H, NC**H**$_2$CH$_2$ *core*, NCH$_2$C**H**$_2$CH$_2$N *branch*), 2.39 (s, 12H, C**H**$_3$ *p-cye*), 2.59 (br m, 4H, C**H**(CH$_3$)$_2$ *p-cye*), 3.39 (br m, 8H, NC**H**$_2$CH$_2$CH$_2$N *branch*), 4.70 & 4.81 (br m, 8H, NCH$_2$CH$_2$C**H**$_2$N *branch*), 6.12 (br m, 8H, Ar *p-cye*), 6.51 (br d, 8H, Ar *p-cye*), 7.79 (br m, 4H, Pyr), 8.28 (br m, 8H, Pyr), 9.24 (br s, 4H, C**H** *imine*), 9.54 (br m, 4H, Pyr). **^{13}C{^{1}H} NMR** ((CD$_3$)$_2$CO): δ (ppm) = 18.3, 21.6, 22.0 (**C**H$_3$ *p-cye*); 24.6, 51.2, 52.8, 65.1 (**C**H$_2$); 31.2, 75.0, 76.0, 77.3,79.7 (**C**H *p-cye*); 97.3, 97.9 (**C** *p-cye*); 129.5, 140.0, 155.5 (**C**H *pyr*); 156.1 (**C** *pyr*); 169.7 (**C**H *imine*). **Elemental analysis** for C$_{80}$H$_{108}$N$_{10}$Cl$_4$P$_4$F$_{24}$Os$_4$.5EtOH (2922.725): Found C, 36.44; H, 4.69; N, 4.59 %; calcd. C, 36.99; H, 4.76; N, 4.79 %. **MS** (HR-ESI-TOF, *m/z*): 528.1338 [M]$^{4+}$ (where M = [**46**][PF$_6$]$_4$ - 4PF$_6$). **MP**: 194 ºC (decompose without melting).

6.5.7.2 [DAB-G_2-PPI-{(η^6-*p*-cye)Os(($C_6H_5N_2$)-κ^2-*N*,*N*)Cl}$_8$][PF_6]$_8$ ([**47**][PF_6]$_8$)

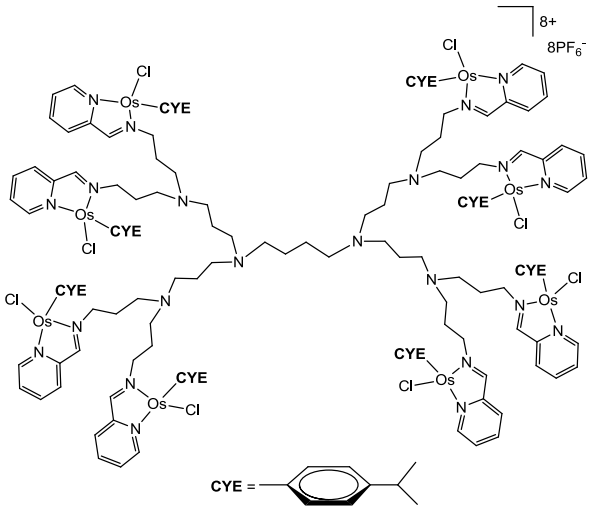

Yellow -brown solid. **Yield**: 0.186 g, 75.7 %. **IR** (KBr pellets): ν (cm^{-1}) = 1619 (s, imine, C=N), 1596 (s, pyridyl, C=N). **^{1}H NMR** ($(CD_3)_2CO$): δ (ppm) = 1.01 (br m, 48H, $CH(CH_3)_2$ *p-cye*), 1.30 (br m, 4H, NCH_2CH_2 *core*), 1.94 - 2.77 (overlapping m, 56H, $NCH_2CH_2CH_2N$ *1st branch*, $NCH_2CH_2CH_2N$ *2nd branch*, $CH(CH_3)_2$ *p-cye*, CH_3 *p-cye*), 3.26 - 3.61 (overlapping m, 32H, NCH_2CH_2 *core*, $NCH_2CH_2CH_2N$ *1st branch*, $NCH_2CH_2CH_2N$ *1st branch*, $NCH_2CH_2CH_2N$ *2nd branch*,), 4.80 (br m, 16H, $NCH_2CH_2CH_2N$ *2nd branch*), 6.15 & 6.52 (br m, 32H, Ar *p-cye*), 7.77 (br m, 8H, Pyr), 8.24 (br m, 8H, Pyr), 8.32 (br m, 8H, Pyr), 9.33 (br m, 8H, CH *imine*), 9.53 (br m, 8H, Pyr). **^{13}C{^{1}H} NMR** ($(CD_3)_2CO$): δ (ppm) = 18.4, 21.7, 22.1 (CH_3 *p-cye*); 24.5, 50.9, 53.0, 65.1 (CH_2); 31.2, 75.0, 76.0, 77.3,79.7 (CH *p-cye*); 97.2, 97.8 (C *p-cye*); 129.4, 140.0, 155.5 (CH *pyr*); 156.1 (C *pyr*); 169.7 (CH *imine*). **Elemental analysis** for $C_{168}H_{232}N_{22}Cl_8P_8F_{48}Os_8$.12EtOH (5524.995): Found C, 37.86; H, 5.29; N, 5.95 %; calcd. C, 37.94; H, 5.04; N, 5.07 %. **MS** (HR-ESI-TOF, *m/z*): 545.6624 $[M]^{8+}$ (where M = [**47**][PF_6]$_8$ - $8PF_6$). **MP**: 193 ºC (decompose without melting).

6.5.7.3 $CH_3CH_2CH_2$-(η^6-*p*-cye)Os(($C_6H_5N_2$)-κ^2-*N*,*N*)Cl][PF_6] ([51][PF_6])

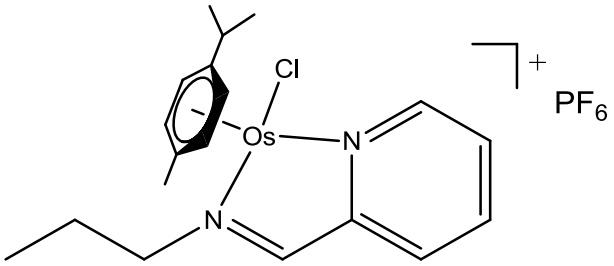

Red solid. **Yield**: 0.120 g, 62.3 %. **IR** (KBr pellets): ν (cm^{-1}) = 1615 (s, imine, C=N), 1596 (s, pyridyl, C=N). **^{1}H NMR** ($(CD_3)_2CO$): δ (ppm) = 1.00 (m, 3H, $NCH_2CH_2C\mathbf{H}_3$), 1.03 & 1.10 (d, ^3J = 6.9 Hz, 6H, $CH(C\mathbf{H}_3)_{2\ p\text{-}cye}$), 1.82 & 1.98 (m, 2H, $NCH_2C\mathbf{H}_2CH_3$), 2.36 (s, 3H, $C\mathbf{H}_{3\ p\text{-}cye}$), 2.68 (m, 1H, $C\mathbf{H}(CH_3)_{2\ p\text{-}cye}$), 4.62 (m, 2H, $NC\mathbf{H}_2CH_2CH_3$), 6.12 (d, ^3J = 6.0 Hz, 1H, $Ar_{p\text{-}cye}$), 6.18 (d, ^3J = 5.9 Hz, 1H, $Ar_{p\text{-}cye}$), 6.50 (d, ^3J = 5.8 Hz, 1H, $Ar_{p\text{-}cye}$), 6.63 (d, ^3J = 5.6 Hz, 1H, $Ar_{p\text{-}cye}$), 7.79 (t, ^3J = 7.5 Hz, 1H, Pyr), 8.26 (t, ^3J = 7.5 Hz, 1H, Pyr), 8.45 (d, ^3J = 7.8 Hz, 1H, Pyr), 9.39 (s, 1H, $C\mathbf{H}_{\ imine}$), 9.66 (d, ^3J = 5.6 Hz, 1H, Pyr). **^{13}C{^{1}H} NMR** ($(CD_3)_2CO$): δ (ppm) = 10.8 ($\mathbf{C}H_3$); 21.5, 22.0, 22.9 ($\mathbf{C}H_{3\ p\text{-}cye}$); 17.9, 69.4 ($\mathbf{C}H_2$); 31.2, 75.5, 76.0, 76.8, 79.7 ($\mathbf{C}H_{\ p\text{-}cye}$); 96.7, 97.0 ($\mathbf{C}_{\ p\text{-}cye}$); 128.8, 129.2, 139.7, 155.8 ($\mathbf{C}H_{\ pyr}$); 156.4 ($\mathbf{C}_{\ pyr}$); 168.2 ($\mathbf{C}H_{\ imine}$). **Elemental analysis** for $C_{19}H_{26}N_2ClPF_6Os$ (653.073): Found C, 34.85; H, 5.98; N, 4.21 %; calcd. C, 34.94; H, 4.01; N, 4.29 %. **MS** (ESI, *m*/*z*): 508 $[M+H]^+$. **MP**: 181 ºC (decompose without melting).

6.6 Synthesis of Ferrocenyl-Derived Conjugates (53 - 55)

6.6.1 Vinyl Ferrocene (53)

53 was prepared from a known literature reported procedure.[10]

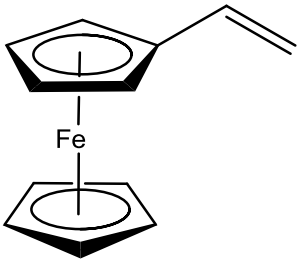

2.5 M *n*-BuLi (2.96 mL, 7.40 mmol) was added dropwise to a stirred light yellow suspension of methyltriphenylphosphonium iodide (2.64 g, 6.53 mmol) in dry THF (100 mL) at -78 ºC. The reaction was warmed to RT and stirred for 1.5 h. The light yellow suspension turns bright yellow. To this suspension, a solution of ferrocene carboxaldehyde **52** (1.03 g, 4.83 mmol) in dry THF (20 mL) was added dropwise at -78 ºC. The mixture was warmed to RT and stirred for 20 h. Following stirring, the reaction mixture was quenched by slow addition of a saturated solution of NH_4Cl (40 mL) at 0 ºC. The organic layer was separated and the aqueous layer washed with Et_2O (3 x 50 mL). The organic fractions were combined, stirred over $MgSO_4$ and filtered. The solvent of the filtrate was reduced and excess Et_2O added. A brown precipitate was observed and filtered off. The solvent of the filtrate was removed to afford the desired product.

Orange solid. **Yield**: 0.933 g, 86.0 %. **IR** (ATR): ν (cm^{-1}) = 1627 (m, alkene, C=C). **^{1}H NMR** ($CDCl_3$): δ (ppm) = 4.10 (s, 5H, Cp-C**H** *unsubst. ring*), 4.20 (t, ^3J = 1.8 Hz, 2H, Cp-C**H**), 4.35 (t, ^3J = 1.9 Hz, 2H, Cp-C**H**), 5.02 (dd, ^3J = 10.7 Hz *cis* & ^2J = 1.6 Hz *geminal*, 1H, Cp-CH=C**H**$_2$), 5.33 (dd, ^3J = 17.5 Hz *trans* & ^2J = 1.6 Hz *geminal*, 1H, Cp-CH=C**H**$_2$), 6.45 (dd, ^3J = 17.5 Hz *trans* & ^3J = 10.7 Hz *cis*, 1H, Cp-C**H**=CH_2). **^{13}C{^{1}H} NMR** ($CDCl_3$): δ (ppm) = 66.7, 68.6 (Cp-**C**H); 69.2 (Cp-**C**H *unsubst. ring*); 83.6 (**C** *Cp*); 111.0 (Cp-CH=**C**H_2); 134.7 (Cp-**C**H=CH_2). **MP**: 48 - 49 ºC (lit. 48 - 50 ºC).[11]

Spectroscopic data in agreement with reported literature.[11]

6.6.2 (4*E*)-(4-ferrocenyl-vinyl)-2-hydroxy-benzaldehyde (54)

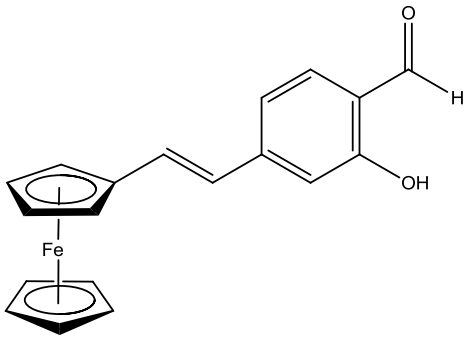

Triethylamine (0.59 mL, 4.25 mmol) was syringed into a solution of **53** (0.300 g, 1.42 mmol), 4-bromo-2-hydroxybenzaldehyde (0.284 g, 1.42 mmol), triphenylphosphine (0.0743 g, 0.283 mmol, 20 mol %) and palladium acetate (0.0159 g, 0.0708 mmol, 5.0 mol % Pd) in 1.4-dioxane (30 mL). The reaction mixture was heated under reflux for 3 days. The orange solution turned into a dark red solution. The reaction mixture was cooled to RT and filtered over a small pad of silica (~2 cm in height). The silica was washed with Et_2O, and the solvent of the filtrate removed. The crude product was purified by flash column chromatography on silica. The column was eluted with a 10:90 (EtOAc/Pet. Ether) solution and the last red band collected. The solvent was removed *in vacuo* to afford the pure product.

Purple solid. **Yield**: 0.0614 g, 13.0 %. **IR** (ATR): ν (cm^{-1}) = 1614 (s, alkene, C=C), 1652 (m, carbonyl, C=O). **^{1}H NMR** ($CDCl_3$): δ (ppm) = 4.16 (s, 5H, Cp-C**H** *unsubst. ring*), 4.37 (t, ^3J = 1.8 Hz, 2H, Cp-C**H**), 4.51 (t, ^3J = 1.8 Hz, 2H, Cp-C**H**), 6.65 (d, ^3J = 16.1 Hz *trans*, 1H, C**H** *alkene*), 7.00 (d, ^4J = 1.2 Hz, 1H, Ar), 7.06 (dd, ^3J = 8.0 Hz & ^4J = 1.5 Hz, 1H, Ar), 7.09 (d, ^3J = 16.1 Hz *trans*, 1H, C**H** *alkene*), 7.48 (d, ^3J = 8.1 Hz, 1H, Ar), 9.83 (s, 1H, C**H**O), 11.10 (s, 1H, O**H**). **^{13}C{^{1}H} NMR** ($CDCl_3$): δ (ppm) = 67.5, 69.9 (Cp-**C**H); 69.4 (Cp-**C**H *unsubst. ring*); 81.9 (**C** *Cp*); 113.8, 117.6, 134.0 (**C**H *Ar*); 119.3, 146.7, 162.2 (**C** *Ar*); 124.3, 133.0 (**C**H *alkene*); 195.2 (**C**HO). **HPLC** (MeOH/H_2O (gradient, 5 - 90 %, flow rate, 0.6 mL/min)): t_R = 17.4 min. **MS** (HR-ESI-TOF, *m*/*z*): 333.0562 $[M+H]^+$. **MP**: 152 ºC (decompose without melting).

6.6.3 (5*E*)-(5-ferrocenyl-vinyl)-2-pyridinecarboxaldehyde (55)

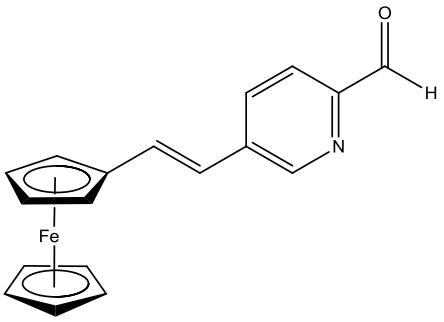

Triethylamine (0.70 mL, 5.01 mmol) was syringed into a solution of **53** (0.354 g, 1.67 mmol), 5-bromo-2-pyridinecarboxaldehyde (0.311 g, 1.67 mmol), triphenylphosphine (0.0876 g, 0.334 mmol, 20 mol %) and palladium acetate (0.0188 g, 0.0835 mmol, 5.0 mol % Pd) in 1.4-dioxane (30 mL). The reaction mixture was heated under reflux for 3 days. The orange solution turned into a dark red solution. The reaction mixture was cooled to RT and filtered over a small pad of silica. The silica was washed with Et_2O, and the solvent of the filtrate removed. The crude product was purified by flash column chromatography on silica (~2 cm in height). The column was eluted with a 10:90 (EtOAc/Pet. Ether) solution and the last red band collected. The solvent was removed *in vacuo* to afford the pure product.

Dark purple solid. **Yield**: 0.1314 g, 24.8 %. **IR** (ATR): ν (cm^{-1}) = 1575 (s, alkene, C=C), 1629 (m, pyridyl, C=N), 1703 (m, carbonyl, C=O). **^{1}H NMR** ($CDCl_3$): δ (ppm) = 4.16 (s, 5H, Cp-C**H** *unsubst. ring*), 4.39 (t, ^{3}J = 1.8 Hz, 2H, Cp-C**H**), 4.50 (t, ^{3}J = 1.8 Hz, 2H, Cp-C**H**), 6.70 (d, ^{3}J = 16.2 Hz *trans*, 1H, C**H** *alkene*), 7.14 (d, ^{3}J = 16.1 Hz *trans*, 1H, C**H** *alkene*), 7.91 (m, 2H, Pyr), 8.77 (s, 1H, Pyr), 10.05 (s, 1H, C**H**O). **^{13}C{^{1}H} NMR** ($CDCl_3$): δ (ppm) = 67.5, 70.1 (Cp-**C**H); 69.5 (Cp-**C**H *unsubst. ring*); 81.7 (**C** *Cp*); 120.9, 122.0 (**C**H *alkene*); 127.9, 135.2 (**C** *Pyr*); 132.3, 133.7, 148.0 (**C**H *Pyr*); 192.8 (**C**HO). **HPLC** (MeOH/H_2O (gradient, 5 - 90 %, flow rate, 0.6 mL/min)): t_R = 15.5 min. **MS** (HR-ESI-TOF, *m*/*z*): 318.0580 $[M+H]^+$. **MP**: 184 - 186 ºC.

6.7 General Procedure for the Preparation of Ferrocenyl-Derived *N,O*-Salicylaldiminato Dendritic Ligands (56 & 57)

DAB-**G$_1$**-PPI-$(NH_2)_4$ (0.0203 g, 0.0641 mmol for **56**) or DAB-**G$_2$**- PPI-$(NH_2)_8$ (0.0249 g, 0.0322 mmol for **57**) in DCM (5.00 mL), was added dropwise to a stirred dark purple solution of (4*E*)-(4-ferrocenyl-vinyl)-2-hydroxy-benzaldehyde (0.0863 g, 0.260 mmol for **56**, 0.0861 g, 0.259 mmol for **57**) in 30 mL DCM. Anhydrous $MgSO_4$ (~10 g) was added and the reaction mixture stirred overnight at room temperature. The reaction mixture was filtered and the solvent removed from the filtrate under reduced pressure, yielding a solid residue. The solid residue was dissolved in a minimum amount of DCM and the products were precipitated with petroleum ether (40 - 60 ºC). The solid was isolated by filtration, washed with petroleum ether (40 - 60 ºC), followed by excess pentane and dried under reduced pressure.

6.7.1 DAB-G$_1$-(4-ferrocenyl-vinyl-$C_7H_5NOH)_4$ (56)

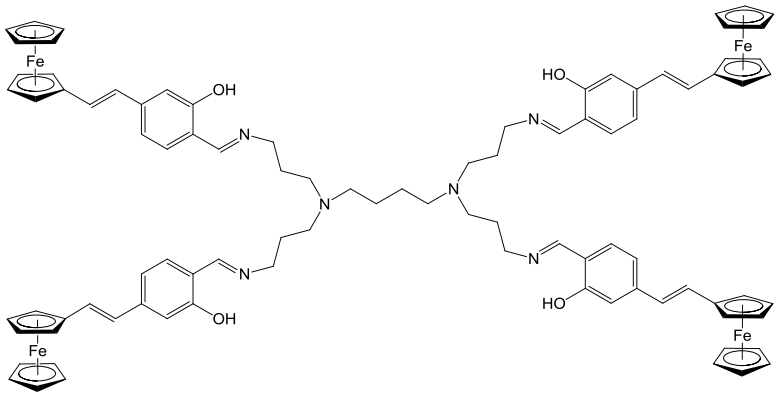

Orange solid. **Yield**: 0.0614 g, 60.9 %. **IR** (ATR): ν (cm^{-1}) = 1614 (s, alkene, C=C & imine, C=N). **^{1}H NMR** ($CDCl_3$): δ (ppm) = 1.42 (br m, 4H, $NCH_2C\mathbf{H}_2$ *core*), 1.82 (br m, 8H, $NCH_2C\mathbf{H}_2CH_2N$ *branch*), 2.40 - 2.51 (overlapping m, 12H, $NC\mathbf{H}_2CH_2$ *core*, $NC\mathbf{H}_2CH_2CH_2N$ *branch*), 3.60 (br m, 8H, $NCH_2CH_2C\mathbf{H}_2N$ *branch*), 4.14 (br s, 20H, Cp-C**H** *unsubst. ring*), 4.30 (br t, ^3J = 1.7 Hz, 8H, Cp-C**H**), 4.47 (br t, ^3J = 1.7 Hz, 8H, Cp-C**H**), 6.63 (d, ^3J = 16.1 Hz *trans*, 4H, C**H** *alkene*), 6.63 (d, ^3J = 16.1 Hz *trans*, 4H, C**H** *alkene*), 6.90 (br d, ^3J = 8.1 Hz, 4H, Ar), 6.94 (d, ^3J = 16.1 Hz *trans*, 4H, C**H** *alkene*), 7.00 (br s, 4H, Ar), 7.14 (d, ^3J = 8.0 Hz, 4H, Ar), 8.27 (br s, 4H, C**H** *imine*). **^{13}C{^{1}H} NMR** ($CDCl_3$): δ (ppm) = 25.2, 28.6, 51.5, 54.1, 57.2 (**C**H_2); 67.2, 69.4 (Cp-**C**H); 69.3 (Cp-**C**H *unsubst. ring*); 82.3 (**C** *Cp*); 113.8, 116.3, 131.4 (**C**H *Ar*); 117.5, 141.8, 162.1 (**C** *Ar*); 125.4, 129.5 (**C**H *alkene*); 164.4 (**C**H *imine*). **Elemental analysis** for $C_{92}H_{96}N_6O_4Fe_4$.4DCM (1912.920): Found C, 60.95; H, 5.41; N, 4.61 %; calcd. C, 60.28; H, 5.48; N, 4.39 %. **MS** (HR-ESI-TOF, *m*/*z*): 525.1727 $[M+3H]^{3+}$. **MP**: 87 ºC (decompose without melting).

6.7.2 DAB-G_2-(4-ferrocenyl-vinyl-$C_7H_5NOH)_8$ (57)

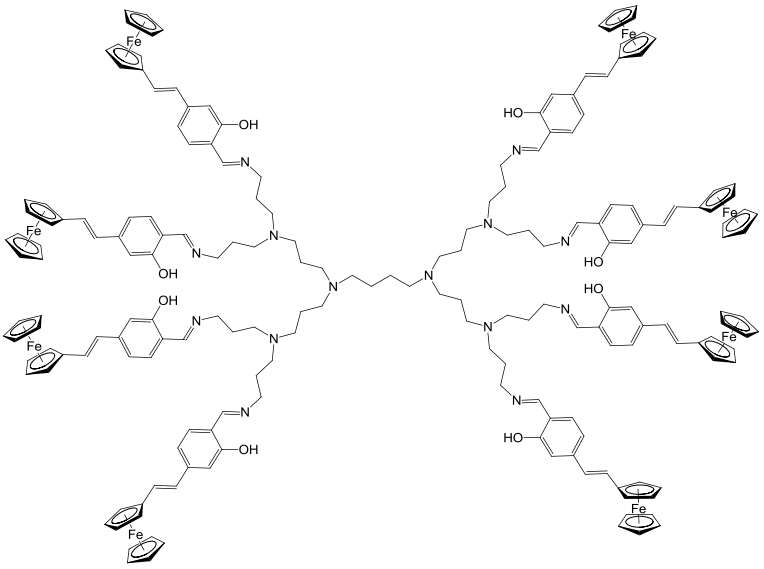

Orange solid. **Yield**: 0.0683 g, 64.6 %. **IR** (ATR): ν (cm^{-1}) = 1613 (s, alkene, C=C & imine, C=N). **^{1}H NMR** ($CDCl_3$): δ (ppm) = 1.41 (m, 4H, NCH_2CH_2 *core*), 1.56 (m, 8H, $NCH_2CH_2CH_2N$ *1st branch*), 1.79 (m, 16H, $NCH_2CH_2CH_2N$ *2nd branch*), 2.41 - 2.50 (overlapping m, 32H, $NCH_2CH_2CH_2N$ *1st branch*, $NCH_2CH_2CH_2N$ *1st branch*, $NCH_2CH_2CH_2N$ *2nd branch*), 2.69 (br m, 4H, NCH_2CH_2 *core*), 3.57 (br m, 16H, $NCH_2CH_2CH_2N$ *2nd branch*), 4.13 (m, 40H, Cp-CH *unsubst. ring*), 4.30 (m, 16H, Cp-CH), 4.46 (m, 16H, Cp-CH), 6.62 (br d, 8H, CH *alkene*), 6.87 - 6.99 (overlapping m, 24H, 2 x Ar, CH *alkene*), 7.06 (m, 8H, Ar), 8.18 (br s, 8H, CH *imine*). **^{13}C{^{1}H} NMR** ($CDCl_3$): δ (ppm) = 24.7, 25.2, 28.6, 40.8, 51.6, 52.3, 54.3, 57.3 (CH_2); 67.2, 69.4 (Cp-CH); 69.3 (Cp-CH *unsubst. ring*); 82.8 (C *Cp*); 113.8, 116.3, 131.4 (CH *Ar*); 117.5, 141.8, 161.9 (C *Ar*); 125.4, 129.5 (CH *alkene*); 164.4 (CH *imine*). **Elemental analysis** for $C_{192}H_{208}N_{14}O_8Fe_8$.6DCM (3796.202): Found C, 62.73; H, 5.90; N, 5.50 %; calcd. C, 62.65; H, 5.84; N, 5.17 %. **MS** (HR-ESI-TOF, *m*/*z*): 822.8010 $[M+4H]^{4+}$. **MP**: 285 ºC (decompose without melting).

6.8 Synthesis of Ferrocenyl-Derived *N,N*-Pyridylimine Ligands (58 & 59)

DAB-**G_1**-PPI-$(NH_2)_4$ (0.0300 g, 0.0948 mmol for **58**) or DAB-**G_2**- PPI-$(NH_2)_8$ (0.0606 g, 0.0784 mmol for **59**) in DCM (5.00 mL), was added dropwise to a stirred dark purple solution of (5*E*)-(5-ferrocenyl-vinyl)-2-pyridinecarboxaldehyde (0.122 g, 0.384 mmol for **58**, 0.200 g, 0.631 mmol for **59**) in 30 mL DCM. Anhydrous $MgSO_4$ (~10 g) was added and the reaction mixture stirred overnight at room temperature. The reaction mixture was filtered and the solvent removed from the filtrate under reduced pressure, yielding a solid residue. The solid residue was dissolved in a minimum amount of DCM and the products were precipitated with petroleum ether (40 - 60 ºC). The solid was isolated by filtration, washed with petroleum ether (40 - 60 ºC), followed by excess pentane and dried under reduced pressure.

6.8.1 DAB-G_1-(5-ferrocenyl-vinyl-$C_6H_5N_2)_4$ (58)

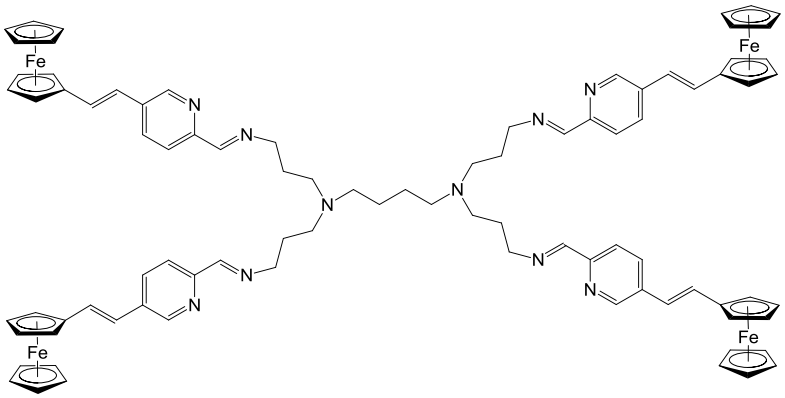

Orange solid. **Yield**: 0.0701 g, 48.9 %. **IR** (ATR): ν (cm^{-1}) = 1579 (m, alkene, C=C), 1628 (s, pyridyl, C=N), 1640 (m, imine, C=N). **^{1}H NMR** ($CDCl_3$): δ (ppm) = 1.45 (br m, 4H, $NCH_2C\mathbf{H}_2$ *core*), 1.88 (br m, 8H, $NCH_2C\mathbf{H}_2CH_2N$ *branch*), 2.45 - 2.55 (overlapping m, 12H, $NC\mathbf{H}_2CH_2$ *core*, $NC\mathbf{H}_2CH_2CH_2N$ *branch*), 3.69 (br m, 8H, $NCH_2CH_2C\mathbf{H}_2N$ *branch*), 4.15 (br s, 20H, Cp-C**H** *unsubst. ring*), 4.33 (br m, 8H, Cp-C**H**), 4.48 (br m, 8H, Cp-C**H**), 6.66 (d, ^3J = 16.3 Hz *trans*, 4H, C**H** *alkene*), 6.99 (br d, ^3J = 16.4 Hz *trans*, 4H, C**H** *alkene*), 7.77 (br d, ^3J = 8.3 Hz, 4H, Pyr), 7.92 (br d, ^3J = 8.1 Hz, 4H, Pyr), 8.37 (br s, 4H, C**H** *imine*), 8.61 (br s, 4H, Pyr). **^{13}C{^{1}H} NMR** ($CDCl_3$): δ (ppm) = 25.2, 28.4, 51.8, 54.1, 59.7 ($C\mathbf{H}_2$); 67.2, 69.5 (Cp-**C**H); 69.3 (Cp-**C**H *unsubst. ring*); 82.4 (**C** *Cp*); 121.2, 121.7 (**C**H *alkene*); 130.6, 132.2, 147.4 (**C**H *Pyr*); 134.5, 152.7 (**C** *Pyr*); 161.7 (**C**H *imine*). **Elemental analysis** for $C_{88}H_{92}N_{10}Fe_4$.1.5DCM (1640.544): Found C, 65.54; H, 6.28; N, 8.51 %; calcd. C, 65.53; H, 5.84; N, 8.54 %. **MS** (HR-ESI-TOF, *m*/*z*): 500.0750 $[M+3H]^{3+}$. **MP**: 82 ºC (decompose without melting).

6.8.2 DAB-G_2-(5-ferrocenyl-vinyl-$C_6H_5N_2$)$_8$ (59)

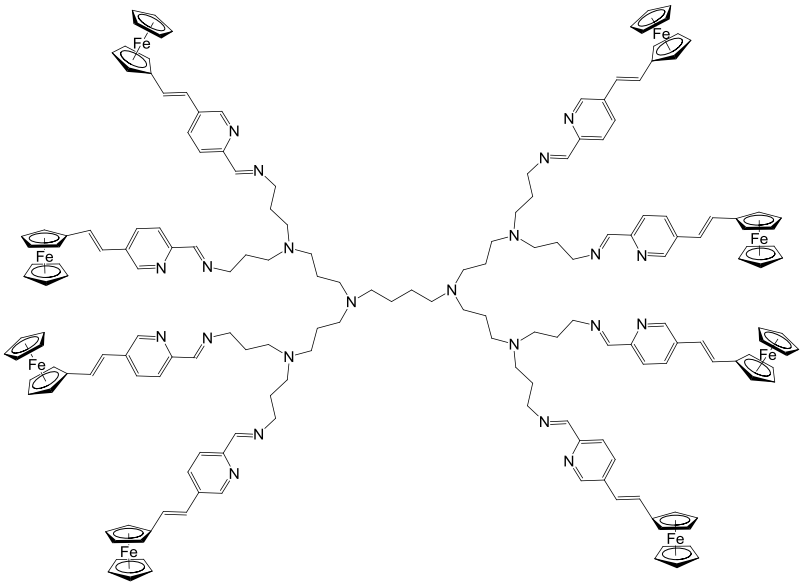

Orange solid. **Yield**: 0.125 g, 50.2 %. **IR** (ATR): ν (cm^{-1}) = 1581 (m, alkene, C=C), 1628 (s, pyridyl, C=N), 1643 (m, imine, C=N). **^{1}H NMR** ($CDCl_3$): δ (ppm) = 1.41 (m, 4H, $NCH_2C\mathbf{H}_2$ *core*), 1.58 (m, 8H, $NCH_2C\mathbf{H}_2CH_2N$ *1st branch*), 1.87 (m, 16H, $NCH_2C\mathbf{H}_2CH_2N$ *2nd branch*), 2.43 - 2.55 (overlapping m, 32H, $NC\mathbf{H}_2CH_2CH_2N$ *1st branch*, $NCH_2CH_2C\mathbf{H}_2N$ *1st branch*, $NC\mathbf{H}_2CH_2CH_2N$ *2nd branch*), 2.72 (br m, 4H, $NC\mathbf{H}_2CH_2$ *core*), 3.68 (br m, 16H, $NCH_2CH_2C\mathbf{H}_2N$ *2nd branch*), 4.14 (br s, 40H, Cp-C**H** *unsubst. ring*), 4.32 (m, 16H, Cp-C**H**), 4.47 (br m, 16H, Cp-C**H**), 6.64 (br d, 8H, C**H** *alkene*), 6.98 (br d, 8H, C**H** *alkene*), 7.76 (m, 8H, Pyr), 7.90 (m, 8H, Pyr), 8.35 (br s, 8H, C**H** *imine*), 8.60 (br s, 8H, Pyr). **^{13}C{^{1}H} NMR** ($CDCl_3$): δ (ppm) = 24.8, 25.2, 28.4, 40.8, 51.8, 52.4, 54.4, 59.7 ($C\mathbf{H}_2$); 67.2, 69.6 (Cp-**C**H); 69.3 (Cp-**C**H *unsubst. ring*); 82.3 (**C** *Cp*); 121.2, 121.7 (**C**H *alkene*); 130.6, 132.2, 147.4 (**C**H *Pyr*); 134.5, 152.6 (**C** *Pyr*); 161.7 (**C**H *imine*). **Elemental analysis** for $C_{184}H_{200}N_{22}Fe_8$.4DCM (3506.249): Found C, 64.33; H, 6.22; N, 8.75 %; calcd. C, 64.40; H, 5.98; N, 8.79 %. **MS** (HR-ESI-TOF, *m*/*z*): 633.1572 $[M+5H]^{5+}$. **MP**: 86 - 87 ºC

6.9 Synthesis of Ferrocenyl-Derived *N,O*-Salicylaldiminato Monomeric Ligand (60)

n-Propylamine (0.025 mL, 0.303 mmol) was added dropwise to a stirred solution of **54** (0.0504 g, 0.152 mmol) in DCM (20.0 mL). The reaction mixture was stirred at RT for 2 h. The orange reaction mixture was filtered over a small pad of silica (2 cm in height), and washed with EtOAc. The solvent was removed from the filtrate under vacuum, to afford the desired product without further purification.

6.9.1 (5*E*, 2*E*)-(5-ferrocenyl-vinyl)-2-((propylimino)methyl)phenol (60)

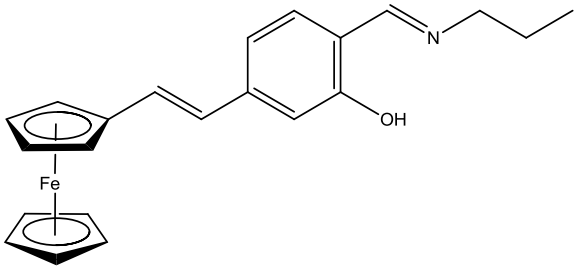

Orange solid. **Yield**: 0.0316 g, 55.8 %. **IR** (ATR): ν (cm^{-1}) = 1607 (s, alkene, C=C & imine, C=N). **^{1}H NMR** ($CDCl_3$): δ (ppm) = 0.99 (t, ^{3}J = 7.4 Hz, 3H, $NCH_2CH_2C\mathbf{H}_3$), 1.72 (m, 2H, $NCH_2C\mathbf{H}_2CH_3$), 3.55 (t, ^{3}J = 6.8 Hz, 2H, $N\mathbf{H}_2CH_2CH_3$), 4.14 (s, 5H, Cp-C**H** *unsubst. ring*), 4.30 (d, ^{3}J = 1.8 Hz, 2H, Cp-C**H**), 4.47 (d, ^{3}J = 1.9 Hz, 2H, Cp-C**H**), 6.64 (d, ^{3}J = 16.1 Hz *trans*, 1H, C**H** *alkene*), 6.94 (m, 2H, C**H** *alkene*, Ar), 7.00 (br s, 1H, Ar), 7.17 (d, ^{3}J = 7.9 Hz, 1H, Ar), 8.29 (s, 1H, C**H** *imine*). **^{13}C{^{1}H} NMR** ($CDCl_3$): δ (ppm) = 11.7 (**C**H_3); 24.1, 61.1 (**C**H_2); 67.2, 69.4 (Cp-**C**H); 69.3 (Cp-**C**H *unsubst. ring*); 82.8 (**C** *Cp*); 113.8, 116.3, 131.3 (**C**H *Ar*); 117.5, 141.8, 162.1 (**C** *Ar*); 125.4, 129.5 (**C**H *alkene*); 164.0 (**C**H *imine*). **HPLC** (MeOH/H_2O (gradient, 5 - 90 %, flow rate, 0.6 mL/min)): t_R = 17.5 min. **MS** (HR-ESI-TOF, *m*/*z*): 374.1206 $[M+H]^+$. **MP**: 152 ºC (decompose without melting).

6.10 Synthesis of Ferrocenyl-Derived *N,N*-Pyridylimine Monomeric Ligands (61)

n-Propylamine (0.026 mL, 0.316 mmol) was added dropwise to a stirred solution of **55** (0.0501 g, 0.158 mmol) in DCM (20.0 mL). The reaction mixture was stirred at RT for 2 h. The orange reaction mixture was filtered over a small pad of silica, and washed with EtOAc. The solvent was removed from the filtrate under vacuum, to afford the desired product without further purification.

6.10.1 (5*E*, 2*E*)-*N*-((5-ferrocenyl-vinyl-pyridin-2-yl)methylene)propan-1-amine (61)

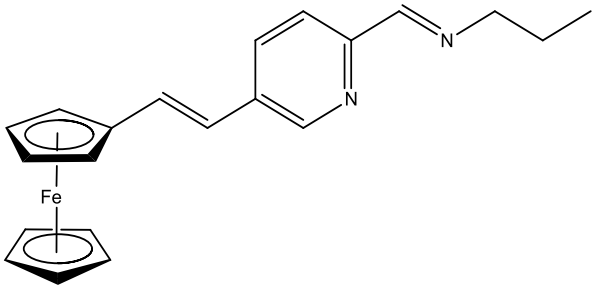

Orange-red solid. **Yield**: 0.0401 g, 70.9 %. **IR** (ATR): ν (cm^{-1}) = 1579 (s, alkene, C=C), 1630 (s, pyridyl, C=N), 1643 (m, imine, C=N). **^{1}H NMR** ($CDCl_3$): δ (ppm) = 0.90 (t, ^{3}J = 7.4 Hz, 3H, $NCH_2CH_2C\mathbf{H}_3$), 1.68 (m, 2H, $NCH_2C\mathbf{H}_2CH_3$), 3.55 (m, 2H, $NC\mathbf{H}_2CH_2CH_3$), 4.08 (s, 5H, Cp-C**H** *unsubst. ring*), 4.27 (m, 2H, Cp-C**H**), 4.42 (m, 2H, Cp-C**H**), 6.61 (d, ^{3}J = 16.2 Hz *trans*, 1H, C**H** *alkene*), 6.95 (d, ^{3}J = 16.2 Hz *trans*, 1H, C**H** *alkene*), 7.73 (d, ^{3}J = 8.8 Hz, 1H, Pyr), 7.87 (d, ^{3}J = 8.2 Hz, 1H, Pyr), 8.29 (s, 1H, C**H** *imine*), 8.57 (s, 1H, Pyr). **^{13}C{^{1}H} NMR** (($CDCl_3$): δ (ppm) = 12.7 ($C\mathbf{H}_3$); 23.9, 63.4 ($C\mathbf{H}_2$); 67.2, 69.6 (Cp-**C**H); 69.4 (Cp-**C**H *unsubst. ring*); 82.3 (**C** *Cp*); 121.2, 121.7 (**C**H *alkene*); 130.7, 132.2, 147.4 (**C**H *Pyr*); 134.6, 152.7 (**C** *Pyr*); 161.6 (**C**H *imine*). **HPLC** (MeOH/H_2O (gradient, 5 - 90 %, flow rate, 0.6 mL/min)): t_R = 17.8 min. **MS** (HR-ESI-TOF, *m*/*z*): 359.1208 $[M+H]^+$. **MP**: 184 - 186 ºC.

6.11 General Procedure for the Preparation of Ferrocenyl-Derived Cationic *N,O*-Ru(II)-Arene-PTA Metallodendrimers ([62][PF_6]$_4$ & [63][PF_6]$_8$)

Triethylamine (0.017 mL, 0.122 mmol for [**62**][PF_6]$_4$; 0.039 mL, 0.279 mmol for [**63**][PF_6]$_8$) was added dropwise to a stirred solution of ligand **56** (0.473 g, 0.0301 mmol for [**62**][PF_6]$_4$) or **57** (0.114 g, 0.0347 mmol for [**63**][PF_6]$_8$) in a EtOH:DCM (50:50, 60 mL) solution. The resulting orange solution was stirred at room temperature for 0.5 h. Next, [Ru(η^6-*p*-Pr^iC_6H_4Me)Cl_2]$_2$ (0.0377 g, 0.0616 mmol for [**62**][PF_6]$_4$; 0.0860 g, 0.140 mmol for [**63**][PF_6]$_8$) was added to the reaction mixture. The reaction mixture was stirred overnight at room temperature, then the reaction mixture was filtered and PTA (0.0191 g, 0.122 mmol for [**62**][PF_6]$_4$; 0.0438 g, 0.279 mmol for [**63**][PF_6]$_8$) was added to the filtrate. The solution was stirred for 6 h and filtered. A solution of $NaPF_6$ (0.0205 g, 0.122 mmol for [**62**][PF_6]$_4$; 0.0495 g, 0.279 mmol for [**63**][PF_6]$_8$) in EtOH (5 mL) was added to the filtrate at 0 ºC and stirred for 1 h. The DCM was removed from the reaction mixture under reduced pressure, which resulted in the precipitation of an orange solid. The solid was isolated by filtration, washed with cold EtOH, followed by Et_2O and dried *in vacuo*.

6.11.1 [DAB-G_1-PPI-{(η^6-*p*-cye)Ru((C_7H_5NO)-κ^2-*N*,*O*)PTA-(5-ferrocenyl-vinyl)}$_4$][PF_6]$_4$ ([**62**][PF_6]$_4$)

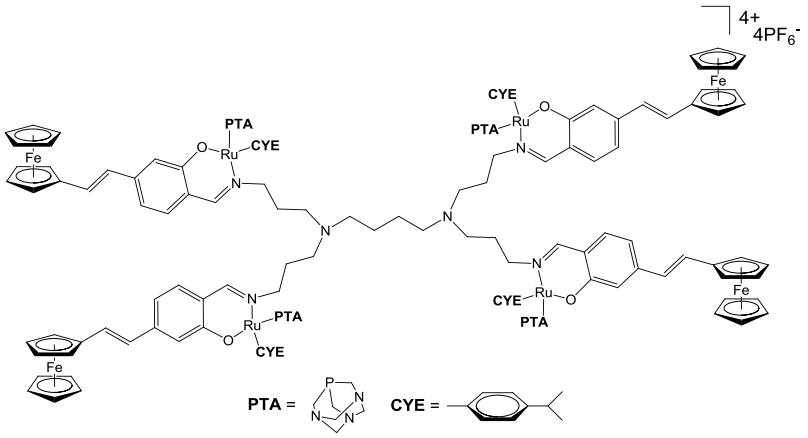

Orange solid. **Yield**: 0.0807 g, 72.2 %. **IR** (ATR): ν (cm^{-1}) = 1590 (br s, alkene, C=C & imine, C=N). **^{1}H NMR** ($(CD_3)_2CO$): δ (ppm) = 1.13 & 1.27 (br m, 24H, $CH(CH_3)_2$ *p-cye*), 1.66 (br m, 4H, NCH_2CH_2 *core*), 2.00 (m, 8H, $NCH_2CH_2CH_2N$ *branch*), 2.09 (br s, 12H, CH_3 *p-cye*), 2.16 - 2.26 (overlapping m, 12H, NCH_2CH_2 *core*, $NCH_2CH_2CH_2N$ *branch*), 2.63 (br m, 4H, $CH(CH_3)_2$ *p-cye*), 3.96 (br m, 8H, $NCH_2CH_2CH_2N$ *branch*), 4.13 (br s, 20H, Cp-CH *unsubst. ring*), 4.22 - 4.55 (overlapping m, 64H, PTA, 2 x Cp-CH), 5.58 (br d, 4H, Ar *p-cye*), 5.83 (br d, 4H, Ar *p-cye*), 6.24 (br d, 4H, Ar *p-cye*), 6.40 (br d, 4H, Ar *p-cye*), 6.66 (d, ^3J = 16.2 Hz *trans*, 4H, CH *alkene*), 6.78 (br d, 4H, Ar), 6.85 (br s, 4H, Ar), 7.07 (d, ^3J = 16.0 Hz *trans*, 4H, CH *alkene*), 7.17 (m, 4H, Ar), 8.08 (br s, 4H, CH *imine*). **^{13}C{^{1}H} NMR** ($(CD_3)_2CO$): δ (ppm) = 17.9, 20.9, 21.5 (CH_3 *p-cye*); 25.0, 53.9, 65.5, 68.3 (CH_2); 51.1, 51.2, 72.4, 72.5 (CH_2 *PTA*); 67.1, 67.3, 69.4 (Cp-CH); 69.1 (Cp-CH *unsubst. ring*); 83.2 (C *Cp*); 30.7, 82.9, 87.5, 88.8, 91.7 (CH *p-cye*); 97.5, 119.9 (C *p-cye*); 112.9, 119.3, 135.4 (CH *Ar*); 118.5, 145.0, 164.5 (C *Ar*); 125.4, 130.4 (CH *alkene*); 165.6 (CH *imine*). **^{31}P{^{1}H} NMR** ($(CD_3)_2CO$): δ (ppm) = -32.7 (s, PTA), -144.1 (sep, ^1J = 709.7 Hz, PF_6). **Elemental analysis** for $C_{156}H_{196}N_{18}O_4P_8F_{24}Fe_4Ru_4$·3DCM (3973.589): Found C, 48.27; H, 5.76; N, 6.44 %; calcd. C, 48.06; H, 5.12; N, 6.35 %. **MS** (HR-ESI-TOF, *m/z*): 627.7885 $[M+2H]^{6+}$ (where M = [**62**][PF_6]$_4$ - 4PF_6). **MP**: 166 ºC (decompose without melting).

6.11.2 [DAB-G_2-PPI-{(η^6-*p*-cye)Ru((C_7H_5NO)-κ^2-*N*,*O*)PTA-(5-ferrocenyl-vinyl)}$_8$][PF_6]$_8$ ([**63**][PF_6]$_8$)

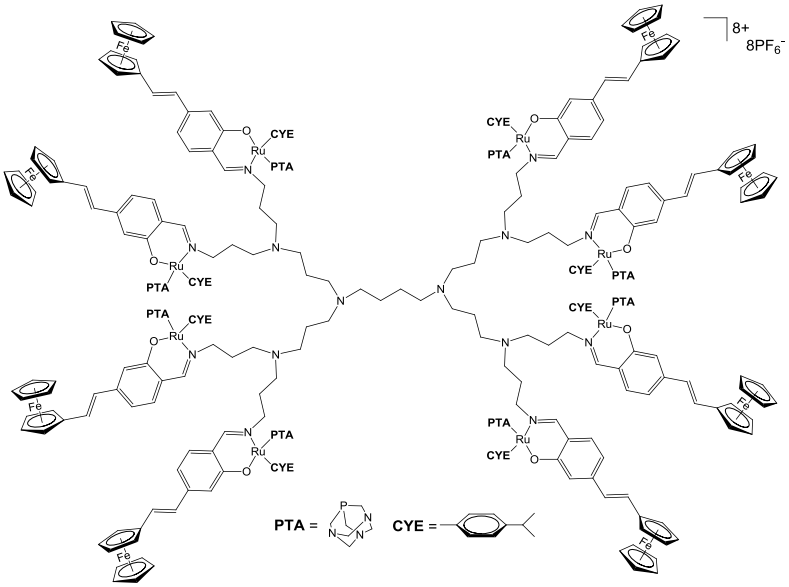

Orange solid. **Yield**: 0.2013 g, 76.6 %. **IR** (ATR): ν (cm^{-1}) = 1590 (br s, alkene, C=C & imine, C=N). **^{1}H NMR** ($(CD_3)_2CO$): δ (ppm) = 1.12 & 1.26 (br d, 48H, CH(C**H**$_3$)$_2$ *p-cye*), 1.81 - 3.25 (overlapping m, 64H, NC**H**$_2$CH$_2$ *core*, NCH$_2$C**H**$_2$ *core*, NC**H**$_2$CH$_2$CH$_2$N *1st branch*, NCH$_2$C**H**$_2$CH$_2$N *1st branch*, NCH$_2$CH$_2$C**H**$_2$N *1st branch*, NC**H**$_2$CH$_2$CH$_2$N *2nd branch*, NCH$_2$C**H**$_2$CH$_2$N *2nd branch*), 2.20 (s, 24H, CH$_3$ *p-cye*), 2.60 (br m, 8H, C**H**(CH$_3$)$_2$ *p-cye*), 3.89 & 4.00 (br m, 16H, NCH$_2$CH$_2$C**H**$_2$N *2nd branch*), 4.13 (br s, 40H, Cp-C**H** *unsubst. ring*), 4.13 - 4.61 (overlapping m, 128H, PTA, 2 x Cp-C**H**), 5.52 (m, 8H, Ar *p-cye*), 5.82 (m, 8H, Ar *p-cye*), 6.19 (m, 8H, Ar *p-cye*), 6.38 (m, 8H, Ar *p-cye*), 6.65 (br d, 8H, C**H** *alkene*), 6.71 (m, 8H, Ar), 6.84 (br s, 8H, Ar), 7.05 (br d, 8H, C**H** *alkene*), 7.22 (m, 8H, Ar), 8.13 (br s, 8H, C**H** *imine*). **^{13}C{^{1}H} NMR** ($(CD_3)_2CO$): δ (ppm) = 18.0, 21.0, 21.4 (**C**H$_3$ *p-cye*); 23.5, 43.2, 59.2, 68.2 (**C**H$_2$); 51.1, 51.2, 72.5 (**C**H$_2$ *PTA*); 67.1, 67.4, 69.5 (Cp-**C**H); 69.2 (Cp-**C**H *unsubst. ring*); 83.0 (**C** *Cp*); 30.7, 82.9, 87.6, 88.8, 91.8 (**C**H *p-cye*); 97.2, 120.0 (**C** *p-cye*); 112.9, 119.2, 135.5 (**C**H *Ar*); 118.6, 145.0, 164.5 (**C** *Ar*); 125.5, 130.4 (**C**H *alkene*); 165.7 (**C**H *imine*). **^{31}P{^{1}H} NMR** ($(CD_3)_2CO$): δ (ppm) = -31.5 (s, PTA), -144.0 (sep, ^1J = 711.5 Hz, **P**F$_6$). **Elemental analysis** for $C_{320}H_{414}N_{38}O_8P_{16}F_{48}Fe_8Ru_8$.9DCM (8348.252): Found C, 47.29; H, 6.60; N, 6.46 %; calcd. C, 47.33; H, 5.22; N, 6.38 %. **MS** (HR-ESI-TOF, *m/z*): 247.1670 $[M+18H]^{26+}$ (where M = [**63**][PF_6]$_8$ - 8PF_6). **MP**: 285 ºC (decompose without melting).

6.12 General Procedure for the Preparation of Ferrocenyl-Derived Cationic *N,N*-Ru(II)-Arene Metallodendrimers ([64][PF_6]$_4$ & [65][PF_6]$_8$)

[Ru(η^6-*p*-Pr^iC_6H_4Me)Cl_2]$_2$ (0.0906 g, 0.148 mmol for [**64**][PF_6]$_4$; 0.0516 g, 0.0843 mmol for [**65**][PF_6]$_8$) was added to a stirred orange-red solution of ligand **58** (0.0553 g, 0.0365 mmol for [**64**][PF_6]$_4$) or **59** (0.0659 g, 0.0208 mmol for [**65**][PF_6]$_8$) in a EtOH:DCM (50:50, 60 mL) solution. The dark purple reaction mixture was stirred overnight at room temperature, and then the reaction mixture was filtered. A solution of $NaPF_6$ (0.0249 g, 0.148 mmol for [**64**][PF_6]$_4$; 0.0281 g, 0.168 mmol for [**65**][PF_6]$_8$) in EtOH (5 mL) was added to the filtrate at 0 ºC and stirred for 1 h. The DCM was removed from the reaction mixture under reduced pressure, which resulted in the precipitation of a dark purple solid. The solid was isolated by filtration, washed with cold EtOH, followed by Et_2O and dried *in vacuo*.

6.12.1 [DAB-G_1-PPI-{(η^6-*p*-cye)Ru(($C_6H_5N_2$)-κ^2-*N*,*N*)Cl-(5-ferrocenyl-vinyl)}$_4$][PF_6]$_4$ ([**64**][PF_6]$_4$)

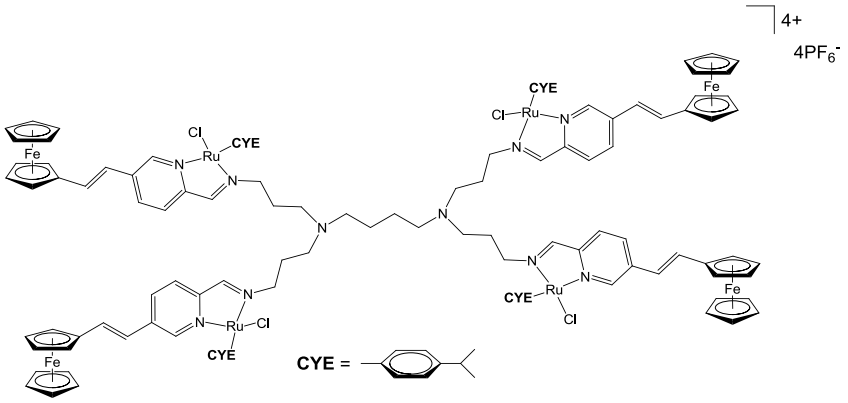

Dark-purple solid. **Yield**: 0.0983 g, 84.7 %. **IR** (ATR): ν (cm^{-1}) = 1586 (s, alkene, C=C), 1623 (s, pyridyl & imine, C=N). **^{1}H NMR** ($(CD_3)_2CO$): δ (ppm) = 1.09 (br m, 24H, CH(C**H**$_3$)$_2$ *p-cye*), 1.30 (br m, 4H, NCH$_2$C**H**$_2$ *core*,), 2.00 (br m, 8H, NCH$_2$C**H**$_2$CH$_2$N *branch*), 2.24 (br m, 4H, NC**H**$_2$CH$_2$ *core*,), 2.32 (br d, 12H, C**H**$_3$ *p-cye*), 2.62 (br m, 4H, C**H**(CH$_3$)$_2$ *p-cye*), 3.26 (br m, 8H, NC**H**$_2$CH$_2$CH$_2$N *branch*), 4.19 (s, 20H, Cp-C**H** *unsubst. ring*), 4.43 - 4.78 (overlapping m, 24H, NCH$_2$CH$_2$C**H**$_2$N *branch*, 2 x Cp-C**H**), 6.00 & 6.30 (m, 16H, Ar *p-cye*), 6.97 & 7.56 (m, 8H, C**H** *alkene*), 8.10 (m, 4H, Pyr), 8.39 (m, 4H, Pyr), 8.88 (br s, 4H, C**H** *imine*), 9.52 (br s, 4H, Pyr). **^{13}C{^{1}H} NMR** ($(CD_3)_2CO$): δ (ppm) = 18.6, 21.5, 22.0 (**C**H$_3$ *p-cye*); 24.5, 25.0, 51.2, 51.8, 52.7, 64.1 (**C**H$_2$); 68.0, 69.1, 70.6 (Cp-**C**H); 69.5 (Cp-**C**H *unsubst. ring*); 81.4 (**C** *Cp*); 31.1, 83.9, 85.2, 85.6, 87.5 (**C**H *p-cye*); 104.9, 105.3 (**C** *p-cye*); 119.1, 137.3 (**C**H *alkene*); 129.1, 133.4, 153.7 (**C**H *Pyr*); 139.3, 151.5 (**C** *Pyr*); 168.1 (**C**H *imine*). **Elemental analysis** for $C_{128}H_{148}N_{10}Cl_4P_4F_{24}Fe_4Ru_4$.4.5DCM (3558.1648): Found C, 44.45; H, 4.68; N, 3.84 %; calcd. C, 44.73; H, 4.45; N, 3.94 %. **MS** (HR-ESI-TOF, *m/z*): 649.1115 $[M+H]^{5+}$ (where M = [**64**][PF_6]$_4$ - 4PF_6). **MP**: 236 ºC (decompose without melting).

6.12.2 [DAB-G_2-PPI-{(η^6-*p*-cye)Ru(($C_6H_5N_2$)-κ^2-*N*,*N*)Cl-(5-ferrocenyl-vinyl)}$_8$][PF_6]$_8$ ([**65**][PF_6]$_8$)

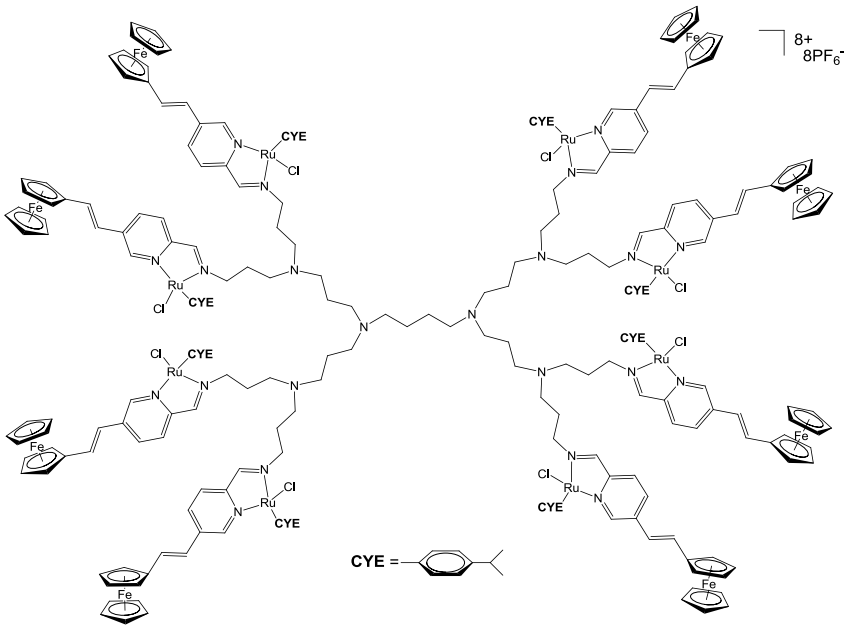

Dark-purple solid. **Yield**: 0.0985 g, 72.9 %. **IR** (ATR): ν (cm^{-1}) = 1588 (s, alkene, C=C), 1625 (s, pyridyl & imine, C=N). **^{1}H NMR** ($(CD_3)_2CO$): δ (ppm) = 1.06 & 1.11 (br m, 48H, CH(C**H**$_3$)$_2$ *p-cye*), 1.28 (br m, 4H, NCH$_2$C**H**$_2$ *core*), 1.86 - 2.30 (overlapping m, 48H, NCH$_2$C**H**$_2$CH$_2$N *1st branch*, NCH$_2$C**H**$_2$CH$_2$N *2nd branch*, C**H**$_3$ *p-cye*), 2.54 - 3.23 (overlapping m, 44H, NC**H**$_2$CH$_2$ *core*, NC**H**$_2$CH$_2$CH$_2$N *1st branch*, NCH$_2$CH$_2$C**H**$_2$N *1st branch*, NC**H**$_2$CH$_2$CH$_2$N *2nd branch*, C**H**(CH$_3$)$_2$ *p-cye*), 4.19 (br s, 40H, Cp-C**H** *unsubst. ring*), 4.43 - 4.71 (overlapping m, 48H, NCH$_2$CH$_2$C**H**$_2$N *2nd branch*, 2 x Cp-C**H**), 5.90 & 6.21 (m, 32H, Ar *p-cye*), 6.98 & 7.55 (m, 16H, C**H** *alkene*), 8.06 (m, 8H, Pyr), 8.34 (m, 8H, Pyr), 8.73 (br s, 8H, C**H** *imine*), 9.50 (br s, 8H, Pyr). **^{13}C{^{1}H} NMR** ($(CD_3)_2CO$): δ (ppm) = 18.5, 21.4, 22.0 (**C**H$_3$ *p-cye*); 26.7, 50.8, 51.4, 51.7, 64.9 (**C**H$_2$); 68.1, 70.6 (Cp-**C**H); 69.5 (Cp-**C**H *unsubst. ring*); 81.5 (**C** *Cp*); 31.1, 84.3, 85.2, 85.3, 87.4 (**C**H *p-cye*); 103.9, 105.4 (**C** *p-cye*); 119.0, 137.1 (**C**H *alkene*); 128.6, 133.4, 151.7 (**C**H *Pyr*); 139.1, 151.7 (**C** *Pyr*); 166.8(**C**H *imine*). **Elemental analysis** for $C_{264}H_{312}N_{22}Cl_8P_8F_{48}Fe_8Ru_8$.9DCM (7256.558): Found C, 45.41; H, 4.11; N, 4.37 %; calcd. C, 45.19; H, 4.58; N, 4.25 %. **MS** (HR-ESI-TOF, *m/z*): 667.4059 $[M]^{8+}$ (where M = [**65**][PF_6]$_8$ - 8PF_6). **MP**: 203 -204 ºC.

6.13 Synthesis of Ferrocenyl-Derived Cationic *N,O*-Ru(II)-Arene-PTA Mononuclear Complex ([66][PF_6])

To a stirred solution of **60** (0.0812 g, 0.218 mmol) in a EtOH:DCM (50:50, 30 mL) solution, triethylamine (0.032 mL, 0.228 mmol) was added. The resulting orange solution was stirred at room temperature for 0.5 h. Next, [Ru(η^6-*p*-Pr^iC_6H_4Me)Cl_2]$_2$ (0.0666 g, 0.109 mmol) was added to the reaction mixture. The reaction mixture was stirred for 2 h at room temperature, then the reaction mixture was filtered and PTA (0.0359 g, 0.228 mmol) was added to the red-orange filtrate. The solution was stirred for 6 h and filtered. A solution of $NaPF_6$ (0.0384 g, 0.228 mmol) in EtOH (5 mL) was added to the filtrate at 0 ºC and stirred for 0.5 h. The DCM was removed from the reaction mixture under reduced pressure, which resulted in the precipitation of an orange solid. The solid was isolated by filtration, washed with cold EtOH, followed by Et_2O and dried under vacuum. Crystals were grown by slow evaporation of a solution of [**66**][PF_6] in acetone.

6.13.1 [$CH_3CH_2CH_2$-(η^6-*p*-cye)Ru((C_7H_5NO)-κ^2-*N,O*)PTA-(5-ferrocenyl-vinyl)][PF_6] ([66][PF_6])

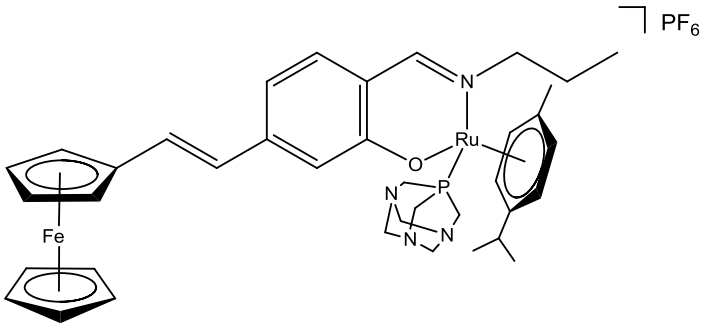

Orange solid. **Yield**: 0.1033 g, 52.2 %. **IR** (ATR): ν (cm^{-1}) = 1587 (s, alkene, C=C), 1619 (w, imine, C=N). **^{1}H NMR** ($(CD_3)_2CO$): δ (ppm) = 1.07 (t, ^3J = 7.3 Hz, 3H, $NCH_2CH_2C\mathbf{H}_3$), 1.17 & 1.30 (d, ^3J = 6.9 Hz, 6H, $CH(C\mathbf{H}_3)_{2\ p\text{-}cye}$), 2.02 & 2.06 (m, 2H, $NCH_2C\mathbf{H}_2CH_3$), 2.22 (s, 3H, $C\mathbf{H}_{3\ p\text{-}cye}$), 2.71 (m, 1H, $C\mathbf{H}(CH_3)_{2\ p\text{-}cye}$), 3.81 & 3.98 (m, 2H, $NC\mathbf{H}_2CH_2CH_3$), 4.15 (s, 5H, Cp-C**H** $_{unsubst.\ ring}$), 4.27 & 4.39 (2d, 6H, PTA), 4.34 (t, ^3J = 1.9 Hz, 2H, Cp-C**H**), 4.53 (s, 6H, PTA), 4.56 (m, 2H, Cp-C**H**), 5.64 (br d, 1H, Ar $_{p\text{-}cye}$), 5.86 (br d, 1H, Ar $_{p\text{-}cye}$), 6.34 (br d, 1H, Ar $_{p\text{-}cye}$), 6.46 (m, 1H, Ar $_{p\text{-}cye}$), 6.67 (d, ^3J = 16.2 Hz $_{trans}$, 1H, C**H** $_{alkene}$), 6.78 (d, ^3J = 8.1 Hz, 1H, Ar), 6.86 (s, 1H, Ar), 7.09 (d, ^3J = 16.2 Hz $_{trans}$, 1H, C**H** $_{alkene}$), 7.16 (d, ^3J = 8.3 Hz, 1H, Ar), 8.09 (s, 1H, C**H** $_{imine}$). **^{13}C{^{1}H} NMR** ($(CD_3)_2CO$): δ (ppm) = 10.5 ($C\mathbf{H}_3$); 17.7, 20.8, 21.5 ($\mathbf{C}H_{3\ p\text{-}cye}$); 24.7, 72.0 ($\mathbf{C}H_2$); 51.1, 51.3, 72.4, 72.5 ($\mathbf{C}H_{2\ PTA}$); 67.1, 67.3, 69.4 (Cp-**C**H); 69.1 (Cp-**C**H $_{unsubst.\ ring}$); 82.9 (**C** $_{Cp}$); 30.6, 83.9, 87.5, 88.9, 91.1 (**C**H $_{p\text{-}cye}$); 98.3, 119.9 (**C** $_{p\text{-}cye}$); 112.8, 119.2, 135.3 (**C**H $_{Ar}$); 117.9, 145.0, 161.1 (**C** $_{Ar}$); 125.5, 130.3 (**C**H $_{alkene}$); 165.8 (**C**H $_{imine}$).

^{31}P{^{1}H} NMR ($(CD_3)_2CO$): δ (ppm) = -32.7 (s, PTA), -144.2 (sep, ^{1}J = 707.7 Hz, **P**F_6). **HPLC** (MeOH/H_2O (gradient, 5 - 90 %, flow rate, 0.6 mL/min)): t_R = 15.6 min. **MS** (HR-ESI-TOF, *m/z*): $[M]^+$ (where M = [**66**][PF_6] - PF_6). **MP**: 198 ºC (decompose without melting).

6.14 Synthesis of Ferrocenyl-Derived Cationic *N,N*-Ru(II)-Arene Mononuclear Complex ([67][PF_6])

$[Ru(\eta^6\text{-}p\text{-}Pr^iC_6H_4Me)Cl_2]_2$ (0.0489 g, 0.0798 mmol) was added to a stirred orange-red solution of ligand **61** (0.0572 g, 0.160 mmol) in a EtOH:DCM (50:50, 20 mL) solution. The dark purple reaction mixture was stirred for 1 h at room temperature, and then the reaction mixture was filtered. A solution of $NaPF_6$ (0.0282 g, 0.168 mmol) in EtOH (5 mL) was added to the filtrate at 0 ºC and stirred for 0.5 h. The DCM was removed from the reaction mixture under reduced pressure, which resulted in the precipitation of a dark purple solid. The solid was isolated by filtration, washed with cold EtOH, followed by Et_2O and dried *in vacuo*.

6.14.1 [$CH_3CH_2CH_2$-(η^6-*p*-cye)Ru(($C_6H_5N_2$)-κ^2-*N,N*)Cl-(5-ferrocenyl-vinyl)][PF_6] ([67][PF_6])

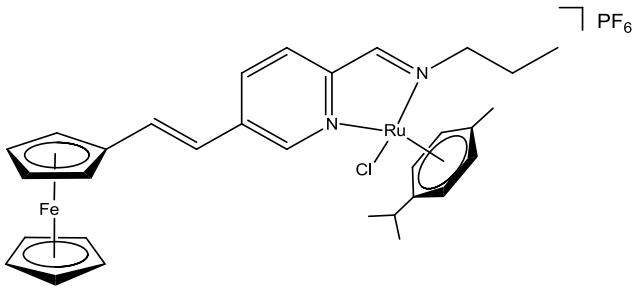

Dark purple solid. **Yield**: 0.0551 g, 96.3 %. **IR** (ATR): ν (cm^{-1}) = 1586 (s, alkene, C=C), 1625 (s, pyridyl & imine, C=N). **^{1}H NMR** ($(CD_3)_2CO$): δ (ppm) = 1.00 (t, ^{3}J = 7.4 Hz, 3H, $NCH_2CH_2C\mathbf{H}_3$), 1.12 & 1.17 (d, ^{3}J = 6.9 Hz, 6H, $CH(C\mathbf{H}_3)_{2\ p\text{-}cye}$), 1.99 & 2.10 (br m, 2H, $NCH_2C\mathbf{H}_2CH_3$), 2.33 (s, 3H, $C\mathbf{H}_{3\ p\text{-}cye}$), 2.82 (m, 1H, $C\mathbf{H}(CH_3)_{2\ p\text{-}cye}$), 4.21 (s, 5H, Cp-C**H** *unsubst. ring*), 4.38 & 4.62 (m, 2H, $NC\mathbf{H}_2CH_2CH_3$), 4.50 (m, 2H, Cp-C**H**), 4.65 (br d, 2H, Cp-C**H**), 5.95 & 6.27 (m, 4H, Ar *p-cye*), 6.98 (d, ^{3}J = 16.2 Hz *trans*, 1H, C**H** *alkene*), 7.59 (d, ^{3}J = 16.2 Hz *trans*, 1H, C**H** *alkene*), 8.13 (d, ^{3}J = 8.3 Hz, 1H, Pyr), 8.43 (d, ^{3}J = 8.2 Hz, 1H, Pyr), 8.71 (s, 1H, C**H** *imine*), 9.56 (s, 1H, Pyr). **^{13}C{^{1}H} NMR** ($(CD_3)_2CO$): δ (ppm) = 10.8 ($C\mathbf{H}_3$); 18.1, 67.6 ($\mathbf{C}H_2$); 21.2, 21.9, 22.9 ($\mathbf{C}H_{3\ p\text{-}cye}$); 68.2, 68.4, 70.5 (Cp-**C**H); 69.5 (Cp-**C**H *unsubst. ring*); 81.5 (**C** *Cp*); 31.1, 84.2, 85.2, 85.3, 87.4 (**C**H *p-cye*); 104.0, 105.4 (**C** *p-cye*); 119.1, 136.9 (**C**H *alkene*); 128.4, 133.5, 153.6 (**C**H *Pyr*); 139.0, 151.9 (**C** *Pyr*); 166.1 (**C**H *imine*). **HPLC** (MeOH/H_2O (gradient, 5 - 90 %, flow rate, 0.6 mL/min)): t_R = 15.6 min. **MS** (HR-ESI-TOF, *m/z*): 629.0955 $[M]^+$ (where M = [**67**][PF_6] - PF_6). **MP**: 165 - 166 ºC.

6.15 Synthesis of Bipyridyl Conjugate (71)

6.15.1 4'-Methyl-2,2'-bipyridine-4-carboxaldehyde (71)

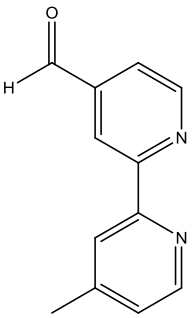

Selenium dioxide (6.64 g, 59.9 mmol) and 4,4'-dimethyl-2,2'-bipyridyl (10.0 g, 54.4 mmol) was dissolved in 1,4-dioxane (40 mL with 4 % H_2O) and gently heated under reflux for 24 h. The reaction was filtered through Celite whilst hot, and washed with 100 mL of EtOH. The filtrate and EtOH washings were combined and the solvent removed. The resulting residue was suspended in a saturated solution of sodium bicarbonate (50 mL), stirred for 1 h and extracted with DCM (5 x 50 mL). The organic fractions were combined and dried over Na_2SO_4. The solution was filtered and the solvent removed. The resulting orange residue was suspended in a solution of 0.3 M sodium metabisulfite (50 mL) and stirred for 1 h. The solution was filtered and the filtered solid suspended in a fresh solution of 0.3 M sodium metabisulfite (50 mL) and stirred for 1 h. The solution was filtered and the pH of the combined filtrates was adjusted to pH 6 with sodium carbonate (slow addition). The aqueous solution was extracted with EtOAc (4 x 100 mL). The organic layers were combined, dried over Na_2SO_4, filtered and solvent removed.

White solid, **Yield**: 5.3453 g, 49.6 %. **IR** (KBr pellets): ν (cm^{-1}) = 1703 (s, carbonyl, C=O), 1596 (s, bpy C=N). **^{1}H NMR** ($CDCl_3$): δ (ppm) = 2.46 (s, 3H, C**H**$_3$), 7.18 (m, 1H, C**H** $_{bpy}$), 7.71 (m, 1H, C**H** $_{bpy}$), 8.27 (s, 1H, C**H** $_{bpy}$), 8.57 (m, 1H, C**H** $_{bpy}$), 8.82 (s, 1H, C**H** $_{bpy}$), 8.88 (m, 1H, C**H** $_{bpy}$), 10.17 (s, aH, C**H**O). **^{13}C{^{1}H} NMR** ($CDCl_3$): δ (ppm) = 21.2 (**C**H$_3$); 120.6, 121.4, 122.1, 125.4, 149.2, 150.3 (**C**H $_{bpy}$); 142.7, 148.4, 154.8, 158.4 (C $_{bpy}$); 191.7 (**C**HO). Spectroscopic data in agreement with reported literature.[12-14]

6.16 Synthesis of Bipyridyl Ligands (72 - 74)

A solution of DAB-**G$_1$**-PPI-$(NH_2)_4$ (0.481 g, 1.51 mmol for **72**), DAB-**G$_2$**-PPI-$(NH_2)_8$ (0.822 g, 1.06 mmol for **73**), or *n*-propylamine (0.360 g, 6.08 mmol for **74**) in DCM (10 mL) was added dropwise to a stirred solution of 4'-methyl-2,2'-bipyridine-4-carboxaldehyde (**71**) (1.22 g, 6.15 mmol for **72**; 1.70 g, 8.56 mmol for **73**; 1.21 g, 6.39 mmol for **74**) in DCM (25 mL) and stirred for 48 h (for **72** and **73**) or overnight (for **74**) at room temperature. The solvent was then removed under vacuum to afford a dark yellow oil. This was dissolved in DCM (30 mL) and washed with copious amounts of ultrapure H_2O (15 × 30 mL). The organic layer was separated, dried over sodium sulfate (~10 g), and filtered. The solvent was then removed under reduced pressure and the resulting oil dried *in vacuo*.

6.16.1 DAB-G$_1$-$(C_{12}H_{10}N_3)_4$ (72)

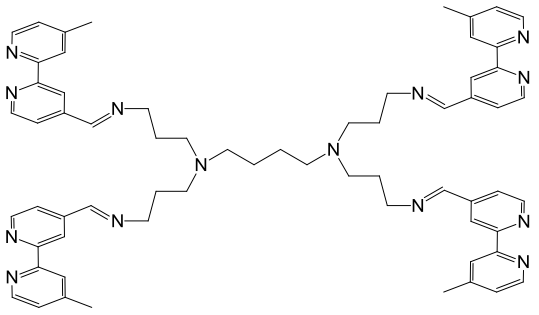

Red-brown oil. **Yield**: 1.41 g, 89.5 %. **IR** (NaCl cells, DCM): ν (cm^{-1}) = 1648 (s, imine, C=N), 1596 (s, bpy, C=N). **^{1}H NMR** ($CDCl_3$): δ (ppm) = 1.45 (br m, 4H, $NCH_2C\mathbf{H}_2$ *core*), 1.84 (br m, 8H, $NCH_2C\mathbf{H}_2CH_2N$ *branch*), 2.42 (s, 16H, $NC\mathbf{H}_2CH_2$ *core*, $C\mathbf{H}_3$), 2.52 (br m, 8H, $NC\mathbf{H}_2CH_2CH_2N$ *branch*), 3.68 (br m, 8H, $NCH_2CH_2C\mathbf{H}_2N$ *branch*), 7.11 (br d, ^3J = 4.8 Hz, 4H, C**H** *bpy*), 7.64 (br d, ^3J = 5.0 Hz, 4H, C**H** *bpy*), 8.21 (br s, 4H, C**H** *bpy*), 8.33 (br s, 4H, C**H** *imine*), 8.51 (br d, ^3J = 4.9 Hz, 4H, C**H** *bpy*), 8.56 (br s, 4H, C**H** *bpy*), 8.67 (br d, ^3J = 5.0 Hz, 4H, C**H** *bpy*). **^{13}C{^{1}H} NMR** ($CDCl_3$): δ (ppm) = 21.2 (**C**H_3); 25.3, 28.4, 51.7, 54.1, 59.9 (**C**H_2); 120.5, 120.9, 122.0, 124.9, 149.1, 149.6 (**C**H *bpy*); 144.2, 148.1, 155.6, 157.2 (**C** *bpy*); 159.3 (**C**H *imine*). **Elemental analysis** for $C_{64}H_{72}N_{14}$ (1037.37): Found C, 73.92; H, 7.11; N, 18.97 %; calcd. C, 74.10; H, 7.00; N, 18.90 %. **MS** (HR-ESI-TOF, *m*/*z*): 1038.79 $[M+H]^+$.

6.16.2 DAB-G_2-$(C_{12}H_{10}N_3)_8$ (73)

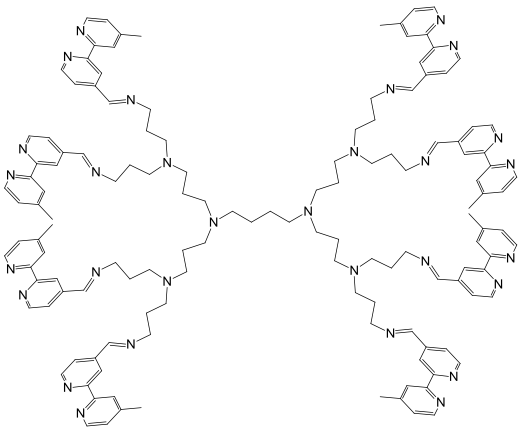

Red-brown oil. **Yield**: 2.09 g, 88.7 %. **IR** (NaCl cells, DCM): ν (cm^{-1}) = 1648 (s, imine, C=N), 1596 (s, bpy, C=N). **^{1}H NMR** ($CDCl_3$): δ (ppm) = 1.39 (br m, 4H, $NCH_2C\mathbf{H}_2$ *core*), 1.57 (br m, 8H, $NCH_2C\mathbf{H}_2CH_2N$ *1st branch*), 1.83 (br m, 16H, $NCH_2C\mathbf{H}_2CH_2N$ *2nd branch*), 2.31 - 2.59 (overlapping m, 60H, $NC\mathbf{H}_2CH_2$ *core*, $NC\mathbf{H}_2CH_2CH_2N$ *1st branch*, $NCH_2CH_2C\mathbf{H}_2N$ *1st branch*, $NC\mathbf{H}_2CH_2CH_2N$ *2nd branch*, $C\mathbf{H}_3$), 3.65 (br m, 16H, $NCH_2CH_2C\mathbf{H}_2N$ *2nd branch*), 7.09 (br m, 8H, C**H** *bpy*), 7.62 (br d, 8H, ^3J = 5.0 Hz, C**H** *bpy*), 8.19 (br s, 8H, C**H** *bpy*), 8.30 (br s, 8H, C**H** *imine*), 8.49 (br d, ^3J = 4.9 Hz 8H, C**H** *bpy*), 8.56 (br s, 8H, C**H** *bpy*), 8.64 (br d, ^3J = 5.0 Hz, 8H, C**H** *bpy*). **^{13}C{^{1}H} NMR** ($CDCl_3$): δ (ppm) = 21.1 (**C**H_3); 24.7, 25.2, 28.3, 51.7, 52.3, 53.4, 54.2, 59.9 (**C**H_2); 120.4, 120.9, 121.9, 124.8, 149.0, 149.5 (**C**H *bpy*); 144.2, 148.1, 155.6, 157.2 (**C** *bpy*); 159.2 (**C**H *imine*). **Elemental analysis** for $C_{136}H_{160}N_{30}$ (2214.96): Found C, 73.74; H, 7.58; N, 18.68 %; calcd. C, 73.75; H, 7.28; N, 18.97 %. **MS** (HR-ESI-TOF, *m*/*z*): 560.25 $[M+4H]^{4+}$.

6.16.3 (4*E*)-*N*-((4'-methyl-[2,2'-bipyridin]-4yl)methylene)propan-1-amine (74)

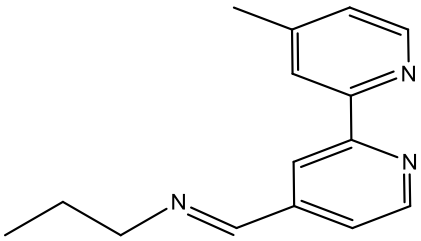

Dark yellow oil. **Yield**: 0.920 g, 63.2 %. **IR** (NaCl cells, DCM): ν (cm^{-1}) = 1649 (s, imine, C=N), 1596 (s, bpy, C=N). **^{1}H NMR** ($CDCl_3$): δ (ppm) = 0.94 (t, ^3J = 7.4 Hz, 3H, $NCH_2CH_2C\mathbf{H}_3$), 1.73 (m, 2H, $NCH_2C\mathbf{H}_2CH_3$), 2.41 (s, 3H,$C\mathbf{H}_3$ *bpy*), 4.20 (td, ^3J = 6.9 Hz, ^4J = 1.4 Hz, 2H, $NC\mathbf{H}_2CH_2CH_3$), 7.11 (d, ^3J = 2.4 Hz, 1H, C**H** *bpy*), 7.67 (dd, ^3J = 5.0 Hz, ^4J = 1.6 Hz, 1H, C**H** *bpy*), 8.22 (s, 1H, C**H** *bpy*), 8.32 (s, 1H, C**H** *imine*), 8.52 (d, ^3J = 5.4 Hz, 1H, C**H** *bpy*), 8.58 (s, 1H, C**H** *bpy*), 8.69 (d, ^3J = 5.26 Hz, 1H, C**H** *bpy*). **^{13}C{^{1}H} NMR** ($CDCl_3$): δ (ppm) = 11.8, 21.1 (**C**H_3); 23.8, 63.6 (**C**H_2); 120.5, 120.9, 122.0, 124.9, 149.0, 149.5 (**C**H *bpy*); 144.3, 148.1, 155.6, 157.2 (**C** *bpy*); 159.1 (**C**H *imine*). **Elemental analysis** for $C_{15}H_{17}N_3$ (239.32): Found C, 75.26; H, 7.19; N, 17.55 %; calcd. C, 75.28; H, 7.16; N, 17.56 %. **MS** (EI, *m*/*z*): 239.28 $[M]^+$.

6.17 Synthesis of $Mn(CO)_3$-Functionalized Complexes (75 - 77)

A solution of ligand **72** (0.112 g, 0.108 mmol for **75**), **73** (0.116 g, 0.053 mmol for **76**), or **73** (0.103 g, 0.429 mmol for **77**) in DCM (5 mL) was added dropwise to a stirred suspension of $[Mn(CO)_5Br]$ (0.120 g, 0.439 mmol for **75**, 0.116 g, 0.423 mmol for **76**, and 0.112 g, 0.408 mmol for **77**) in DCM (30 mL). The reaction mixture was stirred overnight at room temperature while protected from light by wrapping in aluminium foil, then filtered by gravity and the filtrate reduced to ~5 mL. The addition of Et_2O (for **75** and **76**) or *n*-pentane (for **77**) resulted in the precipitation of the desired product. The solids were filtered, washed with copious amounts of Et_2O or *n*-pentane and dried under vacuum. Single crystals of complex **77** were obtained by slow diffusion of *n*-pentane into a concentrated DCM solution of the compound but did not diffract well enough for a good structure solution due to disorder.

6.17.1 [DAB-G_1-PPI-{$(CO)_3Mn((C_{12}H_{10}N_3)$-$\kappa^2$-*N*,*N*)Br}$_4$] (75)

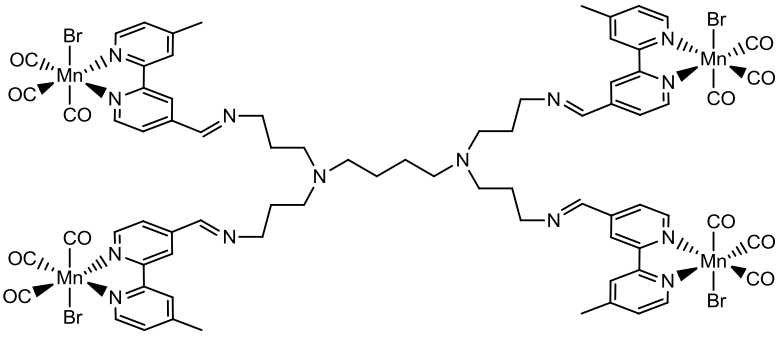

Yellow-orange solid. **Yield**: 0.165 g, 79.1 %. **IR** (ATR): ν (cm^{-1}) = 2022 (s, carbonyl, C≡O), 1921 (s, carbonyl, C≡O), 1905 (s, carbonyl, C≡O), 1644 (m, imine, C=N), 1618 (m, bpy, C=N). **^{1}H NMR** ($(CD_3)_2SO$): δ (ppm) = 1.39 (overlapping m, 12H, $NCH_2C\mathbf{H}_{2\ core}$, $NCH_2C\mathbf{H}_2CH_2N_{\ branch}$), 1.77 (overlapping m, 12H, $NC\mathbf{H}_2CH_{2\ core}$, $NC\mathbf{H}_2CH_2CH_2N_{\ branch}$), 2.36 (br m, 12H, $C\mathbf{H}_3$), 3.69 (br m, 8H, $NCH_2CH_2C\mathbf{H}_2N_{\ branch}$), 7.52 (br m, 4H, C**H** $_{bpy}$), 7.89 (br m, 4H, C**H** $_{bpy}$), 8.46 (br s, 4H, C**H** $_{imine}$), 8.51 (br s, 4H, C**H** $_{bpy}$), 8.76 (br s, 4H, C**H** $_{bpy}$), 8.98 (br m, 4H, C**H** $_{bpy}$), 9.19 (br m, 4H, C**H** $_{bpy}$). **^{13}C{^{1}H} NMR** ($(CD_3)_2SO$): δ (ppm) = 20.6 ($\mathbf{C}H_3$); 24.7, 27.8, 50.9, 53.4, 58.9 ($\mathbf{C}H_2$); 121.0, 123.5, 124.2, 127.8, 153.9, 154.3 (**C**H $_{bpy}$); 145.2, 151.2, 152.8, 156.0 (**Cbpy**$_r$); 158.0 (**C**H $_{imine}$); 221.0, 221.7, 222.0 (**C**O). **HPLC** (CH_3CN/H_2O (gradient, 5 - 90 %, flow rate, 0.6 mL/min)): t_R = 23.1 min. **MS** (HR-ESI-TOF, *m*/*z*): 961.57 $[M+2H]^{2+}$.

6.17.2 [DAB-G_2-PPI-{$(CO)_3Mn((C_{12}H_{10}N_3)$-$\kappa^2$-*N*,*N*)Br}$_8$] (76)

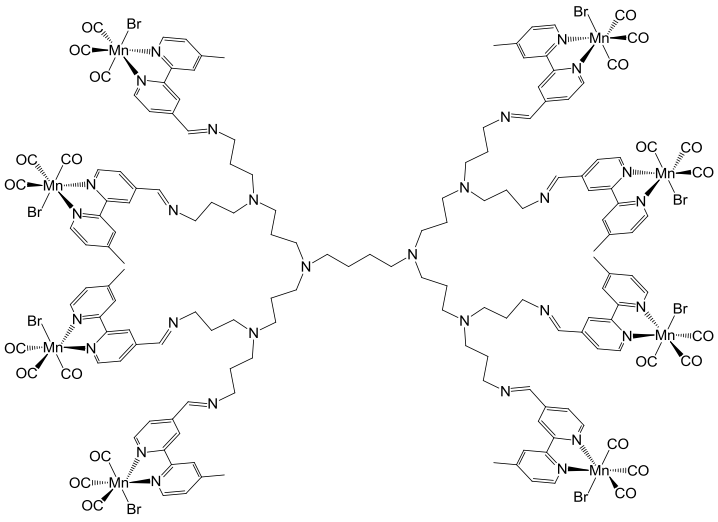

Yellow-orange solid. **Yield**: 0.139 g, 65.4 %. **IR** (ATR): ν (cm^{-1}) = 2022 (s, carbonyl, C≡O), 1920 (s, carbonyl, C≡O), 1904 (s, carbonyl, C≡O), 1644 (m, imine, C=N), 1619 (m, bpy, C=N). **^{1}H NMR** ($(CD_3)_2SO$): δ (ppm) = 1.23 (overlapping m, 28H, $NCH_2C\mathbf{H}_2$ *core*, $NCH_2C\mathbf{H}_2CH_2N$ *1st branch*, $NCH_2C\mathbf{H}_2CH_2N$ *2nd branch*), 1.38 (overlapping m, 20H, $NC\mathbf{H}_2CH_2$ *core*, $NC\mathbf{H}_2CH_2CH_2N$ *1st branch*, $NCH_2CH_2C\mathbf{H}_2N$ *1st branch*), 1.71 (br m, 16H, $NC\mathbf{H}_2CH_2CH_2N$ *2nd branch*), 2.42 (br m, 24H, C**H**$_3$), 3.63 (br m, 16H, $NCH_2CH_2C\mathbf{H}_2N$ *2nd branch*), 7.48 (br m, 8H, C**H** *bpy*), 7.84 (br m, 8H, C**H** *bpy*), 8.43 (br m, 16H, C**H** *imine*, C**H** *bpy*), 8.69 (br s, 8H, C**H** *bpy*), 8.95 (br m, 8H, C**H** *bpy*), 9.14 (br m, 8H, C**H** *bpy*). **^{13}C{^{1}H} NMR** ($(CD_3)_2SO$): δ (ppm) = 20.6 (**C**H_3); 24.2, 24.9, 27.8, 51.0, 51.5, 53.8, 54.7, 58.9 (**C**H_2); 121.0, 123.4, 124.1, 127.8, 153.8, 154.3 (**C**H *bpy*); 145.2, 151.1, 152.8, 156.0 (**C** *bpy*); 157.8 (**C**H *imine*); 220.9, 221.6, 222.9 (**C**O). **HPLC** (CH_3CN/H_2O (gradient, 5 - 90 %, flow rate, 0.6 mL/min)): t_R = 23.1 min. **MS** (HR-ESI-TOF, *m*/*z*): 1344.59 $[M+3H]^{3+}$.

6.17.3 [$CH_3CH_2CH_2$-$(CO)_3Mn((C_{12}H_{10}N_3)$-$\kappa^2$-*N*,*N*)Br] (77)

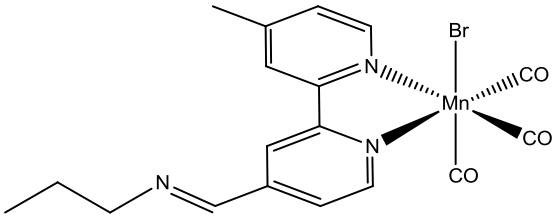

Orange solid. **Yield**: 0.0731 g, 39.1 %. **IR** (ATR): ν (cm^{-1}) = 2021 (s, carbonyl, C≡O), 1928 (s, carbonyl, C≡O), 1899 (s, carbonyl, C≡O), 1644 (m, imine, C=N), 1616 (m, bpy, C=N). **^{1}H NMR** ($(CD_3)_2SO$): δ (ppm) = 0.93 (br t, ^3J = 6.85 Hz, 3H, $NCH_2CH_2C\mathbf{H}_3$), 1.72 (br m, 2H, $NCH_2C\mathbf{H}_2CH_3$), 2.55 (br s, 3H, C**H**$_3$ *bpy*), 3.69 (br t, ^3J = 6.23 Hz, 2H, $NC\mathbf{H}_2CH_2CH_3$), 7.58 (br m, 1H, C**H** *bpy*), 7.97 (br m, 1H, C**H** *bpy*), 8.53 (br s, 1H, C**H** *imine*), 8.59 (br s, 1H, C**H** *bpy*), 8.82 (br s, 1H, C**H** *bpy*), 9.02 (br m, 1H, C**H** *bpy*), 9.25 (br m, 1H, C**H** *bpy*). **^{13}C{^{1}H} NMR** ($(CD_3)_2SO$): δ (ppm) = 11.7, 20.6 (**C**H_3); 23.3, 62.5 (**C**H_2); 120.9, 124.0, 124.3, 127.9, 154.1, 154.4 (**C**H *bpy*); 145.4, 151.3, 152.8, 158.1 (**C** *bpy*); 158.2 (**C**H *imine*); 221.0, 221.7, 222.0 (**C**O). **HPLC** (CH_3CN/H_2O (gradient, 5 - 90 %, flow rate, 0.6 mL/min)): t_R = 22.9 min. **MS** (HR-ESI-TOF, *m*/*z*): 462.02 $[M+H]^+$.

6.18 Electrochemical Studies

Electrochemical studies were not performed on the ferrocenyl-derived ligands **56** - **61**, as the focus of this study was on the ferrocenyl-derived complexes [**62**][PF_6]$_4$ - [**67**][PF_6]. Cyclic voltammetric studies were performed at ambient temperature using a Bioanalytical Systems Inc. BAS 100W Electrochemical Analyser with a one-compartment three-electrode system comprising of a Pt disk working electrode, a platinum wire auxiliary electrode and a Ag/Ag^+ reference electrode (0.01 M $AgNO_3$ and 0.1 M [*n*-Bu_4N][ClO_4] in anhydrous CH_3CN). The reported electrochemical potentials (listed in Tables 3.3 & 3.4 of Chapter 3) are with reference to this electrode. Measurements were made on anhydrous CH_3CN solutions which were 2 mM in sample and contained 0.1 M [*n*-Bu_4N][ClO_4] as the background electrolyte. San rates were optimised in an effort to obtain a smoother voltammogram. Unless otherwise stated, the scan rate used was 100 $mV.s^{-1}$. Under these conditions the ferrocene/ferrocenium couple, which was used as a reference, had an $E_{1/2}$ of +0.12 V and ΔE_p = 0.10 V. All solutions were purged with argon and voltammograms were recorded under a blanket of argon. The platinum working electrode was polished between runs.

6.19 X-ray Crystallography

Crystals of mononuclear complexes [**38**][PF_6], [**39**][PF_6], [**49**][PF_6], [**51**][PF_6] and [**66**][PF_6] were mounted on a STOE Image Plate Diffraction system equipped with a ϕ circle goniometer, using Mo-Kα graphite monochromated radiation (λ = 0.71073 Å) with ϕ range 0-200°. The structures were solved by direct methods using the program SHELXS-97, while the refinement and all further calculations were carried out using SHELXL-97.[15] The H-atoms were found on Fourier difference map or included in calculated positions and treated as riding atoms using the SHELXL default parameters. The non-H atoms were refined anisotropically, using weighted fullmatrix least-square on F^2.

Single-crystal X-ray diffraction data of **48** were collected on a Bruker KAPPA APEX II DUO diffractometer using graphite-monochromated Mo-Kα radiation (χ = 0.71073 Å). Data collection was carried out at 173(2) K. Temperature was controlled by an Oxford Cryostream cooling system (Oxford Cryostat). Cell refinement and data reduction were performed using the program SAINT.[16] The data were scaled and absorption correction performed using SADABS.[17] The structure was solved by direct methods using SHELXS-97 and refined by full-matrix least-squares methods based on F^2 using SHELXL-97.[15]

Crystallographic details are summarized in Tables 6.1, 6.2 and 6.3. Figures 2.8, 2.10, 2.11 and 3.18 were drawn with ORTEP.[18]

Table 6.1 *Crystallographic and selected experimental data for mononuclear complexes [**38**][PF_6] and [**39**][PF_6].*

	[**38**][PF_6]	[**39**][PF_6]
Chemical formula	$C_{26}H_{38}F_6N_4OP_2Ru$	$C_{28}H_{42}F_6N_4OP_2Ru$
Formula weight	699.61	727.67
Crystal system	Triclinic	Orthorhombic
Space group	*P* -1 (no. 2)	*P bca* (no. 61)
Crystal colour and shape	orange block	Yellow plate
Crystal size	0.17 x 0.15 x 0.09	0.22 x 0.18 x 0.16
a (Å)	9.2116(5)	14.364(3)
b (Å)	11.0549(6)	15.552(3)
c (Å)	15.4803(8)	28.435(6)
α (°)	102.868(4)	90
β (°)	97.444(4)	90
γ (°)	102.792(4)	90
V (Å^3)	1471.91(14)	6352(2)
Z	2	8
T (K)	173(2)	293(2)
D_c (g·cm^{-3})	1.579	1.522
μ (mm^{-1})	0.707	0.658
Scan range (°)	3.19 < 2θ < 55.71	4.04 < 2θ < 52.16
Unique reflections	7938	5901
Reflections used [$I>2\sigma(I)$]	6403	1639
R_{int}	0.0879	0.0836
Final *R* indices [$I>2\sigma(I)$][a]	R_1 0.0998, wR_2 0.2413	R_1 0.0451, wR_2 0.0870
R indices (all data)	R_1 0.1209, wR_2 0.2491	R_1 0.1792, wR_2 0.1061
Goodness-of-fit	1.217	0.642
Max, Min $\Delta\rho$ (e Å^{-3})	3.733, -2.034	0.588, -0.653

[a] Structures were refined on F_0^2: $wR_2 = [\Sigma[w(F_0^2 - F_c^2)^2] / \Sigma w(F_0^2)^2]^{1/2}$, where $w^{-1} = [\Sigma (F_0^2) + (aP)^2 + bP]$ and $P = [\max(F_0^2, 0) + 2F_c^2]/3$

Table 6.2 *Crystallographic and selected experimental data for mononuclear complexes* ***48****,* ***[49][PF$_6$]*** *and* ***[51][PF$_6$]****.*

	48	[**49**][PF$_6$]	[**51**][PF$_6$]
Chemical formula	$C_{20}H_{26}ClNOOs$	$C_{26}H_{38}F_6N_4OP_2Os$	$C_{19}H_{26}ClF_6N_2POs$
Formula weight	522.07	788.74	653.04
Crystal system	Orthorhombic	Triclinic	Triclinic
Space group	*Pbca*	*P* -1	*P* -1
Crystal colour and shape	Yellow needles	Orange block	Red block
Crystal size	0.15 x 0.13 x 0.08	0.22 x 0.19 x 0.18	0.17 x 0.16 x 0.13
a (Å)	12.8543(7)	9.2386(4)	9.2552(11)
b (Å)	18.2467(9)	11.0355(5)	9.8786(11)
c (Å)	32.5773(15)	15.4940(7)	12.2867(16)
α (°)	90.00	103.275(4)	82.159(15)
β (°)	90.00	97.262(4)	80.047(14)
γ (°)	90.00	102.771(4)	84.028(14)
V (Å^3)	7641.0(7)	1473.06(11)	1092.4(2)
Z	16	2	2
T (K)	173(2)	173(2)	173(2)
D_c (g·cm^{-3})	1.815	1.778	1.985
μ (mm^{-1})	6.821	4.503	6.092
Scan range (°)	5.04 < 2θ < 51.02	4.50 < 2θ < 55.55	4.10 < 2θ < 52.00
Unique reflections	7862	7950	4029
Reflections used [$I>2\sigma(I)$]	5977	6973	3263
R_{int}	0.0599	0.0590	0.0705
Final *R* indices [$I>2\sigma(I)$][a]	R_1 0.0289, wR_2 0.0504	R_1 0.0366, wR_2 0.0758	R_1 0.0503, wR_2 0.1184
R indices (all data)	R_1 0.0487, wR_2 0.0556	R_1 0.0467, wR_2 0.0780	R_1 0.0633, wR_2 0.1238
Goodness-of-fit	1.004	1.128	1.001
Max, Min $\Delta\rho$ (e Å^{-3})	0.758, -0.779	1.496, -2.190	3.053, -4.257

[a] Structures were refined on F_0^2: $wR_2 = [\Sigma[w(F_0^2 - F_c^2)^2] / \Sigma\, w(F_0^2)^2]^{1/2}$, where $w^{-1} = [\Sigma\,(F_0^2) + (aP)^2 + bP]$ and $P = [\max(F_0^2, 0) + 2F_c^2]/3$

Table 6.3 *Crystallographic and selected experimental data for mononuclear complexes [**66**][PF_6].*

	[**66**][PF_6]·H_2O
Chemical formula	$C_{38}H_{48}F_6N_4OP_2RuFe$
Formula weight	909.68
Crystal system	Monoclinic
Space group	*P* 2_1/c
Crystal colour and shape	Red block
Crystal size	0.25 x 0.22 x 0.20
a (Å)	11.0255(8)
b (Å)	8.6471(5)
c (Å)	41.358(3)
α (°)	90.00
β (°)	98.991(6)
γ (°)	90.00
V (Å^3)	3894.6(5)
Z	1
T (K)	293(2)
D_c (g·cm^{-3})	1.577
μ (mm^{-1})	0.911
Scan range (°)	1.87 < 2θ < 29.32
Unique reflections	10516
Reflections used [$I>2\sigma(I)$]	4523
R_{int}	0.2698
Final *R* indices [$I>2\sigma(I)$][a]	R_1 0.0736, wR_2 0.1298
R indices (all data)	R_1 0.1895, wR_2 0.1686
Goodness-of-fit	0.883
Max, Min Δ*ρ* (e Å^{-3})	0.733, -1.666

[a] Structures were refined on F_0^2: $wR_2 = [\Sigma[w(F_0^2 - F_c^2)^2] / \Sigma w(F_0^2)^2]^{1/2}$, where $w^{-1} = [\Sigma (F_0^2) + (aP)^2 + bP]$ and $P = [\max(F_0^2, 0) + 2F_c^2]/3$

6.20 NMR Experiments

6.20.1 Degradation Test

The first-generation metallodendrimer [**33**][PF_6]$_4$ (~0.1 mg/mL) and its mononuclear analog [**39**][PF_6] (~0.1 mg/mL) were dissolved in $(CD_3)_2SO$. $^{31}P\{^1H\}$ NMR experiments were performed at 37 ºC, at 15 min intervals over a 2h period. The $^{31}P\{^1H\}$ NMR spectra were recorded on a Bruker Biospin GmbH spectrometer at 162.00 MHz.

6.20.2 Aquatic Stability

For the hydrolysis studies first-generation metallodendrimer [**33**][PF_6]$_4$ (~0.1 mg/mL) was dissolved in D_2O:$(CD_3)_2SO$ (95:5 % *v*/*v*) because of limited solubility, and the sample was analyzed using ^1H and $^{31}P\{^1H\}$NMR experiments at 37 ºC over 14 days. ^1H and $^{31}P\{^1H\}$ NMR spectra were recorded daily on a Bruker Biospin GmbH spectrometer (^1H: 400.22 MHz, $^{31}P\{^1H\}$: 162.00 MHz).

6.20.3 Interactions with 5'GMP

For the 5'GMP binding studies, the mononuclear complex [**39**][PF_6] (used to model the higher generation metallodendrimers) was dissolved in a solution of 5'GMP (10 mg/mL) in D_2O:$(CD_3)_2SO$ (95:5 % *v*/*v*, because of limited solubility). The mixtures were incubated at 37 ºC for 2h before ^1H NMR experiments were performed. ^1H NMR spectra were recorded on a Bruker Biospin GmbH spectrometer (^1H: 400.22 MHz).

6.21 Biological Studies

6.21.1 Cell Culture and Inhibition of Cell Growth

The human A2780 and A2780cisR ovarian carcinoma cell lines were obtained from the European Collection of Cell Cultures (Salisbury, UK). Cells were grown routinely in RPMI-1640 medium with 10 % fetal calf serum (FCS) and antibiotics at 37 ºC and 5 % CO_2. Cytotoxicity was determined using the MTT assay (MTT = 3-(4,5-dimethyl-2-thiazolyl)-2,5-diphenyl-2H-tetrazolium bromide) (in triplicate).[19] Cells were seeded in 96-well plates as monolayers with 100 mL of cell solution (approximately 20,000 cells) per well and pre-incubated for 24 h in medium supplemented with 10 % FCS. Compounds were prepared as DMSO stock solutions, then immediately dissolved in the culture medium and serially diluted to the appropriate concentration, to give a final DMSO concentration of 0.5 %. Thus, the probability of DMSO-mediated ligand dissociation occurring is low. A 100 mL portion of drug solution was added to each well and the plates were incubated for another 72 h. Subsequently, MTT (5 mg/mL solution) was added to the cells and the plates were incubated for a further 2 h. The culture medium was aspirated, and the purple formazan crystals formed by the mitochondrial dehydrogenase activity of vital cells were dissolved in DMSO. The optical density, directly proportional to the number of surviving cells, was quantified at 590 nm using a multiwell plate reader and the fraction of surviving cells was calculated from the absorbance of untreated control cells. Evaluation is based on means from two independent experiments, each comprising three microcultures per concentration level.

6.21.2 DNA Binding Study

Samples were prepared by mixing a solution of 75 ng/mL pBR322 plasmid DNA with the appropriate complex at the appropriate concentration to give the required r value (0.5 and 0.25, r being the ratio of the metal centre to DNA base pairs). The samples were incubated for 24 h at 37 °C. The mobility of the plasmid DNA was analyzed by gel electrophoresis on 0.8 % at a constant voltage of 100 V for 1 h in tris-acetate-EDTA buffer. The gel was stained for 30 min in 0.5 mg/mL (*w*/*v*) ethidium bromide and the bands were then analyzed with an UVP gel scanner.

6.21.3 Cell Viability Study

Testing is done with cells growing in 96 well microtiter plates at 37 °C with 5 % CO_2/air. Shortly before confluency, cells are trypsinized and a single cell suspension is prepared. Cells are then plated out at a density of 250-2000 cells/well in 100 μL medium, depending on the cell line. Plates returned to the incubator and cells allowed to attach and begin growing for 24 h before adding test substances. On the day of testing, one untreated plate for each cell line is removed, fixed with glutaraldehyde and stored in the refrigerator; this plate serves later as the control. To prepare stock dilutions of test substances, five serial dilutions of substance in DMF or DMSO at 1000-fold the target concentration are performed. Next, these solutions are diluted 500-fold into culture medium to give five dilutions of test substance at 2-fold the target concentration. Then, 100 μL of medium containing test substance is added to each well, which already contains 100 μL of medium. The final solvent concentration (*i.e.* DMF or DMSO) in each well is 0.1 %. Plates are returned to the back of the incubator for 96 h. The method for quantifying growth inhibition is based on staining cells with crystal violet. After 96 h incubation with substance, culture medium is discarded and replace with 100 μL/well of a 1 % glutaraldehyde-buffer solution for 20 min to fix the cells. The fixing solution is discarded and the cells stored under 100 µl/well PBS at 4 °C until staining. Before staining, PBS medium is removed from all plates. Staining is done for 30 min with 100 μL/well of a 0.02 % solution of crystal violet dissolved in PBS buffer solution. After discarding the excess dye and washing the cells for 30 min in clear water, the cell bound dye is re-dissolved in 100 μL/well 70 % ethanol/water and the optical densities of the wells are measured at λ = 570 nm with a microtiter plate reader.

6.21.4 Myoglobin Assay

A solution of horse skeletal muscle myoglobin in phosphate buffer (PBS, 0.1 M, pH 7.4) was degassed by bubbling with dinitrogen and reduced by addition of sodium dithionite (100 mM, 100 μL) in PBS buffer (0.1 M, pH 7.4). The PBS buffer solution was prepared according to literature methods.[20] A concentrated stock solution of metal compounds **75**, **76**, or **77** in DMSO/H_2O (10:90, *v*/*v*) was added, followed by PBS to give a total volume of 1000 μL and final concentrations of 60 μM of myoglobin, 10 mM of sodium dithionite and 4 μM of **75**, 2 μM of **76**, or 10 μM of **77**. Solutions were freshly prepared for the dark stability and photoactivation experiments. Irradiations were carried out under dinitrogen with a custom-built LED setup at 410 nm (5 mm round type UV-LEDs, wavelength range 407-412 nm, model YDG-504VC, Kingbright Elec. Co., Taipei, Taiwan, http://www.kingbright.com, part no. 181000-05), positioned perpendicular to the cuvette at a distance of 5 cm (Figure 5.17, Chapter 5). The irradiation was interrupted in 1 min intervals during the initial 10 min, followed by 2 min intervals for the next 10 min, and then 5 min intervals to collect UV/Vis spectra on an Agilent 8453 UV/Vis diode array spectrophotometer until no more spectral changes were observed in the Q-band region of myoglobin. Dark control spectra were automatically collected for an extended period of time set by the spectrometer software. All irradiation experiments were carried out in triplicate

6.22 Ferrioxalate Actinometry

Ferrioxalate actinometry was used to determine the photon flux of the 410 nm LED array because of its sensitivity, wide spectral range including ultraviolet, and the ease of use.[21, 22] The entire ferrioxalate actinometry procedure including the preparation of solutions was carried out under dim red light. The moles of ferrous iron formed were determined spectrophotometrically by complexation with 1,10-phenanthroline (phen) to give the coloured tris-phenanthroline complex, $[Fe(phen)_3]^{2+}$ with λ_{max} = 510 nm. In a 1 cm quartz cell, 0.006 M (3 ml) of potassium ferrioxalate in 0.05 M sulfuric acid as the chemical actinometer was irradiated with a 410 nm LED array under efficient stirring. 1 ml of this irradiated solution was mixed with 0.1 % 1,10-phenanthroline in H_2O and 0.5 ml of sodium acetate buffer in H_2O (1 M, pH 3.5) and further diluted to 10 ml by H_2O. A reference was prepared in the same way except that it has not been irradiated. Both solutions were placed in the dark (about an hour) to allow the complexation to complete. The absorbance was then measured at 510 nm (ε = 11.100 $M^{-1}cm^{-1}$). The absorbance (A_{510}) was kept within the range of 0.4 - 1.0. The photon flux of the 410 nm LED array was then calculated by using $\Phi_{410\ nm}$ = 1.14 following the equation:[23]

$$\boldsymbol{\phi_P = \frac{\Delta A \cdot V_1 \cdot 10^{-3} \cdot V_3}{\phi_\lambda \cdot \varepsilon_{510} \cdot V_2 \cdot t}}$$

6.23 References

1. G. R. Fulmer, A. J. M. Miller, N. H. Sherden, H. E. Gottlieb, A. Nudelman, B. M. Stoltz, J. E. Bercaw and K. I. Goldberg, *Organometallics*, 2010, **29**, 2176-2179.
2. R. Malgas, S. F. Mapolie, S. O. Ojwach, G. S. Smith and J. Darkwa, *Catal. Commun.*, 2008, **9**, 1612-1617.
3. M. A. Torzilli, S. Colquhoun, D. Doucet and R. H. Beer, *Polyhedron*, 2002, **21**, 697-704.
4. M. A. Bennett and A. K. Smith, *J. Chem. Soc., Dalton Trans.*, 1974, **2**, 233-241.
5. M. A. Bennett, T. W. Matheson, G. B. Robertson, A. K. Smith and P. A. Tucker, *Inorg. Chem.*, 1980, **19**, 1014-1021.
6. R. Castarlenas, M. A. Esteruelas and E. Onate, *Organometallics*, 2005, **24**, 4343-4346.
7. J. Cloete and S. F. Mapolie, *J. Mol. Catal A: Chem.*, 2006, **243**, 221-225.
8. G. Smith, R. Chen and S. Mapolie, *J. Organomet. Chem.*, 2003, **673**, 111-115.
9. G. S. Smith and S. F. Mapolie, *J. Mol. Catal A: Chem.*, 2004, **213**, 187-192.
10. M. Gallei, R. Klein and M. Rehahn, *Macromolecules*, 2010, **43**, 1844-1854.
11. A. Sonoda, I. Moritani, T. Saraie and T. Wada, *Tetrahedron Lett.*, 1969, 2943-2946.
12. B. M. Peek, G. T. Ross, S. W. Edwards, G. J. Meyer, T. J. Meyer and B. W. Erickson, *Int. J. Peptide Protein Res.*, 1991, **38**, 114-123.
13. C. Busche, P. Comba, A. Mayboroda and H. Wadepohl, *Eur. J. Inorg. Chem.*, 2010, 1295-1302.
14. L. D. Ciana, I. Hamachi and T. J. Meyer, *J. Org. Chem.*, 1989, **54**, 1731-1735.
15. G. M. Sheldrick, *Acta Cryst.*, 2008, **A64**, 112-122.
16. G. M. Sheldrick, SAINT Version 7.60a, Brucker AXS Inc., Madison, WI, USA, 2006.
17. G. M. Sheldrick, SADABS, University of Gottingen, Germany, 1997.
18. L. Farrugia, *J. Appl. Cryst.*, 1997, **30**, 565.
19. J. van Meerloo, G. J. L. Kaspers and J. Cloos, in *Cancer Cell Culture: Methods and Protocols (Methods in Molecular Biology)*, ed. I. A. Cree, Humana Press, 2011, pp. 237-245.
20. N. Metzler-Nolte and U. Schatzschneider, *Bioinorganic Chemistry: A Practical Course*, Walter de Geuyter GmbH & Co., Berlin, 2009.
21. C. A. Parker, *Proc. Roy. Soc. A.*, 1953, **220**, 104-116.
22. C. G. Hatchard and C. A. Parker, *Proc. Roy. Soc. A.*, 1956, **235**, 518-536.
23. H. J. Kuhn, S. E. Braslavsky and R. Schmidt, *Pure Appl. Chem.*, 1989, **61**, 187-210.

Chapter 7

Overall Summary, Conclusions and Future Outlook

7.1 Conclusions

The main objectives of this study were to prepare new bioorganometallic metallodendrimers as potential metal-based therapeutic agents. These would contribute towards the development of the field of bioorganometallics.

7.1.1 Synthesis of Ruthenium-Arene and Osmium-Arene Metallodendrimers

A series of new ruthenium-arene and osmium-arene metallodendrimers were prepared and characterized using an array of spectroscopic and analytical techniques. The complexes were based on four generations of the 1,4-diaminobutane-poly(propylene) dendritic scaffold.

Two new third- and fourth-generation *N,O*-salicylaldiminato dendritic ligands **23** and **24** were prepared *via* Schiff base condensation between salicylaldehyde and the appropriate dendritic scaffold. Four new third- and fourth-generation neutral *N,O*-ruthenium-arene (arene = *p*-cymene or hexamethylbenzene) metallodendrimers **25** - **28** were prepared by coupling the appropriate ruthenium precursor (*i.e.* $[Ru(\eta^6\text{-}p\text{-}Pr^iC_6H_4Me)Cl_2]_2$ or $[Ru(\eta^6\text{-}C_6Me_6)Cl_2]_2$) and the appropriate *N,O*-salicylaldiminato dendritic ligand **23** or **24**. All these compounds (ligands and complexes) were characterized with ^1H, $^{13}C\{^1H\}$ NMR and FT-IR spectroscopy, MALDI-TOF or HR-ESI mass spectrometry, and elemental analysis.

Eight new first-, second-, third- and fourth-generation cationic *N,O*-ruthenium-arene-PTA (arene = *p*-cymene or hexamethylbenzene) metallodendrimers [**29**][PF_6]$_4$ - [**36**][PF_6]$_{32}$ were synthesized *via* a bridge-splitting reaction of the appropriate metal dimer (*i.e.* $[Ru(\eta^6\text{-}p\text{-}Pr^iC_6H_4Me)Cl_2]_2$ or $[Ru(\eta^6\text{-}C_6Me_6)Cl_2]_2$) and the *N,O*-salicylaldiminato dendritic ligand **21** - **24**. This was followed by the displacement of the chlorido ligand with PTA, to afford cationic compounds that were isolated as hexafluorophosphate salts in good yields. The cationic metallodendrimers were characterized with ^1H, $^{13}C\{^1H\}$, $^{31}P\{^1H\}$ NMR and FT-IR

spectroscopy, MALDI-TOF or HR-ESI mass spectrometry, and elemental analysis. Two new mononuclear complexes [**38**][PF_6] and [**39**][PF_6] were synthesized as models of the larger metallodendrimers [**29**][PF_6]$_4$ - [**36**][PF_6]$_{32}$, in order to compare size dependency on the antiproliferative activity. Single-crystal X-ray diffraction of [**38**][PF_6] and [**39**][PF_6] confirmed the expected pseudo-tetrahedral geometry around the Ru(II) ion and the coordination of the monomeric salicylaldiminato ligand **37**, in a bidentate-chelating manner through its phenolic oxygen and imine nitrogen.

To investigate whether the type of metal has influence on the biological activity, six new neutral and cationic osmium-arene complexes (**40** - [**43**][PF_6]$_8$, [**46**][PF_6]$_4$, [**47**][PF_6]$_8$) of their ruthenium analogs were prepared, by reacting the osmium-arene dimer [Os(η^6-*p*-Pr^{i}C$_6$H$_4$Me)Cl$_2$]$_2$ and the appropriate dendritic ligand (**21**, **22**, **44**, **45**). These metallodendrimers were characterized with ^{1}H, ^{13}C{^{1}H}, ^{31}P{^{1}H} NMR and FT-IR spectroscopy, HR-ESI mass spectrometry, and elemental analysis. The molecular structure of three new mononuclear osmium-arene complexes (**48**, [**49**][PF_6] & [**51**][PF_6]) were unambiguously determined by single-crystal X-ray diffraction and showed the expected pseudo-tetrahedral geometry around the osmium center.

7.1.2 Synthesis of Heterometallic Ferrocenyl-Derived Ruthenium-Arene Metallodendrimers

Two new *N,O*- and *N,N*- ferrocenyl-derived conjugates **54** and **55**, were prepared *via* a Heck coupling reaction of vinyl ferrocene **53** and the appropriate aryl-bromide. These conjugates were subsequently reacted with the appropriate dendritic scaffold, *via* a Schiff base condensation reaction, to afford four new *N,O*- and *N,N*- ferrocenyl-derived dendritic ligands **56** - **59**.

Four new heterometallic first- and second-generation cationic *N,O*- and *N,N*- ferrocenyl-derived ruthenium-*p*-cymene metallodendrimers [**62**][PF_6]$_4$ - [**65**][PF_6]$_8$ were synthesized *via* a bridge-splitting reaction between [Ru(η^6-*p*-Pr^{i}C$_6$H$_4$Me)Cl$_2$]$_2$ and the appropriate dendritic ligand **56** - **59**. All of the compounds were characterized using various analytical and spectroscopic techniques including FT-IR solid state, ^{1}H, ^{13}C{^{1}H} and ^{31}P{^{1}H} NMR spectroscopy, elemental analysis and HR-ESI mass spectrometry.

Two new *N,O*- and *N,N*- monomeric ligands **60** and **61**, were prepared *via* similar methods to the dendritic ligands **56** - **59**, with subsequent complexation to the ruthenium-*p*-cymene dimer $[Ru(\eta^6\text{-}p\text{-}Pr^iC_6H_4Me)Cl_2]_2$, afforded mononuclear derivatives [**66**][PF_6] and [**67**][PF_6]. The molecular structure of [**66**][PF_6] was elucidated by a single-crystal X-ray diffraction.

7.1.3 *In Vitro* Biological Activity

A series of new neutral and cationic ruthenium-arene metallodendrimers were evaluated for *in vitro* antitumor activity. Essentially the mononuclear analogs are inactive, whilst, the neutral *N,O*-ruthenium-arene metallodendrimers **25** - **28** exhibited moderate to high antiproliferative activity against both the A2780 and A2780cisR human ovarian cancer cell lines. Furthermore, the fourth-generation neutral *N,O*-ruthenium-arene metallodendrimers **26** and **28** displayed potent activity compared to cisplatin. The neutral *N,O*-ruthenium-hexamethylbenzene derivatives (**27**, **28**) displayed better activity, in both the A2780 and A2780cisR cell lines, compared to their *p*-cymene counter-parts (**25**, **26**), and was attributed to the improvement of the lipophilicity and improved hydrophobic interactions between the arene ring and DNA. The neutral *N,O*-ruthenium-*p*-cymene metallodendrimers (**25**, **26**) displayed an increase in resistance with an increase in dendrimer generation, whilst the neutral *N,O*-ruthenium-hexamethylbenzene metallodendrimers (**27**, **28**) displayed no cross-resistance to cisplatin. Furthermore, the neutral *N,O*-ruthenium-arene metallodendrimers **25** - **28** demonstrated lower toxicity against human embryonic kidney (HEK) cells.

The cationic *N,O*-ruthenium-arene-PTA metallodendrimers [**29**][PF_6]$_4$ - [**36**][PF_6]$_{32}$ displayed a similar trend in activity to their neutral derivatives **25** - **28**, with an excellent increase in cytotoxicity observed with an increase in dendrimer generation. Furthermore, incorporation of the PTA moiety does appear to improve the pharmacological properties of the dendritic systems. The fourth-generation cationic ruthenium-*p*-cymene metallodendrimer [**32**][PF_6]$_{32}$ displayed the highest activity in the high nanomolar range, with a two-fold increase in activity over the neutral chlorido-derivative **26**. The cationic *N,O*-ruthenium-hexamethylbenzene metallodendrimers [**29**][PF_6]$_4$ - [**32**][PF_6]$_{32}$ displayed a modest improvement in activity compared to their *p*-cymene counter-parts [**33**][PF_6]$_4$ - [**36**][PF_6]$_{32}$. With an increase in dendrimer generation, there was a decrease in resistance of the cationic ruthenium-hexamethylbenzene-PTA metallodendrimers [**33**][PF_6]$_4$ - [**36**][PF_6]$_{32}$ towards A2780cisR cells. These multinuclear complexes were consistently selective for cancer cells over the healthy cells.

First-generation cationic ruthenium-hexamethylbenzene metallodendrimer [**33**][PF_6]$_4$ and mononuclear derivative [**39**][PF_6] demonstrated good stability in DMSO-d_6 over a 2h period. The first-generation cationic ruthenium-hexamethylbenzene metallodendrimer [**33**][PF_6]$_4$ was stable in D_2O for 14 days with no side-products or aqua-species observed. The introduction of the *N,O*-chelate ligand resulted in enhanced stability of the complexes, and appeared that covalent binding to biomolecules might be a prerequisite for the compounds to exhibit such activity. Hence, preliminary ^{1}H and $^{31}P\{^{1}H\}$ NMR experiments used to monitor interactions between [**39**][PF_6] and nucleotide guanosine 5'-monophosphate (5'GMP), confirmed the coordination of the 5'GMP to the ruthenium centre *via* the *N*7 atom, and suggest that hydrolysis may not be a prerequisite in the mode of action of these complexes.

The metallodendrimers bearing chlorido ligands do not seem to interact with DNA. Whilst the metallodendrimers bearing the PTA ligand, that contained eight or more metal centres, appeared to form extensive DNA aggregates that was unable to migrate in the gel.

The antiproliferative activity of the neutral and cationic osmium-arene complexes (**40** - [**43**][PF_6]$_8$, [**46**][PF_6]$_4$, [**47**][PF_6]$_8$) presented in this study, were investigated *in vitro*. The neutral metallodendrimers showed no activity, whilst the cationic metallodendrimers displayed moderate activity in both cell lines (A2780 & A2780cisR). Once again, the PTA ligand improved biological properties of the dendritic systems, leading to improved antitumor activity. However, replacing ruthenium with osmium did not show vast improvement in the cytotoxicity of these complexes compared to their ruthenium analogs. Nevertheless, these were the first osmium-based metallodendrimers investigated as anticancer agents.

Preliminary cell viability studies performed on the ferrocenyl-derived ligands **56** - **61** and ferrocenyl-derived ruthenium-*p*-cymene complexes [**62**][PF_6]$_4$ - [**67**][PF_6] displayed activity at the 5 μM dose concentration in both the A2780 and A2780cisR cell lines, with no cross resistance to cisplatin observed. The data for the first- and second-generation ferrocenyl-derived *N,O*-ruthenium-*p*-cymene-PTA metallodendrimers [**62**][PF_6]$_4$ and [**63**][PF_6]$_8$ are the most active of the series. It does seem preparation of the mixed heterometallic ferrocenyl-derived ruthenium-arene systems do show better activity than the ferrocenyl-derived ligands, for at least two of the metallodendrimers.

Though a select number of complexes displayed low to moderate *in vitro* cytotoxicity compared to the benchmark drug cisplatin, they may display effective *in vivo* activity against metastasis cells, similarly observed for the ruthenium-based drugs RAPTA-C[1, 2] and NAMI-A.[3, 4]

7.1.4 Synthesis and CO-Release Properties of $Mn(CO)_3$-Functionalized Metallodendrimers

Two new *N*,*N*-bipyridylimine dendritic ligands **72** and **73** were prepared *via* a Schiff base condensation reaction of 4'-methyl-2,2'-bipyridine-4-carboxaldehyde **71** with the appropriate first- and second- generation DAB poly(propelene) dendritic scaffold.

Two new tetranuclear and octanuclear $Mn(CO)_3$-functionalized CO-releasing metallodendrimers **75** and **76**, based on first- and second-generation polypyridyl dendritic scaffolds, were prepared and comprehensively characterized by analytical and spectroscopic methods, such as ^{1}H, $^{31}C\{^{1}H\}$ NMR, FT-IR and UV/Vis spectroscopy and ESI-mass spectrometry. In addition, a new mononuclear analog **77** was synthesized as a model of the larger metallodendrimers in order to study potential size-dependent scaling effects on the photoactivated CO-release.

All three complexes are stable in solution and in air for an extended period of time in the absence of light. The CO-release of the metallodendrimers **75**, **76** and closest mononuclear analog **77** was investigated using the myoglobin assay, which showed that at least two of the three carbonyl ligands per $Mn(CO)_3$ moiety can be liberated under these conditions. The total amount of CO-released per molecular unit increases with the dendrimer generation, reaching a value of 15 CO per molecule of the second-generation metallodendrimer **76**. Furthermore, these peripherally functionalized dendritic systems were the first of its kind to contain CO-releasing moieties.

To conclude, although no exhaustive aspects of medicinal chemistry are given in this thesis, there are several key properties that should be addressed, such as tolerability, biocompatibility, pharmacokinetics and stability under physiological conditions. Exhaustive testing in the form of toxicity studies and biodistribution is required, as well as an examination of *in vivo* applications. Nevertheless, research highlighted in this thesis represents exciting developments in the medicinal applications of metallodendrimers that show potential and warrant further exploration in multinuclear metal-based drug discovery.

7.2 Future Outlook

7.2.1 Investigating Higher Dendrimer Generations and Alternative Dendritic Scaffolds

The present study has shown great scope of ruthenium-arene functionalized metallodendrimers as potential biological agents. Improved cytotoxicities may be possible by preparation of higher generation dendritic systems (higher than the 4th generation), in turn exploiting the enhanced permeability and retention (EPR) effect. Generally, all the complexes presented in this study may be structurally modified by replacing the DAB-dendritic scaffold with the highly water-soluble PAMAM dendritic scaffold, in an effort to increase the hydrophilicity of the complexes.[5, 6]

Anionic water-soluble metallodendrimers (bearing sulfonate groups) have been investigated as aqueous biphasic hydroformylation catalysts.[7] By applying this strategy and functionalizing the metallodendrimers with water-soluble sulfonate end-groups, may improve the lipophilicity and anticancer activity of these metallodendrimers presented in this study.

Furthermore, the disulfide bond (-S-S-) is a valuable functional group in a variety of chemical and biological agents that display potent reactivity or biological activities.[8] The disulfide bond has already been found in proteins, oxidized glutathione, and even in numerous natural products including some drugs.[8] Hence, the incorporation of the disulfide bond into the dendritic scaffold may influence the biological activity of these metallodendrimers and thus should be explored.

7.2.2 Exploring Covalently Bound Dendrimer-Drug Conjugates

Extended Ruthenium-Arene Systems

Mononuclear ruthenium-arene systems functionalized with an extended arene ring, such as tetrahydroanthracene, have shown good antiproliferative activity, whilst the biphenyl ring has shown to improve lipophilicity.[9] Hence, preparing ruthenium-arene metallodendrimers which include the extended arene system may improve selectivity and cell-uptake of these complexes presented in this study.

Cyclodextrin Derivatized Metallodendrimers

The regular and highly branched structure of metallodendrimers allows for the placement of repeating moieties on their surface. Terminally functionalized ferrocenyl-derived metallodendrimers have been reported, and each ferrocene moiety encapsulated with *β*-cyclodextrin.[10] The hydrophobic interior cavity and the hydrophilic exterior surface, makes cyclodextrins very attractive.[11] Hence, encapsulation of the ferrocenyl-derived ruthenium-arene moiety with such molecular hosts may afford improved lipophilicity and improved solubility in aqueous buffer solutions, which in turn may result in enhanced biological activities of the presented metallodendrimers.

Improved Heck Reaction

Chapter 3 discussed the preparation of ferrocenyl-derived ruthenium-arene complexes, where the key step in these reactions was to incorporate the ferrocenyl moiety *via* the Heck reaction. These reactions were successful; however the yields were low. Improvement on the reaction conditions may afford better yields, such as changing the reaction solvent to DMF or DMSO, to ascertain higher boiling temperatures. One could use the more reactive aryl-iodide as a substrate, utilize a different base such as Cs_2CO_3, changing the Pd-catalyst to the bulkier $Pd_2(dba)_3$ and/or varying the phosphine ligand to the bulkier P(*t*-Bu)$_3$. A number of alterations to the reaction conditions can be attempted in an effort to maximize the yield of the Heck reaction used in the preparation of these compounds.

Tagged Metallodendrimers

By functionalizing the arene ring with a fluorescent tag, a series of metallodendrimers can be prepared, and with the use of fluorescence microscopy the cell uptake of the drugs can be monitored. Furthermore, with this technique possible drug targets may be identified. Radiolabelled metallodendrimers, bearing the ruthenium isotope ^{106}Ru, can be prepared in an effort to show the biodistribution of the compounds within the cell, similarly observed by Sadler and co-workers.[12]

7.2.3 Exploring the Biology

Further Biological Studies

In order to make a comparison, further *in vitro* experiments to calculate the IC_{50} values of the heterometallic ferrocenyl-derived ruthenium-arene metallodendrimers described in Chapter 3 should be performed, in both the A2780 and A2780cisR human ovarian cancer cell lines.

A series of biological experiments can be employed such as, screening across several cell lines to show selectivity, *in vivo* experiments, DNA binding experiments, circular dichroism experiments, reactive-oxygen species (ROS) studies and atomic force microscopy (AFM) studies. These are just some of the biological studies and experiments that may assist in elucidating the mode of action of these potential therapeutic agents.

In Vitro Testing of CO-Releasing Metallodendrimers

The next step in the discovery of new CO-realising agents, involves investigating the *in vitro* photoactivity of these metallodendrimers presented here, against cancer cells, more specifically against adherent HT29 human colon cancer cells, in the form of cell viability studies. Variation of the bidentate ligand, will allow for the discovery of new CO-releasing molecules with varying CO-release and biological activities.

7.3 References

1. C. Scolaro, A. Bergamo, L. Brescacin, R. Delfino, M. Cocchietto, G. Laureneczy, T. J. Geldbach, G. Sava and P. J. Dyson, *J. Med. Chem.*, 2005, **48**, 4161-4171.
2. S. Chatterjee, S. Kundu, A. Bhattacharyya, C. G. Hartinger and P. J. Dyson, *J. Biol. Inorg. Chem.*, 2008, **13**, 1149-1155.
3. S. Zorzet, A. Bergamo, M. Cocchietto, A. Sorc, B. Gava, E. Alessio, E. Iengo and G. Sava, *J. Pharmcol. Exp. Ther.*, 2000, **295**, 927-933.
4. G. Sava, S. Zorzet, C. Turrin, F. Vita, M. R. Soranzo, G. Zabucchi, M. Cocchietto, A. Bergamo, S. Di Giovine, G. Pezzoni, L. Sartor and S. Garbisa, *Clin. Cancer Res.*, 2003, **9**, 1898-1905.
5. R. Duncan and L. Izzo, *Adv. Drug Delivery Rev.*, 2005, **57**, 2215-2237.
6. M. El-Sayed, M. Ginski, C. Rhodes and H. Ghandehari, *J. Controlled Release*, 2002, **252**, 355-365.
7. E. B. Hager, C. E. Makhubela and G. S. Smith, *Dalton Trans.*, 2012, **41**, 13927-13935.
8. M. H. Lee, Y. Z., C. W. Lim, Y. H. Lee, S. Dongbang, C. Kang and J. S. Kim, *Chem. Rev.*, 2012, **113**, 5071-5109.
9. R. E. Aird, J. Cummings, A. A. Ritchie, M. Muir, R. E. Morris, H. Chen and P. J. Sadler, *Br. J. Cancer.*, 2002, **86**, 1652-1657.
10. R. Castro, I. Cuadrado, B. Alonso, C. M. Casado, M. Moran and A. E. Kaifer, *J. Am. Chem. Soc.*, 1997, **119**, 5760-5761.
11. E. Bilensoy, in *Handbook of Particulate Drug Delivery*, ed. M. N. V. R. Kumar, 2008, vol. 1, pp. 187-204.
12. J. D. Hoeschele, A. Habtemariam, M. Muir and P. J. Sadler, *Dalton Trans.*, 2007, **43**, 4974-4979.